NANOFABRICATION FOR SMART NANOSENSOR APPLICATIONS

Edited by
Kaushik Pal
Fernando Gomes

ELSEVIER

Micro & Nano Technologies Series

Nanofabrication for Smart Nanosensor Applications

Nanofabrication for Smart Nanosensor Applications

Edited by

Kaushik Pal

International and Inter University Centre for Nanoscience and Nanotechnology (IIUCN), School of Energy Materials, Mahatma Gandhi University, Kottayam, Kerala, India; Wuhan University, Wuchang District, Wuhan, Hubei Province, Republic of China

Fernando Gomes

Macromolecule Institute Professor Eloisa Mano; Civil Engineering Program, COPPE, Technology Center - University City, Federal University of Rio de Janeiro, Rio de Janeiro, Brazil

ELSEVIER

Elsevier
Radarweg 29, PO Box 211, 1000 AE Amsterdam, Netherlands
The Boulevard, Langford Lane, Kidlington, Oxford OX5 1GB, United Kingdom
50 Hampshire Street, 5th Floor, Cambridge, MA 02139, United States

© 2020 Elsevier Inc. All rights reserved.

No part of this publication may be reproduced or transmitted in any form or by any means, electronic or mechanical, including photocopying, recording, or any information storage and retrieval system, without permission in writing from the publisher. Details on how to seek permission, further information about the Publisher's permissions policies and our arrangements with organizations such as the Copyright Clearance Center and the Copyright Licensing Agency, can be found at our website: www.elsevier.com/permissions.

This book and the individual contributions contained in it are protected under copyright by the Publisher (other than as may be noted herein).

Notices

Knowledge and best practice in this field are constantly changing. As new research and experience broaden our understanding, changes in research methods, professional practices, or medical treatment may become necessary.

Practitioners and researchers must always rely on their own experience and knowledge in evaluating and using any information, methods, compounds, or experiments described herein. In using such information or methods they should be mindful of their own safety and the safety of others, including parties for whom they have a professional responsibility.

To the fullest extent of the law, neither the Publisher nor the authors, contributors, or editors, assume any liability for any injury and/or damage to persons or property as a matter of products liability, negligence or otherwise, or from any use or operation of any methods, products, instructions, or ideas contained in the material herein.

Library of Congress Cataloging-in-Publication Data
A catalog record for this book is available from the Library of Congress

British Library Cataloguing-in-Publication Data
A catalogue record for this book is available from the British Library

ISBN: 978-0-12-820702-4

For information on all Elsevier publications
visit our website at https://www.elsevier.com/books-and-journals

Publisher: Matthew Deans
Acquisitions Editor: Simon Holt
Editorial Project Manager: Fernanda Oliveira
Production Project Manager: Prem Kumar Kaliamoorthi
Cover Designer: Greg Harris

Typeset by SPi Global, India

Contributors

M.M. Abdullah Promising Centre for Sensors and Electronic Devices (PCSED), Department of Physics, Faculty of Science and Arts, Najran University, Najran, Saudi Arabia

Mostafa G. Aboelkheir Macromolecule Institute Professor Eloisa Mano, Technology Center - University City, Federal University of Rio de Janeiro, Rio de Janeiro, Brazil

Gulzar Ahmad Department of Physics, University of Agriculture, Faisalabad, Pakistan

Mazhar S. Al Zoubi Department of Basic Medical Studies, Yarmouk University, Irbid, Jordan

Khalid M. Al-Batanyeh Department of Biological Sciences, Yarmouk University, Irbid, Jordan

Norma Alias Center for Sustainable Nanomaterials, Ibnu Sina Institute for Scientific and Industrial Research, Universiti Teknologi Malaysia, Skudai, Malaysia

Alaa A.A. Aljabali Department of Pharmaceutics and Pharmaceutical Technology, Faculty of Pharmacy, Yarmouk University, Irbid, Jordan

Lorca Alzoubi Department of Pharmaceutics and Pharmaceutical Technology; Medicinal Chemistry and Pharmacognosy Department, Faculty of Pharmacy, Yarmouk University, Irbid, Jordan

Nidhi Asthana National Centre of Experimental Mineralogy and Petrology, University of Allahabad, Allahabad, India

Murthy Chavali Shree Velagapudi Rama Krishna Memorial College (PG Studies), Affiliated to Acharya Nagarjuna University, Nagaram; PG Department of Chemistry, Dharma Appa Rao College, Affiliated to Krishna University, Nuzvid; NTRC, MCETRC, Tenali, Andhra Pradesh, India

Ramchander Chepyala FPC@DCU – Fraunhofer Project Centre for Embedded Bioanalytical Systems at Dublin City University, Dublin City University, Dublin, Ireland

Shiplu Roy Chowdhury Tissue Engineering Centre, Faculty of Medicine, Universiti Kebangsaan Malaysia, Kuala Lumpur, Malaysia

Vítor Corrêa da Costa Macromolecule Institute Professor Eloisa Mano, Technology Center - University City, Federal University of Rio de Janeiro, Rio de Janeiro, Brazil

Michael K. Danquah Chemical Engineering Department, University of Tennessee, Chattanooga, TN, United States

Krishna Chitanya Etika Department of Chemical Engineering, Birla Institute of Technology and Science, Pilani, Rajasthan, India

Irene S. Fahim Industrial Engineering Department, Smart Engineering Systems Research Center (SESC), Nile University, Giza, Egypt

Romildo Dias Toledo Filho Civil Engineering Program, COPPE, Technology Center - University City, Federal University of Rio de Janeiro, Rio de Janeiro, Brazil

Sanjeev Gautam Netaji Subhas University of Technology, Delhi, India

Ganesh Gollavelli Centre of Excellence of Nanotechnology; Department of Industrial Chemistry, College of Applied Sciences, Addis Ababa Science and Technology University, Addis Ababa, Ethiopia

Hazidatul Akma Hamlan Center for Sustainable Nanomaterials, Ibnu Sina Institute for Scientific and Industrial Research, Universiti Teknologi Malaysia, Skudai, Malaysia

Ahmed M. Hassanein Nanoelectronics Integrated Systems Center (NISC), Nile University, Giza, Egypt

Md Enamul Hoque Department of Biomedical Engineering, Military Institute of Science and Technology (MIST), Dhaka, Bangladesh

Saiqa Ikram Bio/Polymer Research Laboratory, Department of Chemistry, Jamia Millia Islamia, New Delhi, India

Purnima Jain Netaji Subhas University of Technology, Delhi, India

Yasir Javed Department of Physics, University of Agriculture, Faisalabad, Pakistan

Jaison Jeevanandam Department of Chemical Engineering, Curtin University, Miri, Sarawak, Malaysia

Rocktotpal Konwarh Department of Biotechnology, College of Biological and Chemical Engineering; Centre of Excellence of Nanotechnology, Addis Ababa Science and Technology University, Addis Ababa, Ethiopia

Samo Kralj Faculty of Natural Sciences and Mathematics, University of Maribor, Maribor, Slovenia

Amit Kumar Dyal Singh College, University of Delhi, Delhi, India

Enamala Manoj Kumar Bioserve Biotechnologies (India) Private Ltd., Hyderabad, Telangana, India

Ahmed H. Madian Nanoelectronics Integrated Systems Center (NISC), Nile University, Giza; Radiation Engineering Department, NCRRT, Egyptian Atomic Energy Authority, Cairo, Egypt

Tariq Mahbub Department of Mechanical Engineering, Military Institute of Science and Technology, Dhaka, Bangladesh

Zaid Bin Mahbub Department of Mathematics and Physics, North South University, Dhaka, Bangladesh

Ahmed Nawaz Department of Physics, University of Agriculture, Faisalabad, Pakistan

Somia Nawaz Department of Physics, University of Agriculture, Faisalabad, Pakistan

Mohammad A. Obeid Department of Pharmaceutics and Pharmaceutical Technology, Faculty of Pharmacy, Yarmouk University, Irbid, Jordan

Kaushik Pal International and Inter University Centre for Nanoscience and Nanotechnology (IIUCN), School of Energy Materials, Mahatma Gandhi University, Kottayam, Kerala, India; Wuhan University, Wuchang District, Wuhan, Hubei Province, Republic of China

Periasamy Palanisamy Department of Physics, Gnanamani College of Engineering, Namakkal, Tamil Nadu, India

Suresh Babu Palanisamy Department of Biotechnology, College of Biological and Chemical Engineering, Addis Ababa Science and Technology University, Addis Ababa, Ethiopia

Mamun Rabbani Department of Biomedical Physics and Technology, University of Dhaka, Dhaka, Bangladesh

Lobna A. Said Nanoelectronics Integrated Systems Center (NISC), Nile University, Giza, Egypt

M. Munir Sajid Department of Physics, Government College University, Faisalabad, Pakistan

Naveed Akhtar Shad Department of Physics, Government College University, Faisalabad, Pakistan

Bhasha Sharma Netaji Subhas University of Technology, Delhi, India

Shreya Sharma Netaji Subhas University of Technology, Delhi, India

Zayed Bin Zakir Shawon Department of Mathematics and Natural Sciences, BRAC University, Dhaka, Bangladesh

Shashank Shekhar Netaji Subhas University of Technology, Delhi, India

Asiya S.I. Bharath Institute of Higher Education and Research (BIHER), Bharath University, Chennai, Tamil Nadu, India

Preeti Singh Bio/Polymer Research Laboratory, Department of Chemistry, Jamia Millia Islamia, New Delhi, India

Fernando Gomes Macromolecule Institute Professor Eloisa Mano; Civil Engineering Program, COPPE, Technology Center - University City, Federal University of Rio de Janeiro, Rio de Janeiro, Brazil

Murtaza M. Tambwala SAAD Centre for Pharmacy and Diabetes, School of Pharmacy and Pharmaceutical Science Ulster University, Coleraine, United Kingdom

Sabu Thomas International and Inter University Centre for Nanoscience and Nanotechnology (IIUCN), School of Chemical Sciences, Mahatma Gandhi University, Kottayam, Kerala, India

Editors' biography

Professor (Dr.) Kaushik Pal is an Indian citizen. He did his PH.D. in Physics (e.g. Nanotechnology, Multidisciplinary Sciences, Advanced Materials Science, Spectroscopy) from University of Kalyani, West-Bengal, India. Most recently he awarded with honorable **DOCTOR OF SCIENCE (D.SC.)** from **Higher National Youth Skill Institute, Sepang, Selangor, Malaysia**. He is the "Distinguish Research Professor" at ***Federal University of Rio de Janeiro, Brazil*** and acting as "Chair Professor and Group Leader, (Chief-Scientist & Faculty Fellow)" position in ***Wuhan University, Wuchang Dist., Hubei Province, Republic of China***. Most recently, he has been a visiting professor working and contributing at the International and Inter University Centre for Nanoscience and Nanotechnology (IIUCN), School of Energy Materials, Mahatma Gandhi University, Kottayam, Kerala. He awarded international prestigious awards e.g. awarded the Marie-Curie Experienced Researcher (Postdoctoral Fellow) by the European Commission Network in Greece, and received the Brain Korea (BK-21) National Research Foundation Visiting Scientist Fellowship in South Korea. He was appointed Senior Postdoctoral Fellow at Wuhan University, China and within a year achieved the prestigious position of Chief-Scientist and Faculty (CAS) Fellow by the Chinese Academy of Science. He served as research professor (Group Leader and Independent Scientist), at Bharath University (BIHER), Research and Development, Chennai. His current research spans are focusing on e.g. Molecular Nanoscience and nanofabrication, functional materials, condensed matter physics (expt.), CNTs/graphene, liquid crystal, polymeric nanocomposite, switchable device, electron microscopy and spectroscopy, bioinspired materials, drug delivery, integration, switchable device modulation, stretchable electronics, supercapacitors, optoelectronics, green chemistry, and biosensor applications. He supervises a significant number of bachelor's, master's, PhD, and postdoctoral scholar's theses, and his research has been published in several international top-tier journals from publishers e.g. Royal Chemical Society, Elsevier, Springer, IEEE, and InTech. He has edited 25 book chapters with significant publishers, contributed 10 review articles, and has edited several books for Elsevier, Apple Academic Press, and InTech. Dr. Pal is an expert group leader and the associate member of various scientific societies, organizations, and professional bodies. In his academic and professional research, he has received a number of significant

awards and prizes. He has been the chairperson of 30 national and international events, symposia, conferences, and workshops, and has contributed to 10 plenary, 28 keynote, and 30 invited lectures worldwide.

Professor Fernando Gomes graduated in chemistry from the Federal University of Espírito Santo (1999), and received a Master in Engineering and Materials Science from the State University of the North Fluminense Darcy Ribeiro (2002), a PhD in Science and Technology of Polymers from the Federal University of Rio de Janeiro (2006), and a postdoctorate in the chemical engineering program at COPPE/UFRJ, Brazil. He is currently Associate Professor at the Macromolecules Institute at UFRJ, Collaborated Professor at the Civil Engineering Program at COPPE/UFRJ and Young Scientist in the State of Rio de Janeiro (FAPERJ-2015). He mainly works with polymeric nanocomposites obtained from renewable resources in three main lines: (I) in the field of environmental recovery, coordinating research projects focused on the use of renewable resources for the removal of oil in spills; (II) in the field of human health, coordinating projects that seek kinetic and spatial control of the drug release process; and (III) in the field of sensors, where he coordinates projects that seek to obtain plant fibers that conduct electricity for their use in sensors for intelligent devices. Supervisor of **103** undergraduate students; **28** M.Sc. students, **8** Ph.D. students and **5** Post Doc. Nowadays I am the supervisor of **4** undergraduate students; **2** M.Sc. students, **14** Ph.D. students and **2** Post Doc. Member of the editorial board of Current Applied Polymer Science (ISSN 2452-2716), Associate Editor of the MedCrave Online Journal (MOJ) Polymer Science (ISSN: 2574-9773), and Editor of the Academic Journal of Polymer Science. He also awarded Young Scientist of Rio de Janeiro State (FAPERJ 2011 and 2014), member of Post Graduate Program in Science and Technology of Polymers of the Federal University of Rio de Janeiro since 2008.

CHAPTER 1

Introduction to nanomaterials and nanomanufacturing for nanosensors

Tariq Mahbub[a], **Md Enamul Hoque**[b]

[a]*Department of Mechanical Engineering, Military Institute of Science and Technology, Dhaka, Bangladesh*
[b]*Department of Biomedical Engineering, Military Institute of Science and Technology (MIST), Dhaka, Bangladesh*

1.1 Nanosensors

Sensors are devices used to detect the presence of a specific substance or to measure a physical property such as temperature, mass, or electrical or optical characteristics and produce a signal for recording or further postprocessing. The history of sensors is a long one. The first thermostat came into existence in the 1880s, and the first infrared sensor was developed in 1940. Nanosensors are similar to macrolevel sensors but have at least one dimension in nanoscale and can be used to measure signals available at that scale. Nanotechnology, with its rapid developments in recent years, has shown great potential in almost all industries. Various electronics industries have fueled these developments to satisfy their need for miniaturization, and the nanosensor field has taken advantage of these advances for its own development. A large volume of research has been conducted over the last two decades in the area of nanomaterials for wider applications, including nanosensors [1–10]. Since nanosensors can deal with signals produced at the nanoscale, the sample quantities needed are quite small and detection is very rapid. All of these qualities have helped the applications of various types of nanosensors in different fields, especially in the medical and homeland security fields. Gaining a clearer understanding of the special properties offered at the nanoscale by nanomaterials, evolution of the various techniques for nanomaterial production, and exploitation of the special properties of nanomaterials have all advanced nanosensor development.

Nanofabrication for Smart Nanosensor Applications. https://doi.org/10.1016/B978-0-12-820702-4.00001-5
© 2020 Elsevier Inc. All rights reserved.

1.1.1 Types of nanosensors

During the short history of nanosensors, this technology has experienced substantial developments. Since a variety of nanosensors are available today, classification can be somewhat difficult. However, nanosensors can be classified based on two general factors: (1) structure and (2) application.

Based on structure, nanosensors can be further classified into two groups:

Optical nanosensors: Optical nanosensors use the sensitivity of fluorescence for qualitative and quantitative measurement.

Electrochemical nanosensors: This class of nanosensor mainly detects electronic or chemical properties of a respective substance and transduces a signal. Recently, major developments have taken place in this type of nanosensor technology.

Based on application, nanosensors can be classified into chemical nanosensors, nanoscale electrometers, nanobiosensors, deployable sensors, and so on.

1.1.2 Applications of nanosensors

Nanosensors are gradually assuming roles in almost every aspect of human life. A number of sensors can detect the presence of hazardous materials or microorganisms in food, water, and air. These sensors are saving lives in different corners of the world. In the medical field nanosensors are having a huge impact: for example, a variety of nanosensors are being used in cancer detection, DNA and protein detection, and targeted drug delivery. Deployable sensors have found applications in homeland security. Various chemical sensors are now added to unmanned aerial vehicles to detect the presence of poisonous gas on the battlefield, to save the lives of soldiers. Various tagging systems employ RFID chips, which are also an application of nanosensors.

1.2 Nanomaterials for nanosensors

For centuries the beauty of the 400 CE Lycurgus Cup and the strength and beauty of a Damascus steel blade have amazed people, but it has been only decades since we discovered the secret behind these extraordinary ancient artifacts: nanomaterials [11,12]. Nanomaterials are defined as those nanoparticles (NPs) that have at least one dimension in nanometer scale and that exhibit some special property that is not available in the bulk form of the same material. Though unknowingly used in several ancient artifacts, the modern-day extensive research, informed fabrication, and utilization of nanomaterials began in 1857, when Michael Faraday reported the synthesis of so-called “activated gold,” which was a colloidal solution

of Au NPs [13]. Since that time, the use of nanomaterials has slowly but surely spread, due to their extraordinary properties associated with their size. Nanomaterials show extraordinary properties different than their bulk size because of their nanoscale dimension. The surface-to-volume ratio of nanomaterials is very high, which results in variations in chemical, mechanical, optical, and magnetic nature [14]. To explore the properties and applications of nanomaterials properly, it is judicious to classify them. However, several factors can be considered in classifying nanomaterials, such as physical and chemical properties, manufacturing process, dimensionality, uniformity, composition, and so forth [15]. From the point of view of this chapter, we classify nanomaterials into four classes based on their chemical composition: (1) carbon-based, (2) organic-based, (3) inorganic-based, and (4) composite-based nanomaterials. In the following sections, we discuss different nanomaterials that fall within these four categories and their applications, especially as nanosensors.

At this point, a brief introduction to nanosensors may be very helpful for those new to this field. A sensor is a device that detects and responds to any change in its environment. Daily life is full of sensors, such as light sensors, rain sensors, lane assist in automobiles, smoke and fire alarm sensors, electrical sensors, and so forth. Nanosensors perform the same function, but on a much smaller scale (1–100 nm), capable of sensing pathogens, viruses, molecules, or even a single chemical element. The main advantages of nanosensors are the minute sample quantities required, speed, portability, and low cost in mass production, among others.

The history of nanosensors is only decades old. Since the beginning of the current century, the world has experienced a rapid escalation of production and use of nanosensors as a consequence of two factors. First, nanosensors, due to their excellent performance, have convinced the world that they can be successfully used in different applications varying from the food industry, fire and hazardous gas detection, to various critical fields like military and advanced medical applications. Secondly, there is a tremendous advancement of different manufacturing processes used for manufacturing nanosensors, increased availability, and development of new nanomaterials and more clear understanding of nanoscale phenomena [16].

1.2.1 Properties of nanomaterials for nanosensors

Nanomaterials, due to high surface-to-volume ratio and the manufacturing process, offer some extraordinary properties that can be explored to produce various applications in drug manufacturing, environmental sensing and protection, materials and manufacturing industries, electronics, energy harvesting, etc. A few properties that are relevant to nanosensors are briefly described in the following sections.

1.2.1.1 Optical properties

Nanomaterials offer some excellent optical properties, such as light absorption, color, light emission, and magnetooptical properties due to their sizes; these properties are quite different from their bulk properties and make nanomaterials a good choice for optical nanosensors. One of the first nanosensors devised to measure inhomogeneous pH distribution in three-dimensional resolution was fluorescein-based, using a polyacrylamide nanoparticle incorporated with pH-sensitive fluorescein-acrylamide [17]. Fluorescent nanosensors can respond to some specific stimuli provided by the surrounding environment and transduce a fluorescence signal to the detector to sense environmental changes. These nanosensors are used to make oxygen sensors [18] and temperature sensors. The localized surface plasmon (LSP) effect of the noble metal nanoparticle is a current active field of research for making nanosensors (Fig. 1.1). When a nanoparticle confines surface plasmon, due to its dimension, comparable to the wavelength of light, the free electron of the nanoparticle participates in the collective oscillation. This phenomenon is called localized surface plasmon (LSP) [19]. The LSP effect greatly enhances the electric field near the nanoparticle surface and at the plasmon resonant frequency the particle shows maximum optical extinction. A number of gas sensors [20,21] and pH sensors [22,23] are manufactured using LSP.

1.2.1.2 Electronic properties

Nanomaterials can offer quite exceptional electronic properties that originate from the shape and structure of the nanomaterial. When talking about exceptional electronic properties, the name that comes to mind first is graphene. Graphene has a single-layer 2D honeycomb structure in which both surfaces are available for molecule absorption. The structure causes the electron seemly to be massless [24] and the electron moves at an average speed which is 300 times less than the speed of light at vacuum. This allows many relativistic events to be

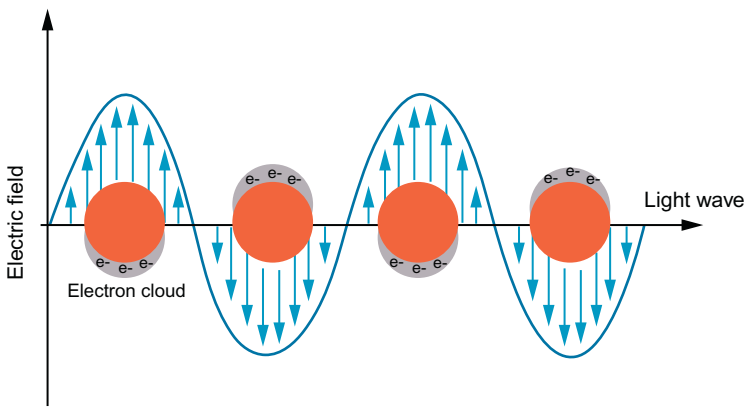

Fig. 1.1
Schematic diagram of localized surface plasmon effect.

observable without a particle accelerator [15]. The carbon nanotube (CNT) in which graphene acts as a building block also offers some excellent electronic properties. The sp^2 hybridization of the carbon orbitals in the CNT leaves free electrons at the surface of the tubes, which yields these excellent properties. CNT can show metallic, semiconducting, or insulating behavior, which can be controlled by controlling the diameter, chirality of the CNT, and any functionalization or doping done on CNT [25]. Nanosensors using these properties detect using two methods: (a) current enhancement, and (b) current inhibition. Various electrochemical sensors have been developed for different purposes, such as detecting dopamine [26], histamine [27], bacteria [28], glucose [29], and so forth, using the electronic properties of nanomaterials.

1.2.1.3 Magnetic properties

Due to the uneven arrangement and orientation of electrons in nanomaterials, and their size, nanomaterials exhibit excellent magnetic properties too. Magnetic properties of nanomaterials are becoming a center of interest in different branches of engineering, including but not limited to different types of catalysis, biomedicine for cancer treatment, magnetic fluids, nuclear magnetic resonance imaging (NMR), magnetic resonance imaging (MRI), and environmental remediation [30]. Magnetic nanosensors use different techniques to perform detection, like the effect magnetic particles exert on water proton relaxation rates, by determining the relaxation of the magnetic moment within the magnetic particle, by detecting the presence of a magnetic particle using magnetoresistivity, etc. Koh et al. explain different biosensors using the previously mentioned methods. The following figures show schematic representations of the three procedures [31]. Fig. 1.2A represents how magnetic nanoparticles dephase the protons of water for a better MRI scan. Magnetic particles generally stay dispersed in a liquid solvent. But when a target analyte (triangle in Fig. 1.2A) appears, the dispersed nanoparticles produce an aggregate around it and eventually this aggregate dephases the spins of water protons more efficiently than the dispersed state. This reduces the spin-spin relaxation time T_2 to produce a better MRI image. Fig. 1.2B shows the application of magnetic moment relaxation within a magnetic nanoparticle for bacterial detection. The type of relaxation used here is Neel relaxation. In the upper figure A, a magnetic field is applied to the nanoparticles and they orient themselves along the applied field. Some of the nanoparticles are bonded with the target bacteria. Later, in figure B, the field is removed and many of the particles experience Brownian relaxation and randomly orient in a different direction. But the nanoparticles bonded to the bacteria cannot undergo Brownian relaxation and rather show Neel relaxation, which is comparatively slower and detectable. The superconducting quantum interference devices (SQUIDs) detect the slower Neel relaxation and bacterial detection is performed. Fig. 1.2C shows the operation of a magnetoresistive sensor. The basic principle that a magnetoresistive sensor applies is that the magnetic particle bonds to the surface of the sensor and eventually alters its magnetic field. This causes a change in sensor current and the detection is performed. There are two mechanisms through which magnetic particles bind to the sensor surface: (i) direct labeling, and (ii) indirect labeling. In the case of direct labeling, magnetic nanoparticles directly

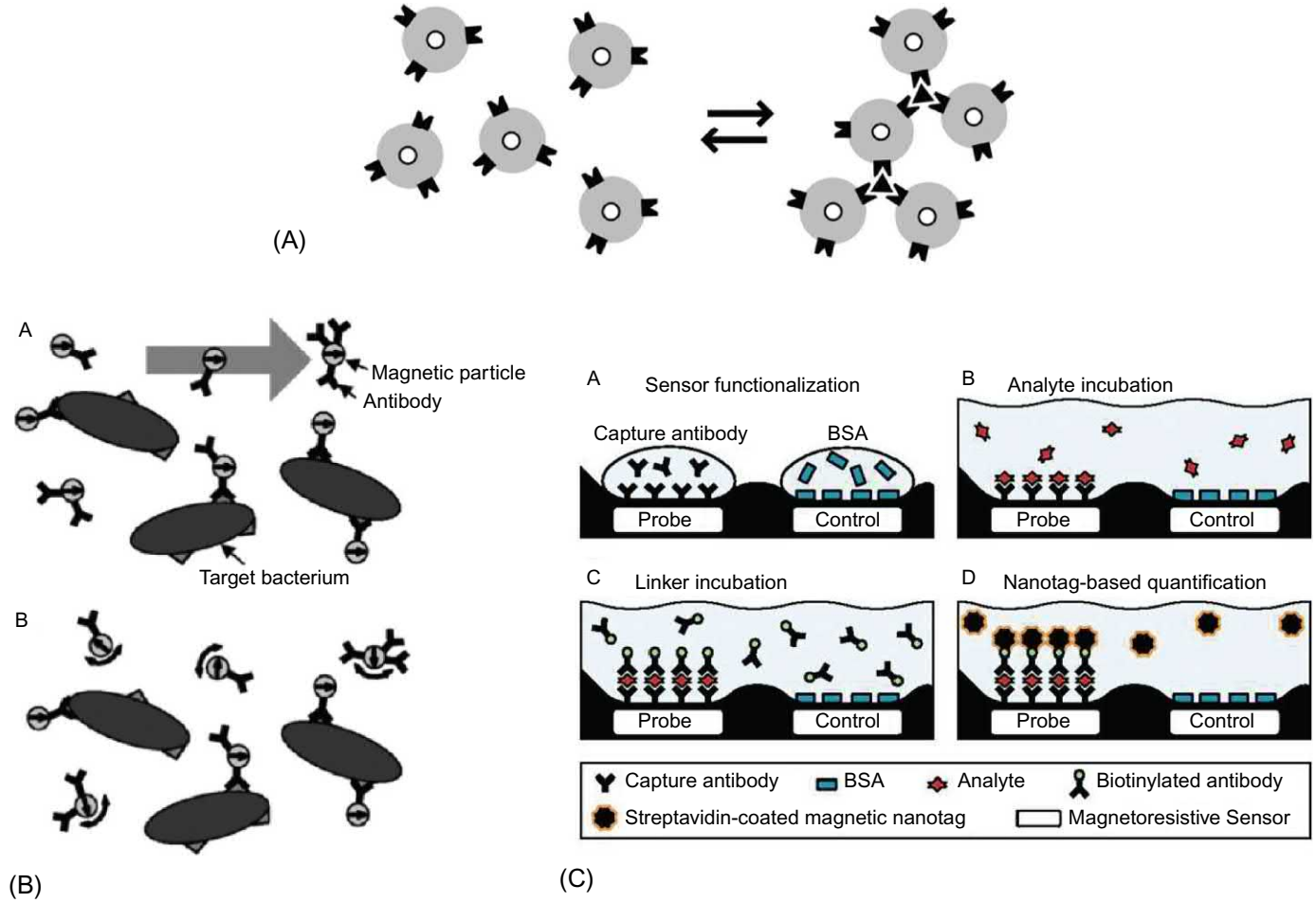

Fig. 1.2

(A) Magnetic property of nanomaterials used for sensing applications [31]. (B) Magnetic property of nanomaterials used for sensing applications (working principle of SQUID) [31]. (C) Schematic diagram of giant magnetoresistive sensor application [31].

bind to the surface functionality, while for indirect labeling a sandwich assay is created. Fig. 1.2C schematically shows the detection of protein by creating a sandwich assay.

Nanoparticles possess many more extraordinary properties including mechanical and thermal properties, but these properties are not very important to the current subject point of view.

1.2.2 Different nanomaterials for nanosensors

To discuss and understand the use of nanomaterials in developing nanosensors, it is helpful to classify them into different groups. But classifying nanomaterials into different groups is a formidable job. Nanomaterials can be prepared using a number of bottom-up processes such as cutting, ball milling, extruding, chipping, pounding, and many more [32] and top-down approaches [33] resulting in different types of structures, with different surface coatings, which can cause the classification to be obscure. For that reason, here we do not put too much concentration on classifying nanomaterials, but rather we shed some light on some commonly used nanomaterials. A schematic representation of carbon-based nanomaterials is provided in Fig. 1.3 for a better understanding of the diverse nature of nanomaterials.

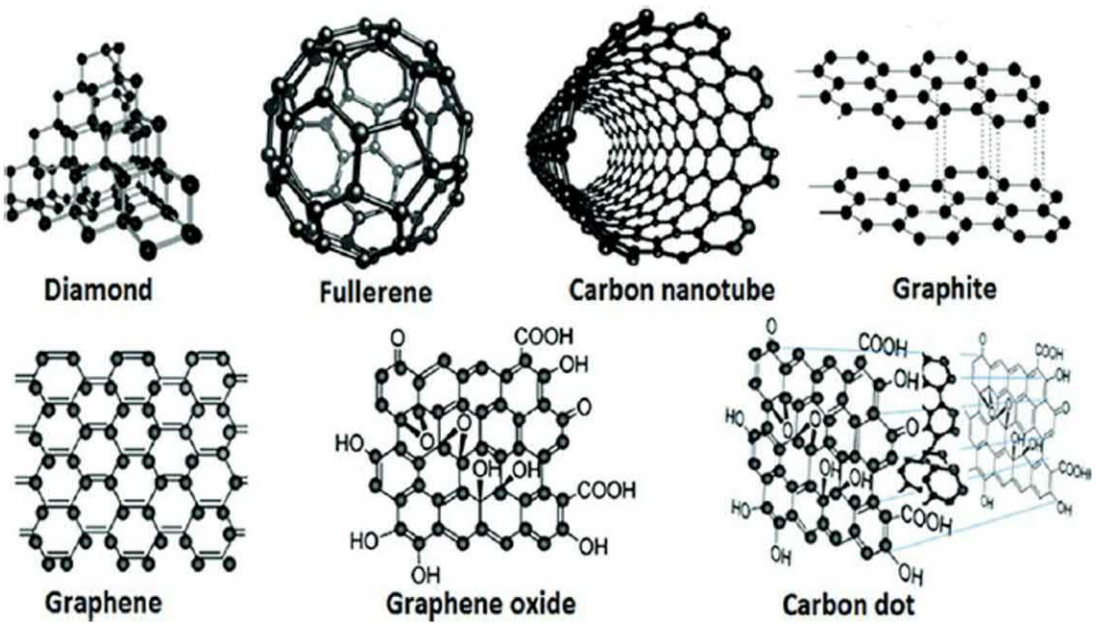

Fig. 1.3
Different carbon-based nanomaterials [34].

1.2.2.1 Carbon nanotube

First developed in 1991 by Iijima, the carbon nanotube (CNT) is by far the most-used carbon-based nanomaterial. It is a cylinder having diameters from fractions to tens of nanometers and a length up to several micrometers. There exist both single-walled (SWCNTs) and multiwalled (MWCNTs) nanotubes that are formed by single and multiple layers of graphene lamella, respectively, seamlessly rolled up [14]. The CNT is commonly produced by a chemical vapor deposition (CVD) technique or vaporization of graphite in a furnace in an inert (argon gas) atmosphere. The CNT possesses some excellent properties, such as high strength caused by its hexagonal structure, exceptional electronic properties caused by the free electron available after sp^2 hybridization, and ease of functionalization with different organic molecules that provide a means to interact selectively with different analytes. This easy-to-functionalize property enables CNTs to be used as probe tips for a wide range of chemical and biological applications.

The main application of the CNT as a sensor is in the field-effect transistor (FET). Though the CNT is robust and inert in nature, it is highly sensitive to chemical doping. A wide variety of FETs are manufactured by chemical doping of CNTs. Fig. 1.4 shows a schematic diagram of CNT-FET.

CNT-FETs are used to detect different types of gases like CO_2, NH_3, O_2 [35], NO_2, N_2 [36], and so forth. CNT-FETs are also used for detection in biological science. A variety of sensors have already been developed by researchers for detecting proteins [37], enzymes, and β-D glucose [38], among others.

1.2.2.2 Nanowires

Nanowires are also commonly used in making nanosensors, just like CNTs. Nanowires are produced through a variety of processes such as chemical vapor deposition (CVD), laser ablation, alternating current electrodeposition, and thermal evaporation [25]. Nanowires can be made up of different materials but silicone nanowires have drawn recent interest. The electrical properties and sensitivity of silicon nanowires can be tuned properly and reproducibly by

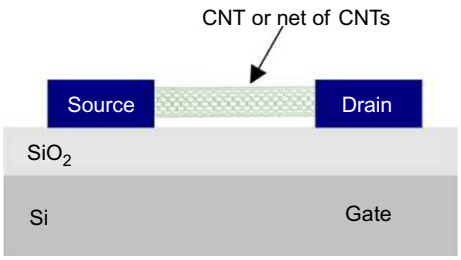

Fig. 1.4
Schematic diagram of CNT-FET [25].

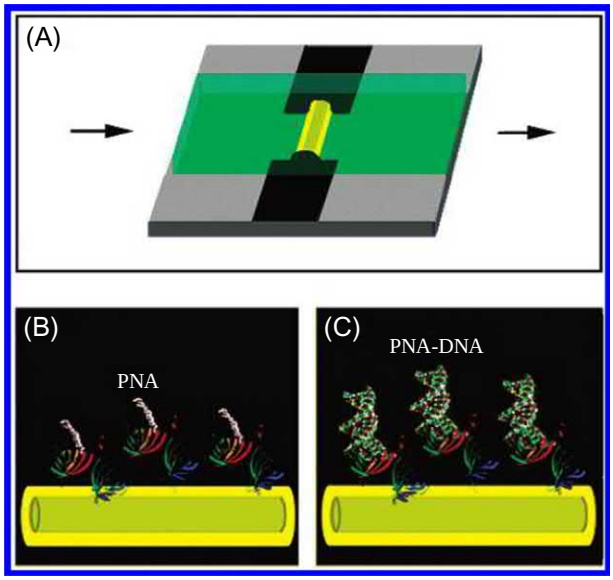

Fig. 1.5
(A) Schematic of a sensor device consisting of a SiNW (*yellow*) and a microfluidic channel (*green*), where the *arrows* indicate the direction of sample flow. (B) The SiNW surface with PNA receptor. (C) PNA-DNA duplex formation [40].

controlling the nanowire diameter and dopant concentration [39]. Hahm et al. produced a SiNW-based sensor to detect DNA and DNA mismatches [40] in which the silicon nanowire devices were modified with peptide nucleic acid receptors. The gold nanocluster catalyzed chemical vapor deposition technique was employed to prepare the nanowires used in this sensor. The nanowires were assembled on the sensor along with peptide nucleic acid. A schematic diagram of the device is given in Fig. 1.5 [40]. When a wild type or mutant DNA is introduced to the sensor via the microfluidic channel, peptide nucleic acid binds with the DNA and creates a tiny change of the conductance of the silicon nanowire. This change of conductance enables the sensor to differentiate between fully complementary or mismatched DNA.

Nanowires are also used to make gas sensors that can qualitatively detect NH_3.

1.2.2.3 Nanoparticles

Nanoparticles are a commonly used nanomaterial not only in sensor manufacturing but also in many other engineering applications. Although the name suggests a nanoparticle is a single molecule, NPs are not just simply one molecule but rather a combination of three layers. These layers are (a) the surface layer, which can be used to functionalize the nanoparticle; (b) the shell layer; and (c) the core, which is essentially the central portion of the NP [41]. Nanoparticles are

prepared using various approaches like bottom-up synthesis, including but not limited to chemical vapor deposition (CVD), spinning, plasma spraying synthesis, and laser pyrolysis, and top-down approaches, including but not limited to mechanical milling, sputtering, and laser ablation. Nanoparticles can be classified into various classes, for example (a) carbon-based nanoparticle, (b) metal nanoparticle, (c) ceramic nanoparticle, (d) semiconductor nanoparticle, and (e) polymer nanoparticle. Fig. 1.6 shows the SEM and TEM images of different nanoparticles (NPs). Nanoparticles offer exceptional electronic, optical, magnetic, mechanical, and thermal properties. Among these, the first three properties are exploited to produce many sensors. Metallic nanoparticles are used to enhance surface plasmon resonance sensitivity. The surface plasmon resonance technique is used in many optical sensors described in the previous section. Palladium nanoparticles deposited on etched porous silicon are used to detect hydrogen in the environment, while carbon electrodes with deposited gold nanoparticles are used to detect copper in water [16].

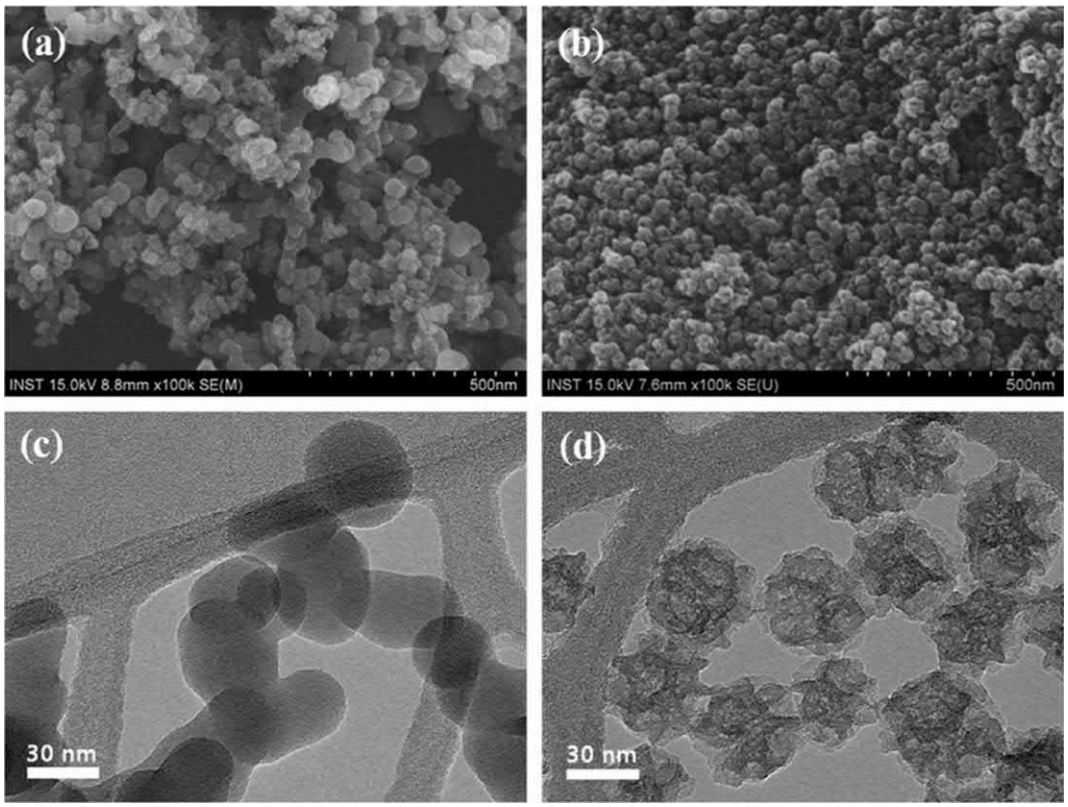

Fig. 1.6
SEM image of (A) nonporous MA-SiO_2 NPs, (B) mesoporous MA-SiO_2 NPs. TEM images of (C) nonporous $MASiO_2$ NPs and (D) mesoporous MA-SiO_2 NPs [18].

1.2.2.4 Fullerenes

Due to their unique properties, fullerenes are now receiving major attention from the scientific community. Fullerenes have a hexagonal ground state with sp^2 hybridization and are highly symmetric with 120 symmetry operations. Fullerenes are very strong and bounce back to their initial shape after deformation [15]. Among other properties, fullerenes have high surface-to-volume ratio, high electron affinity, and a hydrophobic surface. A good number of sensors have been developed using fullerenes along with other nanomaterials to form nanocomposites. Brahman et al. developed a C60-MWCNT nanosensor for detecting pyruvic acid [42]. Another electrochemical sensor was developed by the same researcher that uses a fullerene, copper nanoparticle-fullerene, MWCNT composite to detect paracetamol [43]. Here they used a pretreated carbon paste electrode (CPE) on which fullerene-C60 and multiwalled carbon nanotubes (MWCNTs) were dropped to produce a modified CPE. Later copper nanoparticles (CuNPs) were deposited electrochemically on the modified CPE and a nanocomposite film of CuNPs/C60-MWCNTs/CPE was formed. This composite showed excellent performance in paracetamol recognition and determination.

1.3 Nanomanufacturing

Nanomanufacturing is the process of manufacturing nanomaterials or various structures in nanoscale for different applications. This can be considered an updated version of micromanufacturing/microfabrication in which the dimension at which the manufacturing is done is several orders smaller. The term *nanofabrication* is sometimes used as analogous to *nanomanufacturing*, but sometimes nanofabrication refers more to a nanoscale fabrication process that is used in funded research work and nanomanufacturing is used to refer to manufacturing products for revenue generation [44]. However, in this chapter, we are not very concerned about the lack of a specific definition for the term nanomanufacturing; rather, we provide a general idea of current prevailing nanomanufacturing processes for manufacturing nanosensors.

A schematic diagram of an ultrasonic assisted nanomanufacturing process is shown in Fig. 1.7. In the figure, various possible types of vibration configurations are shown for the machining process. The research group reported that this method can be successfully applied to produce 3D nanoobjects of discrete height levels and also of continuously varying height [45].

1.3.1 Nanomanufacturing processes

The main drive behind the nanomanufacturing process is the ever-increasing hunger of the electronics industry to obtain smaller sizes. Currently, a microchip that we can hold on our fingertips can store gigabytes of data. To satiate this hunger, different types of nanomanufacturing processes have been developed that can be classified into three broad

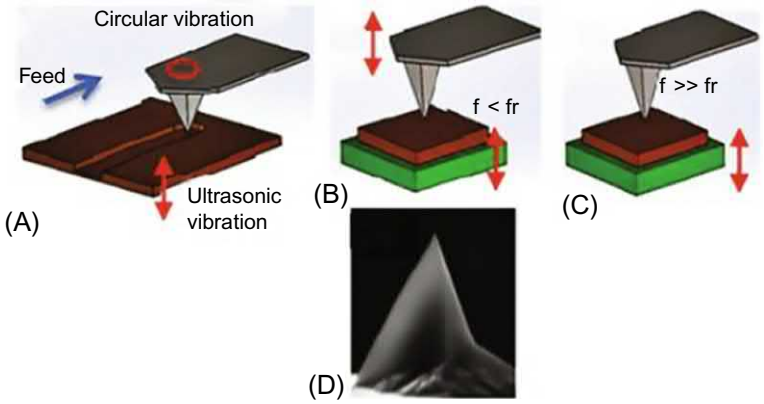

Fig. 1.7

(A) Ultrasonic assisted AFM-based nanomanufacturing process. (B) Low-frequency tip-sample interacting. (C) Ultrasonic tip-sample interaction while the tip is stationary. (D) SEM image of AFM tip [45].

approaches: (1) top-down approach, (2) bottom-up approach, and (3) molecular assembly. These three approaches are briefly described in the following sections.

1.3.1.1 Top-down approach

David, the famous statue created by Michelangelo, is one of the most notable sculptures of all time. However, if someone asks how David or any other stone or wooden sculpture is made, the answer is simple: a large block of stone or wood is gradually trimmed to the final shape. This is a top-down approach. In nanomanufacturing, this approach is used when a large block of material is taken and, by machining, the material is removed little by little till the final shape is obtained. The top-down approach consists of two steps: (1) nanolithography and (2) transfer of pattern.

In nanolithography, the desired pattern is created on a special type of sacrificial layer called a resist. There are a number of nanolithography techniques, such as photolithography, electron beam lithography, X-ray lithography, soft lithography, and so forth. The basic idea in every case is similar. First, a layer of resist is applied to the substrate. Then with the help of a pattern the photoresist is exposed to an energy source: for example, photolithography uses ultraviolet rays while electron beam lithography uses an electron beam and X-ray lithography uses an X-ray. Due to this patterned exposure, the resist undergoes a chemical process and the chemical and mechanical properties vary throughout the whole coating. Later, some part of the resist (exposed or unexposed part) is removed, depending on the positive or negative resist, and a pattern is created. Now the metal layer (SiO_2 in Fig. 1.8) is ready for the etching process. After etching the pattern created by the resist is removed mechanically or chemically. The simplified process is graphically represented in Fig. 1.8.

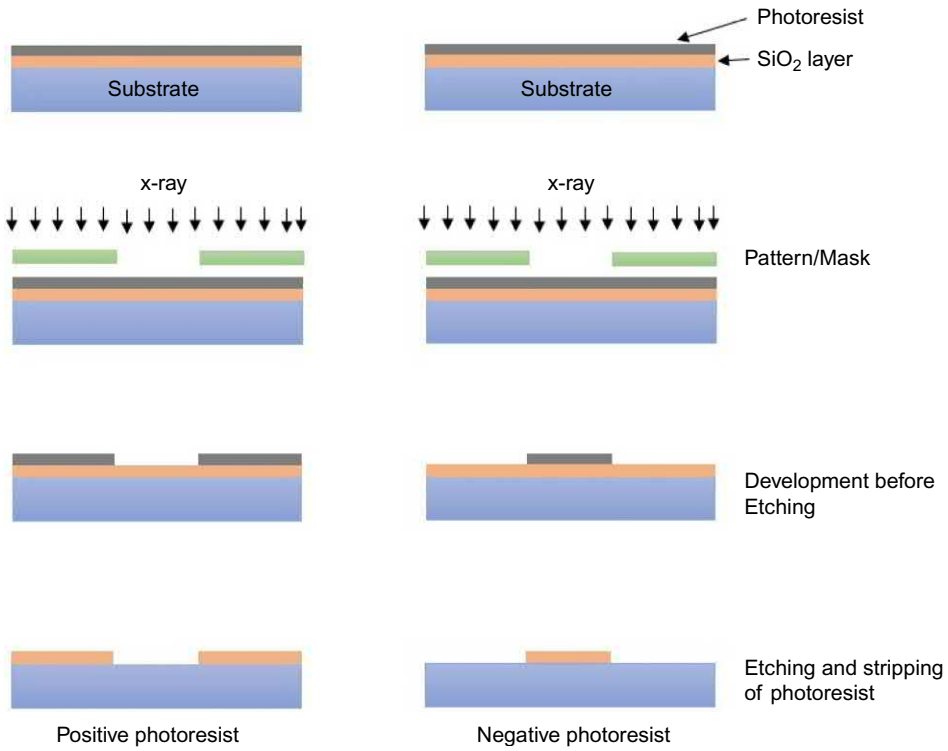

Fig. 1.8
Image of positive and negative resist in X-ray lithography.

Currently, the top-down approach prevails as the most popular and widely used approach in the nanomanufacturing industry. But the other two approaches are also beginning to have their own positions in nanomanufacturing.

1.3.1.2 Bottom-up approach

The bottom-up approach is similar to building up a house brick by brick (Fig. 1.9). In this approach, the final structure is developed by assembling or joining small components, even molecules. Typically there are several bottom-up approaches, including physical or chemical vapor deposition, contact printing, imprinting, assembly and joining, and coating. The bottom-up approach has high potential in healthcare and medical applications. Carbon nanomaterials and carbon nanotubes can be used for a bottom-up approach and a device that can work on an individual cell can be nanofabricated using this approach (Fig. 1.9).

1.3.1.3 Molecular self-assembly

Molecular self-assembly is the newest approach, in which the components, especially molecules, assemble themselves in the desired fashion to produce a nanoobject without the direction of an outside force. This process involves different properties such as shape, surface

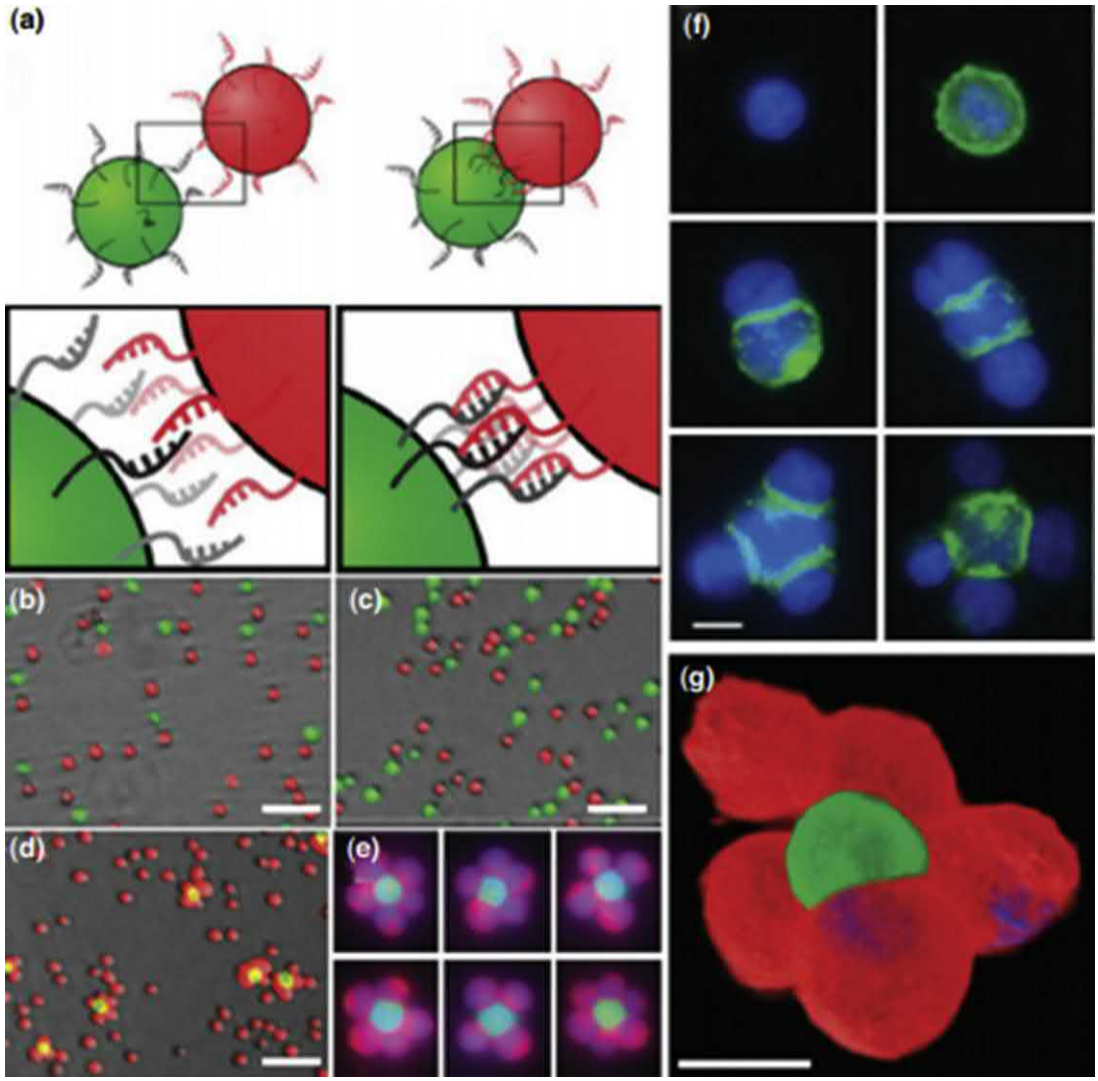

Fig. 1.9

Bottom-up approach used in tissue engineering. (A) Complementary oligonucleotides were covalently coupled to the surfaces of different cells by click chemistry. (B–E) Two nonadherent cell types were mixed, and did not aggregate if their surfaces were modified with: (B) no oligonucleotides, (C) noncomplementary oligonulceotides. However, specific aggregation was observed if the cell surfaces were modified with complementary oligonucleotides (D, E). (F) Aggregation of DAPI stained cells (*blue*), with the central cell modified with fluorescein-conjugated oligonucleotides (*green*). (G) 3D reconstruction of an aggregate of Texas Red-labeled (*red*) and fluorescein-labeled cells (*green*) [46].

properties, charge, polarizability, and magnetic dipole of the molecule to drive them to assemble together to form a particular structure. This is still a growing field and various developments are required before this approach is used in industry.

1.4 Nanomanufacturing processes for nanosensors

Nanomanufacturing can be defined as the ability to measure, predict, and manufacture on atomic and molecular scales and to exploit the unique properties shown by nanomaterials at that scale. Nanomanufacturing is a multidisciplinary field and researchers from various backgrounds are contributing to it. Fig. 1.10 shows graphically how researchers from different, but strongly related, research disciplines approach the science of the nanomanufacturing process.

However, in this chapter we are only concerned with the nanomanufacturing processes used in manufacturing nanosensors. In the previous section, it was shown that there are two broad approaches, namely the bottom-up approach and the top-down approach. A detailed discussion of these two approaches is not necessary here, as they have already been described. In this current section, we will discuss several nanomanufacturing processes that are commonly used in nanosensor preparation.

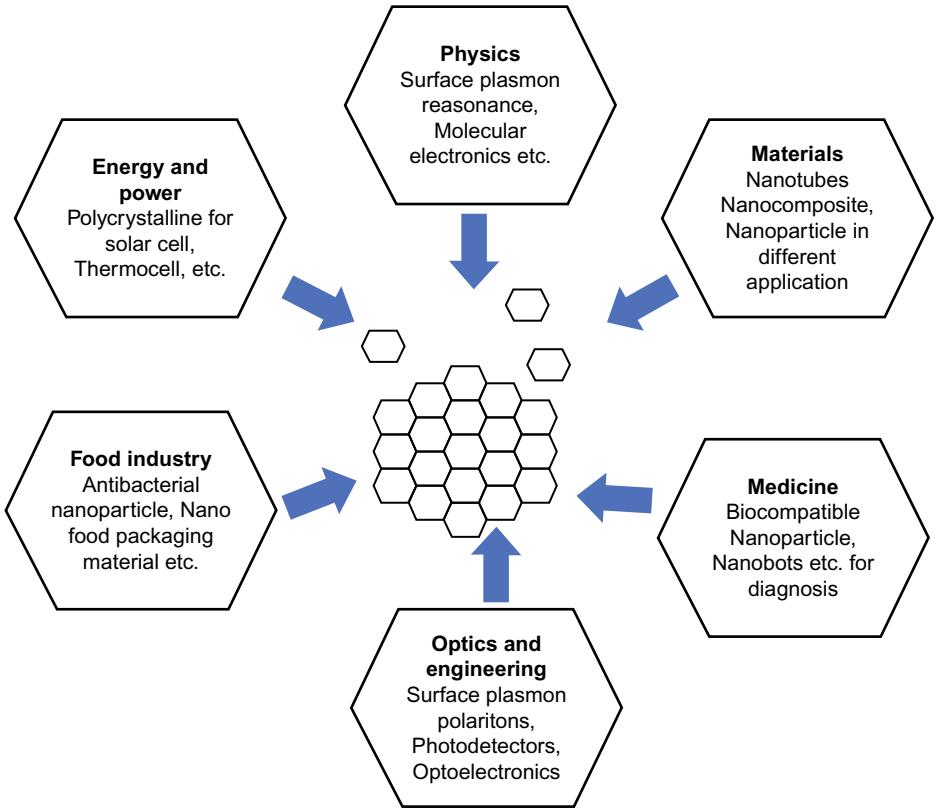

Fig. 1.10
Nanomanufacturing approached from different disciplines.

1.4.1 Electron beam lithography

Lithography is the technique of transferring patterns from one medium to another medium with the help of a material called resist. Previously, different particle beams were used in lithography, but with the application of the electron beam, nanometer-sized features have become possible. Due to its precious pattern-making capability, electron beam lithography (EBL) is frequently used in sensor manufacturing. Among various electron beam lithography technologies, here we will discuss direct writing EBL technology due to its simplicity and frequent use. In direct writing EBL, a finely focused Gaussian round beam is used that moves with the wafer and a single pixel of the wafer is exposed at a time (Tseng et al., 2003). The basic setup for direct writing EBL is shown in Fig. 1.11. The beam creates a desired pattern on the wafer and, supported with the etching and deposition process, a very complicated nanostructure can be produced. Though this technique is very cheap and popular, its main drawback is the large time requirement. However, researchers are trying to improve the technology to make this process more applicable.

1.4.2 Focused ion beam lithography

Focused ion beam lithography is another nanomanufacturing technique similar to electron beam lithography, but here ions are used to perform the lithography instead of an electron beam (Fig. 1.12). Since the ions are much heavier than electrons, focused ion beam lithography can be more efficient than electron beam lithography. The focused ion beam lithography technique also has some different classifications, but direct writing is the simplest and cheapest one and hence that is the one discussed here. In this method, a resist is not used and by varying the distance of the wafer, the dose of ions can be controlled, resulting

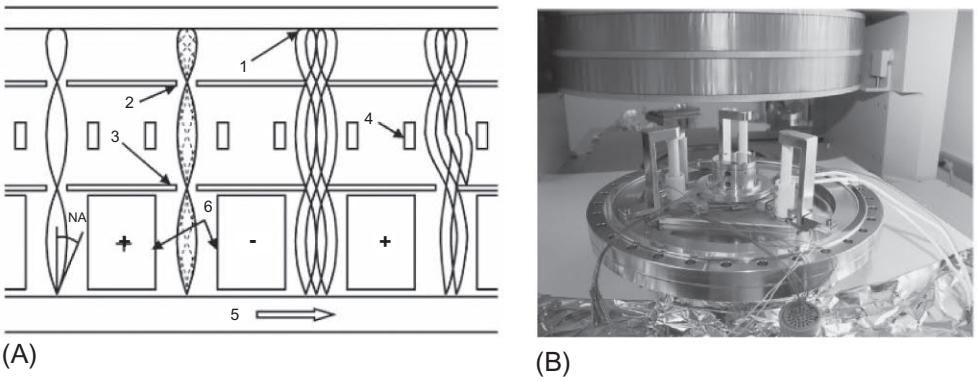

Fig. 1.11

(A) Conceptual diagram of DiVa: 1. Planar cathode, 2. Shaping apparatus, 3. Shaping apparatus second set, 4. deflector, 5. Wafer, 6. Deflection plates; (B) Experimental DiVa apparatus at Stanford University [47].

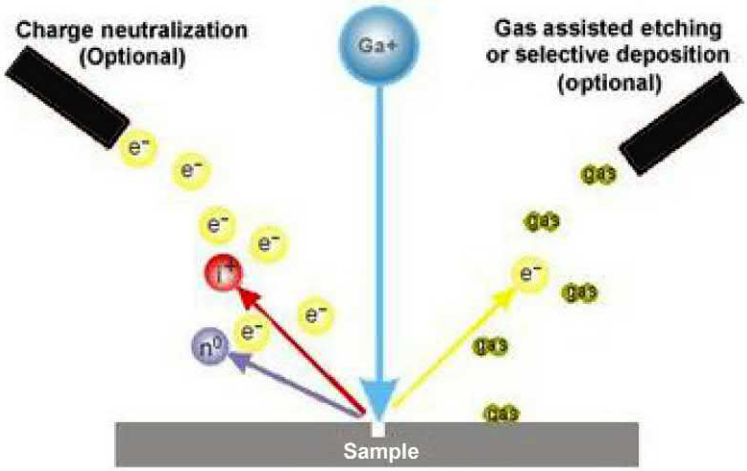

Fig. 1.12
Schematic diagram of focused ion beam lithography.

in a trench of different depth on the wafer. Heavy-ion species such as Ga^+ and Au^+ can also be used in this lithography to produce a stronger effect. When a beam is passed over the wafer, a trench having inverse Gaussian shape is obtained. With increase in strength, the trench becomes more sharp, narrow, and V-shaped [48]. Multiple passes are also possible to create complicated shapes.

1.4.3 X-ray lithography

X-ray lithography (XRL) is an advanced version of optical lithography in which shorter wavelengths are used. In this method, a special type of mask is used with different local X-ray absorption areas to define the pattern. This pattern is replicated on an X-ray sensitive material called a resist, which is previously deposited on a substrate (usually a silicon wafer). When the X-ray passing through the pattern falls on the resist, it may cause cross-linking (for negative resists) or bond breaking (for positive resists), depending on the chemical nature of the resist. After exposure, the whole thing is dipped in a specific solvent and, depending on its nature, either the exposed area resist will dissolve and create a pattern or vice versa. The other part of the resist will stay intact [49]. This is how X-ray lithography creates nanopatterns on the substrate.

1.5 Conclusions and future directions

The beginnings of nanotechnology are popularly dated back to the famous lecture given by Nobel laureate Richard Feynman, "There's Plenty of Room at the Bottom," in 1959. But the application of this technology became evident at the beginning of 1980. Since then, nanotechnology has gained huge momentum and currently is being applied in various aspects of

our daily life. In this chapter, we mainly focused on different nanomaterials that are used in making nanosensors, along with different nanomanufacturing processes used to develop those sensors. In nanoscale, materials exhibit some extraordinary properties that are not visible in bulk form and nanosensors take advantage of those properties. Nanosensors are gradually making their way into various fields, including but not limited to biomedicine and biotechnology, hazardous material detection, water purification, food industry, electronics and optoelectronics, and forensics. The main advantages of nanosensors include (a) rapidness, (b) low quantities of samples required, (c) robustness, (d) point of care capability, and (e) cost-effectiveness. More and more research is being conducted to improve the current nanomanufacturing methods, create new nanomaterials, and develop new sensors using the properties of nanomaterials.

References

[1] A. Kumar, N. Das, N.K. Satija, K. Mandrah, S.K. Roy, R.G. Rayavarapu, A novel approach towards synthesis and characterization of non-cytotoxic gold nanoparticles using taurine as capping agent, Nanomaterials 10 (1) (2020) 45, https://doi.org/10.3390/nano10010045.

[2] M.E. Hoque, A.M. Peiris, S.M. Atiqure Rahman, M.A. Wahab, New generation antibacterial nanofibrous membrane for potential water filtration, Curr. Anal. Chem. 14 (3) (2018) 278–284, https://doi.org/10.2174/1573411013666171009162832.

[3] M. Golieskardi, M. Satgunam, D. Ragurajan, M.E. Hoque, A.M.H. Ng, L. Shanmuganantha, Advanced 3Y-TZP bioceramic doped with Al_2O_3 and CeO_2 potentially for biomedical implant applications, Mater. Technol. 34 (8) (2019) 480–489, https://doi.org/10.1080/10667857.2019.1578912.

[4] D. Ragurajan, et al., Advanced 3Y-TZP bioceramic doped with Al_2O_3 and MnO_2 particles potentially for biomedical applications: study on mechanical and degradation properties, J. Mater. Res. Technol. 7 (4) (2018) 432–442, https://doi.org/10.1016/j.jmrt.2017.05.015.

[5] A. Wahab, N. Islam, M.E. Hoque, D.J. Young, Recent advances in silver nanoparticle containing biopolymer nanocomposites for infectious disease control—a mini review, Curr. Anal. Chem. 14 (2018) 198–202.

[6] S. Sagadevan, K. Pal, Z.Z. Chowdhury, M.E. Hoque, Structural, dielectric and optical investigation of chemically synthesized Ag-doped ZnO nanoparticles composites, J. Sol-Gel Sci. Technol. 83 (2) (2017) 394–404, https://doi.org/10.1007/s10971-017-4418-8.

[7] F.M. Michael, M. Khalid, C.T. Ratnam, W. Rashmi, M.E. Hoque, M.R. Ketabchi, Nanohydroxyapatite synthesis using optimized process parameters for load-bearing implant, Bull. Mater. Sci. 39 (1) (2016) 133–145, https://doi.org/10.1007/s12034-015-1120-8.

[8] S.M.M. Nainar, et al., Effect of compatibilizers on in vitro biocompatibility of PLA–HA bioscaffold, Bioinspired Biomim. Nanobiomater. 3 (4) (2014) 208–216, https://doi.org/10.1680/bbn.14.00014.

[9] P. Malik, V. Katyal, V. Malik, A. Asatkar, G. Inwati, T.K. Mukherjee, Nanobiosensors: concepts and variations, ISRN Nanomater. 2013 (2013) 1–9, https://doi.org/10.1155/2013/327435.

[10] L.M. Bellan, D. Wu, R.S. Langer, Current trends in nanobiosensor technology, Wiley Interdiscip. Rev. Nanomed. Nanobiotechnol. 3 (3) (2011) 229–246, https://doi.org/10.1002/wnan.136.

[11] D.J. Barber, I.C. Freestone, An investigation of the origin of the colour of the Lycurgus cup by analytical transmission electron microscopy, Archaeometry 32 (1990) 33–45, https://doi.org/10.1111/j.1475-4754.1990.tb01079.x.

[12] J.D. Verhoeven, D.T. Peterson, What is a Damascus steel? Mater. Charact. 29 (1992) 335–341, https://doi.org/10.1016/1044-5803(92)90105-Q.

[13] M. Faraday, The Bakerian lecture: experimental relations of gold (and other metals) to light, Philos. Trans. R. Soc. Lond. 147 (1857) 145–181.

[14] B.-T. Zhang, X. Zheng, H.-F. Li, J.-M. Lin, Application of carbon-based nanomaterials in sample preparation: a review, Anal. Chim. Acta 784 (2013) 1–17, https://doi.org/10.1016/j.aca.2013.03.054.
[15] P.N. Sudha, K. Sangeetha, K. Vijayalakshmi, A. Barhoum, Chapter 12: Nanomaterials history, classification, unique properties, production and market, in: A. Barhoum, A.S.H. Makhlouf (Eds.), Emerging Applications of Nanoparticles and Architecture Nanostructures, Micro and Nano Technologies, Elsevier, 2018, pp. 341–384, https://doi.org/10.1016/B978-0-323-51254-1.00012-9.
[16] R. Bogue, Nanosensors: a review of recent research, Sens. Rev. 29 (2009) 310–315, https://doi.org/10.1108/02602280910986539.
[17] K. Sasaki, Z.-Y. Shi, R. Kopelman, H. Masuhara, Three-dimensional pH microprobing with an optically-manipulated fluorescent particle, Chem. Lett. 25 (1996) 141–142, https://doi.org/10.1246/cl.1996.141.
[18] J.E. Lee, N. Lee, T. Kim, J. Kim, T. Hyeon, Multifunctional mesoporous silica nanocomposite nanoparticles for theranostic applications, Acc. Chem. Res. 44 (2011) 893–902, https://doi.org/10.1021/ar2000259.
[19] K.M. Mayer, J.H. Hafner, Localized surface plasmon resonance sensors, Chem. Rev. 111 (2011) 3828–3857, https://doi.org/10.1021/cr100313v.
[20] C.-S. Cheng, Y.-Q. Chen, C.-J. Lu, Organic vapour sensing using localized surface plasmon resonance spectrum of metallic nanoparticles self assemble monolayer, Talanta 73 (2007) 358–365, https://doi.org/10.1016/j.talanta.2007.03.058.
[21] T. Karakouz, A. Vaskevich, I. Rubinstein, Polymer-coated gold island films as localized plasmon transducers for gas sensing, J. Phys. Chem. B 112 (2008) 14530–14538, https://doi.org/10.1021/jp804829t.
[22] N.H. Mack, J.W. Wackerly, V. Malyarchuk, J.A. Rogers, J.S. Moore, R.G. Nuzzo, Optical transduction of chemical forces, Nano Lett. 7 (2007) 733–737, https://doi.org/10.1021/nl0629759.
[23] M. Nuopponen, H. Tenhu, Gold nanoparticles protected with pH and temperature-sensitive diblock copolymers, Langmuir 23 (2007) 5352–5357, https://doi.org/10.1021/la063240m.
[24] J.C. Meyer, C. Kisielowski, R. Erni, M.D. Rossell, M.F. Crommie, A. Zettl, Direct Imaging of Lattice Atoms and Topological Defects in Graphene Membranes (WWW Document), 2008, https://doi.org/10.1021/nl801386m.
[25] J. Riu, A. Maroto, F.X. Rius, Nanosensors in environmental analysis, Talanta 69 (2006) 288–301. 1st swift-WFD workshop on validation of robustness of sensors and bioassays for screening pollutants, https://doi.org/10.1016/j.talanta.2005.09.045.
[26] L. Jiao, G. Lu, C. Zhang, Y. Yuan, J. Wang, Q. Zhang, P. Li, Aptamer and graphene-based electrochemical biosensor for dopamine determination with high sensitivity and selectivity, Micro Nano Lett. 8 (2013) 903–905, https://doi.org/10.1049/mnl.2013.0626.
[27] L. Saghatforoush, M. Hasanzadeh, N. Shadjou, Polystyrene–graphene oxide modified glassy carbon electrode as a new class of polymeric nanosensors for electrochemical determination of histamine, Chin. Chem. Lett. 25 (2014) 655–658, https://doi.org/10.1016/j.cclet.2014.01.014.
[28] L. Soleymani, Z. Fang, B. Lam, X. Bin, E. Vasilyeva, A.J. Ross, E.H. Sargent, S.O. Kelley, Hierarchical nanotextured microelectrodes overcome the molecular transport barrier to achieve rapid, direct bacterial detection, ACS Nano 5 (2011) 3360–3366, https://doi.org/10.1021/nn200586s.
[29] K. Dawson, M. Baudequin, A. O'Riordan, Single on-chip gold nanowires for electrochemical biosensing of glucose, Analyst 136 (2011) 4507–4513, https://doi.org/10.1039/C1AN15279C.
[30] I. Khan, K. Saeed, I. Khan, Nanoparticles: properties, applications and toxicities, Arab. J. Chem. 12 (2017) 908–931, https://doi.org/10.1016/j.arabjc.2017.05.011.
[31] I. Koh, L. Josephson, Magnetic nanoparticle sensors, Sensors 9 (2009) 8130–8145, https://doi.org/10.3390/s91008130.
[32] A. Magasinski, P. Dixon, B. Hertzberg, A. Kvit, J. Ayala, G. Yushin, High-performance lithium-ion anodes using a hierarchical bottom-up approach, Nat. Mater. 9 (2010) 353–358, https://doi.org/10.1038/nmat2725.
[33] P.A. Sabatier, Top-down and bottom-up approaches to implementation research: a critical analysis and suggested synthesis, J. Public Policy 6 (1986) 21–48, https://doi.org/10.1017/S0143814X00003846.
[34] Q.-L. Yan, M. Gozin, F.-Q. Zhao, A. Cohen, S.-P. Pang, Highly energetic compositions based on functionalized carbon nanomaterials, Nanoscale 8 (2016) 4799–4851, https://doi.org/10.1039/C5NR07855E.

[35] K.G. Ong, K. Zeng, C.A. Grimes, A wireless, passive carbon nanotube-based gas sensor, IEEE Sensors J. 2 (2002) 82–88, https://doi.org/10.1109/JSEN.2002.1000247.
[36] B.-Y. Wei, M.-C. Hsu, P.-G. Su, H.-M. Lin, R.-J. Wu, H.-J. Lai, A novel SnO_2 gas sensor doped with carbon nanotubes operating at room temperature, Sens. Actuators B Chem. 101 (2004) 81–89, https://doi.org/10.1016/j.snb.2004.02.028.
[37] R.J. Chen, S. Bangsaruntip, K.A. Drouvalakis, N.W.S. Kam, M. Shim, Y. Li, W. Kim, P. J. Utz, H. Dai, Noncovalent functionalization of carbon nanotubes for highly specific electronic biosensors, Proc. Natl. Acad. Sci. U. S. A. 100 (2003) 4984–4989, https://doi.org/10.1073/pnas.0837064100.
[38] P.W. Barone, S. Baik, D.A. Heller, M.S. Strano, Near-infrared optical sensors based on single-walled carbon nanotubes, Nat. Mater. 4 (2005) 86–92, https://doi.org/10.1038/nmat1276.
[39] Y. Cui, C.M. Lieber, Functional nanoscale electronic devices assembled using silicon nanowire building blocks, Science 291 (2001) 851–853, https://doi.org/10.1126/science.291.5505.851.
[40] J. Hahm, C.M. Lieber, Direct ultrasensitive electrical detection of DNA and DNA sequence variations using nanowire nanosensors, Nano Lett. 4 (2004) 51–54, https://doi.org/10.1021/nl034853b.
[41] W.-K. Shin, J. Cho, A.G. Kannan, Y.-S. Lee, D.-W. Kim, Cross-linked composite gel polymer electrolyte using mesoporous methacrylate-functionalized SiO_2 nanoparticles for lithium-ion polymer batteries, Sci. Rep. 6 (2016) 26332, https://doi.org/10.1038/srep26332.
[42] P.K. Brahman, N. Pandey, S.N. Topkaya, R. Singhai, Fullerene–C60–MWCNT composite film based ultrasensitive electrochemical sensing platform for the trace analysis of pyruvic acid in biological fluids, Talanta 134 (2015) 554–559, https://doi.org/10.1016/j.talanta.2014.10.054.
[43] P.K. Brahman, L. Suresh, V. Lokesh, S. Nizamuddin, Fabrication of highly sensitive and selective nanocomposite film based on CuNPs/fullerene-C60/MWCNTs: an electrochemical nanosensor for trace recognition of paracetamol, Anal. Chim. Acta 917 (2016) 107–116, https://doi.org/10.1016/j.aca.2016.02.044.
[44] K. Mohamed, 2.16 – Nanoimprint lithography for nanomanufacturing, in: D.L. Andrews, R.H. Lipson, T. Nann (Eds.), Comprehensive Nanoscience and Nanotechnology, second ed., Academic Press, Oxford, 2019, pp. 357–386, https://doi.org/10.1016/B978-0-12-803581-8.10508-9.
[45] J. Deng, J. Dong, P. Cohen, High rate 3D nanofabrication by AFM-based ultrasonic vibration assisted nanomachining, in: Procedia Manuf., 44th North American Manufacturing Research Conference, NAMRC 44, June 27–July 1, 2016, Blacksburg, Virginia, United States, 5, 2016, pp. 1283–1294, https://doi.org/10.1016/j.promfg.2016.08.100.
[46] D.L. Elbert, Bottom-up tissue engineering, Curr. Opin. Biotechnol. 22 (2011) 674–680, https://doi.org/10.1016/j.copbio.2011.04.001.
[47] T.R. Groves, D. Pickard, B. Rafferty, N. Crosland, D. Adam, G. Schubert, Maskless electron beam lithography: prospects, progress, and challenges, Microelectron. Eng. Micro- Nano-Eng. 61–62 (2002) 285–293, https://doi.org/10.1016/S0167-9317(02)00528-2.
[48] K. Arshak, M. Mihov, A. Arshak, D. McDonagh, D. Sutton, Focused ion beam lithography-overview and new approaches, in: 2004 24th International Conference on Microelectronics (IEEE Cat. No.04TH8716). Presented at the 2004 24th International Conference on Microelectronics (IEEE Cat. No.04TH8716), vol. 2, 2004, pp. 459–462, https://doi.org/10.1109/ICMEL.2004.1314862.
[49] J.R. Maldonado, M. Peckerar, X-ray lithography: some history, current status and future prospects, Microelectron. Eng. 161 (2016) 87–93, https://doi.org/10.1016/j.mee.2016.03.052.

CHAPTER 2

Features and complex model of gold nanoparticle fabrication for nanosensor applications

Norma Alias, Hazidatul Akma Hamlan

Center for Sustainable Nanomaterials, Ibnu Sina Institute for Scientific and Industrial Research, Universiti Teknologi Malaysia, Skudai, Malaysia

2.1 Introduction

In recent years, many researchers and engineers have been shifting the focus of their studies toward nanosensors because of their unique sensitivity and selectivity, which mostly originate from modifications and reactions that occur at nanoscales [1]. Due to their unique features, nanosensors are widely chosen for detecting chemical and physical properties in many fields such as environmental, biomedical, and food processing.

Dahman [2] expressed that nanosensors have a plethora of environmental applications. The ability to detect chemical components of air and water strengthen the choice of nanosensors in the environmental field. Nanosensors are mainly used in water monitoring quality [3], monitoring plant signaling pathways [4], and detecting and determining quantities of acetamiprid (insecticide) in food and the environment [5] and agriculture [6]. Vikesland [3] stated that an abundance of existing nanosensors can be developed into consumer- and operator-friendly tools. The author emphasized that nanotechnology-enabled sensors or nanosensors can provide extensive and potentially low-cost monitoring of chemicals, microbes, and other analytes in drinking water. Meanwhile, Kwak et al. [4] discussed how nanosensors can act as monitoring tools to observe and monitor plant signaling pathways and metabolism.

Verdian [5] highlighted a current major concern of food safety experts, which is pesticide residues. Despite the small amounts of toxicity from pesticide residues, insecticides that contain acetamiprid can represent a health risk to human beings who are exposed to polluted food and environments. Hence, nanosensors can be used in detecting and determining amounts of acetamiprid in food and the environment.

Nanofabrication for Smart Nanosensor Applications. https://doi.org/10.1016/B978-0-12-820702-4.00002-7
© 2020 Elsevier Inc. All rights reserved.

Srivastava et al. [6] explained applications of nanosensors in agriculture in which wireless nanosensors are used to monitor the soil fertility, moisture level, insects, temperature, crop nutrient status, and diseases of crops. Using advances in nanotechnology, crop growth can be monitored by employing networks of wireless nanosensors across cultivated fields. The network can provide crucial data for agronomic intelligence processes such as optimal times for crop planting and harvesting.

One of the most popular nanosensor technologies makes use of gold nanoparticles [7], whose flexible surface chemistry allows them to be coated with biological recognition molecules, polymers, and small molecules, hence broadening their range of applications. Gold nanoparticles as substrates can also be used as a nanosensor technology for the detection of pollutants and label-free detection of other molecules and proteins [8]. Based on the facts described, this chapter presents established mathematical modeling based on partial differential equations (PDEs) for nanoparticle materials fabrication, to control the process of gold nanoparticle manufacturing. The modeling is created to investigate the feature properties and boundaries in the development process. One-dimensional PDEs with respect to time and space are employed to visualize the growth of gold nanoparticles (AuNPS).

An accurate and precise result can be achieved by governing complex mathematical modeling and obtaining a large sparse matrix of linear system equations (LSEs). Meanwhile, the parallelization of LSE is chosen in order to accelerate and speed up the simulation for a large sparse matrix. Therefore, the main focus of this chapter is the parallelization of a mathematical model of the fabrication of nanoparticles.

Nanoparticles have played an important role in advanced catalysts, ceramics, and electronic devices as well as polymer composites and coatings for the last two decades [9]. Their physical and chemical properties are different from those of conventional materials. A nanoparticle can best be defined as a small object that behaves as a whole unit with regard to its properties, and is classified according to its diameter.

Schmid [10] defined nanoparticles as nanomaterials with an average diameter that is less than 100 nm. Nowadays, nanoparticle technology plays an important role in providing opportunities and possibilities for the development of a new generation of sensing tools. The targeted sensing of selective biomolecules using functionalized gold nanoparticles (Au NPs) has become a major research thrust in the last decade [11]. Researchers normally use gold nanoparticles due to their stability and unique optical, electronic, biolabeling, and molecular-recognition properties.

In fabricating gold nanoparticles, several features need to be controlled – for example, size, shape, and structure. The parameters will be changed according to functionality. This is due to the strong correlation between the parameters and optical, electrical, and catalytic properties [12]. Nanoparticles with controlled size and shape are of great interest because of their morphology-dependent properties [10] and potential applications in a variety of fields.

The application of gold growth is so significant that, in recent years, some researchers have been reporting mainly on the analysis of gold growth, especially chemical properties. However, only a few studies focus on mathematical modeling and simulation in visualizing the growth of gold nanoparticles [13]. Due to this situation, this research investigates the rate of growth for gold nanoparticles using a one-dimensional parabolic PDE approach.

Since nanoparticle fabrication is being dealt with through nanoscale approaches, the focus of this chapter is on fine-grain parallelism involving a large-scale matrix from the mathematical model discretization. In solving the problem of a large-scale matrix, parallel computing systems with huge memory space are needed to produce a good result. Therefore, parallel computing systems are employed throughout this study. The parameter change from phase change simulation is the code from the Linux operating system using DPCS based on the approximation of numerical scheme and parallel algorithms, as well as their sequential flows. The PVM software integrated with the C language is used to support the message passing paradigm and simulation for the parallel algorithm program.

2.1.1 Applications of nanoparticles

Nanotechnology deals with the particular technological goal of specifically manipulating atoms and molecules for fabrication of macroscale merchandise. Nowadays, this is also known as molecular nanotechnology [14]. In nanotechnology, sensitivity experiments are carried out for various physical processes, involving a large-scale structure of modeling and reformation of the nanoscale system, which appearance as nanoparticles [15].

Gold nanoparticles (AuNPs) display irreplaceable properties that make them a very attractive material for nanosensing applications, especially in the environmental field. Besides that, the "additional attractive feature of AuNPs is their interaction with thiols, providing effective and selective means of controlled intracellular release" [16]. Liu et al. [17], Park et al. [18], and Rejiya et al. [19] have investigated the application of gold particles as nanoparticles. Various sizes of gold nanoparticles and their morphologies have attracted considerable interest for researchers, especially in medical applications [20] and [21].

2.1.2 Growth of gold nanoparticles

As mentioned, gold nanoparticles (AuNPs) have attracted much attention among researchers, due to their unique properties and encouraging applications in areas of biotechnology, catalysis [22], and optoelectronics [23]. In preparing AuNPs, the homogeneous mixing of continuous flows of an aqueous tetrachloroauric acid solution and a sodium borohydride solution is applied using a microstructured static mixer [24]. Their studies have provided a profound understanding of gold nanoparticle growth and small angle X-ray scattering (SAXS), combined with X-ray absorption near-edge structure (XANES). In predicting the size, shape, and

polydispersity of gold nanoparticles, one paper [25] stressed that it is necessary to interpret the underlying process using SAXS that offers integral information on the growth of nanoparticles.

However, Polte et al. [26], despite their widespread use, in countless cases and applications, a deeper understanding and consideration of the underlying formation of the processes is missing. Due to this phenomenon, the size and shape control of gold nanoparticles often remained. Therefore, in this chapter, a great deal of attention has been focused on understanding the process of gold nanoparticle formation pertaining to its growth rate. In predicting and visualizing the growth of gold nanoparticles, mathematical modeling using one-dimensional parabolic PDEs as the integrated methodology is proposed instead of conducting experimental laboratory studies.

The gold nanoparticle fabrication correlates with longer systemic circulation and a high-cost fabrication for small-scale limited process. Although the nanoparticles are small, mathematical modeling and large sparse simulation can be presented in the fabrication process.

2.2 Mathematical model of gold nanoparticle fabrication

The focus of this chapter is on the application of one-dimensional parabolic equations from PDEs to governing mathematical modeling. The prediction and visualization of the growth rate of gold nanoparticles are obtained by employing one-dimensional parabolic PDEs with respect to time, space, and some independent and dependent variables.

2.2.1 Governing equation of gold nanoparticle fabrication

This section deals with the mathematical modeling and simulation of one-dimensional parabolic PDEs as an integrated methodology for predicting and visualizing the growth of gold nanoparticles with respect to time and space. The modeling is formulated as a boundary value problem of PDEs. The PDE modeling with significant features and its parameter identification that influences on gold nanoparticles (AuNPs) of diameter Φ, ultraviolet radiation λ, and rate of gold growth U are investigated.

The integrated methodology for predicting and visualizing the growth rate of gold nanoparticles for nanosensor applications with respect to time and space involves predicting and visualizing using one-dimensional parabolic PDEs. The governing equation of the mathematical model for this problem is:

$$\frac{\partial U}{\partial t} = \Phi \frac{\partial^2 U}{\partial x^2} + \lambda,\ 0 \le x \le 1,\ t > 0. \tag{2.1}$$

Initial and boundary conditions are given by [27].

$$U(x, 0) = \sin(\pi x),\ 0 \le x \le 1,$$

$$U(0,t)=0,\ 0\le t\le 1,$$
$$U(1,t)=0,\ 0\le t\le 1.$$

The exact solution is given by

$$U(x,t)=\mathrm{e}^{-\pi t}\sin(\pi x), \tag{2.2}$$

where λ represents the incoherent ultraviolet radiation (nm), Φ is the diameter of gold growth, U is the rate of gold growth, t is time (duration taken for the growth rate), and x is the spatial coordinate of direction.

2.2.2 Nondimensionalized parameter for governing equations

In mathematics, a transformation from dimensional to nondimensional variables is required so the relevant parameter identification and changes of the required parameters for mathematical modeling can be specified. However, for engineering applications, nondimensionalizing the governing equation is not necessary since real physical quantities are dealt with as the solution progresses. Since this study focuses on mathematical analysis, the nondimensional rule is needed because the nondimensionalized variables reduce the complexity of solving the governing equation.

Therefore, Eqs. (2.1), (2.2) are nondimensionalized using the following dimensional scaling from Blest et al. [28]. The nondimensional scaling is denoted with a tilde:

$$\tilde{T}_i=\frac{T_i-T_{ini}}{T_c-T_{ini}},\ \ \tilde{x}=\frac{x}{d},\ \tilde{y}=\frac{y}{d},\ \ \tilde{u}^i=\frac{u^i}{d},\ \tilde{v}^i=\frac{v^i}{d},\ \ \tilde{t}=\frac{K_r t}{d^2},\ \ \tilde{L}=\frac{L}{d},$$
$$\tilde{h}_k=\frac{h_k}{d},\ \text{and}\ \ \tilde{\delta}_k=\frac{\delta_k}{d},$$

where $i=r,f$ are the respective resin and saturated fiber layer. By applying these transformations and omitting tildes for clarity, Eqs. (2.1), (2.2) can be simplified as

$$\frac{\partial T_f}{\partial t}+\mathrm{Pe}\left(u^f\frac{\partial T_f}{\partial x}+v^f\frac{\partial T_f}{\partial y}\right)=D\left(\frac{\partial^2 T_f}{\partial x^2}+\frac{\partial^2 T_f}{\partial y^2}\right)+J_1\frac{\partial \alpha}{\partial t}, \tag{2.3}$$

$$\frac{\partial T_r}{\partial t}+\mathrm{Pe}\left(u^r\frac{\partial T_r}{\partial x}+v^r\frac{\partial T_r}{\partial y}\right)=\left(\frac{\partial^2 T_r}{\partial x^2}+\frac{\partial^2 T_r}{\partial y^2}\right)+J_2\frac{\partial \alpha}{\partial t}, \tag{2.4}$$

and

$$\frac{\partial \alpha}{\partial t}=(C_1+C_2\alpha)(1-\alpha)(0.47-\alpha)\qquad \textit{for}\ \alpha\le 0.3, \tag{2.5}$$

$$\frac{\partial \alpha}{\partial t} = C_3(1-\alpha) \quad for\ \alpha > 0.3, \tag{2.6}$$

where D, J_1 and J_2 are dimensionless constants given by

$$D = {}^{K_f}/_{K_r},\ J_1 = \frac{\emptyset \rho_r H_R}{\rho_f c_f (T_c - T_{ini})},\ J_2 = \frac{H_R}{c_r (T_c - T_{ini})}$$

Pe, which is the Peclet number, and the constant C_i are given by

$$\mathrm{Pe} = \frac{Vd}{K_r} \quad C_i = \frac{d^2 c_i}{K_r},\ i = 1,2,3$$

2.2.3 Discretization using finite difference method for gold nanoparticle fabrication problem

The specific parameter value of the finite difference method (FDM) is a numerical strategy for discretizing the parabolic equation. Approximate derivatives in Eq. (2.3) produce the approximation solution of the gold growth, which can be analyzed to be used in environmental analysis for nanosensors. The discretization of Eq. (2.3) is given by

$$\frac{U_{i,j+1} - U_{i,j}}{\Delta t} = \Phi\left(\theta\left(\delta_x^2\right)U_{i,j+1} + (1-\theta)\left(\delta_x^2\right)U_{i,j}\right) + \lambda, \tag{2.7}$$

where $0 \le \theta \le \frac{1}{2}$ and $\frac{1}{2} \le \theta \le 1$.

Transferring the continuity equation of the PDE into the discrete solution by FDM with the forward difference formula for a first-order derivative and three points discretization for a second-order derivative, Eq. (2.7) is expanded as follows:

$$\begin{aligned} -r\theta U_{i-1,j+1} + (1+2r\theta)U_{i,j+1} - r\theta U_{i+1,j+1} = {} & r(1-\theta)U_{i-1,j} + (1-2r(1-\theta))U_{i,j} \\ & + r(1-\theta)U_{i+1,j} + \lambda \Delta t \end{aligned} \tag{2.8}$$

with $i = 1, 2, \ldots, m$ and $j = 1, 2, \ldots, n$.

The step sizes of nanoscale gold nanoparticle growth during the photochemical reduction process can be considered as explicit, implicit, and Crank-Nicolson methods with respect to time and space variables. In equation, the convergent explicit methodology is able to express the growth dynamics of a particle at a new time step, depending on the few forms of points at the previous time. The explicit scheme of the FDM is uniquely designed in the closed domain and available to generate a large sparse fine domain for high resolution of the growth visualization.

2.2.4 Linear system equation formulation for gold nanoparticle fabrication

The next steps of the numerical solution involve formulation of the linear system equation (LSE) for Eq. (2.8). In addition, three important solution tools for solving LSEs—Jacobi, Gauss-Seidel, and Alternating Group Explicit (AGE) by Evans and Sahimi [29], Abdurrahman et al. [30], Sahimi et al. [31], and Abu Mansor et al. [32]—are focused on in this chapter.

The standard scheme for the three-point discretization of a one-dimensional parabolic PDE can be visualized in matrix form as

$$AU = F \tag{2.9}$$

where U and f are one-dimensional vectors defined as

$$U = \left(U_{1,j+1}, U_{2,j+1}, U_{3,j+1}, \ldots, U_{m,j+1}\right)^T,$$
$$F = (F_1, F_2, F_3, \ldots, F_m).$$

Eq. (2.7) can be written in matrix form as:

$$\begin{bmatrix} a & b & & & & \\ c & a & b & & & 0 \\ & c & a & b & & \\ & & \ddots & \ddots & \ddots & \\ 0 & & & c & a & b \\ & & & & c & a \end{bmatrix}_{(m\times m)} \begin{bmatrix} U_1 \\ U_2 \\ U_3 \\ \vdots \\ U_{m-1} \\ U_m \end{bmatrix}_{(m\times 1)} = \begin{bmatrix} F_1 \\ F_2 \\ F_3 \\ \vdots \\ F_{m-1} \\ F_m \end{bmatrix}_{(m\times 1)} \tag{2.10}$$

where

$$a = 1 + 2r\theta,\ b = c = -r\theta$$

and

$$F_1 = r(1-\theta)U_0^j + (1-2r(1-\theta))U_1^j + r(1-\theta)U_2^j + r\theta U_0^{j+1} + \lambda\Delta t$$
$$F_i = r(1-\theta)U_{i-1}^j + (1-2r(1-\theta))U_i^j + r(1-\theta)U_{i+1}^j + \lambda\Delta t,\ for\ i = 2,3,\ldots.m-1$$
$$F_m = r(1-\theta)U_{m-1}^j + (1-2r(1-\theta))U_m^j + r(1-\theta)U_{m+1}^j + r\theta U_{m+1}^{j+1} + \lambda\Delta t \tag{2.11}$$

2.2.5 Visualization of the mathematical model for gold nanoparticle fabrication

Visualization of the mathematical model of the one-dimensional problem of gold nanoparticles is acquired based on a simulation using Microsoft Visual Studio 2012 and the visualization graphs are plotted using Matlab R2013b and Comsol Multiphysics. The results obtained are validated using experimental data for the one-dimensional problem.

In this section, the visualization of the growth of gold nanoparticles from the mathematical model simulation is compared with the experimental data. From the data obtained, the growth of the gold nanoparticles is described in Fig. 2.1, which shows the spectral absorption measured using photon correlation spectroscopy for Samples A and D. Samples A and D used different synthesis methods, such as UVA and UVC photo-initiation.

In the experiment involving photochemical synthesis of AuNPs, tri-sodium citrate was added into a boiling gold chloride dilution and produced relatively monodisperse AuNPs with diameter between 10 and 20 nm. The changes in solution appearance during the experiment were carried out in order to indicate the presence of AuNP size for each sample used.

Different diameters of AuNPs are used in order to visualize the rate of growth for gold nanoparticles. Hence, the computational molecule for AGE methodology at level p+1, as depicted in Fig. 2.5, an average particle size (diameter) from 5 nm to 100 nm, depending on ultraviolet wavelength, was used. In this study, six different sizes of AuNPs were measured: 5, 20, 40, 60, 80 and 100 nm. From Fig. 2.1, it can be concluded that the largest diameter Φ gives the highest rate of gold growth $U(x,t)$.

By focusing on the highest rate of gold growth, with a diameter of 100 nm, the mathematical model simulation of Eq. (2.1) is charged by a different amount of UV radiation, with wavelengths of 366 nm and 253.7 nm. The visualization graph from the simulation of the governing equation is described by Figs. 2.2 and 2.3.

2.3 Numerical implementation and parallelization for gold nanoparticle fabrication

This section consists of the numerical implementation of the solution of the governing equation of the one-dimensional parabolic model for growth of gold nanoparticles, which will aid in promoting the usage of nanosensors in environmental analysis. The numerical implementations

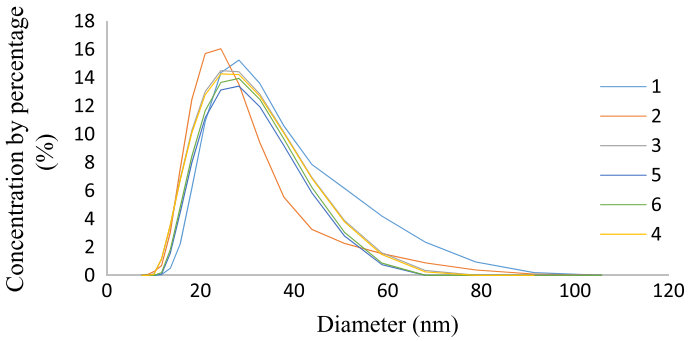

Fig. 2.1
Experimental data for particle size distribution (diameter) of gold nanoparticle growth using different samples.

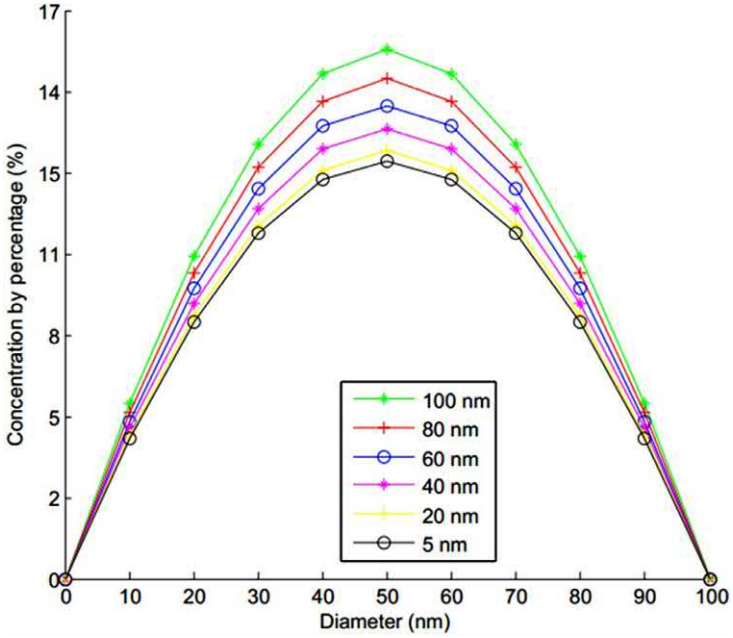

Fig. 2.2
Visualization of gold nanoparticle growth based on the mathematical model with different values of diameters.

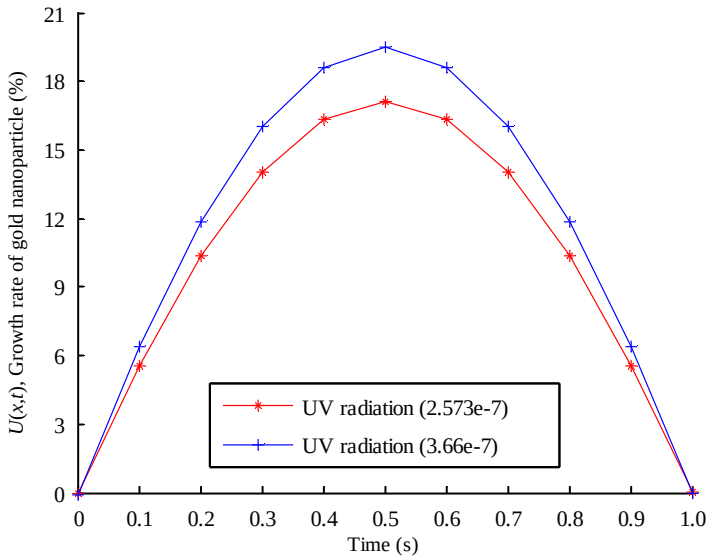

Fig. 2.3
Visualization of gold nanoparticle growth with different UV light radiation wavelengths (366 and 253.7 nm) using AGE method.

involved are alternating group explicit (AGE), red-black Gauss-Seidel (RBGS), and Jacobi (JB) methods. These are then applied using sequential and parallel algorithms that are computed using Parallel Virtual Machine (PVM) programming on a Linux platform by distributed parallel computing systems. Numerical analysis and parallel performance evaluation based on execution time, speed-up, efficiency, effectiveness, temporal performance, and granularity are discussed at the end of this chapter.

2.3.1 Numerical implementation

This section is divided into three subsections: Section 2.3.1.1 discusses the alternating group explicit (AGE) method, followed by the red-black Gauss-Seidel (RBGS) and Jacobi (JB) methods for solving the LSE. In 1985, Evans introduced the AGE method for solving the parabolic PDE problem [33]. It has been shown that this method is extremely powerful and flexible, and provides users with many advantages. This so-called advanced iterative method employs a fractional splitting strategy, which is applied alternately at each half time step on tridiagonal systems of different schemes and which has proven to be stable. The Jacobi (JB) and red-black Gauss-Seidel schemes represent basic numerical schemes and are the benchmarks for simulating the AGE scheme.

2.3.1.1 Alternating group explicit (AGE)

As mentioned earlier, this iterative scheme employs a fractional splitting strategy which is applied alternately at each half time step on tridiagonal systems of difference schemes. This method has already proven to be stable. The linear system equation for the AGE scheme is given by $Au = f$, also illustrated.

The AGE method for obtaining the growth rate of a gold nanoparticle uses the Douglas-Rachford (DR) variant instead of the Peaceman-Rachford (PR). This is so as to ensure its unconditional stability [34] with stationary case (r is constant) and $p \geq 0$ are given by the following equations. The computational molecule for the AGE method in determining the value of U at level $p + \frac{1}{2}$ is (Fig. 2.4):

The molecule diagram of the AGE method for level $p + 1$ can be drawn as follows (Fig. 2.5):

2.3.1.2 Red-Black Gauss-Seidel method (RBGS)

The second iterative scheme of basic numerical analysis used for solving the linear system is the Gauss-Seidel (GS) method. This method was modified and improved from the Jacobi method, so it is no more difficult to apply and it often requires fewer iterations to produce the same degree of accuracy.

When the Jacobi scheme is applied, the value of x_i that is obtained in the n^{th} approximation remains unchanged until the entire $(n + 1)^{th}$ approximate has been calculated, while for the

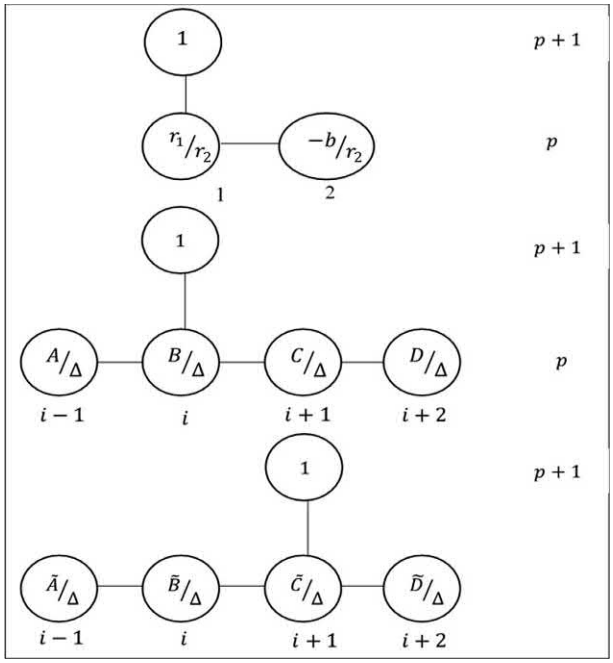

Fig. 2.4
Computational molecule for AGE method at level $p + \frac{1}{2}$.

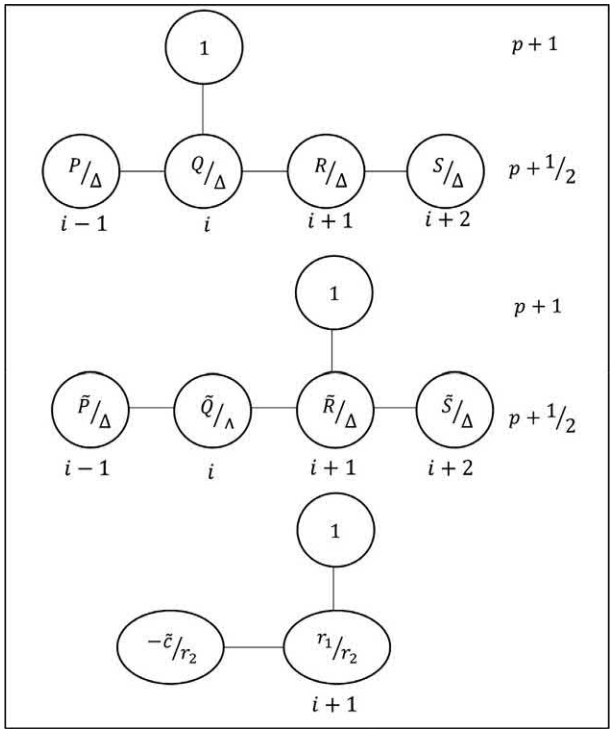

Fig. 2.5
Computational molecule for AGE method at level $p + 1$.

Gauss-Seidel scheme, new values of each $x_i$will be used as soon as they are known. Once x_1 is determined in the first equation, the value is then used in the second equation to obtain a new x_2. Similarly, the new x_1 and x_2 are used in the third equation to obtain the new x_3 and so forth. Tavakoli and Davami [35] considered a parallel Gauss-Seidel in solving a one-dimensional elliptic partial differential equation with a Dirichlet boundary condition. The solution to the linear system $AU = f$ can be obtained starting with $U^{(0)}$ and using the iteration scheme

$$U^{(k+1)} = M_S U^k + C_{S,} \tag{2.12}$$

where M_S and C_S are defined as

$$M_S = -(D+L)^{-1}U \text{ and } C_S = (D+L)^{-1}b.$$

This method is described using the formulae

$$U_i^{(k+1)} = \frac{1}{a_{ii}}\left(b_i - \sum_{j>i} a_{ij}U_j^{(k)} - \sum_{j<i} a_{ij}U_j^{(k+1)}\right), i = 1,2,3,\ldots,m \tag{2.13}$$

However, the GS scheme can only solve sequential algorithms of mathematical modeling, so this scheme has been enhanced to solve algorithms in parallel, called the Red-Black Gauss-Seidel (RBGS). The RBGS contains two subdomains Ω^R and Ω^M. The red point depends on the black point, and vice versa. The loop starts by computing the odd points, from the bottom left, and then going up to the next row and so on. As all of the odd points are finished, the computation of the black ones continues. The red-black grid is illustrated in Figs. 2.6–2.8.

2.3.1.3 Jacobi method (JB)

The third numerical iterative method employed for solving LSEs is the Jacobi method (JB), which is an algorithm for determining the solutions of a diagonally dominant system of linear equations. Each diagonal element is solved and the approximate value is plugged in. The

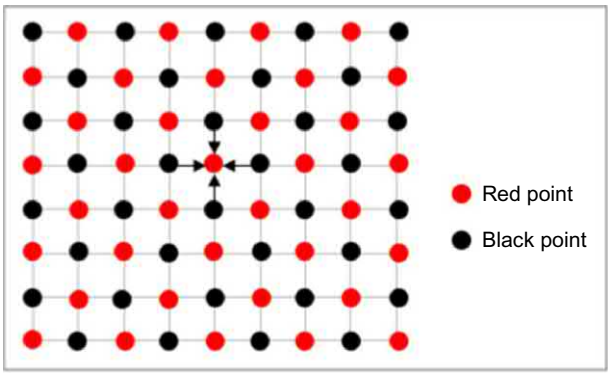

Fig. 2.6
The grid for red and black points.

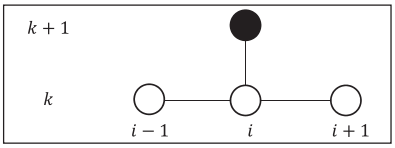

Fig. 2.7
Molecule diagram at Ω^R.

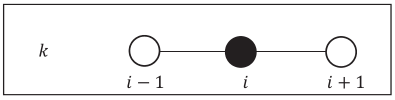

Fig. 2.8
Molecule diagram at Ω^M.

process is then iterated until it converges. The solution to the linear system $Au = b$ can be obtained by beginning with $U^{(0)}$ and using iteration with

$$U^{(k+1)} = M_J u^k + C_J \tag{2.14}$$

where vector M_J and C_J can be defined as

$$M_J = -D^{-1}(L+U) \text{and} C_J = D^{-1}b$$

If $U^{(0)}$ is carefully chosen, a sequence $U^{(1)}$, $U^{(2)}$, $U^{(3)}$… is generated, which converges to the solution $\hat{U}$. A sufficient condition for the method to be applied is that A is a strictly diagonally dominant matrix. Before implementing the simulation of the numerical scheme, an algorithm must be constructed. The purpose of constructing this algorithm is to monitor our programming language. In this study, we develop sequential and parallel algorithms to assist in monitoring our programming. If constructed the programming having error, that can be solved by help of algorithms.

2.3.2 Parallelization of iterative methods for solving one-dimensional mathematical model

A parallel algorithm is constructed based upon the combination of several sequential algorithms. However, this algorithm has two types of server, the "master" and "slave." The "master" will control all the activities that are conducted by the "slave," such as receiving and sending the data. The parallel algorithm is constructed based on a SIMD architecture. A SIMD processor has a single control unit reading instructions pointed to by a single program counter, parallel decoding and sending control signals to the processing elements (PEs). The principle of SIMD is illustrated in Fig. 2.9. The SIMD architecture based on distributed computing system is shown in Fig. 2.10.

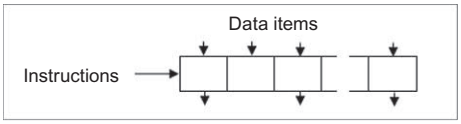

Fig. 2.9
Principle of SIMD processor.

Fig. 2.10
The SIMD architecture based on distributed computer systems.

In this research, C is used as a language that is planted in PVM with the Linux Fedora 21 operating system. The program is linked with the PVM library using the ***#include < pvm3.h >*** command for starting the program. From Fig. 2.11, it is clearly seen that the "master" sends the data of the start, end, initial, and boundary conditions for all slaves. The computational task is run by the "slave" until the local stopping criteria ε is fulfilled by each slave. The results obtained by slaves are sent toward the master. The master will process and store the results. If the global stopping criterion that is declared in the master is satisfied, the computation task is then stopped.

The computation will be running if the condition (global stopping criterion) is still not satisfied. The servers will perform the calculation until the condition declared by the master is reached. The file programs contain message passing in order to communicate the purpose between master and slave as the program is compiled in the host pool for each architecture. The resulting object files are located at a location accessible by machines in the host pool.

The PVM header file should be included with every PVM program. This is due to the important information regarding the interface of PVM programming. The techniques for the one-dimensional algorithm were illustrated in Fig. 2.11A, while the communication between processors is shown in Fig. 2.11B.

In this research, techniques of domain decomposition were employed due to the presence of independent domains in the problem proposed. The grid of domain decomposition for each

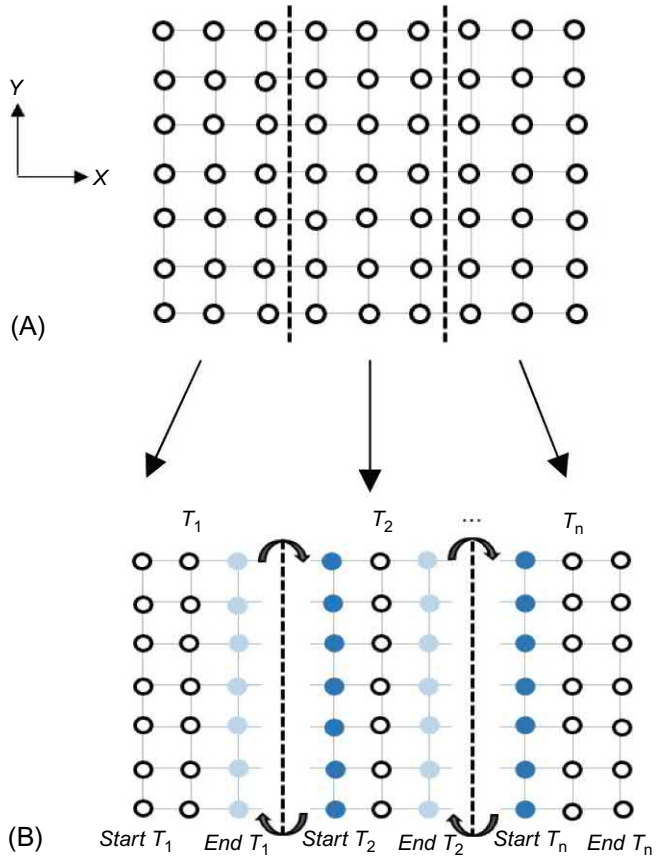

Fig. 2.11

(A) Domain decomposition technique for one-dimensional. (B) Communication between slaves.

one-dimensional parallel algorithm is shown in Tables 2.1A, 2.1B, and 2.1C, which are AGE, RBGS, and JB, respectively. Based on Table 2.1A, we can conclude that the grid of domain decomposition for one-dimensional parallel AGE and JB was similar since the domain is independent. This differs from one-dimensional parallel RBGS since the domain decomposition for those algorithms involves even and odd domain partitioning. This is to avoid the overlapping subdomain problem.

The mapping subdomain processes for sending and receiving data from the one-dimensional parallel algorithm at each time level were summarized in Tables 2.1A–2.1C. Based on that illustrated in Tables 2.1A, 2.1B, and 2.1C, the grid point of u_i required data from the x-direction, which is left and right, while the updating activities are needed for implementing the latest iteration of time level $(k + 1)$. Thus, for this case, the algorithm for sending and receiving data from neighborhood processors $u_{i\pm1}$ is needed to make sure the program functions well.

Table 2.1A: Domain decomposition of one-dimensional molecule for parallel AGE algorithm.

One-dimensional Parallel Alternating Group Explicit (1D-PAGE)

At time level $\left(k+\frac{1}{2}\right)$:

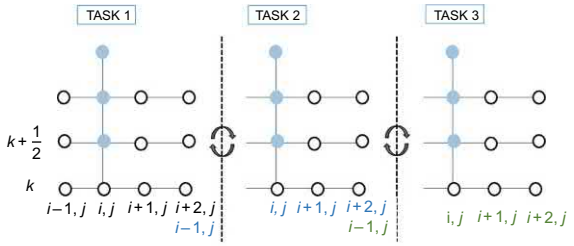

At time level (k + 1):

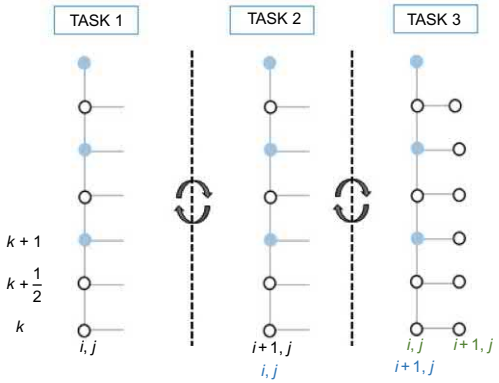

Table 2.1B: Domain decomposition of one-dimensional molecule for parallel RBGS algorithm.

One-dimensional Parallel Red-BlackGauss-Seidel (1D-PRBGS)

Notes:

- Red molecules for odd numbers domain of i^{th}
- Black molecules for even numbers domain of i^{th}

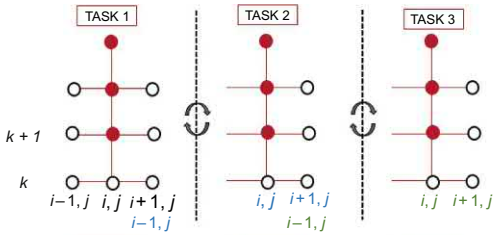

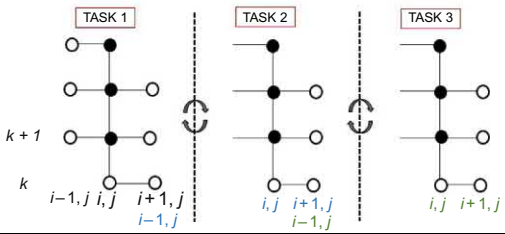

Table 2.1C: Domain decomposition of one-dimensional molecule for parallel JB algorithm.

One-dimensional Parallel Jacobi (1D-PJB)
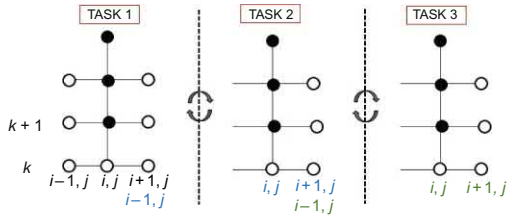

Communication among processors is important for parallel computing, especially for sending and receiving data domain. To ensure the programming runs smoothly, "master" will send the information to data, left, right, start and end to every slave. Subsequently, as slaves receiving the information, computing task would start automatically. The task-to-task communication between slaves happened in sending and receiving neighbourhood data and it is done using massage passing [36].

Besides communication activities and algorithm of data distribution between slaves, the programming of parallel computing would be complete if the global and local convergence's algorithm of master and slave were written well.

2.3.2.1 1D parallel alternating group explicit method (1D PAGE)

AGE method is an advance numerical method that stands with independent domain for each time level. The parallel algorithm for one-dimensional AGE is constructed based on domain decomposition technique shown in Table 2.1A. While, synchronization of domain that decomposed into p number of slave processors and sub-domain of one-dimensional Parallel AGE disintegrated according to processors through Fig. 2.12.

Computation of one-dimensional Parallel AGE is begun by slave receiving the parameters involved and initial condition from the master. Since this method consist of two time level, the

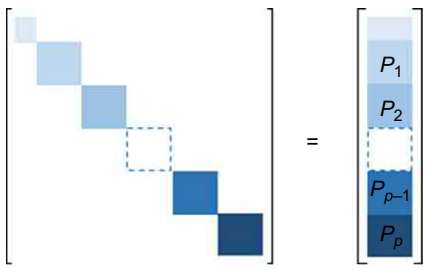

Fig. 2.12
Data partitioning by number of processors.

algorithm defined it as $U_1[i]$ and $U_2[i]$ represent the time level of $\left(k+\frac{1}{2}\right)$ and $(k+1)$ respectively. According to Fig. 2.13, the communication between slaves is needed for sending $U_1[i-1]$ and $U_1[i+1]$ grid data at the time level of $\left(k+\frac{1}{2}\right)$ to neighbour slaves. While, for completing the computation at the time level of $(k+1)$ the grid points of $U_1[i-1]$ and $U_1[i+1]$ is anticipated. It is important to calculate the convergence for completing the computation at time level $(k+1)$. The computation will generate until convergence criterion for local error, $|U_i^{k+1}(p) - U_i^k((p)| < \varepsilon(p)$ is satisfied.

2.3.2.2 1D parallel Red-Black Gauss-Seidel method (1D PRBGS)

Parallel RBGS is a method that has been modified from Gauss-Seidel (GS) iterative method. Since Gauss-Seidel iterative method is not compatible for parallel computing the modification has been made and approved to compute in parallel platform. This is due to the overlapping sub-domain. However, by having the improvement method of GS, which is RBGS, the domain has been partitioned into odd and even number known as red and black points respectively. By having this scenario, the overlapping sub-domain has been avoided successfully. In order to gain new updating value of $U_i[1]$, which is red point, new value of black point is used and vice versa. This phenomenon shown there is no data enslavements between groups. Fig. 2.14,

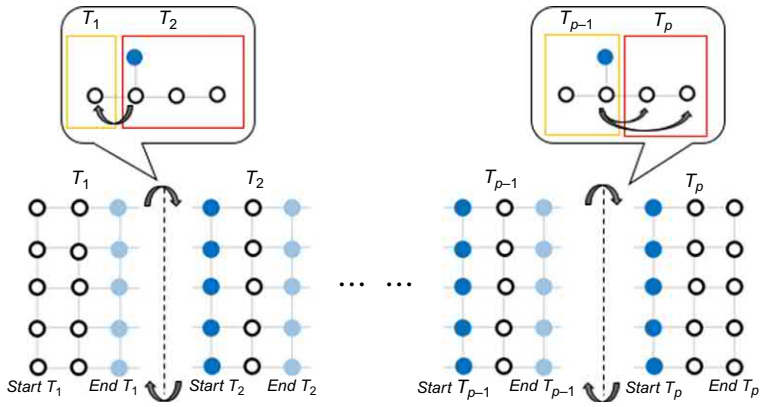

Fig. 2.13
Communication activities of one-dimensional Parallel AGE in sending and receiving domain.

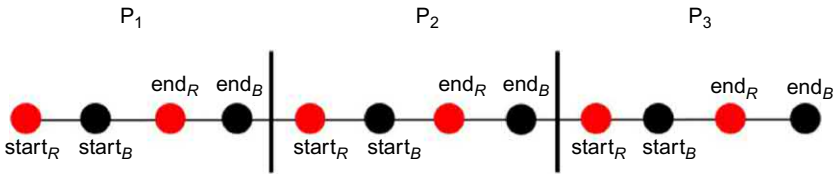

Fig. 2.14
Molecule ordering for one-dimensional parallel RBGS.

illustrated the computational molecule for computation of RBGS ordering toward three processors. The ordering is not simplest as JB method since it involves red and black points.

One-dimensional parallel RBGS is classified into two groups of grid-points through the different colour point red and black represent the odd and even number of grid respectively. In order for obtaining good load balancing, the alternate numbers for the red and black need to be same for conveying toward processors as shown in the figure above. Depending on the colour of the grid-point, the first two starting grid points in a processor were labelled as "start$_R$" and followed by "start$_B$". While the other two end grid points were labelled as "end$_R$" followed by "end$_B$". The computation using this method begin by computing the red point from the bottom left (refer Fig. 2.15A) until finished, then followed black point (refer Fig. 2.15B). In computing black points, the updated value of red points at grid $(i - 1)$ and $(i + 1)$ is needed.

The algorithm begins by providing slave the initial condition as well as independent parameters involve from the master and end up by calculating the global error of the computation. As receiving the initial condition and parameters from the slave, the computation for this method started by computing new value of odd grid (red points) through the communication with neighbourhood slave for sending and receiving data purpose. The computation will carried out until the solution is converged as the global maximum error satisfied the convergence criteria.

2.3.2.3 1D parallel Jacobi method (1D PJB)

One-dimensional Parallel JB method dealing with an independent sub-domain. This method is the simplest method compared with another two iterative method employed for this research. Based on Fig. 2.16 below, we can summarize that the new updating value of U, at time level of $k + 1$, this method hold on value from previous time level of k which are u_{i-1} and u_{i+1}. Fig. 2.16 illutrated the sending and receiving data in order of computing new value for $i - 1$ grid form

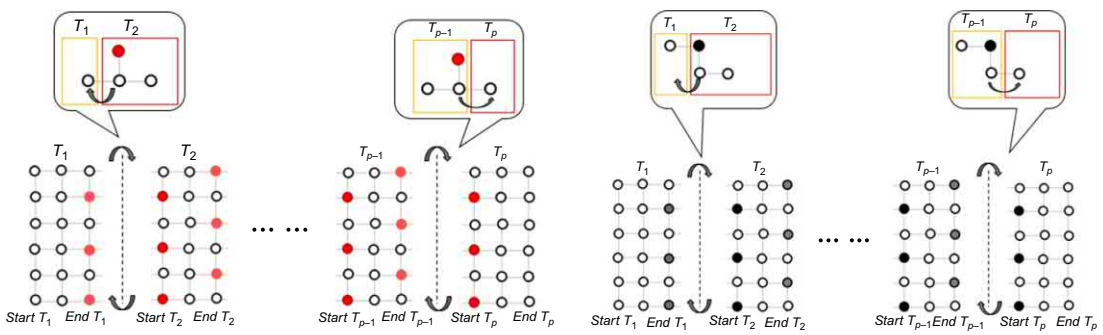

Fig. 2.15

(A) Communication activities of one-dimensional Parallel RBGS in sending and receiving red points. (B) Communication activities of one-dimensional Parallel RBGS in sending and receiving black points.

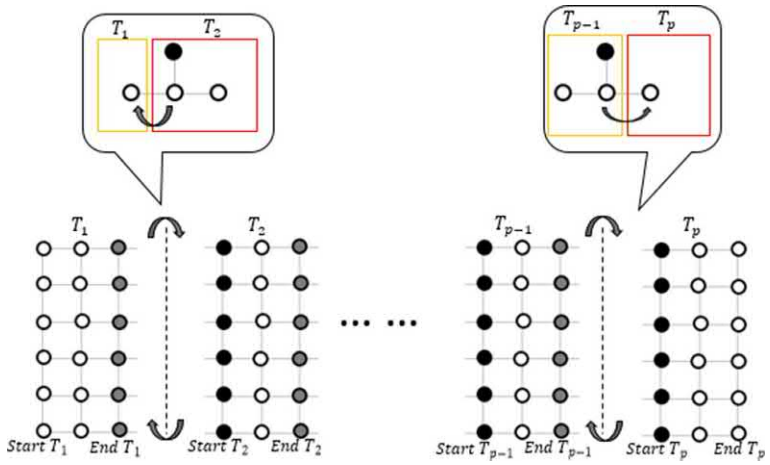

Fig. 2.16
Communication activities of one-dimensional Parallel JB in sending and receiving points.

left and right neighbourhood which are (T_1) and (T_2) respectively. While, that figure also clearly shows the transferring data for $i + 1$.

This Parallel Jacobi algorithm is implemented in the slave's command in order for computing the approximation solution. The algorithm begins by receiving parameters involves from the master such as independent parameters, initial condition and matrix size for computation. Then, the computation will start calculating the new value of U_i based on specified equation. The computation will generate as the approximation solution converged by satisfying the condition of $|U_i^{k+1} - U_i^k| < \varepsilon$. Value of ε, is constant as it is defined by the master. For this research, we use $\varepsilon = 1 \times 10^{-10}$. However, the slaves have to communicate with the neighbour slaves to pass up the neighbourhood data if the solution still not converged. Thus the iteration will be calculated in order for computing new updating value of U_i. As the solution converged, the local maximum error will be sent to master in order to calculate the global maximum error of the parallel algorithms. If the condition of global maximum error were satisfied, the computation will stopped and the result were printed.

2.3.3 Parallel performance evaluation for fabricating gold nanoparticles

By comprising eight number of processors, Parallel Virtual Machine (PVM) with the Fedora version of 21 is installed in distributed memory architecture in order to test and implement the advance as well as the classical numerical methods. The parallel performance that evaluated based on the simulation from parallel algorithm are examined through solving the large sparse problem. Both case studies are being simulated using parallel evaluation and the comparisons of each method known as PAGE, PRBGS and PJB are analyse based on run time, speedup, efficiency, effectiveness, temporal performance and granularity. In order to examine and

measure the performance of the parallel algorithm by the use of numerical methods, the computational complexity and communication cost are calculated. If the computational complexity and communication cost is higher, the longer computational time takes for solving the model problem. Before the matrix size are being decided, the simulation are test for different values of matrix size. Below, in Fig. 2.17 is the speedup results for six value of matrix size that tested using AGE methods.

Based on the graft shown in Fig. 2.17, the performance of the linear speedup and graft value of $m = 50000$, 100000, 150000, 200000, 250000, and 5000000 were reasonable. However, the size matrix for $m = 5000000$ is categorized as superlative size matrix since $S_p \geq p$ and that size of the matrix was not appropriate for large sparse implementation due to some reasons such as the optimization of the usage of cache memory in parallel systems, poor sequential and parallel coding program, and unstable parallel system. For this research, the selected matrix size for undergo the parallelization is $m = 250000$ since the speedup line is converged, stable and has approximately small difference between the linear speedup compared with other size matrix. Since PRBGS and PJB are considered as benchmark methods for PAGE method, thus the size matrixes chosen should be the similar to all methods in this experiment.

The performance evaluation of the parallel algorithms for the 1D problem was done by solving a large sparse matrix size, where $m = 250000$ as an optimum large sparse matrix for predicting the growth of gold nanoparticles (AuNPs). While the other parameters involved were $\Delta x = 0.000004$, $\Delta t = 0.01, r = \left[{}^{\Delta x}/_{\Delta t}\right] \cdot \Delta t$ and $\varepsilon = 10^{-10}$. In addition, the additional calculation that required for the artificial boundary value on the overlapping subdomains also influence the results.

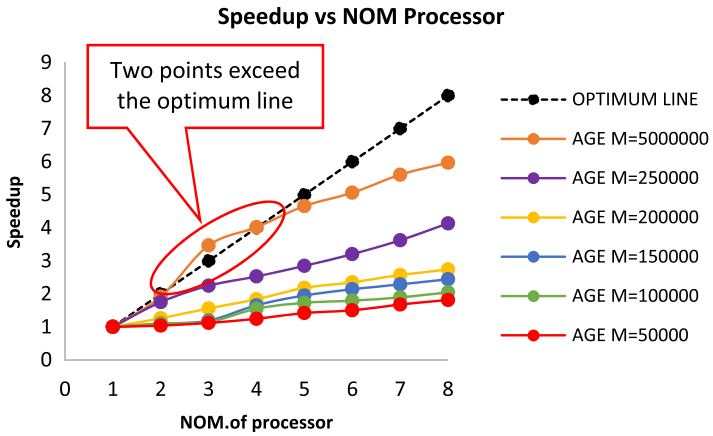

Fig. 2.17
Speedup versus number of processors for different values of matrix size, m for one-dimensional problem.

While the communication cost is important in measuring the time taken for the communication process between processors in the parallel algorithm. Time execution for parallel AGE is in the lowest rank compared to corresponding parallel algorithms because it has the smallest communication cost.

This research concludes that the parallelization approach to the computation of the solution of numerical methods is successful. This is due to the time reducing compared to the serial computing. The parallel performance evaluation is appraised based on six indicators which are execution time, speedup, efficiency, effectiveness, temporal performance and granularity versus eight number of processors. The large sparse matrix dealing with big data set can be easily handled by the high computing platform.

Consuming the same feature dealing with changes parameter, the parallel performance of all the tested schemes is evaluated. Fig. 2.18 shows the execution time versus the number of processors, P with resulting JB implicit scheme with the largest amount of time with $P = 1$. However the time execution were extremely reduced as the number of processors, P increase. Clearly, in Fig. 2.18 parallel AGE with implicit scheme has provided the fastest execution time compared with a corresponding parallel one-dimensional scheme named as RBGS and JB. This is due to the limited domain decomposition technique and message passing activities. Furthermore, the solution domain is divided into small sub domains and distributed to each processor as well as computed synchronously. Despite the one-dimensional Parallel AGE have greater computational complexity, its parallelization enables to execute in shorter time for every p number of processors compared to the parallel algorithm of classical methods.While the speedup, S_p has been improved as the number of processors increases as demonstrated in Fig. 2.19A.

Through the statement described above, this situation has shown that, the parallel computation improves the performance in serial computation based the execution time and speedup indicators. At highest numbers of processors, which is $P = 8$, the speedup of one-dimensional Parallel AGE with implicit scheme is 51.64%, while, the corresponding algorithm which are

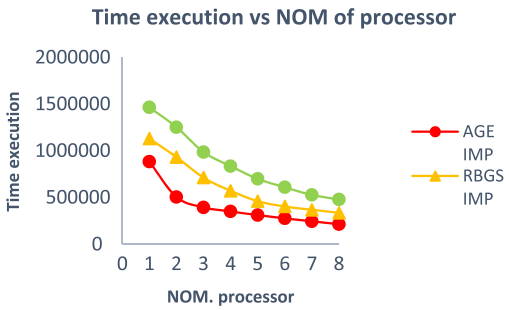

Fig. 2.18
Time execution versus numbers of processors.

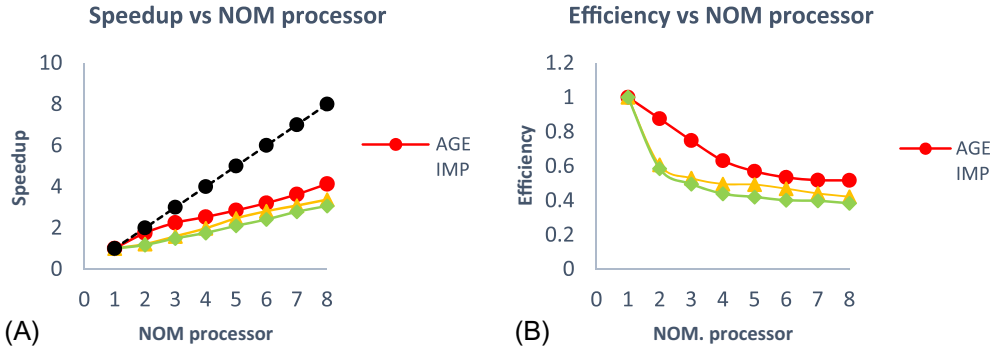

Fig. 2.19

(A) Speed up versus numbers of processors. (B) Efficiency versus numbers of processors.

one-dimensional Parallel RBGS and JB resulting 42.11% and 38.29% respectively. This shows that, one-dimensional Parallel AGE has the closest percentage with the linear speedup which is 48.36%, while the corresponding algorithm resulting in 57.89% and 61.71% respectively. It can be concluded that one-dimensional Parallel AGE has the best speedup performance and makes it the most efficient algorithms among the tested algorithms.

The one-dimensional Parallel AGE with an implicit scheme achieves a speedup that equates to a higher efficiency about 6.45%. Due to overheads, by all the algorithm, as the number of processors increasse, a clear reduction of efficiency were takes place as shown in Fig. 2.19B. Besides that, the efficiency measurement also affected by the idle, starting and waiting time that consumed in completing all the process by the slave. Imbalance task distributed among the different processors caused by poor load balance also becomes one of the reasons that affect the decreasing of efficiency. In contrast, the performance of effectiveness is evaluated by considering the speedup and efficient of the algorithm. Based on Fig. 2.20A, the effectiveness performance and numbers of processors extremely rose up due to the speedup performance.

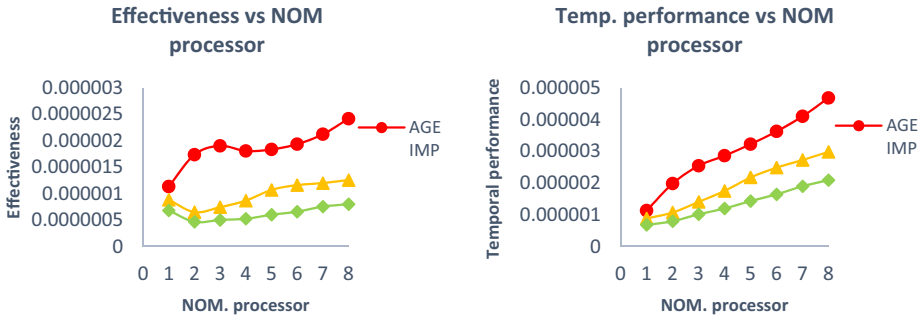

Fig. 2.20

(A) Effectiveness up versus numbers of processors. (B) Temporal performance versus numbers of processors.

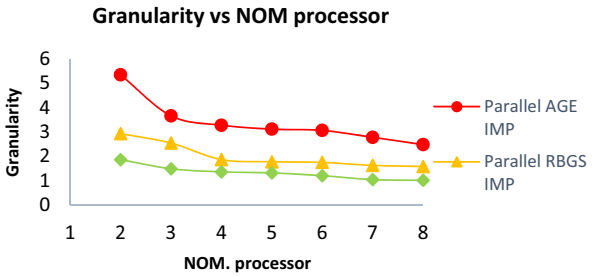

Fig. 2.21
Granularity versus number of processors for one-dimensional parallel algorithm of implicit scheme, $\theta = 1$.

Additionally, aside of speedup, efficiency and effectiveness, the temporal performance as shown in Fig. 2.20B also plays the important role in appraising the parallel performance evaluation of parallel algorithm. Fig. 2.21 shows a huge difference between one-dimensional Parallel AGE algorithm with the corresponding classical parallel algorithm. This difference in term of temporal performance showed the one-dimensional Parallel AGE algorithm is more accomplished than the other classical algorithm. The last measurement of PPE for this research is granularity. Excellence definition of granularity is ratio between the computational and communication time.

Decreasing and increasing the computational as well as communication time respectively has influence the decrement of granularity. It is clearly shows the decreasing of $\boldsymbol{T_{comp}}$ percentage from **84.22**% to **71.17**% with the number of processors from $\boldsymbol{p = 2}$ to $\boldsymbol{p = 8}$ for one-dimensional Parallel AGE. While, from the same range of processor's number and algorithm, the $\boldsymbol{T_{comm}}$ recording an increasing percentage which are from **15.78**% to **28.83**%. This is due to the high communication activities among the master and slaves. Thus, it is conclude that, the computation of algorithm takes longer time compared with communication.

The one-dimensional Parallel JB resulting the smallest percentage of granularity followed by RBGS. This is due to the greater time execution were spent in communication of one-dimensional Parallel JB resulting higher from $\boldsymbol{T_{idle}}$ since the algorithm takes a large number of iterations to have a converged solution. While, the greatest granularity is conquered by one-dimensional Parallel AGE with implicit scheme.

Next, the PPE of one-dimensional Parallel AGE, RBGS and JB with Crank Nicolson, $\boldsymbol{\theta = 0.5}$ are discussed through the tabulated table and plotted a graph below as well as the result of granularity. The matrix size for this result is same as an implicit scheme which is $\boldsymbol{m = 250000}$.

Execution time is needed for measuring the time duration in completing each program routine. Each algorithm showing a reducing in time execution as the number of processors employed is increased. However, Fig. 2.22A, the algorithm of one-dimensional Parallel AGE showing the

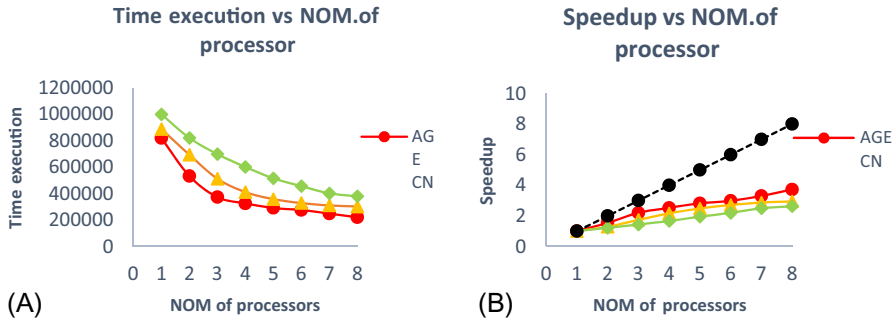

Fig. 2.22

(A) Time execution versus numbers of processors. (B) Speed up versus numbers of processors.

least time execution compared the other two corresponding algorithms. As explained before, this phenomenon is caused by the domain decomposition technique and message passing activities which are limited and domain is divided into small subdomains, distributed to each processor and computed synchronously. Since that algorithm has greater computational complexity, its parallelization enable it to be executed in much shorter time for each number of processors compared with one-dimensional Parallel RBGS and JB algorithm.

Referring to Fig. 2.22B, the speedup of each algorithm was in good condition since all plotted line is below linear speedup dotted. This shows all tested parallel algorithm satisfied Amdahl's law since its resulting each speedup is less than p. According to the plotted graph in Fig. 2.22B, one-dimensional Parallel JB has the worst speedup which indicated 32.90% as it is farther to the super linear line with the difference percentage of 67.10% followed by RBGS which is 63.21%. However, the superior algorithm which is one-dimensional Parallel AGE indicates 46.48% as it is closest to the super linear line.

Fig. 2.23A, however, showing an improvement of efficiency percentage that affected by the increasing number of processors. Commonly, the ratio between speedup and number of

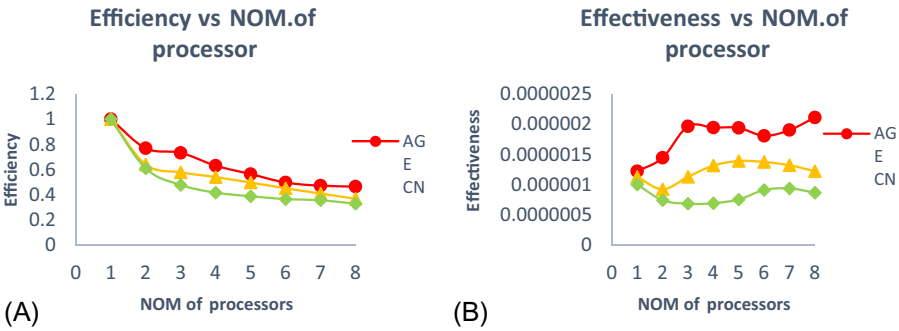

Fig. 2.23

(A) Efficiency versus numbers of processors. (B) Effectiveness versus numbers of processors.

processors affected the values of efficiency. Comparing all tested algorithm for one-dimensional problem, parallel algorithm of AGE recorded the highest percentage of efficiency, which is 5.81% and make it the most efficient algorithm.

In this research, we have found that, there is strong relation between effectiveness and speedup evaluation. As the speedup increase, the effectiveness also indicates as increasing and vice versa. Referring to Fig. 2.23B it is obviously shown that there is gigantic diverse of effectiveness versus the number of processors between one-dimensional Parallel AGE with other corresponding parallel algorithms.

On the other hand, temporal performance of the algorithm is measured as the inverse of time execution. The algorithm is said to be greatest algorithm if it records the shortest execution time. From Fig. 2.24 we conclude that, one-dimensional Parallel RBGS is among the worst algorithm since it is indicating the lowest temporal performance, which is 17.1% if compared with other two corresponding algorithms. This resulting one-dimensional Parallel AGE becomes superior algorithm that is recording the highest percentage of temporal performance which is 18.5%.

This section is concluded by explaining the granularity performance for one-dimensional Parallel AGE, RBGS and JB with Crank Nicolson scheme. The granularity performance for all tested algorithm are summarized in Fig. 2.25. From the plotting graph based on Fig. 2.25 it is undoubtedly shown that the granularity performance of all tested algorithm is decreasing as the number of processors increases. This is due to the dependency of granularity on computational time, T_{comp} and communication time, $T_{comp} = T_{comm1} + T_{idle}$ for any $P \leq 8$. The larger value of granularity, indicating the good feasibility of the parallelization.

Based on all tested algorithm proposed in this research, the one-dimensional Parallel AGE (PAGE) algorithm significantly outperforms their counterparts compared with another two algorithms in term of accuracy, convergence rate and parallel measures such as execution time, speedup, efficiency, effectiveness, temporal performance and granularity for Implicit and

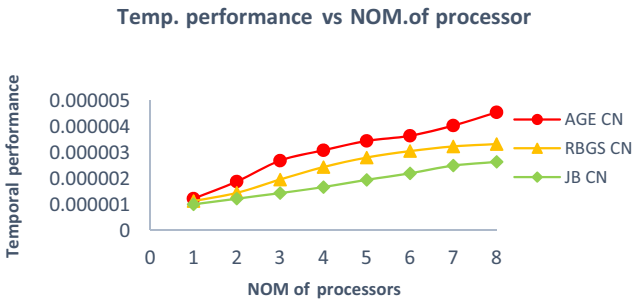

Fig. 2.24
Temporal performance versus numbers of processors.

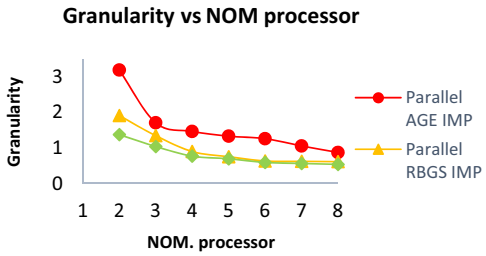

Fig. 2.25
Granularity versus number of processors for one-dimensional parallel algorithm of Crank-Nicolson scheme, $\theta = 0.5$.

Crank-Nicolson scheme, $\theta = 1$ and $\theta = 0.5$, respectively. Numerical analysis also shown PAGE algorithm has the fastest execution time compared with another algorithm. Despite their higher computational complexities, the increase in the number of iterations yields faster rate of convergence with higher level of accuracy for a large size matrix. The relatively less granularity delivery by PJB algorithm and PAGE algorithm implementation gives a good indication of the feasibility of its parallelization.

2.4 Conclusion and recommendation

This chapter is discussing the solving methods of large sparse systems using parallelization to find the best result results of gold nanoparticle development to use in nanosensors environmental application. As discussed the solving methods, a problem was arose which is the fabrication of nanoparticles. To be exact, this problem introduces the visualization of the growth of gold nanoparticles (AuNPs) using one dimensional Partial Differential Equation, (PDEs) with respect to time and space. The mathematical modeling represent the industrial problem was successfully discretized numerically by employing central FDM with weighted parameter $\boldsymbol{\theta}$.

In this study, two weighted parameters were considered which are, $\boldsymbol{\theta = 1}$ and $\boldsymbol{\theta = 0.5}$ represent Fully Implicit and Crank-Nicolson schemes respectively.The Linear System Equation (LSE) that acquired from the discretization are then solved by three iterative methods named as Alternating Group Explicit (AGE), Red Black Gauss Seidel (RBGS) and Jacobi (JB). The LSE for all tested methods were solved sequentially using in C programming language. The numerical results in term of time execution, number of iterations, rate of convergence, maximum error, computational complexity and Root Mean Square Error (RMSE) were discussed details in Section 2.3 for one-dimensional problem. While, in order to accelerate the sequential execution as well as the convergence rate, the parallelization based on distributed computing using PVM platform that plant on Fedora 21 has been successfully done.

Based on the discussion in Section 2.3, Parallel AGE has provided significantly outperform their counterparts compared with the benchmark classical methods for one dimensional problem. Despites having huge computational complexity, results obtained from Parallel AGE methods prove valuable since it enables to provide solution with higher accuracy and stability compared with the benchmark methods either for sequential and parallel algorithm. In addition, these techniques were verified as convergent and unconditionally stable for the rate of convergence for solving one-dimensional problem.

References

[1] C. Fang, R. Dharmarajan, M. Megharaj, R. Naidu, Gold nanoparticle-based optical sensors for selected anionic contaminants, TrAC Trends Anal. Chem. 86 (2017) 143–154.
[2] Y. Dahman, Nanotechnology and Functional Materials for Engineers, Elsevier, 2017.
[3] P.J. Vikesland, Nanosensors for water quality monitoring, Nat. Nanotechnol. 13 (8) (2018) 651–660.
[4] S.-Y. Kwak, M.H. Wong, T.T.S. Lew, G. Bisker, M.A. Lee, A. Kaplan, et al., Nanosensor technology applied to living plant systems, Annu. Rev. Anal. Chem. 10 (2017) 113–140.
[5] A. Verdian, Apta-nanosensors for detection and quantitative determination of acetamiprid – A pesticide residue in food and environment, Talanta 176 (2018) 456–464.
[6] A.K. Srivastava, A. Dev, S. Karmakar, Nanosensors and nanobiosensors in food and agriculture, Environ. Chem. Lett. 16 (1) (2018) 161–182.
[7] R.A. Sperling, P.R. Gil, F. Zhang, M. Zanella, W.J. Parak, Biological applications of gold nanoparticles, Chem. Soc. Rev. 37 (9) (2008) 1896–1908.
[8] S. Aldrich, Gold Nanoparticles: Properties and Applications, Sigma-Aldrich, St. Louis, MO, 2015.
[9] T. Hanemann, D.V. Szabó, Polymer-nanoparticle composites: From synthesis to modern applications, Materials 3 (6) (2010) 3468–3517.
[10] G. Schmid, Clusters and Colloids: From Theory to Applications, John Wiley & Sons, 2008.
[11] S. Zeng, K.-T. Yong, I. Roy, X.-Q. Dinh, X. Yu, F. Luan, A review on functionalized gold nanoparticles for biosensing applications, Plasmonics 6 (3) (2011) 491.
[12] Y. Sun, Y. Xia, Shape-controlled synthesis of gold and silver nanoparticles, Science 298 (5601) (2002) 2176–2179.
[13] R.A. Petros, J.M. DeSimone, Strategies in the design of nanoparticles for therapeutic applications, Nat. Rev. Drug Discov. 9 (8) (2010) 615.
[14] K.E. Drexler, Nanosystems: Molecular Machinery, Manufacturing, and Computation, John Wiley & Sons, Inc, 1992.
[15] T. Schlick, Molecular Modeling and Simulation: An Interdisciplinary Guide: An Interdisciplinary Guide, Vol. 21, Springer Science & Business Media, 2010.
[16] P. Ghosh, G. Han, M. De, C.K. Kim, V.M. Rotello, Gold nanoparticles in delivery applications, Adv. Drug Deliv. Rev. 60 (11) (2008) 1307–1315.
[17] Y. Liu, W. Meyer-Zaika, S. Franzka, G. Schmid, M. Tsoli, H. Kuhn, Gold-cluster degradation by the transition of B-DNA into A-DNA and the formation of nanowires, Angew. Chem. Int. Ed. 42 (25) (2003) 2853–2857.
[18] J.H. Park, G. von Maltzahn, L.L. Ong, A. Centrone, T.A. Hatton, E. Ruoslahti, et al., Cooperative nanoparticles for tumor detection and photothermally triggered drug delivery, Adv. Mater. 22 (8) (2010) 880–885.
[19] C. Rejiya, J. Kumar, V. Raji, M. Vibin, A. Abraham, Laser immunotherapy with gold nanorods causes selective killing of tumour cells, Pharmacol. Res. 65 (2) (2012) 261–269.
[20] E. Boisselier, D. Astruc, Gold nanoparticles in nanomedicine: Preparations, imaging, diagnostics, therapies and toxicity, Chem. Soc. Rev. 38 (6) (2009) 1759–1782.
[21] P. Zhao, N. Li, D. Astruc, State of the art in gold nanoparticle synthesis, Coord. Chem. Rev. 257 (3) (2013) 638–665.

[22] G.C. Bond, D.T. Thompson, Status of catalysis by gold following an AURICAT workshop, Appl. Catal. A Gen. 302 (1) (2006) 1–4.
[23] M. Treguer, F. Rocco, G. Lelong, A. Le Nestour, T. Cardinal, A. Maali, B. Lounis, Fluorescent silver oligomeric clusters and colloidal particles, Solid State Sci. 7 (7) (2005) 812–818.
[24] J. Polte, R. Erler, A.F. Thunemann, S. Sokolov, T.T. Ahner, K. Rademann, et al., Nucleation and growth of gold nanoparticles studied via in situ small angle X-ray scattering at millisecond time resolution, ACS Nano 4 (2) (2010) 1076–1082.
[25] P. Fratzl, Small-angle scattering in materials science – a short review of applications in alloys, ceramics and composite materials, J. Appl. Crystallogr. 36 (3) (2003) 397–404.
[26] J. Polte, R. Kraehnert, M. Radtke, U. Reinholz, H. Riesemeier, A.F. Thünemann, F. Emmerling, New insights of the nucleation and growth process of gold nanoparticles via in situ coupling of SAXS and XANES, in: Paper Presented at the Journal of Physics: Conference Series, 2010.
[27] G. Smith, Numerical Solution of Partial Differential, Oxford University Press, New York, 1979.
[28] D. Blest, B. Duffy, S. McKee, A.K. Zulkifle, Curing simulation of thermoset composites, Compos. A: Appl. Sci. Manuf. 30 (11) (1999) 1289–1309.
[29] D.J. Evans, M.S. Sahimi, The alternating group explicit (AGE) iterative method to solve parabolic and hyperbolic partial differential equations, in: C.L. Tien, T.C. Chawla (Eds.), Annual Review of Numerical Fluid Mechanics and Heat Transfer, Vol. 1, Hemipshere Publishing, Berlin, 1989, , pp. 283–390.
[30] A. Abdurrahman, A.K. Zulkifle, N. Alias, I. Hashim, Implementation of parallel computational tools for the curing simulation of thermoset composites using the double sweep two-stage AGE algorithm, Malays. J. Sci. 26 (2007) 5–15.
[31] M. Sahimi, E. Subdararajan, M. Subramaniam, N. Hamid, A new high order iterative alternating decomposition explicit method to solve the heat conduction equation, Sains Malaysiana 29 (2000) 93–102.
[32] N. Abu Mansor, A.K. Zulkifle, N. Alias, M.K. Hasan, M.J.N. Boyce, The higher accuracy fourth-order IADE algorithm, J. Appl. Math. (2013) 2013.
[33] D. Evans, Alternating group explicit method for the diffusion equation, Appl. Math. Model. 9 (3) (1985) 201–206.
[34] D. Evans, M. Sahimi, The alternating group explicit method (AGE) to solve parabolic and hyperbolic partial differential equations, Annu. Rev. Numer. Fluid Mech. Heat Transf. 2 (1987).
[35] R. Tavakoli, P. Davami, A new parallel gauss–Seidel method based on alternating group explicit method and domain decomposition method, Appl. Math. Comput. 188 (1) (2007) 713–719.
[36] G. Ghiani, P. Legato, R. Musmanno, F. Vocaturo, Optimization via simulation: Solution concepts, algorithms, parallelcomputing strategies and commercial software, Int. J. Comput. 3 (3) (2014) 7–12.

CHAPTER 3

Designing of novel nanosensors for environmental aspects

Rocktotpal Konwarh[a,b], **Ganesh Gollavelli**[b,c], **Suresh Babu Palanisamy**[a]

[a]*Department of Biotechnology, College of Biological and Chemical Engineering, Addis Ababa Science and Technology University, Addis Ababa, Ethiopia*
[b]*Centre of Excellence of Nanotechnology, Addis Ababa Science and Technology University, Addis Ababa, Ethiopia*
[c]*Department of Industrial Chemistry, College of Applied Sciences, Addis Ababa Science and Technology University, Addis Ababa, Ethiopia*

3.1 Introduction

Climate change, constantly growing local and global populations, rural-to-urban human migration, and their associated detrimental consequences on environmental health, primarily attributed to anthropogenic sources, need no further elaboration [1–3]. Be it hazardous water quality with teeming populations of pathogenic microbes and heavy metal contamination, the toxic air we breathe, or the pesticide/insecticide-loaded agricultural fields used to cultivate crops—all pose serious impediments to realization of the UN Sustainable Development Goals [4–6]. As evidence, dearth of safe drinking water is the key reason for the death of nearly 2 million people (primarily children under the age of 5 years) every year [7]. The age-old proverb states that "prevention is better than cure." From this standpoint, facile, timely, and inexpensive detection/sensing of ecological contaminants and toxicants is a prerequisite for effective strategies to prevent dire consequences (diseases and deaths) from environmental pollution.

Among other technologies, nano-enabled sensors have grabbed considerable attention of late. These sensors are opening up novel avenues in biological, chemical, and physical sensing that have facilitated greater detection sensitivity, specificity, multiplexing capability, and portability for a plethora of health, safety, and environmental analysis. The scientific fraternity has witnessed a growing number of reports and patents using these sensors for low-cost and rapid sensing of chemicals, microbes, and other analytes in air, water, and soil. A number of comprehensive write-ups are available on the employed nanomaterials, signal transduction approaches, analytes of interest, and contaminant class [7–9]. In this chapter, we intend to

Nanofabrication for Smart Nanosensor Applications. https://doi.org/10.1016/B978-0-12-820702-4.00003-9
© 2020 Elsevier Inc. All rights reserved.

present an overview of the basic make-up and working principle of nano-enabled sensors, with special emphasis on innovative design approaches. Sensing of various analytes in the environment is of crucial relevance; however, we have streamlined our discussion in the context of sensors fabricated for the detection of heavy metals, pesticides, and a few representative microbes. At this juncture, it would be prudent to delve into the fundamental construct of a nanosensor from an environmental perspective.

3.2 ABCs of the design strategy for nano-enabled sensors

The word sensor has its genesis in the Latin word *sentio* – to observe or perceive. Based on the specific contaminant or specific analyte to be detected, researchers have documented various strategies for fabrication of nano-enabled sensors. Depending on the requirements and appropriate design strategy, either single or multiple (multiplex) analyte detection may be mediated. The basic design consists of a nanomaterial (with dimension between 1 and 100 nm) and a recognition element (responsible for the specificity), while the presence of the analyte is relayed by a specific signal-transduction strategy. Generation of a signal, a decrease in signal, and turn-on and turn-off mechanisms are used as indicators for the presence of analytes. However, strict distinction of these components may not always be apparent in the sensors. Microfluidic devices, solutions, substrates/scaffolds, etc. serve as deployment formats of the sensors.

3.2.1 A note on the signal transduction mechanism

Willner and Vikesland [7, 9] elaborately reviewed the current status of nanosensors employed from an environmental perspective, particularly for water quality monitoring in the context of the signal transduction mechanism as well as the nature of specific environmental contaminants.

3.2.1.1 Electrical signal transduction

High conductivity and electrochemical stability of materials such as graphene, carbon nanotubes, noble metal nanoparticles, silicon, and so forth dictate the electrical signal transduction mechanism. *Chemiresistors* rely on alteration of resistance of an electrical circuit post interaction of the analyte with the sensor surface. As exemplary evidence of chemiresistors, gold nanowires for sensing of halides, polymer nanowires for Fe^{III}, volatile organic compounds (VOCs), and ammonia, and metal oxide semiconductor nanowires for VOCs and NO_2 can be cited [10–16]. *Electrochemical sensors* are dependent on the electron transfer between the surface of the sensor and target analyte/intermediate resulting in voltage or current modulations. Pertinent representatives of electrochemical sensors include graphene for bacterial sensing [17]; carbon nanotubes for ammonium, Co^{2+}, and pesticides [18–20]; copper nanowire electrodes for nitrate [21]; polymeric nanocomposite membranes for Ag^{1+}, Hg^{2+}, and Cu^{2+} [22]; and reduced graphene oxide/gold nanoparticle nanocomposite for organophosphate

pesticides [23]. *Field-effect transistors (FETs)* quantify the mobility of a charge carrier (analyte) moving via a channel subjected to an applied electric field regulated by a conductive gate electrode. Entry of an analyte into the channel leads to a change in signal. FET-dependent nanosensing platforms have been exploited for detection of Hg^{2+} using gold nanoparticle functionalized polymeric FETs [24]; glucose, H_2O_2, proteins, Hg^{2+}, pH using two-dimensional transition metal dichalcogenides [25, 26]; and nucleic acids and flu diagnosis using silicon nanowires (SiNWs) [27, 28].

3.2.1.2 Optical signal transduction

The optical signal transduction mode relies on the generation of a signal postinteraction of a target analyte with a nanomaterial. Fast readout, facile operation, and practical sensitivity of *fluorescence* (fluorophore emission on returning to its ground state postexcitation by light) have been exploited in various optically active nanosensors, based on quantum dots, metal nanoparticles, and up-conversion nanoparticles (UCNPs) for detection of heavy metals such as Cd^{2+}, Pb^{2+}, Hg^{2+}, Cu^{2+}, and Ag^{1+} [29–38]. On the other hand, signal transduction based on *localized surface plasmon resonance (LSPR)* (dictated by shape-size-identity-surface functionality-local ambient accord of nanoparticles), categorized into *surface-enhanced Raman spectroscopy (SERS)* and *colorimetric (absorption) sensing*, has been widely documented for the detection of a plethora of analytes. Colorimetric assays for various analytes (amenable for field-deployable, inexpensive, and easy-to-use paper-based colorimetric sensing) relies on the monitoring of nanoparticle aggregation state. Coupling of surface plasmons on nearby nanoparticles leads to alteration in color (which may be visually observed or spectrophotometrically monitored) as an offshoot of the destabilization of nanoparticles (e.g., yellow to brown for spherical silver nanoparticles). In this regard, noble metal nanoparticles have been employed for detection of NO_{2^-}, NO_{3^-}, cocaine, Pb^{2+}, Cu^{2+}, Hg^{2+} [39–44]. On the other hand, the SERS spectrum is an indicator of the covalent bonds of an analyte. A considerably intense signal emanating from the "fingerprint" spectrum may be employed to directly specify an analyte's presence in a complex media. An indispensable requisite for SERS-based sensing of environmental pollutants is the close interaction of the analyte and the noble metal nanoparticles. Functionalization of the nanoparticle surface with affinity ligands could offer a plausible solution. Noble metal nanoparticles have been employed for the SERS-based detection of pesticides and microorganisms like bacteria, protozoa, and viruses [43–50]. Availability of hand-held Raman spectrometers and the features of high sensitivity and multiplexing capacity are gradually endowing a special niche in the SERS approach in the domain of nanosensing.

3.2.1.3 Magnetic signal transduction

Materials such as metallic iron, oxides of iron, cobalt, nickel, etc. are used to fabricate magnetic nanoparticles (MNPs), responsive to external magnetic fields and amenable for surface functionalization with analyte-specific biomolecules. Sensors based on this category are

grouped according to the principle of *magnetoresistance*, *T2 relaxation nuclear magnetic resonance*, or *hydrodynamic property assessment*. Modulations in electrical resistance postbinding of analyte-tagged MNPs have been exploited in magnetoresistance sensors (e.g., use of magnetite and maghemite for detection of *Mycobacterium bovis* and influenza virus) [51–53]. On the other hand, tracking the alteration in the T2 relaxation time of water protons postaggregation of MNPs in the presence of analyte is possible via magnetic resonance imaging. Recent reports on the use of magnetic beads for sensing *Salmonella enterica* and Newcastle disease virus, and *E. coli* 0157:H7 [54, 55], testify to the prospects. Furthermore, assessment of nanoparticle relaxation dynamics in a temporal-dictated magnetic field may be used to unveil the modulations in hydrodynamic features attributed to analyte-mediated clustering of nanoparticles. Detection of *Bacillus globigii* spores using magnetite nanoparticles [56] stands in testimony to the exploitation of this principle.

3.2.2 A few representative nanomaterials and recognition elements

Quantum effects, high surface area-to-volume ratio, and facile surface functionalization approaches endow intriguing properties to *nanomaterials* [57–61] in contrast to their bulk counterparts, particularly to achieve extremely low detection limits in the context of sensing. Furthermore, the size resemblance of nanomaterials in many cases to the analyte under perusal (antibodies, metallic ions, DNA, etc.) has permitted the scrutiny of formerly unconquered domains in the niche of sensor technology. A spectrum of nanomaterials have found applications in the designing of novel nanosensors. Some of these are listed in Table 3.1.

On the other hand, a wide variety of recognition elements are used in chemical sensors and biosensors. Saini et al. [84] provided an excellent overview on the various *recognition elements* used in nanobiosensors for environmental applications, with special reference to detection of pesticides. A brief note is presented later, while exemplary studies are cited in the subsequent section of this chapter. In *enzymatic biosensors*, biocatalysts serve as a recognition element. In *inhibition based enzymatic biosensors* (e.g., based on choline esterase, ChE; tyrosinase; alkaline phosphatase, ALP; peroxidase), inhibition of the enzyme by the analyte and consequent decrease in enzymatic product yield is correlated with the concentration of the analyte [85]. On the contrary, in *catalysis based enzymatic biosensors* (e.g., those based on organophosphorus hydrolase, OPH; glutathione-S-transferase, GST), catalytic conversion of the analyte by the enzyme is quantified to measure the analyte concentration [84]. Specificity, sensitivity, and simplicity of apparatus and protocol are the advantages, while costly and time-consuming purification, poor stability, and demonstration of efficiency only at optimum pH and temperature are some of the practical snags in enzymatic biosensors. On the other hand, low cost of preparation, high stability, and reduced purification requirements are some of the advantages (in comparison to enzyme-based sensors) of *whole cell biosensors* (e.g., microbial biosensors; electrochemical microbial biosensors and plant tissue- and photosynthesis-based

Table 3.1 Plethora of nanomaterials and their properties, exploited in the fabrication of nanobiosensors.

Nanomaterials	Representative members	Exploitable intrinsic properties	What purpose do they serve in nanosensors?	References
Quantum dots	Combination of semiconductor materials from periodic table's groups: 12–16, 13–15, or 14–16 (CdSe, CdSe/ZnS, CdTe, CdTe/CdS, ZnS, ZnSe/ZnS)	- Tunable fluorescence, depending on material and size - Higher photostability and higher quantum yield than organic fluorophores - Narrow emission band for multiplexing	- Fluorescent probe - FRET donor	[62–64]
Metal nanoparticles (mNPs)	Gold, silver	- Localized surface plasmon resonance (LSPR) - Visible color change by particle aggregation or ambient dielectric constant change - Quenching or enhancement of proximate fluorophore emission, depending on mNP size, the distance to fluorophores, and spectral overlap. - Electromagnetic field enhancement to increase Raman scattering intensity	- Colorimetric probe - FRET acceptor, quench fluorescence - Fluorescence enhancer - SERS probe	[65–68]
Magnetic nanoparticles	Pure iron, iron oxide (Fe_3O_4, γ-Fe_2O_3), iron-based alloy	- Magnetism, depending on materials, size, and shape - Superparamagnetism (no magnetism retained after removal of magnetic field) typically in MNPs <20 nm - Magnetic relaxation difference between dispersed and assembled state	- Capture probe - Target analytes separation and enrichment from complex matrices - Magnetic relaxometry probe	[55, 69]

Continued

Table 3.1 Plethora of nanomaterials and their properties, exploited in the fabrication of nanobiosensors—cont'd

Nanomaterials	Representative members	Exploitable intrinsic properties	What purpose do they serve in nanosensors?	References
Up-conversion nanoparticles (UCNPs)	Lanthanide ion (Er^{3+}, Tm^{3+}, Ho^{3+}, Yb^{3+}) in nanocrystals host (lanthanide compounds)	Up-conversion process, i.e., low energy excitation (infrared) to generate high energy emission (NIR, visible light) - Tunable fluorescence depending on size, dopant, and host materials - Infrared excitation with deep penetration and low photodamage	- Fluorescent probe - FRET donor	[49, 50, 70]
Carbon nanotubes (CNTs)—SWCNTs and MWCNTs	Carbon	- High conductivity - Fluorescence quenching - Peroxidase catalytic activity	- Nanoelectrode - FRET acceptor, quench fluorescence - Fluorescent probe	[71–73]
Carbon dots (CDs) and graphene quantum dots (GQDs)	Carbon	- Tunable fluorescence - Up-conversion photoluminescence - High photostability - Low toxicity - Facile synthesis and surface modification	- Fluorescent probe - FRET donor	[33, 34, 74–77]
Graphene	Carbon	- High conductivity - Fluorescence quenching - Peroxidase catalytic activity - Photoluminescence - Enhance Raman signals	- Nanoelectrode - Fluorescence quencher, FRET acceptor - Fluorescent probe - SERS	[72, 73, 78–81]
Silica nanoparticles	Silica	- High porosity and high surface area for encapsulation of fluorophores	Fluorescent probe	[82, 83]

Adapted from Sutarlie, L., Ow, S.Y., Su, X., 2017. Nanomaterials-based biosensors for detection of microorganisms and microbial toxins. Biotechnol. J. 12 (4). https://doi.org/10.1002/biot.201500459, Copyright 2017, Wiley-VCH Verlag GmbH & Co. KGaA, Weinheim.

biosensors), used efficiently for detection of pollutants such as phenols and heavy metals [86, 87]. Along similar veins, specificity, sensitivity, and stability are the hallmark features of *phage biosensors*. The advantages of high affinity and specificity of antibodies used in *immunosensors* are handicapped by limited target (protein), cumbersome production protocol involving animals, and the lack of stability. A myriad of transducers based on optical (SPR, fluorescence polarization, etc.), piezoelectric, electrochemical (amperometric, potentiometric, conductometric detection) and mechanical principles (microcantilever sensor based) has been employed in immunosensors. Of late, researchers are also delving into the prospects of using affibodies (tailored affinity proteins with single domain and three-helical structures having 13 amino acid positions on the helices; diversity being created by randomization of 1 and 2), capable of reaching commendable affinity and specificity to any target analyte postisolation [88] in *affibody-based biosensors*. Although comparatively stable, the use of nucleic acids in *genosensors* is challenged by limited target (complementary sequence). In this regard, ease of modification, custom-made structural design with thermal stability, in vitro synthesis, feasibility for reversible denaturation as well as the possibility of differentiating targets with varied functionalities all provide a special niche for aptamers (considered as nucleic acid analogs of antibodies) used in *aptasensors* for detecting a plethora of targets, including pathogenic microbes, cocaine, peptides, toxins, metal ions, etc. [84]. *Molecularly imprinted polymeric (MIPs)* nanomaterials have garnered special impetus in recent years. These cross-linked materials with molecularly imprinted cavities have artificial recognition sites, biomimicking the action of natural receptors, and consequently are exploited for fabrication of biosensors. High thermochemical and mechanical tolerance, low cost, and reusability are the preferred aspects, while intricate fabrication protocol, incompatibility with aqueous media, and outflow of template molecules limit their practical applications.

3.3 Pertinent attributes for the design of nano-enabled sensors for environmental monitoring

High sensitivity, low detection limit (LoD), stability and selectivity, rapid response time, small hysteresis, good linearity, considerable life cycle/recyclability, ease of use/portability, and cost-effectiveness are some of the attributes of an ideal nano-enabled sensor [89]. One of the critical factors is the *response time*, namely the rapidity with which the detector exhibits a response to a signal modulation. This is particularly relevant for those nanosensors that find applications in gas-sensing/air-quality monitoring to prevent accidental situations. High surface-to-volume ratio and high reactivity of nanomaterials as well as the porosity of the transducer material used (which facilitates fast adsorption and analyte diffusion) may be correlated to the rapid response time of various nano-enabled sensors for environmental monitoring. To cite as evidence, the response times for detection of ammonia using carbon nanotubes [90]; trinitrotoluene (TNT) using graphene [91]; nitrogen oxide using single-walled

carbon nanotube (SWCNT) [92], and organophosphorus pesticides using Zr-based metal organic frameworks (MOFs) [93] were 20 μs, 1 min, 5 s and minutes, respectively. On the other hand, the *high sensitivity (low detection limit)* of nano-enabled sensors (particularly for sensing heavy metal ions) over the complex and expensive conventional methods (e.g., atomic absorption spectroscopy, X-ray fluorescence, optical emission spectroscopy) has been documented in a number of studies. Table 3.2 reflects some of the exemplary nanosensors for detection of environmental pollutants with high sensitivity.

Selective detection of the analyte (e.g., sensing of a specific gas in a mixture of gases) of interest from a complex media, i.e., in the presence of various interfering entities, has conferred special impetus to nanosensor technology. As an example, the atypical response of SWCNT conductance to exposure to Hg^{2+} ions has been exploited for a facile yet fast and highly selective single-walled carbon nanotube (SWCNT) based FET sensor for Hg^{2+} sensing. Surface functionalization of the transducer substance with precise receptor moieties (e.g., biocatalyst, immunoglobulins, etc.) for the analyte of interest is a common strategy to achieve the objective of selectivity while designing nanosensors for environmental applications. Furthermore, the recent use of an array of synchronized sensors has made it possible to detect multiple analytes with the desired selectivity [102]. On the other hand, a spectrum of gases (CO, LPG, CO_2, NH_3, H_2S, H_2, and C_2H_5OH) could also be specifically detected using a recent nanosensor innovation based on an NiO nanowire that could provide a "thermal fingerprint" type response for each of the gases [103]. Another prime feature of nano-enabled sensors is their *sensitivity* or *resolution*, an indicator of the signal-to-noise ratio. This refers to the magnitude of the monitored signal per analyte concentration unit. In a similar manner, the practical applications of nano-enabled sensing technology rely on the aspect of *portability* of the devices, particularly in the field of quality assessment and control. A portable, user-friendly, field-deployable device (for air, water, and soil quality monitoring) with low energy requisite, low ecological footprint, resilience, and cost-effectivity qualifies as a "smart nano-enabled sensor technology for environmental perspective" with prospects for commercialization. Colorimetric strips, SPEs, FET-dictated online and real-time monitoring chips, as well as lateral flow assays are some of the prime platforms developed in the form of portable nanosensors. As an example, a portable polydimethylsiloxane (PDMS) microfluidic chip with an integrated SPE was fabricated for sensing (with a very low detection limit of 0.018 ppb) and removal of polybrominated diphenyl ethers (PBDEs) [104]. The coating of reduced graphene oxide (rGO) (functioning as the transducer) on the PDMS chip supported the physisorption and eventual removal of the PBDE residues (Fig. 3.1A). Similarly, real-time rapid (response time: 1 s) selective mercury detection in mixed metal solutions has been enabled using a liquid-gated graphene FET array [105] (Fig. 3.1B). The selective detection of the Hg^{2+} was facilitated by the multiple thymine of the DNA aptamer, adhered to the graphene film of the sensor. Similarly, exploitation of a carbon dot (amine functionalized)-based portable paper sensor was reported for the visual detection of TNT (detection limit: 0.213 M) in groundwater [106]. On the other hand, intrinsic cross-

Table 3.2 Examples of highly sensitive nanosensors for different environmental pollutants.

Nanosensor material	Type of sensor	Signal measurement technique	Pollutant detected	Detection limit (M)	Reference
TiO_2 and PbO_2	Adsorption	Amperometric	Trichlorfon	10^{-10}	[94]
Au NPs	Antigen-antibody	Amperometric	Monocrotophos	2.7×10^{-9}	[95]
CNTs	Affinity	Field-effect transistor (FET)	Acephate	5.4×10^{-14}	[96]
CdTe QDs	Enzymatic hydrolysis	Amperometric	Carbaryl	3×10^{-9}	[97]
MOF-5	Chemosensor	Fluorescence response	Organophosphate	5×10^{-9}	[98]
MoS_2	Optical	Photoluminescence	NO_2 and NH_3 molecules	$0.2–50 \times 10^{-9}$	[99]
Au NPs	Colorimetric	Choromophoric changes	Hg^{2+}	1×10^{-6}	[100]
In-doped ZnO nanoparticles	Chemiresistive	–	Trinitrotoluene (TNT)	9×10^{-9}	[101]

Adapted from Kaur, R., Sharma, S.K., Tripathy, S.K., 2019. Advantages and limitations of environmental nanosensors. In: Advances in Nanosensors for Biological and Environmental Analysis. Elsevier, pp. 119–132. Copyright 2019, Elsevier.

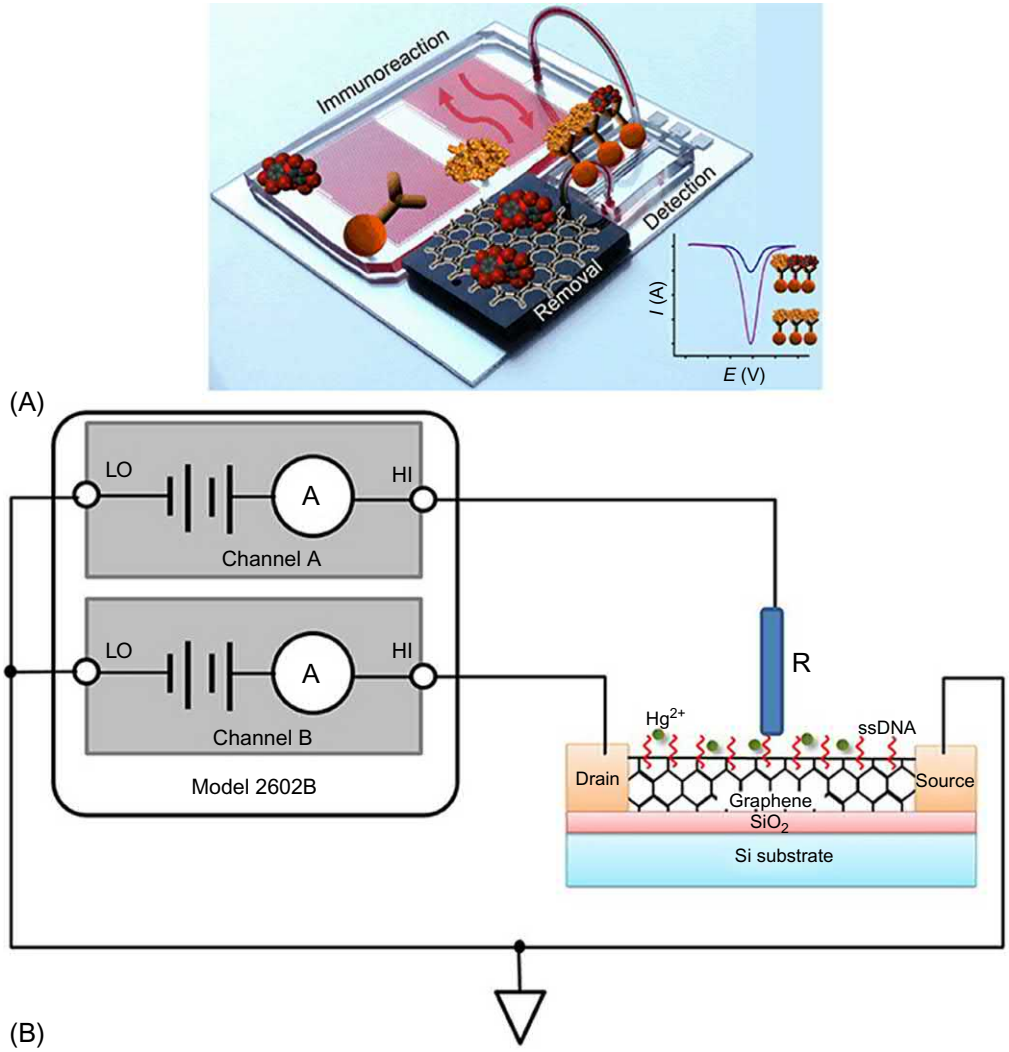

Fig. 3.1

(A) A lab-on-a-chip portable nanosensor with integrated microfluidic channels. (B) Graphene field-effect transistor test configuration using multiple source measurement unit (SMUs) for the real-time analysis of mercury ions, Model 2602B: HI: Force HI terminal, LO: Force LO terminal, R: an external Ag/AgCl reference electrode with saturated KCl. *A: Reproduced from Chalupniak, A., Merkoçi, A., 2017. Toward integrated detection and graphene-based removal of contaminants in a lab-on-a-chip platform. Nano Res. 10 (7), 2296–2310. Copyright 2016 Springer Nature; B: Reproduced from Tu, J., Tao Liang, Y.G., Hu, Q., Wang, Q., Ren, T., Sun, Q., et al., 2018. Graphene FET array biosensor based on ssDNA aptamer for ultrasensitive Hg^{2+} detection in environmental pollutants. Front. Chem. 6. Copyright 2018, Tu, Gan, Liang, Hu, Wang, Ren, Sun, Wan and Wang under the terms of the Creative Commons Attribution License (CC BY).*

verification of the sensor's integrity and elimination of false-positive responses is a hallmark feature of lateral flow-based nanosensors [107, 108].

3.4 Exemplary evidence of novel nanosensor design strategies for environmental applications

In the following section we focus on concepts, presented earlier in the context of design strategies for nanosensors, related to detection of some environmentally relevant contaminants: a few selected pathogenic microbes, some heavy metals, and representative pesticides.

3.4.1 Pathogen detections

The real constraint in understanding the environment is the nature of hazardous contaminants, including pathogenic microorganisms, their collection process, and handling of bulk data [9]. Understanding these microbes and their physiochemical attributes by proper diagnostic and sensing techniques is of utmost pertinence. This necessitates innovation in reliable and persistent diagnostic techniques with instant response, dynamic range, and selective sensing of pathogens [109]. In this regard, nanosensors are promising to meet these requirements with complete flexibility, reliability, target sensitivity, etc., with varied configurations, including multifaceted devices that permit us to visualize their implementation [110]. The illustration in Fig. 3.2 recapitulates the operational principle and elements (as mentioned in preceding sections) of a few representative nanosensors used in microbial detection.

Numerous unique nanomaterials, including quantum dots, carbon nanotubes, nanoribbons, nanorods, nanowires, nanoarrays, nanoprisms, nanospheres, nanofibers, and nanoparticles, have been proposed and successfully demonstrated by the scientific community in the realm of pathogen detection [111–117]. As evidence, Tripathy et al. [118] resorted to the application of electrospun manganese (III) oxide nanofiber as a nanobiosensor to detect dengue consensus primer with outstanding LoD (120×10^{-21} M) in both control and spiked serum samples. The nanobiosensor amalgamated the inherent merits of low band-gap metal oxide nanofibers in addition to electrochemical transduction methods. In yet another report, Sun et al. [119] demonstrated rapid bacterial detection using magnetic nanoparticle-urease nanosensors with extraordinary sensitivity. It is pertinent to note that the interaction between the gold nanoparticles and DNA molecules has been exploited to develop ultrasensitive and selective sensors in a range of various diagnostic applications. A novel attempt reported by Baetsen-Young et al. [120] involved the detection of unamplified genomic DNA by dextrin-capped gold nanoparticles (d-AuNPs) in elevated ionic conditions. The approach enabled the direct colorimetric detection of plant pathogenic DNA. The researchers reported successful detection of as little as 2.9 fM of pathogen DNA, as well as the use of crude extractions of a pathogen matrix—as little as 18 spores/μL. Similarly, Mannoor et al. [17] reported the printing of

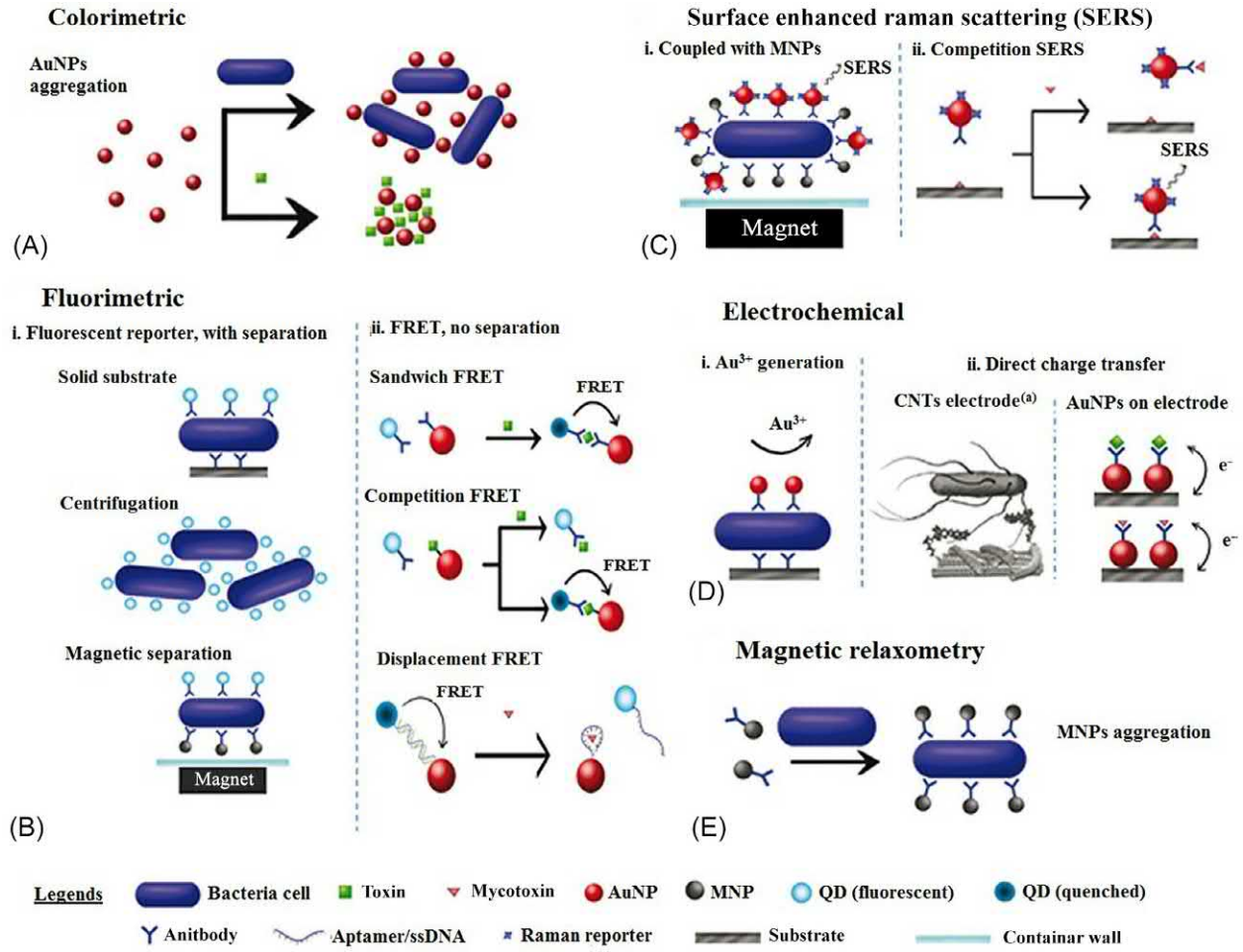

Fig. 3.2

Schematic of various signal transduction modes using nanomaterials to detect microbial analytes. The signal transduction methods include: (A) colorimetric typically through metal nanoparticle aggregation, (B) fluorometric: (i) fluorescent reporter direct binding coupled with separation methods (i.e., solid substrate, centrifugation, or magnetic separation) or (ii) FRET-based assay without separation, (C) SERS: (i) SERS probes binding coupled with magnetic nanoparticles, or (ii) SERS-based competition assay, (D) electrochemical: (i) metal ion generation from mNPs such as Au^{3+} from AuNPs, or (ii) direct charge transfer through nanomaterials (CNTs, graphene, AuNPs) on electrodes (a), and (E) magnetic relaxometry (typically through MNPs aggregation). *A–E: Reproduced from Sutarlie, L., Ow, S.Y., Su, X., 2017. Nanomaterials-based biosensors for detection of microorganisms and microbial toxins. Biotechnol. J. 12 (4). https://doi.org/10.1002/biot.201500459. Copyright 2017, Wiley-VCH Verlag GmbH & Co. KGaA, Weinheim; D ii a: Reproduced from Zelada-Guillen, G.A., Riu, J., Duezguen, A., Rius, F.X., 2009. Immediate detection of living bacteria at ultralow concentrations using a carbon nanotube based potentiometric aptasensor. Angew. Chem. Int. Ed. 48, 7334–7337. Copyright 2009, John Wiley & Sons.*

graphene onto water-soluble silk for wireless bacterial detection on tooth enamel. In addition, Wang et al. [121] emphasized the significance of silver nanospheres and their potential in SERS-based detection of pathogens. Moreover, they also made an attempt to differentiate three various pathogens (*E. coli* O157:H7, *Salmonella typhimurium*, *Staphylococcus aureus*) including live and dead cells using canonical variate analysis in conjunction with Raman spectra. Having said that, let us peruse some specific nanosensor-based detection strategies for a few environmentally/biomedically relevant pathogenic microbes.

Escherichia coli is a familiar Gram-negative bacterium and a common waterborne pathogen. In general, detecting and quantifying *E. coli* using conventional methods is time consuming (24–72 h). PCR and ELISA are considered rapid techniques and hence are used to sense *E. coli*. Still, these approaches have some disadvantages, such as complex and costly procedures and requirements for skilled personnel. Of late, advancements in nanosensors have made the specific sensing of *E. coli* in aqueous samples, even in minimal concentrations, hassle-free, easier, ultrasensitive, and selective [122]. Massad-Ivanir et al. [123] fabricated an antibody functionalized nanostructured oxidized porous silicon dioxide ($PSiO_2$) based sensor assembly to sense *E. coli* by a direct cell-capture technique. The Fabry – Pérot fringes (hallmark of thin-film interference), as observed in the optical reflectivity spectrum of the $PSiO_2$ nanostructure, facilitated the direct, real-time visualization of bacteria attachment within minutes. So et al. [124] developed a sensing method to detect *E. coli* DH5α using an aptamer associated SWCNT-FET combined with most probable number assay. The assembled nanoarray displayed a conductance that dropped to a maximum of more than 50% after binding with the *E. coli* cells within 20 min. No considerable response was noticed when tested for *Salmonella typhimurium* KCTC 1925, indicating the high selectivity of the nanosensor system. The recent thrust in pathogen detection has been directed towards the development of integrated platforms capable of concomitant capture, detection, and inactivation/killing. In this backdrop, Wang et al. [125] exploited the hydrophilic side chains of cationic conjugated polyelectrolytes (CPs) to capture *E. coli*, followed by induction of plasmon-enhanced fluorescence from Ag nanostructure in a bioassay for bacterial detection and inactivation, mediated by the reactive oxygen species (ROS) generated by the CPs and further augmented due to the use of Ag as substrate (Fig. 3.3).

Salmonella typhi is a ubiquitous waterborne pathogenic Gram-negative bacteria found both in rural and urban environmental settings. It is the main causative organism of typhoid fever. Jackeray and team members [126] fabricated bioconjugated nanocrystal-based quantum dots for detecting *S. typhi* from water samples. The core-shell quantum dots were surface functionalized for enhanced hydrophilic attributes using a ligand exchange technique. Carboxyl ended side chains were allowed to attach with *S. typhi*-specific IgG antibodies for the preparation of light stable fluorescent tag. Further, the fruitful bioconjugation and photoluminescence characteristics were analyzed using spectrofluorimetry and ELISA. The prepared quantum dots were forwarded as promising and potential candidates for the method of

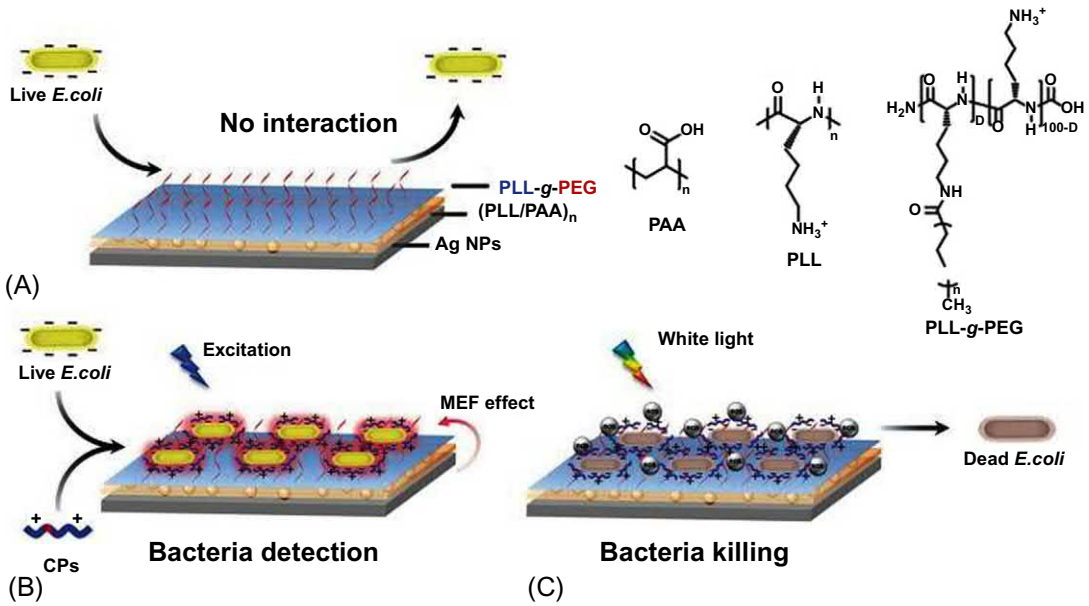

Fig. 3.3

Schematic representation of the bioassay structure and scheme illustrating mechanisms of bacterial detection and disinfection. (A) Adsorbed PLL-g-PEG form stretched PEG brushes for preventing adsorption of proteins and bacteria. (B) *E. coli* were mixed with CPs and captured on the surface of the platform. The excited CPs produced a fluorescent signal in response to binding with bacteria for bacteria detection. With the MEF effect of Ag NPs, the fluorescence intensity of CPs could be enhanced. (C) CPs produced ROS under white light irradiation for disinfection. *Reproduced from Wang, X., Cui, Q., Yao, C., Li, S., Zhang, P., Sun, H., et al., 2017. Conjugated polyelectrolyte–silver nanostructure pair for detection and killing of bacteria. Adv. Mater. Technol. 2 (7), 1700033. Copyright 2017, WILEY-VCH Verlag GmbH & Co. KGaA, Weinheim.*

standardization with enhanced sensitivity and improved specificity to sense the pathogenic bacteria within 90 min postoptimization. On the other hand, Razavilar et al. [127] fabricated a fluorescence nanobiosensor to identify the presence of *S. typhi* using MIP. Interestingly, the *S. typhi* concentration was quantified at 10 colony/mL (minimum) in polluted water. The performance and sensitivity of the nanosensor was established even postintroduction of *E. coli* cells in the test sample. The nanobiosensor was found to be stable and efficient for almost 8 weeks.

Along a similar vein, transmission of cholera is attributed to the consumption of drinking water and foodstuffs contaminated with *Vibrio cholerae* [128]. Mostly, the symptoms of this fatal infectious disease are observed only after the colonization of the bacteria in the small intestine and after release of cholera toxin, one of the major virulence factors of *Vibrio cholerae* [129]. Detection of this pathogen in water is of immense significance. In this regard, Yu et al. [80, 81] reported an immunochromatography-based diagnostic approach to simultaneously unveil

epidemic and pandemic cholera-causing *Vibrio cholerae* 01 and 0139 serogroups using alkaline peptone water culture. Due to the antigen-antibody reactions, agglomeration of gold nanoparticles led to the formation of a red line on the sensor strip. The reported methodology was facile, rapid, and user friendly in terms of visual detection and operational feasibility, even under resource limited settings. On the other hand, Khan et al. [130] reported a facile, feasible, and quick method to sense cholera toxin (CT) by mere agglomeration of antibody-associated gold nanoparticles, resulting in distinct color change (a red shift in the plasmon band of the nanoparticles). The LoD for the reported protocol was as low as 10 nM with excellent specificity towards cholera toxin in comparison to diarrhetic toxins. Furthermore, the feasibility of the approach was assessed in detecting CT in local lake water. Similarly, Tam and Thang [131] demonstrated the performance of a cerium oxide nanowire based immunosensor to detect *Vibrio cholerae* 01. The limit of detection was recorded as 1×10^2 CFU/mL with the sensitivity of 56.82 Ω/CFU/mL and linear response, ranging between 1×10^4 CFU/mL and 1×10^4 CFU/mL. Specificity of the nanosensor (with impressive regeneration) was exceptional in detecting *V. cholera*, as attested to by no response to other pathogens like *Herpes simplex* virus, *E. coli* O157: H7 and *Salmonella* sp. Ahn et al. [132] proposed a facile FRET-inhibition bioassay (linear response for CT: 23.6 nM-2.36 μM, theoretical detection limit: 280 pM) with instant response (within 10 min) to sense CT using galactose-stabilized AuNPs and amine-terminated CdTe quantum dots. In the reported sensor (stable up to 6 months), the selective interaction of CT to the galactose derivative immobilized on AuNPs prevented the formation of H-bonding between the QDs (donor) and AuNPs (acceptor), consequently resulting in the fluorescence recovery. In another recent report, Thiramanas et al. [133] demonstrated a novel and sensitive magneto – PCR – colorimetry based method to detect *V. cholera* (Fig. 3.4). The approach was based on covalent labeling of magnetic polymeric nanoparticles (MPNPs) with an amino-modified forward primer, followed by the interaction

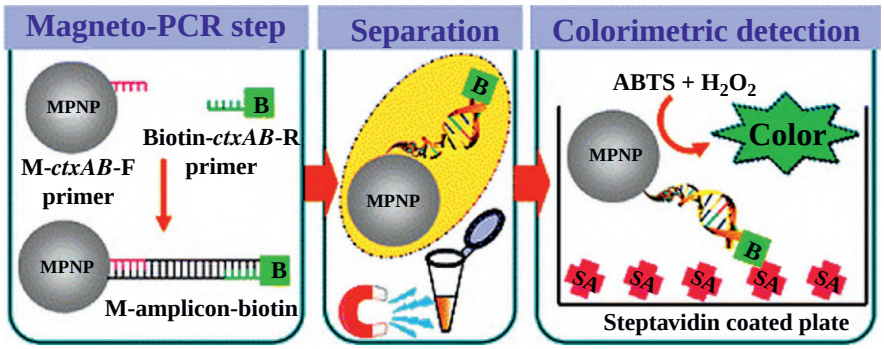

Fig. 3.4

Schematic representation of M-amplicon-biotin detection by the magneto-PCR -colorimetry technique. *Reproduced from Thiramanas, R., Jangpatarapongsa, K., Tangboriboonrat, P., Polpanich, D., 2013. Detection of* Vibrio cholerae *using the intrinsic catalytic activity of a magnetic polymeric nanoparticle. Anal. Chem. 85 (12), 5996–6002. Copyright 2013 American Chemical Society.*

with the PCR product during PCR cycling. Following amplification of *V. cholerae* DNA on the MPNP surface, the colorimetric detection of the target gene was based on the innate catalytic activity of the MPNPs. The sensitivity of the sensor in the buffer system was appreciable (10^3 CFU/mL) while the total time required for detection was below 4 h. The specificity and efficacy of the approach was further vouched for by analysis using bacterial genetic material in drinking and tap water.

Legionella pneumophila is a pathogenic Gram negative bacterium, commonly found in soil and aquatic-related environmental settings. This opportunistic human pathogen is the main causative agent of Pontiac fever [134] and Legionnaires' disease (a pneumonia-like disease), which affect elderly people with poor immunity and also those with smoking habits or chronic lung infections. The transmission mode of this pathogen is exclusively through the air route from artificial aquatic systems and contrivances like cooling towers, showers, and waterspout spas [135]. A couple of nanosensor-based works have been reported for this microbe. Almost a decade back, an attempt [115] was made to detect *L. pneumophila* using a pristine MWCNT electrode-based sensor, functionalized using oxygen plasma treatment for enhanced DNA detection. It could sense the microbial DNA even at the concentration of 10 pM, up to 100 nM. Meneghello et al. [134] reported the fabrication of an ultrasensitive and highly selective grating-based SPR nanostructured sensor under azimuthal control to sense *L. pneumophila* down to 10 colony forming units. The observed results were more promising in terms of the detection sensitivity (more than 1000 times efficient when compared to conventional fluorescence-assays). The proposed approach was forwarded to open up new avenues in the facile detection of bacterium in both water and air samples. On a similar note, Martin et al. [136] reported core-shell magnetic nanoparticles and screen-printed carbon electrodes dictated an amperometric magnetoimmunoassay for the selective sensing of *L. pneumophila* SG1. Park et al. [137] reported an extremely sensitive electrochemical zinc oxide nanorod matrix electrode to detect the pathogen. The performance and efficacy of the developed immunosensor was assessed using cyclic voltammetry in a 0.1 mM acetate buffer at pH 5 in the presence of 0.05 mM 3,3′,5,5′-tetramethylbenzidine and 1 mM hydrogen peroxidase solution. The observed results depicted an excellent selectivity and sensitivity (detection limit: ∼1 pg/mL). The immunosensor efficacy increased logarithmically with *L. pneumophila* antigen concentration in the range of 1–5000 pg/mL with respect to the analyzed antibody concentrations (1 and 2 μg/mL). Melaine et al. [113] demonstrated the detection of *Legionella* sp. using a 16S rRNA-based sensing method. The researchers had employed SPR-based imaging as a detection strategy in conjunction with DNA probe sandwich assemblies and AuNPs for signal amplification. Another similar work reported by Foudeh et al. [138] involved the SPR imaging based successful detection of the metabolically active *Legionella* pathogen and sensing of 16 s rRNA in solutions as diluted as 1 pM at 450 μL (0.45 femtomole) within 3 h. Rai et al. [139] made an attempt to identify *Legionella* sp. using an electrochemically amplified molecular beacon (EAMB) based biosensor, fabricated using thiolated hairpin DNA-ferrocene

probes on gold electrodes. Its potential was assessed against PCR amplicons derived from genomic DNA of live *L. pneumophila*. The researchers also demonstrated commendable specificity down to 1–3 nucleotides mismatches in a different strain of the pathogen as well as a different bacterial species. In another work, Rai et al. [140] immobilized 5′- aminated DNA probes into alumina nanochannels to fabricate a label-free DNA biosensor for the detection of *Legionella* sp. With a broad linear range over seven orders of magnitude, an LoD of 3.1×10^{-13} M for the enumeration of a single-stranded 21 mer DNA sequence was documented.

Pseudomonas aeruginosa is an opportunistic and highly infectious Gram negative pathogen with exceptional antibiotic resistance and is well known for most of the nosocomial infections, like ventilator-associated pneumonia. Disarming this critical and deadly pathogen requires novel diversified approaches, including development of new antibiotics and creation of promising antivirulence factors. For detailed retrospective information about *Pseudomonas* infections and its resistance mechanism, readers are directed to peruse [141]. The pathogen occurs in contaminated soil and aquatic environments including fecal matters, grey water, etc. Whole cell detections, DNA/16S rRNA based detections, oligonucleotide recognition elements, antibodies, and bacteriophages are the major strategies used to sense and recognize *Pseudomonas* specifically [9]. Hu et al. [142] developed a quick, ultrasensitive nano-aptasensor to detect whole-cell *Pseudomonas aeruginosa* PA 01 using an LSPR detection platform. Here, surface confined aptamer was utilized as an affinity tag and nanosphere lithography was employed to construct the sensor surface encompassing a hexagonal arrangement of gold nanotriangles. The sensor surface was altered to a sandwich format using biotinylated poly(ethylene glycol) and poly(ethylene glycol) thiol in the ratio of 1:3 with neutravidin and biotinylated aptamer. In an endeavor to develop a sensitive and fast sensing of *Pseudomonas aeruginosa*, postlysis of sample, genomic DNA was adsorbed onto MNPs, followed by PCR amplification of *gyrB* specific sequence of the pathogen [143]. Chemiluminescence-based detection of the biotin-labeled PCR products was documented on incubation with the probes-modified MNPs and alkaline phosphatase (ALP) labeled streptavidin (SA); 400 nm-sized MNPs were the best suited for the purpose, yielding successful detection results with detection limits as low as 10 cfu/mL.

3.4.2 Detection of heavy metals

Heavy metals are placed in the *d-block* (also known as transition metals) and *p-block* in the periodic table. The presence of these metals, even at very low concentrations (as low as parts per billion, ppb), could pose potential health risks to living beings. We present some of the recent endeavors in the design and applications of nanosensors to detect a few of them.

Chromium (Cr) exists in two oxidation states, III and VI, in the environment. It is pertinent to note that Cr (VI) is a potential toxicant [144] and a carcinogen. In order to detect the presence of

Cr (IV), a limited number of nanobased platforms and immunoassays have been designed. Based on the speed and robustness of lateral flow immunoassays (LFIAs) and the high sensitivity of surface-enhanced Raman scattering (SERS), a SERS-LFIA strip sensor was fabricated for rapid and semiquantitative assessment of Cr^{3+}, with LoD of 10^{-5} ng/mL within 15 min [145]. On the other hand, a low-cost, stable (for at least 12 weeks at 37 °C) and rapid result-yielding (within 5 min) one step-test strip was developed for on-site large-scale monitoring and measurement of chromium speciation in water samples (collected from Pearl River (Guangzhou, China) and the West Lake (Huizhou, China)) and biomonitoring of Cr exposure in serum samples [146]. Gold nanoparticles coated with affinity-purified monoclonal antibodies against isothiocyanobenzyl-EDTA (iEDTA)-chelated Cr^{3+} were used as the detecting reagent (Fig. 3.5A); 50.0 ng/mL was documented as the visual lowest detection limit.

Similarly, *lead* is associated with cancer and neurological disorders [147] and has a tendency to accumulate in the body. Furthermore, increasing global water pollution incidents (e.g., the Flint water crisis in the United States) caused by lead contamination have irked the nerves of the global scientific fraternity and the safety of drinking water distribution systems is at stake. In this context, both label-free and labeled Pb nanosensors have been reported. Tang et al. [148] developed an electrochemical sensor (with an LoD of 7.8 pM), based on the combination of QDs and 8–17 DNAzyme with rolling circle amplification (RCA). Similarly, Brenneman et al. [149] demonstrated micromolar and nanomolar level detections using DNA aptamers (thrombin binding aptamer (TBA) that folds into G-quadruplex structure in the presence of lead) and quantum dots. The interaction of quantum dot and gold nanoparticle with TBA permitted the optical sensing of Pb^{2+} ions via fluorescence resonant energy transfer (FRET). In a similar manner, Qian et al. [150] made a biocompatible graphene QDs -aptamer and GO fluorescent turn-on nanosensor, which could induce G-quadraplex, mediated by Pb(II). This nanosensor (with LOD of 0.6 nM and response time of a minute) was specific to Pb(II) with high sensitivity and reproducibility. Memon et al. [151] resorted to truncated 8–17 DNAzyme to facilitate the desorption of single-stranded DNA pieces following substrate breakdown in the presence of Pb^{2+}, followed by the adsorption of the detached fragments onto AuNPs, without allowing salt-concentration mediated aggregation (Fig. 3.5B). The sensor exhibited an LoD value of 0.2×10^{-9} mol/L Pb^{2+} while the linear working range was between from 0.5×10^{-9} mol/L and 5×10^{-9} mol/L. The authors had proposed the use of the label-free colorimetric nanosensor for fast, selective, and sensitive Pb^{2+} detection in drinking water distribution systems and even other environmental water samples.

In addition, long-term exposure to ***c****admium* (Cd) through various modes: air, water, soil, and food paves the way to cancer and numerous organ system toxicities [152]. A number of nanomaterials have proved to be useful for the detection of cadmium. As evidence, Li et al. [153] designed a fluorescence sensor, based on dithizone-etched CdTe and working on an off/on mechanism for the detection of cadmium ions in environmental aqueous samples. With remarkable sensitivity to Cd^{2+} over other metals, the sensor exhibited a low detection limit (0.13 μM) and a wide linear response range (0.4–15.4 μM). On the other hand, Gui et al. [154]

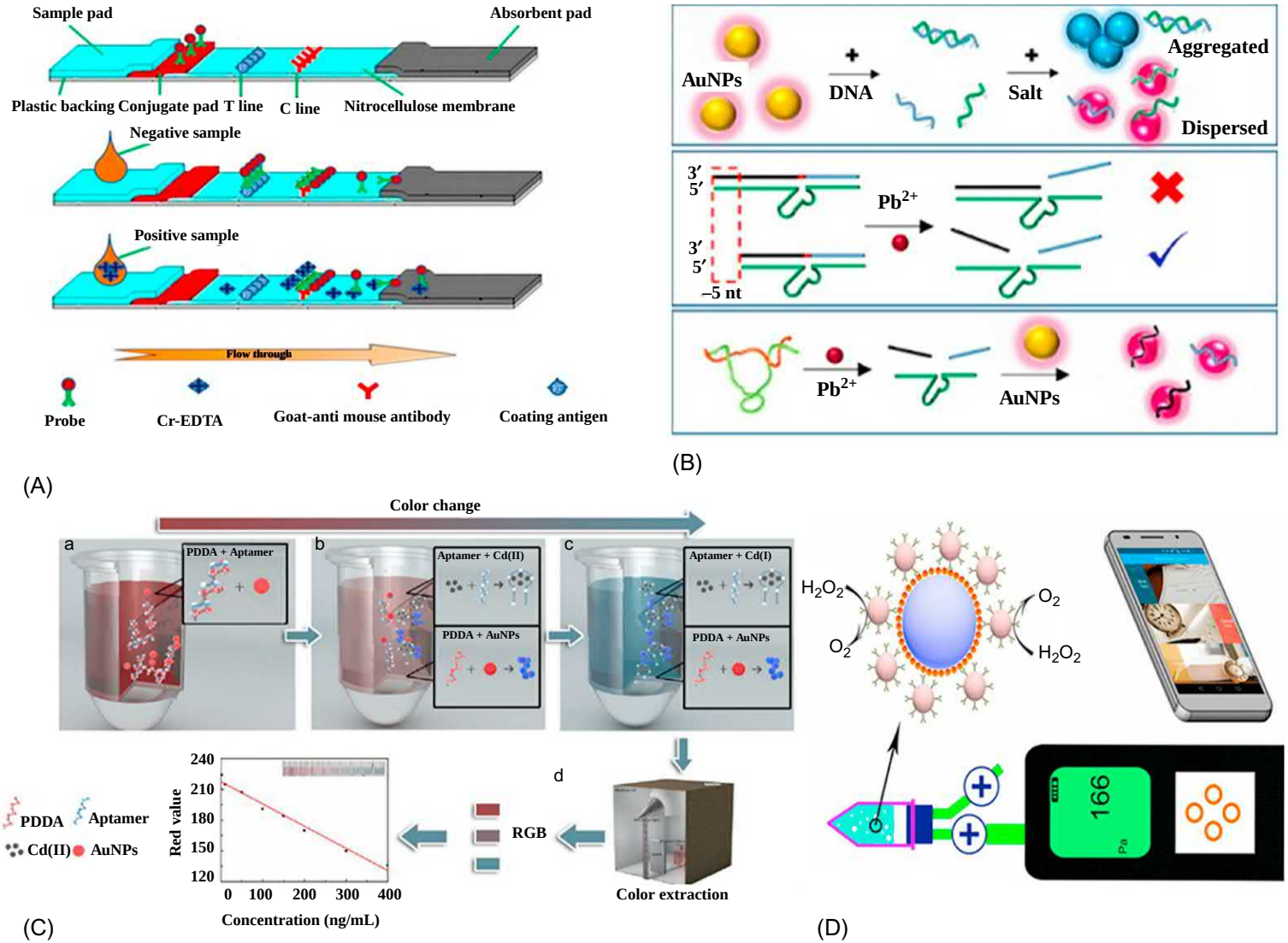

Fig. 3.5

See figure legend on next page

Fig. 3.5 (A) A schematic representation of the immunochromatographic assay, the principles of negative detection and positive detections of Cr^{3+} in water and serum samples. (B) Principle of label-free colorimetric nanosensor for Pb^{2+} in water based on truncated 8–17 DNAzyme. (C) Schematic illustration of the colorimetric method. (a) Gold nanoparticles (AuNPs) incubated with aptamer and polydiene dimethyl ammonium chloride (PDDA); the color of the free AuNP solution was wine red; (b) AuNPs incubated with the aptamer, PDDA, and a few Cd(II); the color of partial aggregation of the AuNP solution changed to *reddish*; (c) AuNPs incubated with the aptamer, PDDA, and sufficient Cd(II); the color of aggregation of the AuNP solution changed to *blue*; and (d) The *red* (R) values of the solution recorded with a smartphone. (D) Versatile Barometer Biosensor Based on Au@Pt Core/Shell Nanoparticle Probe for detecting Hg^{2+}, thrombin, carcinoembryonic antigen (CEA), and ractopamine (Rac). *A: Reproduced from Liu, X., Xiang, J.-J., Tang, Y., Zhang, X.-L., Fu, Q.-Q., Zou, J.-H., et al., 2012. Colloidal gold nanoparticle probe-based immunochromatographic assay for the rapid detection of chromium ions in water and serum samples. Anal. Chim. Acta 745, 99–105. Copyright 2012 Elsevier; B: Reproduced from Memon, A.G., Zhou, X., Xing, Y., Wang, R., Liu, L., Khan, M., He, M., 2019. Label-free colorimetric nanosensor with improved sensitivity for Pb^{2+} in water by using a truncated 8–17 DNAzyme. Front. Environ. Sci. Eng. 13 (1), 12. Copyright 2019, Higher Education Press and Springer-Verlag GmbH Germany, part of Springer Nature; C: Reproduced from Xu, L., Liang, J., Wang, Y., Ren, S., Wu, J., Zhou, H., et al., 2019. Highly selective, aptamer-based, ultrasensitive nanogold colorimetric smartphone readout for detection of Cd (II). Molecules 24 (15), 2745. Copyright 2019 by the authors, Licensee MDPI, Basel, Switzerland, under Creative Commons Attribution (CC BY) license; D: Reproduced from Fu, Q., Wu, Z., Du, D., Zhu, C., Lin, Y., Tang, Y., Versatile barometer biosensor based on Au@ Pt core/shell nanoparticle probe. ACS Sens. 2 (6), 789–795. Copyright 2017 American Chemical Society.*

demonstrated a fluorescence-based off/on-sensor for Cd^{2+} detection. Here, photoluminescence of CdTe/CdS QDs was first quenched by ammonium pyrrolidine dithiocarbamate (APDC). The quenching was effected by the fractional loss of the Cd–SH surface layer and the consequent surface passivation. The addition of Cd^{2+} displaced the APDC from the QD surface and reestablished the photoluminescence (PL). A threefold upturn was observed in the PL intensity, and the LoD was documented as 6 nM. In yet another study, a ratiometric sensor (RMS) was designed in order to upgrade the accuracy of Cd^{2+} detection [155]. To abate the faults due to fluctuation in the photoluminescence of the QDs, the fluorescence of two different chromophores was quantified. In order to minimize the interactions between the QDs and the secondary dye, polyethylenimine (PEI) was coated onto the cores of the CdTe QDs, prior to conjugation with fluorescein isothiocyanate (FITC). Without compromising the FITC signal, the QDs were quenched using sulfides (S_2^-). Again, the sensor was turned on, leading to restoration of photoluminescence after introduction of the cadmium ions. A slight enrichment was observed in the LoD (12 nM) of Cd for this RMS, compared to the LoD (6 nM) of the CdTe/CdS QDs sensors, reported earlier [154]. Recently, a colorimetric smartphone readout coupled to aptamer and gold nanoparticle based Cd^{2+} sensing was reported [156] (Fig. 3.5C). Cd^{2+} concentration in solution dictated the color and red (R) value of the solution. A linear range of 1–400 ng/mL and an LoD of

1 ng/mL were documented. The quantified values of Cd^{2+} in water and rice samples, using this method, tallied well with those obtained by atomic absorption spectrometry.

Ionic *mercury* (one of the high-ranked hazardous substances) in the II state has a potential impact on the nervous system and causes renal infections. It is infamous for mad hatter syndrome and Minamata disease [157]. The detection of Hg^{2+} in water and food is of immense concern. Recently, Pokhrel et al. [158] reviewed the use of carbon nanotube based ultrasensitive sensors for trace Hg^{2+} detection in water. A major focus in designing Hg^{2+} nanosensors has been streamlined on the use of DNA-based probes [159, 160]. Hg^{2+} can easily form a complex with DNA base pairs and subsequently be detected through fluorescence activation or quenching. There are numerous reports based on thiol mediated assays for Hg^{2+}. Diversified nanoparticles such as silver [161], gold [162, 163], or quantum dots [31] have been adopted for this strategy. Aggregation [163] or disaggregation [164] are the mechanisms for colorimetric detection of mercury. Huang et al. [165] fabricated an on-sensor for Hg^{2+} based on emission of fluorescence signal postdisplacement of rhodamine 6G from the nanoparticle surface. Furthermore, thiol coatings increased the specificity of the assay. The reported LoD was found to be 2.0 ppb and the analysis time was 10 min. Zhang et al. [166] prepared a ratiometric colorimetric sensor based on silicon nanodots (Si NDs), covalently functionalized with Hg^{2+} selective 6-carboxy-X-rhodamine (Rox)-tagged DNA. In an Hg (II)-rich environment the blue-emitting Si NDs quenched the red fluorescence of Rox. The fluorescence was attributed to the structural changes in the DNA as Hg (II) complexed with it, hence acting as a response signal. The LoD for this RMS was 9.2 nM and the reported precision was 8.8%. Rao et al. [167] published a turn-on nanosensor comprising Se-doped ZnO nanorods (coated with 3-mercaptopropionic acid), based on a dual emission-quenching mechanism, while Satapathi et al. [168] reported a multimodal nanosensor (with fluorescent and magnetic functionality) for sensitive detection of Hg^{2+}, followed by simple removal of the analyte using a bar magnet. Xiao et al. [169] reported a smartphone read-out device-based aptamer-assay nanosensor. In yet another report, Wei et al. [170] worked on a graphene oxide (GO) sensor based on exonuclease III assisted target recycling amplification methodology. The prepared GO-based fluorescence turn-on sensor showed the sensitive detection of Hg^{2+} down to subnanomolar levels. In a recent innovative endeavor, a barometer-based biosensor for sensitive detection of a number of analytes (carcinoembryonic antigen (CEA) and thrombin in serum samples; ractopamine (Rac) in urine samples; and Hg^{2+} in river water samples), based on the principle of quantifying pressure modulation due to oxygen (O_2) generation in a limited chamber, was fabricated [171]. The researchers employed core-shell Au@Pt nanoparticles (Au@PtNPs) as the bioassay probe that catalyzed the breakdown of H_2O_2 to release O_2. The LoDs were 0.021 ng/mL, 2.4 U/L, 0.051 ng/mL and 0.22 ng/mL, while the linear detection ranges were 0.025–1.6 ng/mL, 4–128 U/L, 0.0625–4 ng/mL, and 0.25–16 ng/mL for CEA, thrombin, Rac, and Hg^{2+} respectively. Furthermore, the authors reported the development of smartphone software for calculation, storage, and transmission of the results wirelessly (Fig. 3.5D).

Although we have highlighted the use of nanosensing platforms for just a few metals in the preceding discussion, the greatest needs are for simple, robust, economic, field-deployable systems that could be applied by commoners across the globe to ensure safe living in healthier environments.

3.4.3 Unraveling the presence of pesticides

Nanotechnology-enabled sensors offer promising avenues to detect the trace amounts of pesticides present in water, food, and contaminated environments. A couple of literature reports [172, 173] on the design and application of various advanced nanosensors for tracing out pesticides are available in the scientific repositories.

Triazines (e.g., atrazine, cyanazine, and simazine) represent a persistent class of herbicides. They bind to the plastoquinone-binding protein in photosystem II and act as an endocrine disruptor in humans [9]. In this milieu, the detection of atrazine (the EPA's prescribed limit being 3 ng/mL) via nanosensors has been a prime thrust of research in recent years. With this backdrop, Singh et al. [174] prepared a simple, stable, and nontoxic antiatrazine functionalized gold nanostructure based stable nanosensor for selective detection of atrazine. The sensor technology design was based on square-wave voltammetry and the dynamic linear range was found to be 50 aM to 1 nM in a 60 s exposure time. Shoji et al. [175] prepared an atrazine sensor based on molecular imprinted technology. They imprinted atrazine-recognizing polymer by using methacrylic acid and ethylene glycol dimethacrylate on a gold electrode surface. The sensor was much more selective to the atrazine than the nonimprinted polymer modified electrode. Yang et al. [176] designed a gold core-shell nanostructure-based LSPR sensor via molecular self-assembly and evaporation techniques. The refractive index sensitivity (RIS) of the sensor depended on the thickness of the gold shell. The detection limits were reported as 10 ng/mL. Recently, Yilmaz et al. [173] fabricated a plastic antibody-based SPR sensor. The sensor was a technology blend of molecular imprinting and SPR. The affinity sensor was designed by the addition of atrazine-imprinted nanoparticles onto the gold surface of an SPR chip. The authors used a polymerizable form of aspartic acid as the recognition element of the nanosensor, displaying better selectivity towards atrazine than to simazine and amitrole. Bhardwaj et al. [177] resorted to an antiatrazine antibody functionalized silica-modified copper-metal organic framework (Cu-MOF), assembled on conducting thin films for sensitive detection of atrazine. In yet another recent endeavor, Bhardwaj et al. [178] developed antibody conjugated glycine doped polyaniline (g-PAni) nanofilms as a conductometric immunoatrazine nanosensor with high sensitivity and specificity for atrazine, documented over a wide concentration scale and LOD of 0.07 ng/mL.

Neonicotinoids (e.g., acetamiprid, clothlanidin, imidacloprid, nitenpyram, nithiazine, thiacloprid, thiamethoxam) represent the largest group of insecticides, introduced almost four decades ago [9, 179]. There exists huge concern with respect to the persistence and

bioaccumulation of this water-soluble class of insecticides. A few reports exist on the design of some innovative nano-enabled sensors for neonicotinoids. Recently, Wang et al. [180] demonstrated a fluorescent lateral flow immunoassay based on QDs to detect imidacloprid, imidaclothiz, and clothianidin in tea leaves. The sensitivity of the sensor was 0.104–0.33 ng/mL, while the visual detection limit of 0.5–1 ng/mL was noted. Verdian [172] discussed the prospects of apta-nanosensors for sensing and quantitation of acetamiprid, while Weerathunge et al. [181] exploited the intrinsic peroxidase-like nanozyme activity of AuNPs and high specificity of the acetamiprid-specific S-18 aptamer for a rapid detection of 0.1 ppm acetamiprid within an assay time of 10 min. Urbanová et al. [182] prepared a GO-based electrochemical sensor to detect thiamethoxam and imidacloprid (with the corresponding LoD being 8.3 μmol/L and 7.3 μmol/L, respectively). Analogously, Zhang et al. [183] fabricated an electrochemical sensor based on β-cyclodextrin-graphene modified glassy carbon electrode (*β*-CD-rGO/GCE) to detect the neonicotinoid insecticide Paichongding (IPP) (Fig. 3.6). The (*β*-CD-rGO/GCE) has better sensitivity than bare GCE and rGO/GCE, even at low temperatures. The LoD of 0.11 μM and quantification limit of 0.37 μM were documented in the study.

Pyrethroids (e.g., fenpropathrin, deltamethrin, cypermethrin) are a well-known class of target-specific insecticides and are particularly toxic to aquatic species [9]. Li et al. [184] reported the

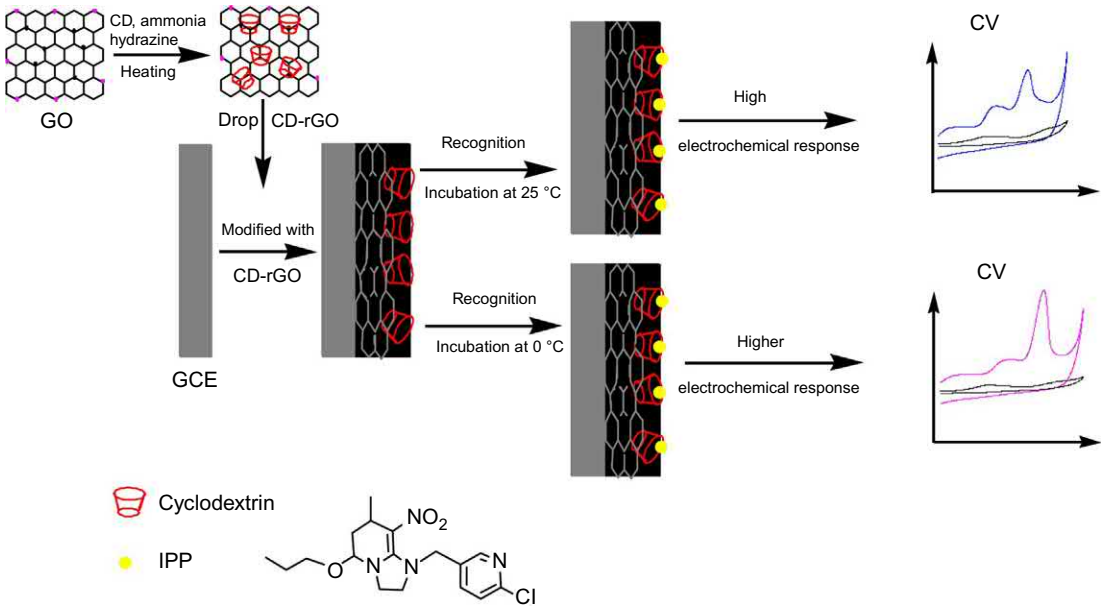

Fig. 3.6

Schematic procedure for the preparation of β-CD-rGO/GCE and the concept for enhancing the sensitivity of electrochemical IPP detection. *Reproduced from Zhang, M., Zhao, H.T., Yang, X., Dong, A.J., Zhang, H., Wang, J., et al., 2016. A simple and sensitive electrochemical sensor for new neonicotinoid insecticide Paichongding in grain samples based on β-cyclodextrin-graphene modified glassy carbon electrode. Sensors Actuators B Chem. 229, 190–199. Copyright 2016 Elsevier.*

fabrication of fluorescent, uniform core-shell lamba-cyhalothrin (LC)-imprinted silica nanospheres (CdSe@SiO_2@MIP) (Fig. 3.7A). The luminescence of CdSe@SiO_2@MIP was quenched by LC in concentration-dependent fashion (explained in terms of the Stern-Volmer type equation). In a similar study, fluorescence quenching of FeSe quantum dots formed the basis for excellent selectivity and high sensitivity of molecularly imprinted silica appended to the quantum dots (MIP-FeSe-QDs) toward cyfluthrin (a pyrethroid insecticide and common household pesticide) with detection limits being 1.3 and 1.0 μg/kg for sediment and fish samples, respectively [185]. Ye et al. [186] recently introduced yet another simple colorimetric sensor based on MIP for detection of 3-phenoxybenzaldehyde (3-PBD), the metabolite of pyrethroid pesticides. In this study, 3-aminopropyltriethoxysilane (APTES) and phenyltrimethoxysilane (PTES) were used as monomers to coat the MIP layer on the surface of monodispersed silica nanoparticles via a sol-gel process. A linear concentration range of 3-PBD from 0.1–1 μg/mL, lower detection limit of 0052 μg/mL, and 90% to 98.9% recovery were registered for the fabricated nanosensor. Furthermore, efficacy was demonstrated for the detection of the target analyte in river water, fruit juice, and beverages.

As another example, *organophosphates* (OPs) (e.g., schradan, parathion, malathion) are used as insecticides and acaricides. Although nonpersistent, these pesticides exhibit cholinesterase-inhibiting action and pose serious toxicity to humans [9, 187]. The quest for innovative sensors for OP nerve agents and pesticides is ever increasing, particularly in defense and food safety. As evidence, Mishra et al. [188] fabricated a wearable, flexible, stretchable, organophosphorus hydrolase (OPH) based wireless glove biosensor (GB) for onsite detection of OPs. Along similar lines, a range of electrochemical sensors based on acetylcholinesterase (AChE) has been developed for detection of OPs [9]. Yang et al. [23] encapsulated AChE in a silica matrix and immobilized it onto an AuNPs-polypyrrole-reduced graphene oxide nanocomposite by codeposition with $(NH_4)_2SiF_6$. A rapid and sensitive detection of paraoxon-ethyl from 1 nM to 5 μM with a detection limit of 0.5 nM was reported. By the same token, Cui et al. [189] prepared a highly stable AChE—chitosan-TiO_2-graphene biosensor for OP detection. The LoD of the electrochemical sensor was 29 nM (6.4 ppb) for dichlorvos (a model OP compound) with a detection time of 25 min. The sensor was stable and reproducible to detect dichlorvos in cabbage juice. Liu et al. [190] used zirconia (ZrO_2) nanoparticles, subjected to cyclic voltammetry mediated electrodynamic deposition onto a polycrystalline gold electrode, for fabrication of electrochemical sensors to detect OPs and nerve agents. The sensor exhibited an LoD of 1 ng/mL (ppb) at 10 min of adsorption time.

Organochlorines (e.g., aldrin, chlordane, dieldrin, endrin, lindane, DDT, pentachlorophenol (PCP), hexachlorobenzene (HCB)) find applications as insecticides, acaricides, and fungicides. This persistent and bioaccumulative class of pesticide is known to affect the reproductive, nervous, endocrine, and immune systems [9]. In this regard, Guerrini et al. [191] prepared a SERS nanosensor-based system to detect endosulfan. Bis-acridinium dication lucigenine served as a molecular assembler while functionalizing AgNPs to aid the pesticide's approach to the metal surface. In a similar fashion, Kubackova et al. [192] resorted to functionalization of

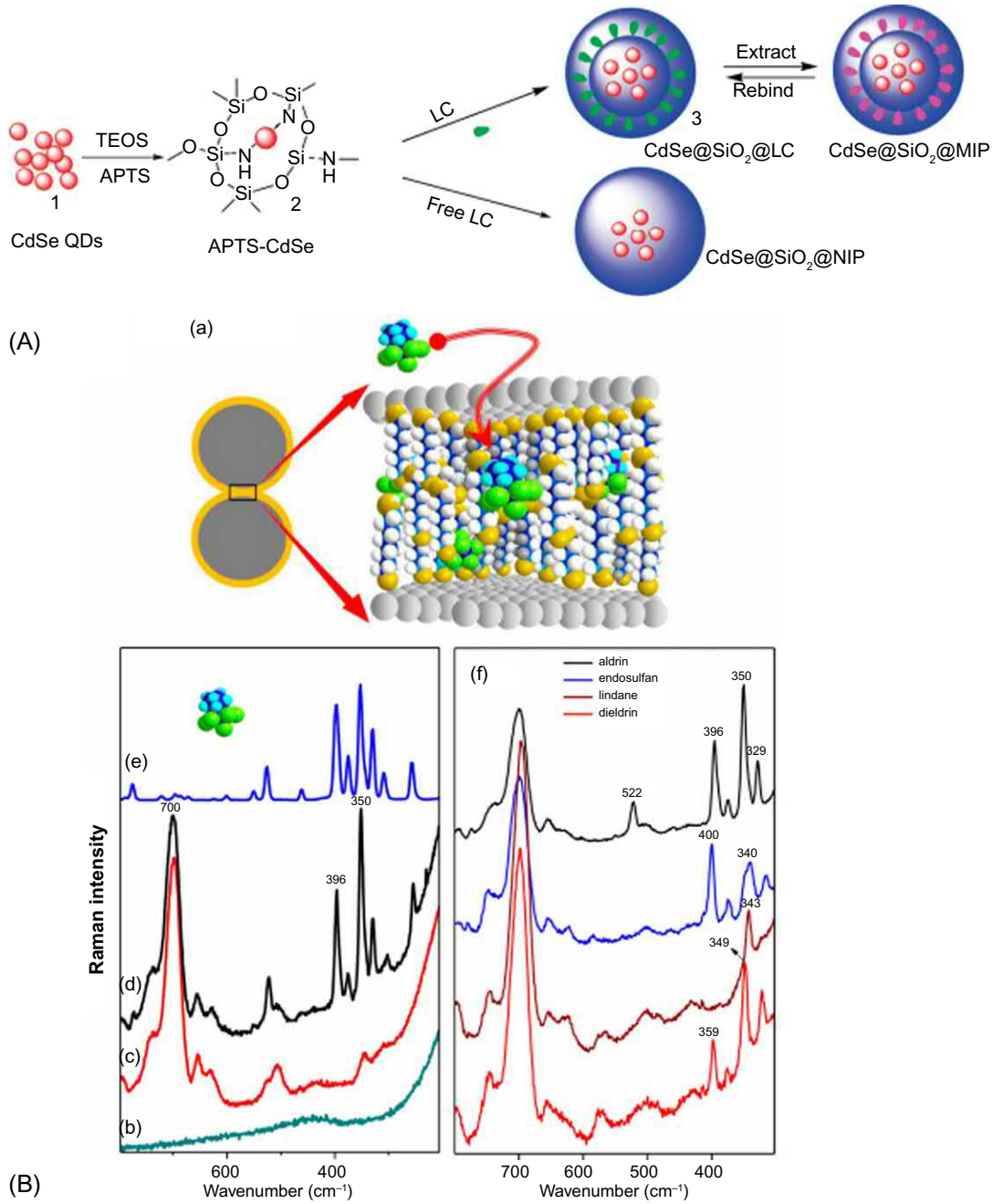

Fig. 3.7

(A) Schematic illustration for the molecular imprinting process of LC-imprinted silica nanospheres embedded CdSe quantum dots. (B) (a) Scheme displaying the pesticide hosting (in this case, for aldrin) in the dithiol layer organized in interparticle gaps. SERS spectra of aldrin (10^{-5} M); (b) on citrate Ag NPs (AgC) in the absence of dithiols and (d) on 1,8-octanedithiol (DT8)-functionalized AgC.

(Continued)

Fig. 3.7, Cont'd The latter spectrum shows the bands corresponding to DT8 that are seen in panel (c) for AgC functionalized with DT8 (10^{-5} M). The Raman of the solid aldrin is presented in spectrum (e). All spectra were obtained at 785 nm excitation. (f) SERS spectra of the analyzed pesticides (10^{-5} M) on DT8-functionalized AgC NPs exciting at 785 nm, showing the C-Cl stretching bands of the fingerprint region (300–400 cm^{-1}) and the C-S stretching bands of DT8 in the deduced multilayer highly ordered conformation employed as reference band for quantitative analysis. *A: Reproduced from Li, H., Li, Y., Cheng, J., 2010. Molecularly imprinted silica nanospheres embedded CdSe quantum dots for highly selective and sensitive optosensing of pyrethroids. Chem. Mater. 22 (8), 2451–2457. Copyright 2010 American Chemical Society; B: Reproduced from Kubackova, J., Fabriciova, G., Miskovsky, P., Jancura, D., Sanchez-Cortes, S., 2015. Sensitive surface-enhanced Raman spectroscopy (SERS) detection of organochlorine pesticides by alkyl dithiol-functionalized metal nanoparticles-induced plasmonic hot spots. Anal. Chem. 87 (1), 663–669. Copyright © 2014 American Chemical Society.*

metal nanoparticles with alkyl dithiols for highly sensitive SERS-based detection of aldrin, dieldrin, lindane, and α-endosulfan. This strategy assisted in generating interparticle junctions with sensitive "hot-spots," requisite for SERS enhancement. Furthermore, this led to creation of specific ambience in the inter-nanoparticles' nanogaps, thereby facilitating the assembly and SERS-based sensing of the pesticides (Fig. 3.7B).

Having stated some of the representative studies on the use of various nano-enabled sensors for detection of pathogens, heavy metals, and pesticides in the earlier sections, the authors would like to highlight an important aspect: identification of the target analytes in the initial stages of device fabrication should be of prime concern. Besides the regulated contaminants [7], research on nanosensors should also be directed towards emerging pathogens and chemicals with established toxicity. Certainly scientific documentation of novel design strategies for nanosensors for a single heavy metal ion or a pathogenic microbe in the form of research papers and patents is highly rewarding; however, cost-effective, field-deployable sensors for high-priority targets must be developed. In the subsequent section, we have highlighted some of the challenges and plausible future research directions for nano-enabled sensors for environmental monitoring.

3.5 Practical snags and future perspectives on nano-enabled sensors for environmental monitoring

After perusal of the earlier sections, one may easily comprehend that nano-enabled sensors have immense prospects for applications in environmental monitoring. Fabrication of various nanomaterials of different shapes and sizes along with exploitation of various bioactive molecules have enabled precise and rapid detection of a plethora of environmental pollutants. However, the translation of lab-based nanosensor research to markets and final acceptance and use by end-users is a highly circuitous path [84].

It is pertinent to note that fabrication approaches and characterization tools and techniques in the course of development and deployment of nanomaterials for sensing systems may not necessarily be cost-effective. As evidence, 1 g (purity >80%, diameter = 1.3 nm) of single-walled carbon nanotubes (SWCNTs), used in electrochemical nanosensors for gases, heavy metals, pathogens, etc., may cost ~$1000 USD (Sigma Aldrich) while 25 mg (COOH functionalized, fluorescence emission at 610 nm) of CdTe quantum dots, used in fluorescent nanosensors for water quality monitoring, is priced at ~$380 USD (Sigma Aldrich) [89]. This *cost factor* may explain the current preference of the commercial units towards conventional cellulose/carbon/fiber-based platforms for pathogen detection or heavy metal ion sensing over nanoenabled sensors. Furthermore, appropriate *sample preparation* and *preconcentration steps* (that involve *analyte isolation and purification*, thereby contributing to *additional analysis cost and complexity of the process*) are prerequisites to abate cross-interference and acquire precise signals. Integration of microfluidic channels in robustly packed devices (which is a challenge in itself) could be a plausible solution to this issue.

In recent years, the scientific repositories have been flooded with reports on nanosensors for prospective environmental applications. However, the functionality of these nanosensors is mostly established in synthetic solutions/media. Furthermore, *lack of calibration and self-standardization* of the nanosensors poses questions on the reliability of the test results. *Collection and validation of data on the operation of these sensors in real complex media* (e.g., detection of heavy metals, pathogens, and pesticides in river and municipality supply water) are mandatory prior to their commercialization. At this juncture, it is pertinent to mention that Vikesland [7] emphasized that nanosensors used for water quality monitoring would make sense in reality if and only if monitoring of the water distribution system is improved using approaches like the Internet of Things (IoT). An integrated network of nanosensors would facilitate real-time monitoring of water quantity and quality, both within the distribution systems and at specific nodes within premise plumbing (Fig. 3.8). However, the nanosensors for such proposed *avant-garde* applications must (a) be able to support device operation under variable ambient parameters, (b) be amenable for in-field replacement, (c) be resistant to fouling, and (d) mediate data communication effectively. Furthermore, it has also been emphasized that use of *nano-enabled sensors must not be skewed towards the detection of only regulated contaminants/analytes* and the framework of water-quality sensing should be democratized [7].

On the other hand, despite the fact that research in the *domain of nanotoxicity* is growing by leaps and bounds, with numerous research groups focusing on the transport/mobility, transformation and in vitro, in vivo, and ecological toxicity of various nanomaterials, *we still have very little information at our disposal*. The requirement of the hour is the development of nontoxic nanosensor designs with the desired functionality, using the dictates of green chemistry applied to nanotechnology. Additionally, *apt, tested, and ratified disposal strategies for disposable types of nanosensors* after use must be available to the public from the suppliers.

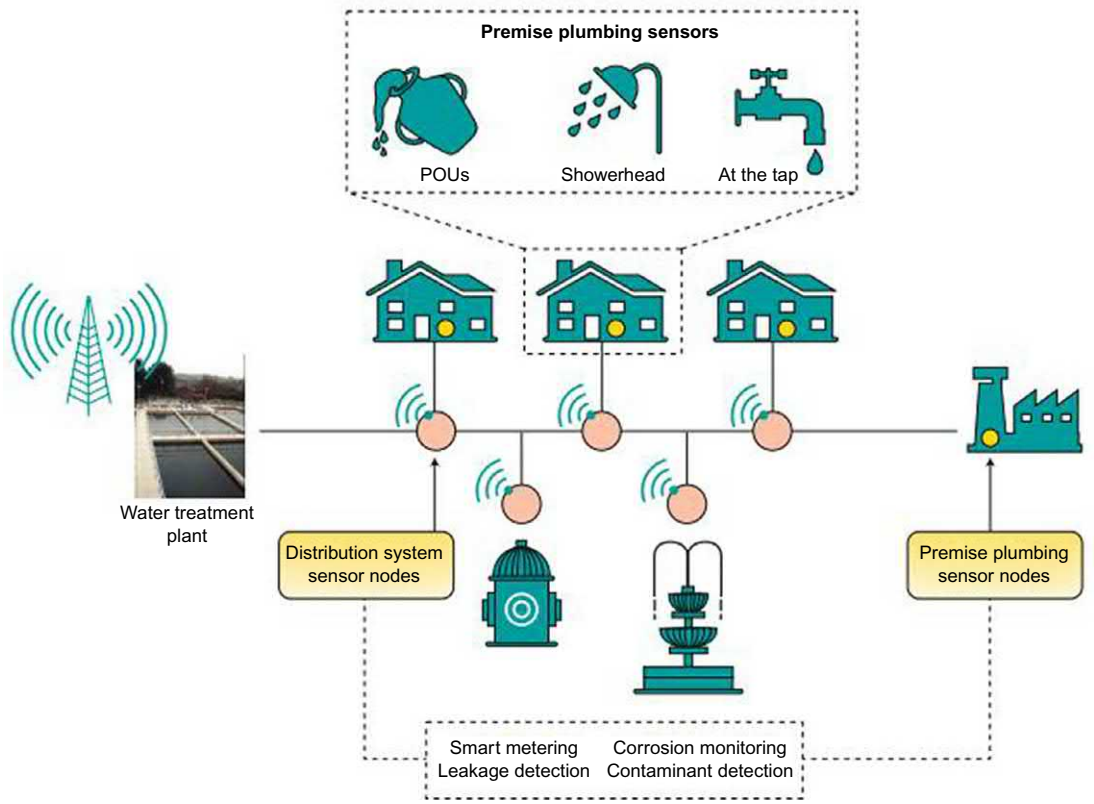

Fig. 3.8
Internet of Things (IoT)-enabled water sensing both within the distribution system and at selected points within premise plumbing. At each sensor node, a suite of nanosensors can be deployed for water-quality monitoring. *Reprinted with permission from Vikesland, P.J., 2018. Nanosensors for water quality monitoring. Nat. Nanotechnol. 13 (8), 651. Copyright 2018 Springer Nature.*

3.6 Conclusion

Though "small," nanomaterials hold prospects of "playing big" in the realm of environmentally relevant analyte sensing. The attributes of simplicity, specificity, sensitivity cum stability, rapidness, size compatibility, ergonomic compatibility, and onsite deployment feasibility with tailorable real-time monitoring with requirements for small sample volumes have led to an immense research effort put forth towards nano-enabled sensors for environmental purposes. The scientific repositories are constantly being updated with numerous innovative design approaches and applications of nanobiosensors. The sensing of analytes in laboratory-spiked samples must be complemented by field-sample assessments. Furthermore, the issues of cost-effectiveness and nanotoxicity must be addressed. As noted in the chapter, nanosensors could play a vital role in the surveillance of ambient health status. This could go a long way towards better policymaking and implementation, eventually ensuring a safe and green environment for us and our posterity.

References

[1] A. Bryndum-Buchholz, D.P. Tittensor, J.L. Blanchard, W.W.L. Cheung, M. Coll, E. D. Galbraith, S. Jennings, O. Maury, H.K. Lotze, Twenty-first-century climate change impacts on marine animal biomass and ecosystem structure across ocean basins, Glob. Chang. Biol. 25 (2) (2019) 459–472.

[2] E. Guermazi, M. Milano, E. Reynard, M. Zairi, Impact of climate change and anthropogenic pressure on the groundwater resources in arid environment, Mitig. Adapt. Strateg. Glob. Chang. 24 (1) (2019) 73–92.

[3] S.X. Wang, F. Yu Benjamin, Labor mobility barriers and rural-urban migration in transitional China, China Econ. Rev. 53 (2019) 211–224.

[4] A.E.V. Evans, J. Mateo-Sagasta, M. Qadir, E. Boelee, A. Ippolito, Agricultural water pollution: key knowledge gaps and research needs, Curr. Opin. Environ. Sustain. 36 (2019) 20–27.

[5] F.E. Greven, J.M. Vonk, P. Fischer, F. Duijm, N.M. Vink, B. Brunekreef, Air pollution during New Year's fireworks and daily mortality in the Netherlands, Sci. Rep. 9 (1) (2019) 5735.

[6] G. Quaglia, I. Joris, S. Broekx, N. Desmet, K. Koopmans, K. Vandaele, P. Seuntjens, A spatial approach to identify priority areas for pesticide pollution mitigation, J. Environ. Manag. 246 (2019) 583–593.

[7] P.J. Vikesland, Nanosensors for water quality monitoring, Nat. Nanotechnol. 13 (8) (2018) 651.

[8] A. Antonacci, F. Arduini, D. Moscone, G. Palleschi, V. Scognamiglio, Nanostructured (bio) sensors for smart agriculture, TrAC Trends Anal. Chem. 98 (2018) 95–103.

[9] M.R. Willner, P.J. Vikesland, Nanomaterial enabled sensors for environmental contaminants, J. Nanobiotechnol. 16 (1) (2018) 95.

[10] S. Chen, G. Sun, High sensitivity ammonia sensor using a hierarchical polyaniline/poly (ethylene-co-glycidyl methacrylate) nanofibrous composite membrane, ACS Appl. Mater. Interfaces 5 (14) (2013) 6473–6477.

[11] S.-Y. Cho, H.-W. Yoo, J.Y. Kim, W.-B. Jung, M.L. Jin, J.-S. Kim, H.-J. Jeon, H.-T. Jung, High-resolution *p*-type metal oxide semiconductor nanowire array as an ultrasensitive sensor for volatile organic compounds, Nano Lett. 16 (7) (2016) 4508–4515.

[12] J.F. Fennell Jr., S.F. Liu, J.M. Azzarelli, J.G. Weis, S. Rochat, K.A. Mirica, J.B. Ravnsbæk, T.M. Swager, Nanowire chemical/biological sensors: status and a roadmap for the future, Angew. Chem. Int. Ed. 55 (4) (2016) 1266–1281.

[13] J.-H. Kim, A. Katoch, S.-H. Kim, S.S. Kim, Chemiresistive sensing behavior of SnO_2 (n)–Cu_2O (p) core–shell nanowires, ACS Appl. Mater. Interfaces 7 (28) (2015) 15351–15358.

[14] L.R. Kindra, C.J. Eggers, A.T. Liu, K. Mendoza, J. Mendoza, A.R. Klein Myers, R.M. Penner, Lithographically patterned PEDOT nanowires for the detection of iron (III) with nanomolar sensitivity, Anal. Chem. 87 (22) (2015) 11492–11500.

[15] I.S. Muratova, K.N. Mikhelson, Y.E. Ermolenko, A. Offenhäusser, Y. Mourzina, Chemiresistors based on ultrathin gold nanowires for sensing halides, pyridine and dopamine, Sensors Actuators B Chem. 232 (2016) 420–427.

[16] O. SeokáKwon, S. JooáPark, Highly sensitive and selective chemiresistive sensors based on multidimensional polypyrrole nanotubes, Chem. Commun. 48 (85) (2012) 10526–10528.

[17] M.S. Mannoor, T. Hu, J.D. Clayton, A. Sengupta, D.L. Kaplan, R.R. Naik, N. Verma, F.G. Omenetto, M.C. McAlpine, Graphene-based wireless bacteria detection on tooth enamel, Nat. Commun. 3 (2012) 763.

[18] A.J. Bandodkar, I. Jeerapan, J.-M. You, R. Nuñez-Flores, J. Wang, Highly stretchable fully-printed CNT-based electrochemical sensors and biofuel cells: combining intrinsic and design-induced stretchability, Nano Lett. 16 (1) (2015) 721–727.

[19] P. Gou, N.D. Kraut, I.M. Feigel, A. Star, Rigid versus flexible ligands on carbon nanotubes for the enhanced sensitivity of cobalt ions, Macromolecules 46 (4) (2013) 1376–1383.

[20] G. Yu, W. Wu, Q. Zhao, X. Wei, L. Qing, Efficient immobilization of acetylcholinesterase onto amino functionalized carbon nanotubes for the fabrication of high sensitive organophosphorus pesticides biosensors, Biosens. Bioelectron. 68 (2015) 288–294.

[21] A.M. Stortini, L.M. Moretto, A. Mardegan, M. Ongaro, P. Ugo, Arrays of copper nanowire electrodes: preparation, characterization and application as nitrate sensor, Sensors Actuators B Chem. 207 (2015) 186–192.

[22] X.-G. Li, J.-L. Zhang, M.-R. Huang, Chemical response of nanocomposite membranes of electroactive polydiaminonaphthalene nanoparticles to heavy metal ions, J. Phys. Chem. C 118 (22) (2014) 11990–11999.
[23] Y. Yang, A.M. Asiri, D. Du, Y. Lin, Acetylcholinesterase biosensor based on a gold nanoparticle–polypyrrole–reduced graphene oxide nanocomposite modified electrode for the amperometric detection of organophosphorus pesticides, Analyst 139 (12) (2014) 3055–3060.
[24] O. Knopfmacher, M.L. Hammock, A.L. Appleton, G. Schwartz, J. Mei, T. Lei, J. Pei, Z. Bao, Highly stable organic polymer field-effect transistor sensor for selective detection in the marine environment, Nat. Commun. 5 (2014) 2954.
[25] S. Jiang, R. Cheng, R. Ng, H. Yu, X. Duan, Highly sensitive detection of mercury (II) ions with few-layer molybdenum disulfide, Nano Res. 8 (1) (2015) 257–262.
[26] D. Sarkar, W. Liu, X. Xie, A.C. Anselmo, S. Mitragotri, K. Banerjee, MoS_2 field-effect transistor for next-generation label-free biosensors, ACS Nano 8 (4) (2014) 3992–4003.
[27] A. Gao, N. Lu, Y. Wang, P. Dai, T. Li, X. Gao, Y. Wang, C. Fan, Enhanced sensing of nucleic acids with silicon nanowire field effect transistor biosensors, Nano Lett. 12 (10) (2012) 5262–5268.
[28] F. Shen, J. Wang, Z. Xu, Y. Wu, Q. Chen, X. Li, X. Jie, et al., Rapid flu diagnosis using silicon nanowire sensor, Nano Lett. 12 (7) (2012) 3722–3730.
[29] M.-R. Chao, Y.-Z. Chang, J.-L. Chen, Hydrophilic ionic liquid-passivated CdTe quantum dots for mercury ion detection, Biosens. Bioelectron. 42 (2013) 397–402.
[30] T.-T. Gan, Y.-J. Zhang, N.-J. Zhao, X. Xue, G.-F. Yin, S.-H. Yu, H.-B. Wang, J.-B. Duan, C.-Y. Shi, W.-Q. Liu, Hydrothermal synthetic mercaptopropionic acid stabled CdTe quantum dots as fluorescent probes for detection of Ag^+, Spectrochim. Acta A Mol. Biomol. Spectrosc. 99 (2012) 62–68.
[31] J. Ke, X. Li, Y. Shi, Q. Zhao, X. Jiang, A facile and highly sensitive probe for Hg (II) based on metal-induced aggregation of ZnSe/ZnS quantum dots, Nanoscale 4 (16) (2012) 4996–5001.
[32] M. Koneswaran, R. Narayanaswamy, L-Cysteine-capped ZnS quantum dots based fluorescence sensor for Cu^{2+} ion, Sensors Actuators B Chem. 139 (1) (2009) 104–109.
[33] L. Li, G. Wu, G. Yang, J. Peng, J. Zhao, J.-J. Zhu, Focusing on luminescent graphene quantum dots: current status and future perspectives, Nanoscale 5 (10) (2013) 4015–4039.
[34] M. Li, X. Zhou, S. Guo, W. Nianqiang, Detection of lead (II) with a "turn-on" fluorescent biosensor based on energy transfer from CdSe/ZnS quantum dots to graphene oxide, Biosens. Bioelectron. 43 (2013) 69–74.
[35] W. Luan, H. Yang, Z. Wan, B. Yuan, X. Yu, T. Shan-tung, Mercaptopropionic acid capped CdSe/ZnS quantum dots as fluorescence probe for lead (II), J. Nanopart. Res. 14 (3) (2012) 762.
[36] T.-W. Sung, Y.-L. Lo, Highly sensitive and selective sensor based on silica-coated CdSe/ZnS nanoparticles for Cu^{2+} ion detection, Sensors Actuators B Chem. 165 (1) (2012) 119–125.
[37] Y.-Q. Wang, L. Yang, X.-W. He, W.-Y. Li, Y.-K. Zhang, Highly sensitive synchronous fluorescence determination of mercury (II) based on the denatured ovalbumin coated CdTe QDs, Talanta 99 (2012) 69–74.
[38] H. Wu, J. Liang, H. Han, A novel method for the determination of Pb^{2+} based on the quenching of the fluorescence of CdTe quantum dots, Microchim. Acta 161 (1–2) (2008) 81–86.
[39] L. Beqa, A.K. Singh, S.A. Khan, D. Senapati, S.R. Arumugam, P.C. Ray, Gold nanoparticle-based simple colorimetric and ultrasensitive dynamic light scattering assay for the selective detection of Pb (II) from paints, plastics, and water samples, ACS Appl. Mater. Interfaces 3 (3) (2011) 668–673.
[40] W.L. Daniel, M.S. Han, J.-S. Lee, C.A. Mirkin, Colorimetric nitrite and nitrate detection with gold nanoparticle probes and kinetic end points, J. Am. Chem. Soc. 131 (18) (2009) 6362–6363.
[41] J. Liu, L. Yi, Fast colorimetric sensing of adenosine and cocaine based on a general sensor design involving aptamers and nanoparticles, Angew. Chem. Int. Ed. 45 (1) (2006) 90–94.
[42] D. Vilela, M.C. González, A. Escarpa, Sensing colorimetric approaches based on gold and silver nanoparticles aggregation: chemical creativity behind the assay. A review, Anal. Chim. Acta 751 (2012) 24–43.
[43] C. Zhang, L. Wang, T. Zhui, X. Sun, Q. He, Z. Lei, C. Xu, et al., Organophosphorus pesticides detection using broad-specific single-stranded DNA based fluorescence polarization aptamer assay, Biosens. Bioelectron. 55 (2014) 216–219.
[44] Z. Zhang, Z. Chen, Q. Chengli, L. Chen, Highly sensitive visual detection of copper ions based on the shape-dependent LSPR spectroscopy of gold nanorods, Langmuir 30 (12) (2014) 3625–3630.

[45] K.R. Ackermann, T. Henkel, J. Popp, Quantitative online detection of low-concentrated drugs via a SERS microfluidic system, ChemPhysChem 8 (18) (2007) 2665–2670.
[46] K. Hadjigeorgiou, E. Kastanos, C. Pitris, Multi-bacteria multi-antibiotic testing using surface enhanced Raman spectroscopy (SERS) for urinary tract infection (UTI) diagnosis, in: European Conference on Biomedical Optics, Optical Society of America, 2013, p. 87980L.
[47] R.A. Halvorson, P.J. Vikesland, Surface-enhanced Raman spectroscopy (SERS) for environmental analyses, Environ. Sci. Technol. 44 (2010) 7749–7755.
[48] R.M. Jarvis, R. Goodacre, Characterisation and identification of bacteria using SERS, Chem. Soc. Rev. 37 (5) (2008) 931–936.
[49] H. Zhou, D. Yang, N.P. Ivleva, N.E. Mircescu, R. Niessner, C. Haisch, SERS detection of bacteria in water by in situ coating with Ag nanoparticles, Anal. Chem. 86 (3) (2014) 1525–1533.
[50] J. Zhou, Q. Liu, W. Feng, Y. Sun, F. Li, Upconversion luminescent materials: advances and applications, Chem. Rev. 115 (1) (2014) 395–465.
[51] T.G. Barroso, R.C. Martins, E. Fernandes, S. Cardoso, J. Rivas, P.P. Freitas, Detection of BCG bacteria using a magnetoresistive biosensor: a step towards a fully electronic platform for tuberculosis point-of-care detection, Biosens. Bioelectron. 100 (2018) 259–265.
[52] V.D. Krishna, K. Wu, A.M. Perez, J.-P. Wang, Giant magnetoresistance-based biosensor for detection of influenza A virus, Front. Microbiol. 7 (2016) 400.
[53] K. Wu, T. Klein, V.D. Krishna, S. Diqing, A.M. Perez, J.-P. Wang, Portable GMR handheld platform for the detection of influenza A virus, ACS Sens. 2 (11) (2017) 1594–1601.
[54] T. Banerjee, S. Sulthana, T. Shelby, B. Heckert, J. Jewell, K. Woody, V. Karimnia, J. McAfee, S. Santra, Multiparametric magneto-fluorescent nanosensors for the ultrasensitive detection of *Escherichia coli* O157: H7, ACS Infect. Dis. 2 (10) (2016) 667–673.
[55] Y. Chen, Y. Xianyu, W. Yu, X. Zhang, R. Cha, J. Sun, X. Jiang, One-step detection of pathogens and viruses: combining magnetic relaxation switching and magnetic separation, ACS Nano 9 (3) (2015) 3184–3191.
[56] G. de la Torre, T. Zardán, R. Ke, A. Mezger, P. Svedlindh, M. Strømme, M. Nilsson, Sensitive detection of spores using volume-amplified magnetic nanobeads, Small 8 (14) (2012) 2174–2177.
[57] R. Konwarh, B. Dhandayuthapani, Sustainable bioresource, silk at the nanoscale for biomedical applications, in: Dynamics of Advanced Sustainable Nanomaterials and Their Related Nanocomposites at the Bio-Nano Interface, Elsevier Science, 2019, p. 125.
[58] R. Konwarh, M. Shail, T. Medhi, M. Mandal, N. Karak, Sonication assisted assemblage of exotic polymer supported nanostructured bio-hybrid system and prospective application, Ultrason. Sonochem. 21 (2) (2014) 634–642.
[59] R. Konwarh, N. Karak, M. Misra, Electrospun cellulose acetate nanofibers: the present status and gamut of biotechnological applications, Biotechnol. Adv. 31 (4) (2013) 421–437.
[60] R. Konwarh, S. Pramanik, K.S.P. Devi, N. Saikia, R. Boruah, T.K. Maiti, R.C. Deka, N. Karak, Lycopene coupled 'trifoliate' polyaniline nanofibers as multi-functional biomaterial, J. Mater. Chem. 22 (30) (2012) 15062–15070.
[61] J.P. Kumar, R. Konwarh, M. Kumar, A. Gangrade, B.B. Mandal, Potential nanomedicine applications of multifunctional carbon nanoparticles developed using green technology, ACS Sustain. Chem. Eng. 6 (1) (2017) 1235–1245.
[62] W.R. Algar, A.J. Tavares, U.J. Krull, Beyond labels: a review of the application of quantum dots as integrated components of assays, bioprobes, and biosensors utilizing optical transduction, Anal. Chim. Acta 673 (1) (2010) 1–25.
[63] F.A. Esteve-Turrillas, A. Abad-Fuentes, Applications of quantum dots as probes in immunosensing of small-sized analytes, Biosens. Bioelectron. 41 (2013) 12–29.
[64] X.-Q. Liu, Q. Liu, S.-H. Cao, W.-P. Cai, Y.-H. Weng, K.-X. Xie, Y.-Q. Li, Directional surface plasmon-coupled emission of CdTe quantum dots and its application in Hg (II) sensing, Anal. Methods 4 (12) (2012) 3956–3960.
[65] S. Schlücker, SERS microscopy: nanoparticle probes and biomedical applications, ChemPhysChem 10 (9–10) (2009) 1344–1354.
[66] E. Petryayeva, U.J. Krull, Localized surface plasmon resonance: nanostructures, bioassays and biosensing—a review, Anal. Chim. Acta 706 (1) (2011) 8–24.

[67] B. Sepúlveda, P.C. Angelomé, L.M. Lechuga, L.M. Liz-Marzán, LSPR-based nanobiosensors, Nano Today 4 (3) (2009) 244–251.
[68] J. Griffin, A.K. Singh, D. Senapati, P. Rhodes, K. Mitchell, B. Robinson, E. Yu, P.C. Ray, Size-and distance-dependent nanoparticle surface-energy transfer (NSET) method for selective sensing of hepatitis C virus RNA, Chem Eur J 15 (2) (2009) 342–351.
[69] C. Kaittanis, S.A. Naser, J.M. Perez, One-step, nanoparticle-mediated bacterial detection with magnetic relaxation, Nano Lett. 7 (2) (2007) 380–383.
[70] J. Chen, J.X. Zhao, Upconversion nanomaterials: synthesis, mechanism, and applications in sensing, Sensors 12 (3) (2012) 2414–2435.
[71] F.R. Baptista, S.A. Belhout, S. Giordani, S.J. Quinn, Recent developments in carbon nanomaterial sensors, Chem. Soc. Rev. 44 (13) (2015) 4433–4453.
[72] B. Garg, T. Bisht, Y.-C. Ling, Graphene-based nanomaterials as efficient peroxidase mimetic catalysts for biosensing applications: An overview, Molecules 20 (8) (2015) 14155–14190.
[73] S. Kumar, W. Ahlawat, R. Kumar, N. Dilbaghi, Graphene, carbon nanotubes, zinc oxide and gold as elite nanomaterials for fabrication of biosensors for healthcare, Biosens. Bioelectron. 70 (2015) 498–503.
[74] Z. Fan, S. Li, F. Yuan, L. Fan, Fluorescent graphene quantum dots for biosensing and bioimaging, RSC Adv. 5 (25) (2015) 19773–19789.
[75] A.L. Himaja, P.S. Karthik, S.P. Singh, Carbon dots: the newest member of the carbon nanomaterials family, Chem. Rec. 15 (3) (2015) 595–615.
[76] S.Y. Lim, W. Shen, Z. Gao, Carbon quantum dots and their applications, Chem. Soc. Rev. 44 (1) (2015) 362–381.
[77] X.T. Zheng, A. Ananthanarayanan, K.Q. Luo, P. Chen, Glowing graphene quantum dots and carbon dots: properties, syntheses, and biological applications, Small 11 (14) (2015) 1620–1636.
[78] S. Ge, F. Lan, F. Yu, Y. Jinghua, Applications of graphene and related nanomaterials in analytical chemistry, New J. Chem. 39 (4) (2015) 2380–2395.
[79] S.K. Pal, Versatile photoluminescence from graphene and its derivatives, Carbon 88 (2015) 86–112.
[80] C.Y. Yu, G.Y. Ang, A.L. Chua, E.H. Tan, S.Y. Lee, G. Falero-Diaz, O. Otero, et al., Dry-reagent gold nanoparticle-based lateral flow biosensor for the simultaneous detection of *Vibrio cholerae* serogroups O1 and O139, J. Microbiol. Methods 86 (3) (2011) 277–282.
[81] X. Yu, H. Cai, W. Zhang, X. Li, N. Pan, Y. Luo, X. Wang, J.G. Hou, Tuning chemical enhancement of SERS by controlling the chemical reduction of graphene oxide nanosheets, ACS Nano 5 (2) (2011) 952–958.
[82] A. Burns, H. Ow, U. Wiesner, Fluorescent core–shell silica nanoparticles: towards "lab on a particle" architectures for nanobiotechnology, Chem. Soc. Rev. 35 (11) (2006) 1028–1042.
[83] A. Burns, P. Sengupta, T. Zedayko, B. Baird, U. Wiesner, Core/shell fluorescent silica nanoparticles for chemical sensing: towards single-particle laboratories, Small 2 (6) (2006) 723–726.
[84] R.K. Saini, L.P. Bagri, A.K. Bajpai, Smart nanosensors for pesticide detection, in: New Pesticides and Soil Sensors, Academic Press, 2017, pp. 519–559.
[85] X. Wang, X. Lu, J. Chen, Development of biosensor technologies for analysis of environmental contaminants, Trends Environ. Anal. Chem. 2 (2014) 25–32.
[86] F. Lagarde, N. Jaffrezic-Renault, Cell-based electrochemical biosensors for water quality assessment, Anal. Bioanal. Chem. 400 (4) (2011) 947.
[87] L. Su, W. Jia, C. Hou, L. Yu, Microbial biosensors: a review, Biosens. Bioelectron. 26 (5) (2011) 1788–1799.
[88] C.I.L. Justino, A.C. Duarte, T.A.P. Rocha-Santos, Analytical applications of affibodies, TrAC Trends Anal. Chem. 65 (2015) 73–82.
[89] R. Kaur, S.K. Sharma, S.K. Tripathy, Advantages and limitations of environmental nanosensors, in: Advances in Nanosensors for Biological and Environmental Analysis, Elsevier, 2019, pp. 119–132.
[90] A. Modi, N. Koratkar, E. Lass, B. Wei, P.M. Ajayan, Miniaturized gas ionization sensors using carbon nanotubes, Nature 424 (6945) (2003) 171.
[91] S. Avaz, R.B. Roy, V.R.S.S. Mokkapati, A. Bozkurt, S. Pandit, I. Mijakovic, Y.Z. Menceloglu, Graphene based nanosensor for aqueous phase detection of nitroaromatics, RSC Adv. 7 (41) (2017) 25519–25527.
[92] J. Li, Y. Lu, Q. Ye, M. Cinke, J. Han, M. Meyyappan, Carbon nanotube sensors for gas and organic vapor detection, Nano Lett. 3 (7) (2003) 929–933.

[93] X. Zhu, B. Li, J. Yang, Y. Li, W. Zhao, J. Shi, G. Jinlou, Effective adsorption and enhanced removal of organophosphorus pesticides from aqueous solution by Zr-based MOFs of UiO-67, ACS Appl. Mater. Interfaces 7 (1) (2014) 223–231.
[94] Y. Wei, Y. Li, Q. Yunhe, F. Xiao, G. Shi, L. Jin, A novel biosensor based on photoelectro-synergistic catalysis for flow-injection analysis system/amperometric detection of organophosphorous pesticides, Anal. Chim. Acta 643 (1–2) (2009) 13–18.
[95] D. Du, S. Chen, J. Cai, A. Zhang, Immobilization of acetylcholinesterase on gold nanoparticles embedded in sol–gel film for amperometric detection of organophosphorous insecticide, Biosens. Bioelectron. 23 (1) (2007) 130–134.
[96] A. Ishii, S. Takeda, S. Hattori, K. Sueoka, K. Mukasa, Ultrasensitive detection of organophosphate insecticides by carbon nanotube field-effect transistor, Colloids Surf. A Physicochem. Eng. Asp. 313 (2008) 456–460.
[97] D. Du, S. Chen, D. Song, H. Li, X. Chen, Development of acetylcholinesterase biosensor based on CdTe quantum dots/gold nanoparticles modified chitosan microspheres interface, Biosens. Bioelectron. 24 (3) (2008) 475–479.
[98] P. Kumar, A.K. Paul, A. Deep, Sensitive chemosensing of nitro group containing organophosphate pesticides with MOF-5, Microporous Mesoporous Mater. 195 (2014) 60–66.
[99] B. Cho, M.G. Hahm, M. Choi, J. Yoon, A.R. Kim, Y.-J. Lee, S.-G. Park, et al., Charge-transfer-based gas sensing using atomic-layer MoS_2, Sci. Rep. 5 (2015) 8052.
[100] J.-.S. Lee, M.S. Han, C.A. Mirkin, Colorimetric detection of mercuric ion (Hg^{2+}) in aqueous media using DNA-functionalized gold nanoparticles, Angew. Chem. Int. Ed. 46 (22) (2007) 4093–4096.
[101] Y. Ge, Z. Wei, Y. Li, Q. Jiang, Z. Baiyi, X. Dou, Highly sensitive and rapid chemiresistive sensor towards trace nitro-explosive vapors based on oxygen vacancy-rich and defective crystallized In-doped ZnO, Sensors Actuators B Chem. 244 (2017) 983–991.
[102] D. Zhang, J. Liu, P. Li, B. Xia, Sensor array based on metal oxide modified graphene for the detection of multi-component mixed gas, in: 2016 IEEE 29th International Conference on Micro Electro Mechanical Systems (MEMS), IEEE, 2016, pp. 920–923.
[103] M. Tonezzer, D.T.T. Le, S. Iannotta, N. Van Hieu, Selective discrimination of hazardous gases using one single metal oxide resistive sensor, Sensors Actuators B Chem. 277 (2018) 121–128.
[104] A. Chalupniak, A. Merkoçi, Toward integrated detection and graphene-based removal of contaminants in a lab-on-a-chip platform, Nano Res. 10 (7) (2017) 2296–2310.
[105] J. Tu, Y. Gan, T. Liang, Q. Hu, Q. Wang, T. Ren, Q. Sun, H. Wan, P. Wang, Graphene FET array biosensor based on ssDNA aptamer for ultrasensitive Hg^{2+} detection in environmental pollutants, Front. Chem. 6 (2018) 333.
[106] X. Tian, H. Peng, Y. Li, C. Yang, Z. Zhou, Y. Wang, Highly sensitive and selective paper sensor based on carbon quantum dots for visual detection of TNT residues in groundwater, Sensors Actuators B Chem. 243 (2017) 1002–1009.
[107] L. Gong, E. Liu, J. Che, J. Li, X. Liu, H. Xu, J. Liang, Multiple cross displacement amplification coupled with gold nanoparticles-based lateral flow biosensor for detection of the mobilized colistin resistance gene mcr-1, bioRxiv (2019) 579904.
[108] Y. Wang, W. Yan, F. Shanshan, S. Hu, Y. Wang, J. Xu, C. Ye, Multiple cross displacement amplification coupled with nanoparticles-based lateral flow biosensor for detection of *Staphylococcus aureus* and identification of methicillin-resistant *S. aureus*, Front. Microbiol. 9 (2018) 907.
[109] L. Sutarlie, S.Y. Ow, X. Su, Nanomaterials-based biosensors for detection of microorganisms and microbial toxins, Biotechnol. J. 12 (4) (2017), https://doi.org/10.1002/biot.201500459.
[110] G.A. Zelada-Guillen, J. Riu, A. Duezguen, F.X. Rius, Immediate detection of living bacteria at ultralow concentrations using a carbon nanotube based potentiometric aptasensor, Angew. Chem. Int. Ed. 48 (2009) 7334–7337.
[111] A. Jyoti, R.S. Tomar, Detection of pathogenic bacteria using nanobiosensors, Environ. Chem. Lett. 15 (1) (2017) 1–6.
[112] P. Koedrith, T. Thasiphu, J.-I. Weon, R. Boonprasert, K. Tuitemwong, P. Tuitemwong, Recent trends in rapid environmental monitoring of pathogens and toxicants: potential of nanoparticle-based biosensor and applications, Sci. World J. 2015 (2015) 510982 (12 pp.).

[113] F. Melaine, M. Saad, S. Faucher, M. Tabrizian, Selective and high dynamic range assay format for multiplex detection of pathogenic *Pseudomonas aeruginosa*, *Salmonella typhimurium*, and *Legionella pneumophila* RNAs using surface plasmon resonance imaging, Anal. Chem. 89 (14) (2017) 7802–7807.
[114] F. Mustafa, R. Hassan, S. Andreescu, Multifunctional nanotechnology-enabled sensors for rapid capture and detection of pathogens, Sensors 17 (9) (2017) 2121.
[115] E.J. Park, J.-Y. Lee, J.H. Kim, C.J. Lee, H.S. Kim, N.K. Min, Investigation of plasma-functionalized multiwalled carbon nanotube film and its application of DNA sensor for *Legionella pneumophila* detection, Talanta 82 (3) (2010) 904–911.
[116] M.L. Verma, Enzymatic nanobiosensors in the agricultural and food industry, in: Nanoscience in Food and Agriculture, 4, Springer, Cham, 2017, pp. 229–245.
[117] Y. Zhang, T.-H. Wang, Quantum dot enabled molecular sensing and diagnostics, Theranostics 2 (7) (2012) 631.
[118] S. Tripathy, S.R.K. Vanjari, S. Vikrant, S. Swaminathan, S.G. Singh, Electrospun manganese (III) oxide nanofiber based electrochemical DNA-nanobiosensor for zeptomolar detection of dengue consensus primer, Biosens. Bioelectron. 90 (2017) 378–387.
[119] Y. Sun, L. Fang, Y. Wan, G. Zhifeng, Pathogenic detection and phenotype using magnetic nanoparticle-urease nanosensor, Sensors Actuators B Chem. 259 (2018) 428–432.
[120] A.M. Baetsen-Young, M. Vasher, L.L. Matta, P. Colgan, E.C. Alocilja, B. Day, Direct colorimetric detection of unamplified pathogen DNA by dextrin-capped gold nanoparticles, Biosens. Bioelectron. 101 (2018) 29–36.
[121] Y. Wang, K. Lee, J. Irudayaraj, Silver nanosphere SERS probes for sensitive identification of pathogens, J. Phys. Chem. C 114 (39) (2010) 16122–16128.
[122] M.R. Nurliyana, M.Z. Sahdan, K.M. Wibowo, A. Muslihati, H. Saim, S.A. Ahmad, Y. Sari, Z. Mansor, The detection method of *Escherichia coli* in water resources: a review, J. Phys. Conf. Ser. 995 (1) (2018) 012065. IOP Publishing.
[123] N. Massad-Ivanir, G. Shtenberg, A. Tzur, M.A. Krepker, E. Segal, Engineering nanostructured porous SiO_2 surfaces for bacteria detection via "direct cell capture", Anal. Chem. 83 (9) (2011) 3282–3289.
[124] H.-.M. So, D.-.W. Park, E.-.K. Jeon, Y.-.H. Kim, B.S. Kim, C.-.K. Lee, S.Y. Choi, S.C. Kim, H. Chang, J.-.O. Lee, Detection and titer estimation of *Escherichia coli* using aptamer-functionalized single-walled carbon-nanotube field-effect transistors, Small 4 (2) (2008) 197–201.
[125] X. Wang, Q. Cui, C. Yao, S. Li, P. Zhang, H. Sun, F. Lv, L. Liu, L. Li, S. Wang, Conjugated polyelectrolyte–silver nanostructure pair for detection and killing of bacteria, Adv. Mater. Technol. 2 (7) (2017) 1700033.
[126] R. Jackeray, G. Singh, S. Jain, Z.A. Ckv, H. Singh, N.H. Zaidi, U. Soni, S. Sapra, T.G. Shrivastav, Bioconjugated quantum dots based rapid detection of pathogenic bacteria from water samples, Int. J. Nanosci. 10 (01n02) (2011) 199–203.
[127] V. Razavilar, H. Ahari, B. Akbari Adergani, A.A. Anvar, A central composite face-centered design for optimizing the detection of *Salmonella typhi* with a fluorescence nanobiosensor using the microcontact method, Int. J. Environ. Sci. Technol. 16 (2018) 4637–4646.
[128] R. Rafique, M.-u. Rashid, S. Monira, Z. Rahman, M. Mahmud, M. Mustafiz, K.M. Saif-Ur-Rahman, et al., Transmission of infectious *Vibrio cholerae* through drinking water among the household contacts of cholera patients (CHoBI7 trial), Front. Microbiol. 7 (2016) 1635.
[129] E.S. Rasti, A.C. Brown, Cholera toxin encapsulated within several *Vibrio cholerae* O1 serotype Inaba outer membrane vesicles lacks a functional B-subunit, Toxins 11 (4) (2019) 207.
[130] S.A. Khan, J.A. DeGrasse, B.J. Yakes, T.R. Croley, Rapid and sensitive detection of cholera toxin using gold nanoparticle-based simple colorimetric and dynamic light scattering assay, Anal. Chim. Acta 892 (2015) 167–174.
[131] P.D. Tam, C.X. Thang, Label-free electrochemical immunosensor based on cerium oxide nanowires for *Vibrio cholerae* O1 detection, Mater. Sci. Eng. C 58 (2016) 953–959.
[132] K.-S. Ahn, K.R. Lim, D. Jeong, B.Y. Lee, K.S. Kim, W.-Y. Lee, Fluorescence energy transfer inhibition bioassay for cholera toxin based on galactose-stabilized gold nanoparticles and amine-terminated quantum dots, Microchem. J. 124 (2016) 9–14.

[133] R. Thiramanas, K. Jangpatarapongsa, P. Tangboriboonrat, D. Polpanich, Detection of *Vibrio cholerae* using the intrinsic catalytic activity of a magnetic polymeric nanoparticle, Anal. Chem. 85 (12) (2013) 5996–6002.
[134] A. Meneghello, A. Sonato, G. Ruffato, G. Zacco, F. Romanato, A novel high sensitive surface plasmon resonance *Legionella pneumophila* sensing platform, Sensors Actuators B Chem. 250 (2017) 351–355.
[135] A.C. Llewellyn, C.E. Lucas, S.E. Roberts, E.W. Brown, B.S. Nayak, B.H. Raphael, J. M. Winchell, Distribution of *Legionella* and bacterial community composition among regionally diverse US cooling towers, PLoS One 12 (12) (2017) e0189937.
[136] M. Martín, P. Salazar, C. Jiménez, M. Lecuona, M.J. Ramos, J. Ode, J. Alcoba, et al., Rapid *Legionella pneumophila* determination based on a disposable core–shell Fe_3O_4@ poly (dopamine) magnetic nanoparticles immunoplatform, Anal. Chim. Acta 887 (2015) 51–58.
[137] J. Park, X. You, Y. Jang, Y. Nam, M.J. Kim, N.K. Min, J.J. Pak, ZnO nanorod matrix based electrochemical immunosensors for sensitivity enhanced detection of *Legionella pneumophila*, Sensors Actuators B Chem. 200 (2014) 173–180.
[138] A.M. Foudeh, J.T. Daoud, S.P. Faucher, T. Veres, M. Tabrizian, Sub-femtomole detection of 16s rRNA from *Legionella pneumophila* using surface plasmon resonance imaging, Biosens. Bioelectron. 52 (2014) 129–135.
[139] V. Rai, Y.T. Nyine, H.C. Hapuarachchi, H.M. Yap, L.C. Ng, C.-S. Toh, Electrochemically amplified molecular beacon biosensor for ultrasensitive DNA sequence-specific detection of *Legionella* sp, Biosens. Bioelectron. 32 (1) (2012) 133–140.
[140] V. Rai, J. Deng, C.-S. Toh, Electrochemical nanoporous alumina membrane-based label-free DNA biosensor for the detection of *Legionella* sp, Talanta 98 (2012) 112–117.
[141] M. Bassetti, A. Vena, A. Croxatto, E. Righi, B. Guery, How to manage *Pseudomonas aeruginosa* infections, Drugs Context 7 (2018) 212527.
[142] J. Hu, F. Kaiyu, P.W. Bohn, Whole-cell *Pseudomonas aeruginosa* localized surface plasmon resonance aptasensor, Anal. Chem. 90 (3) (2018) 2326–2332.
[143] Y. Tang, J. Zou, C. Ma, Z. Ali, Z. Li, X. Li, N. Ma, et al., Highly sensitive and rapid detection of *Pseudomonas aeruginosa* based on magnetic enrichment and magnetic separation, Theranostics 3 (2) (2013) 85.
[144] R. Jindal, K. Handa, Hexavalent chromium-induced toxic effects on the antioxidant levels, histopathological alterations and expression of Nrf2 and MT2 genes in the branchial tissue of *Ctenopharyngodon idellus*, Chemosphere 230 (2019) 144–156.
[145] J. Liang, H. Liu, C. Lan, F. Qiangqiang, C. Huang, Z. Luo, T. Jiang, Y. Tang, Silver nanoparticle enhanced Raman scattering-based lateral flow immunoassays for ultra-sensitive detection of the heavy metal chromium, Nanotechnology 25 (49) (2014) 495501.
[146] X. Liu, J.-J. Xiang, Y. Tang, X.-L. Zhang, F. Qiang-Qiang, J.-H. Zou, Y.H. Lin, Colloidal gold nanoparticle probe-based immunochromatographic assay for the rapid detection of chromium ions in water and serum samples, Anal. Chim. Acta 745 (2012) 99–105.
[147] A. Rocha, K. Trujillo, Neurotoxicity of low-level lead exposure: history, mechanisms of action, and behavioral effects in humans and preclinical models, Neurotoxicology 73 (2019) 58–80.
[148] S. Tang, P. Tong, H. Li, J. Tang, L. Zhang, Ultrasensitive electrochemical detection of Pb^{2+} based on rolling circle amplification and quantum dots tagging, Biosens. Bioelectron. 42 (2013) 608–611.
[149] K.L. Brenneman, S. Poduri, M.A. Stroscio, M. Dutta, Optical detection of lead (II) ions using DNA-based nanosensor, IEEE Sensors J. 13 (5) (2013) 1783–1786.
[150] Z.S. Qian, X.Y. Shan, L.J. Chai, J.R. Chen, H. Feng, A fluorescent nanosensor based on graphene quantum dots–aptamer probe and graphene oxide platform for detection of lead (II) ion, Biosens. Bioelectron. 68 (2015) 225–231.
[151] A.G. Memon, X. Zhou, Y. Xing, R. Wang, L. Liu, M. Khan, M. He, Label-free colorimetric nanosensor with improved sensitivity for Pb^{2+} in water by using a truncated 8–17 DNAzyme, Front. Environ. Sci. Eng. 13 (1) (2019) 12.
[152] M.R. Rahimzadeh, M.R. Rahimzadeh, S. Kazemi, A.-a. Moghadamnia, Cadmium toxicity and treatment: an update, Caspian J. Intern. Med. 8 (3) (2017) 135.

[153] L. Li, L. Liao, Y. Ding, H. Zeng, Dithizone-etched CdTe nanoparticles-based fluorescence sensor for the off–on detection of cadmium ion in aqueous media, RSC Adv. 7 (17) (2017) 10361–10368.
[154] R. Gui, X. An, S. Hongjuan, W. Shen, Z. Chen, X. Wang, A near-infrared-emitting CdTe/CdS core/shell quantum dots-based OFF–ON fluorescence sensor for highly selective and sensitive detection of Cd^{2+}, Talanta 94 (2012) 257–262.
[155] R. Gui, X. An, W. Huang, An improved method for ratiometric fluorescence detection of pH and Cd^{2+} using fluorescein isothiocyanate–quantum dots conjugates, Anal. Chim. Acta 767 (2013) 134–140.
[156] L. Xu, J. Liang, Y. Wang, S. Ren, J. Wu, H. Zhou, Z. Gao, Highly selective, aptamer-based, ultrasensitive nanogold colorimetric smartphone readout for detection of Cd (II), Molecules 24 (15) (2019) 2745.
[157] R.B. Kanarek, R. Marks-Kaufman, Heavy metals, nutrition, and behavior, in: Nutrition and Behavior, Springer, Boston, MA, 1991, pp. 102–130.
[158] L.R. Pokhrel, N. Ettore, Z.L. Jacobs, A. Zarr, M.H. Weir, P.R. Scheuerman, S.R. Kanel, B. Dubey, Novel carbon nanotube (CNT)-based ultrasensitive sensors for trace mercury (II) detection in water: a review, Sci. Total Environ. 574 (2017) 1379–1388.
[159] M. Liu, Z. Wang, S. Zong, H. Chen, D. Zhu, L. Wu, G. Hu, Y. Cui, SERS detection and removal of mercury (II)/silver (I) using oligonucleotide-functionalized core/shell magnetic silica sphere@ Au nanoparticles, ACS Appl. Mater. Interfaces 6 (10) (2014) 7371–7379.
[160] Y. Miyake, H. Togashi, M. Tashiro, H. Yamaguchi, S. Oda, M. Kudo, Y. Tanaka, et al., Mercury(II)-mediated formation of thymine− Hg(II)− thymine base pairs in DNA duplexes, J. Am. Chem. Soc. 128 (7) (2006) 2172–2173.
[161] A. Alam, A. Ravindran, P. Chandran, S. Sudheer Khan, Highly selective colorimetric detection and estimation of Hg^{2+} at nano-molar concentration by silver nanoparticles in the presence of glutathione, Spectrochim. Acta A Mol. Biomol. Spectrosc. 137 (2015) 503–508.
[162] W. Chansuvarn, T. Tuntulani, A. Imyim, Colorimetric detection of mercury (II) based on gold nanoparticles, fluorescent gold nanoclusters and other gold-based nanomaterials, TrAC Trends Anal. Chem. 65 (2015) 83–96.
[163] Y.-R. Kim, R.K. Mahajan, J.S. Kim, H. Kim, Highly sensitive gold nanoparticle-based colorimetric sensing of mercury (II) through simple ligand exchange reaction in aqueous media, ACS Appl. Mater. Interfaces 2 (1) (2009) 292–295.
[164] X. Yang, H. Liu, J. Xu, X. Tang, H. He, D. Tian, A simple and cost-effective sensing strategy of mercury (II) based on analyte-inhibited aggregation of gold nanoparticles, Nanotechnology 22 (27) (2011) 275503.
[165] C.-C. Huang, H.-T. Chang, Selective gold-nanoparticle-based "turn-on" fluorescent sensors for detection of mercury (II) in aqueous solution, Anal. Chem. 78 (24) (2006) 8332–8338.
[166] Y. Zhang, S. Guo, Z. Jiang, G. Mao, X. Ji, Z. He, Rox-DNA functionalized silicon nanodots for ratiometric detection of mercury ions in live cells, Anal. Chem. 90 (16) (2018) 9796–9804.
[167] A.V.R.K. Rao, R.B. Reddy, S. Sengupta, V. Chelvam, Efficient "turn-on" nanosensor by dual emission-quenching mechanism of functionalized Se doped ZnO nanorods for mercury (II) detection, Appl. Nanosci. 8 (8) (2018) 1973–1987.
[168] S. Satapathi, V. Kumar, M.K. Chini, R. Bera, K.K. Halder, A. Patra, Highly sensitive detection and removal of mercury ion using a multimodal nanosensor, Nano-Struct. Nano-Object. 16 (2018) 120–126.
[169] W. Xiao, M. Xiao, F. Qiangqiang, S. Yu, H. Shen, H. Bian, Y. Tang, A portable smart-phone readout device for the detection of mercury contamination based on an aptamer-assay nanosensor, Sensors 16 (11) (2016) 1871.
[170] Y. Wei, W. Zhou, Y. Xu, Y. Xiang, R. Yuan, Y. Chai, Graphene nanosensor for highly sensitive fluorescence turn-on detection of Hg^{2+} based on target recycling amplification, RSC Adv. 4 (73) (2014) 39082–39086.
[171] Q. Fu, Z. Wu, D. Dan, C. Zhu, Y. Lin, Y. Tang, Versatile barometer biosensor based on Au@ Pt core/shell nanoparticle probe, ACS Sens. 2 (6) (2017) 789–795.
[172] A. Verdian, Apta-nanosensors for detection and quantitative determination of acetamiprid—a pesticide residue in food and environment, Talanta 176 (2018) 456–464.

[173] E. Yılmaz, E. Özgür, N. Bereli, D. Türkmen, A. Denizli, Plastic antibody based surface plasmon resonance nanosensors for selective atrazine detection, Mater. Sci. Eng. C 73 (2017) 603–610.
[174] A. Singh, Y. Joshi, M.P. Singh, K. Arora, Anti-atrazine functionalized gold nano structures for environmental monitoring, Biosens. J. 3 (1) (2013) 105.
[175] R. Shoji, T. Takeuchi, I. Kubo, Atrazine sensor based on molecularly imprinted polymer-modified gold electrode, Anal. Chem. 75 (18) (2003) 4882–4886.
[176] S. Yang, T. Wu, X. Zhao, X. Li, W. Tan, The optical property of core-shell nanosensors and detection of atrazine based on localized surface plasmon resonance (LSPR) sensing, Sensors 14 (7) (2014) 13273–13284.
[177] S.K. Bhardwaj, N. Bhardwaj, G.C. Mohanta, P. Kumar, A.L. Sharma, K.-H. Kim, A. Deep, Immunosensing of atrazine with antibody-functionalized Cu-MOF conducting thin films, ACS Appl. Mater. Interfaces 7 (47) (2015) 26124–26130.
[178] S.K. Bhardwaj, A.L. Sharma, K.-H. Kim, A. Deep, Antibody conjugated glycine doped polyaniline nanofilms as efficient biosensor for atrazine, Mater. Res. Express 4 (12) (2017) 125022.
[179] N. Simon-Delso, V. Amaral-Rogers, L.P. Belzunces, J.-M. Bonmatin, M. Chagnon, C. Downs, L. Furlan, et al., Systemic insecticides (neonicotinoids and fipronil): trends, uses, mode of action and metabolites, Environ. Sci. Pollut. Res. 22 (1) (2015) 5–34.
[180] S. Wang, Y. Liu, S. Jiao, Y. Zhao, Y. Guo, M. Wang, G. Zhu, Quantum-dot-based lateral flow immunoassay for detection of neonicotinoid residues in tea leaves, J. Agric. Food Chem. 65 (46) (2017) 10107–10114.
[181] P. Weerathunge, R. Ramanathan, R. Shukla, T.K. Sharma, V. Bansal, Aptamer-controlled reversible inhibition of gold nanozyme activity for pesticide sensing, Anal. Chem. 86 (24) (2014) 11937–11941.
[182] V. Urbanová, A. Bakandritsos, P. Jakubec, T. Szambó, R. Zbořil, A facile graphene oxide based sensor for electrochemical detection of neonicotinoids, Biosens. Bioelectron. 89 (2017) 532–537.
[183] M. Zhang, H.T. Zhao, X. Yang, A.J. Dong, H. Zhang, J. Wang, G.Y. Liu, X.C. Zhai, A simple and sensitive electrochemical sensor for new neonicotinoid insecticide Paichongding in grain samples based on β-cyclodextrin-graphene modified glassy carbon electrode, Sensors Actuators B Chem. 229 (2016) 190–199.
[184] H. Li, Y. Li, J. Cheng, Molecularly imprinted silica nanospheres embedded CdSe quantum dots for highly selective and sensitive optosensing of pyrethroids, Chem. Mater. 22 (8) (2010) 2451–2457.
[185] X. Li, H.F. Jiao, X.Z. Shi, A. Sun, X. Wang, J. Chai, et al., Development and application of a novel fluorescent nanosensor based on FeSe quantum dots embedded silica molecularly imprinted polymer for the rapid optosensing of cyfluthrin, Biosens. Bioelectron. 99 (2018) 268–273.
[186] T. Ye, W. Yin, N. Zhu, M. Yuan, H. Cao, J. Yu, Z. Gou, et al., Colorimetric detection of pyrethroid metabolite by using surface molecularly imprinted polymer, Sensors Actuators B Chem. 254 (2018) 417–423.
[187] M.S. Forde, L. Robertson, E.A. Laouan Sidi, S. Côté, E. Gaudreau, O. Drescher, P. Ayotte, Evaluation of exposure to organophosphate, carbamate, phenoxy acid, and chlorophenol pesticides in pregnant women from 10 Caribbean countries, Environ Sci Process Impacts 17 (9) (2015) 1661–1671.
[188] R.K. Mishra, L.J. Hubble, A. Martín, R. Kumar, A. Barfidokht, J. Kim, M.M. Musameh, I.L. Kyratzis, J. Wang, Wearable flexible and stretchable glove biosensor for on-site detection of organophosphorus chemical threats, ACS Sens. 2 (4) (2017) 553–561.
[189] H.-F. Cui, W.-W. Wu, M.-M. Li, X. Song, Y. Lv, T.-T. Zhang, A highly stable acetylcholinesterase biosensor based on chitosan-TiO_2-graphene nanocomposites for detection of organophosphate pesticides, Biosens. Bioelectron. 99 (2018) 223–229.
[190] G. Liu, Y. Lin, Electrochemical sensor for organophosphate pesticides and nerve agents using zirconia nanoparticles as selective sorbents, Anal. Chem. 77 (18) (2005) 5894–5901.
[191] L. Guerrini, A.E. Aliaga, J. Carcamo, J.S. Gómez-Jeria, S. Sanchez-Cortes, M.M. Campos-Vallette, J.V. Garcia-Ramos, Functionalization of Ag nanoparticles with the bis-acridinium lucigenin as a chemical assembler in the detection of persistent organic pollutants by surface-enhanced Raman scattering, Anal. Chim. Acta 624 (2) (2008) 286–293.
[192] J. Kubackova, G. Fabriciova, P. Miskovsky, D. Jancura, S. Sanchez-Cortes, Sensitive surface-enhanced Raman spectroscopy (SERS) detection of organochlorine pesticides by alkyl dithiol-functionalized metal nanoparticles-induced plasmonic hot spots, Anal. Chem. 87 (1) (2015) 663–669.

CHAPTER 4

Applications and success of MIPs in optical-based nanosensors

Ramchander Chepyala

FPC@DCU – Fraunhofer Project Centre for Embedded Bioanalytical Systems at Dublin City University, Dublin City University, Dublin, Ireland

4.1 Introduction

A biosensor is defined as a device containing a biological sensing element and a transduction unit to produce an electrochemical, optical, mass, or other type of signal in proportion to the quantitative information on the analyte of interest in a given sample. Traditionally, these sensing devices have been classified based on their signal transduction mechanisms; for example, a sensor is called electrochemical if the output is an electrical signal, and it is called optical if the readout is based on an optical output like absorption, fluorescence, and so forth. Recently, interest has grown throughout the research community as well as the commercial sector in the unprecedented applications of various sensing devices in food and agriculture, medical diagnostics, biological threat detection, forensics, and environmental monitoring. Conventionally, to meet the desired requirements of a biosensor, natural receptors such as antibodies and enzymes have been used extensively as the capture and detection molecules. Although there have been significant technological and commercial developments of sensing devices based on these natural receptors, their usage in many other fields is limited due to their intrinsic nature. The natural receptors suffer from serious limitations, such as denaturation, inability to withstand high temperatures, requirements for optimal pH conditions, and challenges in immobilization, among others. Therefore, to circumvent these limitations and to broaden the scope of biosensors for their utilization in harsh field conditions across the domains, there is an urgent need to find alternative solutions. Hence, over the past several years research has been accelerating towards developing artificial receptors by molecular imprinting polymer (MIP) technology, in order to overcome the limitations posed by natural receptors.

Molecularly imprinted polymers (MIPs) are synthetic analogs to the natural biological antibody-antigen systems, selectively developed using various polymeric materials for specific

Nanofabrication for Smart Nanosensor Applications. https://doi.org/10.1016/B978-0-12-820702-4.00004-0
© 2020 Elsevier Inc. All rights reserved.

molecular recognition sites, which are created during the polymerization process with selective molecular templates (e.g., molecules, ions, atoms, and microorganisms) [1–5]. Similar to natural antibody-antigen systems, these MIPs operate by a "lock and key" mechanism to bind to the molecules present on the template during the production process [1]. Owing to the qualities of the MIPs, such as high selectivity and affinity towards the target molecules, MIPs have found applications in separation science [2, 6, 7], enzyme catalysis [8], chemosensing [9], drug delivery, and diagnostics. Further, in contrast to the biological counterparts (i.e., proteins, nucleic acids, cells, miRNAs, and metabolites), MIPs have inherent properties such as higher physical strength, robustness, and capacity to withstand various conditions. In addition, MIPs can be tuned to obtain desired properties, such as compressible and tensile properties along with required strength, softness, and porosity. Moreover, the resistance to elevated temperatures and pressures along with inertness to acids, bases, metal ions, and organic solvents all combine to make these MIPs a most attractive alternative to the natural receptors. Apart from that, their easy and cost-effective synthesis methods, longer shelf life, and tunability to heating, cooling, and varying pH conditions make them versatile materials. Moreover, electrical stimulation of MIPs to obtain desired properties as well as their higher stability over natural biomolecules makes them as the most attractive material for multitude of applications.

There are multiple production methods for preparing MIPs, ranging from simple synthesis methods to advanced surface stamping techniques. Further, the generation of receptors via the MIP method for a specified target is much simpler and faster compared to the generation of biomolecules (e.g., antibodies) by animal models. As shown in Fig. 4.1, the majority of MIPs production methods consist broadly of three basic steps. The first step involves the synthesis of a polymer as a template or target molecule, which binds (i.e., covalently or noncovalently) to the functional group of the polymer host. In the second step, the template molecule is removed from the host polymer to leave the target-specific empty cavity for rebinding the target molecule. In the third step, the resulting MIP is exposed to the sample containing the target for selective rebinding from the complex sample system. Despite the increased significance of MIPs in sensing applications utilizing various detection methods such as electrochemical, gravimetric, magnetic, and mechanical techniques, their use with optical-based detection methods has not been widely explored. Therefore, this review

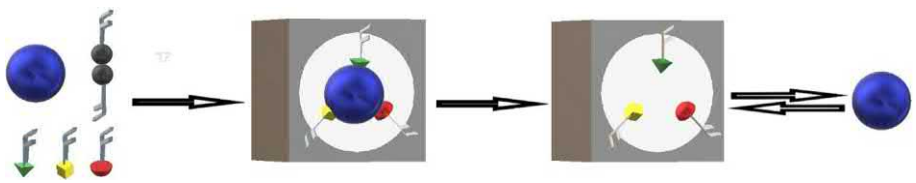

Fig. 4.1

Schematic showing a general procedure for making molecularly imprinted polymers. *Adapted from R. Li, Y. Feng, G. Pan, L. Liu, Advances in molecularly imprinting technology for bioanalytical applications, Sensors (Switzerland) 19 (177) (2019) 177, under the Creative Commons Attribution License, 2019.*

highlights the importance and applications of MIPs using optical-based nanosensing methods for detection of analytes in various domains. This chapter in general presents a broader critical overview of the past and future trends in usage of MIPs with optical sensing methods. In particular, by introducing the general synthesis methods of MIPs, an in-depth discussion and analysis are presented of their applications in detecting various analytes by means of optical nanosensing systems in the domain of immuno-diagnostics, pharmaceuticals, and food and environment samples. In addition, a critical analysis is presented by emphasizing the serious challenges that must be addressed in order to develop MIPs for a wide range of applications. Finally, appropriate critiques are made and the outlook for future developments of MIPs for optical sensing applications is presented.

4.2 MIPs synthesis methods

The process of synthesizing a highly cross-linked network of polymers, capable of selective molecular recognition, is known as molecular imprinting (Fig. 4.1). This process primarily involves three basic steps: self-assembly and polymer curing, template removal, and rebinding. The parameters that play a critical role in preparation of MIPs are stronger reversible binding affinity of the monomer to the imprint molecule and the ability to fixate in the polymer matrix. In addition, the choice of the polymer depends on the complementary functional groups to those present on the template, nature of their reversibility, and the porosity of the polymer to allow the removal and rebinding of template. So far, several synthesis strategies have been developed for preparation of MIPs, and the basic principle is to consider different kinds of interactions between templates and functional monomers in the binding site and during the template rebinding. Based on this, one can categorize MIPs synthesis methods broadly into three categories [1]. The first is synthesis from monomers in the presence of a template [10] (Fig. 4.2); the second is phase inversion using polymer precipitation by addition of incompatible solvent or by evaporation of solvent from the networked solution [11, 12]; and the third is soft lithography or a surface stamping method. Based on the interactions between the template and functional monomer, the imprinting process can be further classified into (a) covalent imprinting (Fig. 4.3), (b) noncovalent imprinting (Fig. 4.3), (c) semicovalent imprinting, and (d) ion imprinting [11, 12]. The phase inversion precipitation polymerization is usually carried out by addition of an incompatible solvent to the original polymer mixture or by causing the solvent to evaporate from the networked solution [13, 14]. In this broad phase inversion method, the MIPs are usually prepared by free radical polymerization in which raw materials based on alkenyl groups are typically used. Other methods that can serve the purpose are bulk polymerization, in-situ polymerization, emulsion polymerization, suspension polymerization, and precipitation polymerization [15, 16]. Under the soft lithography or surface stamping method, various other strategies have been developed, such as solid-phase imprinting, localized photo-polymerization, nanoprecipitation imprinting, self-assembly imprinting, and monomolecular imprinting methods. In addition, other methods based on nonfree radical

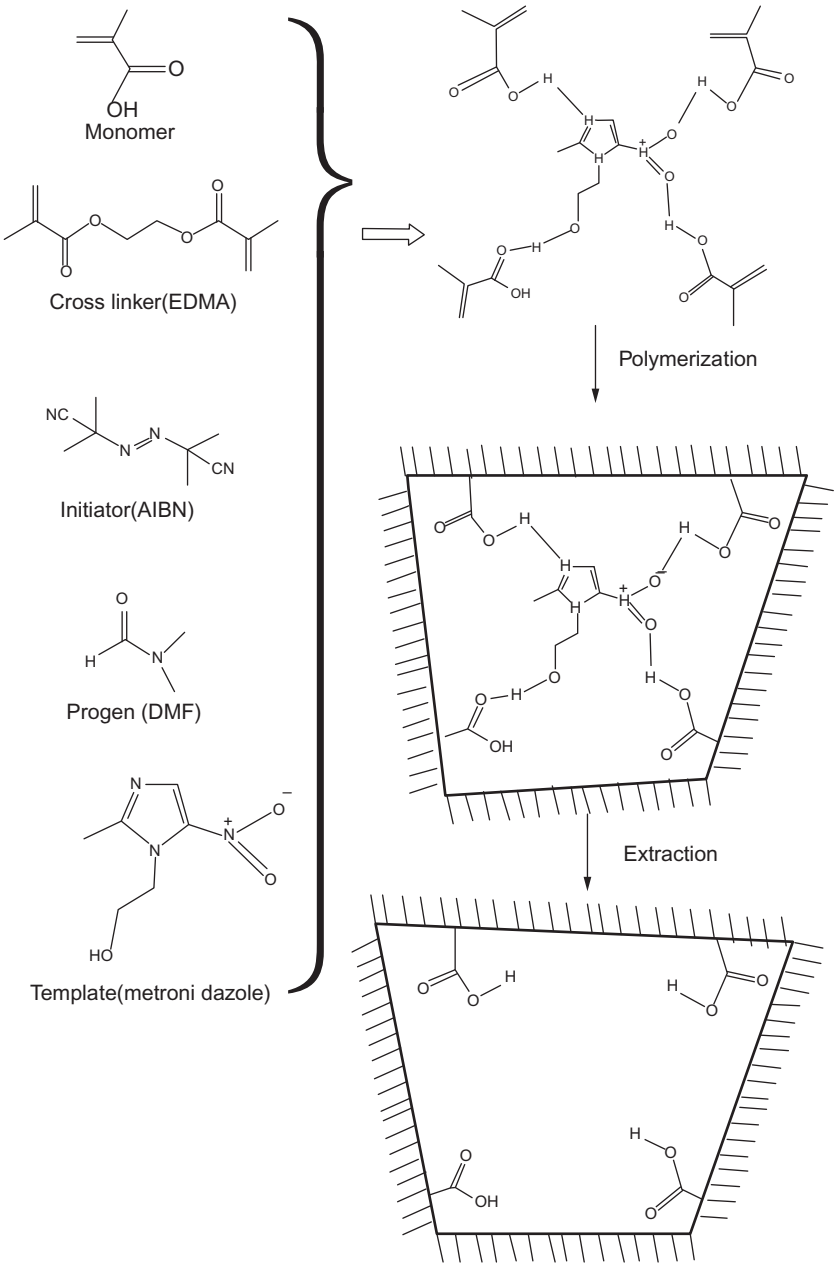

Fig. 4.2

Schematic showing the production of MIPs via the template-monomer method. *Reproduced from M.T. Jafari, B. Rezaei, B. Zaker, Ion mobility spectrometry as a detector for molecular imprinted polymer separation and metronidazole determination in pharmaceutical and human serum samples, Anal. Chem. 81 (9) (2009) 3585–3591, Copyright 2019, with permission from American Chemical Society.*

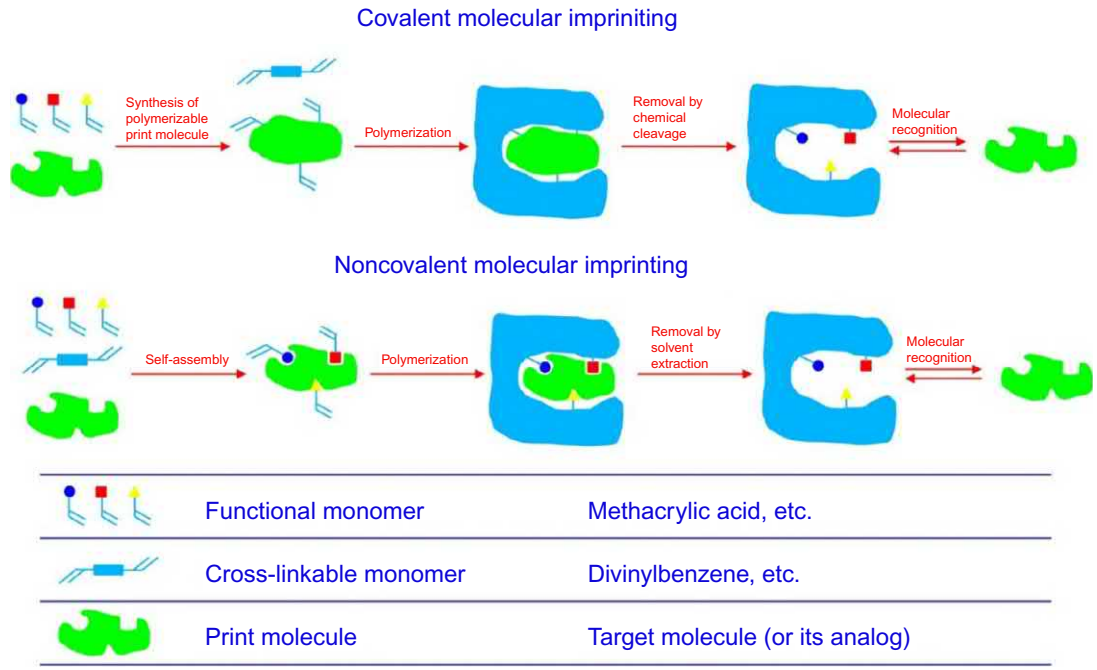

Fig. 4.3

Schematic showing the covalent and noncovalent imprinting method for MIPs. *Reproduced from M. Yoshikawa, K. Tharpa, Ş.-O. Dima, Molecularly imprinted membranes: past, present, and future, Chem. Rev. 116 (19) (2016) 11500–11528, Copyright 2019, with permission from American Chemical Society.*

polymerization methods, such as sol-gel processes, are used for preparing MIPs. Interestingly, in a sol-gel method, green solvents such as ethanol and DI water are primarily used for preparation of nanoMIPs, unlike toluene, chloroform, and acetonitrile, which are often used in free radical polymerization. In addition, methods based on nonradical polymerization also include synthesis of MIPs through polymer-based assembly, using either chemical polymers or natural polymers or by using hydrophilic resins (e.g., phenols, aldehydes, amines) [17]. Similarly, with the increasing interest in synthesizing novel functional materials, various types of synthetic strategies for MIPs, including nonfree radical techniques, have emerged to address future needs. Therefore, instead of presenting numerous elaborate process methods for synthesizing MIPs, three basic strategies are briefly introduced here, for greater ease of understanding.

4.2.1 Synthesis from monomers in the presence of the template

Synthesis of MIPs through the template-monomer method is a general production method involving an interaction between the functional monomer in solution/porogen with the target molecule via covalent, noncovalent, or metal coordination interactions with the target molecule

under the participation of cross-linked and initiator to form a template-monomer complex during the polymerization process. After dissolving the template, a three-dimensional matrix with specific sites complementary to the functional groups of the template results. There are various kinds of functional monomers [17], including acrylamide, methyl methacrylate (MMA), methacrylic acid (MAA), aniline, pyrrole and 2-acrylamido-2-methylpropanesulfonic acid (AMPS), alkenyl glycosides glucose (AGG), and 2-hydroxyethyl methacrylate (HEMA) [18], that have been used. Additionally, cross-linking agents such as dimethacrylate (EGDMA), ethylene glycol, *N*,*N*-methylene diacrylamide, dimethyl ether, ethylene glycol dimethacrylate (EGDMA), along with initiators such as 2,2-azoisobutyronitrile (AIBN) were mixed in required proportions, followed by either UV irradiation or a thermally driven polymerization reaction. The resulting polymerization reaction was initiated to obtain the MIPs either in powder or film form by coating a suitable substrate material. Fig. 4.2 shows the detailed synthesis procedures for the production of MIPs using methacrylic acid (MAA) as functional monomer and metronidazole as template, as MAA is known to establish selective hydrogen bonding with metronidazole. The reaction mixture in the molar ratio of 1:5:25 template-monomer-cross-linker, respectively, was prepared with template (metronidazole), functional monomer (MAA), the cross-linker (EGDMA) and AIBN initiator, dissolved in dimethylformamide (DMF) which is a porogen. The reaction mixture was then deoxygenated followed by polymerization at 60°C for 24 h, and then the resulting polymer was ground in a mortar and sieved mechanically for obtaining <200 μm particles, and this was followed by applying a Soxhlet extraction to separate the analyst from the polymer to result in MIP particles.

Within the template-monomer method, the MIPs can be synthesized via covalent or noncovalent molecular imprinting schemes, as shown in Fig. 4.3. As explained earlier, the choice of an appropriate monomer with functional moieties to form the desired molecular interactions with the template is highly desirable in addition to the suitable cross-linker, initiator for successful synthesis of stable and high affinity functional MIPs. In the case of a noncovalent molecular imprinting approach, all steps remain the same except the interaction forces between the monomer and template during the imprinting and the target molecular recognition, which is due to noncovalent forces such as hydrogen bonding, van der Waals forces, π-π stacking/hydrophobic interactions, and even electrostatic interactions [19, 20].

4.2.2 Production of MIPs by phase inversion using polymer precipitation

The phase inversion method has been developed to improve the homogeneity of the binding sites in MIPs, which may be hindered due to the usage of the cross-linker in the previous method. In this method, a solvent is compatible with the monomer and with the template usually applied to dissolve the polymer. After the formation of a monomer-template complex, to lead the precipitation of the monomer-template complex a nonsolvent is added, or the solvent is usually allowed to evaporate either in bulk or after casting on to the substrate material. This

particular method has been developed to address the drawbacks rendered by using the cross-linker in the synthesis process, to avoid a resulting rigid polymer, which further complicates removal of the template. Additionally, the resulting polymer obtained from the synthesis method needs to be ground into fine particles, followed by sieving for extraction of the template. The downside of this process is that there is a high possibility of the binding sites being buried in the packed state, thereby reducing the effectivity of the MIPs. Moreover, the grinding process results in irregular cracking of the binding sites, leading to poor selectivity of the MIPs in the end application. Therefore, as an alternative to these mentioned synthesis methods, the phase inversion method became popular among the research community for preparation of MIPs. The schematic (Fig. 4.4) shows the detailed process steps for the preparation of MIPs through the phase inversion method after a sol-gel process.

As shown in Fig. 4.4, the phase inversion method involves the preparation of sol-gel particles by mixing triethoxy orthosilicate (TEOS) and 3-(trimethoxysilyl) propyl methacrylate (MPS) in ethanol and tetrahydrofuran (THF) with NH_4OH in required molar ratios [21, 22]. The resulting wetted sol-gel particles are dispersed in a mixture of dioxane, styrene/acrylic acid, and azo-bis-isobutyronitrile (AIBN). After degassing and polymerization at 80°C, the polymer composite grafted sol-gel particles were obtained. Here, 4-Ethylaniline (EA) is used as a template to react with the carboxyl groups present on the sol-gel composite by suspending the

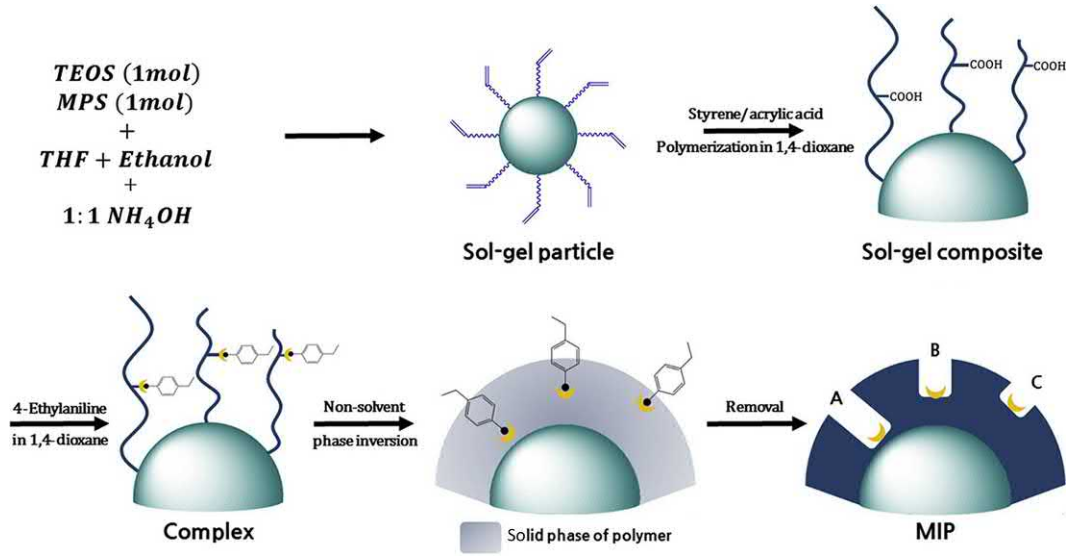

Fig. 4.4

Schematic showing the detailed process steps for the preparation of MIPs by the phase inversion process. *Reproduced from H.M. Lee, S.G. Lee, H.R. Park, S.H. Chough, Sorption behaviors and relation between selectivity and possible cavity shapes of the molecularly imprinted materials, Microporous Mesoporous Mater. 251 (2017) 42–50, Copyright 2019, with permission from Elsevier.*

composite and EA in the dioxane to form a template-monomer complex. During the phase inversion process, water is added as a nonsolvent for formation of a complex between EA and the movable portion of styrene/acrylic acid. This step leads to the coagulation of the complex surrounded by template molecules by styrene, followed by template removal by HCl to form MIPs.

4.2.3 Soft lithography or surface stamping

Although the previous methods are efficient with respect to various applications, usually larger templates are needed (e.g., bacteria) to work with large molecules. Surface imprinting or soft lithography is preferred over other methods for imprinting MIPs for large molecules. Since MIPs prepared by other methods have smaller pores, penetration of macromolecules and their assemblies into these tiny pores becomes difficult, with a high possibility of being trapped during polymerization [1, 22, 23]. In the surface imprinting process, usually a self-assembled array of the template is deposited onto a stamp and then transferred onto a partially polymerized thin film, followed by allowance for completing the polymerization process. The detailed process steps of the surface imprinting process are shown in Fig. 4.5, in which the MIPs are imprinted to *Escherichia coli* [24] to use as receptors for bacterial detection. Specifically, the MIP host was created by using a commercial epoxy (Epon 1002F) in cyclopentanone. The MIP solution

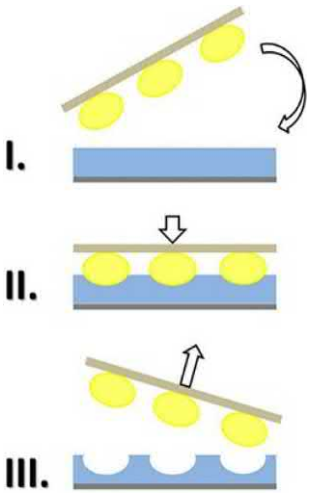

Fig. 4.5

Schematic of soft lithography or surface imprinting method for preparation of MIPs. Step (I) shows the stamp on polymer produced by self-assembly, followed by the step enclosing the stamp for polymerization (II). The final step (III) shows the generation of binding cavities by removal of the stamp. *Reproduced from A.-M. Poller, E. Spieker, P.A. Lieberzeit, C. Preininger, Surface imprints: advantageous application of Ready2use materials for bacterial quartz-crystal microbalance sensors, ACS Appl. Mater. Interfaces 9 (1) (2017) 1129–1135, Copyright 2019, with permission from American Chemical Society.*

was spin coated onto microscopic glass slides, pressing the stamps on coated film, followed by UV curing and baking at 95°C for 10 min. The stamps, which were produced in PDMS, were incubated with an aqueous *E. coli* suspension for 45 min, followed by removal of excess suspension by spin-off and then coating of a glucose layer to serve as a release layer. After the stamps were pressed onto the film, they were lifted off from the imprint cavities and washed to remove remaining bacteria. The imprinted cavities usually match the template in terms of size, shape, and polarity, allowing noncovalent interactions between the polymer and the template, mimicking the interactions between natural antibody-antigen systems [24]. Further, the MIPs imprinted by the surface imprinting method tend to be physically robust due to the presence of the backing solid support, and hence can be effectively used for sensing applications [23].

The choice as to which synthesis strategy is used in the production of MIPs is usually driven by the kind of application being addressed, and hence new methods are constantly emerging to improve on the previous ones. Despite the various methods available for developing MIPs, several factors need to be considered in preparing MIPs. For example, choosing a suitable polymer, template, cross-linker, initiator and porogen, concentration, rate and duration of the polymerization, temperature, pressure, and, most importantly, reaction kinetics are just a few of the factors of interest.

4.3 Characterization studies of MIPs

Usually the polymers used in MIPs are insoluble in various organic and inorganic solvents. Hence, the characterization of these MIPs with traditional techniques is quite challenging. Despite this fact, the chemical, structural, and morphological characteristics of MIPs have been studied by modified sample preparation methods by utilizing analytical techniques such as solid-state NMR, elemental microanalysis, FTIR, and UV-Vis, for obtaining useful information about the polymers. Among all the available methods, FTIR turns out to be a popular method for identifying the pre- and postpolymerization functional groups, and the attachment or formation of new functional groups on the polymer network. By looking for the appearance or disappearance of the functional groups in the polymer and by comparing the polymer and functional group's spectra, one can easily characterize the polymer. The morphological characteristics of MIPs were studied by using light microscopy for verifying the natural integrity of the polymers and their network, along with visualizing the large entities such as beads, ligands, etc. Moreover, scanning electron microscopy (SEM) or atomic force microscopy (AFM) are applied quite often to characterize the internal morphology of the polymers (i.e., the polymer's macropores). The BET (Brunauer, Emmett and Teller) analysis also commonly used to characterize the MIPs for investigating the specific surface area of the polymer, specific pore volume, pore size distribution, along with average diameter of the pore. Usually, nitrogen sorption porosimetry is used for analyzing the smaller pores of the polymers, whereas mercury intrusion porosimetry is used for the larger pores.

The most important property to be characterized in MIPs is the molecular recognition capacity. There are two methods, which are usually applied for evaluating the binding capacity and selectivity. The first method is the batch-binding method and the second is the chromatographic method. In the chromatographic method, the MIPs are used as a stationary phase to provide a quick and easier method for evaluating the binding properties. The Scatchard analysis [25] (Fig. 4.6) is a common method used to characterize the binding and rebinding properties of MIPs. In this procedure, the binding behavior of the MIPs is evaluated with batch binding experiments and the binding data processed with the Scatchard equation. The result from this equation provides the information on noncovalent binding between the functional monomer and the template, which results in a Scatchard plot, as shown in Fig. 4.6. This plot usually contains two straight lines, indicating the heterogeneous affinities of the binding sites. These binding

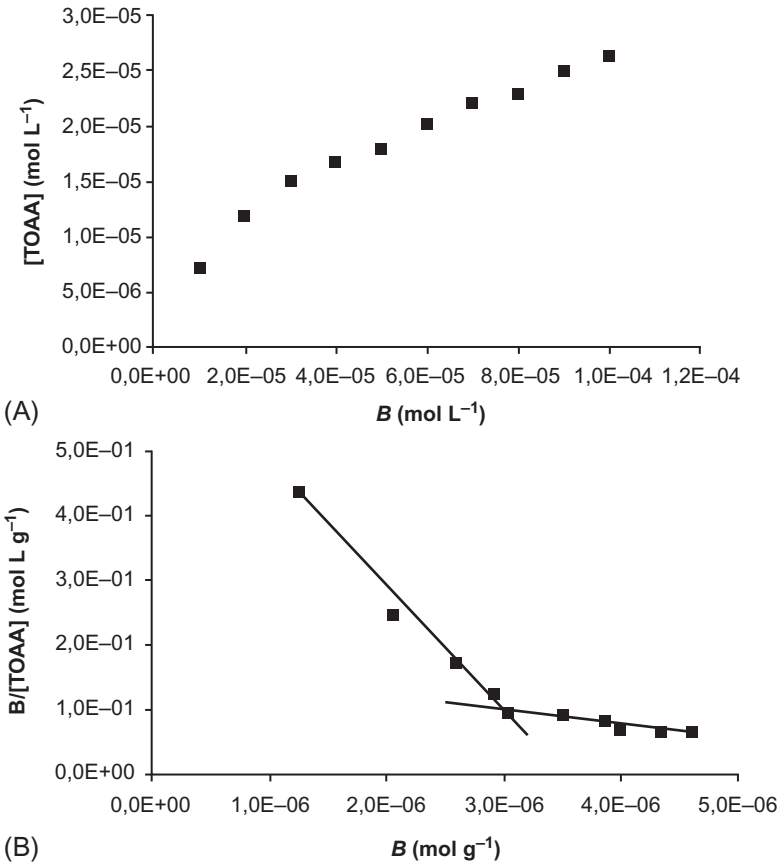

Fig. 4.6

Scatchard plots showing binding isotherm for $PP_{Zn}M$(TOAA) in (A) and Scatchard plot for $PP_{Zn}M$ (TOAA) in (B). *Reproduced from L. Longo, S. Scorrano, G. Vasapollo, RNA nucleoside recognition by phthalocyanine-based molecularly imprinted polymers, J. Polym. Res. 17 (5) (2010) 683–687, Copyright 2019, with permission from Springer Nature.*

properties can be calculated from the plots with corresponding association constants for high and low-affinity binding. Here, in Fig. 4.6, a new class of functional MIPs was prepared by MAA as a functional monomer with a zinc phthalocyanine and ethylene glycol dimethacrylate (EGDMA) as cross-linker and AIBN as an initiator and a tri-*O*-acetyladenosine (TOAA) as a template. Here, UV-Vis spectroscopy was used to study the binding and Scatchard analysis was used for obtaining the batch binding characteristics on the imprinted polymer receptor ($PP_{Zn}M(TOAA)$). As it can be seen from Fig. 4.6A, the curve shows the binding isotherm of the $PP_{Zn}M(TOAA)$ as a function of initial concentration of TOAA and amount of TOAA bound to the polymer. In Fig. 4.6B, the two straight lines indicate the affinities of binding sites in MIPs. These affinities can be estimated, as mentioned earlier, with corresponding association constants in the Scatchard equation. This kind of Scatchard analysis is usually carried out for noncovalent binding sites between template and functional monomers within MIPs.

4.4 Application of MIPs in optical nanosensors

MIPs have found several applications in the scientific as well as commercial sectors, ranging from sensors to targeted drug delivery [26], contaminant detection in foods [27], purification, separation of biological and chemical analytes [28], environmental monitoring [29], and diagnostics. However, in this chapter the focus is on applications of MIPs in optical sensors and specifically the state-of-the-art in immunoassay-diagnostics, pharmaceuticals, and drugs, along with applications in food and environmental sensing. MIPs have been specifically tuned to suit various applications ranging from detecting analytes from biological entities to inorganic, metallic entities (e.g., heavy metals). Thus it is difficult to categorize the MIP-based sensors based on their sensitivities. In addition, it is difficult to compare between any two different sensing techniques (e.g., electrochemical, optical, or magnetic). Further, the limit of detection depends on the type of technique used as well as the specific application.

4.4.1 Optical sensor

The sensing devices that use light sources such as infrared, visible, or ultraviolet for probing chemical/biological interactions at solid or liquid interfaces and transduce the resulting outcome as an optical signal are called optical biochemical sensors [30]. These optical sensors are further classified as absorbance, scattering, diffraction, reflectance, refraction, photoluminescence, fluorescence, chemiluminescence, bioluminescence, and plasmon resonance (to probe refractive index), based on the signal transduction mechanisms [31]. In general, any optical sensor consists of four key elements, as illustrated in Fig. 4.7 [31]: the light source; a wavelength selection device (i.e., a filter or monochromator); a substrate/sample cell having an analyte to be detected and where changes in absorbance or emitted light occur due to the interference of light with the analytes; and a detector that is specific to capture the wavelength of interest. Recent advancements in the technological domain have led to

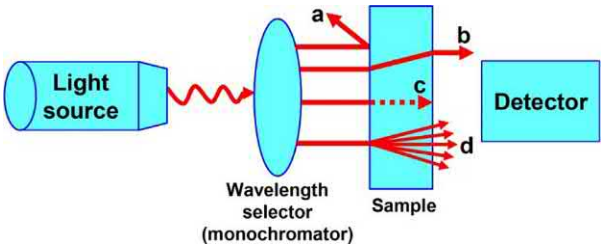

Fig. 4.7

Schematic of an optical spectroscopy sensing system with key elements: (a) reflection, (b) refraction, (c) absorption, and (d) fluorescence emission. *Reproduced from Z. Li, J.R. Askim, K.S. Suslick, The optoelectronic nose: colorimetric and fluorometric sensor arrays, Chem. Rev. 119 (1) (2019) 231–292, Copyright 2019, with permission from American Chemical Society.*

rapid growth of more efficient and integrated optical sensing platforms, such as fiber optic sensors [32, 33], planar wave guides [34], and surface enhanced Raman spectroscopy (SERS) [35]. However, their applicability for MIP-based sensing methods is still in the nascent stages.

4.4.2 Immunoassay/diagnostic applications

4.4.2.1 Cancer diagnosis

Cancer is the term describing the group of diseases involving abnormal growth of cells followed by spreading to other parts of the body beyond their natural boundaries [36]. Early diagnosis of cancers with highly sensitive and specific sensors could lead to timely therapeutic intervention and further improve the lives of patients and result in reduced mortality. Current methods of cancer diagnosis rely on histopathological evaluation of biopsy tissue samples by staining and further evaluation by techniques such as enzyme-linked immunosorbent assay (ELISA), radioimmunoassay, and immunofluorescence along with visual examination of the stained slides with light microscope. Though these techniques quite often are used in tertiary hospital settings, usually they are laborious, time consuming, and require longer waiting times, resulting in failure to provide timely results and making early diagnosis difficult. All these methods are based on detection of specific biomarkers for precise diagnosis of the disease condition. In general, the biomarkers act as an indicator of a normal or a pathogenic biological process in the living organisms and the variation in the concentration of these molecules (e.g., proteins, enzymes, nucleic acids such as miRNA, DNA, mRNA, etc.) in the body is linked to a disease or a particular health condition. Therefore, these biomarkers play a critical role in detecting disease or a condition in early stages for possible therapeutic interventions.

As there are serious limitations of the current detection methods in terms of using natural biomolecules such as antibodies, enzymes, etc., the search for efficient new bio-affinity, high selectivity markers as opposed to natural biomarkers is emerging. It has been demonstrated that MIPs can mimic the biological recognition process for efficient diagnosis of cancers and

these MIPs are used in sensing technologies, and are also called plastic antibodies [37]. Similar to the natural receptors, these synthetic receptors are able to recognize and bind to the target molecules by a "lock and key" mechanism, as mentioned in an earlier section. The detection of the target analyte by the MIPs can be sensed either by a change in the refractive index in the case of SPR, or by a change in the impedance, in the case of electrochemical impedance spectroscopy (EIS), or by a change in the mass by a quartz crystal microbalance (QCM). Most importantly, the polymers of MIPs can also be tuned for generating an optical signal upon the target binding to the imprinting site, even in cases involving molecules/analytes that do not have optical properties [38]. In the following sections, the state-of-the-art methods in which MIPs have been used for detection of various biomarkers are discussed.

The incidence of prostate cancer has increased worldwide, making it the second leading cause of death in men. Early detection helps in reducing the mortality rate [39]. Further, detection of the prostate specific antigen (PSA) biomarker from real samples is crucial for making appropriate clinical decisions for timely therapeutic interventions. Therefore, in this particular direction, the Denizli group [40] developed an SPR-based sensor for detection of PSA by microcontact imprinting, as shown in Fig. 4.8. The PSA protein stamps on the microscopic glass slides were prepared by silane chemistry followed by cross-linking with glutaraldehyde and then PSA, as shown in steps from D–F in Fig. 4.8. The SPR chip was prepared by treating with allyl groups, followed by a polymerization with solution of functional monomer (MAA) and cross-linker (EGDMA) with initiator (AIBN). In addition, it is used for contacting with the protein stamp, followed by initiation of polymerization by exposure under UV light for a specified time (Fig. 4.8B–C) resulting in microcontact-PSA imprinted SPR chips. The PSA-MIP sensor was tested with standard PSA solutions in the concentration range from 0.1–50 ng/mL, where the limit of detection (LOD) was 91 pg/mL and with PSA spiked (concentration 10 ng/mL) human serum samples to test for reliability of the sensor. The selectivity of the sensor was also tested with human serum albumin (HSA) and lysozyme (Lyz) as competitive agents on nonimprinted template proteins PSA. The PSA-MIP sensor was tested with real samples of the prostate cancer patients and results were compared with the standard ELISA. Further, the sensor was tested for its reusability by subjecting it to detection of PSA more than 50 times, with less than 20% standard deviation resulting, demonstrating that this sensor could potentially be used for detection of PSA in clinical samples.

In another study, Zhang et al. [41] developed a fluorescence nanosensor based on molecularly imprinting spatial structure and boronate affinity on CdTe nanocrystals for detection of glycoproteins. These glycoproteins are significant cancer biomarkers and convey information about the physiological state of cells for clinical diagnosis [42]. The recognition performance of the sensor was regulated by controlling the pH and temperature during the detection process. The nanosensor was prepared by coating CdTe nanocrystals with octadecyl-p-vinylbenzyldimethylammonium chloride (OVDAC). In addition, the monomers N-isopropylacrylamide (NIPAAm) and 4-vinylphenylboronic acid (VPBA) were coated onto

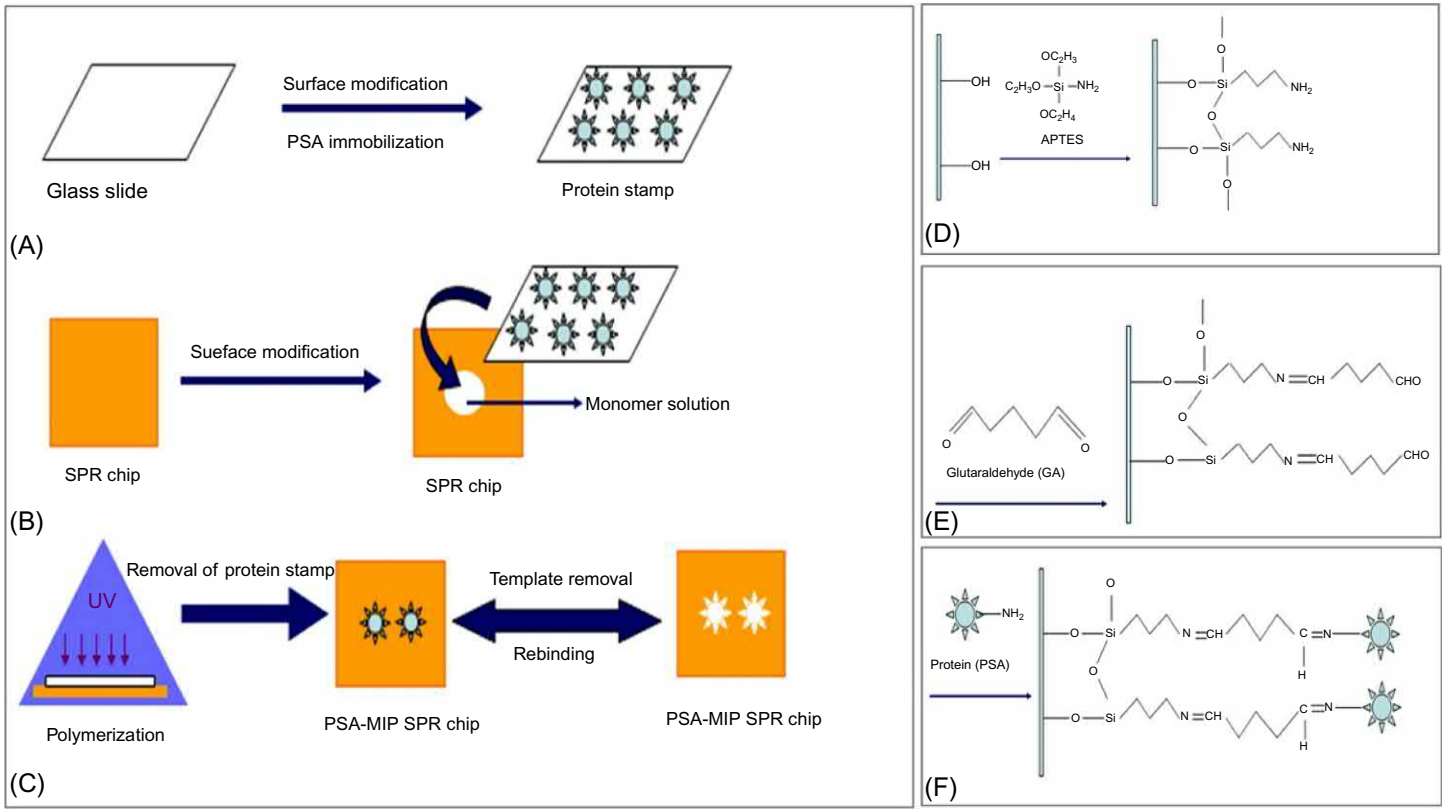

Fig. 4.8

Schematic of microcontact imprinting of PSA onto SRP sensor chip and surface modification of glass slides. Step (A) shows the preparation of glass slides, i.e., protein stamps followed by preparation of SPR chip (B), and microcontact imprinting of PSA by UV polymerization (C). Step (D) shows functionalization of glass slides with APTES followed by cross-linking step (E) and immobilization of PSA (F). *Reproduced from G. Ertürk, H. Özen, M.A. Tümer, B. Mattiasson, A. Denizli, Microcontact imprinting based surface plasmon resonance (SPR) biosensor for real-time and ultrasensitive detection of prostate specific antigen (PSA) from clinical samples, Sensors Actuators B Chem. 224 (2016) 823–832, Copyright 2019, with permission from Elsevier.*

CdTe nanocrystals in the presence of glycoprotein template, followed by polymerization. In this type of nanosensor, the NIPAAm was used as a thermosensitive material, which can swell and shrink with temperatures. In addition, the reversible interaction of VPBA with glycoprotein was regulated by altering the pH values as required. The sensor's performance was tested with a model marker horseradish peroxidase (HRP) and ovalbumin, followed by a fluorescence detection of HRP in biological fluids. The specificity of the nanosensor was tested with a protein solution, demonstrating the sensor's specific affinity adsorption of the target protein in the presence of structurally related proteins. The specificity test resulted in a lower cross-reactivity, showing that the MIP-based nanosensor can detect proteins based on molecular shape rather than size. Interestingly, through this work the authors proved that the selective adsorption of proteins on a MIP nanosensor was due to the synergistic effect of glycosyl groups and molecular imprinting. Finally, the MIP-based nanosensor detected the HRP in human urine samples in the range of 1 to 10 μM with LOD of 1 μM, which clearly indicates the broad applicability of a MIP-based sensor for detection of glycoproteins in biological fluids.

Along the same lines, a liver cancer biomarker a-fetoprotein (AFP) in human serum was demonstrated by Ye et al. [43] with a boronate-affinity sandwich assay (BASA) on MIP-based sensors. In this work, the authors combined the MIPs with SERS for demonstrating a boronate-affinity sandwich assay (BASA) for detection of glycoproteins (e.g., AFP) in complex human serum samples. As shown in Fig. 4.9, the target glycoprotein is bound to the boronate-affinity MIP, followed by labeling with AgNPs (boronate-affinity-functionalized silver nanoparticles (AgNPs)) and detection by SERS. Here, the boronate-affinity MIP array

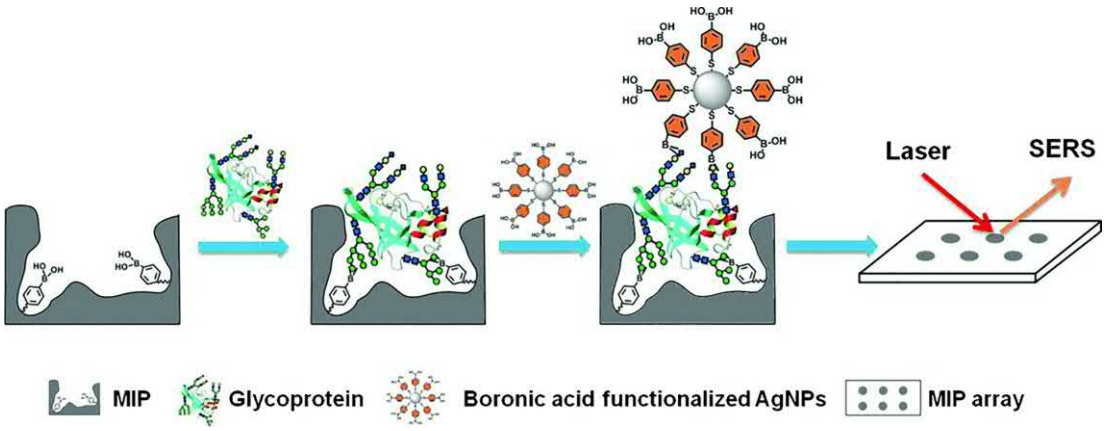

Fig. 4.9

Schematic of the boronate affinity sandwich assay of glycoproteins. *Reproduced from J. Ye, Y. Chen, Z. Liu, A boronate affinity sandwich assay: an appealing alternative to immunoassays for the determination of glycoproteins, Angew. Chemie Int. Ed. 53 (39) (2014) 10386–10389, Copyright 2019, with permission from John Wiley and Sons.*

was prepared by a photolithographic boronate-affinity molecular imprinting method, while the SERS-probe AgNPs were prepared by modifying AgNPs with 4-mercaptophenyl-boronic acid (MPBA). Here, they preferably used boronate-affinity macroporous monolith and it demonstrated a 2.6-fold higher SERS signal compared to the nonporous layer. It was found that the enhanced signal was due to the macroporous monolith-induced secondary Raman scattering in which the macroporous monolith reflected and scattered the laser light, in addition to the normal Raman signal directly from incident laser with almost 35.6% less noise compared to the nonporous layer. The sensor performance was evaluated by a model HRP detection in the concentration range from 0.1 ng/mL to 100 ng/mL, with a detection limit in the range of 1 ng/mL to 10 μg/mL. The cross-reactivity of the HRP-imprinted MIP was tested for different proteins, in which ovalbumin showed 9.7% cross-reactivity, as the HRP and ovalbumin molecular weights are close to each other (44.6 kDa for ovalbumin and 44.2 kDa for HRP), which shows excellent specificity of the boronate affinity MIP sensor. Similarly, when this sensor was subjected to detection of the AFP, it exhibited a linear range of detection from 1 ng/mL to 10 μg/mL with dissociation constant (K_d) value of 0.7 nM, which demonstrates the effectiveness of the sensor and shows that it is a potential method for detection of various biomarkers for diagnostic applications.

Besides biomarker detection, as discussed previously, nanosized MIPs also proving to be very promising for imaging tumor cells, due to nano-MIPs' excellent stability, ease of functionalization, and ease of tunability in different formats and sizes. Therefore, several research groups have demonstrated nano-MIPs for imaging targeted tumor cells. The current practice of cell imaging is based on recognition of specific glycans on the cell surface (e.g., glucuronic acid, sialic acid, fucose, and mannose) [3]. As shown in the schematic (Fig. 4.10), Yin et al. [44] used SERS for imaging and detecting cancer cells on sialic acid-templated MIPs for detection of cancer cells against the normal cells and tissues. In this method, Raman active silver nanoparticles (AgNPs) were prepared as a signal reporting core. Using a boronate affinity-oriented surface imprinting approach, the sialic acid (SA) as template was imprinted onto the thin shell. The SA-imprinted SERS nanotags were then used as a platform for differentiating the tumor cells and tissues from those of normal cells and tissues. The characterization studies showed that the average diameter and thickness of the silica shell SA-imprinted SERS were around 95 nm and 15 nm, respectively. When compared to adsorption isotherms between SA-imprinted and nonimprinted NPs, the SA-imprinted NPs showed higher binding strength towards the template than the nonimprinted NPs with the K_d value of 2.2×10^{-4} M, showing a two orders of magnitude higher binding strength of SA. When SA-imprinted NPs were tested for specificity towards various sugars, they demonstrated an excellent specificity towards the template with cross-reactivity towards monosaccharides of less than 5.6%. Most importantly, this imprinting method was 43% more efficient compared to other methods with greater binding equilibrium within 20 min, with low cytotoxicity of SA-imprinted NPs. This method also demonstrated an excellent

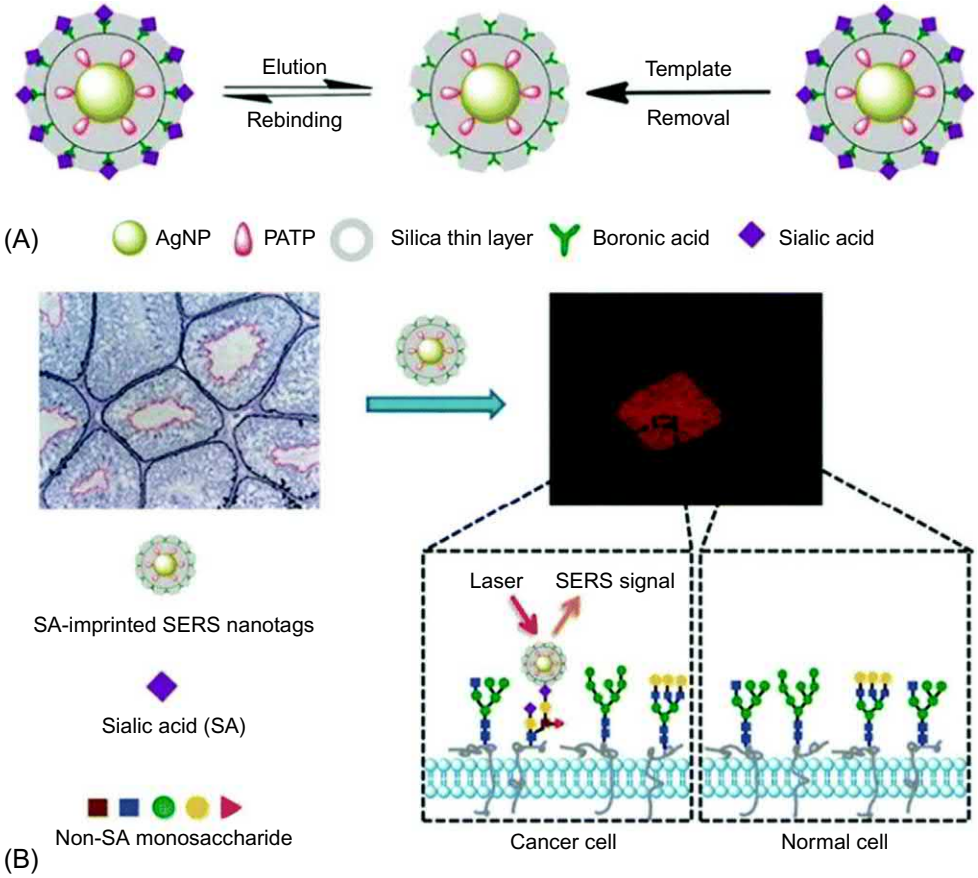

Fig. 4.10

(A) The SA-imprinted Ag@SiO_2SERS nanoparticles. Schematic of SERS imaging of cancer cells and tissues via SA-imprinted nanoparticles (B). *Reproduced from D. Yin et al., Surface-enhanced Raman scattering imaging of cancer cells and tissues via sialic acid-imprinted nanotags, Chem. Commun. 51 (100) (2015) 17696–17699, Copyright 2019, with permission from The Royal Society of Chemistry.*

stability and repeatability of specificity of SA-imprinted NPs. In this method, human hepatoma carcinoma cells (HepG-2) and normal hepatic cells (L-02) were used as model cells for imaging with an intense peak at 1435 cm^{-1} for SERS imaging. The fluorescently labeled lectin was used as positive control for cell imaging and it differentiated the cancer cells from the normal, which confirmed the overexpression of SA on the surface of the cancer cells. Moreover, the authors also demonstrated the imaging and detection of cancer liver tissues using SERS nanotags. Through this work, they demonstrated that the molecularly imprinted SERS nanotags were superior compared to the biomolecules, particularly antibodies. Further, research needs to be undertaken to demonstrate the possibility of extending this technology to detect other types of tumor cells and tissues, which opens up an enormous opportunity for rapid cancer screening and diagnosis.

4.4.3 Applications in detection of pharmaceuticals and drugs

Molecularly imprinted polymer sensors have been developed for detection of various pharmaceuticals and drugs [45–49]. There is a great variation in the type of pharmaceuticals, from antibiotics to nonsteroidal antiinflammatory drugs (e.g., ibuprofen, or anticancer drugs), which have unique properties to treat diseases in humans and animals but also have serious issues with the environment due to their poor biodegradable properties [50–52]. Here, the state-of-the-art technological developments for the detection of key pharmaceuticals and drugs with MIP-based systems are reviewed and discussed.

Conventionally, cocaine abuse and overdose have been diagnosed with complex laboratory procedures; a simple yet effective alternative method for screening these drugs at the point of need is highly desirable. One such method was developed by the Moreda-Piñeiro et al. [49] group using molecularly imprinted polymers with selective functional sites for cocaine on the surface of polyethylene glycol (PEG) modified Mn-doped ZnS quantum dots. The PEG-coated ZnS quantum dots were shown to have lower toxicity, along with having higher fluorescence sensitivity property as compared to other commonly used QDs. Here, the MIPs and QDs showed highest selectivity by fluorescence quenching when only cocaine or its metabolites were present in the samples, but not in the presence of other drugs of abuse such as tetrahydrocannabinol (THC), codeine, or morphine. A lower limit of detection of 250 nM was reported by analyzing the 1:20 diluted human urine samples without any work-up and any standard addition method. The limit of detection was shown to be far better than the prescribed levels to determine cocaine abuse. For analytical comparison, the accuracy of the MIP-based test results were confirmed with the results of the HPLC-MS/MS system. The sensor was reported to provide the results in 15 min with imprinting factor of 23, which shows that this MIP-ZnS QD-based sensor can be used on-site for screening of cocaine drug abuse. Along the same lines, a highly sensitive and selective graphene quantum dots (GQDs) embedded silica molecularly imprinted polymer (SMIP) nanosensor was developed for the detection of nonfluorescent pharmaceutical compound metronidazole (MNZ) in plasma samples [53]. Metronidazole is generally used in the treatment of antianaerobic infections and acne diseases, and due to its low price and high efficiency in treating bacterial infection, it has been illegally used in cosmetic products, causing serious toxic health issues to consumers, and leading to drug resistance [54]. The GQDs-SMIP sensor quenched fluorescently at 365 nm in the presence of metronidazole, showing a linear range of detection from 0.2 μM to 15 μM. The sensor was tested in the plasma samples, where it has shown the lower detection limit of 0.15 μM for metronidazole. The selectivity of the nanosensor was demonstrated in the presence of compounds such as ornidazole (ONZ) and dimetridazole (DMZ), which are analogs to metronidazole in terms of chemical structure. For NIPs (nonimprinted polymers), the fluorescence quenching for all the analogs and MNZ was quite close, signifying highly selective GQD-SMIP sensor. Similarly, the nanosensor also tested for interference ions and was

found to have no effect on the assaying MNZ, further proving high selectivity of the GQD-SMIP sensor, with great potential for analyzing the samples at point of use.

Pharmaceutical compounds such as diclofenac play an important role in treating inflammation and analgesic conditions. However, due to serious matrix effects of the samples in the current detection methods, namely liquid chromatography (LC) and mass spectroscopy (MS), the usage of these methods limits the effective screening of such drugs. In order to address these kinds of challenges, Altintas et al. [55] developed a highly sensitive nanoMIP based SPR based optical sensor for monitoring diclofenac in samples. Fig. 4.11 shows step-by-step details of solid-phase synthesis with the photopolymerization method for preparing the nanoMIPs as well as the detection of diclofenac on a sensor array [55]. The synthesis method was so effective that it resulted in a nanoMIP particle size of 132 nm with low polydispersity index (0.1). After the immobilization of the MIPs on the SPR gold sensor chip via covalent coupling, an affinity based-diclofenac assay was carried out, resulting in the detection of diclofenac in the concentration range of 1.24–80 ng/mL with LOD of 1.2 ng/mL. From kinetic data, the dissociation constant was found to be 1.48×10^{-9} M with the least cross-reactivity against other pharmaceuticals, which clearly suggests that this technique can be applied in field conditions. In another work, Weber et al. [56] developed a nanoMIP-based sensor array for detection of penicillin G (PenG), an antibiotic using an inverse mini-emulsion polymerization

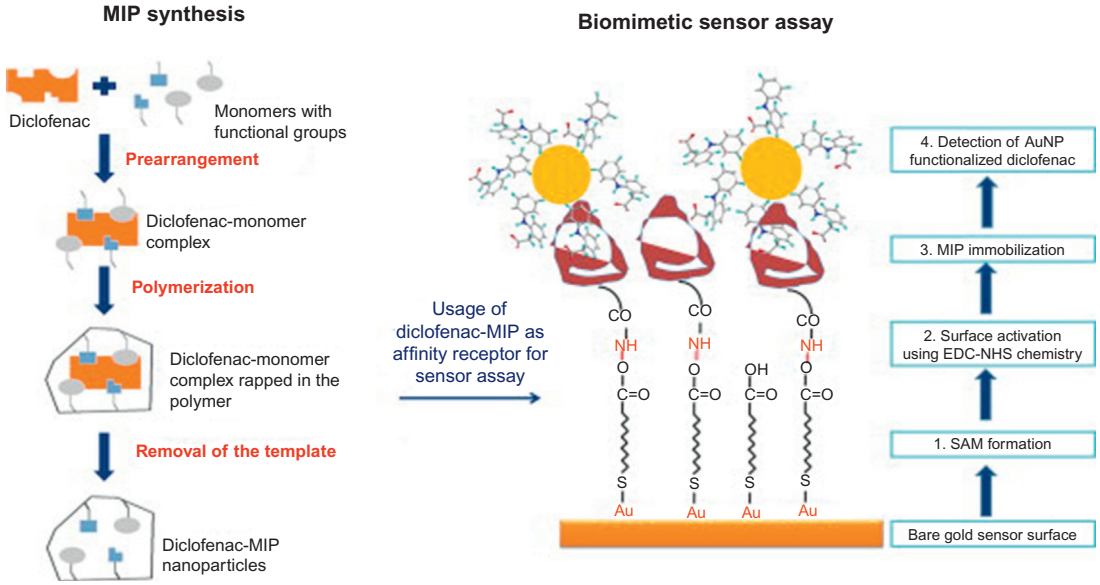

Fig. 4.11

Schematic illustrates the complete process from MIP synthesis to diclofenac sensor assay. *Reproduced from Z. Altintas, A. Guerreiro, S.A. Piletsky, I.E. Tothill, NanoMIP based optical sensor for pharmaceuticals monitoring, Sensors Actuators B Chem. 213 (2015) 305–313, Copyright 2019, with permission from Elsevier.*

method. The functionalized particles with PenG were approximately 400 nm in size with low polydispersity index (0.05). Further, to prepare a sensing layer for the optical sensor setup reflectometric interference spectroscopy (RIfS), the azide modified MIPs were covalently immobilized on alkyne-modified glass transducers by Cu(I) catalyzed 1.3 dipolar cycloaddition. The RIfS system works on the direct optical detection method, in which a white light interferes with the thin sensing layer. The changes in the optical thickness of the sensing layer indicate the effective interaction of the molecules on the sensor surface. The PenG was detected on this sensor platform in the concentration range of 0.0015–0.0195 mol/L with lower LOD of 4.32×10^{-3} mol/L, with high reproducibly and stability for more than 70 measurements over 24 h time. Further, the sensor showed high selectivity when subjected to cross-sensitives between PenG and its structural building blocks phenylacetic acid and 6-aminopenicillanic acid. Overall, this nanoMIP sensor has shown great promise for detecting PenG with the highest reproducibility. Through this study, the authors showed that this sensor can potentially be applied for actual detection of analytes in real samples. Besides the preceding detailed discussion, a brief survey of the current pharmaceutical analytes and their MIP-based detection schemes are presented in Table 4.1.

4.4.4 Applications in food and environmental sensing

The application of MIPs for detection of pesticides, insecticides, and herbicides along with antibiotics in food and environmental samples has recently gained tremendous interest owing to the intriguing properties of MIPs, including their excellent tunability based on the specific requirements. One such sensor based on a fluorescence switch sensing mechanism was developed by Li et al. [65] on graphene oxide supported carbon quantum dots (GO/C-dots) on indium tin oxide (ITO) as signal indicator and a molecularly imprinted polymer as a recognition template for detection of virginiamycin, a type of antibiotic commonly used for treatment of bacterial infections in animals. Usually, traces are found in meat products and they are extremely harmful to human health. As shown in Fig. 4.12, when the cavity of the MIP sensor is empty and once the fluorescence of GO/C-dot is detected, then the sensor turns on, whereas the sensor turns off when virginiamycin adsorbs onto the surface, leading to decreased fluorescence intensity of the GO/C-dots. Likewise, the the GO/C-dot switch can be controlled by elution and readsorption of virginiamycin on the MIP sensor. This sensor has shown excellent stability and sensitivity with a linearity of 5.0×10^{-10} to 8.0×10^{-8} mol/L and a limit of detection of 1.56×10^{-11} mol/L when tested for virginiamycin in actual meat samples. For cross-verification of the results, the same meat samples were tested with gold standard methods such as HPLC-MS. Along similar lines, for detection of beta-cyfluthrin (BC), a well-known pesticide routinely used in agriculture and known to be dangerous to humans, fish, and shrimp, Qiu et al. [67] developed a fluorescent MIP (FMIPs) based sensor using precipitation polymerization. In this method, SiO_2, BC, and fluorescein were used as carrier, target molecule, and functional monomer, respectively. In addition, trimethylolpropane trimethacrylate (TRIM) was used as the cross-linker. The 300 nm

Table 4.1 Molecularly imprinted polymers for detection of pharmaceuticals and drugs by optical sensing methods.

Type of MIPs	Type of analyte	Type of sample	Detection method	LOD	Linear range	Reference
SiO_2@MIPs	λ-Cyhalothrin (LC)	Canal water	FL	10.26 nM	0–160 nM	[9]
NanoMIP-SPR	Ciprofloxacin (CIP)	Standard solution	SPR	~0.08 μg L^{-1}	10^{-11}–10^{-7} mol L^{-1}	[46]
PEG-ZnS-QDs	Cocaine	Urine	FL	76 μg L^{-1}	0.0–1.0 mg L^{-1}	[49]
GQD-SMIP	Metronidazole	Human plasma	FL	0.15 μM	0.2 μM–15 μM	[53]
NanoMIP	Diclofenac	Water	SPR	1.2 ng m L^{-1}	1.2–25 ng m L^{-1}	[55]
PenG-MIPs	Penicillin G (PenG)	Aqueous buffer	RIfS	4.32×10^{-3} mol L^{-1}	0.0015–0.0195 mol L^{-1}	[56]
CDs@MIPs	Tetracycline	Milk	FL	5.5 nM	0.02–14 μM	[57]
Mn-ZnS QDs	Cyphenothrin	Water	FL	9.0 nmol L^{-1}	0.1–80 μmol L^{-1}	[58]
MIP-GQD	Paranitrophenol	River water	FL	9.0 ng/mL	0.02–3.00 μg/mL	[59]
MIP-C-dots	Paranitrophenol	River water	FL	60 nmol L^{-1}	0.2–50 μmol L^{-1}	[60]
COOH@MWCNT-MIP-QDs	Ciprofloxacin	Milk	FL	0.066 μg L^{-1}	0.10–1.0 μg L^{-1}; 1.0–100.0 μg L^{-1}	[61]
MIP-FeSe-QDs	Cyfluthrin (CYF)	Fish	FL	1.0 μg kg^{-1}	0.010–0.20 mg L^{-1}	[62]
mMIP@CDs/QDs	Diniconazole (DNZ)	Soil, river water, wastewater	FL	6.4 μg L^{-1}	20–160 μg L^{-1}	[63]
CdTe-MIP-QDs	Amoxicillin	Egg, milk, honey	PL	0.14 g L^{-1}	0.20–50 μg L^{-1}	[64]
GO/C-dots	Virginiamycin (antibiotic)	Meat	FL	1.56×10^{-11} mol L^{-1}	5.0×10^{-10} to 8.0×10^{-8} mol L^{-1}	[65]
MIP-EGDMA	Clenbuterol	Water	Absorbance	10^{-7} μg L^{-1}	10^{-5} to 1000 μg L^{-1}	[66]

FL, fluorescence; *SPR*, surface plasmon resonance; *RIfS*, reflectometric interference spectroscopy; *PL*, photoluminescence; *SiO_2 @MIPs*, molecularly imprinted fluorescent hollow SiO_2 nanoparticles; *PEG-ZnS-QDs*, polyethylene glycol coated ZnS quantum dots; *GQD-SMIP*, graphene quantum dots-embedded silica molecular imprinted polymer; *PenG-MIPs*, penicillin G-imprinted nanoMIPs; *CDs@MIPs*, carbon quantum dots-molecularly imprinting polymer; *Mn-ZnS QDs*, manganese doped-zinc sulfide quantum dots; *MIP-C-dots*, carbon dot embedded MIP; *MIP-GQDs*, graphene quantum dots embedded molecular imprinted polymer; *MIP-C-dots*, carbon quantum dots embedded molecular imprinted polymer; *COOH@MWCNT-MIP-QDs*, carboxylic functionalized multiwall carbon nanotubes-molecular imprinted polymer quantum dots; *MIP-FeSe-QD*, iron-selenium-quantum dots embedded molecular imprinted polymer; *mMIP@CDs/QDs*, mesorporous-molecular imprinted polymer carbon dots-quantum dots; *CdTe-MIP-QDs*, cadmium telluride quantum dots based molecular imprinted polymer; *GO/C-dots*, graphene oxide-modified carbon dots; *MIP-EGDMA*, molecular imprinted polymer-ethylene glycol dimethacrylate.

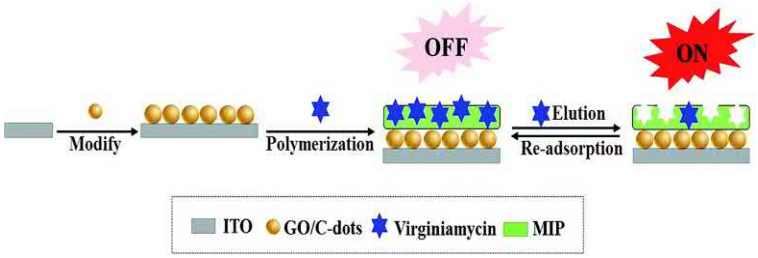

Fig. 4.12

Fabrication of the switch sensor for the detection of virginiamycin. *Reproduced from S. Li, J. Li, J. Luo, Q. Zhang, L. Zhang, A fluorescence switch sensor for detection of virginiamycin based on graphene oxide-supported carbon quantum dots and molecularly imprinted polymer, RSC Adv. 7 (89) (2017) 56359–56364, under the Creative Commons Attribution License, 2019.*

diameter particles with 50 nm shell thickness of SiO_2-MPTMS@FMIPs (methacryloyloxy) propyltrimethoxysilane (MPTMS) showed a lower detection limit of 10.11 BCE nM in water with a linear range of 10.11–80 nM with high stability.

Another type of toxic fungal metabolite called Patulin (PAT), produced by certain molds of the genera Penicillium, has been shown to be present in various moldy fruits, cereals, cheese, and specifically in apple juice, and is harmful to humans. Therefore, in order to detect this harmful chemical, the Li et al. [68] group devised a Mn-doped ZnS quantum dots-based nanosensor with 6-hydroxynicotinic acid (6-HNA) as template via a surface molecular imprinting sol-gel process. As shown clearly in Fig. 4.13, the fabrication of the nanosensor involves usage of the APTES as functional monomer and tetraethoxysilane (TEOS) as cross-linker through a surface imprinting process. In this method, PAT was detected using the phosphorescent method. Also, this MIP-based optical sensor demonstrated high selectivity to the target PAT compared to different analogs and various mycotoxins with an imprinting factor of 2.02. The real apple juice samples were run through phosphorescent spectra from 400 to 700 nm in a fluorescence spectrophotometer with excitation wavelength of 320 nm. It was demonstrated that this MIPs-QDs based nanosensor was able to detect the PAT with a lower limit of detection of 0.32 μmol/L in the linear range of 0.43–6.50 μmol/L. In this work, the generation of the phosphorescence signal was known to occur due to binding of the high-polarity PAT with the imprinted cavities of the sensor, which resulted in a quenching of phosphorescence through a photo-induced electron transfer mechanism. Further, better sensitivity along with specific binding performance of the Mn-doped ZnS QDs towards PAT and its analogs demonstrates this method as a potential screening device for routine monitoring of PAT in apple juice. Subsequently, for the detection of toxic small molecules such as tributyltin pesticide (TBT), a genotoxic and endocrine disruptive chemical, the Merkoçi group [69] developed a novel MIP-based graphene quantum dots photoluminescent sensor. In this study, the authors devised a multifunctional composite material based magnetic silica beads/graphene quantum dots/molecularly imprinted polypyrrole (mSGP) sensor by imprinting tributyltin. Fig. 4.14 shows the

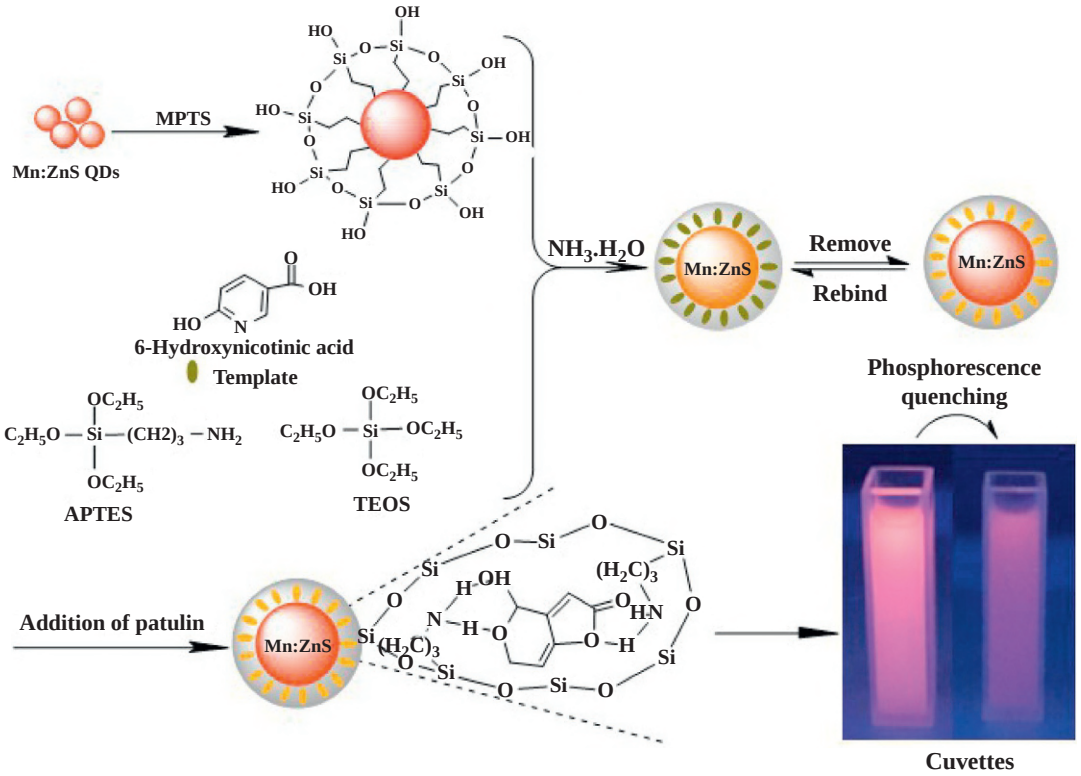

Fig. 4.13

Schematic of MIP-QDs synthesis process for making nanosensor for detection of PAT using phosphorescence method. *Reproduced from W. Zhang et al., Surface molecularly imprinted polymer capped Mn-doped ZnS quantum dots as a phosphorescent nanosensor for detecting patulin in apple juice, Food Chem. 232 (2017) 145–154, Copyright 2019, with permission from Elsevier.*

mSGP sensor and its sensing mechanism. The MIP-GQDs-based sensor was shown to work on an energy transfer mechanism which, upon recognition of the analyte (TBT), quenches the photoluminescence of graphene quantum dots, resulting in a lower limit of detection of 12.78 ppb in spiked sea water samples. Further, this sensor was shown to be highly specific to TBT compared to its analogs, which is a desirable quality for any sensor to be potentially used in field settings. In addition to the preceding discussion, Table 4.2 presents a brief review of various types of analytes present in food and environmental samples and their detection methods by MIPs.

4.5 Challenges of MIPs for optical sensing systems

With the many unquestioned advantages of MIPs, it is not surprising that, over the last several years, molecular imprinting technology has attracted great attention across various domains, due to extremely rapid developments in the field of biology, translational medicine, and

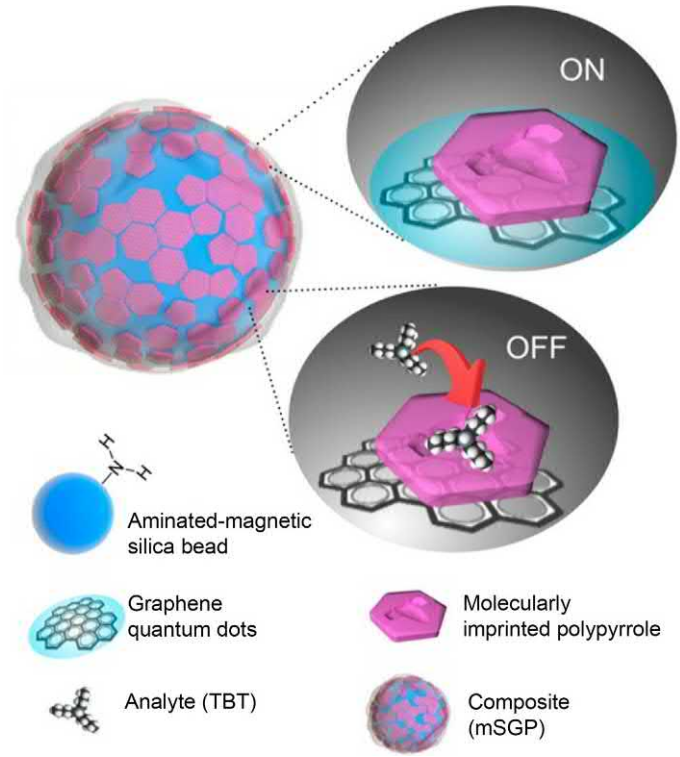

Fig. 4.14
Schematic showing the mSGP composite along with sensing mechanism. *Reproduced from E. Zor, E. Morales-Narváez, A. Zamora-Gálvez, H. Bingol, M. Ersoz, and A. Merkoçi, Graphene quantum dots-based photoluminescent sensor: a multifunctional composite for pesticide detection, ACS Appl. Mater. Interfaces 7 (36) (2015) 20272–20279, Copyright 2019, with permission from American Chemical Society.*

diagnostics. This has strongly motivated the continuous developments seen in MIPs research for sensing applications. In this chapter, a systematic review has been presented on the latest developments and applications of MIPs in optical-based nanosensors, particularly focused on biomolecular detection in the domains of immuno-diagnostics, food, and environmental sensing, along with pharmaceuticals and drugs. In order to realize MIPs as mainstream sensing technologies, there are two major challenges that need to be addressed. The first one is at the research and developmental stage and the other is on the commercial scale. At the outset of the research and developmental stage, several studies focused on the usage of MIPs for sensing applications as compared to conventional natural receptor systems. This is due to their tunability and flexibility for custom decoration of the imprinted polymers to produce unique structures specific to the desired applications. Though on the one hand MIPs are very attractive for custom modification as per required applications, on the other hand they pose a number of challenges in their properties for nanosensing applications. The basic criteria for any technology to be eligible for sensing applications is having high selectivity and high specificity

Table 4.2 Molecularly imprinted polymers for detection of analytes present in food and environmental samples by optical sensing methods.

Type of MIPs	Type of analyte	Type of sample	Detection method	LOD	Linear range	Reference
SiO_2-PTMS@FMIPs	Beta-Cyfluthrin	Water	FL	10.11 nM	10.11–80 nM	[67]
MIP-QDs	Patulin (PAT)	Apple juice	PS	0.32 μmol L^{-1}	0.43–6.50 μmol L^{-1}	[68]
MIPs-OVDAC/ CdTe-QDs	λ-Cyhalothrin (LC).	Water	FL	0.03 μmol L^{-1}	0.1–16 μmol L^{-1}	[70]
IA-MIP	Dimethoate	Olive oil	UV	0.012 μg g^{-1}	0–40 μg g^{-1}	[71]
Fe_3O_4-NH_2-MMIPs	Phosalone, Diazinon, Chlorpyrifos	Aqueous solution	UV-Vis	0.8 mg mL^{-1}	0–82.8, 0–80.5, 0–72.8 mg g^{-1}	[72]
Fe_3O_4@PDA NPs	Chlorpyrifos	Spiked solution	SPR	0.76 nM	0.001 to 10 μM	[73]
HFMT-MIPs	Atriazine	Lake water	UV	0.18	10 to 100 μg L^{-1}	[74]
MIP-Monolith fibers	s-Triazine	Lake water	UV	0.8 μg L^{-1}	2.5–80 μg L^{-1}	[75]
MIP-SPE-nanoTiO_2	Propazine	Water, soil, maize	UV-Vis	2.95–3.0 nmol L^{-1} (water)	0.1–16 μmol L^{-1}	[76]
MIP-SPE	Organophosphorus pesticides (Diazinon, Quinalphos, Chlorpyrifos)	Fruits	UV	0.83–2.8 μg L^{-1}	4–200 μg L^{-1}	[77]
mSGP-GQDs	Tributyltin (TBT)	Sea water	PL	42.56 ppb	~500 ppb	[69]
P-MIP-MMP	2,4-Dichlorophenoxyaceticacid (2,4-D)	Spiked water	CL	1.0 pM	5.0–10.0 μM	[78]
AgNPs-MIPs-SERS	Melamine	Tap water, milk	SERS	0.0019 mmol L^{-1} (water), 0.0165 mmol L^{-1} (skim milk)	0–7.5 × 10^{-3} mmol L^{-1} (water), 0–0.1 mmol L^{-1} (milk)	[79]

PS, phosphorescence; *CL*, chemiluminescence; *SiO_2-MPTMS@FMIPs*, core-shell SiO_2–3-(methacryloyloxy) propyltrimethoxysilane (MPTMS)-fluorescent molecularly imprinted polymers (FMIP); *MIP-QDs*, Mn-doped ZnS quantum dots; *MIPs-OVDAC/CdTe QDs*, octadecyl-4-vinylbenzyl-dimethyl-ammonium chloride (OVDAC)/CdTe quantum dots embedded molecularly imprinted polymer; *IA-MIP*, imprinted-itaconic acid; *Fe_3O_4-NH_2-MMIPs*, Fe_3O_4-NH_2-magnetic molecularly imprinted polymers; *Fe_3O_4@PDA NPs*, Fe_3O_4-based polydopamine molecularly imprinting polymers nanoparticles; *HFMT-MIPs*, hollow fiber membrane tube molecularly imprinted polymer; *MIP-SPE-nanoTiO_2*, TiO_2 embedded molecularly imprinted polymers by solid phase extraction; *mSGP-GQDs*, magnetic silica beads/graphene quantum dots/molecularly imprinted polypyrrole (mSGP)-graphene quantum dots; *P-MIP-MMP*, paper-based molecular imprinted polymer (MIP)-grafted multidisk microdisk plate; *AgNPs-MIPs-SERS*, silver nanoparticles-molecularly imprinted polymers-surface enhanced Raman spectroscopic-active substrate.

concurrently towards the target analyte. However, MIPs are shown to demonstrate these qualities for selective molecules only. Therefore, significant work needs to be carried out for ultimately qualifying MIPs for nanosensing applications in the future. Further, as the detection of any target analyte from a real sample is quite challenging due to the complexity and the presence of several undesirable entities in the sample. Therefore, the development of highly specific MIP-based sensors for selective capture/detection of analytes in mixed media conditions is highly desirable.

The polymers used for synthesizing MIPs are adsorbent in nature and hence there is a high possibility of weaker interactions with the target molecules. Therefore, new binding chemistries need to be explored to optimize the molecular interactions for avoiding nonspecific, nonhomogeneous binding to the template materials. Novel strategies are required to minimize the noncovalent interactions between the functional monomer and template by incorporating appropriate functional groups. In addition, tuning of interactions to permit the extraction of the target molecule from the synthesized polymers is highly desirable, as this avoids the interference between unextracted targets and the template during the rebinding process with the target of interest in the actual sample. A key factor, which decides the stability of the template and its collapsibility after template extraction, is the cross-linker. Therefore, more studies are required to understand its critical role in the diffusion rate of the template to the target sites. So far, a significant amount of progress has been achieved in developing MIPs for detection of analytes present in conventional organic-rich solvents. However, novel strategies are required to produce MIPs with ideal selectivity for aqueous solutions, since a majority of the analytes are usually present in aqueous solutions. This particular advancement at the core level will open up new avenues for MIPs for potential applications ranging from food, water, soil, and diagnostics to environmental monitoring.

Fundamentally, there are a few key challenges that make preparation of MIPs difficult for aqueous media conditions, such as hydrogen bonding, which stabilizes the template-monomer complex. During the application of MIPs in aqueous media, the water molecules tend to destroy hydrogen bonding during the imprinting and recognition process. As water molecules are known to be both hydrogen bonding acceptors and donors, this has led to reduced efficiency in imprinting and recognition. Another challenge for recognition of analytes from aqueous solutions occurs with loss of active sites due to differences in swelling and shrinking of MIPs in response to the aqueous conditions. This problem arises because these MIPs are usually prepared in nonpolar or low polar solvents. Moreover, new synthesis methods are required to bypass the usage of MIPs synthesized with hydrophobic raw materials, such as alkenyl monomer and cross-linkers for detection of analytes from aqueous solutions. In addition, the hydrophobic MIPs are known to have lower dispersibility in water with limited diffusion of the target analyte due to nonspecific adsorption. Further, these hydrophobic MIPs tend to attract macromolecules such as lipids and proteins on their surfaces by hydrophobic interactions, leading to the blockage of imprinted sites, which further results in reduced functionality of the

sensor. To obtain the desired performance of MIPs in different media, it is highly desirable to optimize the co-monomer concentration at the prepolymerization stage along with the feed ratio of hydrophilic/hydrophobic monomers during synthesis.

Moreover, new synthesis approaches are needed for developing mesoporous MIPs with thinner films, along with sensing mechanisms for detection of macromolecules such as proteins, DNA, cells, bacteria, and viruses for optical sensing applications with distinct signals. However, obtaining the desired porosity of MIPs is quite challenging, unless the role of the solvents (porogen) in inducing the micro- to mesoscale pores in the polymer networks without affecting the stability of the functional monomer and the template is clearly understood. Overall, an ideal MIP synthesized at laboratory scale needs to have specific qualities such as rapid binding kinetics and high surface-to-volume ratio in the case of nanoMIPs, and easy removal of template, good dispensability, and little or no nonspecific binding, with high sensitivity and specificity to the target analyte.

In the case of nanoparticle-based MIPs, the uniformity in particle size, controlled surface properties, and well-defined surface chemistries have to be understood from first principles for obtaining reproducible results. Additionally, more studies are required to optimize the MIPs by selecting appropriate functional monomers, cross-linkers, solvents and their concentrations, polymerization processes, and reaction conditions, along with appropriate design parameters for reactors. Besides the fundamental studies, as discussed before, several other challenges have to be addressed to increase the functionality of MIPs in nanosensing applications at commercial scale. As a primary step for commercial scale, new imprinting strategies have to be devised by adapting the computational and combinatorial tools that help in discovering the most appropriate polymers, functional monomers, templates, and cross-linkers along with appropriate reaction conditions. By adopting the design for manufacture approach and by keeping tight key performance indices, one can minimize the dissimilarities and bridge the gap between laboratory-scale development processes to large-scale production methods. Further, significant efforts at attention to detail are highly desirable while developing the synthesis conditions and operating procedures at the laboratory scale by considering their immediate scale-up for commercial production. It is also desirable to develop miniaturized versions of various optical detection systems for ease of usage and for routine monitoring of target analytes at point of need. Hence, academia and industry should work together in order to make MIPs a success at the commercial scale for addressing various real-time challenges.

4.6 Critiques and future outlook

Though there are a great many challenges that need to be addressed in the domain of MIP-based optical sensing, the potential opportunities that MIPs opens up in the research and commercial sectors, along with the benefits that incur to society, should be the guiding principle to progress

further in finding newer applications. Due to the outstanding advantages that MIPs bring, the first and foremost significant aspect is to develop multifunctional sensing kits over single molecular detection systems, as this augments value in terms of effective screening of multiple markers of interest for practically broader applications, with greater simplicity and reduced cost per analysis to the user. As discussed in this chapter, the application of MIP sensors has stretched far beyond simple biomolecule detection for general-purpose chemistries, to the detection and screening of more complex pharmaceuticals and drugs along with pesticides and insecticides screening in food and environmental samples. Recently, researchers have focused on making a three-dimensional bioMEMs-based MIP sensor, due to its exceptional advantages over two-dimensional MIPs sensing systems. Though there are devices in development based on bioMEMs-MIP sensors, such as an electronic tongue and MIPs-based handheld analyzers, still there is a great need for developing MIPs-based optical sensing systems for their utilization at point of use. Though the conventional systems, such as high-performance liquid chromatography and ion mobility spectrometry, are routinely employed in centralized laboratories for detection and analysis of various samples, they cannot be used in the field settings for monitoring or diagnosing target analytes. Therefore, recently several research groups and startups, such as Semorex, are focusing on developing MIPs-based sensing devices for commercial applications.

As evidenced in the literature, significant developments have been made in MIPs-based nanosensors for detection of a range of analytes, from cancer markers to contaminants in food and environmental samples. The domain of MIPs has seen various technological breakthroughs from polymer science, nanotechnology, biology, and physics to material science and has demonstrated novel nanoMIP-based optical sensors. Further, MIPs have proved their key functional role in sensing applications and have quickly gained much attention as a promising alternative to natural receptors due to various intriguing properties, as discussed earlier. This represents a significant breakthrough, as these systems can be effectively applied in harsh environments without the problem of degradation, and thus can potentially address innumerable applications in the sensing domain. Another important advancement in the purview of MIPs is the development of various polymerization imprinting methods, including solid phase imprinting, which truly revolutionized this space by opening numerous possibilities for tuning MIPs for a range of applications.

Despite all these noteworthy developments and success stories in detection of various biomolecules using MIPs, the detection/screening of different cells by MIP-based sensors is still in a nascent stage. Therefore, novel strategies have to be formulated to increase cell capture on MIPs-based sensing surfaces by effectively modifying the MIP's surface properties to prevent undesirable interactions while capturing the cells onto the sensing surfaces. Therefore, new surface chemistries with appropriate hydrophilic functional groups/polymers for covalent or noncovalent attachment of cells onto MIP surfaces seem to be a suitable approach for further consideration. Although many nanosensing applications of MIPs are still in their

infancy, much more work remains to be carried out to make MIPs suitable for real-time uses. It is anticipated that this situation will certainly improve with further exploration and development of innovative molecular imprinting strategies and by considering rational design approaches for MIP-based sensing systems. In addition, deeper understanding of polymer chemistry, surface chemistry, and ligand interaction mechanisms is highly desirable for further success. Most importantly, multidisciplinary efforts are essential, teaming people from different backgrounds, for example chemists, engineers, biologists, material scientists, and stakeholders, for the successful design and implementation of MIPs. So far, based on the progressive developments and functionality of MIPs with optical nanosensing capabilities in various applications, this technology has established sufficient confidence as a reliable and robust tool for bioanalysis. Therefore, in the future, MIPs-based optical sensing systems are expected to become a routine tool for detecting/screening simple to complex analytes of interest in a wide variety of samples across various application areas.

References

[1] J.J. BelBruno, Molecularly imprinted polymers, Chem. Rev. 119 (1) (2019) 94–119.
[2] L. Chen, X. Wang, W. Lu, X. Wu, J. Li, Molecular imprinting: Perspectives and applications, Chem. Soc. Rev. 45 (8) (2016) 2137–2211.
[3] J. Pan, W. Chen, Y. Ma, G. Pan, Molecularly imprinted polymers as receptor mimics for selective cell recognition, Chem. Soc. Rev. 47 (15) (2018) 5574–5587.
[4] M. Jia, Z. Zhang, J. Li, X. Ma, L. Chen, X. Yang, Molecular imprinting technology for microorganism analysis, TrAC Trends Anal. Chem. 106 (2018) 190–201.
[5] T. Takeuchi, H. Sunayama, Beyond natural antibodies—a new generation of synthetic antibodies created by post-imprinting modification of molecularly imprinted polymers, Chem. Commun. 54 (49) (2018) 6243–6251.
[6] H. Zhang, L. Ye, K. Mosbach, Non-covalent molecular imprinting with emphasis on its application in separation and drug development, J. Mol. Recognit. 19 (4) (2006) 248–259.
[7] J. Ashley, et al., Molecularly imprinted polymers for sample preparation and biosensing in food analysis: progress and perspectives, Biosens. Bioelectron. 91 (November 2016) (2017) 606–615.
[8] G. Wulff, J. Liu, Design of biomimetic catalysts by molecular imprinting in synthetic polymers: the role of transition state stabilization, Acc. Chem. Res. 45 (2) (2012) 239–247.
[9] J. Wang, et al., Molecularly imprinted fluorescent hollow nanoparticles as sensors for rapid and efficient detection λ-cyhalothrin in environmental water, Biosens. Bioelectron. 85 (2016) 387–394.
[10] M.T. Jafari, B. Rezaei, B. Zaker, Ion mobility spectrometry as a detector for molecular imprinted polymer separation and metronidazole determination in pharmaceutical and human serum samples, Anal. Chem. 81 (9) (2009) 3585–3591.
[11] H. Zhang, Molecularly imprinted nanoparticles for biomedical applications, Adv. Mater. 32 (2020) 1806328.
[12] S. Ansari, M. Karimi, Novel developments and trends of analytical methods for drug analysis in biological and environmental samples by molecularly imprinted polymers, TrAC Trends Anal. Chem. 89 (2017) 146–162.
[13] Z. Huang, P. Zhang, Y. Yun, Preparing molecularly imprinted membranes by phase inversion to separate kaempferol, Polym. Adv. Technol. 28 (3) (2017) 373–378.
[14] H.Y. Wang, T. Kobayashi, T. Fukaya, N. Fujii, Molecular imprint membranes prepared by the phase inversion precipitation technique. 2. Influence of coagulation temperature in the phase inversion process on the encoding in polymeric membranes, Langmuir 13 (20) (1997) 5396–5400.
[15] H. Zhang, Water-compatible molecularly imprinted polymers: promising synthetic substitutes for biological receptors, Polymer (Guildf) 55 (3) (2014) 699–714.

[16] Y. Hu, J. Pan, K. Zhang, H. Lian, G. Li, Novel applications of molecularly-imprinted polymers in sample preparation, TrAC Trends Anal. Chem. 43 (2013) 37–52.
[17] T. Zhou, L. Ding, G. Che, W. Jiang, L. Sang, Recent advances and trends of molecularly imprinted polymers for specific recognition in aqueous matrix: preparation and application in sample pretreatment, TrAC Trends Anal. Chem. 114 (2019) 11–28.
[18] Q. Zhang, et al., Surface plasmon resonance sensor for femtomolar detection of testosterone with water-compatible macroporous molecularly imprinted film, Anal. Biochem. 463 (2014) 7–14.
[19] H. Nishide, J. Deguchi, E. Tsuchida, Selective adsorption of metal ions on crosslinked poly(vinylpyridine) resin prepared with a metal ion as a template, Chem. Lett. 5 (2) (1976) 169–174.
[20] R.S. Hutchins, L.G. Bachas, Nitrate-selective electrode developed by electrochemically mediated imprinting/doping of polypyrrole, Anal. Chem. 67 (10) (1995) 1654–1660.
[21] B. Gao, J. Wang, F. An, Q. Liu, Molecular imprinted material prepared by novel surface imprinting technique for selective adsorption of pirimicarb, Polymer (Guildf) 49 (5) (2008) 1230–1238.
[22] H.M. Lee, S.G. Lee, H.R. Park, S.H. Chough, Sorption behaviors and relation between selectivity and possible cavity shapes of the molecularly imprinted materials, Microporous Mesoporous Mater. 251 (2017) 42–50.
[23] D.R. Kryscio, N.A. Peppas, Critical review and perspective of macromolecularly imprinted polymers, Acta Biomater. 8 (2) (2012) 461–473.
[24] A.-M. Poller, E. Spieker, P.A. Lieberzeit, C. Preininger, Surface imprints: advantageous application of Ready2use materials for bacterial quartz-crystal microbalance sensors, ACS Appl. Mater. Interfaces 9 (1) (2017) 1129–1135.
[25] L. Longo, S. Scorrano, G. Vasapollo, RNA nucleoside recognition by phthalocyanine-based molecularly imprinted polymers, J. Polym. Res. 17 (5) (2010) 683–687.
[26] P. Luliński, Molecularly imprinted polymers based drug delivery devices: a way to application in modern pharmacotherapy. A review, Mater. Sci. Eng. C 76 (2017) 1344–1353.
[27] F. Barahona, M. Díaz-Álvarez, E. Turiel, A. Martín-Esteban, Molecularly imprinted polymer-coated hollow fiber membrane for the microextraction of triazines directly from environmental waters, J. Chromatogr. A 1442 (2016) 12–18.
[28] M. Pourfarzib, R. Dinarvand, B. Akbari-adergani, A. Mehramizi, H. Rastegar, M. Shekarchi, Water-compatible molecularly imprinted polymer as a sorbent for the selective extraction and purification of adefovir from human serum and urine, J. Sep. Sci. 38 (10) (2015) 1755–1762.
[29] A. Martín-Esteban, Recent molecularly imprinted polymer-based sample preparation techniques in environmental analysis, Trends Environ. Anal. Chem. 9 (2016) 8–14.
[30] F. Zaera, Probing liquid/solid interfaces at the molecular level, Chem. Rev. 112 (5) (2012) 2920–2986.
[31] Z. Li, J.R. Askim, K.S. Suslick, The optoelectronic nose: colorimetric and fluorometric sensor arrays, Chem. Rev. 119 (1) (2019) 231–292.
[32] X. Wang, O.S. Wolfbeis, Fiber-optic chemical sensors and biosensors (2013–2015), Anal. Chem. 88 (1) (2016) 203–227.
[33] C. Caucheteur, T. Guo, F. Liu, B.-O. Guan, J. Albert, Ultrasensitive plasmonic sensing in air using optical fibre spectral combs, Nat. Commun. 7 (1) (2016) 13371.
[34] J. Guo, C. Yang, Q. Dai, L. Kong, Soft and stretchable polymeric optical waveguide-based sensors for wearable and biomedical applications, Sensors 19 (17) (2019) 3771.
[35] C. Zong, et al., Surface-enhanced Raman spectroscopy for bioanalysis: reliability and challenges, Chem. Rev. 118 (10) (2018) 4946–4980.
[36] G. Selvolini, G. Marrazza, MIP-based sensors: promising new tools for cancer biomarker determination, Sensors (Switzerland) 17 (4) (2017) 718.
[37] M. Cieplak, W. Kutner, Artificial biosensors: how can molecular imprinting mimic biorecognition? Trends Biotechnol. 34 (2016) 922–941.

[38] E. Mazzotta, A. Turco, I. Chianella, A. Guerreiro, S.A. Piletsky, C. Malitesta, Solid-phase synthesis of electroactive nanoparticles of molecularly imprinted polymers. A novel platform for indirect electrochemical sensing applications, Sensors Actuators B Chem. 229 (2016) 174–180.
[39] C.E. DeSantis, et al., Cancer treatment and survivorship statistics, 2014, CA Cancer J. Clin. 64 (4) (2014) 252–271.
[40] G. Ertürk, H. Özen, M.A. Tümer, B. Mattiasson, A. Denizli, Microcontact imprinting based surface plasmon resonance (SPR) biosensor for real-time and ultrasensitive detection of prostate specific antigen (PSA) from clinical samples, Sensors Actuators B Chem. 224 (2016) 823–832.
[41] W. Zhang, W. Liu, P. Li, H. Xiao, H. Wang, B. Tang, A fluorescence nanosensor for glycoproteins with activity based on the molecularly imprinted spatial structure of the target and boronate affinity, Angew. Chem. Int. Ed. 53 (46) (2014) 12489–12493.
[42] E. Georges, G. Bradley, J. Gariepy, V. Ling, Detection of P-glycoprotein isoforms by gene-specific monoclonal antibodies, Proc. Natl. Acad. Sci. U. S. A. 87 (1) (1990) 152–156.
[43] J. Ye, Y. Chen, Z. Liu, A boronate affinity sandwich assay: an appealing alternative to immunoassays for the determination of glycoproteins, Angew. Chem. Int. Ed. 53 (39) (2014) 10386–10389.
[44] D. Yin, et al., Surface-enhanced Raman scattering imaging of cancer cells and tissues via sialic acid-imprinted nanotags, Chem. Commun. 51 (100) (2015) 17696–17699.
[45] M. Hassanzadeh, M. Ghaemy, An effective approach for the laboratory measurement and detection of creatinine by magnetic molecularly imprinted polymer nanoparticles, New J. Chem. 41 (6) (2017) 2277–2286.
[46] Q. Luo, N. Yu, C. Shi, X. Wang, J. Wu, Surface plasmon resonance sensor for antibiotics detection based on photo-initiated polymerization molecularly imprinted array, Talanta 161 (2016) 797–803.
[47] H. Niu, Y. Yang, H. Zhang, Efficient one-pot synthesis of hydrophilic and fluorescent molecularly imprinted polymer nanoparticles for direct drug quantification in real biological samples, Biosens. Bioelectron. 74 (2015) 440–446.
[48] Y. Zhang, et al., SiO2-MIP core-shell nanoparticles containing gold nanoclusters for sensitive fluorescence detection of the antibiotic erythromycin, Microchim. Acta 184 (7) (2017) 2241–2248.
[49] M.P. Chantada-Vázquez, et al., Simple and sensitive molecularly imprinted polymer – Mn-doped ZnS quantum dots based fluorescence probe for cocaine and metabolites determination in urine, Anal. Chem. 88 (5) (2016) 2734–2741.
[50] R. Peltomaa, B. Glahn-Martínez, E. Benito-Peña, M.C. Moreno-Bondi, Optical biosensors for label-free detection of small molecules, Sensors (Basel) 18 (12) (2018) 4126.
[51] S. Mompelat, B. Le Bot, O. Thomas, Occurrence and fate of pharmaceutical products and by-products, from resource to drinking water, Environ. Int. 35 (5) (2009) 803–814.
[52] K. Kümmerer, Drugs in the environment: emission of drugs, diagnostic aids and disinfectants into wastewater by hospitals in relation to other sources—a review, Chemosphere 45 (6) (2001) 957–969.
[53] M. Mehrzad-Samarin, F. Faridbod, A.S. Dezfuli, M.R. Ganjali, A novel metronidazole fluorescent nanosensor based on graphene quantum dots embedded silica molecularly imprinted polymer, Biosens. Bioelectron. 92 (2017) 618–623.
[54] N. Xiao, et al., Carbon paste electrode modified with duplex molecularly imprinted polymer hybrid film for metronidazole detection, Biosens. Bioelectron. 81 (2016) 54–60.
[55] Z. Altintas, A. Guerreiro, S.A. Piletsky, I.E. Tothill, NanoMIP based optical sensor for pharmaceuticals monitoring, Sensors Actuators B Chem. 213 (2015) 305–313.
[56] P. Weber, B.R. Riegger, K. Niedergall, G.E.M. Tovar, M. Bach, G. Gauglitz, Nano-MIP based sensor for penicillin G: sensitive layer and analytical validation, Sensors Actuators B Chem. 267 (2018) 26–33.
[57] J. Hou, et al., Rapid microwave-assisted synthesis of molecularly imprinted polymers on carbon quantum dots for fluorescent sensing of tetracycline in milk, Talanta 146 (2016) 34–40.
[58] X. Ren, L. Chen, Quantum dots coated with molecularly imprinted polymer as fluorescence probe for detection of cyphenothrin, Biosens. Bioelectron. 64 (2015) 182–188.

[59] Y. Zhou, Z. Qu, Y. Zeng, T. Zhou, G. Shi, A novel composite of graphene quantum dots and molecularly imprinted polymer for fluorescent detection of paranitrophenol, Biosens. Bioelectron. 52 (2014) 317–323.
[60] T. Hao, X. Wei, Y. Nie, Y. Xu, Y. Yan, Z. Zhou, An eco-friendly molecularly imprinted fluorescence composite material based on carbon dots for fluorescent detection of 4-nitrophenol, Microchim. Acta 183 (7) (2016) 2197–2203.
[61] N. Yuphintharakun, et al., A nanocomposite optosensor containing carboxylic functionalized multiwall carbon nanotubes and quantum dots incorporated into a molecularly imprinted polymer for highly selective and sensitive detection of ciprofloxacin, Spectrochim. Acta A Mol. Biomol. Spectrosc. 201 (2018) 382–391.
[62] X. Li, et al., Development and application of a novel fluorescent nanosensor based on FeSe quantum dots embedded silica molecularly imprinted polymer for the rapid optosensing of cyfluthrin, Biosens. Bioelectron. 99 (May 2017) (2018) 268–273.
[63] M. Amjadi, R. Jalili, Molecularly imprinted mesoporous silica embedded with carbon dots and semiconductor quantum dots as a ratiometric fluorescent sensor for diniconazole, Biosens. Bioelectron. 96 (January) (2017) 121–126.
[64] K. Chullasat, P. Nurerk, P. Kanatharana, F. Davis, O. Bunkoed, A facile optosensing protocol based on molecularly imprinted polymer coated on CdTe quantum dots for highly sensitive and selective amoxicillin detection, Sensors Actuators B Chem. 254 (2018) 255–263.
[65] S. Li, J. Li, J. Luo, Q. Zhang, L. Zhang, A fluorescence switch sensor for detection of virginiamycin based on graphene oxide-supported carbon quantum dots and molecularly imprinted polymer, RSC Adv. 7 (89) (2017) 56359–56364.
[66] Y. Tang, et al., Ultrasensitive detection of clenbuterol by a covalent imprinted polymer as a biomimetic antibody, Food Chem. 228 (2017) 62–69.
[67] H. Qiu, L. Gao, J. Wang, J. Pan, Y. Yan, X. Zhang, A precise and efficient detection of Beta-Cyfluthrin via fluorescent molecularly imprinted polymers with ally fluorescein as functional monomer in agricultural products, Food Chem. 217 (2017) 620–627.
[68] W. Zhang, et al., Surface molecularly imprinted polymer capped Mn-doped ZnS quantum dots as a phosphorescent nanosensor for detecting patulin in apple juice, Food Chem. 232 (2017) 145–154.
[69] E. Zor, E. Morales-Narváez, A. Zamora-Gálvez, H. Bingol, M. Ersoz, A. Merkoçi, Graphene quantum dots-based photoluminescent sensor: A multifunctional composite for pesticide detection, ACS Appl. Mater. Interfaces 7 (36) (2015) 20272–20279.
[70] X. Wei, et al., Facile polymerizable surfactant inspired synthesis of fluorescent molecularly imprinted composite sensor via aqueous CdTe quantum dots for highly selective detection of λ-cyhalothrin, Sensors Actuators B Chem. 224 (2016) 315–324.
[71] I. Bakas, et al., Computational and experimental investigation of molecular imprinted polymers for selective extraction of dimethoate and its metabolite omethoate from olive oil, J. Chromatogr. A 1274 (2013) 13–18.
[72] A. Masoumi, K. Hemmati, M. Ghaemy, Recognition and selective adsorption of pesticides by superparamagnetic molecularly imprinted polymer nanospheres, RSC Adv. 6 (55) (2016) 49401–49410.
[73] G.-H. Yao, R.-P. Liang, C.-F. Huang, Y. Wang, J.-D. Qiu, Surface plasmon resonance sensor based on magnetic molecularly imprinted polymers amplification for pesticide recognition, Anal. Chem. 85 (24) (2013) 11944–11951.
[74] J. Chen, L. Bai, M. Tian, X. Zhou, Y. Zhang, Hollow-fiber membrane tube embedded with a molecularly imprinted monolithic bar for the microextraction of triazine pesticides, Anal. Methods 6 (2) (2014) 602–608.
[75] J. Chen, L. Bai, L. Zhang, M. Hu, Y. Zhang, Novel liquid-liquid-solid microextraction using molecularly imprinted polymer monolithic fibres and its application to the extraction of s-triazine herbicides from water samples, Adsorpt. Sci. Technol. 32 (4) (2014) 331–342.
[76] H.R. Geng, S.S. Miao, S.F. Jin, H. Yang, A newly developed molecularly imprinted polymer on the surface of TiO2 for selective extraction of triazine herbicides residues in maize, water, and soil, Anal. Bioanal. Chem. 407 (29) (2015) 8803–8812.
[77] M.M. Sanagi, et al., Molecularly imprinted polymer solid-phase extraction for the analysis of organophosphorus pesticides in fruit samples, J. Food Compos. Anal. 32 (2) (2013) 155–161.

[78] S. Wang, L. Ge, L. Li, M. Yan, S. Ge, J. Yu, Molecularly imprinted polymer grafted paper-based multi-disk micro-disk plate for chemiluminescence detection of pesticide, Biosens. Bioelectron. 50 (2013) 262–268.
[79] Y. Hu, X. Lu, Rapid detection of melamine in tap water and milk using conjugated 'one-step' molecularly imprinted polymers-surface enhanced Raman spectroscopic sensor, J. Food Sci. 81 (5) (2016) N1272–N1280.

Further reading

R. Li, Y. Feng, G. Pan, L. Liu, Advances in molecularly imprinting technology for bioanalytical applications, Sensors (Switzerland) 19 (177) (2019) 177.
M. Yoshikawa, K. Tharpa, Ş.-O. Dima, Molecularly imprinted membranes: past, present, and future, Chem. Rev. 116 (19) (Oct. 2016) 11500–11528.

CHAPTER 5

Recent developments in nanostructured metal oxide-based electrochemical sensors

M.M. Abdullah[a], **Preeti Singh**[b], **Saiqa Ikram**[b]

[a]*Promising Centre for Sensors and Electronic Devices (PCSED), Department of Physics, Faculty of Science and Arts, Najran University, Najran, Saudi Arabia*
[b]*Bio/Polymer Research Laboratory, Department of Chemistry, Jamia Millia Islamia, New Delhi, India*

5.1 Introduction

Recent progress in various segments of science and technology worldwide unfortunately has adverse effects in other aspects of life on our planet, such as health, water, air, environment, and ecosystems, which has led to direct threats to ecosystems and disturbed natural processes through incorporation of undesirable pollutants. In view of the current alarming situations, comprehensive efforts are required to plan suitable approaches and to design simple, highly efficient, easily applicable, and reliable tools for the precise quantification and elucidation of these threatening situations. Various monitoring agencies and scientific communities are putting forth major efforts to hold the line against rapidly growing environmental disturbances from urbanization, with rapid increases in industrialization, deforestation, water pollution, and human population, which are some of the basic reasons behind the direct and indirect threats to the ecosystem and natural cycling processes.

Among the various sources of pollution, direct discharge of harmful untreated chemicals and toxic moieties into the surrounding atmosphere is of major concern, because it generates many health-related problems [1–4]. Therefore, designing sensing devices having good selectivity and sensitivity with robust performance for the precise detection of different harmful gases and liquid chemicals remains a serious challenge. To address these lethal ecological issues, highly targeted and exhaustive efforts are required, and simple, reliable, reusable, cost-effective, target-specific, efficient, lightweight, and durable electrochemical sensors with the ability to detect a wide range of concentrations, starting at very low levels, are urgently needed for early detection and quantification of harmful and toxic environmental pollutants.

Nanofabrication for Smart Nanosensor Applications. https://doi.org/10.1016/B978-0-12-820702-4.00005-2
© 2020 Elsevier Inc. All rights reserved.

Electrochemical sensors are devices that provide information on the composition of a system in synchronized way by coupling a chemically selective layer (the acknowledgment component) to an electrochemical transducer. Electrochemical sensors are a well-known technology, based on chemical reactions and delivering an electrical signal that corresponds to the analyte concentration. This type of sensor has significant potential as a device for monitoring environmental pollutants. Electrochemical strategies are among the more established estimation procedures, and furthermore include a very wide scope of systematic potential outcomes, improved by ongoing technological advancements in signal handling and front-end electronic systems. Technological advances in electrochemical sensors that took place during the 1980s and the beginning of the 1990s smoothed the subsequent progress of the environmental applications of electrochemical devices. Innovations in electrochemical sensors included amperometric or potentiometric sensors, artificially modified electrodes, stripping-based metal sensors, and different apparatuses for on-location field testing. Such innovations are enabling the effective measurement of inorganic and natural pollutants to move from the research center to the field, and the measurements can be performed quickly, cost-effectively, and dependably in field investigations. These advances adjusted the structure of organic layers of atomic gadgets or sensor clusters and thus improves the areas of microfabrication, computerized instrumentation, and flow detectors. A comprehensive picture of the advanced electrochemical cell is presented in the following section [5, 6].

Nanomaterials have been found promising and efficient, as compared to their bulk counterparts, for sensor materials, and they have played a role in improving the sensitivity, precision, and reliability of sensors. Technological advances in sensors utilizing nanostructured metal oxides, conducting and semiconducting oxides, polymers, and nanocomposites are the subject of research into detection and evaluation of various hazardous gases, synthetics, and biochemicals [7]. Metal oxide semiconductors are of particular interest because of their novel attributes and potential applications in electronic and optoelectronic devices. Metal oxide nanostructures have been extensively studied due to their unique surface activities imparted by their large surface-to-volume ratio. Their high chemical and thermal stabilities are also responsible for their advantageous sensing properties [8]. Semiconductor metal oxide nanostructures are currently a favorite contender among researchers, due to these promising sensing capabilities and quite satisfactory results [9–11]; as a target material they have proven to be highly suitable for applications in sensors [12]. Combinations of semiconductor metal oxide nanostructures with other materials in sensors have opened new paths to reliable sensing materials with high sensitivity and selectivity. The beneficial features of semiconductor metal oxide nanostructures, such as simple preparation methods, chemically stable nature, biosafety and biocompatibility, capability of controlling size and morphology, surface modification and catalytic properties, make these materials superior to other candidates [13]. In addition, semiconductor metal oxides are a very efficient material for electron transfer kinetics and demonstrate enhanced adsorption towards biomolecules, resulting in efficient biosensing

performance [14–16]. Semiconductor oxides receive consideration because of their potential applications in different areas, such as sensors, catalysis, batteries, and solar cells.

Remarkable ingenious skills with firm endurance contributes a smooth platform in this pioneer field of nanotechnology. And therefore it is easy to design new synthesis methodology for the controlled synthesis of nanomaterial structure with high desirable features such as high surface area, controlled morphology, long term stability, and reusability. A number of methods for synthesizing nanosize semiconductor metal oxides – for example, hydrothermal, solvothermal, sol gel process, chemical or physical vapor deposition, chemical bath deposition, growth in aqueous solutions, and electrochemical deposition methods – to produce nanoparticles, nanowires, nanorods, nanosheets, nanotubes, nanobelts, and quantum dots have been investigated by a number of researchers [17–25]. However, new methods are still required to prepare more efficient and novel semiconducting material nanostructures, in order to design and fabricate reliable and efficient sensors. The search for an ideal synthesis method for nanostructure sensor material still encounters many obstacles and this remains a demanding but required task. Appropriate exploitation and modern tailoring of developed material with proper choice of working electrode for the sensor designing is still in demand.

Over the last few decades, increasing research efforts have been made in the detection and correction of pollutants, including harmful/toxic components in liquid as well as gaseous form, as volatile organic/inorganic compounds. These compounds contain numerous chemical entities that can enter the body through the breath and have harmful effects, whether directly or indirectly, on health [26].

Many alcoholic compounds, including methanol, ethanol, isopropanol, etc., are used in laboratories, medicine, industry, and in the routine work of daily life. Careful usage and appropriate applications of these materials are mandatory. Industrial release and untreated wastes have led to direct exposure to living beings, and prolonged exposure beyond the critical limits can cause liver damage and can reduce brain weight [27]. Methanol is an organic solvent with continuous use in laboratories and industries; long exposure to methanol can lead to eye damage, nervous disorders, and even death [28]. Ethanol is another colorless alcohol with wide applications in almost all sectors of industries as a solvent and as a requirement for the synthesis of various materials [29, 30]. Inhalation of alcohol in combination with H_2O can lead to oxidative damage to brain, liver, stomach, erythrocytes, etc. [31, 32]. Isopropyl alcohol (IPA) is widely used in different sectors of the semiconductor industry for various purposes, including wafer surface washing, cleaning, lithography, pharmaceuticals, printing, paint, and rubber production units [33, 34]. Isopropyl alcohol can enter the body by ingestion, inhalation, or absorption and can adversely affect the central nervous system, causing hypothermia and cardiac arrest [35]. Moreover, hydrazine is a flammable, colorless, and highly toxic fluid with a strong and unpleasant odor similar to that of ammonia; it has been detected as a very common pollutant, regularly entering into the environment [36]. Pure hydrazine and its derivatives also

have potential uses in various sectors, such as fuel cell production units, as a corrosion inhibitor, in agriculture, as a pesticide antioxidant, and as a catalyst for polymer production units [37–40]. Despite these beneficial applications, it is one of the important pollutant components and is therefore on the radar of monitoring agencies; pure hydrazine and its derivatives are neurotoxic, hepatotoxic, and cancer causing agents, and direct exposure can lead to many health problems [41, 42]. The World Health Organization (WHO) and the Environmental Protection Agency (EPA) believe that hydrazine and its forms are carcinogenic and thus these compounds have been selected for inclusion in group B2.

The recent situation demands the urgent development of efficient sensing processes and advanced sensor devices for the prior detection, quantification, and rectification of these dangerous, harmful, and toxic pollutants. Very few well-organized reports concerning the application of approaches for the detection, quantification, and rectification of these pollutants are reported in the literature based on the electrochemical method, chromatography, spectrophotometry, titrimetry, and luminescence analysis techniques [43–50]. Out of various methods, electrochemical sensing has been found the most satisfactory and therefore takes priority over the other methodologies. The electrochemical sensing method for the detection of pollutants is simpler, cheaper, highly efficient, and has a rapid detection response.

The search is thus underway for desirable newly synthesized nanostructures for the improvement of sensor device performances via nanotechnology, to enhance the sensitivity, selectivity, linearity, electrode fouling conditions, and to resolve the over-potential issues [51]. Researchers, academicians, and scientists worldwide are showing interest in developing more advanced and suitable nano-electrochemical sensors and are looking at various methods of synthesis of optimized nanostructures that could represent the ideal sensor material. In addition, they are tailoring or modifying the working electrodes with various appropriate nanostructures, including nanocarbon, metal nanoparticles, metal oxide nanostructures, desirable conducting polymers, and their combinations [52–55]. A number of successfully prepared nanostructures have been widely tested as electrode materials, for use in development of chemical sensors as suitable working electrodes for the detection of pollutant chemicals, such as the alcohols discussed earlier. For this purpose, nickel (Ni), porous silicon (Si), hybrid and conductive polymers, carbon nanotubes (CNTs), semiconductor metal oxides and their nanocomposites, carbon and nitrogen doped nanomaterials, and metal organic frameworks [56–63] were used and evaluated as nanoelectrode materials and were found to improve the sensor properties.

Moreover, nanotechnology has been found to be a successful technology for production of miniscule sensors; extremely small size affects the key sensor features, such as material cost, device weight, and power consumption reductions. Low-power nanomaterial-based sensors have been found suitable for various applications, including incorporation into remote specialized devices to empower far-reaching dispersed monitoring and control, for use as battery-powered handhelds or wearable sensors, in medical uses for blood gas observation,

blood monitoring, tolerance checking, symptom testing, biowarfare recognition, genetic analysis, medicine screening or disclosure, food inspection/testing, environmental and chemical industry monitoring (for example, leak detection), glucose monitoring, and others. Moreover, nanosensors show promise for applications in industry, transportation, communications, building and facilities, medicine, safety, and security including both homeland defense and military operations [5]. The preceding discussion shows that metal oxide nanostructure-based nanosensors are promising devices for the detection, quantification, and monitoring of pollutants.

5.2 Types of sensors

Various types of sensors exist, including chemical, electrochemical, biological, gas, optical, magnetic, temperature and humidity sensors, to name just a few [61]. A sensor is a man-made technological device that facilitates the detection or sensing of signals, substantial circumstances, or chemical entities. Nanostructured devices have been discovered to be proficient in imaging and observing nanomaterial, natural, synthetic/chemical, and pathological samples. Thus nanostructures are playing an effective role in providing more sensitive, accurate, and reliable sensors. The many advances in sensors utilizing nanostructured metal oxides, conducting and semiconducting oxides, polymers, and composites are the subjects of research concentrating on recognition and measurement of different destructive and dangerous gases, synthetic substances, and biochemicals.

5.2.1 Chemical sensors

A chemical sensor is a device that transforms chemical information, such as composition, neighboring elements or ions, absorption, chemical activity, fractional pressure, and so forth, into a diagnostic signal. This chemical information is generated by a chemical reaction that occurs in an analyte when voltage is applied or from a physical property of the framework under scrutiny. Chemical sensors have applications in various areas, for example, medicine, home security, natural contamination, and numerous others. They usually have two basic components connected in series: a chemical (molecular) recognition system (receptor) and a physicochemical transducer. Chemical sensing is used frequently in industry for process control and monitoring, including monitoring for safety. It has an important role in environmental protection processes, and has potential application in the detection of unsafe materials including hazardous, natural, and man-made events, for example, contamination, conduit invasion, movement of species, climate change, and so on. The manufacture of synthetic sensors is extremely basic and pursues the procedures of thick film technologies.

5.2.2 Gas sensors

Gas sensors are devices used to measure the concentration of gases by detecting the inimitable breakdown voltage (ionization potential), which is a unique property of gases and is different for different gases. Sensors detect the gas molecules on the basis of breakdown voltage. Gas concentration can be assessed by estimating the current discharge in the device. Gas sensors are generally utilized in process control industries, environmental monitoring, fire location, alcohol breath analyzer tests, discovery of unsafe gases in mines, home health, reviewing of agro-items like espresso and flavor, etc. Temperature and humidity are the basic operating parameters of gas sensors.

However, these sensors have some disadvantages: they can be bulky, and at some point require high voltage operation. The identification standard of resistive gas sensors depends on the varied estimated resistance value of the thin film employed, in light of the adsorption of the gas particles on the surface of the semiconductor metal oxide nanostructures. The gas-solid interaction influences the resistance of thin film due to the thickness of the electronic species present in the film.

5.2.3 Biosensors

Nanostructured metal oxides such as zinc, iron, cerium, tin, zirconium, titanium, magnesium, and their composites are emerging as potential candidates in various electronic and optoelectronic devices and therefore have become significant materials. In addition, they show fascinating nanomorphology, utilitarian biocompatibility, as well as nondangerous and reactant properties.

In addition, these materials display upgraded electron-transfer energy and good adsorption capacity, provide reasonable microenvironments for the immobilization of biomolecules and consequent upgrading of the transfer of electrons, which improves the biosensing characteristics as biosensors. To investigate the impact of optical and electrochemical properties of nanostructured metal oxide suspended media, strong fluid interfaces and nano-bio-interfaces have been investigated for biosensor applications. A biosensor is a miniaturized device that utilizes an organic component or biological element, such as, for example, immune response, catalyst, receptor protein, nucleic corrosive, entire cell, and tissue segment, as a detecting component associated with a transducer for signal discovery. A biosensor uses the selectivity of the biomolecule and the handling intensity of current microelectronics and optoelectronics and consequently it is a powerful scientific device used in medical diagnostics and other related fields. Biosensors are anticipated to assume a basic role in both clinical and nonclinical applications because of their explicitness, versatility, fast reaction time, and economy.

The existing miniaturization of this device permits stuffing of numerous microscopic electrodes alongside transducers into small traces of a biochip device, prompting the structure of high-thickness bioarrays. Numerous biosensors are based on diverse discovery of different analytes; hydrogen, ammonium, and sodium ions as well as urea, creatinine, triglycerides, acetylcholine, butyrylcholine, pesticides, and heavy metal ions are already reported [64].

Biosensors help in distinguishing developing contaminants, like pharmaceuticals, steroids, xenoestrogens and other endocrine disrupting chemicals (EDCs), algal poisons, giardia (and different pathogens), and an assortment of various chemicals, for example, caffeine, cholesterol [65], etc. To generate an effective biosensor, it is vital to choose nanostructured metal oxides that are reasonable for immobilization of the ideal biomolecule.

The interface framed between the nanostructured metal oxides and a biomolecule influences the performance of the biosensor. The characteristics of a nano-bio-interface rely upon the nature of the nanostructured metal oxide parameters, for example, viable surface area, charge, vitality, porosity, valence/conductance states, functional group, physical states, and hygroscopic nature, which in general impact the arrangement of a bio-interface. In broad-spectrum, a biomolecule has ties with metal oxide nanoparticles through physical adsorption or chemical binding. Weak interaction forces occur, such as van der Waals, electrostatic, and physisorption, and depending on the surface morphology, reaction medium, and net surface charge are responsible for physical adsorption. Also, short-range forces, which are produced by reduction, charge, and solvent interaction, facilitate the fabrication of the nano-bio-interface, whereas the covalent binding of a biomolecule depends on the functional group of nanostructured metal oxides produced by chemical reactions under appropriate conditions [66, 67].

5.3 Electrochemical sensors: Construction, working, and principles

The oldest electrochemical sensors were prepared around 1950, to monitor oxygen content. In view of the day-to-day requirements of detection devices such as sensors, they have been modified and developed to greater capability for the monitoring of toxic and harmful pollutants. By the mid-1980s, miniaturized electrochemical sensors were available to use for the detection of many different toxic gases in PEL ranges, with the sensors exhibiting good sensitivity and selectivity. Recently, nanomaterial-based electrochemical sensors have been found suitable and efficient in many stationary and portable applications for personal safety. An electrochemical sensor produces the signal of current in the presence of voltage. The current-voltage characteristic graph can be plotted by noting the electric current for different applied potentials. The current-voltage characteristic graph of the sensor can be obtained by using a two- or three-electrode system. The electrochemical sensor of a two-electrode system (as shown in Fig. 5.1) consists of a counter and working electrodes. Glassy carbon, or silver, or gold for good conductivity were used to prepare working electrodes. A thin film of nanostructured

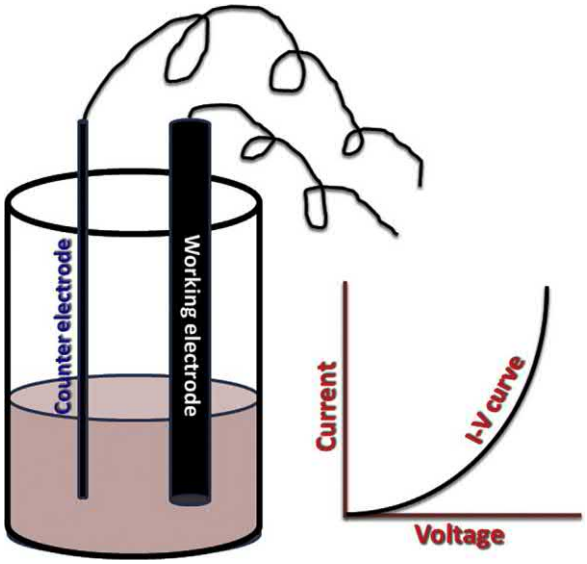

Fig. 5.1
Schematic diagram of electrochemical sensor.

sensor material was deposited onto the working electrode for sensing the current flowing in the electrolyte. By knowing the current for different potentials, a current-voltage graph was plotted to find the response of the sensors.

The sensing mechanism involved in sensor processes basically depends on the morphology of fabricated nanostructures. The mechanism behind the principle of sensor kinetics [8] follows the redox-reaction. Metal-oxide nanostructures react with the oxygen, as shown in Eqs. (5.1) and (5.2). The oxygen is the main element and leads the mechanism of sensing kinetics. Ionized oxygen derivatives (O_2^- and O^-) flow in the system and capture the electron present in surfaces of the sensor material's nanostructures:

$$e^- \text{ (Metal Oxide Nanostructures)} + O_2 \rightarrow O_2^- \tag{5.1}$$

$$e^- \text{ (Metal Oxide Nanostructures)} + O_2^- \rightarrow 2O^- \tag{5.2}$$

The negatively charged electron oxidizes the alcohol to Co_2 and H_2O and discharges electrons ($6e^-$) for conduction, as shown in Eq. (5.3).

$$C_2H_5OH_{(ads)} + 6O^-_{(ads)} \rightarrow 3H_2O + 6e^- \text{(C.B.)} \tag{5.3}$$

The produced electron enhances the conductance of the film deposited on the working electrode and as a result significantly increases the sensing properties of the as-fabricated sensor.

For p-type semiconductors, holes are the majority carriers, due to which its surface is roofed with chemisorbed oxygen. Thus this adsorbed negative-charged oxygen creates the holes for conduction, as represented in Eq. (5.4):

$$\tfrac{1}{2}O_2 \leftrightarrow O^- (\text{ads}) + h^* \tag{5.4}$$

Also, in oxidation of alcohol, the sensing reactions shown in Eq. (5.5) can be considered according to the charges of the adsorbed oxygen species:

$$\text{Alcohol (ads)} + 6O^- (\text{ads}) + 6h^* \rightarrow CO_2 + H_2O \tag{5.5}$$

That is, the oxidation reaction along with the increasing concentration increases the conductivity of the metal oxide nanostructures, and thus reduces the sensor's resistant behavior. The schematic diagram (Fig. 5.2) demonstrates the reactions occurring during the sensing procedure.

The prominent sensitivity is possible due to the small dimension of nanostructures, semiconducting characteristics, optical energy bandgap, and crystallinity of the material. The small dimension of the nanoparticles generates more particles, which substantially increases the overall dynamic exposed surface area for the interaction and, therefore, the adsorption of alcohol occurs at enormous quantities. A semiconductor material releases electrons and holes for conduction. As a result of this, a large number of charge carriers take part in the diffusion. The energy bandgap transition properties of the nanoparticles promote the adsorption of alcohol molecules and thus enhance the rate of reaction. Good crystallinity is favorable to provide directional electron transportation, which accelerates the electrochemical response of target chemical oxidation and thus enhances the reaction kinetics. Thus the sensor's performance could be modified by considering these factors. In such prospects, semiconducting metal oxide nanostructures could be a desirable and capable contender, as they possess feasible bandgap energy, highly exposed active surface area, good sensitivity, and better film thickness and

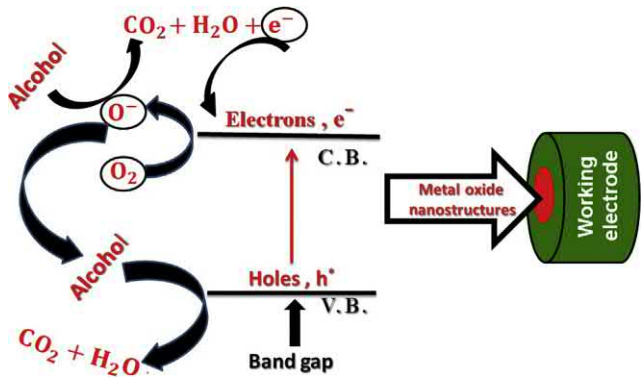

Fig. 5.2
Schematic sketch of reactions occurring in electrochemical sensor.

oxygen content. These salient features have led semiconducting metal oxide nanostructures into a wide range of applications in solar cells, sensors, biomedical imaging, photovoltaic applications, and many more. So the recent developments in electrochemical sensors have seen the use of metal oxide nanostructures, such as ZnO, Fe_2O_3, TiO_2, Co_3O_4, and Cu_2O_3, etc., as sensor materials to boost the properties of electrochemical sensors for more reliable, precise, and rapid electrochemical quantification of toxic and noxious environmental pollutants, down to very low levels of concentration. Various scientific groups have observed that metal oxide nanostructures are potential candidates for electrochemical and biosensing applications [1–4, 68], because of possessing some extraordinary physicochemical properties [9, 17, 69]. Considering these facts, it could be concluded that semiconductor metal oxide nanostructure-based electrochemical sensors will provide a new route for the development of novel nanosensors with the striking features of high efficiency, good selectivity, and long durability and stability.

5.4 Conclusion

Modification of working electrodes of electrochemical sensors with novel nanostructures of metal oxides of good morphological features, high crystalline nature, and a feasible optical energy gap could help to boost the performances of sensing devices. Besides, the fabrication, design, and operational characteristics of the modified electrodes would improve the performances of electrochemical nanosensor devices.

References

[1] R. Doong, H. Shih, Biosens. Bioelectron. 25 (2010) 1439.
[2] H.J. Kim, S.H. Yoon, H.N. Choi, Y.K. Lyu, W.Y. Lee, Bull. Kor. Chem. Soc. 27 (2006) 65.
[3] P. Pandey, M. Datta, B.D. Malhotra, Anal. Lett. 41 (2008) 159.
[4] A.K. Gupta, M. Gupta, Biomaterials 26 (2005) 3995.
[5] J. Wang, K. Rogers, Electrochemical Sensors for Environmental Monitroing: A Review of Recent Technology, U.S. Environmental Protection Agency, Office of Research and Development, Environmental Monitoring and Support Laboratory, 1995. http://www.clu-in.org/download/char/sensr_ec.pdf.
[6] T.S. Dhahi, U.B. Hashim, N.M. Ahmad, A.M. Taib, J. Optoelectron. Adv. Mater. 12 (9) (2010) 1857–1862.
[7] M. Faisal, S.B. Khan, M.M. Rahman, A. Jamal, A.M. Asiri, M.M. Abdullah, Appl. Surf. Sci. 258 (2011) 672–677.
[8] M.M. Abdullah, M.S. Akhtar, S.M. Al-Abbas, Curr. Nanosci. 14 (2018) 1–9.
[9] C. Jianrong, M. Yuqing, H. Nongyue, W. Xiaohua, L. Sijiao, Biotechnol. Adv. 22 (2004) 505.
[10] V. Galstyan, E. Comini, I. Kholmanov, A. Ponzoni, V. Sberveglieri, N. Poli, G. Faglia, G. Sberveglieri, Beilstein J. Nanotechnol. 7 (2016) 1421–1427.
[11] E. Comini, C. Baratto, G. Faglia, M. Ferroni, A. Vomiero, G. Sberveglieri, Prog. Mater. Sci. 54 (2009) 1–67.
[12] P. Singh, M.M. Abdullah, S. Ikram, Nanoresearch and applications, iMedPub J., 1 (2015), pp. 1–10.
[13] A.A. Ismail, F.A. Harraz, M. Faisal, A.M. El-Toni, A. Al-Hajry, M.S. Al-Assiri, Mater. Des. 109 (2016) 530–538.
[14] P. Holt-Hindle, S. Nigro, M. Asmussen, A. Chen, Electrochem. Commun. 10 (2008) 1438.
[15] D. Feng, F. Wang, Z. Chen, Sensors Actuators B Chem. 138 (2009) 539.

[16] J. Wang, D.F. Thomas, A. Chen, Anal. Chem. 80 (2008) 997.
[17] Y. Liua, H. Teng, H. Hou, T. You, Biosens. Bioelectron. 24 (2009) 3329.
[18] B. Liu, H.C. Zeng, J. Am. Chem. Soc. 125 (2003) 4430.
[19] S. Kar, A. Dev, S. Chaudhuri, J. Phys. Chem. B 110 (2006) 17848.
[20] J.M. Wang, L. Gao, J. Mater. Chem. 13 (2003) 2551.
[21] R. Kaur, A.V. Singh, K. Sehrawat, N.C. Mehra, R.M. Mehra, J. Non-Cryst. Solids 23 (2006) 2565.
[22] H.H. Wang, C.S. Xie, J. Cryst. Growth 291 (2006) 187.
[23] N. Tripathy, R. Ahmad, H.-S. Jeong, Y.-B. Hahn, Inorg. Chem. 51 (2012) 1104.
[24] Y.Y. Xi, Y.F. Hsu, A.B. Djurisic, W.K. Chan, J. Electrochem. Soc. 155 (2008) D595.
[25] W. Lee, H.G. Sohn, J.M. Myoung, Mater. Sci. Forum 449 (2004) 1245.
[26] W.I. Park, D.H. Kim, S.W. Jung, G.C. Yi, Appl. Phys. Lett. 80 (2002) 4232.
[27] K.I. Ozoemena, S. Musa, R. Modise, A.K. Ipadeola, L. Gaolatlhe, S. Peteni, G. Kabongo, Curr. Opin. Electrochem. 10 (2018) 82.
[28] S.R. Anjum, V.N. Narwade, K.A. Bogle, R.S. Khairnar, Nano-Struct. Nano-Objects 14 (2018) 98–105.
[29] M.M. Rahman, S.B. Khan, A. Jamal, M. Faisal, A.M. Asiri, Talanta 95 (2012) 18–24.
[30] M.M. Rahman, A. Jamal, S.B. Khan, M. Faisal, Biosens. Bioelectron. 28 (2011) 127–134.
[31] M. Faisal, S.B. Khan, M.M. Rahman, A. Jamal, A.M. Asiri, M.M. Abdullah, Chem. Eng. J. 173 (2011) 178–184.
[32] M. Faisal, S.B. Khan, M.M. Rahman, A. Jamal, A.M. Asiri, K. Akhtar, M.M. Abdullah, J. Mater. Sci. Technol. 27 (7) (2011) 594–600.
[33] M.M. Rahman, A. Jamal, S.B. Khan, M. Faisal, J. Phys. Chem. C 1159 (2011) 9503–9510.
[34] C.-C. Lin, C.-W. Tsai, Sep. Purif. Technol. 209 (2019) 88–93.
[35] S. Raghuvanshi, S. Gupta, B.V. Babu, J. Biotechnol. Biomater. S13 (S) (2012) 002.
[36] A. Wahid, A.M. Asiri, M.M. Rahman, Environ. Nanotechnol. Monit. Manag. 10 (2018) 314–321.
[37] S.M. Golabi, H.R. Zare, J. Electroanal. Chem. 465 (1999) 168–176.
[38] S. Garrod, M.E. Bollard, A.W. Nicholls, S.C. Connor, J. Connelly, J.K. Nichol-son, E. Holmes, Chem. Res. Toxicol. 18 (2005) 115–122.
[39] K.M. Korfhage, K. Ravichandran, R.P. Baldwin, Anal. Chem. 56 (1984) 1514–1517.
[40] W.X. Yin, Z.P. Li, J.K. Zhu, H.Y. Qin, J. Power Sources 182 (2008) 520–523.
[41] A. Umar, M.M. Rahman, S.H. Kim, Y.B. Hahn, Zinc oxide nanonail based chemical sensor for hydrazine detection, Chem. Commun. 2 (2008) 166–168.
[42] S. Ameen, M.S. Akhtar, H.S. Shin, Sensors Actuators B 173 (2012) 177–183.
[43] American Conference of Governmental Industrial Hygienists, Documentation of Threshold Limit Values and Biological Exposure Indices, ACGIH, Cincinnati, OH, 1999.
[44] S.B. Khan, M. Faisal, M.M. Rahman, I.A. Abdel-Latif, A.A. Ismail, K. Akhtar, A. Al-Hajry, A.M. Asiri, K. A. Alamry, New J. Chem. 37 (2013) 1098–1104.
[45] M.M. Alqahtani, A.M. Ali, F.A. Harraz, M. Faisal, A.A. Ismail, M.A. Sayed, M.S. Al-Assiri, Nanoscale Res. Lett. 157 (2018) 1.
[46] A.A. Ismail, A.M. Ali, F.A. Harraz, M. Faisal, H. Shoukry, A.E. Al-Salami, Int. J. Electrochem. Sci. 14 (2019) 15–32.
[47] M. Mori, K. Tanaka, Q. Xu, M. Ikedo, H. Taoda, W. Hu, J. Chromatogr. A 1039 (2004) 135–139.
[48] P.J. Fletcher, J.F. van Staden, Anal. Chim. Acta 499 (2003) 123–128.
[49] M. George, K.S. Nagaraja, N. Balasubramanian, Talanta 75 (2008) 27–31.
[50] Y.A. Gawargious, A. Beseda, Talanta 22 (1975) 757–760.
[51] A. Safavi, M.A. Karimi, Talanta 58 (2002) 785–792.
[52] Y. Liu, B. Li, W. Wei, Q. Wan, N. Yang, Adv. Mater. Res. 7 (2013) 246–251.
[53] B.M. Christopher, E.B. Craig, O.S. Andrew, G.J.J. Timothy, R.G. Compton, Analyst 131 (2006) 106–110.
[54] B. Fang, C.H. Zhang, W. Zhang, G.F. Wang, Electrochim. Acta 55 (2009) 178–182.
[55] G.F. Wang, A.X. Gu, W. Wang, Y. Wei, J.J. Wu, G.Z. Wang, X.J. Zhang, B. Fang, Electrochem. Commun. 11 (2009) 631–634.

[56] M. Faisal, F.A. Harraz, A.E. Al-Salami, S.A. Al-Sayari, A. Al-Hajry, M.S. Al-Assiri, Mater. Chem. Phys. 214 (2018) 126–134.
[57] S. Petralia, E.L. Sciuto, M.A. Messinac, A. Scandurra, S. Mirabella, F. Priolo, S. Conoci, Sensors Actuators B 263 (2018) 10–19.
[58] K. Chebout, A. Iratni, A. Bouremana, S. Sam, A. Keffous, N. Gabouze, Solid State Ionics 253 (2013) 164–168.
[59] A.M. Sanjuán, J.A. Reglero Ruiz, F.C. García, J.M. García, React. Funct. Polym. 133 (2018) 103–125.
[60] S.K.H. Darzi, M.G. Esfidvajani, Int. J. Hydrog. Energy 41 (2016) 20085–20099.
[61] L. Xiao, S. Xu, G. Yu, S. Liu, Sensors Actuators B 255 (2018) 2002–2010.
[62] W.Y. Yana, Q. Zhou, X. Chen, X.J. Huang, Y.-C. Wu, Sensors Actuators B 230 (2016) 761–772.
[63] P. Singh, M.M. Abdullah, S. Sagadevan, C. Kaur, S. Ikram, Optik 182 (2019) 512–518.
[64] Y. Li, A.-S. Xiao, B. Zou, H.-X. Zhang, K.-L. Yan, Y. Lin, Polyhedron 154 (2018) 83–97.
[65] M.H. Huang, S. Mao, H. Feick, H. Yan, Y. Wu, et al., Science 292 (2001) 1897–1899.
[66] Y. Ozaki, S. Suzuki, M. Morimitsu, M. Matsunaga, Sensors Actuators B Chem. 62 (2000) 197–220.
[67] W. Torbicz, D.G. Pijanowska, Semiconductor chemical and biochemical sensors, in: Progress in Electromagnetic Research Symposium, Pisa, Italy, 31 2004, pp. 847–850.
[68] P. Gautam, S. Suniti, A. Prachi Kumari, M. Deepa, et al., A review on recent advances in biosensors for detection of water contamination, Int. J. Environ. Sci. 2 (3) (2012) 1565–1574.
[69] Y.-B. Hahn, R. Ahmad, N. Tripathy, Chem. Commun. 48 (2012) 10369.

CHAPTER 6

Nanosensors and nanobiosensors: Agricultural and food technology aspects

Zayed Bin Zakir Shawon[a], **Md Enamul Hoque**[b], **Shiplu Roy Chowdhury**[c]

[a]*Department of Mathematics and Natural Sciences, BRAC University, Dhaka, Bangladesh*
[b]*Department of Biomedical Engineering, Military Institute of Science and Technology (MIST), Dhaka, Bangladesh*
[c]*Tissue Engineering Centre, Faculty of Medicine, Universiti Kebangsaan Malaysia, Kuala Lumpur, Malaysia*

6.1 Introduction

Nanotechnology is a recent and rapidly growing trend in almost every branch of the sciences. Nanoparticle research is ubiquitous in many different genres, and more and more new nanotechnologies are being adapted in agricultural and food sciences (Fig. 6.1). Recent discoveries in nanotechnology have highlighted its unique properties, such as adsorption capability, surface area, delivery pattern, and so forth. Nanoparticles function on a very small scale, even at the molecular level, which gives them a vast number of potential uses in the agricultural and food industries. For an easy comparison example, the difference between conventional fertilizers and nanofertilizers is shown in Table 6.1. The various uses of nanotechnology in the food and agricultural industries are displayed. The aim of using nanotechnology is to improve the product quality and efficiency of packaging, delivery and preservation of agricultural products, and their derivatives [1, 2].

In recent studies, unique properties of nanomaterials/nanoparticles have been identified, leading these materials into wider applications [3–14]. These unique properties are:

i. Very high surface area
ii. Small size (ranging from 1 to 100 nm)
iii. High adsorption surface area
iv. High mobility of the particles
v. Reproducibility of the particles
vi. Alternative physical properties that can be changed chemically
vii. High surface-to-volume ratio

Nanofabrication for Smart Nanosensor Applications. https://doi.org/10.1016/B978-0-12-820702-4.00006-4
© 2020 Elsevier Inc. All rights reserved.

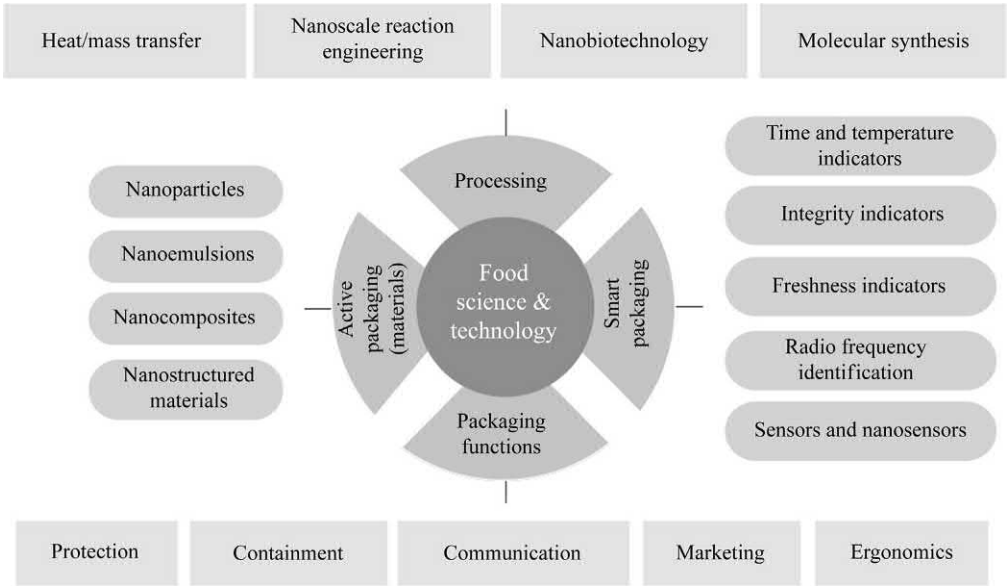

Fig. 6.1
Different applications of nanotechnology in food science and technology [15].

Table 6.1 Comparison of nanotechnology-based formulations and conventional fertilizer applications [16, 17].

Properties	Conventional technology	Nano-fertilizer-enabled technologies
Solubility and dispersion of mineral micronutrients	Less bioavailability to plants due to large particle size and less solubility	Nanosized formulation of mineral micronutrients may improve solubility and dispersion of insoluble nutrients in soil, reduce soil absorption and fixation, and increase the bioavailability
Nutrient uptake efficiency	Bulk composite is not available for roots and decreased efficiency	Nanostructured formulation might increase fertilizer efficiency and uptake ratio of the soil nutrients in crop production and save fertilizer resource
Controlled-release modes	Excess release of fertilizers may produce toxicity and destroy ecological balance of soil Effective duration of nutrient release Nanostructured formulation	Both release rate and release pattern of nutrients for water-soluble fertilizers might be precisely controlled through encapsulation in envelope forms of semipermeable membranes coated by resin-polymer, waxes, and sulfur
Effective duration of nutrient release	Used by plants at the time of delivery, the rest is converted into insoluble salts in the soil	Nanostructured formulation can extend effective duration of nutrient supply of fertilizers into soil
Loss rate of fertilizer nutrients	High loss rate by leaching, rainoff, and drift	Nanostructured formulation can reduce loss rate of fertilizer nutrients into soil by leaching and/or leaking

viii. Rapid or delayed particle agglomeration
ix. High electrical/heat conductivity.

Nanobiosensors, a modern version of biosensors, are basically analytical devices that incorporate biology-based or possibly biologically imitative element joined to a physical-chemical transducer [18,19]. The invention of the first biosensor was reported in 1967 and innovations in this field continue today [20]. History of biosensors can be categorized into three broad fields [18]:

i. First generation (electrical response-based biosensors);
ii. Second generation (mediators between the reaction and the transducer);
iii. Third generation (mediator diffusion is directly involved).

Simply, a nanobiosensor is a biosensor on the nanometer scale. For an easy comparison, in Fig. 6.2 and in Table 6.4 different sizes have been shown for different objects and microorganisms. Fig. 6.3 highlights the uptakes of different nanomaterials in the various parts of a plant body.

Nanotechnology has great potential in many of the more demanding sectors of the agriculture and food industries and is opening up new methodologies for food production, delivery of fertilizers, manufacturing with packaging, plant cropping, animal feeding, animal culture, and other areas. Nanobiosensors in the food sector have a huge potential to improve the quality of food and detect toxicity. Research is ongoing in many nanotechnological fields related to agriculture and food. In reality at this point the applications of nanotechnology are mostly

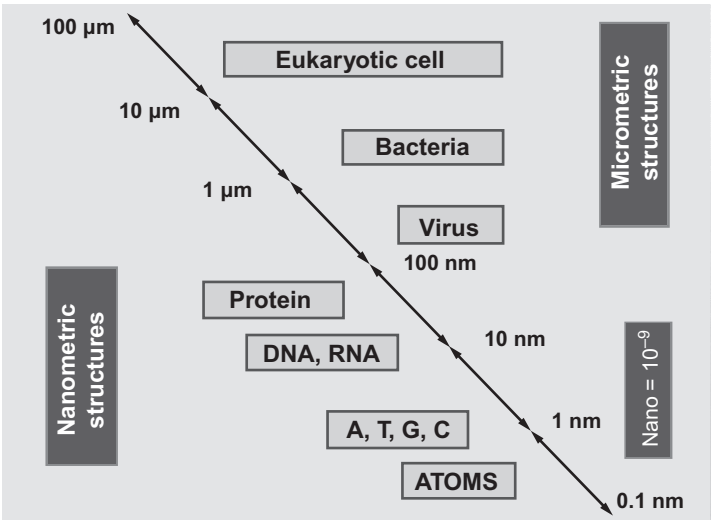

Fig. 6.2
Size comparison between different small objects/microorganisms [8].

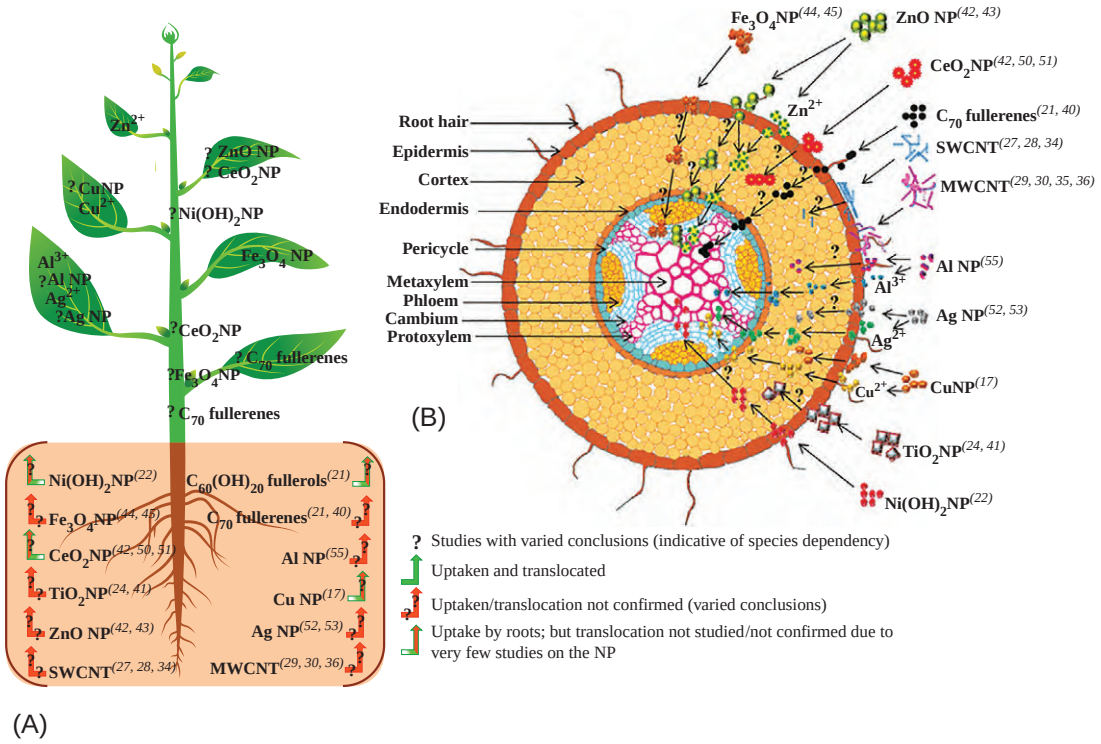

Fig. 6.3
Uptake of different nanomaterials at different sites of a plant (roots and stems) [17, 21].

observed in food processing and packaging and in nanobiosensors to detect food toxins and contaminants. Nanominerals and nanobiosensors have also found applications in the agriculture and food sectors, such as nutrient components in animal feed, quick-detection systems, and smart packaging, and these are making significant improvements in the agriculture sector [22]. This chapter focuses on and reviews various diversified applications and methodologies of nanosensors and nanobiosensors that are trending now, to meet the growing needs for healthy food and solutions to various agricultural issues. A summary of recent uses of nanotechnology in various sectors of the food industry is listed in Table 6.2.

6.2 Nanobiosensors

Nanobiosensors, or nanosensors combined with "immobilized bioreceptor" probes selective for target analyte molecules [18], were first developed in the 21st century, based on nanotechnology advancements. Currently, scientists are utilizing innovative approaches to combine nanoscience, computers, biology, and electronics to develop biosensors with powerful sensing abilities.

Table 6.2 Recent uses of nanotechnology in the food industry (A summary) [23, 24].

Product type	Name and manufacturer	Nanosize content	Reason
Nutritional supplement	Nanoceuticals "mycrohydrin" powder, RBC Lifesciences	Molecular cages 1–5 nm diameter made from silicamineral hydride complex	Nanosized mycrohydrin has increased potency and bioavailability. Exposure to moisture releases H^- ions and acts as a powerful antioxidant
Food contact material	Nanosilver baby mug, baby dream	Nanoparticles of silver	Nanosized silver particles have increased antibacterial properties
Food packaging	Adhesive for McDonald's burger containers, Ecosynthetix	Nanoparticles of silica in a polymer-based nanocomposite	Nanoparticles of silica in the plastic prevent the penetration of oxygen and gas of the wrapping, extending the product's shelf life
Nutritional drink	Durethan KU 2–2601 plastic wrapping, Bayer	300 nm particles of iron (SunActive Fe)	Nanosized iron particles have increased reactivity and bioavailability
Food contact material (cooking equipment)	Oat chocolate Nutritional drink mix nanosilver cutting board, A-Do Global	Nanoparticles of silver	Nanosized silver particles have increased antibacterial properties
Food packaging	Adhesive for McDonald's burger containers, Ecosynthetix	50–150 nm starch nanospheres	These nanoparticles have 400 times the surface area of natural starch particles

Nanobiosensors are constructed on nanoscale to analyze data on a very small scale (e.g., an atomic scale) for real-time biology-based analytical application [18, 25–28], including detection of analytes such as glucose, urea, pesticides, etc.; observing metabolites; and detection of microorganisms and pathogens. They are found both in the field and in the laboratory for analysis.

6.3 General characteristics and categories of nanobiosensors

Ideal characteristics of nanobiosensors were listed by Rai et al. [18] as presented below:

i. Nanosensors should be able to differentiate between analytes and nonanalytes.
ii. At normal storage condition, they should be stable.
iii. Interaction with the analytes should be specific and independent of any physical parameters like agitation, pH, etc.
iv. Minimum reactivity is required.
v. Responses received from the nanosensors should be precise, accurate, and reproducible.
vi. Nanobiosensors should be cheap, biocompatible, nontoxic, portable, and nonantigenic.

A nanobiosensor generally has three components:

(1) Transducer
(2) Probe (biologically sensitized materials)
(3) Detector [18, 29].

Probes are receptors, antibodies, enzymes, nucleic acids, lectins, tissue, molecular imprints, microorganisms, organelles, and so forth; they are generally either biological materials or bioderived components that accept signals from the sample, e.g., the analyte, and after that transmit it to the transducer. We expect this type of nanoreceptor to play a pivotal role in the advancements of future nanosensors. The transducer works as an interface, measures the external or physical change, interacts with the sensitive biological material, and then transforms that energy level into a quantifiable electrical signal in the detector. The detector elements receive the signals from the transducer and pass them to a microprocessor to amplify and analyze. The data is afterwards transferred to user-friendly receptors [18, 30].

There are different types of nanobiosensors, based on their operation, such as mechanical, optical, nanowire, ion channel switch, electronic, viral, pebble, nanoshell biosensors, etc. [18]. These nanobiosensors have advantages over typical biosensors currently in use, making nanobiosensors unique. Some of these advantages are:

i. They have high sensitivity in detecting a virus or even a trace amount of potentially harmful substances.
ii. Their surface-to-volume ratio is very high.
iii. They can function, even in atomic scale, with very high efficiency.

However, nanobiosensors have some drawbacks too. Research is ongoing to meet the design challenges with improvements in the technology [18].

6.4 Nanobiosensors in agriculture

Nanotechnology has already demonstrated its large potential and has a wide range of applications in food and agriculture, electronics, medicine, energy, transport, construction, textiles, water treatments, healthcare, military goods, cosmetics, automobiles, etc. In agriculture, major issues have been detected through nanotechnology, enabling the issues to be addressed, to enhance agricultural production [31, 32]. Some of these issues are:

i. Desired crop's low productivity
ii. Agricultural input efficiency low
iii. Product destruction/wastage

iv. Weak farm management
v. Loss of fertile lands
vi. Postharvest problems associated with packaging, processing, etc.
vii. Large uncultivable area
viii. Low shelf life of seed
ix. Diseases and susceptibilities to climate change
x. Higher demand for growing numbers.

Numerous applications of nanotechnology are now seen in the agricultural sector, with many types of nanocapsules and nanodevices being utilized to detect and handle plant diseases, as nanobiosensors can be targeted to a specific site of interest. Other important uses of nanobiotechnology are treatment of industrial wastewater, water filtration, and absorption of nutrients [3, 4, 32–34]. The targeted delivery of nanocomponents decreases damage to nontargeted sites of plants and also controls the detrimental effects of chemical fertilizers and pesticides on the environment. The unique chemical and mechanical properties of nanomaterials and nanobiosensors make them active electrochemically. Such nanobiosensors may play a valuable role in animal and plant breeding as well as in culturing. Many nanomaterials are being used for wastewater treatment and soil analysis and some are used to deliver nutrients and pesticides to the plants, to a particular targeted point [32, 35]. Particular and gross applications of nanotechnology are shown in Fig. 6.4.

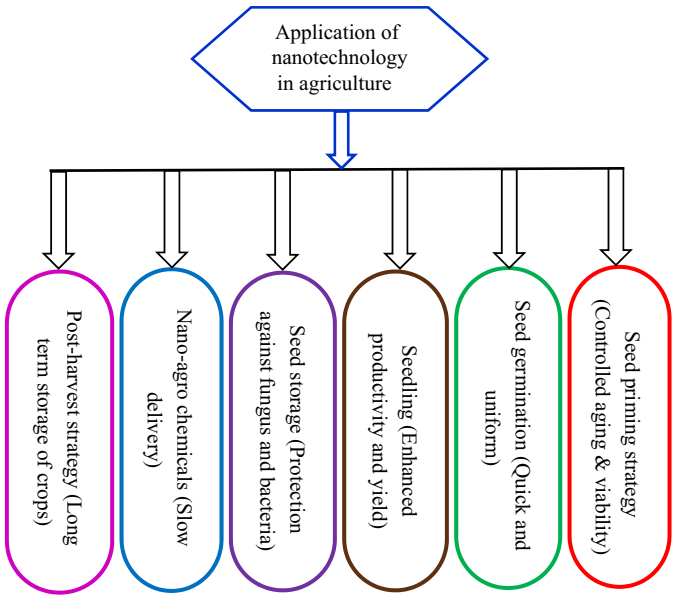
Application of nanotechnology in agriculture
Post-harvest strategy (Long term storage of crops)
Nano-agro chemicals (Slow delivery)
Seed storage (Protection against fungus and bacteria)
Seedling (Enhanced productivity and yield)
Seed germination (Quick and uniform)
Seed priming strategy (Controlled aging & viability)

Fig. 6.4
Uses of nanotechnology at different phases of agriculture [32].

6.5 Detection by nanosensors

Nanosensors represent a powerful tool to identify deficiencies of nutrients, toxicity, plant and animal diseases, and controlled plant health, for improved food quality as well as safety. They can help to expand agricultural yield with higher efficiency, such as applying irrigation, pesticides and fertilizers with minimum loss. Two types of nanosensors are currently used in agriculture: (i) bionanosensors and (ii) electrical nanosensors [36]. The biological organism in bionanosensors can identify an environmental condition; the combination of biology and nanoparticles into sensors has the ability to boost sensitivity and eventually decrease response time for sensing a probable problem [36, 37]. For example, different types of biosensors have been developed for accurate recognition of microcystins toxicity that are formed by cyanobacteria, which poses a severe threat to agricultural products as well as cattle health [36, 38]. Applications of nanosensors for agricultural product safety are listed in Table 6.3.

For pesticide detection in food material and the environment, wireless nanosensors have played an important role. They are also important in quality control and environmental safety. Salicylic acid (phenolic phytohormone) in a plant improves growth, transpiration, photosynthesis, and other aspects. It is a major plant component and the need exists to identify levels of salicylic acid in plants. Electrical-based nanobiosensors with Au electrodes modified with Cu nanoparticles (copper nanoparticles) have been used for this application [36, 39]. Cu nanoparticles detect the electrocatalytic oxidation of salicylic acid and thereby identify the electrochemical nature of salicylic acid. An Au nanoelectrode combined with Cu nanoparticles most precisely identify salicylic acid levels in oilseeds that are infected with the fungal pathogen *Sclerotinia sclerotiorum* [36, 39]. An electrochemical nanobiosensor along with a C-nanotube (carbon nanotube) electrode modified with a deposition of Au nanoparticles was used to recognize triazophos (an insecticide), which was initially present in postharvest crops and vegetables [36, 40]. Silver (Ag) and gold (Au) nanoparticles were used in a nanobiosensor to identify the level of organophorous type of pesticide present in the environment or postharvest food [36, 41–43]. SERS (surface-enhanced Raman scattering spectrum) has been used in different branches of analytical chemistry as well as in the agricultural sector to identify pesticides in both food and the environment. In a recent study, a monolayer of tailored Ag nanoparticles was used to boost the sensitivity for Raman detection and assisted in detecting concentration of methylparathion [36, 44].

Governments of various developed countries continue to expend large amounts of money on advanced research and development of nanotechnology in different sectors, including the food industry and agricultural sectors. The US government spent $862 million in 2003–2005 and proposed $1574.3 million to different agencies under National Nanotechnology Initiative (NNI) for the years 2013–2016. It is quite obvious that the contribution of nanotechnology to boost the economic situation of countries like United States, China, Germany, Russia, and Japan increased substantially. Some other countries, like Taiwan and India, are trying to increase their annual budgets for advanced

Table 6.3 Application of nanosensors for agricultural product safety [36].

NPs	Size (nm)	Sensor type	Target	Detection limit	Reference
Gold (Au)	NA	Biosensor	Neurotoxic organophorous pesticide in environment	Not available	[41]
Cu and Au	<100	Electrochemical	Fungal pathogen *Sclerotiniasclerotiorum* in oilseed rape	0.1 μM	[39]
Au	4–7	Biosensor	Organophorous pesticide and immobilization of protein in food	0.8 pg/mL	[42]
Au coated Carbon-nanotube (CNT)	30–60	Electrochemical biosensor	Triazophos in vegetables and food sample	9.3×10^{-8} M	[40]
Silver (Ag)	<50	Raman detector	Monolayer film to detect pesticide	10^{-7} M	[44]

research and development of nanotechnology, to improve their competitive advantage in the international market as well as to fulfill the demands of the economic situation [36, 45].

6.6 Nanobiosensors in different food sectors

Metallic nanoparticles have many applications in the food technology sector because of their particular shape- and size-dependent properties. The optical, chemical, mechanical, antimicrobial, and electronic properties of metallic nanoparticles make them unique for combination with enzymes, drugs, ligands, antibodies, colorimetric and fluorimetric agents, and other types of biomolecules. Thus these nanoparticles are applicable in sophisticated diagnostic assays, radiotherapy, thermal ablation, gene and drug delivery, optical imaging, effective antimicrobial activities, and decontamination of hazardous compounds, among other functions [46, 47]. Moreover, metallic nanoparticles have a huge impact on food production, consumption, and the ability to quickly respond to pathogens, packaging issues, pesticides, and toxic residues, by detecting microbial weakening of the quality of food as well as contaminants. Of all the metallic nanoparticles currently in use, the colloidal gold nanoparticle is found to be the most commonly applied in a variety of functions, because of its flexible size range of about 10–250 nm; it also possesses shape-dependent optical and mechanical properties as well as being generally complex in nature [47, 48]. Table 6.4 lists different nanomaterials applied in the food sector.

Considering optical properties, the emission spectra of Au nanoparticles are subjugated by local surface plasmon resonance. On excitation of the conduction band coherently, electrons induce oscillation coherently on the positive metal-lattice by an oscillating electromagnetic field. The combination and aggregation of Au nanoparticles in nanosensors or nanobiosensors are expected to significantly increase the sensitivity of local surface plasmon resonance (SPR) two- to tenfold, and also surface-enhanced Raman scattering within 106–109-fold [47, 49]. Strong local SPR absorption along with very high elimination coefficients within the visible wavelength

Table 6.4 Size range of different nanomaterials in the food sector [50].

Different structure	Size (nm) [diameter/length]
DNA	12
Glucose	21–75
Liposome	30–10,000
LDH	40–300
Amylopectin	44–200
Casein micelle	60–100
PLA nanosphere	100–300
Zein	200
Cubosome	500
Nanosensors	<1000

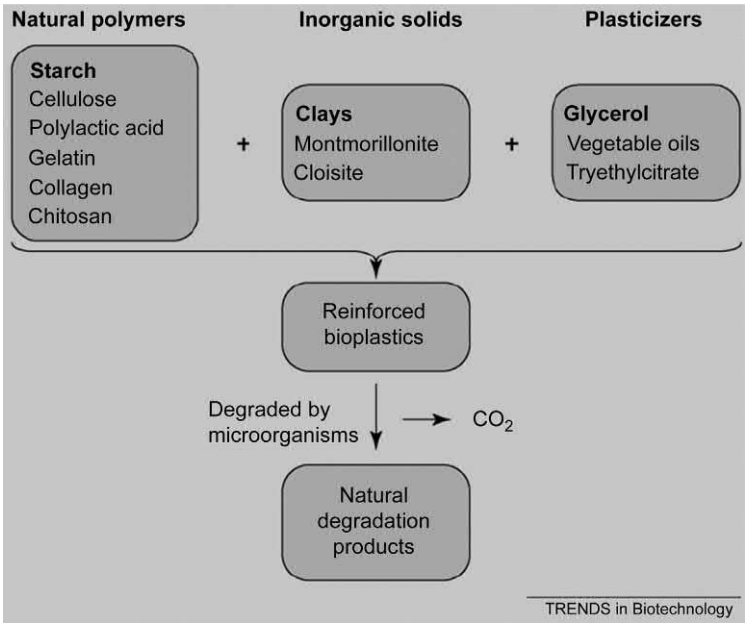

Fig. 6.5
Representation of the formation of bionanocomposites. Besides their improved material properties, their biodegradability makes them an environmentally friendly alternative to traditional packaging [50].

range are the identified characteristics of Au nanoparticles and it generally shows a color transition from deep red to blue after attaining the aggregation state [47]. Fig. 6.5 represents the formation of bionanocomposites and, apart from their improved material properties, the biodegradability, which makes them an environmentally friendly alternative to traditional packaging.

The assessment of residual antibiotics in milk, dairy products, and meat is a crucial scenario in the food technology and agricultural sectors. Au nanoparticles synthesized using pyrocatechol violet (reducing agent) to give a surface OH^- group could be linked with a hydroxyl (OH^-) and amide (NH_2^-) group of an antibiotic through H-bonding. Antibiotics such as kanamycin, streptomycin, neomycin and bleomycin quantity can be identified via color change at a very low concentration level of 10^{-9} mol L^{-1} [47, 51].

The detection sensitivity is improved by joining different functional groups with Au nanoparticles, such as thioaniline and mercaptophenyl boronic acid. Thioaniline acts as an electropolymerized material and mercaptophenyl boronic acid delivers a reversible binding capability that is pH-dependent, and it stabilizes the complex formation, also prevents from precipitation. The thioaniline crosslinked Au nanoparticles generate a matrix which is molecularly imprinted, which exhibits great sensitivity towards identification of the antibiotic analytes. The quantities of antibiotics such as neomycin, streptomycin, kanamycin, and others

are detected by analyzing the SPR curve before and after, with impressive sensitivity of 2.00 ± 0.21 pM, 1.00 ± 0.10 pM, and 200 ± 30 fM, respectively [47, 51].

Pollutants such as the carcinogenic nitrile were sensed using an Ag nanoparticle-based nanosensor containing branched polyethyleneimine. The reaction of nitrite with H_2O_2 (hydrogen peroxide) produces peroxynitrous acid under low pH conditions and prompts the aggregation of Ag nanoparticles. Fluorescence quenching was associated with the concentration of nitrite within the limit of recognition of 100 nM [43, 47]. Au nanoparticle SPR is used for the detection of ochratoxin-A, a mycotoxin made by the *Aspergillus* and *Penicillium* types of agricultural and food toxins or contaminants. Thiolated aptamers are covalently attached to Au nanoparticles via an Au-S (gold-sulfur) bond for the detection of ochratoxin-A toxin [47, 52]. The identifying mechanism is generally based on the capability of the antioxidants to protect fluorescence of Au nanoparticles, and this methodology is used for evaluating the antioxidant quantity in commercially used and consumed fruit juices; it has been demonstrated to be one of the major spectroscopic detecting methods, with regard to rapid response and better biocompatibility [47, 53].

The example of natural honey contamination with sulfonamide residues is a chief concern to modern food industries, because these residues of antibacterial drugs can have toxicological effects and risks, along with allergenic effects. Polyclonal antiserum against sulfathiazole together with colloidal Au nanoparticles assists as a recognition reagent for a lateral flow immunochromatographic assay (shown in Fig. 6.6). C-nanotubes display huge potential in development of nanobiosensors for numerous applications in the area of nanobiosensor technology, because they possess special properties including tiny size, high electrical and thermal conductivity, high strength, and high specific surface area [47, 54]. Quinoxaline-2-carboxylic acid is a type of indicator residue of carbadox, which is a component of food as an additive used in pork, chicken, and fish, having strong carcinogenic and mutagenic effects [47, 55]. In an attempt to distinguish insignificant levels of quinoxaline-2-carboxylic acid, multiwall C-nanotubes are functionalized with chitosan fabricated on a glassy carbon electrode. Sol-gel molecularly imprinted polymer film acts as the detection element [47, 56]. This electrode has been established as a reproducible and reliable electrochemical sensor for the measurement of quinoxaline-2-carboxylic acid at a very low level of concentration in meat samples, with a detection limit of as low as 4.4×10^{-7} mol L^{-1} [47, 57]. Fig. 6.7 shows a typical nanobiosensor comprising essential components starting from the sample analyte to bioreceptor and transducer with integrated nanostructures.

A single-wall C-nanotube was adapted for detecting D-fructose in different liquids such as fruit juices, honey, soft drinks, energy drinks, etc. [47, 58]. An immobilized fructose dehydrogenase enzyme-based nanobiosensor was developed by utilizing polymer (osmium redox polymer as redox mediator) to transport the electrons in between the immobilized fructose dehydrogenase enzymes. A single-wall C-nanotube was inserted as the working electrode. The optimized level biosensor required only 5 units of enzyme and kept 80% of its preliminary sensitivity even after 4 months. This nanobiosensor has a recognition limit for fructose to estimate a minimum level

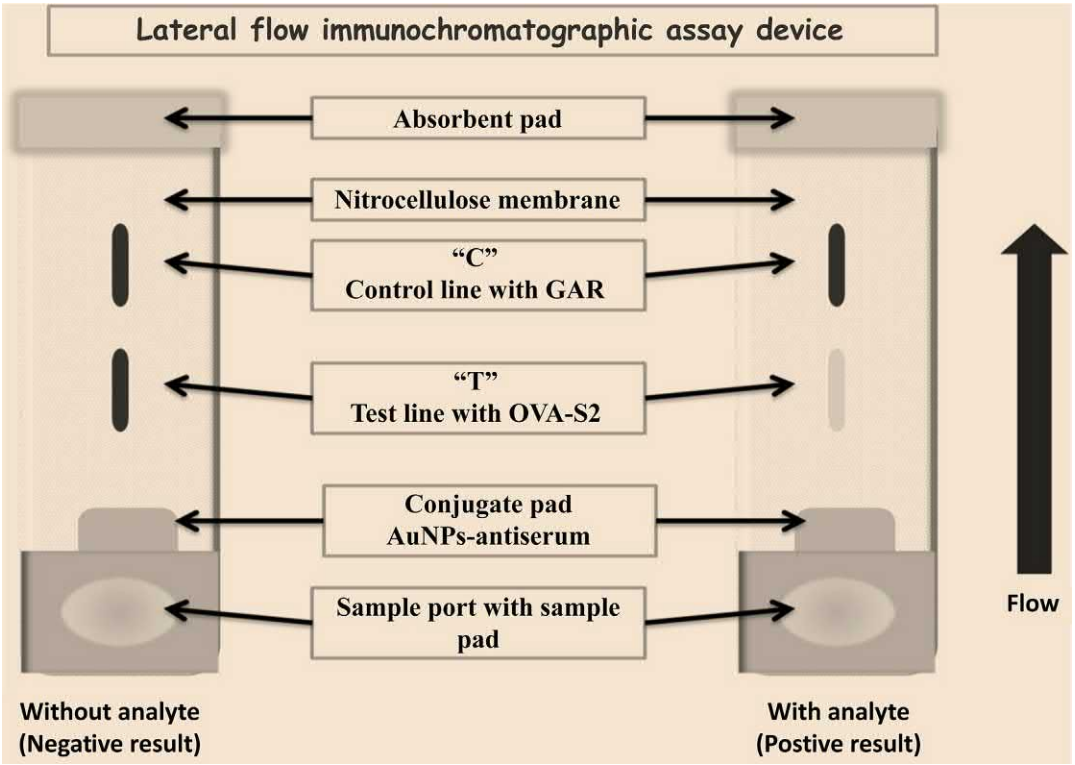

Fig. 6.6
Lateral flow immunochromatographic assay (LFIA) is used for the identification of sulfonamides as a contaminant in a natural honey sample [47].

of 1 μM with high accuracy, good reproducibility, and faster response time for 4 s [47, 59]. Moreover, carcinogenic Sudan-I was detected by a multiwall C-nanotube. Improvements from electrochemical oxidation on the upper surface of the electrode using Sudan-I dye was achieved by an electrochemical method adapted with a limit of detection accuracy up to 5.0 μg L^{-1} [47, 60].

6.7 Development of nanosensors in agrofood sector

Nanosensors or nanobiosensors can be identified as extremely small devices able to bind to whatever is required and send a signal to receptors. These sensors transfer a response into a signal or output that can be understood. Nanosensors have several advantageous properties as compared to other traditional sensors, such as low cost, sensitivity and selectivity, real-time detection, high efficiency, portability, and other necessary features, which can be improved even more by using different metals and nanomaterials in their construction [22, 61]. There are several methods for the development of nanosensors, including top-down lithography,

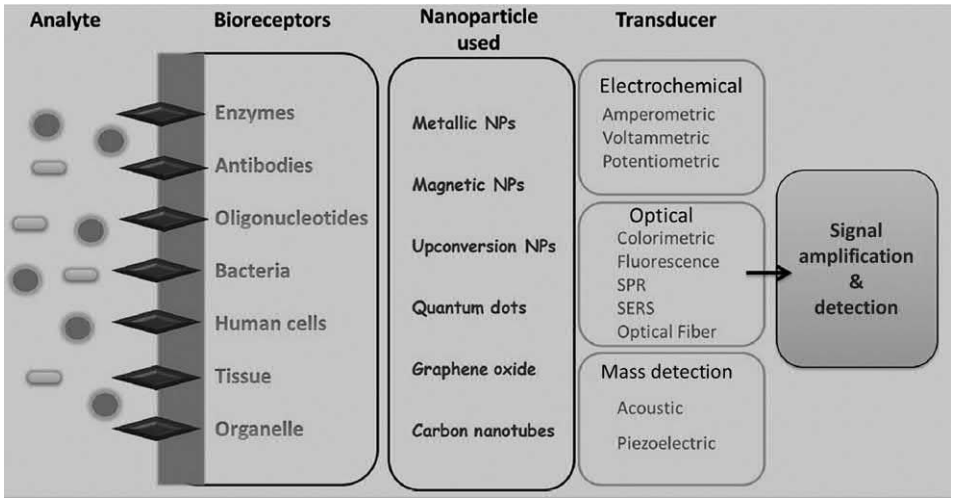

Fig. 6.7
A typical nanobiosensor comprises essential components starting from sample analyte to bioreceptor and transducer with integrated nanostructures [47].

molecular self-assembly, and bottom-up assembly approaches. Current nanosensors being used in the agricultural sectors can be broadly divided into the following categories [22, 57].

- Nanotubes
- Nanoprobes
- Nanoparticles
- Nanosensors having nanowires
- Cantilevers involving nanosystems
- Nano-electromechanical systems (NEMS) [22].

Several nanosensors and nanobiosensors have found practical roles in the agricultural sector and food industry, to quickly identify threats or pollutants in the case of suspected food poisoning or toxicity, or in combination in packaging as nanotracers to trace past records of food products, showing whether they are still within acceptable quality limits at any time. Examples are the application of nanosensors or nanobiosensors in food packaging to identify growth of microorganisms and color changes when an edge level is approached. Nanosensors applied in queue with process control, for monitoring of storage conditions, will be useful in the near future to prevent food poisoning [22, 62]. Nanotechnology has become a proven method in the agricultural sector to increase productivity, improve the quality of the soil, stimulate plant growth, and provide effective monitoring system (Fig. 6.8). Development of atrazine nanopesticides is another innovative nanotechnology development for the healthy growth of plants; a schematic representation of the development of atrazine nanopesticides is presented in Fig. 6.9.

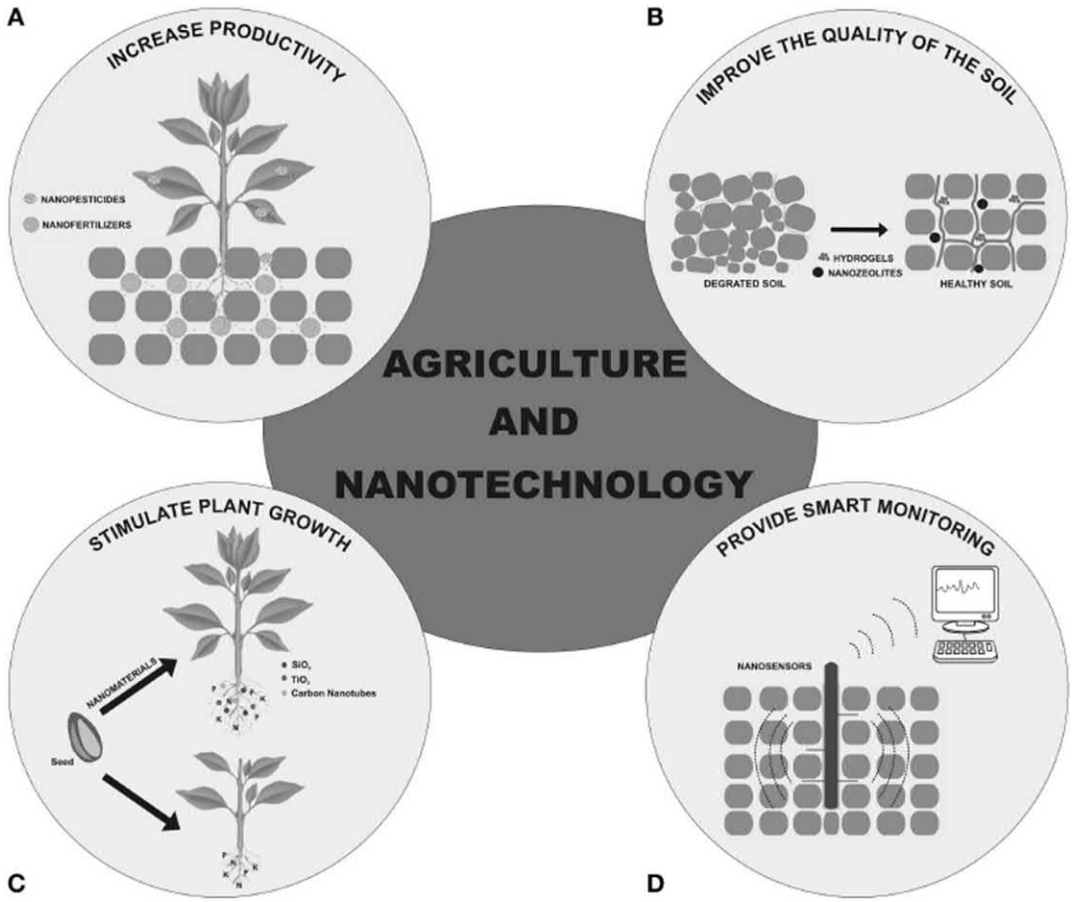

Fig. 6.8
Higher potential application of nanotechnology in agricultural sector. (A) nanopesticides and nanofertilizers; (B) nanozeolites and nanohydrolites; (C) SiO_2, TiO_2, and carbon nanotubes; (D) nanosensors by wireless communication device [63].

Nanosensors used in food analyses employ a combination of nanotechnology, biology, and chemistry. An example is Au-nanoparticles functionalized with different polymers or molecules that can cling to materials such as pesticides, fertilizers, etc. Farmers will be able to spray these nanoparticles on their fields to identify a chemical, such as a particular type of pesticide, at the targeted surface [22]. A summary of comparisons between nanofertilizers and conventional ones is found in Table 6.5.

Another important application involves nanoparticle-based aptasensors, consisting of a particular target-identifying element (aptamer) and a nanomaterial (the signal enhancers of transducers). Aptamers can be defined as single-strand nucleic acids or peptide molecules of

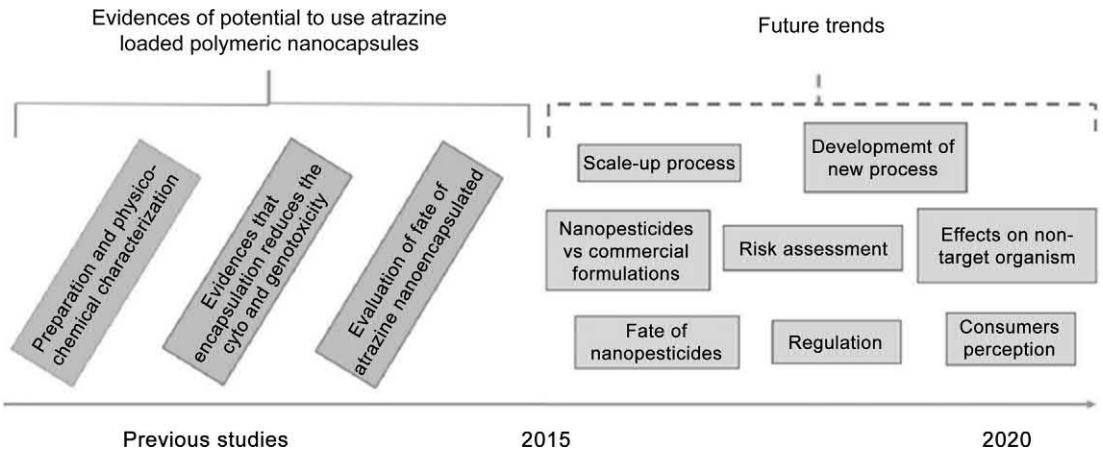

Fig. 6.9
Development of atrazine nanopesticides (now and in future) [63].

Table 6.5 Comparison between nanofertilizers and conventional types [32, 64].

Properties	Conventional fertilizers	Nanofertilizers
Solubility and dispersion of micronutrients	Less bioavailability due to large particle size and less solubility	Improved solubility and dispersion of insoluble nutrients in the soil
Nutrient uptake efficiency	Decrease efficiency and the bulk composite is not available for roots resource	Increase uptake efficiency and uptake ratio of the soil nutrients in crop
Controlled release	Excess release causes toxicity and ecological imbalance of soil	Release rate and release pattern controlled through encapsulation
Effective duration of nutrient release	Much smaller amount used by the plants, rest is converted into insoluble salts	Nanosized formulation can extend effective duration of nutrient supply
Loss rate of fertilizer nutrient	High loss rate by leaching, run off, and drift	Reduces loss rate of nutrients

less than 25 kDa with either natural or artificial origin. These nanosensors are very specific and also selective towards their particular target compounds, such as ions, microbes, proteins, viruses, toxins, etc., due to their precise and well defined 3D assemblies. Aptamers are called artificial antibodies because of their selecting and generating capability through an in vitro molecular technique called SELEX. The dissociation constants of aptamers are found to be within the nM (nanomolar) or pM (picomolar) range. Aptamers are widely used as detecting materials in the fabrication of aptasensors [22, 65]. An extensive variety of nanomaterials can be applied in aptasensors, including metal nanoparticles and nanoclusters, C-nanoparticles, semiconductor nanoparticles, magnetic nanoparticles, and others [22, 65]. A range of transducer systems has been employed in aptasensors for food quality assessment and high-priority health

safety issues. The working principles of aptasensors basically depend on the properties of the nanoparticles incorporated in them.

Additionally, it should be mentioned that nanosensors incorporating Raman spectroscopy can be well suited for food forensic science. Food forensics is an investigation methodology concerned with food origin, adulteration, contamination, or even identifying toxicities. Nanosensor application in these fields can contribute to the specified methodology and allow the application of several analytes to be probed, starting from the macrofood, to proteins, carbohydrates, lipids, dyes, pigments, or preservatives. Some additional examples of nanosensors and their development for agriculture and food applications are depicted in Fig. 6.10 [18, 22, 62, 66]. According to Fig. 6.10 and surveys of research articles [18, 22, 61, 67–71], the list of potential applications of nanosensors in agricultural and food supply chains can be categorized as shown in Table 6.6 [22].

As seen from the examples described, nanosensors or nanobiosensors are useful for detecting and reporting real-time data from a range of food and agricultural products, starting from production, through delivery, to the hand of the consumer. Nanobiosensors are simply the passive, information-accepting devices that can collect information from immediate and isolated backgrounds and be used to investigate, record, and report data to the receiver. They can be designed and manipulated to manage perilous control points in the supply chain, from the point where food is being produced or packaged up to the time it is being consumed. Recent studies show that developments have ensued in nanobiosensors' ability to provide quality assurance by tracing microbes, toxins, or contaminants via the

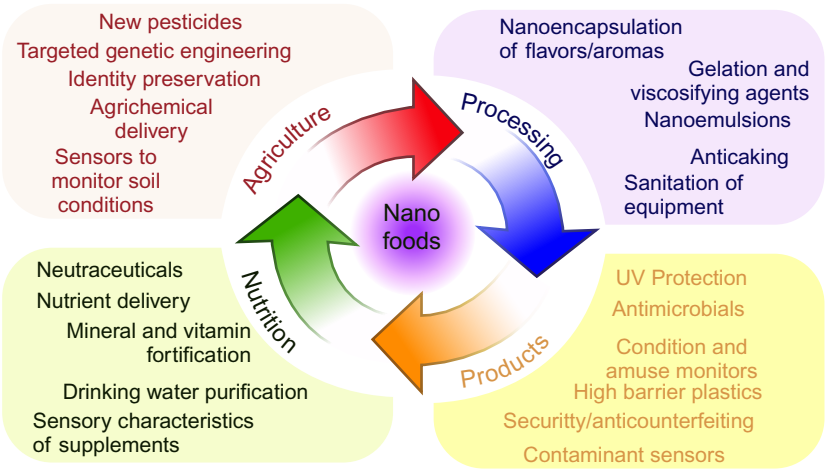

Fig. 6.10
Benefits of nanotechnology in different sectors of the food industry [22, 72]. Reproduced with permission from T.V. Duncan, The communication challenges presented by nanofoods, Nat. Nanotechnol. 6 (2011) 683–688.

Table 6.6 Nanosensor potential applications in the agrifood sector [22].

Agriculture	Food processing	Food packaging	Food transport	Nutrition
• Nanosensors for monitoring soil conditions (e.g., moisture, soil pH), a wide variety of pesticides, herbicides, fertilizers, etc. • Nanosensors for detection of foodborne contaminants or for monitoring environmental conditions at the farm • Nanochips for identity preservation and tracking • Nanocapsules for delivery of pesticides, herbicides, fertilizers, and vaccines • Nanosensors and nano-based smart delivery systems for efficient use of agricultural natural resources	• Nanoencapsulated flavor enhancers • Nanotubes and nanoparticles as gelation and viscosifying agents • Nanocapsule infusion of plant based steroids to replace a meat's cholesterol • Nanoparticles to selectively bind and remove chemicals or pathogens from food • Aptasensors for determination of microbial toxins (e.g., OTA, Fumonisin B1)	• Portable nanosensors to detect chemicals, pathogens, and toxins in food • DNA biochips to detect pathogens and to determine the presence of different kinds of harmful bacteria in meat or fish, or fungi affecting fruit • Nanosensors incorporated into packaging materials for detection of chemicals released during food spoilage and to serve as electronic tongue (e.g., bitter, etc.) • Electromechanical nanosensors to detect ethylene • Nanosensors applied as labels or coating to add an intelligent function to food packaging in terms of ensuring the integrity of the package through detection of leaks, etc.	• Nanosensors for monitoring environmental conditions during distribution and storage • Nanosensors for traceability and monitoring product conditions during transport and storage, which is crucial for products that have a limited shelf life • Smart-sensor technology for monitoring the quality of grain, dairy products, fruit and vegetables in a storage environment in order to detect the source and the type of spoilage • Aptasensors for determination of microbial cells (e.g., *Salmonella typhimurium*, *Escherichia coli*, *Listeria monocytogenes*)	• Nanocapsules incorporated into food to deliver nutrients • Nanocochleates (50 nm coiled nanoparticles) for delivering nutrients (e.g., vitamins, lycopene, and omega fatty acids) more efficiently to cells, without affecting the color or taste of food

food processing queue, by using data capture for automatic control functions and documentation [22, 61].

6.8 Application of nanosensors in food packaging

Nanotechnology has a proven ability to modify food-packaging materials and more applications will be forthcoming in the near future. The nanoscale revolution potentially introduces new improvements to food packaging in the forms of mechanical properties, pathogen identification, and modern packaging systems that ensure the safety of the food and its quality. The coating of an aluminum nanolayer over food packaging is one good example of the role that nanotechnology is already playing in food sector packaging. For food and beverages, the global nanoenabled packaging market attained $6.5 billion in 2013 and was estimated to grow at a compound annual growth rate (CAGR) of 12.7% over 2014–2020 reaching a value of $15.0 billion in 2020 [73, 74]. Nanomaterials are plentiful and several techniques are practical for fabrication of many nanomaterials. Nanoparticles can be formed from larger structures by grinding, pulverizing, laser usage, and vaporization followed by cooling. Other methods are commonly used for the synthesis of complex-type nanoparticles or nanocomposites, including solvent extraction/evaporation, self-assembly, layer-by-layer deposition, crystallization, microbial synthesis, and biomass reactions [74, 75]. Fig. 6.11 represents the effect of interfacial partitioning of molecules on mass transfer between food and packaging materials. This effect is very important for food quality as well as the prediction of food quality degradation.

Nanocomposite packages are predicted to attract a significant portion of the food packaging market in the near future. Many nanocomposite food packages are already on the market or are

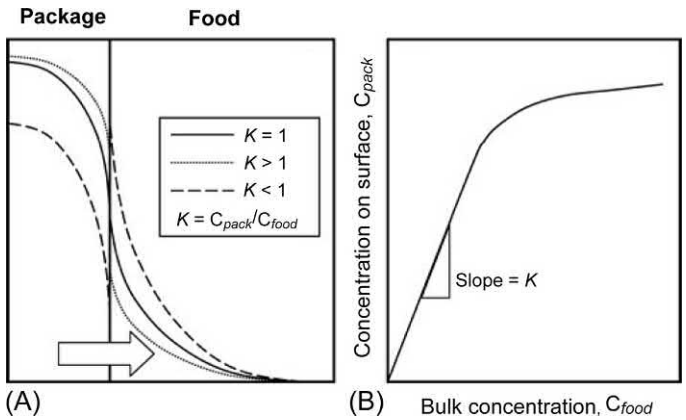

Fig. 6.11

Effect of interfacial partitioning of molecules on mass transfer between food and packaging materials: (A) migration of package constituents into foods, (B) "scalping" (absorption) of food flavor into packaging materials. K is a partition coefficient of a migrant [74].

being developed, the mainstream of these packages being targeted for liquids packaging. Motivations for this predicted growth are the astonishing benefits nanoscience offers to improve food packages. Developments in the fundamental characteristics of food packaging materials, such as strength, barrier properties, antimicrobial properties, and stability to heat and cold, are achieved through use of nanocomposite materials. In 1980s, Toyota was the first company to commercialize nanocomposite materials. According to the company, the addition of nanosized montmorillonite clay (5% by weight) significantly enhanced the mechanical as well as thermal properties of different grades of nylon [74, 76]. Nanocomposite materials are now widely used in gasoline tanks, interior and exterior panels, bumpers, etc. in vehicles [74, 77]. Research on the use of nanocomposites for food packaging began in the 1990s. Montmorillonite clay is used as nanocomponent with various polymers such as polyethylene, polyvinyl chloride, nylon, starch, and so on. The amount of nanoclay added to the polymer ranges from 1% to 5% by weight. The higher surface area of the nanocomposites results in unique properties when they are merged into packages [74]. Fig. 6.12 shows the life cycle of a packaging system.

Three common methods are being introduced to process nanocomposites: the solution method, the interlamellar polymerization technique, and melt processing. The first method (solution method) can be used to form both inserted and exfoliated nanocomposite materials. The nanocomposite clay is at first immersed in a solvent in this method. Then it is mixed into a polymer solution, and then the larger polymer molecules are permitted to spread between the layers of filler. The solvent is afterwards allowed to evaporate. The second method (interlamellar) swells the fillers by absorption of a monomer in liquid form. When the monomer has entered in between the silicate layers, polymerization is started by heat, radiation, or a combination of initiators. The third, or melt, method is commonly used due to the lack of solvent and its cost-effectiveness. In the melting process, the nanocomposite filler is integrated into a polymer in molten condition and later transformed into the final desired material [74, 77].

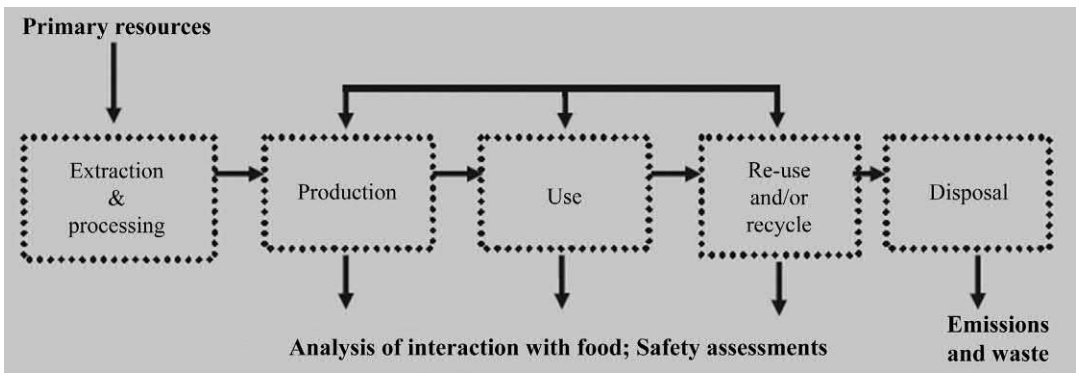

Fig. 6.12
Life cycle of a packaging system [78].

Bayer produces plastic films of transparent nanocomposites; this coating is called Durethan, which has clay nanoparticles isolated throughout the plastic. Large amounts of silicate nanoparticles are scattered in the film of polyamide, and these nanoparticles have the ability to block oxygen and carbon dioxide as well as moisture from reaching fresh meats and other foods. Nanoclay particles represent impermeable obstacles in the diffusion process, thereby helping to extend the shelf life of foods while improving their quality. The package is also found to be considerably lighter, stronger, and more heat-resistant [74, 79].

Plastic bottle beer packaging was not possible because of oxidation and flavor-mixing problems. Recently this challenge has been overcome and beer packaging has been improved by the usage of nanotechnology. For example, a subsidiary of Amcol International Corp., called Nanocor, is making nanocomposites for application in plastic beer bottles. By the combination of nanocomposites along with oxygen scavenging technologies, a new family of barrier nylons was recently developed for use in multilayer, coinjection blow-molded PET bottles. Similar materials are being developed to extend the shelf life of soft drinks. Another advantage of these nanocomposite bottles is that their mass is considerably less, thereby reducing costs [74, 79].

A significant amount of research is also taking place in the field of biodegradable nanocomposites used for food packages. Films can be shaped with exfoliated layers of clay by pumping carbohydrates and clay fillers through cells with high shear. These types of films serve as very effective moisture barriers, because they increase the complexity of the path water must take to penetrate the films. Very large increases in film strength can also be achieved in these types of materials. Starch and chitosan are two of the most-studied biodegradable matrices [74, 76].

Carbon nanotubes are cylindrical shapes of carbon with diameters in the nanoscale range, which can also be used in food packaging to enhance the mechanical properties. Moreover, it was recently shown that they can also exercise powerful antimicrobial effects. *Escherichia coli* was observed to be died immediately upon direct interaction with aggregates of carbon nanotubes. Apparently, long, thin nanotubes punctured the *E. coli* cells, thereby causing damage to the cellular body. Single-wall carbon nanotubes may ultimately serve as building blocks for antimicrobial materials [60, 74]. Nano-wheels are another recently manufactured material to improve food packaging. Inorganic alumina platelets are self-assembled into wagon-wheel shaped structures, and combined into plastics to increase their barrier and mechanical properties [74, 80].

As mentioned earlier, nanosensors can be used to detect pathogens, chemicals, bacteria, viruses, and toxic materials in foods, and abundant research reports designate the detection methods for these materials using nanotechnology. For example, antibodies of Staphylococcus enterotoxin B can stick onto poly(dimethyl-siloxane) chip molded nanobiosensors, with a detection limit of 0.5 ng mL^{-1} [74]. Nanodevices so far have been established to detect *E. coli* 0157:H7 and

Salmonella spp. simultaneously, as well as *Listeria monocytogenes*. Liposome nanovesicles have been devised to detect peanut allergen proteins [74, 75].

Agro-Micron has been established as a nanobioluminescence detection spray that contains a luminescent protein, prepared to bind to the surface of microbes such as Salmonella and *E. coli*. While binding, it emanates a visible glow that varies in intensity according to the amount of contamination found in the sample caused by the bacteria. This product is marketed under the name BioMark [68, 74]. Nanosensors Inc. is another company chasing this potential. Through an agreement with Michigan State University, a nanoporous silicon-based biosensor was developed, thus far to detect Salmonella and *E. coli*. A prototype nanobiosensor was newly verified to detect *Bacillus cereus* and *E. coli* and was identified to be able to detect multiple pathogens quicker and more accurately than current devices [74, 81]. Mahadevan Iyer and his colleagues at Georgia Institute of Technology are investigating the integration of nanocomponents in ultrathin polymer substrates for RFID chips containing biosensors that are found to be able to detect foodborne pathogens or sense the temperature level and moisture content of a product [74, 82].

DNA biochips are already under expansion by the researchers to identify pathogens. Researchers at the University of Pennsylvania and Monell Chemical Sciences Center have used nanosized carbon tubes coated with strands of DNA to produce nanosensors with the ability to distinguish odors and tastes. A single strand of DNA acts as the sensor and a carbon nanotube serves as the transmitter. Using similar technologies and methodologies, electronic tongue nanosensors are being established to detect substances at PPT concentration levels, which could be used to activate color changes in food packages to make consumers aware when food is not in a condition to be used or consumed. A major aspect of these nanobiochips is that the DNA is self-assembled onto the chips and repairs itself if it is damaged [74]. Researchers at Cornell University have designed synthetic DNA barcodes to tag pathogens and monitor their movement. The nanobarcodes fluoresce under ultraviolet light when target compounds are detected [74, 83]. Scientists at the United Kingdom's University of Southampton and the Deutsches Kunststoff Institute in Germany established these exceptional self-assembled structures from arrays of spheres stacked in 3D. Polymer opal films generally belong to a class of materials typically identified as photonic crystals. These types of crystals are constructed of tiny repeating units of carbon nanoparticles wedged between spheres, which lead to deep colors that impersonate the colors associated with the photonic crystals. Photonic crystals can be used to produce exclusive food packaging materials that change color when required [74, 84].

6.9 Conclusions and future directions

The works discussed in this chapter prove that nanotechnology has the ability to offer many improvements and has already established itself at almost every sector of science. Modern science is gradually updating towards nanotechnology because of its efficiency,

cost-effectiveness, reproducibility, and of course because of its size. The agriculture and food sectors are very sensitive areas, as they are directly related to human health. The modern world is much concerned about production levels, quality, health, and environmental safety, and nanosensors and nanobiosensors, having very high efficiency in detecting toxicity levels, can play vital roles in ensuring health safety. Starting from seed preservation through to packaging, we have examined the many uses of nanotechnology in these important fields.

Modern technology is also investigating the usage of Janus nanoparticles in different disciplines. Janus particles are of dual nature and have proven their efficiency in cases such as drug delivery and wastewater management. We expect in the future that properly modified Janus nanobiosensors will play a vital role in detection of plant diseases, drug delivery, and fertilizer distribution to targeted points with specific amounts. However, much more research is required in this area, since the efficient and economically feasible preparation of Janus particles still faces major challenges.

In future, the concept of "smart" packaging will likely become common, with antigen-specific markers being used to make thin films of polymer nanocomposites through incorporating nanoparticles in the food packaging. The specified antigen markers may help to detect and isolate microorganisms responsible for spoilage. These new nanosystem applications should focus on attaining environment-friendly status, as well as have minimal toxic effects on food and consumers.

We expect that the development of novel nanosensors as highlighted in this chapter will enhance manufacturing of affordable and easily operable nanomaterial-based sensing system. However, the full perspective of nanobiosensors in the agriculture and food sectors is yet to be recognized. This chapter has mainly reviewed different aspects and applications of nanosensors and nanobiosensors in the various diversified field of the agriculture and food sectors, which are currently being developed or are already being used.

References

[1] G.N. Rameshaiah, J. Pallavi, S. Shabnam, Nano fertilizers and nano sensors – an attempt for developing smart agriculture, Int. J. Eng. Res. Gen. Sci. 3 (2015) 314–320.

[2] M. Sharon, A.K. Choudhary, R. Kumar, Nanotechnology in agricultural diseases and food safety, J. Phytol. 2 (2010) 83–92.

[3] A.Z.M. Badruddoza, Z.B.Z. Shawon, M.T. Rahman, K.W. Hao, K. Hidajat, M.S. Uddin, Ionically modified magnetic nanomaterials for arsenic and chromium removal from water, Chem. Eng. J. 225 (2013) 607–615.

[4] A.Z.M. Badruddoza, Z.B.Z. Shawon, W.J.D. Tay, K. Hidajat, M.S. Uddin, Fe3O4/cyclodextrin polymer nanocomposites for selective heavy metals removal from industrial wastewater, Carbohydr. Polym. 91 (2013) 322–332.

[5] M. Golieskardi, M. Satgunam, D. Ragurajan, M.E. Hoque, A.M.H. Ng, L. Shanmuganantha, Advanced 3Y-TZP bioceramic doped with Al2O3 and CeO2 potentially for biomedical implant applications, Mater. Technol. 34 (2019) 480–489, https://doi.org/10.1080/10667857.2019.1578912.

[6] M.R. Ketabchi, M. Khalid, C.T. Ratnam, S. Manickam, R. Walvekar, M.E. Hoque, Sonosynthesis of cellulose nanoparticles (CNP) from kenaf fiber: effects of processing parameters, Fibers Polym. 17 (2016) 1352–1358, https://doi.org/10.1007/s12221-016-5813-4.

[7] F.M. Michael, M. Khalid, C.T. Ratnam, W. Rashmi, M.E. Hoque, M.R. Ketabchi, Nanohydroxyapatite synthesis using optimized process parameters for load-bearing implant, Bull. Mater. Sci. 39 (2016) 133–145, https://doi.org/10.1007/s12034-015-1120-8.
[8] A.N. Misra, M. Misra, R. Singh, Nanotechnology in agriculture and food industry, Int. J. Pure Appl. Sci. Technol. 16 (2013) 1.
[9] T. Nuge, K.Y. Tshai, S.S. Lim, N. Nordin, M.E. Hoque, Preparation and characterization of Cu-, Fe-, Ag-, Zn- and Ni- doped gelatin nanofibers for possible applications in antibacterial nanomedicine, J. Eng. Sci. Technol. 12 (2017) 68–81.
[10] S.A. Pradeep, G.P. Kumar, A.R. Phani, R.G.S.V. Prasad, M.E. Hoque, H.L. Raghavendra, Fabrication, characterization and in vitro osteogenic potential of polyvinyl pyrrolidone-titania (PVP-TiO) nanofibers, Anal. Chem. Lett. 5 (2015) 61–72, https://doi.org/10.1080/22297928.2015.1048728.
[11] D. Ragurajan, M. Golieskardi, M. Satgunam, M.E. Hoque, A.M.H. Ng, M.J. Ghazali, A.K. Ariffin, Advanced 3Y-TZP bioceramic doped with Al_2O_3 and MnO_2 particles potentially for biomedical applications: study on mechanical and degradation properties, J. Mater. Res. Technol. 7 (2018) 432–442, https://doi.org/10.1016/j.jmrt.2017.05.015.
[12] M.C. Roco, Handbook on Nanoscience, Engineering and Technology, 2007.
[13] S. Sagadevan, K. Pal, Z.Z. Chowdhury, M.E. Hoque, Structural, dielectric and optical investigation of chemically synthesized Ag-doped ZnO nanoparticles composites, J. Sol-Gel Sci. Technol. 83 (2017) 394–404, https://doi.org/10.1007/s10971-017-4418-8.
[14] A. Wahab, N. Islam, M.E. Hoque, D.J. Young, Recent advances in silver nanoparticle containing biopolymer nanocomposites for infectious disease control – a mini review, Curr. Anal. Chem. 14 (2018) 198–202.
[15] G. Fuertes, I. Soto, R. Carrasco, M. Vargas, J. Sabattin, C. Lagos, Intelligent packaging systems: sensors and nanosensors to monitor food quality and safety, J. Sens. 2016 (2016) 4046061. https://doi.org/10.1155/2016/4046061.
[16] H.X. Cui, C.J. Sun, Q. Liu, J. Jiang, W. Gu, Applications of nanotechnology in agrochemical formulation, perspectives, challenges and strategies, in: International Conference on Nanoagri, Sao Pedro, Brazil, 2010, pp. 28–33.
[17] P. Solanki, A. Bhargava, H. Chhipa, N. Jain, J. Panwar, Nano-fertilizers and their smart delivery system, in: Nanotechnologies in Food and Agriculture, Springer, 2015, pp. 81–101.
[18] V. Rai, S. Acharya, N. Dey, Implications of nanobiosensors in agriculture, J. Biomater. Nanobiotechnol. 3 (2012) 315.
[19] A.P.F. Turner, Biosensors – sense and sensitivity, Science 290 (2000) 1315–1317.
[20] S.J. Updike, G.P. Hicks, The enzyme electrode, Nature 214 (1967) 986.
[21] C.M. Rico, S. Majumdar, M. Duarte-Gardea, J.R. Peralta-Videa, J.L. Gardea-Torresdey, Interaction of nanoparticles with edible plants and their possible implications in the food chain, J. Agric. Food Chem. 59 (2011) 3485–3498.
[22] E. Omanović-Mikličanin, M. Maksimović, Nanosensors applications in agriculture and food industry, Bull. Chem. Technol. Bosnia Herzeg. 47 (2016) 59–70.
[23] A.F. Hamad, J.-H. Han, B.-C. Kim, I.A. Rather, The intertwine of nanotechnology with the food industry, Saudi J. Biol. Sci. 25 (2018) 27–30.
[24] G. Miller, N. Lowrey, R. Senjen, Out of the Laboratory and on to our Plates: Nanotechnology in Food & Agriculture, Friends of the Earth, 2008.
[25] X. Fan, I.M. White, S.I. Shopova, H. Zhu, J.D. Suter, Y. Sun, Sensitive optical biosensors for unlabeled targets: a review, Anal. Chim. Acta 620 (2008) 8–26.
[26] V.K. Khanna, New-generation nano-engineered biosensors, enabling nanotechnologies and nanomaterials, Sens. Rev. 28 (2008) 39–45.
[27] M.N. Velasco-Garcia, Optical biosensors for probing at the cellular level: a review of recent progress and future prospects, in: Seminars in Cell & Developmental Biology, Elsevier, 2009, pp. 27–33.
[28] C. You, M. Bhagawati, A. Brecht, J. Piehler, Affinity capturing for targeting proteins into micro and nanostructures, Anal. Bioanal. Chem. 393 (2009) 1563–1570.

[29] A. Sharma, K.R. Rogers, Biosensors, Meas. Sci. Technol. 5 (1994) 461.
[30] A. Cavalcanti, B. Shirinzadeh, M. Zhang, L. Kretly, Nanorobot hardware architecture for medical defense, Sensors 8 (2008) 2932–2958.
[31] Y. Bhagat, K. Gangadhara, C. Rabinal, G. Chaudhari, P. Ugale, Nanotechnology in agriculture: a review, J. Pure Appl. Microbiol. 9 (2015) 737–747.
[32] P. Shukla, P. Chaurasia, K. Younis, O.S. Qadri, S.A. Faridi, G. Srivastava, Nanotechnology in sustainable agriculture: studies from seed priming to post-harvest management, Nanotechnol. Environ. Eng. 4 (2019) 11.
[33] T. Dhewa, Nanotechnology applications in agriculture: an update, Octa J. Environ. Res. 3 (2015) 204–211.
[34] M.E. Hoque, A.M. Peiris, S.M. Atiqure Rahman, M. Abdul Wahab, New generation antibacterial nanofibrous membrane for potential water filtration, Curr. Anal. Chem. 14 (2018) 278–284.
[35] B.M. Prasanna, Nanotechnology in agriculture, ICAR Natl. Fellow Div. Genet. IARI, New Delhi, 2007.
[36] A. Dubey, D.R. Mailapalli, Nanofertilisers, nanopesticides, nanosensors of pest and nanotoxicity in agriculture, in: Sustainable Agriculture Reviews, Springer, 2016, pp. 307–330.
[37] N. Scott, H. Chen, Nanoscale science and engineering for agriculture and food systems, Ind. Biotechnol. 8 (2012) 340–343.
[38] S. Singh, A. Srivastava, H.-M. Oh, C.-Y. Ahn, G.-G. Choi, R.K. Asthana, Recent trends in development of biosensors for detection of microcystin, Toxicon 60 (2012) 878–894.
[39] Z. Wang, F. Wei, S.-Y. Liu, Q. Xu, J.-Y. Huang, X.-Y. Dong, J.-H. Yu, Q. Yang, Y.-D. Zhao, H. Chen, Electrocatalytic oxidation of phytohormone salicylic acid at copper nanoparticles-modified gold electrode and its detection in oilseed rape infected with fungal pathogen Sclerotinia sclerotiorum, Talanta 80 (2010) 1277–1281.
[40] H. Li, C. Xie, S. Li, K. Xu, Electropolymerized molecular imprinting on gold nanoparticle-carbon nanotube modified electrode for electrochemical detection of triazophos, Colloids Surf. B: Biointerfaces 89 (2012) 175–181.
[41] A.L. Simonian, T.A. Good, S.-S. Wang, J.R. Wild, Nanoparticle-based optical biosensors for the direct detection of organophosphate chemical warfare agents and pesticides, Anal. Chim. Acta 534 (2005) 69–77.
[42] S. Wu, X. Lan, W. Zhao, Y. Li, L. Zhang, H. Wang, M. Han, S. Tao, Controlled immobilization of acetylcholinesterase on improved hydrophobic gold nanoparticle/Prussian blue modified surface for ultra-trace organophosphate pesticide detection, Biosens. Bioelectron. 27 (2011) 82–87.
[43] C. Chen, Z. Yuan, H.-T. Chang, F. Lu, Z. Li, C. Lu, Silver nanoclusters as fluorescent nanosensors for selective and sensitive nitrite detection, Anal. Methods 8 (2016) 2628–2633.
[44] L. Zhang, Self-assembly Ag nanoparticle monolayer film as SERS substrate for pesticide detection, Appl. Surf. Sci. 270 (2013) 292–294.
[45] M.C. Roco, The Long View of Nanotechnology Development: The National Nanotechnology Initiative at 10 Years, 2011.
[46] D.P. O'Neal, L.R. Hirsch, N.J. Halas, J.D. Payne, J.L. West, Photo-thermal tumor ablation in mice using near infrared-absorbing nanoparticles, Cancer Lett. 209 (2004) 171–176.
[47] A.K. Srivastava, A. Dev, S. Karmakar, Nanosensors and nanobiosensors in food and agriculture, Environ. Chem. Lett. 16 (2018) 161–182.
[48] T. Castro, R. Reifenberger, E. Choi, R.P. Andres, Size-dependent melting temperature of individual nanometer-sized metallic clusters, Phys. Rev. B 42 (1990) 8548.
[49] P.K. Jain, X. Huang, I.H. El-Sayed, M.A. El-Sayed, Review of some interesting surface plasmon resonance-enhanced properties of noble metal nanoparticles and their applications to biosystems, Plasmonics 2 (2007) 107–118.
[50] N. Sozer, J.L. Kokini, Nanotechnology and its applications in the food sector, Trends Biotechnol. 27 (2009) 82–89.
[51] M. Frasconi, R. Tel-Vered, M. Riskin, I. Willner, Surface plasmon resonance analysis of antibiotics using imprinted boronic acid-functionalized au nanoparticle composites, Anal. Chem. 82 (2010) 2512–2519.

[52] G. Evtugyn, A. Porfireva, V. Stepanova, M. Kutyreva, A. Gataulina, N. Ulakhovich, V. Evtugyn, T. Hianik, Impedimetric aptasensor for ochratoxin a determination based on au nanoparticles stabilized with hyper-branched polymer, Sensors 13 (2013) 16129–16145.
[53] L. Hu, L. Deng, S. Alsaiari, D. Zhang, N.M. Khashab, "Light-on" sensing of antioxidants using gold nanoclusters, Anal. Chem. 86 (2014) 4989–4994.
[54] S. Iijima, Helical microtubules of graphitic carbon, Nature 354 (1991) 56.
[55] R. Čihák, M. Vontorková, Cytogenetic effects of quinoxaline-1, 4-dioxide-type growth-promoting agents: II. Metaphase analysis in mice, Mutat. Res. Toxicol. 117 (1983) 311–316.
[56] J. Tkac, J.W. Whittaker, T. Ruzgas, The use of single walled carbon nanotubes dispersed in a chitosan matrix for preparation of a galactose biosensor, Biosens. Bioelectron. 22 (2007) 1820–1824.
[57] Y. Yang, G. Fang, G. Liu, M. Pan, X. Wang, L. Kong, X. He, S. Wang, Electrochemical sensor based on molecularly imprinted polymer film via sol–gel technology and multi-walled carbon nanotubes-chitosan functional layer for sensitive determination of quinoxaline-2-carboxylic acid, Biosens. Bioelectron. 47 (2013) 475–481.
[58] M. Stredansky, A. Pizzariello, S. Stredanska, S. Miertu, Determination of D-fructose in foodstuffs by an improved amperometric biosensor based on a solid binding matrix, Anal. Commun. 36 (1999) 57–61.
[59] R. Antiochia, G. Vinci, L. Gorton, Rapid and direct determination of fructose in food: a new osmium-polymer mediated biosensor, Food Chem. 140 (2013) 742–747.
[60] T. Gan, K. Li, K. Wu, Multi-wall carbon nanotube-based electrochemical sensor for sensitive determination of Sudan I, Sens. Actuators B Chem. 132 (2008) 134–139.
[61] J. Lu, M. Bowles, How will nanotechnology affect agricultural supply chains? Int. Food Agribus. Manag. Rev. 16 (2013) 21–42.
[62] M.A. Augustin, P. Sanguansri, Nanostructured materials in the food industry, Adv. Food Nutr. Res. 58 (2009) 183–213.
[63] L.F. Fraceto, R. Grillo, G.A. de Medeiros, V. Scognamiglio, G. Rea, C. Bartolucci, Nanotechnology in agriculture: which innovation potential does it have? Front. Environ. Sci. 4 (2016) 20.
[64] S.B. Manjunatha, D.P. Biradar, Y.R. Aladakatti, Nanotechnology and its applications in agriculture: a review, J. Farm Sci. 29 (2016) 1–13.
[65] R. Sharma, K.V. Ragavan, M.S. Thakur, K. Raghavarao, Recent advances in nanoparticle based aptasensors for food contaminants, Biosens. Bioelectron. 74 (2015) 612–627.
[66] C. Parisi, M. Vigani, E.R. Cerezo, Proceedings of a Workshop on "Nanotechnology for the agricultural sector: From research to the field", Joint Research Centre (Seville site), 2014.
[67] M.M. Berekaa, Nanotechnology in food industry; advances in food processing, packaging and food safety, Int. J. Curr. Microbiol. App. Sci. 4 (2015) 345–357.
[68] T. Joseph, M. Morrison, Nanotechnology in agriculture and food, Nanoforum Rep. 2 (2006) 2–3.
[69] M. Rai, C. Ribeiro, L. Mattoso, N. Duran, Nanotechnologies in Food and Agriculture, Springer, 2015.
[70] B.S. Sekhon, Nanotechnology in agri-food production: an overview, Nanotechnol. Sci. Appl. 7 (2014) 31.
[71] M.G. Valdés, A.C.V. González, J.A.G. Calzón, M.E. Díaz-García, Analytical nanotechnology for food analysis, Microchim. Acta 166 (2009) 1–19.
[72] T.V. Duncan, The communication challenges presented by nanofoods, Nat. Nanotechnol. 6 (2011) 683–688. https://doi.org/10.1038/nnano.2011.193.
[73] Persistence Market Research, Global market study on nano-enabled packaging for food and beverages: intelligent packaging to witness highest growth by 2020, Persistence Market Research Website (2014) Available at. https://www.persistencemarketresearch.com/market-research/nano-enabled-packaging-market.asp. Accessed: April 19, 2020.
[74] A.L. Brody, B. Bugusu, J.H. Han, C.K. Sand, T.H. Mchugh, Innovative food packaging solutions, J. Food Sci. 73 (2008) 107–116.
[75] M.E. Doyle, Nanotechnology: A Brief Literature Review, Food Research Institute Briefings, 2006.
[76] J. Weiss, P. Takhistov, D.J. McClements, Functional materials in food nanotechnology, J. Food Sci. 71 (2006) R107–R116.

[77] S. Ray, S.Y. Quek, A. Easteal, X.D. Chen, The potential use of polymer-clay nanocomposites in food packaging, Int. J. Food Eng. 2 (2006). https://doi.org/10.2202/1556-3758.1149.
[78] C. Silvestre, D. Duraccio, S. Cimmino, Food packaging based on polymer nanomaterials, Prog. Polym. Sci. 36 (2011) 1766–1782.
[79] Group, E.T.C, Down on the farm: the impact of nano-scale technologies on food and agriculture, ETC Group, Ottawa, Canada, 2005. 74pp.
[80] D. Mössinger, J. Hornung, S. Lei, S. De Feyter, S. Höger, Molecularly defined shape-persistent 2D oligomers: the covalent-template approach to molecular spoked wheels, Angew. Chem. Int. Ed. 46 (2007) 6802–6806.
[81] Y. Liu, S. Chakrabartty, E.C. Alocilja, Fundamental building blocks for molecular biowire based forward error-correcting biosensors, Nanotechnology 18 (2007) 424017.
[82] K. Nachay, Analyzing nanotechnology, Food Technol. (2007).
[83] B. Steele, Researchers make synthetic DNA 'barcodes' to tag pathogens, providing an inexpensive, off-the-shelf monitoring system, Cornell Univ. News Service, 2005 (Internet).
[84] O.L.J. Pursiainen, J.J. Baumberg, H. Winkler, B. Viel, P. Spahn, T. Ruhl, Nanoparticle-tuned structural color from polymer opals, Opt. Express 15 (2007) 9553–9561.

CHAPTER 7

Nanosensors in biomedical and environmental applications: Perspectives and prospects

Mamun Rabbani[a], **Md Enamul Hoque**[b], **Zaid Bin Mahbub**[c]

[a]*Department of Biomedical Physics and Technology, University of Dhaka, Dhaka, Bangladesh*
[b]*Department of Biomedical Engineering, Military Institute of Science and Technology (MIST), Dhaka, Bangladesh*
[c]*Department of Mathematics and Physics, North South University, Dhaka, Bangladesh*

7.1 Introduction

Nanotechnology is one of the booming fields of this era, and in most walks of life the gradually increasing presence of nanotechnology can be felt. In general terms, it can be described as the technology dealing with structures having dimensions in the range of 1–100 nm. Using state-of-the-art nanomaterials in developing predefined superstructures from nanoscale structures defines the crucial role nanotechnology will play in this millennium. Many fields, such as biomedical science, optics, energy science, and magnetism, are now flourishing with the results of nanotechnology innovations. Various nanomaterials are currently being used in drug delivery systems [1, 2], antimicrobial drugs [3], biolabeling [4], and sensors [5].

Materials in the nanoscale demonstrate quite different and novel properties as compared to their bulk counterparts. Photoemission, heat, magnetic features, electrical conductivity, luminescent properties, and catalytic activity are some of the unique qualities of nanomaterials. Disease diagnosis, sample separation, signal amplification, and biomolecule detection are some of the areas in which the enhanced qualities of nanomaterials are successfully applied. Moreover, nanomaterials have contributed in increasing the sensitivity of various sensors for detecting biological activities.

Sensors are widely used in the field of biological science and biomedical applications. Some of the basic criteria of a biomedical sensor are that it should be minimally invasive and should cause minimal physiological damage or alteration to the tissue under consideration. Hence,

Nanofabrication for Smart Nanosensor Applications. https://doi.org/10.1016/B978-0-12-820702-4.00007-6
© 2020 Elsevier Inc. All rights reserved.

demands for sensors of nanoscale size are on the rise for biomedical applications. Biosensors are devices that use the high sensitivity of biological reactions to detect analytes. Usually they consist of two parts: a specific target analyte known as the biological recognition element, and a transduction mechanism that transduces the recognition element into an identifiable and measurable quantity, such as an optical emission, electrical signal, or mechanical motion. Another important component of a biosensor is the bioreceptor, which provides binding of a specific analyte to the sensor with minimal interference from other analytes in a mixture. The first biosensor was developed back in 1960 by Clark and Lyons [6] and Updike and Hicks [7]; it sensed the interaction of glucose oxidase enzyme with glucose. Biosensors developed by using nanoscale materials are known as nanobiosensors.

The advancements in nanotechnology over the past years have brought about new techniques and devices for biosensing. Various nanodevices have enabled monitoring of intracellular physiology and biological parameters in microenvironments. This chapter aims to discuss the prospects and perspectives of nanosensors in the field of biomedical applications. To start, a detailed discussion of biosensors is presented in which the fundamental blocks of a typical biosensor are illustrated, along with the basic classifications of biosensors. This is followed by an introduction to nanosensors. An introduction to nanobiosensors is then given in which the relationship between nanosensors and biosensors is discussed. Subsequently, an intricate description of the various types of nanobiosensors is presented. The chapter comes to an end by discussing some of the applications of nanobiosensors in different aspects of biomedical science.

7.2 Biosensors

A sensor is a device or system that converts any form of energy to electrical energy. In this conversion process, if a biological activity is involved, then it is called a biosensor. A biosensor can be defined as an analytical device that includes a physical transducer and a biologically active element producing a signal that is measurable and comparative to the concentration of the biologically active target molecules in a sample [8, 9]. A biosensor is a system specifically designed to sense materials by detecting interactions with biologically active target molecules and interpreting those interactions into a measurable form through a mechanism of transduction and electromechanical interpretation [10]. The difference between a sensor and a biosensor is that biosensors sense a material that is biologic in nature, like antibodies, immunological molecules, enzymes, proteins, etc. The working process of a biosensor can be summarized by the flow chart shown in Fig. 7.1.

7.2.1 Fundamental blocks

A biosensor fundamentally consists of three parts: the bioreceptor, the transducer, and the detector (Fig. 7.2). The bioreceptor is known as the template used to detect the material of interest. For example, to detect an antigen, an antibody is used as a bioreceptor. The output of

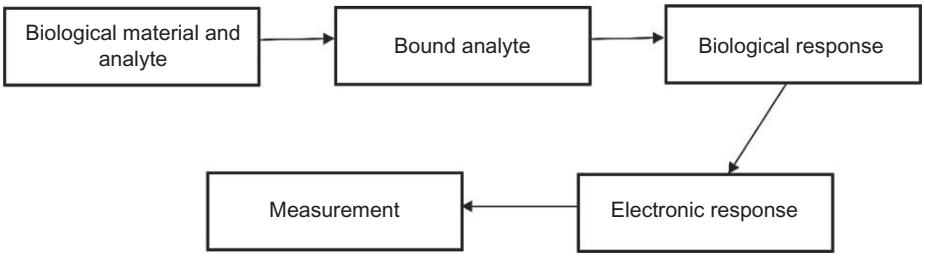

Fig. 7.1
Working process of biosensors.

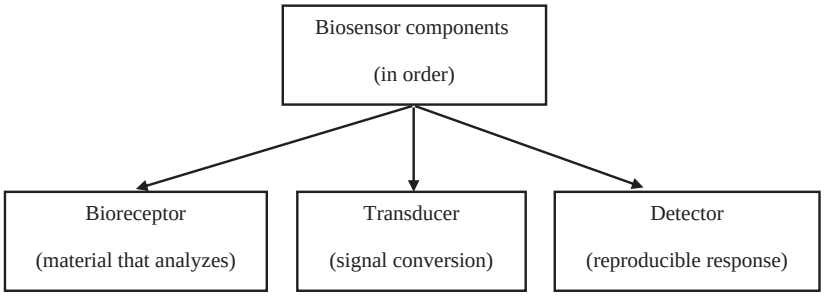

Fig. 7.2
Fundamental blocks of a biosensor.

the bioreceptor is fed into the second system of the biosensor, known as the transducer. The basic purpose of a transducer is to convert one form of energy into another. In the case of biosensors, the first form of energy is biochemical in nature while the later one is electrical. The interaction between bioanalyte and bioreceptor is transduced into electrical signals by the transducer. The last block of a biosensor system is the detector. The electrical signal from the transducer is received in this block and a suitable response is created through amplification and other signal-conditioning methods. Apart from the three fundamental blocks, an important component in biosensors is immobilization schemes. Due to immobilization, the bioreceptors react with the bioanalyte in a faster and more reliable condition, making the sensing technique more sensitive and efficient. Biosensing schemes are cheaper due to immobilization but the process is susceptible to changes in pH, temperature, contaminant interference, and physiochemical variations [11].

7.2.2 Types of biosensors

Biosensors can be classified based on various aspects. Broadly, they are classified on the basis of two schemes: (a) biorecognition element, and (b) principle of signal transduction. As a general scheme, the biorecognition element reacts with the target element, which is commonly

known as the reaction between bioreceptor and bioanalyte. The response of this biological reaction is converted into detectable electrical signals by the transducer through various processes.

According to the biorecognition element, biosensors are categorized into three classes, namely affinity sensor, metabolism sensor, and catalytic sensor [12, 13]. Based on the principle of signal transduction, biosensors can be classified into three categories: electrochemical detection biosensors, optical detection biosensors, and acoustic detection biosensors [10].

7.2.2.1 Affinity biosensor

An affinity sensor senses the binding of the biorecognition element with the target element. The principle of detection is based on the competitive binding of a definite biorecognition element and a fluorescein-labeled analog with receptor sites precise for the biorecognition element and the labeled ligand [14].

7.2.2.2 Metabolism biosensor

In many cases, the interaction between the analyte and biological element results in a chemical change in which the densities of the products or substrates are measurable. The sensor that detects the change in substrate concentration is defined as a metabolism sensor.

7.2.2.3 Catalytic biosensor

In some cases, the binding of bioreceptors and bioanalyte does not change the components chemically but rather influences a chemical change in an auxiliary substrate. The sensors that detect these sorts of changes are defined as catalytic sensors [12, 13].

7.2.2.4 Electrochemical biosensor

The chemical reaction between a restrained biomolecule and a targeted bioanalyte consumes ions or electrons. This changes the electric properties (current or voltage) of the solution [15, 16] and the change of electric properties can be detected as an electrochemical signal. These electrochemical signals can be quantitatively related to the amount of analyte. The electrochemical signal produced due to the changes in electrical properties is the transduction property for electrochemical biosensors. According to the type of signal measured, electrochemical sensors can be of various types, for example, potentiometric, amperometric, voltammetric, etc. A more recent addition to the electrochemical sensor family is the electrochemical impedance spectroscopic measurement. There are various electrochemical devices on the market that are specific for pathogens and toxins [17].

7.2.2.5 Optical biosensor

In optical detection biosensors, optical fibers are used to detect the analyte. Optical fibers are flexible glass cables capable of transmitting light through biological components. The detection of the analyte is done by fluorescence, absorption, or light scattering. Optical biosensors have the advantage over electrochemical biosensors due to the fact that more than one analyte can be detected by using a variety of monitoring wavelengths. As different samples can be addressed with different wavelengths of light, optical methods can be considered readily multiplexed. Among the various optical methods of detection, the most commonly preferred devices are those based on surface plasmon resonance, fluorescence spectroscopy, interferometry, and guided modes spectroscopy in optical waveguides. Optical ring resonators and photonic crystals are also among the emerging technologies. All the methods measure different parameters such as energy, amplitude, decay time, polarization, phase, etc. Among them, amplitude measurement is widely preferred, as it can be easily linked to the density of analytes [18].

7.2.2.6 Acoustic biosensor

The biosensors that detect a change of elastic, viscoelastic, dielectric, electric properties or mass density of a membrane are termed acoustic or electroacoustic detection biosensors. These sensors are fabricated from chemically interactive materials that are in contact with a piezoelectric material. Two types of acoustic biosensors are used commonly, bulk acoustic wave (BAW) transducers and surface acoustic wave (SAW) transducers. In the BAW transducer, an oscillator is formed by a quartz crystal resonator connected to an amplifier. The resonant frequency of the oscillator is dependent on the two membranes connected to it [19]. On the other hand, SAW transducers are based on the propagation of surface acoustic waves along a substrate layer concealed by the membrane. The membrane properties affect the phase velocity of the wave and propagation loss [20]. Although the SAW transducer based biosensing technology has some fabrication drawbacks, it is inexpensive to make and is small in size, which offers an adaptable approach to real-time diagnostics.

7.3 Nanosensors

Devices fabricated on nanoscale dimensions that are capable of measuring physical quantities and converting those quantities into detectable and analyzable signals are known as nanosensors. Having dimensions in the nanoscale range, these sensors can be quite robust and are applied in many state-of-the-art sensing mechanisms. Nanosensors are fabricated from nanomaterials, another gift of the modern era. Nanomaterials have at least one of their dimensions less than 100 nm. This size constraint gives an advantage, as most of the constituent atoms of the materials are located near the surface. This results in a very different physiochemical property in nanomaterials, compared to their bulk counterparts. Nanomaterials

have a very applicable role in the sensing mechanism; hence nanosensors are considered the epitome of modern sensor technology. Integration of nanomaterials in electromechanical systems has led to nanoelectromechanical systems (NEMS), which are very attractive in terms of the electromechanical transduction mechanism.

The widely used nanomaterials include nanoparticles, nanotubes, nanorods, nanowires, and thin films made up of nanocrystalline matter [21]. Nanotubes are nanoscale structures in the form of tubes, which can be made of various materials like carbon, boron nitride, etc. [22]. Nanowires are cylindrical nanostructures having a diameter on the order of a nanometer. They can also be defined as a structure having a ratio of length to width greater than 1000. Various sorts of nanowires are in use, such as superconductor-based yttrium barium copper oxide nanowires, silicon nanowires, and metallic nanowires, to name a few [23]. Nanorods are nanostructures having all of their dimensions less than 100 nm. Nanorods have the ratio of length to width between 3 and 5 [24]. A nanoparticle is defined as a small object that can function independently as a unit in terms of transport properties. Nanoparticles have their dimensions in the range of less than 100 nm and are surrounded by an interfacial layer [25].

7.4 Nanobiosensors

Advances in nanotechnology have boosted the application of nanoscale devices in many aspects. Among them, one of the most evident fields is the application of nanosensors in detecting biochemical and biophysical signals due to some specific disease at the molecular or cellular level. Thus "nanobiosensor" can be seen as nanotechnology used for biosensing purposes. In general terms, nanobiosensors are biosensors made up of nanomaterials. Although nanobiosensors have their dimensions in the nanoscale, they are not sensors for determining nanoscale biological events and happenings.

Nanobiosensors are considered very effective breakthroughs in biosensing technology. Various studies of biosensing devices employing nanostructures have been conducted worldwide. Amperometric devices are used for enzymatic detection of glucose. Quantum dots and bioconjugated nanomaterials are used as fluorescence agents in detecting the binding of specific biomolecules. Nanomaterials are also used in enhancement of detection using electron microscopes. Nanoparticles based on metal are outstanding materials in electronic and optical applications, which are efficiently used for detecting nucleic acid sequences. Carbon nanotubes have the key benefits of higher aspect ratio, improved enzyme loading, ability of being functionalized, and having improved electrical communication [26–28]. Nanoparticles aid in immobilization, allow a better loading of bioanalyte, and possess good catalytic properties [29–32]. Quantum dots have excellent fluorescence capability, size tunable band energy, and good quantum confinement of charge carriers [33–35]. Nanowires are highly versatile. They have good electrical properties along with good biosensing properties. Charge conduction through nanowires is better [36–38]. Nanorods are good plasmonic materials having

size-tunable energy regulation and a good couple sensing phenomenon. They can be coupled with NEMS and included in specific responses [39, 40]. In the later part of this chapter, the various advantages and outcomes of various nanomaterials in biomedical applications will be discussed.

7.5 Types of nanobiosensors

The classification of nanobiosensors is a wide-ranging field. Based on the type of nanomaterial used, nanobiosensors can be classified as nanoparticle-based sensors, nanotube-based sensors, and nanowire-based sensors. The following sections discuss the classifications of nanobiosensors in some detail. Also, cantilever-based nanobiosensors for electromechanical sensing and graphene-based nanobiosensors are discussed.

7.5.1 Nanoparticle-based biosensors

Nanoparticle-based sensors are those that use metallic nanoparticles for enhancement of sensing the biological signal as presented in Fig. 7.3. Nanoparticles have all the three dimensions in the nanoscale range. They are of great interest in research, as they form the connection between bulk materials and molecular or atomic structures. Nanoparticles exhibit a number of properties different from their bulk counterparts. Copper nanoparticles smaller than 50 nm do not show the same ductility and malleability as bulk copper and are considered to be superhard materials. Ferromagnetic nanoparticles having a size less than 10 nm can reverse

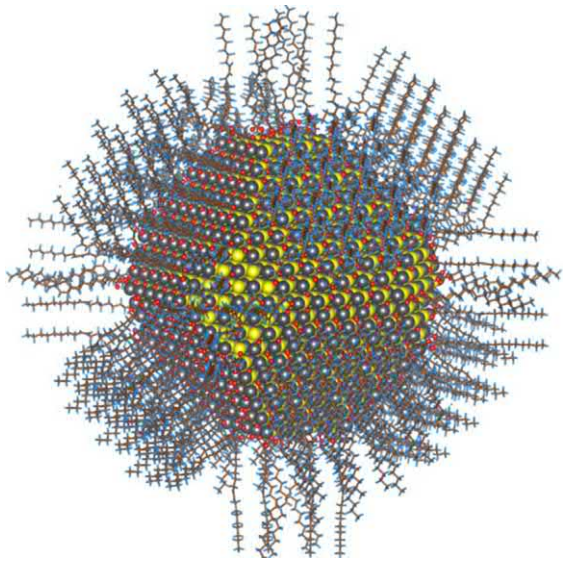

Fig. 7.3
Colloidal nanoparticle of lead sulfide (selenide) [41]/Wikimedia Commons.

their direction of magnetization while at room temperature. Nanoparticles have a very high surface area to volume ratio, providing a huge driving force for diffusion at increased temperatures. Biosensors based on nanoparticles can be further classified into three categories, which are discussed here.

7.5.1.1 Acoustic wave nanobiosensor

Acoustic wave biosensors amplify the sensing response in biodetection. This improves the overall precision of the limits of biodetection. Various stimulation-based effects are seen in this category of nanobiosensors. The mass-based variant of acoustic wave nanobiosensors involves the conjugation of sol particles modified by antibodies that bind themselves on the surface of the electrode. The electrode surface is complexed with particles of the analyte conjugated in such a way that the molecules of the antibody are restrained over the electrode surface. The huge amount of bounded sol particles of the antibody changes the frequency of vibration for the piezoelectric-based sensing platform. Such a change in vibrational frequency acts as the foundation of detection. The diameter of the sol-based antibody particles is preferred to be between 5 and 100 nm. Generally, nanoparticles of gold, cadmium sulfide, platinum, and titanium dioxide are preferred [42, 43].

7.5.1.2 Magnetic nanobiosensor

Specially designed magnetic nanoparticles are used to make magnetic nanobiosensors. These nanoparticles are primarily ferrite-based materials. Magnetic nanobiosensors are highly recommended in biomedical applications, and they offer a great deal of variation in different analytical applications. Magnetic compounds used in screening are made from various transition metals coupled with iron, which gives the compound different properties. Traditional biodetection devices have become more powerful and sensitive by incorporating magnetic nanoparticles. Alloys of iron with transition metals and d-block metals having unpaired electrons exhibit huge versatility in their magnetic behavior. A recent technique has gained popularity that involves a magnetic bioassay technique that is used for specific isolation of biological targets, which are magnetically labeled using a magnetometer [44]. Superconducting quantum interference devices (SQUIDs) use the superparamagnetic property of magnetic nanoparticles for fast recognition of biological targets. These devices are used in biomedical applications to detect specific antigens using magnetic nanoparticle bounded antibodies [45]. Such screening by using superparamagnetic properties is particularly observed in magnetic nanoparticles.

7.5.1.3 Electrochemical nanobiosensor

Electrochemical nanobiosensors basically use electrical means to aid or examine biochemical reactions. They are mostly made of metallic nanoparticles. Nanoparticles ease up the chemical reaction between the biomolecules, which helps by restraining one of the reactants. As a result, the reactions become very specific and the chances of getting any unwanted byproducts are

eliminated. For example, colloidal gold-based nanoparticles are used in immobilizing DNA on gold electrodes, which lowers the detection limit significantly and increases the overall efficiency of the biosensor [46]. Enzyme conjugated gold nanoparticles are used to design biosensors for the detection of glucose, hydrogen peroxide, and xanthine [47–49]. In the work of Xu et al. [48], it was found that a faster amperometric response and better electrocatalytic reduction ability are achievable for horseradish peroxidase (HRP) when immobilized on gold electrodes loaded with carbon nanoparticles. Hence, biosensors incorporated with nanoparticles showed enhanced sensitivity and lower detection limit than those without nanoparticles.

Nanoscale semiconductor crystals can be used to enhance the efficiency of photochemical reactions. They can be used to tag biological entities like enzymes and precursors in designing a novel photoelectrochemical system. For instance, Curri et al. used immobilized cadmium sulfide (CdS) to design a system for enzymatic detection on immobilized formaldehyde dehydrogenase onto gold electrodes for catalytic oxidation of formaldehyde [50]. In many other works, it has been shown that metal-based nanoparticles are coupled with biological probes to perform efficient detection of a particular biomolecule in a mixture [51].

7.5.2 Nanotube-based biosensors

Nanotubes are a specific class of materials. The different properties of nanotubes depend on their geometry along with their composition. The diameter of the tube, number of walls in the nanostructure, van der Waals force, and chirality contributes to the performance and properties of nanotubes. One of the unusual properties of nanotubes is that they stick together, forming strands or bundles. The most popular nanotubes used in the world of nanomaterials are carbon nanotubes (CNTs) (Fig. 7.4). CNTs have their applications in materials science and optoelectronics. Among the extraordinary properties of CNTs are electronic conductivity, high

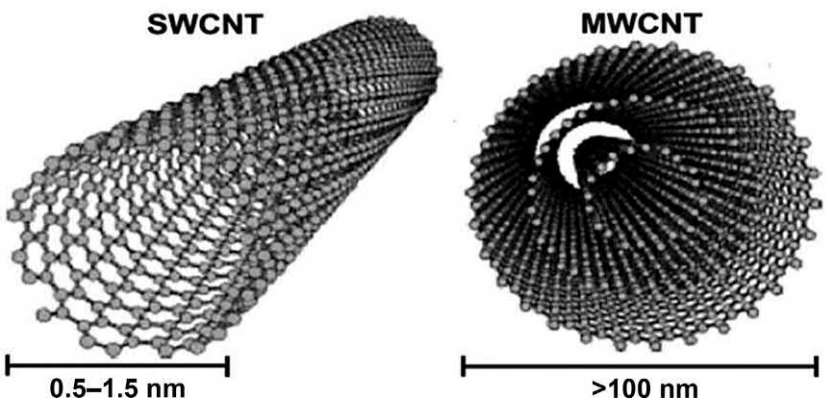

Fig. 7.4
Single-walled carbon nanotube (SWCNT) and multiwalled carbon nanotube (MWCNT) [52].

aspect ratio, flexible physical geometric features, good functionalization abilities, and high mechanical strength. Due to such properties, both single-walled CNTs (SWCNTs) and multiwalled CNTs (MWCNTs) have been used in fabricating biosensors with better performances [26, 27].

One of the most expected advances due to use of nanomaterials in biosensing has to be the development in the design of biosensors for detecting glucose using nanotubes as an immobilizing surface for glucose oxidase. Glucose oxidase is an enzyme used to determine the amount of glucose in various body fluids. The conventional sensing technique uses the enzyme to detect glucose from fundamental body tissues like blood. Incorporation of nanotubes as immobilization assemblies allows the estimation of glucose from minute amounts of body fluids like saliva, tears, etc. Single-walled nanotubes have been successfully adapted for detection of glucose enzymatically and have shown a noteworthy increase in the activity of the enzyme [53]. Such enhanced performance of the biosensor was due to the superior enzyme-loading property and improved electrical conductivities in nanotubes. The enhanced electron transfer flow characteristics of CNTs have paved the way for advances in detection of sensing phenomenon electrically. Such advancements in catalytic biosensors have been reported in several studies. One study shows a better oxidoreductase performance in terms of efficiency and controllability for both glucose oxidase and flavin adenine dinucleotide precursors binding to their substrates [54]. On a similar note, the chemoelectroluminescence effect has been improved by combining CNTs with the sensing molecules of a biosensor. This is due to the enhanced charge carrier conductance and controllability in the flow characteristics in CNTs.

Incorporation of carbon nanotubes has increased the functionality and sensitivity of biosensors. The friendliness of CNTs for being coupled with biomolecules like proteins, DNA, and oligonucleotide probes is the reason for many breakthroughs and advantages in biosensing technology.

7.5.3 Nanowire-based biosensors

Nanowires are nanostructures in cylindrical form quite similar to carbon nanotubes. They have lengths in the range of a few micrometers to centimeters, while their diameters are in the nanometer range. Nanowires are different from nanotubes in terms of aspect ratio (ratio of length to diameter). The aspect ratio of nanotubes is very high, while that of nanowire is in the range of 1000. Nanowires have brilliant electron transport properties and the charge carrier motions are significantly improved in nanowires compared to their bulk counterpart. Although sensors based on nanowires are few in number, studies claim to have mentionable examples of improved performance and recognition of biological target materials through the use of nanowire-based sensors. Such performance enhancement has been reported by the Cui and Leiber group, who used biosensors made from silicon nanowires doped with boron to

detect biological and chemical species [55]. Semiconductor-based nanowires have been used to couple a few biomolecules for detecting their precisely linked substrates. In the detection of streptavidin molecules from a mixture, biotin-coated silicon nanowires have been used.

In regard to their small size and capability, nanowires are ideal components for biodetection of pathogens and biological and chemical species. Nanowires work on specifically termed dimensions, so they are used in in-vivo applications and can be applied in minute environments such as within the living cell. Wang et al. developed a biosensor by fabricating optical fibers with nanowires covered with antibodies to determine the existence of toxicants within the living cell [56]. Cullum et al. synthesized and coated ZnO nanowires over gold electrodes for detection of hydrazine by amperometric responses [57]. They found low detection limit, high sensitivity, and quite lower response time compared to the responses of conventionally used sensor systems.

Nanowires are better than nanotubes and more versatile in performance in two specific ways. First, modification in their design is allowed during their synthesis by controlling operational parameters. Second, many materials are compatible with their surface, which gives the scope for functionalized assembly development. Although the synthesis procedure of nanowires is quite well known, their use in developing sensing devices has met various challenges [58]. Many studies portray the difficulties in incorporating nanowires into detection systems for the overall enhancement in the electrical conductivities. Lieber et al. synthesized nanowires by conventional methods and designed a one-dimensional complex structure of nearly 200 independent nanowire assemblies. They used this structure to conduct a low-level sensing of serum-bone cancer antigens [55].

Yang et al. provided insights about the structural aspects of nanowires and their qualities to improve the sensing mechanism [59]. Cui et al. reported the utility of nanowires in improved conduction and detection of biological signals by exploring the salient attributes of nanowires [36]. In the work of Huang et al. [60], the ability of surface plasmon resonance in nanowires has been explored, which can improve the sensitivity of sensing probes. Stern et al. fabricated nanowires through a simplified process. They used a complementary metal oxide semiconductor (CMOS) approach, which turned out to be easy in control and regulation of the synthesis process of nanowires. Such nanowires have been used to analyze serum fluids to isolate proteins and pathogens in basic form [38].

7.5.4 Cantilever-based biosensors

Cantilever-based biosensors are the best example of nanotransducers. This biosensor utilizes a micromechanically produced cantilever. A cantilever of nearly 100 nm thickness is bent due to interaction with biosensing components. The sensitivity of such nanostructures can be

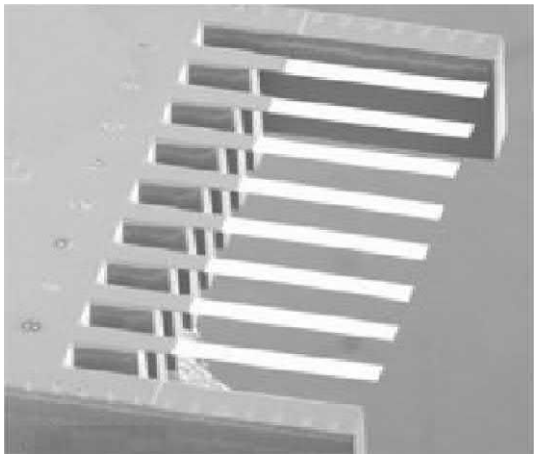

Fig. 7.5
Silicon cantilever array consisting of eight cantilevers and two sidebars [61].

calibrated down to interaction with a single molecule [36]. Cantilever-based nanobiosensors are established as a powerful platform in label-free, time-resolved detection of molecular interactions due to their high sensitivity (Fig. 7.5) [61].

Cantilever-based sensors have versatility in sensing vapors, ions, DNA, proteins, antibiotics, and pathogenic microorganisms. In static mode, these sensors can detect a process by calculating the bend due to stress development by chemosorption of molecules in one side of the cantilever. Mass adsorption on the surface of the cantilever shifts the frequency of resonance in an oscillating cantilever, thus detecting a process in dynamic mode. The mechanical sensitivity in this mode of operation comes from alterations in surface stress due to molecular interaction with the surface and by lateral interactions with the molecular layer [62]. Such sensitivity is suited for measurement of binding processes of DNA, proteins or lipid bilayers. Langmuir et al. studied the behavior of polymethyl methacrylate brushes polymerized from the silicon surface of the cantilever sensor by applying a static mode technique [63]. This method is also known as a "grafting approach." In this approach, they were able to study the in-situ inflammation and collapse of poly(methyl methacrylate) brushes, although the kinetics of the formation of the brush cannot be monitored in real time.

Cantilever-based biosensors can transduce signals of various domains, which include mass, heat, temperature, stress, electromagnetic field, etc., into a mechanical deformation. The deformation, whether in the form of bending or change in resonance frequency, has a higher resolution than that realizable with macroscopic structures. Due to the flexibility of the biosensor, the low consumption of the sample, and the requirement of nonpretreated samples, the number of applications of cantilever-based nanobiosensors has grown rapidly over the past few years.

7.5.5 Graphene-based biosensors

Graphene is a two-dimensional nanomaterial that has some extraordinary electrical and chemical properties, making it one of the first choices in fabricating nanobiosensors. It is fundamentally an allotrope of carbon and commercially synthesized from graphite. Graphene has a noteworthy Young's modulus along with an enormous aspect ratio. It can be considered thermally and electrically superconductive and has a high surface insulating performance. New sensing platforms have been proposed over the past few years with original and modified graphene nanoparticles. Many of such platforms were used for immobilization of biomolecules like antibodies, DNA, and enzymes, in order to come up with highly sensitive and selective biosensors.

Graphene-based nanomaterials are used to make transducers for biosensors. As we know, transducers convert the interaction between the bioreceptor and target biomolecules into measurable and detectable signals. For the interaction to occur, the target molecules are required to attach to the transducer surface. One of the most common methods for attachment of target molecules like antibodies and ssDNA onto graphene is EDC/NHS chemistry, while target molecules like enzymes are usually immobilized using physisorption.

Graphene has been used in designing various biosensors due to its large surface area, high electrical conductivity, high electron transfer rate, and immobilization capacity of various molecules [64]. The nanostructure of graphene enables electron transfer between the bioreceptor and transducer, allowing enhanced signal sensitivity for electrochemical sensing [65–68]. Moreover, graphene-based nanomaterials are used as a quencher in the transducer for generating fluorescent biosensors. Many studies suggest that graphene, graphene oxide, and reduced graphene oxide can be used as highly efficient fluorescent quenchers [69–71].

Some aspects of graphene limit the detection of target molecules. Hence these aspects should be taken into consideration when designing biosensors using graphene. The properties and functionalities of graphene-based nanomaterials vary for different synthesis batch and different synthesis technique. The orientation between a graphene nanomaterial sheet and the bioreceptor also plays a direct role in the selectivity and sensitivity of the biosensors. The number of layers, the amount of functional group, and oxidation state of graphene and its derivatives affect the sensing performance, and also impacts on the bonding between the transducer and bioreceptor. The number of functional groups affects the detection limit of target molecules. Hence, it is essential to restrict any nonspecific adsorption sites on the nanomaterials that might cause unspecific bonding of biomolecules, ignoring the target molecules. Blocking of the surface is often done by covering them with blocking reagents like bovine serum albumin (BSA) [72], casein, or superblock [73]. Treatment of the sensor with tween surfactant is also a possible way of blocking unwanted bondage [74]. Considering these limitations, graphene nanomaterial-based biosensors can

achieve high sensitivity and stability along with fast response time, which aid in advances in healthcare and diagnosis.

7.6 Performance parameters of nanobiosensors

The different components of a nanobiosensor should meet certain requirements to have an optimized and specific performance. These requirements are termed as the performance parameters for nanobiosensors. Some of the performance parameters are discussed here.

7.6.1 Selectivity

The quality of a nanobiosensor to respond to a specific target molecule is known as selectivity [75, 76]. One of the most intimidating challenges in designing a biosensor is to meet the selectivity criteria when sensing real-time complex samples. During the sensing of real-time samples, it is often found that the target biomolecules are in lower concentrations than most of the nonspecific biomolecules. Furthermore, nonspecific and nontarget molecules tend to bind themselves to the transducer probe layer, which obscures the sensing process. This is known as "nonspecific binding" [77]. Due to nonspecific binding, some of the binding locations become occupied, leaving less room for target biomolecules to bind to the transducer. This decreases the sensitivity of the probe and moreover creates a chance for false-positive detection.

7.6.2 Sensitivity

The lowest or smallest amount of the desired biomolecule concentration that can be successfully sensed by the nanobiosensor is known as the sensitivity [76]. Sensitivity is considered the figure of merit of a biosensor. The ratio of the output signal of a sensor to the change in transducing property of the sensor due to analyte binding is known as the internal sensitivity of the biosensor [75]. It can also be said to be the transducing ability of a biosensor. A biosensor with a large sensitivity is capable of picking up minor changes in a transducing property more faithfully, compared to a biosensor with small sensitivity. In many cases, the sensitivity is coined as the output signal with respect to the transducing input signal per unit area of the transducer surface, which rules out the effect of sensor surface area in determining the quality of the sensor. Although a biosensor is sensitive to the amount of analyte bound to it, the actual quantity under consideration is the concentration of the analyte. Therefore, sensitivity should be defined as the output signal per analyte concentration. Apart from analyte concentration, binding interaction kinetics between sensor and analyte and the total exposed surface of the sensor are some of the factors that should be taken into consideration. These factors are specifically important in designing nanobiosensors. For example, a small surface area may reduce the kinetics of interaction

between sensor and analyte and the analyte might show poor affinity to the sensor. Hence, the definition of sensitivity with respect to analyte concentration is much more useful than considering the total mass.

Sensitivity is also known as limit of detection or limit of determination (LOD) [75]. It refers to the minimum quantity that can be detected on top of a background signal. The LOD can be related to the resolution of the sensor. When all the different noise activities of a sensor contribute to a standard deviation of σ, the resolution of the sensor is limited by this deviation and the LOD can be defined as $LOD = {}^{3\sigma}/_{sensitivity}$ [78].

7.6.3 Dose-response curve

The graph representing the detection limit and concentration range that can be sensed by a biosensor is known as the dose-response curve. It is also termed the calibration curve for the nanobiosensor [76]. It shows the relation between the size of the stimulus to the reaction of the bioreceptor. The abscissa represents the measured dose, while the ordinate represents response in a dose-response curve.

7.6.4 Dynamic range

The range of a biosensor over which it is capable of precisely producing an output signal transduced by the analyte quantity is known as the dynamic range [75]. It can also be defined as the ratio of the maximum value of concentration of the target biomolecule and the biosensor's limit of detection (LOD). The LOD confines the lower end of the range. The upper end of the dynamic range is determined by the breakage of the sensor, saturation of the sensor, and other random unexpected changes in the sensitivity of the sensor. The upper end of the range can be extended by taking nonequilibrium measurements by the biosensor instead of taking steady-state measurements.

7.6.5 Multiplex detection

When a nanobiosensor detects more than one biomolecule from a single biological sample, it is known as multiplexing [76]. This is considered one of the most important conditions of a nanobiosensor. Multiplexing can be obtained by localizing various biological probes at different sites on a nanobiosensor. Although the various biological probes are localized, one probe might react with other target biomolecules and hamper the detection of other biological probes on the same nanobiosensor. This is known as cross reactivity and is the prime issue with multiplex detection. Such cross reactions can be reduced by innovative designing of probes and making the probes highly specific to the target molecule.

It is evident from this discussion on performance parameters that the limitations in a nanobiosensor are principally due to the biological affinity probes rather than the detection mechanism. By having good insight into immobilization techniques and minimization of

nonspecific bindings, the detection limitation of nanobiosensors could be addressed. The following section shows some of the biomedical applications of nanobiosensors.

7.7 Applications of nanobiosensors

Nanobiosensors are highly versatile and multifunctional, so their applications are endless. Nanobiosensors are mainly used in approximation and diagnosis of health-related in-vivo features, although they are also used in environmental aspects related to health, such as monitoring of pollutants, toxicants, carcinogens, etc. Some broad fields of nanobiosensors are discussed here.

7.7.1 Diagnostic purpose

Earlier, the detection of many diseases was costly, time consuming, and difficult, but nanobiosensors are now excelling in the diagnosis of these diseases. Use of nanomaterials has enabled the reuse and recycling of expensive enzymes. These materials have also contributed to improving sensitivity and accuracies of sensing systems. Nanobiosensors are used to detect serum antigens, carcinogens and many metabolic disorders. Detection of diabetes, cancer, allergic responses, and many other disorders rely on serum analysis. Some of the widely accepted clinical uses of nanobiosensors are discussed here.

7.7.1.1 Blood glucose detection

Blood glucose monitoring is one of the outstanding breakthroughs of nanobiosensors. Bolincier et al. monitored the absolute concentration of glucose in the subcutaneous adipose tissue using a microdialysis probe [79]. Samples were collected from patients using implanted dialysis probes. The amount of glucose in the adipose tissue correlated to the blood glucose level by about 87%–100%. They proposed this method for continuous monitoring of glucose for diabetic patients. Similar works have been carried out by Pickup et al. [80]

Another novel approach in determining the blood glucose level is by using nanorobotics. The sensor of the nanorobots detects biochemical changes due to hyperglycemia [81]. The outer layer of the nanorobot is made up of carbon metal nanocomposites [82]. The nanorobot has an artificial glycocalyx surface to minimize bioactivity and adsorption, and it utilizes a radiofrequency identification device (RFID) CMOS transponder system to determine the in-vivo positions [83]. The real-time patient information from the nanorobots provides on-the-run healthcare planning and decreases the suffering time of the patient due to hyperglycemia. Bloodborne nanorobots at multiple sites of the body enable the physician to come up with a whole-body map of glucose concentration in the blood serum. This helps in detecting any anomaly in glucose uptake rates and contributes in identifying diabetes-related tissue damage.

7.7.1.2 Cancer detection

In-vivo targeting of cancer cells has been achieved by quantum dot-based multifunctional nanoparticle probes [84]. The quantum dot probes gather at tumors due to their improved permeability and by biomarkers specific to a certain cancer cell. This has led to imaging of cancer cells that are sensitive and have multicolored fluorescence in in-vivo conditions. This method has been successfully applied in human prostate cancer grown on mice.

In-vivo sensing of cancer cells using magnetic nanoparticles is another breakthrough in detection of cancer. In most form of malignancies, a high level of telomerase phase is observed, which can be considered as a promising target for detection purposes. The technique developed by Grimm et al. uses magnetic nanoparticles that change their magnetic state on being annealed with telomerase synthesized TTAGGG repeats [85]. Using MRI to process many images within a short time establishes this technique to be a promising one in in-vivo sensing.

7.7.1.3 HIV detection

The assays used to detect HIV-1 protease measure the effect of HIV inhibitors on the rate of hydrolysis of synthetic peptides. Alterman et al. suggested a new type of assay based on surface plasmon resonance (SPR) [86]. The SPR signal of the assay is proportional to the amount of analyte interacting with the immobilized molecule on the assay. High molecular weight binders were used to amplify the SPR signal. The most sensitive assay gave a detection range between 0.1 nM and 10 μM. Such assays are suitable for rapid detection of probable HIV inhibitors.

7.7.1.4 Immunoassays

An improved version of nanoscale biosensors and chemosensors is in development that utilizes nonspherical nanoparticles. These nanoparticles have a high sensitivity of localized surface plasmon resonance (LSPR) to adsorb induced charges in the local dielectric constant. Changes in refractive index due to the presence of molecules near the surface of noble metal thin films are detected by the sensor [87, 88]. The LSPR nanobiosensor senses the change of local refractive index in an immunoassay, which involves biotin and anti-biotin [89]. The sensing is done by following the LSPR extinction maximum using UV–visible spectroscopy. In binding of anti-biotin with biotinylated nanoparticles, a wavelength shift in the maximum LSPR is found to be +38 nm red shift, which establishes that the LSPR nanobiosensor has minimal reaction to nonspecific bindings [90]. This offers a promising application of the nanosensor in diagnostic purposes as shown in the work of Kim et al., where biomolecular binding is enhanced by LSPR using gold nanoparticles [91]. LSPR sensors could be considered as an alternative to the present immunosensors, as they are completely noninvasive and have the capacity of organelle-specific sensing.

7.7.1.5 Drug discovery

Silicon nanowire field effect transistor-based miniature devices are used for direct and rapid analysis of particular binding of small molecules to proteins. The binding of small molecule inhibitors of long form adenosine triphosphate (ATP) with tyrosine kinase is detected with such devices, which is used in conclusion for chronic myelogenous leukemia [92]. The inhibition of ATP binding due to variation of concentration was also studied by Wang et al. The proposed method successfully differentiates among the affinities of various small molecule inhibitors which can be used as a stage for drug discovery.

7.7.1.6 Nanostructured sensing electrodes

Sensing electrodes made from nanostructures are a new method that produces nucleic acid sensors having large sensitivities. These electrodes are capable of quick analysis. It is proposed that fine structured highly branched electrodes obtain molar sensitivity. Planar chips contain many gold leads, which are electrically independent. They are passivated with silicon dioxide and the lead tips contain apertures. A microelectrode array is constructed by generating various nanostructured electrodes of palladium. Due to the high binding affinity of palladium with thiols, such nanostructured microelectrodes have the capability to be attached with biomolecular probes. Such a relationship between nanosensor structure and sensitivity of biodetection complements the development of high-performing disease diagnostic tools, as seen in the works of Soleymani et al. This work expanded the dynamic range of the sensor system from 2 to 6 orders of magnitude by fabricating arrays of microelectrodes with different levels of nanostructuring [93].

7.7.1.7 Detection of pathogenic bacteria

Detection of bacteria is done by culture and biochemical test. These methods are tedious and, in many cases, bacteria do not grow at all in culture. Hence there is a need to develop a fast, reliable, and sensitive method for detecting bacteria in clinical samples. *Mycobacterium avium* spp. *paratuberculosis* (MAP) have been identified by using supermagnetic iron oxide nanoparticles [94]. Assessing the metabolic activity of pathogens is another way of detecting the presence of pathogens. In the works of Kaittanis et al., nanoparticle-mediated sensors were used to assess the metabolic activity of microbial pathogens [95]. Furthermore, it also suggested whether the pathogen can multiply in the presence of an antibiotic. A novel technique using gold nanoparticles for the assessment of antimicrobial susceptibility was proposed by Nath et al. [96]. Another technique developed by Fu et al. used gold/silicon hetero-structured nanorods for the detection of Salmonella. The silicon nanorods contained dye molecules that produced fluorescence on coming into contact with Salmonella [97].

7.7.2 Environmental monitoring

Environmental monitoring is rather a broader area of application for nanobiosensors. Pollutants, toxic intermediates, and heavy metal wastes are considered hazardous to health. Hence, detection of such pollutants in the environment is a comprehensive task. As nanobiosensors are very versatile in terms of detection, they are incorporated to accomplish such tasks.

7.7.2.1 Detection of toxicants

Carcinogens and harmful intermediates disrupt the proper hormonal system. Isolation of such harmful molecules and compounds has been accomplished through highly sophisticated systems. Such a method has been developed by Kim et al. They used a recombinant fluorescent Chinese hamster ovary cell line for monitoring different toxicants [98]. These cell lines offered 2 to 50 times greater sensitivity for various toxicants as compared to the regular bacterial biosensor systems. Hence, a cheap, fast, and replicated nanobiosensor was proposed for detecting environmental toxicants.

7.7.2.2 Detection of inorganics

Nanobiosensors have been used for detecting nitrates [99] and inorganic phosphates [100, 101]. There are many environmental parameters that are needed to be evaluated on a regular basis. Nanobiosensors are designed and implemented for these evaluations for their superior energy saving, economic, and time saving nature.

7.7.3 Nanomedicine

Nanomedicine is the branch of medicine in which regeneration is involved at a cellular level. This is accomplished by repairing cells one by one that are repairable and triggering apoptosis in those cells that are irreparable.

7.7.3.1 Gene therapy

Gene therapy is used to deliver the target mechanism to a single cell. [102] Multilayer nanoparticle systems are used in this regard. Cleavable shells that contain molecules for targeting, biosensing, and gene therapy are used to deliver nanoparticles to the desired intracellular target. Control switches activated by a biosensor are used to control the therapeutic gene sequences to ensure the proper quantity of gene therapy on a single cell. The prime goal is to establish therapeutic gene sequencing “nanofactories” inside single living cells [103]. The expression of these genes is controlled by molecular biosensors. When the biosensor detects a problem in the cell, it triggers the gene delivery system and halts it when the problem is

resolved. The green fluorescent protein (GFP) reporter sequence has been successful in gene delivery. To increase the expression of these genes, DNA tethering techniques were used [103]. Nanocrystals and nanocapsules are used for cell targeting in combination with fluorescent tracking dyes, flow cytometry, and fluorescence microscopy. Confocal microscopy has been tested for intracellular targeting. Although still in the growth stage, nanomedicine could represent a new age of medicine and rehabilitation, and nanobiosensors play a key role in the development and construction of nanomedicine.

7.8 Conclusions and future directions

In the past years, the development of biosensors has seen a great deal of growth. The incorporation of nanomaterials has been given a noteworthy upper hand in this development. Nanotechnology has particularly revolutionized the sector of biodetection. Today nanobiosensors are getting smarter and quicker while being more user friendly and costing less than before. A great deal of improvement has been observed in the transduction process due to nanomaterials and nanostructures. Nanoparticles used for immobilizing enzymes and nanoelectromechanical (NEMS) structures having various functionalities are paving the way for the future of biosensors. These versatile, dynamic, and quick recognition systems can be considered the epitome, due to their multidimensional potentials. Present works are targeting combinations of chemical and biological sensors so as to achieve better performance and easily executable processes. The ever-rising development of miniaturization and research in nanomaterials has encouraged the use of these materials in sensing various fundamental pathways and controlling events. The biosensing technology is becoming more robust, versatile, and dynamic with the present research and development of nanomaterials. Although the development of a biosensor for a particular task has its own technical difficulties, which makes the process expensive and burdensome, the inclusion of nanomaterials has provided a great boon for this technology. The day might not be far away when nanotechnology-based biosensors will be the key elements in healthcare and medicine and will enable us to provide universal healthcare and effective diagnostic procedures for one and all.

References

[1] Y. Lv, et al., Silver nanoparticle-decorated porous ceramic composite for water treatment, J. Membr. Sci. 331 (1–2) (2009) 50–56.
[2] P. Marcato, N. Duran, New aspects of nanopharmaceutical delivery systems, J. Nanosci. Nanotechnol. 8 (5) (2008) 2216–2229.
[3] M. Rai, A. Yadav, A. Gade, Silver nanoparticles as a new generation of antimicrobials, Biotechnol. Adv. 27 (1) (2009) 76–83.
[4] A. Kulesza, R. Mitrić, V. Bonačić-Koutecký, Silver cluster induced absorption enhancement and conformation control of peptides, Eur. Phys. J. D 52 (1–3) (2009) 203–206.
[5] S. Baruah, J. Dutta, Nanotechnology applications in pollution sensing and degradation in agriculture: a review, Environ. Chem. Lett. 7 (3) (2009) 191–204.

[6] L.C. Clark Jr., C. Lyons, Electrode system for continuous monitoring in cardiovascular surgery, Ann. N. Y. Acad. Sci. 29 (1962) 102.
[7] S. Updike, G. Hicks, The enzyme electrode, Nature 214 (1967) 986–988.
[8] M. Arnold, M. Meheroff, Recent advances in the development and analytical applications of BIosensing probes, Crit. Rev. Anal. Chem. 20 (1988) 149–196.
[9] S. Belkin, Microbial whole-cell sensing systems of environmental pollutants, Curr. Opin. Microbiol. 6 (2003) 206–212.
[10] P. Malik, V. Katyal, V. Malik, A. Asatkar, G. Inwati, T.K. Mukherjee, Nanobiosensors: concepts and variations, ISRN Nanomater (2013) 1–9, Article ID 327435.
[11] P.T. Kissinger, Biosensors—a perspective, Biosens. Bioelectron. 20 (12) (2005) 2512–2516.
[12] F. Schubert, U. Wollenberger, F. Scheller, H. Müller, Artificially coupled reactions with immobilized enzymes: biological analogs and technical consequences, in: D. Wise (Ed.), Bioinstrumentation and Biosensors, Marcel Dekker, Inc., New York, 1991, p. 19
[13] J. Wilson, Sensor Technology Handbook, Elsevier, Amsterdam/Boston, 2005.
[14] J.S. Schultz, S. Mansouri, I.J. Goldstein, Affinity sensor: a new technique for developing implantable sensors for glucose and other metabolites, Diabetes Care 5 (3) (1982) 245–253.
[15] D.R. Thévenot, K. Toth, R.A. Durst, G.S. Wilson, Electrochemical biosensors: recommended definitions and classifications, Anal. Lett. 34 (2001) 635–659.
[16] X. Zhang, H. Ju, J. Wang, Electrochemical Sensors, Biosensors and Their Biomedical Applications, first ed., Elsevier, 2007.
[17] M. Nayak, A. Kotian, S. Marathe, D. Chakravortty, Detection of microorganisms using biosensors—a smarter way towards detection techniques, Biosens. Bioelectron. 25 (4) (2009) 661–667.
[18] H. Sharma, R. Mutharasan, Review of biosensors for foodborne pathogens and toxins, Sensors Actuators B Chem. 183 (2013) 535–549.
[19] M. Deng, Design and Fabrication of High Frequency Bulk Acoustic Wave Transducers Using Interdigital Transducers, IEEE, Honolulu, 2003.
[20] K. Länge, B.E. Rapp, M. Rapp, Surface acoustic wave biosensors: a review, Anal. Bioanal. Chem. 391 (5) (2008) 1509–1519.
[21] C. Jianrong, et al., Nanotechnology and biosensors, Biotechnol. Adv. 22 (7) (2004) 505–518.
[22] A. Rubio, J.L. Corkill, M.L. Cohen, Theory of graphitic boron nitride nanotubes, Phys. Rev. B 49 (7) (1994) 5081–5084.
[23] R. Boston, et al., In situ TEM observation of a microcrucible mechanism of nanowire growth, Science 344 (6184) (2014) 623–626.
[24] S. Rackauskas, et al., A novel method for metal oxide nanowire synthesis, Nanotechnology 20 (16) (2009) 1–8.
[25] C.A.S. Batista, R.G. Larson, N.A. Kotov, Nonadditivity of nanoparticle interactions. Science 350 (6257) (2015) 1242477, https://doi.org/10.1002/chem.200304872.
[26] J.J. Davis, et al., Chemical and biochemical sensing with modified single walled carbon nanotubes, Chemistry 9 (16) (2003) 3732–3739.
[27] S. Sotiropoulou, V. Gavalas, V. Vamvakaki, N. Chaniotakis, Novel carbon materials in biosensor systems, Biosens. Bioelectron. 18 (2–3) (2003) 211–215.
[28] Y.-D. Zhao, et al., Direct electrochemistry of horseradish peroxidase at carbon nanotube powder microelectrode, Sensors Actuators B Chem. 87 (1) (2002) 168–172.
[29] E. Katz, I. Willner, J. Wang, Electroanalytical and bioelectroanalytical systems based on metal and semiconductor nanoparticles, Electroanalysis 16 (1–2) (2004) 19–44.
[30] X. Luo, A. Morrin, A. Killard, M. Smyth, Application of nanoparticles in electrochemical sensors and biosensors, Electroanalysis 18 (4) (2006) 319–326.
[31] A. Merkoçi, M. Aldavert, S. Marı´n, S. Alegret, New materials for electrochemical sensing V: nanoparticles for DNA labeling, TrAC Trends Anal. Chem. 24 (4) (2005) 341–349.
[32] J. Wang, Nanoparticle-based electrochemical DNA detection, Anal. Chim. Acta 500 (1–2) (2003) 247–257.

[33] Y. Huang, W. Zhang, H. Xiao, G. Li, An electrochemical investigation of glucose oxidase at a CdS nanoparticles modified electrode, Biosens. Bioelectron. 21 (5) (2005) 817–821.
[34] J. Wang, G. Liu, R. Polsky, A. Merkoçi, Electrochemical stripping detection of DNA hybridization based on cadmium sulfide nanoparticle tags, Electrochem. Commun. 4 (9) (2002) 722–726.
[35] N. Zhu, A. Zhang, P. He, Y. Fang, Cadmium sulfide nanocluster-based electrochemical stripping detection of DNA hybridization, Analyst 128 (3) (2003) 260–264.
[36] Y. Cui, Q. Wei, H. Park, C.M. Lieber, Nanowire nanosensors for highly sensitive and selective detection of biological and chemical species, Science 293 (5533) (2001) 1289–1292.
[37] R. MacKenzie, et al., Nanowire development and characterization for applications in biosensing, in: Nanosystems Design and Technology, Springer, Boston, MA, 2009, pp. 143–173.
[38] E. Stern, et al., Label-free immunodetection with CMOS-compatible semiconducting nanowires, Nature 445 (2007) 519–522.
[39] A.V. Kabashin, et al., Plasmonic nanorod metamaterials for biosensing, Nat. Mater. 8 (2009) 867–871.
[40] S. Ramanathan, et al., Fluorescence and infrared spectroscopy of electrochemically self assembled ZnO nanowires: evidence of the quantum confined Stark effect, J. Mater. Sci. Mater. Electron. 17 (9) (2006) 651–655.
[41] D. Zherebetskyy, et al., Hydroxylation of the surface of PbS nanocrystals passivated with oleic acid, Science 344 (6190) (2014) 1380–1384.
[42] T. Liu, J. Tang, L. Jiang, The enhancement effect of gold nanoparticles as a surface modifier on DNA sensor sensitivity, Biochem. Biophys. Res. Commun. 313 (1) (2004) 3–7.
[43] X. Su, F.T. Chew, S. Fy Li, Design and application of piezoelectric quartz crystal-based immunoassay, Anal. Sci. 2 (2000) 107–114.
[44] J. Richardson, P. Hawkins, R.W. Luxton, The use of coated paramagnetic particles as a physical label in a magneto-immunoassay, Biosens. Bioelectron. 16 (9–12) (2001) 989–993.
[45] Y.R. Chemla, et al., Ultrasensitive magnetic biosensor for homogeneous immunoassay, Proc. Natl. Acad. Sci. U. S. A. 26 (2000) 14268–14272.
[46] H. Cai, C. Xu, P. He, Y. Fang, Colloid Au-enhanced DNA immobilization for the electrochemical detection of sequence-specific DNA, J. Electroanal. Chem. 510 (1–2) (2001) 78–85.
[47] A.L. Crumbliss, et al., Colloidal gold as a biocompatible immobilization matrix suitable for the fabrication of enzyme electrodes by electrodeposition, Biotechnol. Bioeng. 40 (4) (1992) 483–490.
[48] X. Xu, S. Liu, H. Ju, A novel hydrogen peroxide sensor via the direct electrochemistry of horseradish peroxidase immobilized on colloidal gold modified screen-printed electrode, Sensors 3 (9) (2003) 350–360.
[49] J. Zhao, et al., A xanthine oxidase/colloidal gold enzyme electrode for amperometric biosensor applications, Biosens. Bioelectron. 11 (5) (1996) 493–502.
[50] M. Curri, et al., Development of a novel enzyme/semiconductor nanoparticles system for biosensor application, Mater. Sci. Eng. C 22 (2) (2002) 449–452.
[51] M.B. González-García, C. Fernandez-Sanchez, A. Costa García, Colloidal gold as an electrochemical label of streptavidin–biotin interaction, Biosens. Bioelectron. 15 (5–6) (2000) 315–321.
[52] B. Ribeiro, E.C. Botelho, M.L. Costa, C.F. Bandeira, Carbon nanotube buckypaper reinforced polymer composites: a review, Polímeros 27 (3) (2017) 247–255.
[53] B.R. Azamian, et al., Bioelectrochemical single-walled carbon nanotubes, J. Am. Chem. Soc. 124 (43) (2002) 12664–12665.
[54] A. Guiseppi-Elie, C. Lei, R.H. Baughman, Direct electron transfer of glucose oxidase on carbon nanotubes, Nanotechnology 13 (5) (2002) 75–83.
[55] Y. Cui, C.M. Lieber, Functional nanoscale electronic devices assembled using silicon nanowire building blocks, Science 291 (5505) (2001) 851–853.
[56] J. Wang, Electrochemical nucleic acid biosensors, Anal. Chim. Acta 469 (1) (2002) 63–71.
[57] B.M. Cullum, G.D. Griffin, G.H. Miller, T. Vo-Dinh, Intracellular measurements in mammary carcinoma cells using fiber-optic nanosensors, Anal. Biochem. 277 (1) (2000) 25–32.

[58] A. Umar, M. Rahman, A. Al-Hajry, Y.-B. Hahn, Highly-sensitive cholesterol biosensor based on well-crystallized flower-shaped ZnO nanostructures, Talanta 78 (1) (2009) 284–289.
[59] S. Yang, Nanowires and nanobelts, materials, properties and devices, in: Z.L. Wang (Ed.), Nanowires and Nanobelts of Functional Materials, Kluwer Academic, New York, 2003, pp. 209–238.
[60] B. Huang, F. Yu, R.N. Zare, Surface plasmon resonance imaging using a high numerical aperture microscope objective, Anal. Chem. 79 (7) (2007) 2979–2983.
[61] N. Backmann, et al., Sensing surface PEGylation with microcantilevers, Beilstein J. Nanotechnol. 1 (2010) 3–13.
[62] J. Fritz, Cantilever biosensors, Analyst 133 (7) (2008) 855–863.
[63] I. Pera, J. Fritz, Sensing lipid bilayer formation and expansion with a microfabricated cantilever array, Langmuir 23 (3) (2007) 1543–1547.
[64] C. Rao, A. Sood, K. Subrahmanyam, A. Govindaraj, Graphene: the new two-dimensional nanomaterial, Angew. Chem. 48 (42) (2009) 7752–7777.
[65] N. Chauhan, T. Maekawa, D.N.S. Kumar, Graphene based biosensors—accelerating medical diagnostics to new-dimensions, J. Mater. Res. 32 (15) (2017) 2860–2882.
[66] T. Kuila, et al., Recent advances in graphene-based biosensors, Biosens. Bioelectron. 26 (12) (2011) 4637–4648.
[67] C.S. Park, H. Yoon, O.S. Kwon, Graphene-based nanoelectronic biosensors, J. Ind. Eng. Chem. 38 (2016) 13–22.
[68] M. Pumera, Graphene in biosensing, Mater. Today 14 (7–8) (2011) 308–315.
[69] G.G. Batır, et al., Synthesis and characterization of reduced graphene oxide/rhodamine 101 (rGO-Rh101) nanocomposites and their heterojunction performance in rGO-Rh101/p-Si device configuration, J. Electron. Mater. 47 (1) (2018) 329–336.
[70] A. Kasry, et al., Highly efficient fluorescence quenching with Graphene, J. Phys. Chem. C 116 (4) (2012) 2858–2862.
[71] X. Wu, et al., Study of fluorescence quenching ability of graphene oxide with a layer of rigid and tunable silica spacer, Langmuir 34 (2) (2018) 603–611.
[72] S. Cheng, et al., Label-free detection of tumor markers using field effect transistor (FET)-based biosensors for lung cancer diagnosis, Sensors Actuators B Chem. 212 (2015) 329–334.
[73] F. Wang, et al., Detection of Salmonella Typhimurium on spinach using phage-based magnetoelastic biosensors, Sensors 17 (2) (2017) 386.
[74] A. Benvidi, et al., Simple and label-free electrochemical impedance Amelogenin gene hybridization biosensing based on reduced graphene oxide, Biosens. Bioelectron. 58 (15) (2014) 145–152.
[75] L.M. Bellan, D. Wu, R.S. Langer, Current trends in nanobiosensor technology, Nanomed. Nanobiotechnol. 3 (3) (2011) 229–246.
[76] S. Prasad, Nanobiosensors: the future for diagnosis of disease? Nanobiosens, Dis. Diagn 3 (2014) 1–10.
[77] A. Baszkin, W. Norde, Physical Chemistry of Biological Interfaces, Marcel Dekker, New York, 2000.
[78] M. Cooper, Label-Free Biosensors: Techniques and Applications, Cambridge University Press, Cambridge, 2009.
[79] J. Bolincier, U. Ungerstedt, P. Arner, Microdialysis measurement of the absolute glucose concentration in subcutaneous adipose tissue allowing glucose monitoring in diabetic patients, Diabetologia 35 (12) (1992) 1177–1180.
[80] J.C. Pickup, F. Hussain, N.D. Evans, N. Sachedina, In vivo glucose monitoring: the clinical reality and the promise, Biosens. Bioelectron. 20 (10) (2005) 1897–1902.
[81] A. Cavalcanti, B. Shirinzadeh, L.C. Kretly, Medical nanorobotics for diabetes control, Nanomedicine 4 (2) (2008) 127–138.
[82] R.J. Narayan, Pulsed laser deposition of functionally gradient diamondlike carbon–metal nanocomposites, Diam. Relat. Mater. 14 (8) (2005) 1319–1330.
[83] C. Rutherglen, P. Burke, Carbon nanotube radio, Nano Lett. 7 (11) (2007) 3296–3299.

[84] X. Gao, et al., In vivo cancer targeting and imaging with semiconductor quantum dots, Nat. Biotechnol. 22 (2004) 969–976.
[85] J. Grimm, J.M. Perez, L. Josephson, R. Weissleder, Novel nanosensors for rapid analysis of telomerase activity, Cancer Res. 64 (2) (2004) 639–643.
[86] M. Alterman, et al., P1/P1′ modified HIV protease inhibitors as tools in two new sensitive surface plasmon resonance biosensor screening assays, Eur. J. Pharm. Sci. 13 (2) (2001) 203–212.
[87] J.M. Brockman, B.P. Nelson, R.M. Corn, Surface plasmon resonance imaging measurements of ultrathin organic films, Annu. Rev. Phys. Chem. 51 (2000) 41–63.
[88] C. Huang, et al., An on-chip localized surface plasmon resonance-based biosensor for label-free monitoring of antigen–antibody reaction, Microelectron. Eng. 86 (12) (2009) 2437–2441.
[89] J.C. Riboh, et al., A nanoscale optical biosensor: real-time immunoassay in physiological buffer enabled by improved nanoparticle adhesion, J. Phys. Chem. B 107 (8) (2003) 1772–1780.
[90] A.J. Haes, R.P. Van Duyne, A nanoscale optical biosensor: sensitivity and selectivity of an approach based on the localized surface plasmon resonance spectroscopy of triangular silver nanoparticles, J. Am. Chem. Soc. 124 (35) (2002) 10596–10604.
[91] H.M. Kim, et al., Detection of biomolecular binding through enhancement of localized surface plasmon resonance (LSPR) by gold nanoparticles, Sensors 9 (4) (2009) 2334–2344.
[92] W.U. Wang, et al., Label-free detection of small-molecule–protein interactions by using nanowire nanosensors, Proc. Natl. Acad. Sci. U. S. A. 102 (9) (2005) 3208–3212.
[93] L. Soleymani, Z. Fang, E.H. Sargent, S.O. Kelley, Programming the detection limits of biosensors through controlled nanostructuring, Nat. Nanotechnol. 4 (2009) 844–848.
[94] C. Kaittanis, S.A. Naser, J.M. Perez, One-step, nanoparticle-mediated bacterial detection with magnetic relaxation, Nano Lett. 7 (2) (2007) 380–383.
[95] C. Kaittanis, S. Nath, J.M. Perez, Rapid nanoparticle-mediated monitoring of bacterial metabolic activity and assessment of antimicrobial susceptibility in blood with magnetic relaxation, PLoS One 3 (9) (2008) e3253.
[96] S. Nath, C. Kaittanis, A. Tinkham, J.M. Perez, Dextran-coated gold nanoparticles for the assessment of antimicrobial susceptibility, Anal. Chem. 80 (4) (2008) 1033–1038.
[97] J. Fu, et al., An Au/Si hetero-nanorod-based biosensor for Salmonella detection, Nanotechnology 19 (15) (2008) 1–7.
[98] E. Kim, Y. Lee, J. Lee, M. Gu, Application of recombinant fluorescent mammalian cells as a toxicity biosensor, Water Sci. Technol. 46 (3) (2002) 51–56.
[99] L.H. Larsen, T. Kjær, N.P. Revsbech, A microscale NO3- biosensor for environmental applications, Anal. Chem. 69 (17) (1997) 3527–3531.
[100] J. Kulys, I.J. Higgins, J. Bannister, Amperometric dertermination of phosphate ions by biosensor, Biosens. Bioelectron. 7 (3) (1992) 187–191.
[101] U. Wollenberger, F. Schubert, F.W. Scheller, Biosensor for sensitive phosphate detection, Sensors Actuators B Chem. 7 (1–3) (1992) 412–415.
[102] I.M. Verma, et al., Gene therapy: promises, problems and prospects, in: V. Boulyjenkov, K. Berg, Y. Christen (Eds.), Genes and Resistance to Disease, Springer, Berlin, Heidelberg, 2000, pp. 147–157.
[103] A. Touhami, Biosensors and nanobiosensors: design and applications, in: A. Seifalian, M. Kalaskar (Eds.), Nanomedicine, One Central Press (OCP), Altrincham, UK, 2014, pp. 374–403 (Chapter 15).

CHAPTER 8

Nanosensors for better diagnosis of health

Jaison Jeevanandam[a], **Michael K. Danquah**[b]

[a]*Department of Chemical Engineering, Curtin University, Miri, Sarawak, Malaysia*
[b]*Chemical Engineering Department, University of Tennessee, Chattanooga, TN, United States*

8.1 Introduction

Diagnosis is the starting stage of any disease treatment module [1], and proper clinical diagnosis always helps in reducing the complications of diseases, either in the initial or final stages [2]. Diagnosis is the clinical, medical, or pharmaceutical procedure used for identifying the disease, disorder, or malfunction in a patient via biomolecules that are released due to the disease condition [3]. It is noteworthy that effective diagnosis will facilitate identification and incorporation of proper medication to cure diseases faster and safer [4]. Further, patients with deadly diseases such as cancer [5], diabetes [6] and neurodegenerative diseases [7] have been saved by proper diagnosis of those diseases and prescription of specific drugs in precise dosages to cure them without any side effects [8]. Moreover, infectious diseases that are caused by microbes should also be diagnosed to identify the specific microbes that are causing the disease and their growth patterns, and to inhibit their growth by using a specific dosage of antimicrobial agents [8]. Thus diagnosis is essential in the treatment of diseases, and consequently grabs the attention of researchers in the biomedical sciences. Human body fluids and blood, containing biomolecules, antigens, enzymes, and proteins, may possess unique characteristics of disease diagnosis [9,10]. Certain biomolecules are secreted due to disease progression [11] and another set of existing biomolecules are secreted in excess [12], which indicates the malfunction of metabolism in cells and indicates diseases, their types, and stages [13]. Biosensors are widely used to sense and identify these biomolecules and their concentrations in normal human and patients' bodies, to diagnose diseases and to evaluate the severity of the disease [14]. Conventional biosensors are fabricated via bulk or microparticles (microsensors) to detect compositional and structural deficiencies in human secretions for identifying diseases [15]. Even though they are beneficial in identifying specific biomolecules, they possess limitations such as lack of precision, taking a long time to generate results, and requirements of large sample quantities [16]. Moreover, conventional biosensors utilize materials that are larger in size and can be used only for in vitro detection

Nanofabrication for Smart Nanosensor Applications. https://doi.org/10.1016/B978-0-12-820702-4.00008-8
© 2020 Elsevier Inc. All rights reserved.

[17]. Thus, nanomaterials have been introduced to overcome the limitations of conventional materials for biosensors, to act as superior diagnostic agents for identifying specific disease biomarkers [18]. Nanomaterials possess enhanced surface-to-volume ratio and enhanced diagnostic ability, with elevated sensitivity and precision [19]. These properties make nanomaterials suitable to be used and employed in extensive research as a significant tool for diagnosis of various diseases.

Biosensors are fabricated with three main components: bioreceptor, transducer, and signal processor [20]. The bioreceptor is the component that binds with the analyte (biomolecules), which gives a signal in various forms to indicate the presence of specific biomolecules for disease diagnosis [21]. These signals are amplified by the transducer and are received by signal processors to give a precise reading for identifying the number of biomolecules that are sensed by the biosensor [22]. Nanomaterials can be incorporated in all these components of biosensors to enhance their sensing properties [23]. Nanomaterials can be used to fabricate a bioreceptor substrate, which is beneficial to incorporate several bioreceptor molecules to bind with diagnostic markers, due to their high surface-to-volume ratio [24]. In addition, nanomaterials can be incorporated with the bioreceptor molecules [25] or analyte [26,27] to increase their binding or immobilization efficiency. Likewise, nanomaterials are utilized to fabricate smaller-sized transistors for integrated circuits to be incorporated in transducers and signal processors [28,29]. Thus nanomaterials possess a wide range of applications in biosensors, especially for those that are used for disease diagnosis. The property enhancement ability of nanomaterials has led to the emergence of several novel biosensors, exclusive for disease diagnosis [30]. Dual diagnosis materials [31], skin mountable sensors [32], photoacoustic diagnosis and treatment [33], bioimaging diagnostics [34], and multipurpose [35] and magnetic diagnostic biosensors [36] are novel nanosensors that are under extensive research for disease diagnosis in recent times. Hence, the emergence of bionanomaterials shows promise in rapid sensing of biomolecules for in situ detection of diseases, due to their smaller size, larger surface area, intact stability, and enhanced biocompatibility. The aim of this chapter is therefore to give an account of advancements in nanomaterials fabrication with enhanced biosensing properties and distinct classifications. In addition, nanobiosensors that are used to diagnose specific diseases, along with their challenges and future research directions, are discussed.

8.2 Nanomaterials for biosensors

Several classes of nanomaterials, including metal, metal oxide, carbon-based, nanocomposites, and nanoformulated nanomaterials, are employed for the fabrication of biosensors, as shown in Table 8.1, depending on the desired biodetecting application. It is noteworthy that the synthesis procedure plays a crucial role in fabricating biosensing nanomaterials with the desired size, morphology, and surface charge, which eventually will alter or enhance their efficient biosensing application.

Table 8.1 Various nanomaterial-based biosensors for specific biomolecular detection.

Nanomaterial	Biosensor	References
Metal nanomaterials		
Self-assembled gold nanoparticles	Electrochemical biosensor to microRNA-21	[37]
Gold nanoparticles	Catechol detection in water samples	[38]
Gold nanoparticles	Methyl parathion detection	[39]
Gold nanoparticles	Glucose detection	[40]
Gold nanoparticles	Genomic DNA of *Brucella* species	[41]
Gold nanoparticles	Prostate specific antigen	[42]
Gold nanoparticles	Choline detection	[43]
Gold nanosheets	Human papilloma virus detection	[44]
Gold nanofilms	Glucose biosensors	[45]
Gold nanorods	Biomolecule detection	[46–48]
Silver nanoparticles	SPR biosensor to detect human IgG	[49]
Silver nanoparticles	Catechol detection in green tea samples	[50]
Silver nanoparticles	Human chorionic gonadotropin detection in human serum or urine samples	[51]
Silver nanoparticles	Acetylcholinesterase detection	[52]
Silver nanoparticles	Antibiotics detection in milk	[53]
Silver nanoparticles	Beta-amyloid oligomer detection	[54]
Silver nanoparticles	Guanine and adenine detection	[55]
Porous silver nanofilms	Virus detection	[56]
Concave silver nanosheets	Hydrogen peroxide detection	[57]
Silver nanorods	Dopamine and ascorbic acid detection	[58]
Silver nanofibers	Clonazepam detection	[59]
Silver nanowires	Biosensor chips	[60]
Copper nanoparticles	Protein detection	[61]
Copper nanofibers	Polyphenol pollutant	[62]
Copper nanowires	Organophosphate pesticide	[63]
Copper nanorods	Glucose sensors	[64]
Palladium nanoparticles	Carcinoembryonic antigen detection	[65]
Platinum nanoparticles	Glucose sensors	[66]
Platinum nanowires	Amperometric biosensor	[67]
Transition metal nanosheets	Nucleic acid detection	[68]
Lanthanum hydroxide nanostructure	Oral cancer Cyfra-21-1 biomarker detection	[69]
Metal oxide nanomaterials		
Ocimum tenuiflorum leaf extract synthesized zinc oxide nanoparticles	Glucose biosensor	[70]
Zinc oxide nanoparticles	Urea detection	[71]
Zinc oxide mesocrystal nanoparticles	Glucose biosensor	[72]
Zinc oxide nanosheets	Uric acid detection	[73]
Zinc oxide nanofilms	Glucose and urea detection	[74]
Zinc oxide nanofibers	Breast cancer detection	[75]
Zinc oxide nanorods	Glucose sensor	[76]
Zinc oxide nanowires	Glucose sensor	[77]
Zinc oxide quantum dots	Detection of pesticide in water	[78]
Magnetic iron oxide nanoparticles	Soluble transferrin detection	[79]
Iron oxide nanoparticles	Malathion and chlorpyrifos pesticide detection in water	[80]

Continued

Table 8.1 Various nanomaterial-based biosensors for specific biomolecular detection—cont'd

Nanomaterial	Biosensor	References
Iron oxide nanoparticles	Biotin-streptavidin complex detection	[81]
Iron oxide nanorods	Hydrogen peroxide detection	[82]
Iron oxide nanowires	Glucose sensor	[83]
Iron oxide quantum dots	Hydrogen peroxide detection in live cells	[84]
Copper oxide nanoparticles	Glucose sensors	[85]
Copper oxide nanowire	Glucose and hydrogen peroxide sensors	[86]
Copper oxide nanorods	Chemiluminescent immunosensor	[87]
Copper oxide nanofiber	Glucose sensors	[88]
Silicon dioxide nanoparticles	*Escherichia coli* O157:H7 detection	[89]
Titanium dioxide nanoparticles	Glucose detection	[90]
Cerium oxide nanoparticles	Rutin detection	[91]
Cerium oxide nanorods	DNA sensors	[92]
Cerium oxide nanowires	*Vibrio cholerae* detection	[93]
Bismuth oxide nanoparticles	Cholesterol detection	[94]
Magnesium oxide nanoparticles	Cholera detection	[95]
Manganese dioxide nanoparticles	Choline detection	[96]
Metal dichalcogenide nanosheet	DNA detection	[97]
Nickel oxide quantum dots	Glucose sensors	[98]
Carbon based nanomaterials		
Graphene oxide nanoparticles with zirconia	Oral cancer detection	[99]
Graphene oxide layers with gold nanoparticles	L-lactate tumor biomarker detection	[100]
Graphene nanosheets	Low cholesterol concentration detection	[101]
Graphyne nanosheets	Cytosine and guanine detection	[102]
Graphyne nanotubes	Acrolein detection	[103]
Multiwalled carbon nanotube with polypyrrole	6-mercaptopurine detection	[104]
Carbon nanotubes with chitosan	Lactate detection	[105]
Carbon nanotubes with silver nanoparticles	Glucose biosensor	[106]
Single-walled carbon nanotubes	Ethanol detection in alcoholic beverages	[107]
Carbon dots	Mercury detection	[108]
Self-doped carbon dots	Iron ion and pH detection	[109]
Carbon dots	Hyaluronidase detection	[110]
Carbon dots	Dopamine, DNA, cholesterol and intercellular lead ions	[111–114]
Fullerene	Nanomediator for biosensor	[115]
Fullerene modified ascorbate	Ascorbic acid biosensor	[116]
Fullerenes-rose Bengal dyes	DNA detection	[117]
Fullerenes	Polyphenol, dopamine, fabricate glucose sensor, bacterial sensor and on-site water monitor system	[118–122]
Graphene quantum dots	mecA gene sequence detection in *Staphylococcus aureus*	[123]
Graphene quantum dots	miRNA-155 detection	[124]
Diamond nanoparticles	Glucose, lactate, valproic acid drug, guanine and adenine	[125]

Table 8.1 Various nanomaterial-based biosensors for specific biomolecular detection—cont'd

Nanomaterial	Biosensor	References
Nanocomposites		
Zinc-iron oxide-gold-silver	Lead ion detection	[126]
Transition metal carbide nanosheets-chitosan	Organo-phosphorous pesticide detection	[127]
Porous laser-induced graphene-silver-platinum-gold	Glucose detection	[128]
Copper-hemin-metal organic framework-chitosan reduced graphene oxide	Hydrogen peroxide detection	[129]
Gold-platinum metal organic framework	Protein kinase activity detection	[130]
Silver nanoparticles-two-dimensional transition metal carbides	Malathion detection	[52]
Silver-multiwalled carbon nanotubes-iron oxide	Glucose biosensors	[131]
Nickel-iron-mesoporous carbon	Hydrogen peroxide and glucose detection	[132]
Metal organic framework-carbon	Enzyme immobilization platform for biosensors	[133]
Zinc oxide-porous carbon	Ascorbic acid, uric acid, dopamine, hydrogen peroxide, and hydrazine detection	[134]
Iron oxide-chitosan-graphene	Glucose biosensors	[135]
Graphene oxide-gold	Thrombin detection	[136]
Graphene oxide-gold nanoparticles-beta-cyclodextrin-Prussian blue-chitosan	Malathion and carbaryl	[137]
Graphene oxide-gold-iron oxide-platinum nanoparticles	Hydrogen peroxide detection	[138]
Graphene-zinc oxide	H5 PCR amplicon detection	[139]
Gold nanoparticles-reduced graphene oxide	Mercury ion detection	[140]
Graphene oxide-magnetic nanoparticle	Glucose detection	[141]
Gold nanoparticles-toluidine blue-graphene oxide	DNA detection	[142]
Polypyrrole-nafion functionalized-multiwalled carbon nanotubes-chitosan-glucose oxidase	Glucose biosensor	[143]
Copper oxide nanowires-single-walled carbon nanotubes	DNA biosensors	[144]
Single-walled carbon nanotube-chitosan	Leptin detection	[145]
Multiwalled carbon nanotubes-reduced graphene oxide nanoribbons-chitosan	Hydrogen peroxide and nitrite	[146]
Carbon nanotube-nickel	Glucose sensors	[147]
Fullerene-TOAB-concanavalin A protein	Glucose detection in saliva samples	[148]
Hydroxyl fullerenes-titanium dioxide nanoparticles	Glucose sensors	[149]
Fullerene nanoparticle-nitrogen doped graphene nanosheet-gold nanoparticles	*Mycobacterium tuberculosis* IS6110 fragment detection	[150]
Biotinylated quantum dots-manganese dioxide nanosheet	Glutathione detection	[151]
Cadmium selenide quantum dots-chitosan	Catechol phenolic compounds detection	[152]
Zinc sulfide quantum dots-polyaniline	Clenbuterol detection	[153]
Single/multiwalled carbon nanotubes-poly ethyleneimine	Electrochemical biosensors	[154]

Continued

Table 8.1 Various nanomaterial-based biosensors for specific biomolecular detection—cont'd

Nanomaterial	Biosensor	References
Tin oxide-polyaniline-three-dimensional reduced graphene oxide	Glucose biosensors	[155]
Poly (glycidyl methacrylate-co-vinylferrocene)-multiwalled carbon nanotubes	Xanthine in fish meat detection	[156]
Paper-based optical biosensor-green algae *Chlamydomonas reinhardtii*	Nanoencapsulated atrazine	[157]
Micelle formulated irinotecan hydrochloride and DSPE-mPED$_{2000}$	Endotoxin detection	[158]
Novel nanomaterials		
Gold nanoparticles-DNA supersandwiches	MicroRNA detection	[159]
DNA-modified three-dimensional reduced graphene oxide-chitosan	Mercury detection	[160]
Double stranded DNA-poly (L-cysteine)-iron oxide nanoparticles-graphene oxide	Adenine and guanine detection	[161]
Saccharomyces cerevisiae extract synthesized gold nanoparticles	Acute lymphoblastic leukemia detection	[162]
Convolvulus pluricaulis leaf extracts and polyphenol oxidase from *Manilkara zapota* synthesized silver nanoparticles	Catechol detection	[163]

8.2.1 Metal and metal oxide nanomaterials

Nanosized metals such as gold and silver are the most common metal nanoparticles used in biosensor fabrication. Tian et al. developed an electrochemical biosensor using a superlattice of self-assembled gold nanoparticles for the efficient and rapid detection of microRNA-21. The result revealed that the gold nanoparticles coated with polypyrrole act as a support material and toluidine blue as a redox indicator to detect microRNA, with a detection range of 100 aM to 1 nM and detection limit of 78 aM. These electrochemical biosensors are proven to be beneficial in direct microRNA detection in serum samples without the need of sample preparation, extraction, and amplification [37]. Similarly, gold nanoparticles are used to fabricate a biosensor by modifying a glassy carbon electrode, along with tyrosinase supported by crosslinking agents such as cystamine and glutaraldehyde, within a dihexadecylphosphate film. These biosensors showed efficiency with 95% confidence level, better stability, and repeatability for the amperometric detection of catechol in natural water samples [38]. Chen et al. reported in their review article that gold nanoparticles can be surface functionalized with small molecules to enhance their biochemical detection ability by accelerating signal transduction and intensity [164]. Moreover, gold nanoparticles are also used for the detection of methyl parathion [39], glucose [40], genomic DNA of *Brucella* species [41], prostate specific antigen [42], and choline [43]. Silver nanoparticles were also extensively used in the detection of biochemical components and biological agents. Chen et al. demonstrated that

silver nanoparticles can be used for the preparation of localized surface plasmon resonance-mediated reflective optical fiber biosensors. The antihuman IgG was immobilized onto the biosensor for the specific detection of human IgG via the antigen-antibody interaction [49]. Further, Alessio et al. fabricated a biosensor for the rapid detection of polyphenol using silver nanoparticles, phospholipid, and phthalocyanine films in a layer-by-layer arrangement. These nanofilms are proven to be useful in impedance spectroscopy for the detection of catechol at lower concentrations and they also helped to detect polyphenols in green tea samples [50]. Likewise, Xia et al. reported that the conversion of colorimetric assays into electrochemical analysis via silver nanoparticles helps to enhance peptide aptamer-based biosensors. This biosensor was proven to be highly beneficial in the rapid and sensitive detection of human chorionic gonadotropin in human serum or urine samples [51]. Further, the silver nanoparticles were used to fabricate biosensors to detect acetylcholinesterase [52], antibiotics in milk [53], beta-amyloid oligomer [54], and guanine and adenine [55] in biological samples. In addition, copper nanoparticles for protein detection [61], palladium nanoparticles for carcinoembryonic antigen detection [65], platinum nanoparticles as glucose sensors [66] and lanthanum hydroxide nanostructure for oral cancer Cyfra-21-1 biomarker [69] are other metal nanoparticles that are used in biosensing applications.

Similar to metals, metal oxide nanoparticles are also extensively used in the preparation of biosensors. Oxides of zinc, iron, and copper are the most common nanoparticles used in biosensor fabrication. Dayakar et al. reported that the zinc oxide nanoparticles synthesized using *Ocimum tenuiflorum* leaf extract possess the ability to detect glucose and can be used as a potential glucose biosensor [70]. Likewise, Migliorini et al. illustrated that electrospun nanofibers embedded with zinc oxide nanoparticles exhibit enhanced ability in the detection of urea and can be utilized as impedimetric biosensors [71]. Further, Zhao et al. demonstrated that 20–30 nm sized zinc oxide mesocrystal nanoparticles assembled in an orientation with chitosan can be used as glucose biosensors with high biocompatibility [72]. Furthermore, magnetic iron oxide nanoparticles are functionalized with antibodies as a photonic crystal biosensor to perform a sandwich immunoassay for the detection of soluble transferrin in complex matrices [79]. Chauhan and Jain reported that iron oxide nanoparticles were conjugated with poly (indole-5-carboxylic acid) to fabricate amperometric acetylcholinesterase biosensor for the rapid detection of malathion and chlorpyrifos pesticides in water. The biosensor showed 96%–100% satisfactory level with initial activity of 50% at 4°C within 70 days [80]. Dolci et al. also reported the fabrication of a surface plasmon resonance-based biosensor using iron oxide nanoparticles that are assembled via robust click chemistry. These novel biosensors were proven to detect biotin-streptavidin complex, with high sensitivity and reduced steric hindrance [81]. Zhong et al. revealed that in situ synthesized copper oxide nanoparticles can be useful as an ultrasensitive nonenzymatic glucose sensor [85]. Likewise, silicon dioxide nanoparticles are used to fabricate a shear horizontal surface acoustic wave biosensor for the detection of *Escherichia coli* O157:H7. These biosensors showed the ability to detect the DNA of food

pathogenic *E. coli* with 0.6439 nM/0.1 kHz sensitivity and 1.8 fM of detection limit [89]. In addition, titanium dioxide, cerium oxide, bismuth oxide, magnesium oxide, and manganese dioxides are other metal oxide nanoparticles that are used in biosensor fabrication to detect glucose [90], rutin [91], cholesterol [94], cholera [95], and choline [96], respectively.

Apart from three-dimensional, spherical metal and metal oxide nanoparticles, other dimensional nanoparticles were also used to fabricate biosensors. Two-dimensional metal nanostructures such as nanosheets and nanofilms have also been employed and proven to exhibit better biosensing ability. Recently, it was demonstrated that gold nanosheets can be used as an impedimetric biosensor for the rapid DNA detection of human papilloma virus [44]. Further, gold nanofilms are embedded on the polymer electrode along with graphene oxide, gold, and molybdenum sulfide to be useful as an electrochemical glucose biosensor [45]. Moreover, it can be noted that porous silver nanofilms are used for selective virus detection [56] and concave silver nanosheets to fabricate an electrochemical nonenzymatic biosensor to detect hydrogen peroxide in living cells [57]. Furthermore, two-dimensional metal oxide nanostructures such as zinc oxide nanosheets for detecting uric acid [73], zinc oxide nanofilms for glucose and urea detection [74], transition metal nanosheets for nucleic acid detection [68], and metal dichalcogenide nanosheet for DNA detection [97] are also used in biosensor applications. It is noteworthy that metal nanoparticles can be embedded on the surface of a two-dimensional nanostructure to enhance the biosensing efficiency. The utilization of one-dimensional nanostructures such as nanorods and nanofibers is the latest trend in biosensor applications, to detect various biomolecules. Several studies reported that gold nanorods can be used as an efficient biosensor for the rapid and sensitive detection of biomolecules [46–48]. Silver nanorods [58], silver nanofibers [59], platinum nanowires [67], silver nanowires [60], copper nanowires [63], copper nanorods [64], and copper nanofibers [62] are the common one-dimensional nanostructures that are used as biosensors. Likewise, nanofibers, nanorods, and nanowires of zinc oxide [75–77], copper oxide [86–88], iron oxide [82,83,165], and cerium oxide [92,93] are the various metal oxide one-dimensional nanostructures with biosensing ability. Zero-dimensional nanostructures such as quantum dots are recently gaining significance in the field of biosensors. Mostly, metal nanoparticles are conjugated with quantum dots to enhance their biosensing property [166,167]. Quantum dots of zinc oxide [78], iron oxide [84], and nickel oxide [98] are the recent zero-dimensional nanostructures used in biosensor fabrication and applications.

8.2.2 Carbon-based nanomaterials

Carbon-based nanomaterials such as graphene, graphyne, carbon nanotubes, carbon dots, fullerenes, and diamond are used as biosensors for the detection of specific biomolecules, in addition to metallic nanoparticles. Kumar et al. reported that reduced graphene oxide nanoparticles decorated with zirconia can serve as an effective biosensor for the noninvasive

detection of oral cancer [99]. Likewise, reduced graphene oxide layers were embedded with gold nanoparticles to fabricate an amperometric biosensor for efficient L-lactate tumor biomarker detection [100]. Two-dimensional graphene nanosheets prepared by chemical vapor deposition and coated with cholesterol via an immobilization technique were used to fabricate biosensors based on a field-effect transistor for detection of low cholesterol concentration [101]. It can be noted that individual graphene oxide nanostructures do not possess biomolecule detection ability and the addition or embedding of metallic nanostructures enhances or activates their biosensing property [168]. Graphyne is another allotrope of carbon that has been recently found and employed in various biomedical applications. Madhumitha et al. revealed that graphyne nanosheets possess the ability to effectively adsorb cytosine and guanine nucleobases to be beneficial as biosensors [102]. Likewise, Karami et al. demonstrated via a density functional theory study that graphyne nanotubes have the ability to adsorb acrolein, and can be used as an efficient acrolein biosensor [103]. However, there is very little literature available on the biosensing application of graphyne nanostructures, as they have been only recently introduced in this research.

Recently, carbon nanotubes have been the most common carbon allotrope used in biomedical applications, especially to fabricate biosensors. Karimi-Maleh et al. demonstrated a novel method to fabricate a DNA biosensor using a pencil graphite electrode that is modified with multiwalled carbon nanotubes that are functionalized with polypyrrole. The results revealed that these biosensors are highly useful in the detection of anticancer 6-mercaptopurine drug in salmon sperm samples [104]. Likewise, carbon nanotubes along with chitosan are used to modify screen-printed graphite electrodes and used as an effective biosensor for lactate determination in embryonic cell culture [105]. Moreover, graphene-carbon nanotubes are decorated with gold nanoparticles and are immobilized with glucose oxidase to fabricate a novel amperometric glucose biosensor to detect glucose with high reproducibility, stability, and repeatability [40]. Similarly, silver nanoparticles were also used to decorate carbon nanotubes for the fabrication of nonenzymatic glucose biosensors [106]. Eguilaz et al. further reported that single-walled carbon nanotubes that are functionalized with polytyrosine via covalent bonds exhibited potential for the fabrication of nicotinamide adenine dinucleotide (NADH) based biosensors that are effectively significant for detecting ethanol in alcoholic beverages [107]. All these studies emphasized that carbon nanotubes possess better biosensing properties among the carbon allotropes.

Zero-dimensional nanostructures were also prepared using carbon-based materials and are employed for the effective detection of biomolecules. Cui et al. demonstrated that carbon dots that are labeled with oligodeoxyribonucleotide and graphene oxide possess the ability to act as a fluorescent biosensor for the detection of mercury [108]. Likewise, Wang et al. revealed that self-doped carbon dots have an enhanced photoluminescent property to act as a multifunctional biosensor for iron ion and pH detection [109]. Liu et al. also reported that carbon dots can exhibit fluorescence after being functionalized with amino group and can serve as surface

energy transfer biosensors for the detection of hyaluronidase [110]. Furthermore, carbon dots are used in the fabrication of biosensors to detect biomolecules such as dopamine [111], DNA [112], cholesterol [113], and intracellular lead ions [114]. Another significant zero-dimensional allotrope of carbon is fullerene or C60, which is widely used in several biomedical applications, including biosensors. Afreen et al. reported that functionalized fullerene possesses the ability to be a nanomediator to fabricate highly sensitive biosensors [115]. Berberis et al. fabricated a novel telemetric system with fullerene modified ascorbate to act as a subtractive biosensor for the amperometric detection of ascorbic acid and antioxidant agents in fruit juices such as kiwi, orange, and blueberry [116]. Moreover, fullerenes cosensitized with rose Bengal dyes showed the potential to be an ultrasensitive photoelectrochemical biosensor to detect DNA [117]. In addition, fullerenes are used in the detection of polyphenol [118] and dopamine [119] and to fabricate a bacterial sensor [120], glucose sensor [121], and on-site water monitor systems [122]. Additionally, graphene can be fabricated into quantum dots and employed in the fabrication of fluorescence resonance energy transfer biosensors to detect the mecA gene sequence in *Staphylococcus aureus* [123]. Hu et al. also proposed that graphene quantum dots can be very helpful in the preparation of an electrochemical biosensor for increasing enzyme catalytic amplification to detect miRNA-155 [124]. Also, diamond nanoparticles are used in biosensor fabrication for the rapid and sensitive detection of glucose [169], lactate [170], anticonvulsant valproic acid drug [171], guanine, and adenine [125]. Even though several studies reported the enhanced ability of nanosized carbon allotropes to act as biosensors, extensive research is still encouraged to further elevate their biosensing efficiency and to detect multiple biomolecules.

8.2.3 Nanocomposites

Nanosized composites are formed by blending two unique materials with exclusive properties to enhance their efficiency by foreshadowing their drawbacks [172]. Liang et al. demonstrated the fabrication of a ratiometric fluorescence-naked eye bimodal biosensor via zinc-iron oxide-gold-silver nanocomposites and DNA-cerium oxide complex for the on-time and real-time detection of unknown lead ion concentration in real systems [126]. Similarly, Zhou et al. reported on transition metal carbide nanosheets-chitosan coated with acetylcholinesterase for the fabrication of biosensors to detect organophosphorous pesticides in any samples [127]. Recently, Xuan et al. fabricated a stretchable, conductive, and three-dimensional hybrid biosensor by using porous laser-induced graphene-silver-platinum-gold nanoparticle nanocomposites for the sensitive and rapid detection of glucose [128]. Moreover, a novel copper-hemin-metal organic framework-chitosan reduced graphene oxide nanocomposite was synthesized by Wang et al. for electrochemical biosensor fabrication to detect hydrogen peroxide in complex samples [129]. Likewise, gold-platinum metal organic framework nanocomposites are used to design electrogenerated sensitive chemiluminescence biosensors for improving their signal amplification of bimetallic catalysis to effectively detect protein

kinase activity in cells [130]. Further, silver nanoparticles-two-dimensional transition metal carbides were highly recommended for an electrochemical acetylcholinesterase biosensor for efficient and rapid malathion detection [52].

Several carbon-based nanocomposites were also introduced in biosensor research and are proven to be useful as an efficient biomolecular detector. Recently, silver-multiwalled carbon nanotubes-iron oxide magnetic multilayered nanocomposites were fabricated to be significant as an exclusive glucose biosensor [131]. Likewise, nickel-iron-mesoporous carbon nanocomposites were synthesized by Xiang et al. for the preparation of an amperometric biosensor to detect hydrogen peroxide and glucose in complex samples [132]. Moreover, metal organic framework-carbon nanocomposites were fabricated as an enzyme immobilization platform to be useful as efficient biosensors [133]. Also, Madhu et al. prepared functional zinc oxide-porous carbon nanocomposites as biosensors with high performance to detect ascorbic acid, uric acid, and dopamine in biological samples as well as hydrogen peroxide and hydrazine in environmental samples [134]. Cui et al. revealed that chitosan-titanium dioxide-graphene nanoparticles were used to fabricate potential acetylcholinesterase biosensor for rapid organophosphate pesticides [173]. Similarly, iron oxide-chitosan-graphene nanocomposites were prepared for the fabrication of multifunctional glucose biosensors [135]. Moreover, reduced graphene oxide-gold nanocomposites with aptamer were used for the development of an aptameric biosensor to effectively detect thrombin [136]. Furthermore, electrochemical reduced graphene oxide-gold nanoparticles-beta-cyclodextrin-Prussian blue-chitosan nanocomposites were deposited over a glassy carbon electrode to develop acetylcholinesterase biosensors. These novel biosensors were proven to be highly significant in detecting organophosphate pesticides, such as malathion and carbaryl [137]. Also, reduced graphene oxide blended with gold, iron oxide, and platinum nanoparticles were synthesized as nanocomposites for the development of a highly sensitive electrochemical biosensor. These sensitive biosensors are proposed to be beneficial in detecting hydrogen peroxide, and will eventually report the oxidative stress of any cell or tissue sample [138]. Additionally, graphene-zinc oxide for H5 PCR amplicon detection [139], gold nanoparticles-reduced graphene oxide for mercury ion detection based on a thymine-mercury-thymine structure [140], graphene oxide-magnetic nanoparticles for glucose detection [141], and gold nanoparticles-toluidine blue-graphene oxide for DNA detection [142] are nanocomposites used in biosensing applications.

Carbon nanotubes are also included in the development of novel nanocomposites that have potential biosensing applications. Shrestha et al. demonstrated that polypyrrole-nafion functionalized with multiwalled carbon nanotubes immobilized with chitosan-glucose oxidase was used to fabricate a novel bio-nanohybrid composite film for the development of a glucose biosensor [143]. On the other hand, Chen et al. reported that copper oxide nanowire-single walled carbon nanotubes can be highly significant as DNA biosensors. The results stated that these biocompatible nanostructured, highly conductive biosensors showed efficiency in

detecting even ultralow concentrations of DNA with 3.5×10^{-15} M as the detection limit [144]. Zhang et al. fabricated a nanocomposite using single-walled carbon nanotubes and chitosan via carbodiimide crosslinkers such as 1-ethyl-3-(3-dimethylaminopropyl) carbodiimide, hydrochloric acid (EDC), and N-hydroxysuccinimide (NHS). These nanocomposites are employed in the fabrication of electrochemical biosensors and exhibited enhanced ability in the detection of leptin in human serum [145]. Likewise, Mani et al. emphasized that multiwalled carbon nanotubes-reduced graphene oxide nanoribbons-chitosan heterostructures in the form of core-shell nanocomposites can be used to develop enzymatic biosensors to detect hydrogen peroxide and nitrite in cleaning solutions used to wipe contact lens and meat samples [146]. Also, carbon nanotube-nickel nanocomposites are synthesized via atomic layer deposition methods for the fabrication of nonenzymatic glucose sensors [147]. In addition, fullerenes are also combined with other nanoparticles to form nanocomposites for biosensing purposes. Ye et al. reported that fullerene was blended with tetraoctylammonium bromide (TOAB) and functionalized with glucose binding concanavalin A protein via surface linkage and the nanocomposite was deposited on a glassy carbon electrode. These C60-based nanocomposites are used in glucose biosensor fabrication for effective determination of glucose in saliva samples [148]. Similarly, Li et al. demonstrated that hydroxyl fullerenes are linked with titanium dioxide nanoparticles to form nanocomposites and glucose oxidase was immobilized on its surface. The nanocomposites were coated over glassy carbon electrodes to modify them as a potential glucose sensor to detect glucose in complex samples rapidly with high sensitivity [149]. Further, Bai et al. revealed recently that a fullerene nanoparticle-nitrogen doped graphene nanosheet decorated with gold nanoparticles can serve as a potential ultrasensitive electrochemical nanocomposite-based biosensor for the efficient detection of *Mycobacterium tuberculosis* IS6110 fragments. The nanocomposites aid as a signal tag in biosensors and are highly beneficial in early tuberculosis diagnosis [150].

Quantum dots are next-generation zero-dimensional nanostructures that are extensively used in nanocomposite fabrication. Chen et al. demonstrated that lateral flow biosensors with a fluorescence property were developed using biotinylated quantum dots-manganese dioxide nanosheet composites. These biosensors were combined with test strips of the conjugation pad for rapid and sensitive glutathione detection [151]. Similarly, Han et al. evaluated the effectiveness of a cadmium selenide quantum dots-chitosan nanocomposite in developing a tyrosinase biosensor. These biosensors are proven to be useful in the detection of catechol phenolic compounds with a 0.3 nM detection limit with a low signal-to-noise ratio of 3 [152]. Further, zinc sulfide quantum dots and polyaniline were fabricated as nanocomposites and modified with a gold electrode to develop a novel electrochemical immunosensor for the sensitive detection of clenbuterol without the interaction of salbutamol, ractopamine, as well as urine components including urea, uric acid, calcium, sodium, and potassium ions [153].

Polymer-based nanocomposites are another major nanomaterial used in the development of biosensors. Tertis et al. reported that single and multiwalled carbon nanotubes were linked with

poly ethyleneimine to form nanocomposites for the fabrication of effective electrochemical biosensors [154]. Also, Wu et al. revealed that nanocomposites with tin oxide, polyaniline, and three-dimensional reduced graphene oxide were fabricated via a plasma polymerization method to exhibit an enhanced glucose biosensing property [155]. Moreover, Dervisevic et al. evaluated the biosensing ability of poly (glycidyl methacrylate-co-vinylferrocene) as a polymeric mediator and multiwalled carbon nanotubes in the form of nanocomposites. The results showed that these novel biosensors can be highly useful for the detection of xanthine in fish meat [156]. In recent times, nanoformulations were also introduced as a novel nanomaterial for the fabrication of biosensors. Scognamiglio et al. reported the development of an effective paper-based optical biosensor using green algae *Chlamydomonas reinhardtii*. These biosensors showed enhanced biosensing properties in detecting pico-molar concentrations of nanoencapsulated atrazine [157]. Contrarily, Jin et al. revealed that the conventional endotoxin detection assays such as the rabbit pyrogen test and amebocyte lysate assay may not be applicable to nanoformulated irinotecan hydrochloride and DSPE-mPED$_{2000}$ drug using micelle [158]. Thus, it is evident that nanocomposites will occupy the market of conventional biosensors and eventually replace them.

8.2.4 Other novel nanomaterials

There are numerous novel nanomaterials that are recently under extensive research for the development of novel, rapid, and sensitive biosensors. Wang et al. reported a novel method for the fabrication of a surface plasmon resonance biosensor using gold nanoparticles and DNA supersandwiches. The results revealed that the DNA biosensor effectively helped in the detection of microRNA via enzyme-free amplification [159]. Likewise, Zhang et al. demonstrated an easy fabrication method for developing an electrochemical biosensor using DNA-modified three-dimensional reduced graphene oxide-chitosan nanocomposites. These DNA-included nanocomposites were proven to be highly efficient in the detection of mercury in complex samples with high sensitivity [160]. Similarly, DNA biosensors were developed for the detection of adenine and guanine by using a nanocomposite modified electrode that is made up of double-stranded DNA, poly (L-cysteine), iron oxide nanoparticles, and graphene oxide [161]. Biogenic nanoparticles were recently introduced in biosensor fabrication as chemical synthesized biosensors are toxic to the environment and living cells [174]. Recently, a novel nanocomposite using graphene sheets, conducting polymers, and biosynthesized gold nanoparticles using *Saccharomyces cerevisiae* yeast extracts was fabricated as an effective biosensor for the detection and diagnosis of acute lymphoblastic leukemia [162]. Likewise, silver nanoparticles synthesized via *Convolvulus pluricaulis* leaf extracts and polyphenol oxidase extracted from *Manilkara zapota* were used to fabricate a novel biosensor for sensitive and selective catechol detection [163]. However, the stability of these biosynthesized nanoparticle-based biosensors is the major concern for their large-scale applications, which can be avoided by using hybrid synthesis approaches.

8.3 Classification of biosensing nanomaterials

The biosensor nanomaterials can be classified based on the mechanism used to detect the biomolecules. Thus electrochemical, field effect, spectroscopic, impedance, surface plasmon resonance, microneedle, and terahertz technologies are the major classifications of biosensors, as shown in Table 8.2, used in the diagnosis of various diseases.

Table 8.2 Various nanomaterial-based biosensor classes used to detect biomolecules.

Electrochemical biosensor		
Nanomaterial	**Biomolecules detected**	**References**
HIV-1 oligonucleotide sequence	HIV-1 detection and AIDS diagnosis	[175]
DNA hairpin	Gamma-interferon detection	[176]
Carbon nanotube	p-nitrophenol product, paraoxon, and methyl parathion detection	[177]
RNA aptamer sequence	Theophylline detection in serum samples	[178]
Nanoporous pseudocarbon paste electrode	L-glutamate detection	[179]
Single-walled carbon nanotubes-gold coated palladium nanocubes	Hydrogen peroxide detection	[180]
Gold nanoparticles	Dehydrogenase enzyme detection	[181]
Tetrahedral DNA nanostructure	MicroRNA detection	[182]
Thionine-graphene nanocomposite	DNA oligonucleotide detection	[183]
Graphene oxide-single stranded DNA-poly L-lactide nanoparticles	VEGF and PSA detection	[184]
Gold nanoparticles- two-dimensional molybdenum disulfide nanosheets	Glucose detection	[185]
Gold nanoparticles	Polynucleotide kinase detection	[186]
Gold nanoparticles	DNA of pathogens that cause plant disease	[187]
Nitrogen-doped graphene-gold nanoparticles	Human multidrug resistance microbial gene detection	[188]
Hybrid molybdenum sulfide nanoparticle-graphene oxide	Hydrogen peroxide detection	[189]
Iron oxide nanoparticle-polyvinyl alcohol composite	Glucose detection	[190]
Silver nanoparticle-aptamer	*Staphylococcus aureus* detection	[191]
Gold nanoparticle-molybdenum sulfide nanosheet	MicroRNA-21 detection	[192]
Gold nanoparticle-carbon nanosphere	Protein kinase A detection	[193]
Stainless steel-gold-palladium nanoparticles	Levodopa and uric acid detection	[194]
Field effect transistor biosensors		
Manganese dioxide nanoparticles	Lactate detection	[195]
Silicon dioxide nanoparticles	Glucose detection	[196]
Reduced graphene oxide nanoparticles	DNA detection	[197]
Magnetic nickel ferrite nanoparticles	Triglycerides, trioctanoate, tributyrin and triolein detection	[198]

Table 8.2 Various nanomaterial-based biosensor classes used to detect biomolecules—cont'd

Electrochemical biosensor		
Nanomaterial	**Biomolecules detected**	**References**
Silicon dioxide nanoparticles-polyaniline	Acetylcholine biosensors	[199]
Nanoscale field effect transistor biosensors	Molecular point-of-care blood analysis	[200]
Manganese dioxide nanoparticles	Glucose detection	[201]
Aptamer modified carbon nanotube	Protein detection	[202]
Silicon nanowires	Cell recording	[203]
Aptamer modified graphene	Immunoglobulin E protein detection	[204]
Reduced graphene oxide	DNA detection	[205]
Graphene oxide-gold nanoparticle nanocomposite	Lead ion detection in water	[206]
Gold nanoparticles-graphene	MicroDNA detection	[207]
Silicon nanowire-gold nanoparticles	PSA detection	[42]
Reduced graphene sheets-gold nanoparticles	Ebola antigen detection	[208]
Black phosphorus nanosheets	Human immunoglobulin G detection	[209]
Molybdenum disulfide-gold nanoparticle	Mercury ion detection	[210]
Platinum nanoparticles	Brain natriuretic peptide detection in whole blood sample	[211]
Zinc oxide nanorod arrays	Phosphate detection	[212]
Platinum-conducting polymer hybrid nanoparticles	Dopamine detection	[213]
Zinc oxide nanorod modified nickel oxide quantum dots	Glucose detection	[98]
Graphene-protein	Glucose detection	[214]
Spectroscopic biosensors		
Iron oxide-based magnetic nanoparticles	*E. coli* O157:H7 detection in ground beef samples	[215]
Gold nanoparticles	Sequence specific DNA detection of chronic lymphocytic leukemia	[216]
Gold nanoparticles	Complementary oligonucleotide sequence detection	[217]
Gold nanoparticles	Impedance and capacitance biosensors	[218]
Gold nanoparticle-aptamer	Thrombin detection	[219]
Nanoporous alumina membrane-magnetic nanoparticles	Histamine detection	[220]
Gold nanoparticle	Peptide-based biosensor for *Clostridium difficile* toxin detection	[221]
Magnetic nanoparticles	*Listeria monocytogenes* detection	[222]
Gold nanoparticles-aptamer	Avian influenza virus H5N1 in chicken tracheal samples	[223]
Triangular silver nanoparticles	Streptavidin detection	[224]
Triangular silver nanoparticles	Amyloid beta-derived diffusible ligand detection	[225]
Silver nanoparticles	Poly-L-lysine and 11-mercaptoundecanoic acid detection	[226]

Continued

Table 8.2 Various nanomaterial-based biosensor classes used to detect biomolecules—cont'd

Electrochemical biosensor		
Nanomaterial	**Biomolecules detected**	**References**
Gold nanoparticles	Oral malignant epithelial HOC 313 clone 8 and HSC 3 cell line detection	[227]
Gold nanoparticles	C-reactive protein detection	[228]
Streptavidin coated gold nanoparticles	Carcinoembryonic antigen detection	[229]
Graphene oxide-gold nanoparticles	MicroRNA detection	[230]
Gold nanoparticles-polyaniline-titanium dioxide nanotube	Lactate detection	[231]
Magnetic nanoparticles	CD81 surface marker, annexin V and cholera toxin B detection	[232]
Three-dimensional graphene foam-silver nanoparticle	Methylene blue detection	[233]
Titanium dioxide-silver nanoparticles	Hexavalent chromium detection	[234]
Graphene-copper nanoparticle	Adenosine detection	[235]
Silver-copper oxide-reduced graphene oxide nanocomposite	Peroxidase detection	[236]
Molecularly imprinted polymeric nanoparticles	Propranolol detection	[237]
Molecularly imprinted polymeric nanoparticles	Chlorpyrifos detection in apple juice	[237]
Other novel biosensors		
Graphene oxide nanohybrid	Microneedle biosensor to detect hydrogen peroxide	[238]
Polystyrene embedded carbon nanoparticles	Microneedle biosensor to detect uric acid	[239]
Gold nanoparticles	Microneedle biosensor to detect hydrogen peroxide in rat abdominal wall	[240]
Polymeric nanoparticles	Microneedle biosensor to detect transdermal biomolecules	[241]
Gold nanoparticles	Microneedle biosensor to detect lactate	[242]
Graphene oxide-gold nanoparticles	Microneedle biosensor for uric acid, glucose and cholesterol detection	[243]
Gold nanoparticles	Terahertz metamaterials for antigen-antibody detection	[244]
Gold nanoparticles	Terahertz metamaterials for protein detection	[245]
Indium nitride plasmonic nanoparticles	Terahertz metamaterials for water content detection in skin cancer cells	[246]

8.3.1 Electrochemical biosensors

Generally, electrochemical biosensors are used to detect any biochemical substances and convert them into electrical signals to quantify them. Electrodes, supporting substrates, materials incorporated from biological element immobilization, biocompatible membrane materials, and biological elements are the significant components required for electrochemical biosensor fabrication. Sensor arrays, conventional electrochemical or chemical deposition, polymerization, plasma-induced polymerization at high vacuum conditions, photolithography,

atomic force microscopy, and immobilization are the various methods used in the development of electrochemical biosensors using nanomaterials [247]. The variety and diversity in biosensor fabrication conditions obtained by combining these components and methods have led to several electrochemical biosensors. The very first noticeable modern electrochemical biosensor was designed and developed by Wang et al. The study utilized a nanosized 21- or 42-mer single stranded, human immunodeficiency virus type 1 (HIV-1) U5 long terminal repeat oligonucleotide sequence that was hybridized and immobilized with strip electrodes or carbon paste. The result revealed that these biosensors can be highly significant in trace-level detection of HIV-1 and early acquired immunodeficiency syndrome (AIDS) diagnosis [175]. Liu et al. reported that a nanosized DNA hairpin with thiolated interferon γ-binding aptamer and redox methylene blue tag conjugation and self-assembled gold electrode can be used to fabricate an electrochemical biosensor for the detection of gamma-interferon [176]. Likewise, Deo et al. demonstrated that carbon nanotubes as transducer conjugated with biocatalyst organophosphorus hydrolase in the form of a two-dimensional film can serve as an efficient amperometric electrochemical biosensor for the effective detection of p-nitrophenol product, paraoxon and methyl parathion with excellent sensitivity [177]. Similarly, Ferapontova et al. revealed that an electrochemical biosensor can be developed with a nanosized RNA aptamer sequence that is functionalized with 5′-disulfide and immobilized over gold electrode, whereas, the 3′ end of RNA was functionalized with an amino group and conjugated with a redox probe of ferrocene. These RNA biosensors are proven to be beneficial in the sensitive detection of theophylline in serum samples [178]. Moreover, electrochemical biosensors are fabricated via a nanoporous pseudocarbon paste electrode for L-glutamate detection [179], single-walled carbon nanotubes-gold coated palladium nanocubes for hydrogen peroxide detection [180], gold nanoparticles for dehydrogenase enzyme detection [181], tetrahedral DNA nanostructure probes for microRNA detection [182], and thionine-graphene nanocomposite for complementary DNA oligonucleotide detection [183].

Recently, graphene oxide-single stranded DNA-poly L-lactide nanoparticles were reported to be helpful in the fabrication of an electrochemical biosensor for the simultaneous vascular endothelial growth factor and prostate specific antigen detection in human serum, to increase the chances of early prostate cancer diagnosis [184]. Parlak et al. reported the fabrication of electrochemical biosensors using gold nanoparticles embedded over two-dimensional molybdenum disulfide nanosheets for effective glucose detection [185]. Similarly, Cui et al. demonstrated a novel method for the development of an electrochemical biosensor using gold nanoparticles for the signal amplification of lambda exonuclease cleavage for sensitive and rapid polynucleotide kinase detection [186]. Likewise, Lau et al. emphasized that gold nanoparticles can be utilized as probes in electrochemical biosensors for the effective detection of DNA that belongs to pathogenic *Pseudomonas syringae* in the *Arabidopsis thaliana* plant [187]. Moreover, Chen et al. showed nitrogen-doped graphene-gold nanoparticles can be used

for electrochemical biosensor fabrication to effectively detect genes of a human multidrug resistance microbe [188]. Further, Yoon et al. synthesized a novel hybrid molybdenum sulfide nanoparticle and graphene oxide structure and immobilized it with myoglobin to perform as an electrochemical biosensor. The result showed that these biosensors are effective in detecting hydrogen peroxide in complex samples with high sensitivity, precision, and confidence [189]. Additionally, electrochemical biosensors were fabricated using an iron oxide nanoparticle-polyvinyl alcohol composite for glucose detection [190], silver nanoparticle-aptamer conjugation for *Staphylococcus aureus* detection [191], gold nanoparticle-molybdenum sulfide nanosheet for microRNA-21 detection [192], gold nanoparticle-carbon nanosphere for protein kinase A detection [193], and stainless steel-gold-palladium nanoparticles for levodopa and uric acid detection [194].

8.3.2 Biosensors with field effect transistors

The field effect transistor is an electronic device that controls current flow using an electric field [248]. These transistors are widely incorporated in biosensors for amplification of sensor signals for effective detection of biomolecules [249]. Xu et al. reported that manganese dioxide nanoparticles that are assembled layer-by-layer with lactate oxidase can be useful for the fabrication of biosensors with ion-sensitive field effect transistors to effectively detect lactate [195]. Further, Luo et al. demonstrated that biosensors for the rapid detection of glucose can be fabricated using enzyme field effect transistors that are doped with silicon dioxide nanoparticles [196]. Furthermore, Cai et al. emphasized that field effect transistor biosensors can be fabricated via reduced graphene oxide nanoparticles for the ultrasensitive detection of DNA using peptide nucleic acid (PNA)-DNA hybridization [197]. Moreover, Vijayalakshmi et al. stated that an ion-selective field effect transistor based biosensor can be developed by using magnetic nickel ferrite nanoparticles for the rapid and sensitive detection of triglycerides, trioctanoate, tributyrin, and triolein [198]. Likewise, Liu et al. revealed that polyaniline thin films that are self-assembled as a material for semiconducting channel and thin films of silicon dioxide nanoparticles as dielectric gate material can be utilized for the fabrication of ion sensitive field effect transistor based acetylcholine biosensors [199]. Similarly, it was proven that nanoscale field effect transistor biosensors can be highly beneficial for molecular point-of-care analysis of blood for the effective diagnosis of diseases and their management [200]. Also, Luo et al. reported that manganese dioxide nanoparticles can be used for the preparation of enzyme field effect transistor-based biosensors for sensitive glucose detection [201]. In addition, aptamer modified carbon nanotubes for protein detection [202], silicon nanowires for cellular recording [203], aptamer modified graphene for immunoglobulin E protein detection [204], reduced graphene oxide for DNA detection [205], and graphene oxide-gold nanoparticle nanocomposites for lead ion detection in water [206] are other nanomaterials used in fabricating field effect transistor biosensors.

In recent times, Cai et al. reported that field effect transistor biosensors can be developed by using graphene decorated with gold nanoparticles for the selective determination of microDNA in femtomolar concentrations [207]. Likewise, Presnova et al. recently demonstrated that a novel biosensor can be developed with field effect transistors that are made of silicon nanowire and are functionalized with gold nanoparticles. These biosensors have proven to be highly significant in the detection of prostate specific antigen and early diagnosis of prostate cancer [42]. Moreover, Chen et al. stated that electrospray reduced graphene sheets decorated with gold nanoparticles will be beneficial in the fabrication of field effect transistor biosensors that can be useful for the rapid, sensitive, and selective detection of Ebola antigen [208]. Similarly, Chen et al. emphasized that two-dimensional black phosphorus nanosheets can be used to fabricate field effect transistor biosensors by exfoliating with aluminum oxide for the effective detection of human immunoglobulin G via antigen-antibody interaction [209]. Further, Zhou et al. experimentally proved that a molybdenum disulfide-gold nanoparticle hybrid that is functionalized with DNA can be used to fabricate a field effect transistor biosensor for the ultrasensitive determination of mercury ion [210]. Furthermore, graphene-based field effect transistor biosensors decorated with platinum nanoparticles were proven to be highly useful in the detection of a heart failure related biomarker, namely brain natriuretic peptide in whole blood sample [211]. Additionally, carbon nanotubes, nano-graphene [250], zinc oxide nanorod arrays for phosphate detection [212], platinum-conducting polymer hybrid nanoparticles for dopamine detection [213], zinc oxide nanorod modified nickel oxide quantum dots [98], and graphene-protein [214] for glucose detection are other nanomaterials that are extensively used in the development of field effect transistor biosensors.

8.3.3 Spectroscopic biosensors

Spectroscopic biosensors utilize light as a source and its optical properties as well as modifications due to interaction with biomolecules for effective and specific detection of biological components [251]. Surface plasmon resonance, impedance, and surface enhanced Raman spectroscopy are the distinct types of spectroscopic sensors used for biomolecule detection. The measurement of properties related to resistance and capacitance of a material by applying a signal of sinusoidal alternating current excitation is known as impedance spectroscopy and the spectrum is obtained by frequency variations over a definite range [252]. Varshney and Li reported that iron oxide-based magnetic nanoparticles coated with streptavidin immobilized with biotin-labeled polyclonal goat anti-*E. coli* antibodies can be highly significant in the development of impedance biosensors with interdigitated array microelectrodes for effective detection of *E. coli* O157:H7 in ground beef samples [215]. Likewise, Ensafi et al. demonstrated that gold nanoparticles and gold-modified electrodes are used to fabricate DNA impedance biosensors for the detection of sequence-specific DNA of chronic lymphocytic leukemia [216]. On the other hand, Zhang et al. used gold nanoparticle modified gold electrodes for the detection of complementary oligonucleotide sequences via

DNA hybridization [217]. Similarly, Wang et al. stated that gold nanoparticles conjugated with a fluorescein-anti-fluorescein system were utilized for the synthesis and signal amplification of impedance and capacitance biosensors [218]. Li et al. mentioned in his experimental article that gold nanoparticles conjugated with aptamer will be beneficial in the preparation of label free impedance biosensors for the effective, rapid, and sensitive detection of thrombin [219]. Recently, Ye et al. reported that a nanoporous alumina membrane with magnetic nanoparticles was used for impedance biosensor preparation for histamine detection via magnetic separation and amplification [220]. Also, Wang et al. demonstrated a novel method to fabricate label-free impedance peptide-based biosensors via gold nanoparticle incorporated carbon electrode for the determination of cardiac troponin 1 [253]. Moreover, Ensafi et al. revealed that insulin can be detected using an electrochemical impedance biosensor that is fabricated using aptamer-gold nanoparticle-o-phenylenediamine modified with a pencil graphite electrode [254]. Gold nanoparticles for *Clostridium difficile* toxin detection [221], magnetic nanoparticles for *Listeria monocytogenes* detection [222], and gold nanoparticles-aptamer for avian influenza virus H5N1 in chicken tracheal samples [223] are other nanomaterials used for impedance biosensor fabrication.

Nanoparticles exhibit localized surface plasmon resonance (SPR), where the incident and transmitted light is in resonance after encountering any molecule. Such resonance is used in the biosensors for the ultrasensitive detection of biomolecules. Haes and Duyne reported that biotin-coated triangular silver nanoparticles with the SPR property help in the development of a nanoscale optical biosensor for the sensitive and rapid detection of streptavidin [224]. Similarly, Haes et al. stated that nanosized triangular silver particles exhibit the SPR property for the effective and rapid detection of amyloid beta-derived diffusible ligands for early diagnosis of Alzheimer's disease [225]. Likewise, Malinsky et al. revealed that SPR exhibiting silver nanoparticles modified with alkanethiol self-assembled monolayers can be utilized for the detection of poly-L-lysine and 11-mercaptoundecanoic acid [226]. Further, gold nanoparticles with SPR properties were conjugated with antiepidermal growth factor receptor antibody (EGFR) for the detection of oral malignant epithelial cell lines such as HOC 313 clone 8 and HSC 3. These SPR nanoparticle-included biosensors were proven to be highly beneficial in early oral cancer detection [227]. Recently, gold nanoparticles with the SPR property were used for biosensor fabrication to detect C-reactive protein in diluted human serum samples [228]. Similar streptavidin-coated gold nanoparticles with the SPR property were used to amplify signals in biosensors for the effective detection of carcinoembryonic antigen in human serum and early diagnosis of cancer [229]. A graphene oxide-gold nanoparticle hybrid for microRNA detection [230], gold nanoparticle-polyaniline-titanium dioxide nanotube for lactate detection [231], and magnetic nanoparticles for extracellular vesicle analysis to detect CD81 surface marker, annexin V, and cholera toxin B [232] are other SPR exhibiting nanomaterials for biosensor fabrication.

In addition, three-dimensional graphene foam with silver nanoparticle decorations exhibited surface enhanced Raman spectroscopy (SERS) properties, which can be fabricated as

biosensors for effective methylene blue detection [233]. Likewise, hollow sea urchin-shaped titanium dioxide-silver nanoparticles were used as a SERS substrate in biosensors for the sensitive detection of hexavalent chromium [234]. Moreover, a graphene-copper nanoparticle for adenosine detection [235], silver-copper oxide-reduced graphene oxide nanocomposite for peroxidase detection [236], and molecularly imprinted polymeric nanoparticles for the detection of propranolol [237] and chlorpyrifos in apple juice [255] are the latest nanomaterials that were introduced with SERS properties for biosensor fabrication.

8.3.4 Latest novel biosensors

Recently, numerous hybrid biosensors using the previously mentioned detection approaches have been developed using nanomaterials. Further, microneedle and terahertz technologies have also been used for novel biosensor fabrication using nanomaterials. Jin et al. reported that a reduced graphene oxide nanohybrid can be utilized as a microneedle to fabricate mini-invasive electrodes for the development of real-time transdermal biosensors to detect hydrogen peroxide [238]. Similarly, Hegarty et al. showed that polystyrene embedded carbon nanoparticles could be used to fabricate conductive microneedle patches in biosensors for the effective detection of uric acid [239]. Moreover, Narayanan and Slaughter revealed that gold nanoparticle-horseradish peroxidase showed high significance in specifically detecting hydrogen peroxide in the rat abdominal wall, by fabricating them as an ultrasensitive microneedle biosensor [240]. Further, polymeric nanoparticles for transdermal detection of biomolecules [241], gold nanoparticles for lactate detection [242], and graphene oxide-gold nanoparticles for uric acid, glucose, and cholesterol [243] are other nanomaterials used to fabricate microneedle-based biosensors. In addition, gold nanoparticles embedded with antibody for virus-envelope proteins were fabricated into terahertz plasmonic metamaterials for the development of biosensors to detect and diagnose diseases via antigen-antibody interaction [244]. Similarly, Xu et al. stated that gold nanoparticles as terahertz metamaterials were used in the fabrication of effective biosensors for protein detection [245]. Furthermore, indium nitride plasmonic nanoparticles were proven to be useful as terahertz metamaterials for enhancing their localized SPR and ultrahigh polarimetric image contrast to detect water content variations in cancer cells, for an effective diagnosis of skin cancer [246].

8.4 Applications of nanomaterials in diagnosis of specific diseases

Nanomaterials are widely employed in the diagnosis of diseases such as cancer, microbial infections, diabetes, cardiovascular diseases, and several other diseases, including malaria, typhoid, cholera, and dengue by using biosensing technology, as shown in Table 8.3.

Table 8.3 Nanomaterial-based biosensors in diagnosis of specific diseases.

Cancer diagnosis		
Nanomaterial	**Biosensor**	**Reference**
Two-dimensional nanomaterials	Electrochemical biosensors	[256]
Silicon nanomaterials	FET and SERS biosensors	[257]
Magnetic beads-gold nanoparticles	Electrochemical biosensor	[258]
Carbon nanotube forest	Electrochemical immunosensor	[259]
Multiwalled carbon nanotube	Electrochemical DNA biosensor	[260]
Oval-shaped gold nanoparticles	Spectroscopic biosensor	[261]
Gold nanoparticles	Immunobiosensors	[262]
Titanium dioxide nanoparticles	Electrochemical biosensors	[263]
Bismuth selenide nanosheets-gold nanoparticles	Spectroscopic biosensor	[264]
Porous graphene-titanium dioxide nanofibers	Microfluidic immunosensor	[265]
Nitrogen-doped nanosized graphene aerogel	Electrochemical DNA biosensor	[266]
Platinum nanoparticles-rubrene microrods	Electrochemiluminescence biosensor system	[267]
Microbial infection diagnosis		
Chitosan-carbon nanotube	*Pseudomonas fluorescens* and *P. putida* detection	[267]
Single-walled carbon nanotube	*Proteus vulgaris*	[268]
Carbon nanotube	*Xanthomonas* species	[269]
Single-walled carbon nanotube	*Gluconobacter oxydans*	[270]
Cadmium selenide quantum dot-multiwalled carbon nanotubes	*Alcaligenes* species	[271]
Gold nanoparticles, magnetic iron oxide nanoparticles, and graphene	Microbial infection and biomolecule detection	[272]
Nanomaterials	Magnetic relaxometry, colorimetric, SERS, fluorometric, electrochemical biosensors	[273]
Graphene nanocomposites	Microbial toxin detection	[274]
Cysteine functionalized silver nanoparticles	Detection of milk spoiling lactic acid bacteria	[275]
Metal oxide, metal nanoparticles, carbon nanotubes and quantum dots	Bacterial pathogens and toxin detection in meat products	[276]
Diabetes diagnosis		
Carbon nanomaterials	Enzymatic biosensors for glucose detection	[277]
Carbon nanotubes-reduced graphene oxide nanosheets-gold nanowire array	Microfluidic injection analysis for glucose detection	[278]
Gold nanoparticles-three-dimensional zinc oxide nanostructures	Glucose-detecting biosensors	[279]
Nanosized metals	Electrochemical biosensors for insulin detection	[280]
Gold nanoparticle-doped beta-cyclodextrin-lead metal-organic framework	Electrochemiluminescent biosensors for insulin detection	[281]
Silver nanoflower-reduced graphene oxide composite	Micro-disk electrode in biosensor for insulin detection	[282]

Table 8.3 Nanomaterial-based biosensors in diagnosis of specific diseases—cont'd

Cancer diagnosis		
Nanomaterial	**Biosensor**	**Reference**
Diagnosis of other diseases		
Boron nitride quantum dots	Imprinted biosensors for cardiac troponin I detection	[283]
Zinc selenium oxide perovskite nanomaterial	Electrochemical biosensors for cardiac troponin T	[284]
Zinc oxide nanostructure	Electrochemical biosensors for cardiac troponin T	[285]
Mesoporous silica and graphene hybrid nanomaterials	Apolipoprotein E gene detection for Alzheimer's disease diagnosis	[286]
Graphene oxide-gold nanowires	Serum microRNA-137 detection for Alzheimer's disease diagnosis	[287]
Carbon-based nanomaterials	A53T alpha-synuclein aggregation detection for Parkinson's disease diagnosis	[288]
Molybdenum sulfide nanosheets	Malarial biomarker detection	[289]
Silicon nanowire-gold nanoparticle	Dengue viral DNA oligomer detection	[290]
Gold and magnetic nanoparticles	*Vibrio cholera* O1 OmpW gene detection	[291]
Graphene	Biosensors for Zika virus detection	[292]
Molybdenum sulfide-reduced graphene oxide nanocomposite	Vi antigen detection for early typhoid diagnosis	[293]

8.4.1 Cancer

Cancer is one of the most common lethal diseases throughout the world. Nanomaterial-based biosensors have been recently introduced and are gaining attention from cancer patients and doctors for the early and effective diagnosis of cancer [256]. Silicon nanomaterials have been commonly employed in recent times to fabricate field effect transistor and SERS biosensors for the effective and sensitive detection of cancer DNA and protein, as well as early diagnosis of cancer via biosensing and bioimaging approaches [257]. Likewise, Jin et al. reported that magnetic beads-gold nanoparticles over a graphene platform could be significant in fabricating an electrochemical biosensor for the detection of carcinoembryonic antigen [258]. Similarly, Malhotra et al. stated that carbon nanotube forest electrodes can be used as an electrochemical immunosensor for the ultrasensitive detection of the interleukin-6 biomarker for the diagnosis of oral cancer [259]. On the other hand, multiwalled carbon nanotubes in aqueous sodium dodecyl sulfate were reported to be beneficial in fabricating an electrochemical DNA biosensor to detect the effect of berberine on the DNA of the cancer cell [260]. Moreover, oval-shaped gold nanoparticles were employed in the detection of breast cancer cells by acting as a simple colorimetric biosensor [261]. Recently, Devi et al. clearly portrayed in their review article that gold nanoparticles can be a potential immunosensor for the detection of cancer biomarkers, to facilitate early diagnosis [262]. Likewise,

Maveric et al. also listed electrochemical biosensors developed using titanium dioxide nanoparticles for the effective and sensitive detection of human cancer biomarker [263]. Moreover, bismuth selenide nanosheets decorated with gold nanoparticles were used to fabricate a colorimetric biosensor for carcinoembryonic antigen detection and early diagnosis of cancer [264]. Additionally, porous graphene with titanium dioxide nanofibers [265], nitrogen-doped nanosized graphene aerogel [266], and platinum nanoparticles with neotype rubrene microrods [267] are recently introduced nanomaterials for the fabrication of distinct biosensors to detect cancer biomarkers and effectively diagnose them at an early stage.

8.4.2 Microbial infection

Apart from cancer, nanomaterials are extensively undergoing research for the detection of infectious microbes and to help in the early diagnosis of microbial-related infections. Carbon nanotubes have proven to be useful in the detection of *Pseudomonas fluorescens*, *P. putida* [267], *Proteus vulgaris* [268], *Xanthomonas* species [269], and *Gluconobacter oxydans* [270]. Moreover, cadmium selenide quantum dot-multiwalled carbon nanotubes are used in the detection of microbes that belong to the *Alcaligenes* species [271]. Likewise, gold nanoparticles, magnetic iron oxide nanoparticles, and graphene are other nanomaterials used in the detection of microbial infection and immobilizing microbial cells to detect other biomolecules [272]. Similarly, Sutarlie et al. stated that nanomaterials are widely used in the detection of microbes as well as microbial toxins to prevent infection. The review article emphasized that nanosized materials are used in the fabrication of magnetic relaxometry, colorimetric, SERS, fluorometric, and electrochemical biosensors for the precise detection of microbial toxins, mycotoxins, and bacterial and protozoan cells [273]. Geleta et al. demonstrated that graphene nanocomposites can be used to develop electrochemical biosensors for the detection of microbial toxins to protect humans from microbial infection [274]. Further, silver nanoparticles that are functionalized with cysteine are used to fabricate spectroscopic biosensors for the detection of lactic acid bacteria that spoils milk [275]. Furthermore, metal oxide, metal nanoparticles, carbon nanotubes, and quantum dots have proved to be highly beneficial in fabricating biosensors for the detection of bacterial pathogens and toxins in meat products [276].

8.4.3 Diabetes

Next to cancer, diabetes is the most predominant metabolic disorder, widespread throughout the world. Diagnosis of diabetes plays a key role in the selection and implication of effective treatment modalities to control or cure it. Biosensors are used in the diagnosis of diabetes to detect either glucose and insulin level in blood. Recently, David et al. reported that acid and base functionalized carbon nanomaterials can be used as electrical bridges in biosensors that are made up of chitosan-poly (styrene sulfonate) loaded with enzymes in a self-assembled layer-by-layer structure for the detection of glucose [277]. Likewise, carbon nanotubes-reduced

graphene oxide nanosheets-gold nanowire array composites were used in microfluidic injection analysis for the sensitive detection of glucose [278]. Similarly, gold nanoparticles-three-dimensional zinc oxide nanostructures were arranged hierarchically for the fabrication of effective glucose-detecting biosensors [279]. Further, Hovancova et al. stated that electrodes made of nanomaterials, especially nanosized metals, were highly beneficial in the development of electrochemical biosensors to detect insulin with high sensitivity and selectivity [280]. Furthermore, Ma et al. demonstrated a gold nanoparticle-doped beta-cyclodextrin-lead metal-organic framework for the sensitive determination of insulin [281]. Moreover, Yagati et al. emphasized that a silver nanoflower-reduced graphene oxide composite can be used as a potential material for the fabrication of microdisk electrodes in biosensors to detect insulin in serum samples [282].

8.4.4 Other diseases

There are numerous other diseases for which nanomaterials are undergoing extensive research to act as biosensors for the detection of disease-related biomarkers that can help in effective diagnosis. It is noteworthy that cardiac troponin I and T are the most common biomarkers related to cardiovascular diseases. Thus, boron nitride quantum dots in molecularly imprinted polymer [283], zinc selenium oxide perovskite nanomaterial [284], and zinc oxide nanostructure [285] are used for the development of biosensors to detect cardiovascular disease biomarkers, for effective and early diagnosis of cardiac diseases. Similarly, mesoporous silica and graphene hybrid nanomaterials for apolipoprotein E gene detection [286] and graphene oxide-gold nanowires to detect serum microRNA-137 for Alzheimer's disease diagnosis [287], and carbon-based nanomaterials for A53T alpha-synuclein aggregation detection for Parkinson's disease diagnosis [288] are nanomaterial-based biosensors used to diagnose neurodegenerative diseases. Also, molybdenum sulfide nanosheets for malarial biomarker detection [289], silicon nanowire-gold nanoparticle electrodes for dengue viral DNA oligomer detection [290], gold and magnetic nanoparticles for *Vibrio cholera* O1 OmpW gene detection [291], graphene-based biosensors for Zika virus detection [292], and molybdenum sulfide-reduced graphene oxide nanocomposite to detect Vi antigen for early typhoid diagnosis [293] are other nanomaterial-based biosensors used in disease diagnosis. Even though nanomaterials are used in the detection of biomolecules for efficient disease diagnosis, it can be noted from Table 8.3 that these nanomaterials are predominantly employed for the fabrication of electrochemical biosensors. Extensive research should be carried out to utilize and employ nanomaterials in the fabrication of other types of biosensors.

8.5 Current challenges and future perspective

There are certain challenges that have to be addressed before the extensive introduction of nanomaterials in biosensors for diagnostic applications. For each type of novel biosensor, there exist certain challenges that impede their large-scale application. Impedance biosensors belong

to the group of electrical sensors that are highly beneficial in point-of-care applications, as they are cheaper to fabricate in smaller size and operate label free. However, limitations such as change in impedance, response curve, differential measurement, and problems with self-assembled monolayers exist in impedance biosensors, which reduce their performance as compared to DNA and protein biosensors [294]. It is noteworthy that the core challenge of using nanomaterials in biosensors, especially in electrochemical sensors, is to market these sensors for usage by patients in their personal care, without compromising their quality, reliability, and accuracy [295]. Estevez et al. reviewed the literature related to localized surface plasmon resonance (LSPR) based refractometric nanoplasmonic biosensors. These novel biosensors possess enormous benefits due to their smaller size, elevated sensitivities, and multiplexed opportunities. However, certain limitations exist, such as the presence of impurities, aggregation of nanoparticles, and damage of the sample, which are obstacles to the standalone usage of refractometric biosensors, similar to conventional SPR sensors with enhanced sensitivity, integration, and robustness for disease diagnosis [296]. Meanwhile, Topkaya et al. reported the benefits of electrochemical biosensors in detecting cancer biomarkers. This review article also reported and recommended that electrochemical biosensors must be integrated with point-of-care devices to increase their large-scale production. These integrated systems will be highly useful for accurate identification of normal and elevated concentrations of target analytes and also resistant to interference of other biomolecules [297]. Likewise, Balasubramaniam and Kangasharju reported several uses of nanomaterials in biosensor applications. In this article, the authors mentioned several uses as well as limitations of incorporating nanomaterials in sensor applications. They emphasized that biosensors containing nanomaterials may cause environmental toxicity after their lifetime as waste. Thus waste management of nanomaterial-based biosensors must be developed in future to avoid environmental toxicity [298]. Similarly, Farka et al. reviewed the advantages and challenges of nanoparticle-based immunochemical biosensors. The authors emphasized that existing heterogeneity in the nanoregime; instability in the size, morphology, and surface charge of nanomaterials; elevated variability of nanobased immunosensors due to lack of optimization; and common limitations related to immobilization of antibodies on the solid state nanoparticle surface are the limitations of immunochemical biosensors that hinder their large-scale applications and their availability in the pharmaceutical market [299]. These reports revealed that there are several research gaps associated with each type of nanobased biosensor that must be addressed in the future.

Currently, nanomaterial-based biosensors for disease diagnosis are at the lab-scale development stage, and it will take a long time for large-scale applications and their introduction into pharmaceutical markets. However, novel biosensors, including dual diagnosis materials [31], skin-mountable sensors [32], photoacoustic diagnosis and treatment [33], bioimaging diagnostics [34], multipurpose [35] and magnetic diagnostic biosensors [36] are

under extensive research for use in advanced diagnostics. The emergence of novel nanomaterial-based biosensors has led to the idea of in situ biochips [300,301], nanorobots [302], smart fabrics [303], and tattoos [304], which will be the next-generation personal diagnostic tools. In situ biochips are fabricated using implantable biosensors, to be injected into the bloodstream of the patient [305]. These biochips will detect an elevation or decrement in the concentration of the target analyte in the body and signals that to a digital receiver [306]. The receiver can be a computer [307], a smartphone app [308], or a smart watch [309], highly useful for diagnosing any changes in the patient's body without the need for medical technicians or doctors [310]. Likewise, these biochips can be coupled with a micro/nanoneedle with nanomedicines, which could inject the drug into the patient's body in the required quantity to balance the target analyte secretion, which eventually could reduce the complications of diseases [311]. Such biochips are termed nanorobots, and they can sense, diagnose, and deliver drugs for the treatment of diseases without the assistance of medical practitioners [312]. Meanwhile, nanomaterial-coated fabrics and tattoos are also under extensive research to monitor changes in the concentration of target analytes [313,314]. These smart fabrics and tattoos change color to indicate the variations in target analyte concentration, which will indicate to the patient to take medication [315,316]. Glucose monitoring tattoos with a similar function to this are currently available, with certain side effects, on the market [317]. Thus the emergence of nanomaterials in the field of biosensors represents the future of diagnosis and point-of-care treatments in biomedical and clinical sciences (Fig. 8.1).

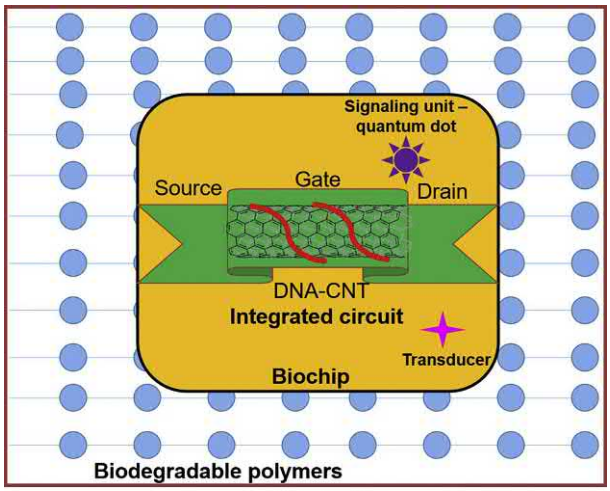

Fig. 8.1

Schematics of futuristic biosensor design with nanomaterials incorporated in gate of integrated circuit transistors, transducers, signal processors, biodegradable polymer, and bioplastic substrates.

8.6 Conclusion

This chapter is an overview of nanomaterial-based biosensors used in the diagnosis of diseases. Metal, metal oxide, carbon nanomaterials, nanocomposites and novel green synthesized nanomaterials are widely used for the fabrication of biosensors. These nanomaterials have paved the way for the emergence of several biosensor classes, namely electrochemical, field effect, and spectroscopic sensors for rapid disease diagnosis. These biosensors are highly beneficial in the diagnosis of diseases and disorders such as cancer, diabetes, cardiovascular and neurodegenerative disease, and microbial infections. However, several limitations exist in each of the biosensor types that must be addressed before employing nanomaterials in biosensors for large-scale clinical diagnostic applications. Once the limitations are reduced, nanomaterial-based biosensors will take over the market of conventional biosensors for diagnosis and can transform into novel wearable, implantable biosensors, nanorobots, smart fabrics, and tattoos for the rapid and sensitive diagnosis of diseases.

References

[1] W.G. Lee, et al., Nano/microfluidics for diagnosis of infectious diseases in developing countries, Adv. Drug Deliv. Rev. 62 (4-5) (2010) 449–457.
[2] A. Giustina, et al., Diagnosis and treatment of acromegaly complications, J. Endocrinol. Investig. 26 (12) (2003) 1242–1247.
[3] J. Gertler, Fault Detection and Diagnosis, Springer, 2013.
[4] J.A. Robertson, Extending preimplantation genetic diagnosis: medical and non-medical uses, J. Med. Ethics 29 (4) (2003) 213–216.
[5] J. Wardle, et al., Screening for prevention and early diagnosis of cancer, Am. Psychol. 70 (2) (2015) 119.
[6] American Diabetes Association, 2. Classification and diagnosis of diabetes: standards of medical care in diabetes—2018, Diabetes Care 41 (Suppl 1) (2018) S13–S27.
[7] G. Singh, L. Samavedham, Unsupervised learning based feature extraction for differential diagnosis of neurodegenerative diseases: a case study on early-stage diagnosis of Parkinson disease, J. Neurosci. Methods 256 (2015) 30–40.
[8] V. Prasad, J. Lenzer, D.H. Newman, Why cancer screening has never been shown to "save lives"—and what we can do about it, BMJ 352 (2016) h6080.
[9] V.N. Shabalin, S.N. Shatokhina, Diagnostic markers in the structures of human biological liquids, Singap. Med. J. 48 (5) (2007) 440.
[10] Y. Wang, et al., Identification of a three-miRNA signature as a blood-borne diagnostic marker for early diagnosis of lung adenocarcinoma, Oncotarget 7 (18) (2016) 26070.
[11] F.N. Soria, et al., Exosomes, an unmasked culprit in neurodegenerative diseases, Front. Neurosci. 11 (2017) 26.
[12] B. Hess, Enzymes in Blood Plasma, Academic Press, 2016.
[13] J.C. Lindon, et al., Metabonomics technologies and their applications in physiological monitoring, drug safety assessment and disease diagnosis, Biomarkers 9 (1) (2004) 1–31.
[14] G.-J. Zhang, Y. Ning, Silicon nanowire biosensor and its applications in disease diagnostics: a review, Anal. Chim. Acta 749 (2012) 1–15.
[15] N.P. Revsbech, Analysis of microbial communities with electrochemical microsensors and microscale biosensors, Methods Enzymol. 397 (2005) 147–166.

[16] D. Franke, S. Binder, G. Gerlach, Performance of fast-responsive, porous crosslinked poly (N-isopropylacrylamide) in a piezoresistive microsensor, IEEE Sens. Lett. 1 (6) (2017) 1–4.
[17] D.J. Maxwell, J.R. Taylor, S. Nie, Self-assembled nanoparticle probes for recognition and detection of biomolecules, J. Am. Chem. Soc. 124 (32) (2002) 9606–9612.
[18] Y. Song, et al., Recent advances in electrochemical biosensors based on graphene two-dimensional nanomaterials, Biosens. Bioelectron. 76 (2016) 195–212.
[19] S. Vigneshvar, et al., Recent advances in biosensor technology for potential applications – an overview, Front. Bioeng. Biotechnol. 4 (2016) 11.
[20] B.R. Eggins, Chemical Sensors and Biosensors, Vol. 28, John Wiley & Sons, 2008.
[21] K.K. Jain, Nanotechnology in clinical laboratory diagnostics, Clin. Chim. Acta 358 (1-2) (2005) 37–54.
[22] J. Wang, E. Katz, Digital biosensors with built-in logic for biomedical applications—biosensors based on a biocomputing concept, Anal. Bioanal. Chem. 398 (4) (2010) 1591–1603.
[23] P.D. Howes, R. Chandrawati, M.M. Stevens, Colloidal nanoparticles as advanced biological sensors, Science 346 (6205) (2014) 1247390.
[24] J. Wang, et al., Facile fabrication of gold nanoparticles-poly (vinyl alcohol) electrospun water-stable nanofibrous mats: efficient substrate materials for biosensors, ACS Appl. Mater. Interfaces 4 (4) (2012) 1963–1971.
[25] Y. Li, H.J. Schluesener, S. Xu, Gold nanoparticle-based biosensors, Gold Bull. 43 (1) (2010) 29–41.
[26] W. Zhou, R. Saran, J. Liu, Metal sensing by DNA, Chem. Rev. 117 (12) (2017) 8272–8325.
[27] N.L. Rosi, C.A. Mirkin, Nanostructures in biodiagnostics, Chem. Rev. 105 (4) (2005) 1547–1562.
[28] H. Heli, et al., Copper nanoparticles-modified carbon paste transducer as a biosensor for determination of acetylcholine, Biosens. Bioelectron. 24 (8) (2009) 2328–2333.
[29] J. Chen, et al., Computational lateral flow biosensor for proteins and small molecules: a new class of strip logic gates, Anal. Chem. 84 (15) (2012) 6321–6325.
[30] W. Cui, X. Zhao, Theranostic Bionanomaterials, Elsevier, 2019.
[31] X. Shen, et al., Biodegradable nanosyringes for intracellular amplification-based dual-diagnosis and gene therapy in single living cells, Chem. Sci. (2019).
[32] E.K. Lee, M.K. Kim, C.H. Lee, Skin-mountable biosensors and therapeutics: a review, Annu. Rev. Biomed. Eng. 21 (2019).
[33] J.M. Morales, et al., DNA-based photoacoustic nanosensor for interferon gamma detection, ACS Sensors 4 (2019) 1313–1322.
[34] M. Mehrzad-Samarin, F. Faridbod, M.R. Ganjali, A luminescence nanosensor for ornidazole detection using graphene quantum dots entrapped in silica molecular imprinted polymer, Spectrochim. Acta A Mol. Biomol. Spectrosc. 206 (2019) 430–436.
[35] S. Mehmood, et al., Aptamer-based biosensors: a novel toolkit for early diagnosis of cancer, Mater. Today Chem. 12 (2019) 353–360.
[36] S. Doswald, W.J. Stark, B. Beck-Schimmer, Biochemical functionality of magnetic particles as nanosensors: how far away are we to implement them into clinical practice? J. Nanobiotechnol. 17 (1) (2019) 73.
[37] L. Tian, et al., Gold nanoparticles superlattices assembly for electrochemical biosensor detection of microRNA-21, Biosens. Bioelectron. 99 (2018) 564–570.
[38] F. Campanhã Vicentini, et al., A biosensor based on gold nanoparticles, dihexadecylphosphate, and tyrosinase for the determination of catechol in natural water, Enzym. Microb. Technol. 84 (2016) 17–23.
[39] Y. Deng, et al., An novel acetylcholinesterase biosensor based on nano-porous pseudo carbon paste electrode modified with gold nanoparticles for detection of methyl parathion, J. Nanosci. Nanotechnol. 16 (9) (2016) 9460–9467.
[40] R. Devasenathipathy, et al., Glucose biosensor based on glucose oxidase immobilized at gold nanoparticles decorated graphene-carbon nanotubes, Enzym. Microb. Technol. 78 (2015) 40–45.
[41] N. Sattarahmady, et al., Gold nanoparticles biosensor of Brucella spp. genomic DNA: visual and spectrophotometric detections, Biochem. Eng. J. 97 (2015) 1–7.

[42] G. Presnova, et al., Biosensor based on a silicon nanowire field-effect transistor functionalized by gold nanoparticles for the highly sensitive determination of prostate specific antigen, Biosens. Bioelectron. 88 (2017) 283–289.
[43] H.S. Magar, et al., A novel sensitive amperometric choline biosensor based on multiwalled carbon nanotubes and gold nanoparticles, Talanta 167 (2017) 462–469.
[44] A. Karimizefreh, et al., Impedimetic biosensor for the DNA of the human papilloma virus based on the use of gold nanosheets, Microchim. Acta 184 (6) (2017) 1729–1737.
[45] J. Yoon, et al., Flexible electrochemical glucose biosensor based on GOx/gold/MoS2/gold nanofilm on the polymer electrode, Biosens. Bioelectron. 140 (2019) 111343.
[46] Z. Shakoori, et al., Electrochemical DNA biosensor based on gold nanorods for detecting hepatitis B virus, Anal. Bioanal. Chem. 407 (2) (2015) 455–461.
[47] W. Wen, et al., Increased electrocatalyzed performance through hairpin oligonucleotide aptamer-functionalized gold nanorods labels and graphene-streptavidin nanomatrix: highly selective and sensitive electrochemical biosensor of carcinoembryonic antigen, Biosens. Bioelectron. 83 (2016) 142–148.
[48] Q. Lang, et al., A sensitive acetylcholinesterase biosensor based on gold nanorods modified electrode for detection of organophosphate pesticide, Talanta 156 (2016) 34–41.
[49] J. Chen, et al., Optimization and application of reflective LSPR optical fiber biosensors based on silver nanoparticles, Sensors 15 (6) (2015) 12205–12217.
[50] P. Alessio, et al., Mimetic biosensors composed by layer-by-layer films of phospholipid, phthalocyanine and silver nanoparticles to polyphenol detection, Sens. Actuators B Chem. 233 (2016) 654–666.
[51] N. Xia, et al., Peptide aptamer-based biosensor for the detection of human chorionic gonadotropin by converting silver nanoparticles-based colorimetric assay into sensitive electrochemical analysis, Sens. Actuators B Chem. 243 (2017) 784–791.
[52] Y. Jiang, et al., Silver nanoparticles modified two-dimensional transition metal carbides as nanocarriers to fabricate acetycholinesterase-based electrochemical biosensor, Chem. Eng. J. 339 (2018) 547–556.
[53] G. Rosati, et al., Silver nanoparticles inkjet-printed flexible biosensor for rapid label-free antibiotic detection in milk, Sens. Actuators B Chem. 280 (2019) 280–289.
[54] Y. Xing, et al., A sensitive and selective electrochemical biosensor for the determination of beta-amyloid oligomer by inhibiting the peptide-triggered in situ assembly of silver nanoparticles, Int. J. Nanomed. 12 (2017) 3171.
[55] Y. Hui, et al., Silver nanoparticles-β-cyclodextrin-graphene nanocomposites based biosensor for guanine and adenine sensing, Ionics 21 (6) (2015) 1751–1759.
[56] N.N. Durmanov, et al., Non-labeled selective virus detection with novel SERS-active porous silver nanofilms fabricated by electron beam physical vapor deposition, Sens. Actuators B Chem. 257 (2018) 37–47.
[57] B. Ma, et al., A sensitive electrochemical nonenzymatic biosensor for the detection of H_2O_2 released from living cells based on ultrathin concave Ag nanosheets, Biosens. Bioelectron. 106 (2018) 29–36.
[58] V. Sharma, et al., Graphene nanoplatelets-silver nanorods-polymer based in-situ hybrid electrode for electroanalysis of dopamine and ascorbic acid in biological samples, Appl. Surf. Sci. 449 (2018) 558–566.
[59] A. Khoshroo, et al., Silver nanofibers/ionic liquid nanocomposite based electrochemical sensor for detection of clonazepam via electrochemically amplified detection, Microchem. J. 145 (2019) 1185–1190.
[60] P. Yang, et al., Facile synthesis of Prussian blue nanocubes/silver nanowires network as a water-based ink for the direct screen-printed flexible biosensor chips, Biosens. Bioelectron. 92 (2017) 709–717.
[61] H.-B. Wang, et al., A fluorescent biosensor for protein detection based on poly (thymine)-templated copper nanoparticles and terminal protection of small molecule-linked DNA, Biosens. Bioelectron. 74 (2015) 581–586.
[62] Y. Fu, et al., Preparation of polyaniline-encapsulated carbon/copper composite nanofibers for detection of polyphenol pollutant, Colloids Surf. A Physicochem. Eng. Asp. 559 (2018) 289–296.
[63] D. Song, et al., Palladium-copper nanowires-based biosensor for the ultrasensitive detection of organophosphate pesticides, Anal. Chim. Acta 982 (2017) 168–175.

[64] X. Liu, et al., Synthesis of copper nanorods for non-enzymatic amperometric sensing of glucose, Microchim. Acta 183 (8) (2016) 2369–2375.
[65] H. Li, et al., Fluorescence resonance energy transfer biosensor between upconverting nanoparticles and palladium nanoparticles for ultrasensitive CEA detection, Biosens. Bioelectron. 86 (2016) 791–798.
[66] L. Meng, et al., Hydrogen microexplosion synthesis of platinum nanoparticles/nitrogen doped graphene nanoscrolls as new amperometric glucose biosensor, Electrochim. Acta 152 (2015) 330–337.
[67] Z. Li, F. Gao, Z. Gu, Vertically aligned Pt nanowire array/Au nanoparticle hybrid structure as highly sensitive amperometric biosensors, Sens. Actuators B Chem. 243 (2017) 1092–1101.
[68] L. Mo, et al., Nucleic acid-functionalized transition metal nanosheets for biosensing applications, Biosens. Bioelectron. 89 (2017) 201–211.
[69] S. Tiwari, et al., L-cysteine capped lanthanum hydroxide nanostructures for non-invasive detection of oral cancer biomarker, Biosens. Bioelectron. 89 (2017) 1042–1052.
[70] T. Dayakar, et al., Novel synthesis and structural analysis of zinc oxide nanoparticles for the non enzymatic glucose biosensor, Mater. Sci. Eng. C 75 (2017) 1472–1479.
[71] F.L. Migliorini, et al., Urea impedimetric biosensing using electrospun nanofibers modified with zinc oxide nanoparticles, Appl. Surf. Sci. 443 (2018) 18–23.
[72] S. Zhao, B. You, L. Jiang, Oriented assembly of zinc oxide mesocrystal in chitosan and applications for glucose biosensors, Cryst. Growth Des. 16 (6) (2016) 3359–3365.
[73] R. Ahmad, et al., Fabrication of highly sensitive uric acid biosensor based on directly grown ZnO nanosheets on electrode surface, Sens. Actuators B Chem. 206 (2015) 146–151.
[74] P.V. Morais, et al., Nanofilm of ZnO nanocrystals/carbon nanotubes as biocompatible layer for enzymatic biosensors in capacitive field-effect devices, J. Mater. Sci. 52 (20) (2017) 12314–12325.
[75] M.A. Ali, et al., Anti-epidermal growth factor receptor conjugated mesoporous zinc oxide nanofibers for breast cancer diagnostics, Nanoscale 7 (16) (2015) 7234–7245.
[76] M. Marie, S. Mandal, O. Manasreh, An electrochemical glucose sensor based on zinc oxide nanorods, Sensors 15 (8) (2015) 18714–18723.
[77] X. Li, C. Zhao, X. Liu, A paper-based microfluidic biosensor integrating zinc oxide nanowires for electrochemical glucose detection, Microsyst. Nanoeng. 1 (2015) 15014.
[78] D. Sahoo, et al., Nanosensing of pesticides by zinc oxide quantum dot: an optical and electrochemical approach for the detection of pesticides in water, J. Agric. Food Chem. 66 (2) (2018) 414–423.
[79] R.D. Peterson, et al., Enhanced sandwich immunoassay using antibody-functionalized magnetic iron-oxide nanoparticles for extraction and detection of soluble transferrin receptor on a photonic crystal biosensor, Biosens. Bioelectron. 74 (2015) 815–822.
[80] N. Chauhan, J. Narang, U. Jain, Amperometric acetylcholinesterase biosensor for pesticides monitoring utilising iron oxide nanoparticles and poly(indole-5-carboxylic acid), J. Exp. Nanosci. 11 (2) (2016) 111–122.
[81] M. Dolci, et al., Robust clicked assembly based on iron oxide nanoparticles for a new type of SPR biosensor, J. Mater. Chem. C 6 (34) (2018) 9102–9110.
[82] C.-Y. Lin, C.-T. Chang, Iron oxide nanorods array in electrochemical detection of H_2O_2, Sens. Actuators B Chem. 220 (2015) 695–704.
[83] D. Manoj, J. Santhanalakshmi, Nanomaterials as an immobilizing platform for enzymatic glucose biosensors, in: Advanced Nanostructured Materials for Environmental Remediation, Springer, 2019, pp. 229–251.
[84] Y. Zhao, et al., Biosensor based on 3D graphene-supported Fe_3O_4 quantum dots as biomimetic enzyme for in situ detection of H_2O_2 released from living cells, Sens. Actuators B Chem. 244 (2017) 1037–1044.
[85] Y. Zhong, et al., Ultrasensitive non-enzymatic glucose sensors based on different copper oxide nanostructures by in-situ growth, Sens. Actuators B Chem. 236 (2016) 326–333.
[86] W. Lu, et al., Direct growth of pod-like Cu_2O nanowire arrays on copper foam: highly sensitive and efficient nonenzymatic glucose and H_2O_2 biosensor, Sens. Actuators B Chem. 231 (2016) 860–866.
[87] J. Li, et al., Efficient label-free chemiluminescent immunosensor based on dual functional cupric oxide nanorods as peroxidase mimics, Biosens. Bioelectron. 100 (2018) 304–311.

[88] A. Esmaeeli, et al., Copper oxide-polyaniline nanofiber modified fluorine doped tin oxide (FTO) electrode as non-enzymatic glucose sensor, Sens. Actuators B Chem. 266 (2018) 294–301.
[89] S.T. Ten, et al., Highly sensitive *Escherichia coli* shear horizontal surface acoustic wave biosensor with silicon dioxide nanostructures, Biosens. Bioelectron. 93 (2017) 146–154.
[90] R. Atchudan, et al., An ultrasensitive photoelectrochemical biosensor for glucose based on bio-derived nitrogen-doped carbon sheets wrapped titanium dioxide nanoparticles, Biosens. Bioelectron. 126 (2019) 160–169.
[91] S.R. Benjamin, et al., Enzymatic electrochemical biosensor based on multiwall carbon nanotubes and cerium dioxide nanoparticles for rutin detection, Int. J. Electrochem. Sci. 13 (2018) 563–586.
[92] N.T. Nguyet, et al., Highly sensitive DNA sensors based on cerium oxide nanorods, J. Phys. Chem. Solids 115 (2018) 18–25.
[93] P.D. Tam, et al., Detection of vibrio cholerae O1 by using cerium oxide nanowires-based immunosensor with different antibody immobilization methods, J. Korean Phys. Soc. 68 (10) (2016) 1235–1245.
[94] A. Umar, et al., Bi2O2CO3 nanoplates: fabrication and characterization of highly sensitive and selective cholesterol biosensor, J. Alloys Compd. 683 (2016) 433–438.
[95] M.K. Patel, et al., A label-free photoluminescence genosensor using nanostructured magnesium oxide for cholera detection, Sci. Rep. 5 (2015) 17384.
[96] G. Yu, et al., A facile and practical biosensor for choline based on manganese dioxide nanoparticles synthesized in-situ at the surface of electrode by one-step electrodeposition, Talanta 146 (2016) 707–713.
[97] Y. Zhang, et al., Single-layer transition metal dichalcogenide nanosheet-based nanosensors for rapid, sensitive, and multiplexed detection of DNA, Adv. Mater. 27 (5) (2015) 935–939.
[98] R. Ahmad, Y.-B. Hahn, Nonenzymatic flexible field-effect transistor based glucose sensor fabricated using NiO quantum dots modified ZnO nanorods, J. Colloid Interface Sci. 512 (2018) 21–28.
[99] S. Kumar, et al., Nanostructured zirconia decorated reduced graphene oxide based efficient biosensing platform for non-invasive oral cancer detection, Biosens. Bioelectron. 78 (2016) 497–504.
[100] S. Azzouzi, et al., A novel amperometric biosensor based on gold nanoparticles anchored on reduced graphene oxide for sensitive detection of L-lactate tumor biomarker, Biosens. Bioelectron. 69 (2015) 280–286.
[101] S. Siddique, M.Z. Iqbal, H. Mukhtar, Cholesterol immobilization on chemical vapor deposition grown graphene nanosheets for biosensors and bioFETs with enhanced electrical performance, Sens. Actuators B Chem. 253 (2017) 559–565.
[102] S. Madhumitha, V. Nagarajan, R. Chandiramouli, Adsorption behavior of cytosine and guanine nucleobases on graphyne nanosheets: a DFT study, Comput. Theor. Chem. 1163 (2019) 112514.
[103] A.R. Karami, Acrolein adsorption on graphyne nanotube: a density functional theory study, Fuller. Nanotub. Carbon Nanostructures 23 (10) (2015) 885–889.
[104] H. Karimi-Maleh, et al., A novel DNA biosensor based on a pencil graphite electrode modified with polypyrrole/functionalized multiwalled carbon nanotubes for determination of 6-mercaptopurine anticancer drug, Ind. Eng. Chem. Res. 54 (14) (2015) 3634–3639.
[105] N. Hernández-Ibáñez, et al., Electrochemical lactate biosensor based upon chitosan/carbon nanotubes modified screen-printed graphite electrodes for the determination of lactate in embryonic cell cultures, Biosens. Bioelectron. 77 (2016) 1168–1174.
[106] M. Baghayeri, A. Amiri, S. Farhadi, Development of non-enzymatic glucose sensor based on efficient loading Ag nanoparticles on functionalized carbon nanotubes, Sens. Actuators B Chem. 225 (2016) 354–362.
[107] M. Eguílaz, et al., Single-walled carbon nanotubes covalently functionalized with polytyrosine: a new material for the development of NADH-based biosensors, Biosens. Bioelectron. 86 (2016) 308–314.
[108] X. Cui, et al., A fluorescent biosensor based on carbon dots-labeled oligodeoxyribonucleotide and graphene oxide for mercury (II) detection, Biosens. Bioelectron. 63 (2015) 506–512.
[109] R. Wang, X. Wang, Y. Sun, One-step synthesis of self-doped carbon dots with highly photoluminescence as multifunctional biosensors for detection of iron ions and pH, Sens. Actuators B Chem. 241 (2017) 73–79.

[110] S. Liu, et al., Amino-functionalized green fluorescent carbon dots as surface energy transfer biosensors for hyaluronidase, Nanoscale 7 (15) (2015) 6836–6842.
[111] L. Zhu, et al., Highly sensitive determination of dopamine by a turn-on fluorescent biosensor based on aptamer labeled carbon dots and nano-graphite, Sens. Actuators B Chem. 231 (2016) 506–512.
[112] S.-S. Liang, et al., Ratiometric fluorescence biosensor based on CdTe quantum and carbon dots for double strand DNA detection, Sens. Actuators B Chem. 244 (2017) 585–590.
[113] T.T. Bui, S.-Y. Park, A carbon dot–hemoglobin complex-based biosensor for cholesterol detection, Green Chem. 18 (15) (2016) 4245–4253.
[114] C. Xiong, et al., In situ electro-polymerization of nitrogen doped carbon dots and their application in an electrochemiluminescence biosensor for the detection of intracellular lead ions, Chem. Commun. 52 (32) (2016) 5589–5592.
[115] S. Afreen, et al., Functionalized fullerene (C60) as a potential nanomediator in the fabrication of highly sensitive biosensors, Biosens. Bioelectron. 63 (2015) 354–364.
[116] A. Barberis, et al., Simultaneous amperometric detection of ascorbic acid and antioxidant capacity in orange, blueberry and kiwi juice, by a telemetric system coupled with a fullerene- or nanotubes-modified ascorbate subtractive biosensor, Biosens. Bioelectron. 67 (2015) 214–223.
[117] H. Wang, et al., An ultrasensitive photoelectrochemical biosensor based on [Ru(dcbpy)2dppz]2+/Rose Bengal dyes co-sensitized fullerene for DNA detection, Biosens. Bioelectron. 120 (2018) 71–76.
[118] C. Tortolini, et al., Application of a nanostructured enzymatic biosensor based on fullerene and gold nanoparticles to polyphenol detection, in: B. Prickril, A. Rasooly (Eds.), Biosensors and Biodetection: Methods and Protocols, Volume 2: Electrochemical, Bioelectronic, Piezoelectric, Cellular and Molecular Biosensors, Springer New York, New York, NY, 2017, pp. 41–53.
[119] H. Wang, et al., An electrochemiluminescence biosensor for dopamine based on the recognition of fullerene-derivative and the quenching of cuprous oxide nanocrystals, RSC Adv. 5 (71) (2015) 58019–58023.
[120] S. Emelyantsev, et al., Biological effects of C60 fullerene revealed with bacterial biosensor—toxic or rather antioxidant? Biosensors (2) (2019) 9, https://doi.org/10.3390/bios9020081.
[121] S. Sutradhar, A. Patnaik, A new fullerene-C60 – nanogold composite for non-enzymatic glucose sensing, Sens. Actuators B Chem. 241 (2017) 681–689.
[122] N.M.M. Pires, T. Dong, Z. Yang, A fluorimetric nitrite biosensor with polythienothiophene-fullerene thin film detectors for on-site water monitoring, Analyst 144 (14) (2019) 4342–4350.
[123] J. Shi, et al., A fluorescence resonance energy transfer (FRET) biosensor based on graphene quantum dots (GQDs) and gold nanoparticles (AuNPs) for the detection of mecA gene sequence of Staphylococcus aureus, Biosens. Bioelectron. 67 (2015) 595–600.
[124] T. Hu, et al., Enzyme catalytic amplification of miRNA-155 detection with graphene quantum dot-based electrochemical biosensor, Biosens. Bioelectron. 77 (2016) 451–456.
[125] B. Habibi, M. Jahanbakhshi, A glassy carbon electrode modified with carboxylated diamond nanoparticles for differential pulse voltammetric simultaneous determination of guanine and adenine, Microchim. Acta 183 (7) (2016) 2317–2325.
[126] L. Liang, et al., Metal-enhanced ratiometric fluorescence/naked eye bimodal biosensor for lead ions analysis with bifunctional nanocomposite probes, Anal. Chem. 89 (6) (2017) 3597–3605.
[127] L. Zhou, et al., Acetylcholinesterase/chitosan-transition metal carbides nanocomposites-based biosensor for the organophosphate pesticides detection, Biochem. Eng. J. 128 (2017) 243–249.
[128] X. Xuan, et al., A highly stretchable and conductive 3D porous graphene metal nanocomposite based electrochemical-physiological hybrid biosensor, Biosens. Bioelectron. 120 (2018) 160–167.
[129] L. Wang, et al., Cu-hemin metal-organic-frameworks/chitosan-reduced graphene oxide nanocomposites with peroxidase-like bioactivity for electrochemical sensing, Electrochim. Acta 213 (2016) 691–697.
[130] Z. Yan, et al., Sensitive electrogenerated chemiluminescence biosensors for protein kinase activity analysis based on bimetallic catalysis signal amplification and recognition of Au and Pt loaded metal-organic frameworks nanocomposites, Biosens. Bioelectron. 109 (2018) 132–138.

[131] M. Baghayeri, H. Veisi, M. Ghanei-Motlagh, Amperometric glucose biosensor based on immobilization of glucose oxidase on a magnetic glassy carbon electrode modified with a novel magnetic nanocomposite, Sens. Actuators B Chem. 249 (2017) 321–330.
[132] D. Xiang, et al., Amperometric hydrogen peroxide and glucose biosensor based on NiFe2/ordered mesoporous carbon nanocomposites, Analyst 140 (2) (2015) 644–653.
[133] S. Dong, et al., Three MOF-templated carbon nanocomposites for potential platforms of enzyme immobilization with improved electrochemical performance, ACS Appl. Mater. Interfaces 10 (17) (2018) 14665–14672.
[134] R. Madhu, et al., Functional porous carbon–ZnO nanocomposites for high-performance biosensors and energy storage applications, Phys. Chem. Chem. Phys. 18 (24) (2016) 16466–16475.
[135] W. Zhang, et al., Multifunctional glucose biosensors from Fe_3O_4 nanoparticles modified chitosan/graphene nanocomposites, Sci. Rep. 5 (2015) 11129.
[136] Q. Wang, et al., Label-free aptamer biosensor for thrombin detection based on functionalized graphene nanocomposites, Talanta 141 (2015) 247–252.
[137] H. Zhao, et al., An ultra-sensitive acetylcholinesterase biosensor based on reduced graphene oxide-Au nanoparticles-β-cyclodextrin/Prussian blue-chitosan nanocomposites for organophosphorus pesticides detection, Biosens. Bioelectron. 65 (2015) 23–30.
[138] L. Wang, et al., Highly sensitive electrochemical biosensor for evaluation of oxidative stress based on the nanointerface of graphene nanocomposites blended with gold, Fe_3O_4, and platinum nanoparticles, ACS Appl. Mater. Interfaces 7 (33) (2015) 18441–18449.
[139] S.S. Low, et al., Facile hydrothermal growth graphene/ZnO nanocomposite for development of enhanced biosensor, Anal. Chim. Acta 903 (2016) 131–141.
[140] N. Wang, et al., Functionalized gold nanoparticles/reduced graphene oxide nanocomposites for ultrasensitive electrochemical sensing of mercury ions based on thymine–mercury–thymine structure, Biosens. Bioelectron. 79 (2016) 320–326.
[141] S. Pakapongpan, R.P. Poo-arporn, Self-assembly of glucose oxidase on reduced graphene oxide-magnetic nanoparticles nanocomposite-based direct electrochemistry for reagentless glucose biosensor, Mater. Sci. Eng. C 76 (2017) 398–405.
[142] H.-P. Peng, et al., Label-free electrochemical DNA biosensor for rapid detection of mutidrug resistance gene based on Au nanoparticles/toluidine blue–graphene oxide nanocomposites, Sens. Actuators B Chem. 207 (2015) 269–276.
[143] B.K. Shrestha, et al., High-performance glucose biosensor based on chitosan-glucose oxidase immobilized polypyrrole/Nafion/functionalized multi-walled carbon nanotubes bio-nanohybrid film, J. Colloid Interface Sci. 482 (2016) 39–47.
[144] M. Chen, et al., An ultrasensitive electrochemical DNA biosensor based on a copper oxide nanowires/single-walled carbon nanotubes nanocomposite, Appl. Surf. Sci. 364 (2016) 703–709.
[145] Q. Zhang, et al., Synthesis of single-walled carbon nanotubes–chitosan nanocomposites for the development of an electrochemical biosensor for serum leptin detection, Mater. Lett. 211 (2018) 348–351.
[146] V. Mani, et al., Core-shell heterostructured multiwalled carbon nanotubes@reduced graphene oxide nanoribbons/chitosan, a robust nanobiocomposite for enzymatic biosensing of hydrogen peroxide and nitrite, Sci. Rep. 7 (1) (2017) 11910.
[147] T. Choi, et al., Synthesis of carbon nanotube–nickel nanocomposites using atomic layer deposition for high-performance non-enzymatic glucose sensing, Biosens. Bioelectron. 63 (2015) 325–330.
[148] C. Ye, et al., Sensing glucose based on its affinity for concanavalin A on a glassy carbon electrode modified with a C60 fullerene nanocomposite, Microchim. Acta 182 (13) (2015) 2215–2221.
[149] L.I. Di, et al., Direct electrochemistry of glucose oxidase immobilized on a hydroxyl fullerenes-Tio2 nanocomposite modified glassy carbon electrode, in: 2nd International Conference on Biomedical and Biological Engineering 2017 (BBE 2017), Atlantis Press, 2017.

[150] L. Bai, et al., Ultrasensitive electrochemical detection of Mycobacterium tuberculosis IS6110 fragment using gold nanoparticles decorated fullerene nanoparticles/nitrogen-doped graphene nanosheet as signal tags, Anal. Chim. Acta 1080 (2019) 75–83.
[151] J. Chen, et al., A facile fluorescence lateral flow biosensor for glutathione detection based on quantum dots-MnO2 nanocomposites, Sens. Actuators B Chem. 260 (2018) 770–777.
[152] E. Han, et al., Development of tyrosinase biosensor based on quantum dots/chitosan nanocomposite for detection of phenolic compounds, Anal. Biochem. 486 (2015) 102–106.
[153] Z. Zhang, et al., Electrochemical clenbuterol immunosensor based on a gold electrode modified with zinc sulfide quantum dots and polyaniline, Microchim. Acta 183 (3) (2016) 1089–1097.
[154] M. Terti, et al., Electrochemical impedance studies on single and multi-walled carbon nanotubespolymer nanocomposites for biosensors development, J. Nanosci. Nanotechnol. 15 (5) (2015) 3385–3393.
[155] S. Wu, et al., Development of glucose biosensors based on plasma polymerization-assisted nanocomposites of polyaniline, tin oxide, and three-dimensional reduced graphene oxide, Appl. Surf. Sci. 401 (2017) 262–270.
[156] M. Dervisevic, et al., Construction of novel xanthine biosensor by using polymeric mediator/MWCNT nanocomposite layer for fish freshness detection, Food Chem. 181 (2015) 277–283.
[157] V. Scognamiglio, et al., An eco-designed paper-based algal biosensor for nanoformulated herbicide optical detection, J. Hazard. Mater. 373 (2019) 483–492.
[158] Y. Jin, et al., LAL test and RPT for endotoxin detection of CPT-11/DSPE-mPEG2000 nanoformulation: What if traditional methods are not applicable? Asian J. Pharm. Sci. 13 (3) (2018) 289–296.
[159] Q. Wang, et al., Surface plasmon resonance biosensor for enzyme-free amplified microRNA detection based on gold nanoparticles and DNA supersandwich, Sens. Actuators B Chem. 223 (2016) 613–620.
[160] Z. Zhang, et al., One-step fabrication of electrochemical biosensor based on DNA-modified three-dimensional reduced graphene oxide and chitosan nanocomposite for highly sensitive detection of Hg(II), Sens. Actuators B Chem. 225 (2016) 453–462.
[161] M. Arvand, M. Sanayeei, S. Hemmati, Label-free electrochemical DNA biosensor for guanine and adenine by ds-DNA/poly(L-cysteine)/Fe3O4 nanoparticles-graphene oxide nanocomposite modified electrode, Biosens. Bioelectron. 102 (2018) 70–79.
[162] M. Mazloum-Ardakani, et al., A new composite consisting of electrosynthesized conducting polymers, graphene sheets and biosynthesized gold nanoparticles for biosensing acute lymphoblastic leukemia, Bioelectrochemistry 121 (2018) 38–45.
[163] S. Sandeep, et al., Detection of catechol using a biosensor based on biosynthesized silver nanoparticles and polyphenol oxidase enzyme, Port. Electrochim. Acta 37 (2017). https://doi.org/10.4152/pea.201904257.
[164] Y. Chen, Y. Xianyu, X. Jiang, Surface modification of gold nanoparticles with small molecules for biochemical analysis, Acc. Chem. Res. 50 (2) (2017) 310–319.
[165] R. Faridi-Majidi, N. Sharifi-Sanjani, In situ synthesis of iron oxide nanoparticles on poly (ethylene oxide) nanofibers through an electrospinning process, J. Appl. Polym. Sci. 105 (3) (2007) 1351–1355.
[166] D. Du, et al., Development of acetylcholinesterase biosensor based on CdTe quantum dots/gold nanoparticles modified chitosan microspheres interface, Biosens. Bioelectron. 24 (3) (2008) 475–479.
[167] Y. Wang, et al., Colorimetric and fluorometric determination of uric acid based on the use of nitrogen-doped carbon quantum dots and silver triangular nanoprisms, Microchim. Acta 185 (6) (2018) 281.
[168] J. Lee, et al., Biosensors based on graphene oxide and its biomedical application, Adv. Drug Deliv. Rev. 105 (2016) 275–287.
[169] M. Briones, et al., Diamond nanoparticles based biosensors for efficient glucose and lactate determination, Biosens. Bioelectron. 68 (2015) 521–528.
[170] M. Briones, et al., Diamond nanoparticles as a way to improve electron transfer in sol–gel l-lactate biosensing platforms, Anal. Chim. Acta 908 (2016) 141–149.
[171] M.D. Petit-Domínguez, et al., Synergistic effect of MoS2 and diamond nanoparticles in electrochemical sensors: determination of the anticonvulsant drug valproic acid, Microchim. Acta 185 (7) (2018) 334.

[172] J. Jeevanandam, et al., Metal oxide nanocomposites: cytotoxicity and targeted drug delivery applications, in: Hybrid Nanocomposites: Fundamentals, Synthesis and Applications, Pan Stanford Publishing, 2019, pp. 111–147.
[173] H.-F. Cui, et al., A highly stable acetylcholinesterase biosensor based on chitosan-TiO_2-graphene nanocomposites for detection of organophosphate pesticides, Biosens. Bioelectron. 99 (2018) 223–229.
[174] S. Andra, et al., Phytosynthesized metal oxide nanoparticles for pharmaceutical applications, Naunyn Schmiedeberg's Arch. Pharmacol. 392 (2019) 755–771.
[175] J. Wang, et al., DNA electrochemical biosensor for the detection of short DNA sequences related to the human immunodeficiency virus, Anal. Chem. 68 (15) (1996) 2629–2634.
[176] Y. Liu, et al., Aptamer-based electrochemical biosensor for interferon gamma detection, Anal. Chem. 82 (19) (2010) 8131–8136.
[177] R.P. Deo, et al., Determination of organophosphate pesticides at a carbon nanotube/organophosphorus hydrolase electrochemical biosensor, Anal. Chim. Acta 530 (2) (2005) 185–189.
[178] E.E. Ferapontova, E.M. Olsen, K.V. Gothelf, An RNA aptamer-based electrochemical biosensor for detection of theophylline in serum, J. Am. Chem. Soc. 130 (13) (2008) 4256–4258.
[179] Y. Deng, et al., Preparation and electrochemical behavior of L-glutamate electrochemical biosensor, J. Biomed. Nanotechnol. 9 (2) (2013) 318–321.
[180] J.C. Claussen, et al., Electrochemical biosensor of nanocube-augmented carbon nanotube networks, ACS Nano 3 (1) (2009) 37–44.
[181] B.K. Jena, C.R. Raj, Electrochemical biosensor based on integrated assembly of dehydrogenase enzymes and gold nanoparticles, Anal. Chem. 78 (18) (2006) 6332–6339.
[182] Z. Ge, et al., Hybridization chain reaction amplification of MicroRNA detection with a tetrahedral DNA nanostructure-based electrochemical biosensor, Anal. Chem. 86 (4) (2014) 2124–2130.
[183] L. Zhu, L. Luo, Z. Wang, DNA electrochemical biosensor based on thionine-graphene nanocomposite, Biosens. Bioelectron. 35 (1) (2012) 507–511.
[184] L.-H. Pan, et al., An electrochemical biosensor to simultaneously detect VEGF and PSA for early prostate cancer diagnosis based on graphene oxide/ssDNA/PLLA nanoparticles, Biosens. Bioelectron. 89 (2017) 598–605.
[185] O. Parlak, et al., Structuring Au nanoparticles on two-dimensional MoS2 nanosheets for electrochemical glucose biosensors, Biosens. Bioelectron. 89 (2017) 545–550.
[186] L. Cui, et al., An ultrasensitive electrochemical biosensor for polynucleotide kinase assay based on gold nanoparticle-mediated lambda exonuclease cleavage-induced signal amplification, Biosens. Bioelectron. 99 (2018) 1–7.
[187] H.Y. Lau, et al., Specific and sensitive isothermal electrochemical biosensor for plant pathogen DNA detection with colloidal gold nanoparticles as probes, Sci. Rep. 7 (2017) 38896.
[188] M. Chen, et al., An electrochemical DNA biosensor based on nitrogen-doped graphene/Au nanoparticles for human multidrug resistance gene detection, Biosens. Bioelectron. 85 (2016) 684–691.
[189] J. Yoon, et al., Electrochemical H_2O_2 biosensor composed of myoglobin on MoS2 nanoparticle-graphene oxide hybrid structure, Biosens. Bioelectron. 93 (2017) 14–20.
[190] N. Sanaeifar, et al., A novel electrochemical biosensor based on Fe_3O_4 nanoparticles-polyvinyl alcohol composite for sensitive detection of glucose, Anal. Biochem. 519 (2017) 19–26.
[191] A. Abbaspour, et al., Aptamer-conjugated silver nanoparticles for electrochemical dual-aptamer-based sandwich detection of staphylococcus aureus, Biosens. Bioelectron. 68 (2015) 149–155.
[192] S. Su, et al., Dual-mode electrochemical analysis of microRNA-21 using gold nanoparticle-decorated MoS2 nanosheet, Biosens. Bioelectron. 94 (2017) 552–559.
[193] Y. Zhou, et al., Electrochemical biosensor for protein kinase A activity assay based on gold nanoparticles-carbon nanospheres, phos-tag-biotin and β-galactosidase, Biosens. Bioelectron. 86 (2016) 508–515.
[194] B. Rezaei, et al., An electrochemical biosensor based on nanoporous stainless steel modified by gold and palladium nanoparticles for simultaneous determination of levodopa and uric acid, Talanta 158 (2016) 42–50.

[195] J.-J. Xu, et al., A sensitive biosensor for lactate based on layer-by-layer assembling MnO2 nanoparticles and lactate oxidase on ion-sensitive field-effect transistors, Chem. Commun. 6 (2005) 792–794.
[196] X.-L. Luo, et al., Glucose biosensor based on ENFET doped with SiO_2 nanoparticles, Sens. Actuators B Chem. 97 (2-3) (2004) 249–255.
[197] B. Cai, et al., Ultrasensitive label-free detection of PNA–DNA hybridization by reduced graphene oxide field-effect transistor biosensor, ACS Nano 8 (3) (2014) 2632–2638.
[198] A. Vijayalakshmi, et al., Enzyme field effect transistor (ENFET) for estimation of triglycerides using magnetic nanoparticles, Biosens. Bioelectron. 23 (11) (2008) 1708–1714.
[199] Y. Liu, A.G. Erdman, T. Cui, Acetylcholine biosensors based on layer-by-layer self-assembled polymer/nanoparticle ion-sensitive field-effect transistors, Sens. Actuators A Phys. 136 (2) (2007) 540–545.
[200] M.S. Makowski, A. Ivanisevic, Molecular analysis of blood with micro-/nanoscale field-effect-transistor biosensors, Small 7 (14) (2011) 1863–1875.
[201] X.-L. Luo, et al., A novel glucose ENFET based on the special reactivity of MnO2 nanoparticles, Biosens. Bioelectron. 19 (10) (2004) 1295–1300.
[202] K. Maehashi, et al., Label-free protein biosensor based on aptamer-modified carbon nanotube field-effect transistors, Anal. Chem. 79 (2) (2007) 782–787.
[203] K.-I. Chen, B.-R. Li, Y.-T. Chen, Silicon nanowire field-effect transistor-based biosensors for biomedical diagnosis and cellular recording investigation, Nano Today 6 (2) (2011) 131–154.
[204] Y. Ohno, K. Maehashi, K. Matsumoto, Label-free biosensors based on aptamer-modified graphene field-effect transistors, J. Am. Chem. Soc. 132 (51) (2010) 18012–18013.
[205] R. Stine, et al., Real-time DNA detection using reduced graphene oxide field effect transistors, Adv. Mater. 22 (46) (2010) 5297–5300.
[206] G. Zhou, et al., Real-time, selective detection of Pb2+ in water using a reduced graphene oxide/gold nanoparticle field-effect transistor device, ACS Appl. Mater. Interfaces 6 (21) (2014) 19235–19241.
[207] B. Cai, et al., Gold nanoparticles-decorated graphene field-effect transistor biosensor for femtomolar MicroRNA detection, Biosens. Bioelectron. 74 (2015) 329–334.
[208] Y. Chen, et al., Field-effect transistor biosensor for rapid detection of Ebola antigen, Sci. Rep. 7 (1) (2017) 10974.
[209] Y. Chen, et al., Field-effect transistor biosensors with two-dimensional black phosphorus nanosheets, Biosens. Bioelectron. 89 (2017) 505–510.
[210] G. Zhou, et al., Ultrasensitive mercury ion detection using DNA-functionalized molybdenum disulfide nanosheet/gold nanoparticle hybrid field-effect transistor device, ACS Sensors 1 (3) (2016) 295–302.
[211] Y.-M. Lei, et al., Detection of heart failure-related biomarker in whole blood with graphene field effect transistor biosensor, Biosens. Bioelectron. 91 (2017) 1–7.
[212] R. Ahmad, M.-S. Ahn, Y.-B. Hahn, ZnO nanorods array based field-effect transistor biosensor for phosphate detection, J. Colloid Interface Sci. 498 (2017) 292–297.
[213] J.S. Lee, et al., Highly sensitive and selective field-effect-transistor nonenzyme dopamine sensors based on Pt/conducting polymer hybrid nanoparticles, Small 11 (20) (2015) 2399–2406.
[214] S. Viswanathan, et al., Graphene–protein field effect biosensors: glucose sensing, Mater. Today 18 (9) (2015) 513–522.
[215] M. Varshney, Y. Li, Interdigitated array microelectrode based impedance biosensor coupled with magnetic nanoparticle–antibody conjugates for detection of *Escherichia coli* O157: H7 in food samples, Biosens. Bioelectron. 22 (11) (2007) 2408–2414.
[216] A.A. Ensafi, et al., Sensitive DNA impedance biosensor for detection of cancer, chronic lymphocytic leukemia, based on gold nanoparticles/gold modified electrode, Electrochim. Acta 56 (24) (2011) 8176–8183.
[217] K. Zhang, et al., Fabrication of a sensitive impedance biosensor of DNA hybridization based on gold nanoparticles modified gold electrode, Electroanalysis 20 (19) (2008) 2127–2133.
[218] J. Wang, et al., Au nanoparticle conjugation for impedance and capacitance signal amplification in biosensors, Anal. Chem. 78 (6) (2006) 1769–1773.

[219] L.-D. Li, et al., Aptamer biosensor for label-free impedance spectroscopy detection of thrombin based on gold nanoparticles, Sens. Actuators B Chem. 157 (1) (2011) 189–194.
[220] W.W. Ye, et al., A nanoporous alumina membrane based impedance biosensor for histamine detection with magnetic nanoparticles separation and amplification, Procedia Technology 27 (2017) 116–117.
[221] Z. Zhu, et al., Single domain antibody coated gold nanoparticles as enhancer for *Clostridium difficile* toxin detection by electrochemical impedance immunosensors, Bioelectrochemistry 101 (2015) 153–158.
[222] D. Wang, et al., Efficient separation and quantitative detection of *Listeria monocytogenes* based on screen-printed interdigitated electrode, urease and magnetic nanoparticles, Food Control 73 (2017) 555–561.
[223] S. Karash, et al., Rapid detection of avian influenza virus H5N1 in chicken tracheal samples using an impedance aptasensor with gold nanoparticles for signal amplification, J. Virol. Methods 236 (2016) 147–156.
[224] A.J. Haes, R.P. Van Duyne, A nanoscale optical biosensor: sensitivity and selectivity of an approach based on the localized surface plasmon resonance spectroscopy of triangular silver nanoparticles, J. Am. Chem. Soc. 124 (35) (2002) 10596–10604.
[225] A.J. Haes, et al., A localized surface plasmon resonance biosensor: first steps toward an assay for Alzheimer's disease, Nano Lett. 4 (6) (2004) 1029–1034.
[226] M.D. Malinsky, et al., Chain length dependence and sensing capabilities of the localized surface plasmon resonance of silver nanoparticles chemically modified with alkanethiol self-assembled monolayers, J. Am. Chem. Soc. 123 (7) (2001) 1471–1482.
[227] I.H. El-Sayed, X. Huang, M.A. El-Sayed, Surface plasmon resonance scattering and absorption of anti-EGFR antibody conjugated gold nanoparticles in cancer diagnostics: applications in oral cancer, Nano Lett. 5 (5) (2005) 829–834.
[228] B. Wu, et al., Detection of C-reactive protein using nanoparticle-enhanced surface plasmon resonance using an aptamer-antibody sandwich assay, Chem. Commun. 52 (17) (2016) 3568–3571.
[229] R. Li, et al., Sensitive detection of carcinoembryonic antigen using surface plasmon resonance biosensor with gold nanoparticles signal amplification, Talanta 140 (2015) 143–149.
[230] Q. Wang, et al., Graphene oxide–gold nanoparticles hybrids-based surface plasmon resonance for sensitive detection of microRNA, Biosens. Bioelectron. 77 (2016) 1001–1007.
[231] J. Zhu, et al., Gold nanoparticles deposited polyaniline–TiO_2 nanotube for surface plasmon resonance enhanced photoelectrochemical biosensing, ACS Appl. Mater. Interfaces 8 (1) (2016) 341–349.
[232] A.T. Reiner, et al., Magnetic nanoparticle-enhanced surface plasmon resonance biosensor for extracellular vesicle analysis, Analyst 142 (20) (2017) 3913–3921.
[233] C. Srichan, et al., Highly-sensitive surface-enhanced raman spectroscopy (SERS)-based chemical sensor using 3D graphene foam decorated with silver nanoparticles as SERS substrate, Sci. Rep. 6 (2016) 23733.
[234] W. Zhou, B.-C. Yin, B.-C. Ye, Highly sensitive surface-enhanced Raman scattering detection of hexavalent chromium based on hollow sea urchin-like TiO2@Ag nanoparticle substrate, Biosens. Bioelectron. 87 (2017) 187–194.
[235] S. Xu, et al., Graphene/Cu nanoparticle hybrids fabricated by chemical vapor deposition as surface-enhanced Raman scattering substrate for label-free detection of adenosine, ACS Appl. Mater. Interfaces 7 (20) (2015) 10977–10987.
[236] Y. Guo, et al., Fabrication of Ag–Cu_2O/reduced graphene oxide nanocomposites as surface-enhanced raman scattering substrates for in situ monitoring of peroxidase-like catalytic reaction and biosensing, ACS Appl. Mater. Interfaces 9 (22) (2017) 19074–19081.
[237] T. Kamra, et al., Photoconjugation of molecularly imprinted polymer nanoparticles for surface-enhanced Raman detection of propranolol, ACS Appl. Mater. Interfaces 7 (49) (2015) 27479–27485.
[238] Q. Jin, et al., Reduced graphene oxide nanohybrid–assembled microneedles as mini-invasive electrodes for real-time transdermal biosensing, Small 15 (6) (2019) 1804298.
[239] C. Hegarty, et al., Microneedle array sensors based on carbon nanoparticle composites: interfacial chemistry and electroanalytical properties, J. Mater. Sci. 54 (15) (2019) 10705–10714.

[240] J.S. Narayanan, G. Slaughter, AuNPs-HRP microneedle biosensor for ultrasensitive detection of hydrogen peroxide for organ preservation, Med. Devices Sens. 1 (2) (2018) e10015.
[241] M. Wang, L. Hu, C. Xu, Recent advances in the design of polymeric microneedles for transdermal drug delivery and biosensing, Lab Chip 17 (8) (2017) 1373–1387.
[242] P. Bollella, et al., Microneedle-based biosensor for minimally-invasive lactate detection, Biosens. Bioelectron. 123 (2019) 152–159.
[243] J. Gao, et al., Simultaneous detection of glucose, uric acid and cholesterol using flexible microneedle electrode array-based biosensor and multi-channel portable electrochemical analyzer, Sens. Actuators B Chem. 287 (2019) 102–110.
[244] A. Ahmadivand, et al., Extreme sensitive metasensor for targeted biomarkers identification using colloidal nanoparticles-integrated plasmonic unit cells, Biomed. Opt. Expr. 9 (2) (2018) 373–386.
[245] W. Xu, et al., Gold nanoparticle-based terahertz metamaterial sensors: mechanisms and applications, ACS Photonics 3 (12) (2016) 2308–2314.
[246] M. Ney, I. Abdulhalim, Ultrahigh polarimetric image contrast enhancement for skin cancer diagnosis using InN plasmonic nanoparticles in the terahertz range, J. Biomed. Opt. 20 (12) (2015) 125007.
[247] S. Zhang, G. Wright, Y. Yang, Materials and techniques for electrochemical biosensor design and construction, Biosens. Bioelectron. 15 (5) (2000) 273–282.
[248] J. Schliemann, J.C. Egues, D. Loss, Nonballistic spin-field-effect transistor, Phys. Rev. Lett. 90 (14) (2003) 146801.
[249] C.-S. Lee, S. Kim, M. Kim, Ion-sensitive field-effect transistor for biological sensing, Sensors 9 (9) (2009) 7111–7131.
[250] T.-T. Tran, A. Mulchandani, Carbon nanotubes and graphene nano field-effect transistor-based biosensors, TrAC Trends Anal. Chem. 79 (2016) 222–232.
[251] N. Gupta, Biosensors technologies: acousto-optic tunable filter-based hyperspectral and polarization imagers for fluorescence and spectroscopic imaging, in: Biosensors and Biodetection, Springer, 2009, pp. 293–305.
[252] K.C. Honeychurch, 13 – Printed thick-film biosensors, in: M. Prudenziati, J. Hormadaly (Eds.), Printed Films, Woodhead Publishing, 2012, pp. 366–409.
[253] B. Wang, et al., Label-free electrochemical impedance peptide-based biosensor for the detection of cardiac troponin I incorporating gold nanoparticles modified carbon electrode, J. Electroanal. Chem. 781 (2016) 212–217.
[254] A.A. Ensafi, E. Khoddami, B. Rezaei, Aptamer@Au-o-phenylenediamine modified pencil graphite electrode: a new selective electrochemical impedance biosensor for the determination of insulin, Colloids Surf. B: Biointerfaces 159 (2017) 47–53.
[255] S. Feng, et al., Development of molecularly imprinted polymers-surface-enhanced Raman spectroscopy/colorimetric dual sensor for determination of chlorpyrifos in apple juice, Sens. Actuators B Chem. 241 (2017) 750–757.
[256] L. Wang, et al., 2D nanomaterials based electrochemical biosensors for cancer diagnosis, Biosens. Bioelectron. 89 (2017) 136–151.
[257] F. Peng, et al., Silicon nanomaterials platform for bioimaging, biosensing, and cancer therapy, Acc. Chem. Res. 47 (2) (2014) 612–623.
[258] B. Jin, et al., Multi-nanomaterial electrochemical biosensor based on label-free graphene for detecting cancer biomarkers, Biosens. Bioelectron. 55 (2014) 464–469.
[259] R. Malhotra, et al., Ultrasensitive electrochemical immunosensor for oral cancer biomarker IL-6 using carbon nanotube forest electrodes and multilabel amplification, Anal. Chem. 82 (8) (2010) 3118–3123.
[260] R. Ovádeková, et al., Nanostructured electrochemical DNA biosensors for detection of the effect of berberine on DNA from cancer cells, Anal. Bioanal. Chem. 386 (7) (2006) 2055–2062.
[261] W. Lu, et al., Multifunctional oval-shaped gold-nanoparticle-based selective detection of breast cancer cells using simple colorimetric and highly sensitive two-photon scattering assay, ACS Nano 4 (3) (2010) 1739–1749.

[262] R. Viswambari Devi, M. Doble, R.S. Verma, Nanomaterials for early detection of cancer biomarker with special emphasis on gold nanoparticles in immunoassays/sensors, Biosens. Bioelectron. 68 (2015) 688–698.
[263] T. Mavrič, et al., Chapter Three: Electrochemical biosensor based on TiO_2 nanomaterials for cancer diagnostics, in: A. Iglič, M. Rappolt, A.J. García-Sáez (Eds.), Advances in Biomembranes and Lipid Self-Assembly, Academic Press, 2018, pp. 63–105.
[264] L. Xiao, et al., Colorimetric biosensor for detection of cancer biomarker by Au nanoparticle-decorated Bi2Se3 Nanosheets, ACS Appl. Mater. Interfaces 9 (8) (2017) 6931–6940.
[265] M.A. Ali, et al., Microfluidic immuno-biochip for detection of breast cancer biomarkers using hierarchical composite of porous graphene and titanium dioxide nanofibers, ACS Appl. Mater. Interfaces 8 (32) (2016) 20570–20582.
[266] H. Kazerooni, B. Nassernejad, A novel biosensor nanomaterial for the ultraselective and ultrasensitive electrochemical diagnosis of the breast cancer-related BRCA1 gene, Anal. Methods 8 (15) (2016) 3069–3074.
[267] J.-L. Liu, et al., Ternary electrochemiluminescence system based on rubrene microrods as luminophore and Pt nanomaterials as coreaction accelerator for ultrasensitive detection of MicroRNA from cancer cells, Anal. Chem. 89 (17) (2017) 9108–9115.
[268] F.J. Rawson, et al., Electron transfer from Proteus vulgaris to a covalently assembled, single walled carbon nanotube electrode functionalised with osmium bipyridine complex: application to a whole cell biosensor, Biosens. Bioelectron. 26 (5) (2011) 2383–2389.
[269] H. Chen, et al., Mechanically strong, electrically conductive, and biocompatible graphene paper, Adv. Mater. 20 (18) (2008) 3557–3561.
[270] I. Vostiar, E.E. Ferapontova, L. Gorton, Electrical "wiring" of viable *Gluconobacter oxydans* cells with a flexible osmium-redox polyelectrolyte, Electrochem. Commun. 6 (7) (2004) 621–626.
[271] S.-K. Kim, H.-D. Kwen, S.-H. Choi, Fabrication of a microbial biosensor based on QD-MWNT supports by a one-step radiation reaction and detection of phenolic compounds in red wines, Sensors 11 (2) (2011) 2001–2012.
[272] J. Šefčovičová, J. Tkac, Application of nanomaterials in microbial-cell biosensor constructions, Chem. Pap. 69 (1) (2015) 42–53.
[273] L. Sutarlie, S.Y. Ow, X. Su, Nanomaterials-based biosensors for detection of microorganisms and microbial toxins, Biotechnol. J. 12 (4) (2017), https://doi.org/10.1002/biot.201500459.
[274] G.S. Geleta, Z. Zhao, Z. Wang, Electrochemical biosensors for detecting microbial toxins by graphene-based nanocomposites, J. Anal. Test. 2 (1) (2018) 20–25.
[275] A.J. Lakade, K. Sundar, P.H. Shetty, Nanomaterial-based sensor for the detection of milk spoilage, LWT 75 (2017) 702–709.
[276] B. Stephen Inbaraj, B.H. Chen, Nanomaterial-based sensors for detection of foodborne bacterial pathogens and toxins as well as pork adulteration in meat products, J. Food Drug Anal. 24 (1) (2016) 15–28.
[277] M. David, et al., Acidic and basic functionalized carbon nanomaterials as electrical bridges in enzyme loaded chitosan/poly(styrene sulfonate) self-assembled layer-by-layer glucose biosensors, Electroanalysis 27 (9) (2015) 2139–2149.
[278] Y. Qin, et al., Integration of microfluidic injection analysis with carbon nanomaterials/gold nanowire arrays-based biosensors for glucose detection, Sci. Bull. 61 (6) (2016) 473–480.
[279] L. Fang, et al., Direct electrochemistry of glucose oxidase immobilized on Au nanoparticles-functionalized 3D hierarchically ZnO nanostructures and its application to bioelectrochemical glucose sensor, Sens. Actuators B Chem. 222 (2016) 1096–1102.
[280] J. Hovancová, et al., Nanomaterial-based electrochemical sensors for detection of glucose and insulin, J. Solid State Electrochem. 21 (8) (2017) 2147–2166.
[281] H. Ma, et al., Sensitive insulin detection based on electrogenerated chemiluminescence resonance energy transfer between Ru(bpy)32+ and Au nanoparticle-doped β-cyclodextrin-Pb (II) metal–organic framework, ACS Appl. Mater. Interfaces 8 (16) (2016) 10121–10127.
[282] A.K. Yagati, et al., Silver nanoflower–reduced graphene oxide composite based micro-disk electrode for insulin detection in serum, Biosens. Bioelectron. 80 (2016) 307–314.

[283] M.L. Yola, N. Atar, Development of cardiac troponin-I biosensor based on boron nitride quantum dots including molecularly imprinted polymer, Biosens. Bioelectron. 126 (2019) 418–424.
[284] P. Supraja, et al., Label free electrochemical detection of cardiac biomarker troponin T using $ZnSnO_3$ perovskite nanomaterials, Anal. Methods 11 (6) (2019) 744–751.
[285] N.R. Shanmugam, et al., Electrochemical nanostructured ZnO biosensor for ultrasensitive detection of cardiac troponin-T, Nanomedicine 11 (11) (2016) 1345–1358.
[286] L. Wu, et al., Label-free ratiometric electrochemical detection of the mutated apolipoprotein E gene associated with Alzheimer's disease, Chem. Commun. 52 (81) (2016) 12080–12083.
[287] M. Azimzadeh, et al., Early detection of Alzheimer's disease using a biosensor based on electrochemically-reduced graphene oxide and gold nanowires for the quantification of serum microRNA-137, RSC Adv. 7 (88) (2017) 55709–55719.
[288] S. Mohammadi, M. Nikkhah, S. Hosseinkhani, Investigation of the effects of carbon-based nanomaterials on A53T alpha-synuclein aggregation using a whole-cell recombinant biosensor, Int. J. Nanomedicine 12 (2017) 8831.
[289] A. Geldert, et al., Highly sensitive and selective aptamer-based fluorescence detection of a malarial biomarker using single-layer MoS2 nanosheets, ACS Sensors 1 (11) (2016) 1315–1321.
[290] J.I.A. Rashid, et al., A novel disposable biosensor based on SiNWs/AuNPs modified-screen printed electrode for dengue virus DNA oligomer detection, IEEE Sensors J. 15 (8) (2015) 4420–4427.
[291] A. Narmani, et al., Highly sensitive and accurate detection of Vibrio cholera O1 OmpW gene by fluorescence DNA biosensor based on gold and magnetic nanoparticles, Process Biochem. 65 (2018) 46–54.
[292] S. Afsahi, et al., Novel graphene-based biosensor for early detection of Zika virus infection, Biosens. Bioelectron. 100 (2018) 85–88.
[293] P.K. Pathania, et al., Aptamer functionalized MoS2-rGO nanocomposite based biosensor for the detection of Vi antigen, Biosens. Bioelectron. 122 (2018) 121–126.
[294] J.S. Daniels, N. Pourmand, Label-free impedance biosensors: opportunities and challenges, Electroanalysis 19 (12) (2007) 1239–1257.
[295] J. Wang, Electrochemical biosensors: Towards point-of-care cancer diagnostics, Biosens. Bioelectron. 21 (10) (2006) 1887–1892.
[296] M.C. Estevez, et al., Trends and challenges of refractometric nanoplasmonic biosensors: a review, Anal. Chim. Acta 806 (2014) 55–73.
[297] S.N. Topkaya, M. Azimzadeh, M. Ozsoz, Electrochemical biosensors for cancer biomarkers detection: recent advances and challenges, Electroanalysis 28 (7) (2016) 1402–1419.
[298] S. Balasubramaniam, J. Kangasharju, Realizing the Internet of nano things: challenges, solutions, and applications, Computer 46 (2) (2013) 62–68.
[299] Z. Farka, et al., Nanoparticle-based immunochemical biosensors and assays: recent advances and challenges, Chem. Rev. 117 (15) (2017) 9973–10042.
[300] J.-H. Choi, J. Lee, B.-K. Oh, Nanomaterial-based in vitro analytical system for diagnosis and therapy in microfluidic device, Biochip journal 10 (4) (2016) 331–345.
[301] C. Wang, et al., Ultrarobust biochips with metal–organic framework coating for point-of-care diagnosis, ACS Sens. 3 (2) (2018) 342–351.
[302] M.T. Nistor, A.G. Rusu, Nanorobots with applications in medicine, in: Polymeric Nanomaterials in Nanotherapeutics, Elsevier, 2019, pp. 123–149.
[303] W.A.D.M. Jayathilaka, et al., Significance of nanomaterials in wearables: a review on wearable actuators and sensors, Adv. Mater. 31 (7) (2019) 1805921.
[304] H. Liu, et al., Clinical translation of nanomaterials, in: Theranostic Bionanomaterials, Elsevier, 2019, pp. 75–111.
[305] K. Scholten, E. Meng, A review of implantable biosensors for closed-loop glucose control and other drug delivery applications, Int. J. Pharm. 544 (2) (2018) 319–334.
[306] X. Zhang, Bio-Inorganic Interfaces for Cellular Signal Detection and Tissue Engineering, University of California, Riverside, 2005.

[307] H.-J. Lee, J.-G. Yook, Graphene nanomaterials-based radio-frequency/microwave biosensors for biomaterials detection, Materials 12 (6) (2019) 952.
[308] N. Cheng, et al., Nanozyme-mediated dual immunoassay integrated with smartphone for use in simultaneous detection of pathogens, ACS Appl. Mater. Interfaces 9 (46) (2017) 40671–40680.
[309] K. Guk, et al., Evolution of wearable devices with real-time disease monitoring for personalized healthcare, Nanomaterials 9 (6) (2019) 813.
[310] P. Chandra, E. Segal, Nanobiosensors for Personalized and Onsite Biomedical Diagnosis, The Institution of Engineering and Technology, 2016.
[311] R. Villanueva, D. Ganta, D.A. Molina, Micro/nanorobotics: propulsion and biosensors, J. Bionanosci. 11 (6) (2017) 461–469.
[312] S. Shrivastava, et al., A review on theranostics: an approach to targeted diagnosis and therapy, Asian J. Pharm. Res. Dev. 7 (2) (2019) 63–69.
[313] M. Sepehri, K.H. Carlsen, J. Serup, Papulo-nodular reactions in black tattoos as markers of sarcoidosis: study of 92 tattoo reactions from a hospital material, Dermatology 232 (6) (2016) 679–686.
[314] A. Ankhili, et al., Comparative study on conductive knitted fabric electrodes for long-term electrocardiography monitoring: silver-plated and PEDOT: PSS coated fabrics, Sensors 18 (11) (2018) 3890.
[315] O. Hosu, et al., Minireview: smart tattoo, microneedle, point-of-care, and phone-based biosensors for medical screening, diagnosis, and monitoring, Anal. Lett. 52 (1) (2019) 78–92.
[316] M. Haque, Nano fabrics in the 21st century: a review, Asian J. Nanosci. Mater. 2 (2) (2019) 120–256. 131-148.
[317] D. Meetoo, L. Wong, B. Ochieng, Smart tattoo: technology for monitoring blood glucose in the future, Br. J. Nurs. 28 (2) (2019) 110–115.

CHAPTER 9

Nanomaterial-based gas sensor for environmental science and technology

Gulzar Ahmad[a], Ahmed Nawaz[a], Somia Nawaz[a], Naveed Akhtar Shad[b], M. Munir Sajid[b], Yasir Javed[a]

[a]*Department of Physics, University of Agriculture, Faisalabad, Pakistan*
[b]*Department of Physics, Government College University, Faisalabad, Pakistan*

9.1 Introduction

Nanostructures are considered the backbone of nanotechnology due to their extraordinary electrical, optical, and magnetic properties. Low-dimensional nanoparticles can be used in the fabrication of gas sensors, nanothermometers, solar cells, fuel cells, and much more. Nanostructures have enhanced properties due to their large surface-to-volume ratio and the emergence of quantum effects at this small scale [1]. One of the major problems of the 21st century is the need for a cleaner and better environment for living. With industrial progress, many factors have degraded environmental quality by releasing different gaseous species during manufacturing processes and by combustion of fossil fuels. The presence of these gases above certain concentrations can harm human as well as plant life [2].

Several hazardous gases, for example ethanol, benzene, toluene, CO, H_2, NO, H_2S, NH_3, and CO_2, are routinely released through various industrial processes including combustion, distillation, and the Haber process [3]. Among these gases, some exhibit dramatic behavior: for example, during exposure methane and hydrogen are highly explosive, and toluene is toxic to the environment as well as to humans when its concentration is increased [4]. As a result, there is an urgent need for gas sensors with outstanding features such as fast response time, high sensitivity, high monitoring capabilities, and good selectivity. Therefore, resistive, electrochemical, and ultrasonic gas sensors have been successfully developed for this purpose. Several quantitate techniques, including gas chromatography (separate species via analytical columns), mass spectrometry (identify molecules), chemical vapor deposition (CVD) (controls significant features), spray pyrolysis (contains heated chemical reaction), and

Nanofabrication for Smart Nanosensor Applications. https://doi.org/10.1016/B978-0-12-820702-4.00010-6
© 2020 Elsevier Inc. All rights reserved.

Fourier transform infrared (FTIR) spectroscopy (uses IR characteristics), are being used for the investigation of absorbed species as well as gas sensing [5].

In the last few years, researchers have been very interested in the development of gas sensing devices with small dimensions, having numerous field and practical applications. Therefore, the scientific community has taken steps to find favorable materials to use as sensing elements in these sensing devices, with promising bulk and surface characteristics such as rapid recovery time, high selectivity, and environmental safety. As a consequence, this new sensor technology is widely used due to its beneficial impacts in improving the quality of the product, energy efficiency, and emission reductions. In pellet form, thin gas sensors have been used as detectors due to low power consumption during operation as well as their rugged surface and low cost [6].

Different types of gas sensors have been used for the various purposes of good selectivity, fast response, low limit detection, high sensitivity, and real-time and in-situ monitoring. For the fabrication of resistive gas sensors, organic semiconductors, carbon materials, and semiconducting metal oxide nanostructures are mainly used. Metal oxides generally have better stability and reversibility, fast recovery speed, and are cost effective as compared to organic semiconductors and carbon materials [7]. N-type metal oxides based on ln_2O_3, Fe_2O_3[80], $^{199}CeO_2$[86], and ZnO have been used for the detection of H_2S gas. The prominent feature of H_2S molecules is their quick decomposition, as a reaction occurs between H_2S molecules and chemisorbed oxygen species on the sensing material surface due to small bonding energy between S—H—S. Doping of gold nanoparticles with TiO_2 thin films has applications for conductometric and optical sensors, to detect H_2 and CO. These sensing capabilities are reproducible and reversible [8]. In this chapter, we discuss different sensor types, materials for sensors, fabrication processes, and the operational principles of different gas sensors.

9.2 Types of sensors

There are three major types of sensors, as discussed in the following paragraphs.

9.2.1 Gas sensor

The properties of stimulated reaction for different gases, such as H_2, H_2O, CO, NO_2, O_2 and CO_2, have made gas sensors more useful for detection in the environment and at different exposure points [9]. While oxygen sensors can be widely used for applications in hospital incubators and mines to identify the presence of oxygen, these sensors can also be applied for controlling the combustion process in furnaces and in various development fields as an analytical instrument [10,11]. Another outstanding application of gas sensor technology is environmental pollution monitoring [12]. The performance of chemical gas sensors, such as their time response, selectivity, sensitivity, reversibility, reproducibility, stability, and durability, is greatly affected by the material properties [13]. Typically, three parameters are used to characterize a sensor: response time, selectivity, and sensitivity of the working

sensor. The response time indicates the relative change with gas concentration and maximum change in the signal, whereas selectivity is the ability of sensing a specific gas free from interference, and sensitivity is the capability of a sensor to measure the gas quantitatively, which is tested under stated conditions. These important parameters are highly influenced by the chemical and physical properties of the sensor material [14–17].

9.2.2 Biosensors

In research fields, biosensors are a well-funded area related to nanosensors [18]. This is due to the potential applications of these sensors for detection of diseases [19], infected cells [20], DNA, pathogens, and enzymes [21]. Nanobiosensors can use different means of detection, such as pH or temperature, and can be reusable [22]. In this set-up, physical changes occur, which can be electrochemical, electrical, piezoelectric, calorimetric, or optical, resulting in a change in chemical composition, electrical distribution, electric charge, heat, or intensity of light, respectively [23].

Biosensors can also be implemented for detection of glucose level, which affects many people worldwide. The first biosensor was established on the principle of enzyme glucose oxidase (GOX) [24]. Current enzyme sensors are based on nanoscale semiconductors, in which the mesoporous surface of an electrode is covered with semiconductor or metallic nanoparticles [25]. This set-up allows electrons to transfer directly between enzyme and electrode, trapped between the pores. In biosensors, the main components consist of a physiochemical transducer, a biological element, and a detector. Target molecules are bound through the biological element, which must be stable in different storage conditions, highly specific, and immobilized. Examples of typical biological elements are enzymes, antibodies, tissues, and microorganisms. A physiochemical transducer is used for measuring the interface: for example, the physical change appearing at the bioreceptor during the reaction. This physiochemical transducer converts the energy into an electrical output up to a measurable range. The final detector gains a signal through the transducer, which is then passed through a microprocessor. At this stage, the signals are analyzed and amplified. The data obtained are then transformed into measurable units and moved to a data storage or display device [26].

9.2.3 Chemical sensor

A chemical sensor is defined as a self-contained device that can provide analytical information in real time about the chemical species present in the environment [27]. A chemical sensor executes two functions, transduction and recognition. Initially the analyte interacts with the recognition element in a selective way. The sensing element consists of recognition receptors that are distinct molecular units [28]. Biosensors are in actuality chemical sensors whose recognition system follows a biological or biochemical mechanism [29]. The interaction of analyte and sensing element results in a certain variation in chemical or physical

properties with analyte concentration [30]. In order to achieve this variation, these changes convert into a measurable quantity through a chemical sensor. This process is known as signaling or signal transduction [31]. The transducer and sensing element are distinct components that are packed together and have the same units. In some chemical sensors, there is no physical distinction between the transducer and the sensing element [27].

The first type of chemical sensor was an ion sensor, which was used and developed on a large scale [32]. The most extensively used ion sensor was a pH glass electrode. Klemensiewicz and Haber developed this type of sensor in 1908 and it was commercially available in 1936 together with the Beckman pH meter [33]. One of the distinctive features of the ion sensor is the electric charge, which is useful for ion recognition. Thus the ion recognition process can be achieved by different reagents and materials, which have opposite analyte ion and electric charge. The selectivity in the process of electrostatic ion recognition appears due to additional characteristics of the sensing material, for example, analyte peculiarity or ionic receptor size [34].

The affinity interaction is associated with the reversible multiple chemical binding of two species due to noncovalent bonds, such as hydrogen bonds, van der Waal interactions, and ionic bonds [35]. A complex molecular association is produced as a result of the affinity interaction. However, in order to form such a complex, the species used must be compatible with respect to chemical reactivity and shape [36]. For instance, if one specie has a hydrogen atom with positive polarization, the other must show a donor electron atom placed in such a manner that hydrogen bond formation in the complex becomes possible [37]. In the affinity interaction, a common type is defined with the antibody-antigen interaction. In actual antibodies, glycoproteins are produced by the immune system for neutralization and identification of pathogen microorganisms like viruses and bacteria. The specific part of a pathogen that is interrelated with specific bodies is known as an antigen [38]. Fig. 9.1 shows the operation of ZnO-based chemical sensors for different concentrations of phenyl hydrazine [39].

9.3 Materials used in nanosensors

There are several types of inorganic nanomaterials employed as sensors. Semiconductor nanomaterials have shown promise in this regard. However, optical materials can also be used. Here, we review properties of different inorganic nanomaterials having potential as gas sensors.

9.3.1 Metal sulfides

9.3.1.1 Zinc sulfide

In the last few decades, the II-VI semiconductor NPs have attained importance due to their size-dependent and tunable electroluminescence characteristics [40]. Among the II-VI semiconductors family, ZnS is a foremost candidate due to its wide direct bandgap. ZnS is an

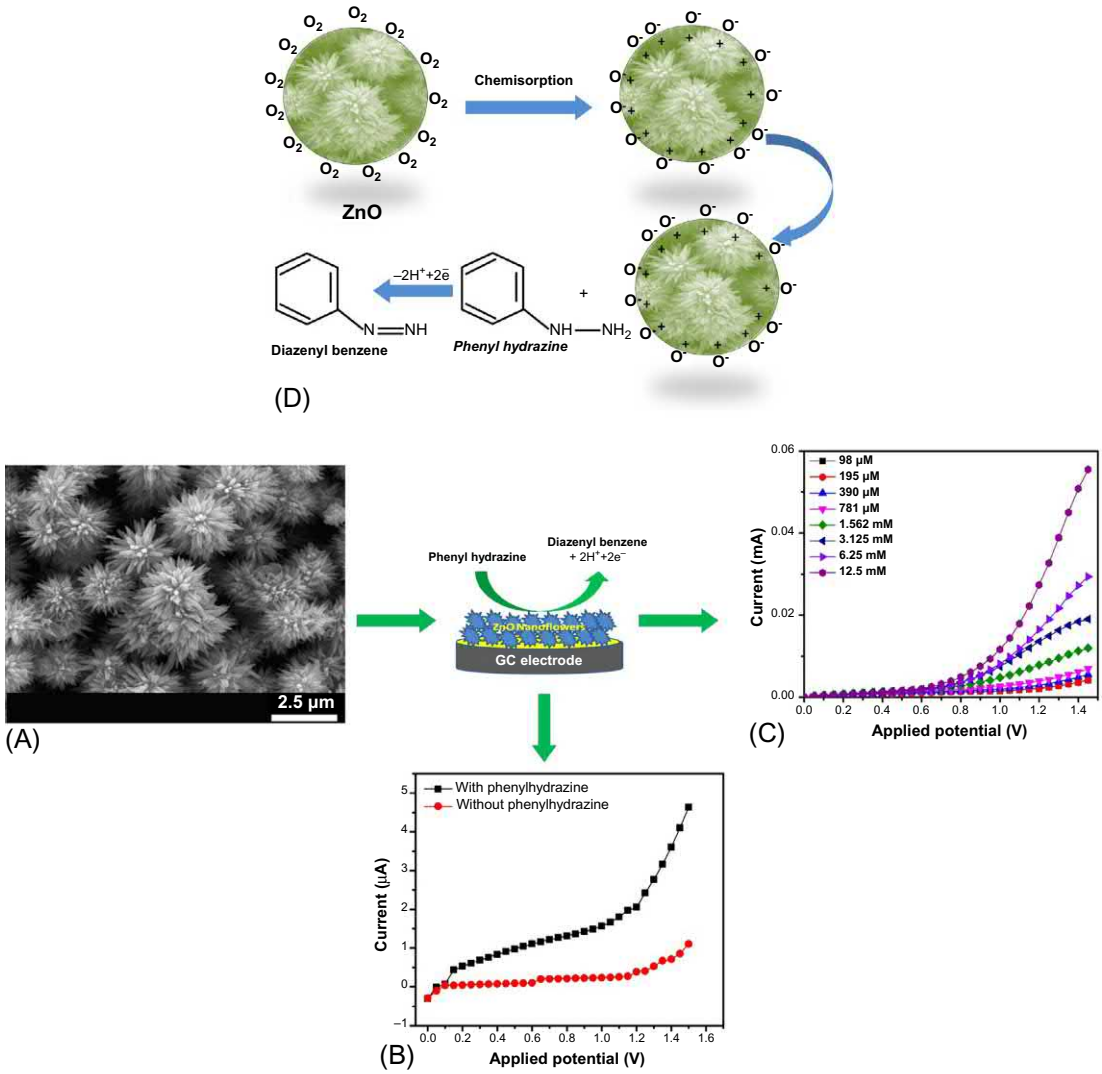

Fig. 9.1

(A) SEM image of ZnO nano-urchins as chemical sensor; (B) Current-voltage measurements in the presence and absence of phenyl hydrazine in phosphate-buffered saline solution; (C) Detection of different concentrations of phenyl hydrazine by nanomaterials; (D) Schematic working representation of ZnO-based chemical sensor. *Reproduced with permission from A. Umar, et al., Enhanced photocatalytic degradation of harmful dye and phenyl hydrazine chemical sensing using ZnO nanourchins, Chem. Eng. J. 262 (2015) 588–596.*

inorganic compound, a favorable host material, transparent, chemically stable, and technologically superior as compared to (ZnSe), an alternative chalcogenide [41]. At nanoscale, ZnS possesses exceptional chemical and physical characteristics, for example, chemical activity, low melting point, increase in optical absorption, thermal resistance, increase in surface-to-volume ratio, and quantum size effect, as compared to bulk ZnS NPs. ZnS semiconductors have attracted growing interest due to their versatile and promising potential applications in solid-state devices, biosensors, and gas sensors [42,43].

Zinc sulfide is a polymorphous material existing in two crystalline structures, namely a cubic phase (zinc blende) with the F-43 m space group and a hexagonal phase (wurtzite) structure with the P63mc space group. The growth mechanism of these crystalline structures depends upon the synthesis techniques. The cubic (zinc blende) structure has four asymmetric units and the hexagonal (wurtzite) structure has two asymmetric units in their unit cells. The neighbor coordination in both cubic and hexagonal structures are similar; however, the angles and distances are quite different. The atomic layer stacking sequence in ZnS is different for the two structure types. The transformation of the cubic structure into the hexagonal structure is achieved at 1020°C. The stoichiometry between zinc and sulfide is the same (1:1). The bond length in Zn—S is about 2.36 Å. The unit cell volume and cell dimensions (a, z) in the cubic phase are 40.476 $Å^3$, and a = 5.41 Å, z = 4, respectively [44,45].

Its attractive luminescent property makes ZnS an interesting semiconductor material. The ZnS wurtzite structure is effective in the ultraviolet region due to its fundamental wide bandgap (3.50 eV) [46]. ZnS semiconductor nanomaterials are widely used for the investigation of photoelectric and luminescent as well as light-based ultraviolet and visible devices at room temperature. The refractive index of ZnS is 2.3677 [47].

9.3.1.2 Cadmium sulfide

In the last few decades, researchers have been very interested in cadmium sulfide NPs due to their size-dependent characteristics. Cadmium sulfide has potential applications in different fields such as optical filters, solar cells, gas sensors, thin-film transistors, and photodetectors due to its cost effectiveness [48].

The semiconducting cadmium sulfide NPs exist in two crystalline structures: a cubic phase (zinc blende) and a hexagonal phase (wurtzite) structure, or a mixture of these two phases. The crystalline structure of CdS NPs is highly dependent upon synthesis techniques as well as on the growth mechanism. Bulk CdS exhibits a highly stable hexagonal phase (wurtzite) structure within the P63mc space group at room temperature, having a melting point of 1600°C. The difference in Cd—S bond lengths is between 2.57 Å to 2.58 Å. The axial ratio (a:c) unit cell volume and cell dimensions (a, c, z) in the hexagonal phase are 1:1.623, 99.45 $Å^3$ and 4.136 Å, 6.713 Å, 4, respectively. The CdS cubic structure is metastable and belongs to the F43m space group. The transformation of the cubic structure into the stable hexagonal structure is achieved via annealing the nanostructure. Nevertheless, the hexagonal structure can also be transformed into the cubic structure by increasing the pressure. The cell dimensions and unit cell volume in the cubic structure are a = 5.832 Å, z = 4, and 196.93 $Å^3$ [49,50].

We know that the properties and performance of optical, electronic, and optoelectronic devices are highly influenced through bandgap energy, surface states, and refractive index of the material. In semiconducting materials, the bandgap and refractive index explain the absorption

threshold of the photon and the transparency of the material to incident radiation, respectively. Considering these aspects, CdS nanomaterials show high transmittance in the visible region. The wide bandgap (2.42 eV) of CdS nanomaterials can be decreased by increasing Cd ion concentration as well as by increasing temperature. The other way to enhance the optical and electrical properties of CdS nanomaterials is by doping or codoping with different materials; for example, CdS can be doped with iron (Fe) [51], copper (Cu) [52], manganese (Mn) [53] or codoped with cobalt and manganese (Co, Mn) [54]. The other advantage of doping is to bring about a successful change in the semiconducting nature of CdS: for example, undoped cadmium sulfide is an n-type while doped cadmium sulfide is a p-type semiconductor material. The CdS wurtzite structure is effective in the UV-visible region due to its fundamental wide bandgap (2.5 eV at 300 K). The hexagonal (wurtzite) CdS structure is optically anisotropic [55].

9.3.1.3 Lead sulfide

Lead sulfide (PbS) is an important material from the IV–VI semiconductor group, due to its relatively small bandgap. For nanoscale structures, PbS exhibits good quantum confinement because of its large Bohr excitation radius. PbS nanomaterials have also exhibited unique characteristics such as high mobility and high value of dielectric constant, as compared to other semiconductors. These unique properties make lead sulfide an important material for applications in infrared sensors, photovoltaic cells, biosensors and gas sensors, IR detectors, and temperature sensors [56].

Lead sulfide is a polar semiconductor material existing in a cubic rock salt crystal structure with the Fm3m space group. The octahedral PbS_6 edge and corner-sharing structure are formed by combining Pb^{2+} atoms with six S^{2-} atoms. The bond length in Pb—S is about 3.00 Å. The unit cell volume (a) of the cubic phase PbS is 5.936 Å. However, lead sulfide exhibits an FCC real lattice [57].

The optical, structural, and electrical characteristics are highly influenced by varying stoichiometry of lead sulfide NPs. PbS is a p-type semiconductor and has a small tunable bandgap value between 0.41 and 2.3 eV. Due to the narrow direct bandgap, PbS is widely utilized to obtain selective sensors, detectors, and sensitive temperature transducers. By increasing the temperature, the percentage of optical transmittance is relatively decreased. The value of the absorption coefficient is high from the visible to infrared region. The bulk PbS exhibits n-type or p-type behavior. The behavior of PbS strongly depends upon the stoichiometry of the lead ion: for example, deficiency of Pb ion makes bulk PbS p-type while an excess makes PbS n-type. Typically, in the visible region, the transmittance is low for undoped lead sulfide; however, this can be increased by increasing the doping concentration of various materials [58,59].

9.3.2 Metal oxides

The most studied semiconductor materials for gas sensors are metal oxides. There are many metal oxides that present a good response for gases, but here we discuss the most important metal oxide nanomaterials.

9.3.2.1 Aluminum oxide

Among the boron group, Al (aluminum) is a ductile metal, silvery-white, with nonmagnetic behavior. Al is treated ideally in passivation due to its low density. In aluminum's shell, the number of electrons is 2, 8, and 3. The electronic configuration of Al is [Ne] $3s^2$ $3p^1$. Corundum is one of the thermodynamically stable and common crystalline forms of Al_2O_3. Al_2O_3 belongs to the trigonal crystal structure with the R-3C space group. Alumina-based sensor devices, especially Al_2O_3, are excellent humidity-sensing materials and operate mainly in structures like a capacitor. These devices show high stability and mostly work at room temperature. When these devices are exposed, no chemical reaction takes place. Usually, alumina-based sensing devices are highly volume-effective devices [60]. The pores on Al_2O_3 films are regarded as a dielectric and by changing the humidity content in the micropores, conductivity can also be varied. The humidity balances the pore walls as well as penetrates/saturates via a top layer of the conductor sensing element [61]. Nevertheless, by varying the moisture content, the capacitive structure can be changed. At 45°C, oxygen, carbon dioxide, and hydrogen were detected with these Al_2O_3-based sensors [62]. As a consequence, Al_2O_3-based devices have shown exceptional quality with 1-min response time [63].

9.3.2.2 Cadmium oxide

Cadmium (Cd) is present in the earth's crust at approximately 0.1 ppm. Cadmium was first isolated and discovered in 1817 by Friedrich Stromeyer and Karl Samuel Leberecht. The atomic weight, radius, and van der Waal's radius of cadmium ions is about 112.411 g/mol, 151 pm, and 230 pm, respectively [64]. In cadmium's shell, the numbers of electrons are 2, 8, 18, 18, and 2. The electronic configuration of Cd is [Kr] $4d^{10}$ $5s^2$. Cadmium in its elemental form is silvery bluish gray. As a result of its unique color, Cd plays a key role in battery construction, specific pigments, and in coatings. Cd has +1 and +2 oxidation states, but in all its compounds, it usually is in the +2 oxidation state. CdO has a cubic structure belongs to the Fm-3 m space group. It serves as a base material for several scientific applications, such as photodiodes, IR detectors, photovoltaic cells, and transparent electrodes [65]. CdO nanomaterials have exhibited *n*-type semiconducting characteristics with direct and indirect bandgaps of 2.28 eV and 0.55 eV, respectively [66].

9.3.2.3 Copper oxide

Cu is a transition metal, a member of d-block. Among the other naturally occurring metals, Cu is one of the directly unstable metallic structures with +1 and +2 oxidation states at its normal chemistry. Copper (I) compounds are usually colorless, exhibiting diamagnetic behavior.

Researchers are very interested in cupric oxide (CuO) due to its numerous commercial applications. Its photochemical and photoconductive characteristics have made CuO a promising candidate for the fabrication of solar cells. From different copper oxide forms, CuO is suitable for gas-sensing materials. CuO exhibits a p-type semiconducting nature with 1.2 eV narrow bandgap, and a low value of electrical resistance. By decreasing the gaseous species, electrical conductivity can be decreased. CuO materials have a $3d_9$ electronic configuration and antiferromagnetic behavior with an 1.4 eV bandgap at the ground state. The bandgap is ideal for the determination of charge transfer origin [67,68].

9.3.2.4 Zinc oxide

Chemically, Zn is an active metal. Zn exhibits +2 or an exclusively divalent oxidation state. Several coordination compounds are formed through Zn metal. ZnO belongs to the hexagonal crystal structure with the P63m space group. Zinc oxide (ZnO) is an important material from II–VI semiconductors, due to the 60 eV binding energy and relatively wide 3.37 eV bandgap with point defects on their surfaces. Considering these aspects, ZnO has become a favorable resistive-type gas sensing candidate in sensing applications. By responding to adsorbed gases, ZnO can be used as a gas sensor at room temperature by changing the surface conductivity [69].

9.3.3 Other nanomaterials

9.3.3.1 Noble metal nanoparticles

In the last few decades, researchers have become very interested in noble metal NPs, especially gold and silver due to their fast reaction times as well as nonlinear optical characteristics. Gold and silver NPs can be produced by reduction of ($HAuCl_4$) chloroauric acid and silver nitrate, respectively [70]. The localized surface plasmon resonance spectrum can be controlled through the external environment along with the shape and size of the nanoparticles. This plasmon spectrum is used for the detection of molecules. These aspects make noble metal NPs (Au, Ag, Pt) a promising material for nanosensing [71] (Fig. 9.2).

9.3.3.2 Quantum dots (QDs)

QDs are defined as *small semiconductor crystals having a size range of a few nanometers*. The common elements used for the preparation of QDs are usually CdS and cadmium selenide (CdSe) [72]. The inert polymer coating is present on QDs to protect the human cells from toxic/harmful effects of Cd. This polymeric coating provides an easy route for the attachment of several other molecules for the detection of target species. The doping of QDs with atoms affects the conductivity as well as the emitted wavelength of QDs. QDs exhibit various optical characteristics due to their size, composition, and shape. Custom design QDs can be formed via controlling the size and composition. Fluorescence-based optical sensors are developed with semiconductor QDs. In the UV-vis spectrum, any fluorescence color can be obtained by adjusting the QD semiconductor size: for example, CdSe exhibits green fluorescence with

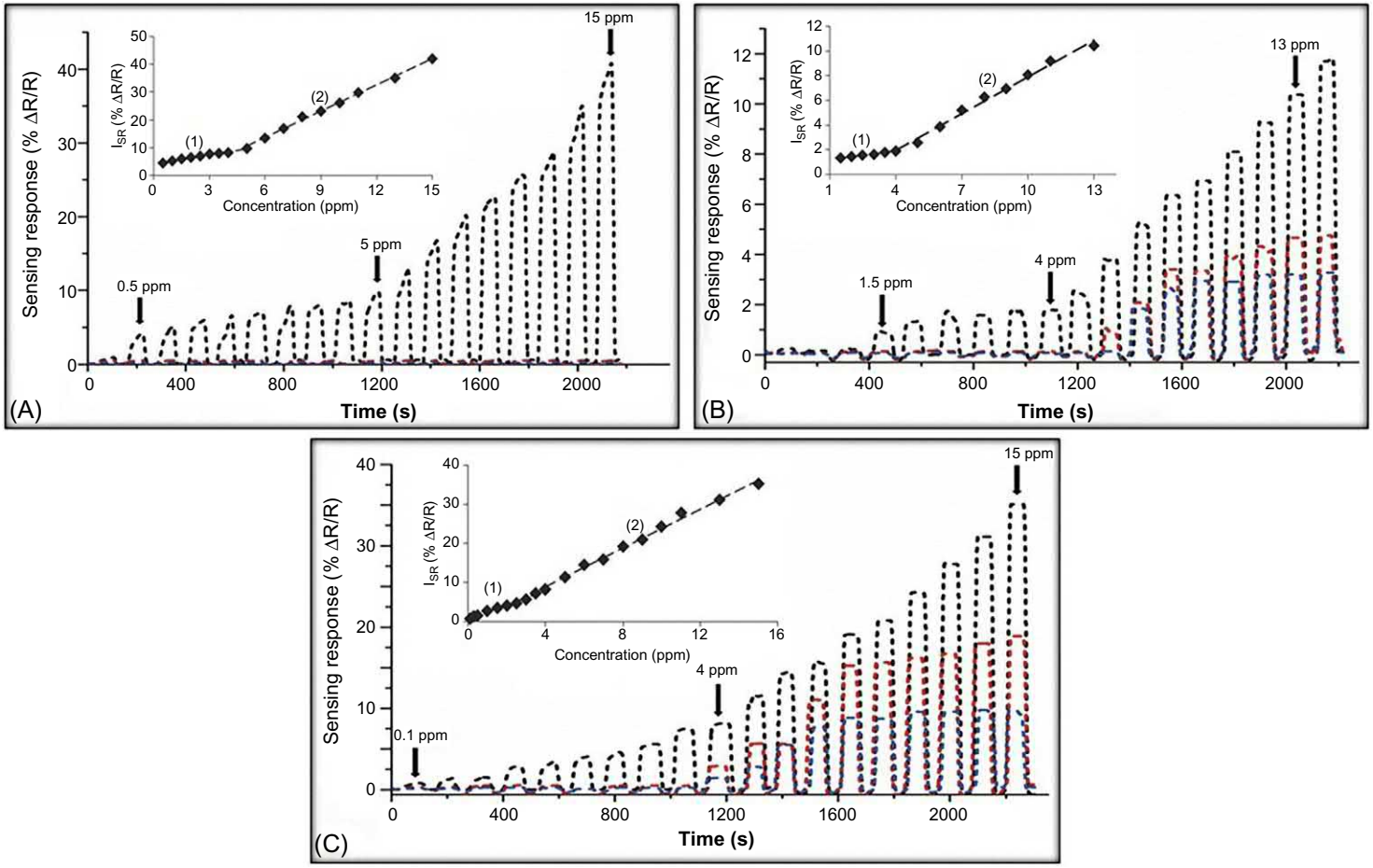

Fig. 9.2

Sensing properties of different noble metals-reduced graphene oxide composites. Gas response of different concentrations of NH3, H, and CO with (A) Ag-rGO, (B) Au-rGO, and (C) Pt-rGO (*Inset*: Calibration plots for NH_3 gas.) *Reprinted with permission from I. Karaduman et al., Room-temperature ammonia gas sensor based on reduced graphene oxide nanocomposites decorated by Ag, Au and Pt nanoparticles, J. Alloys Compd. 722 (2017) 569–578.*

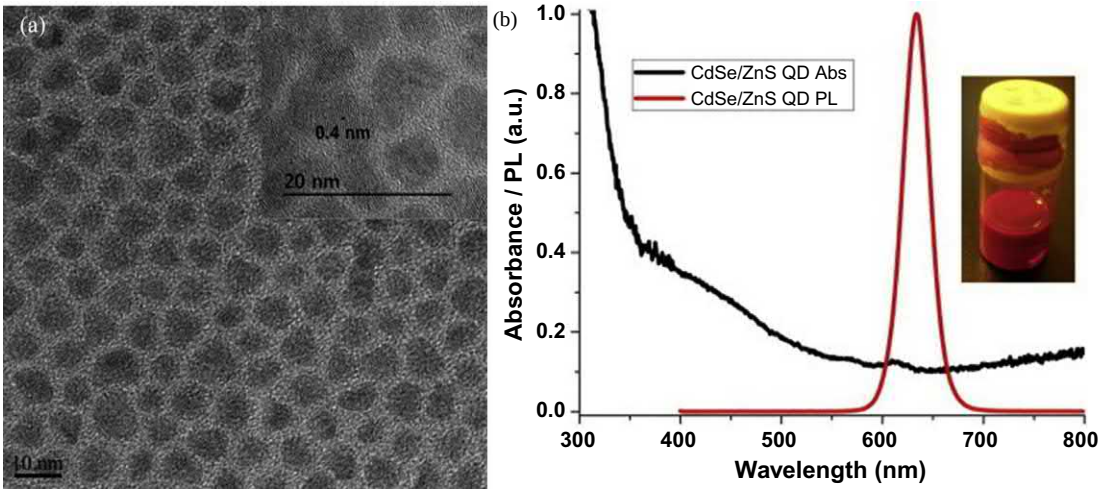

Fig. 9.3

(A) TEM image of CdSe/ZnS quantum dots; (B) UV-vis absorption and photoluminescence spectra of CdSe/ZnS quantum dots. *Reproduced with permission from M. Zubair, et al., Fabrication of CdSe/ZnS quantum dots thin film by electrohydrodynamics atomization technique for solution based flexible hybrid OLED application, Chem. Eng. J. 253 (2014) 325–331.*

a diameter of approximately 2.5 nm or red fluorescence at 7 nm, respectively. The absorption and photoluminescence spectrum of CdSe/ZnS composites are shown in Fig. 9.3 [73]. Forster resonance energy transfer explains the transfer of nonradiative energy from donor to the acceptor fluorophore. Due to this effect, QDs operate as sensors. The energy is successfully transferred between donor to acceptor fluorophore at the 2 to 8 nm range. The fluorescence rate gradually increases or decreases at donor and acceptor, due to the energy transfer [74].

9.3.3.3 Porous silicon

Porous silicon (PSi) is a form of silicon having tiny pores at its surface; it has outstanding applications in various fields, such as humidity sensors, sacrificial layers, gas sensors, and reference electrochemical electrodes. In addition, for chemical sensors, PSi can be used as a substrate [75] (Fig. 9.4). PSi contains a complicated Si thread network of 2–5 nm thickness, and a large (500 m^2/cm_3) surface-to-volume ratio. The emitted wavelength can also be controlled with the unique porosity of the material. The emission of longer or shorter wavelengths depends upon the material porosity: for example, material with 40% or greater than 70% porosity emits red and blue lights, respectively. Due to the quantum confinement effect, light emission has been successfully observed in the UV-vis region [76,77].

9.4 Techniques for designing nanosensors

Different methods are employed for the fabrication of sensor devices for gas analysis. A few of these methods are discussed in the following section.

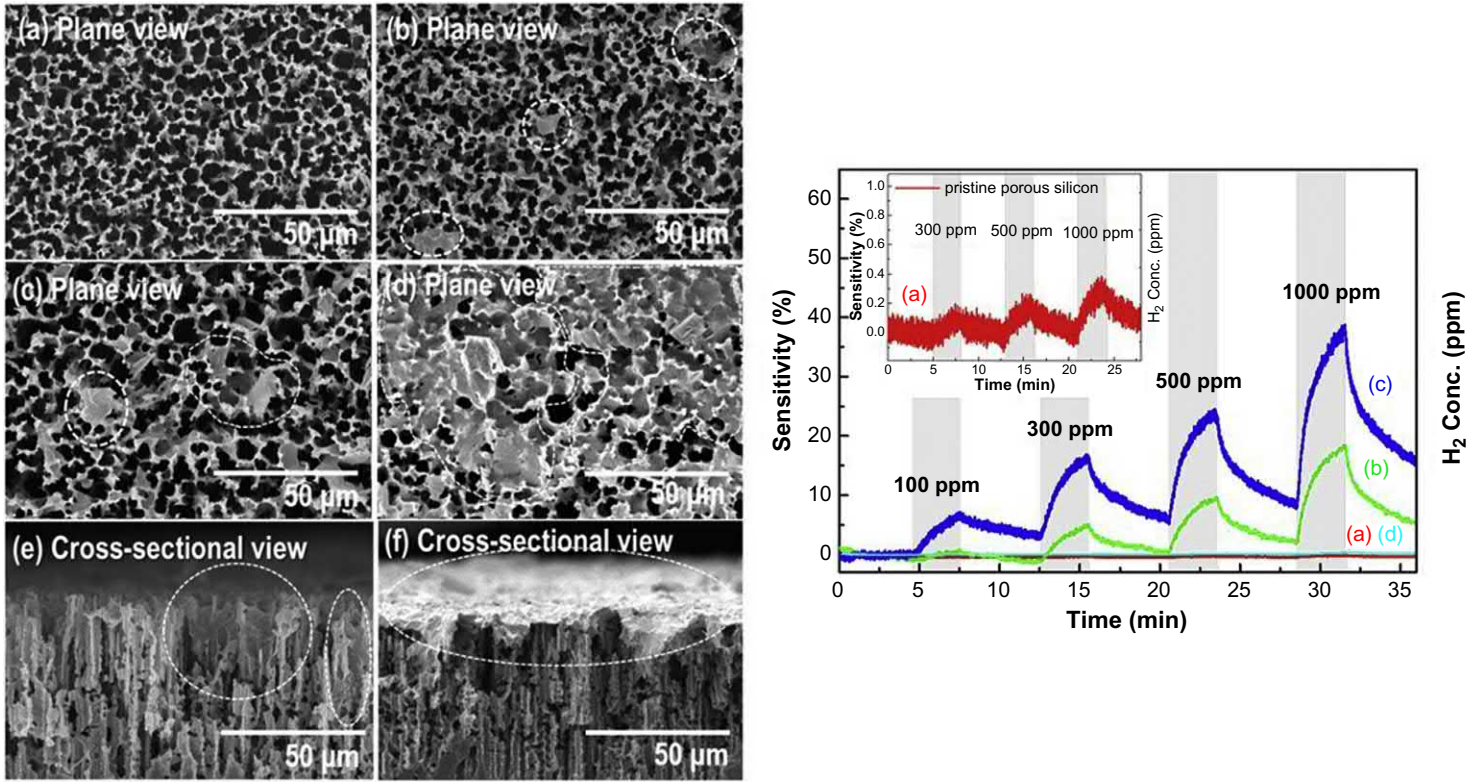

Fig. 9.4

Left: SEM images of graphene-doped porous silicon. (A) PSi, (B) 0.1 mg/mL, (C and E) 1 mg/mL, and (D and F) 10 mg/mL graphene concentrations. *Right*: (A–D) Gas detection response of PSi and graphene-doped PSi. *Reproduced from N.S.A. Eom, et al., Room-temperature H2 gas sensing characterization of graphene-doped porous silicon via a facile solution dropping method, Sensors 17 (12) (2017) 2750.*

9.4.1 Physical vapor deposition technique

In physical vapor deposition (PVD), vaporized solid material is deposited on thin films under vacuum conditions [78]. In this process, atoms/molecules of a material condense onto the substrate physically. The reactive gas is introduced simultaneously to the vapors during the deposition process, known as reactive deposition. Usually, PVD processes are adopted to deposit thin films with a thickness of a few nanometers.

The PVD method can be categorized based on the following steps:

- Formation of vapor phase: This involves a change of the given materials from solid to vapor form by evaporation and sputtering.
- Transporting of the material source to the substrate: Some of these materials to be ionized due to collisions during movement.
- Film development on the surface: The arrangement and microstructure of film can also be changed by bombardment of ions [78].

The major PVD methods with their different variations are discussed in the following paragraphs.

9.4.1.1 Thermal evaporation

Thermal evaporation is an ancient deposition method used for the development of the film on the substrate. This method is still valuable in a normal environment and is widely used in research laboratories and industries for the fabrication of thin films. Fundamental steps for this method are:

- The vapors are generated by raising the temperature of the material,
- The expelled vapors from the target material are shifted to substrate through high vacuum,
- Condensation of the vapors occurs to form solid thin film on substrate.

This process is generally carried out in ultrahigh vacuum and the path of movement of the vaporized material to the substrate remains straight, called line of sight. The vacuum environment generates a safe zone to decrease gaseous impurities in the deposition procedure. The thermal vaporization amount can be very large compared to other PVD methods. Tungsten filament is usually used as the source of thermal heat [79].

9.4.1.2 Sputtering

Sputtering is an important and commonly used process among the PVD procedures. It is a nonthermal vaporization method through which individual atoms discharge from the target surface as atomic collision cascades from sufficiently high-energy ion bombardment. Through the sputtering procedure, atoms are eliminated from the surface of the target material by

transfer of continuous momentum from an atomic-sized strong bombarding particle, generally a gaseous ion accelerated through plasma [80].

The sputtering deposition method employs several sources for power:

- DC sputtering is performed by a pair of parallel electrodes. The material to be deposited is put on the cathode, and the substrate is placed at the anode. Argon gas is used as a working gas in the deposition chamber. DC voltage is applied between the anode and cathode to continue the glow discharge, and these glow discharges create gaseous ions that accelerate the target material. The sputtering results in a thin film deposition on the substrate [81].
- Reactive sputter deposition is used for making multiple thin films. In sputtering, nitrogen or oxygen is used as a reactive gas in the deposition chamber and interacts with the given material to make multiple thin films on the substrate. This method is called reactive sputtering [82].

9.4.1.3 Ion plating

In this technique, the deposited material can be vaporized by different methods, such as evaporation, sputtering, and arc erosion, and then these evaporated atoms pass over the gaseous glow discharge, which can ionize the atoms. The ion bombardment at the time of film growth helps to make thicker films, with a thickness near to the bulk material. This is suitable for depositing a thin film substrate. A reactive gas can be added to make multiple surface coatings, which is called reactive ion plating [83,84].

9.4.1.4 Arc vapor deposition

In the arc vapor deposition method, high current with low voltage is used to vaporize the target material and deposit it on the substrate. Flux is created by making an arc that moves on the surface of the target material. The arc collisions lead to discharge of atoms through the target materials and a considerable amount of the metal atoms are converted into ions. These ionized atoms form a thick layer on the substrate [78].

9.4.2 Chemical vapor deposition

In the CVD technique, a series of chemical reactions are used for the deposition of thin films. The vapors of the target material are deposited on the substrate through chemical processes. The CVD method gives control over significant features of gas sensing materials, such as electrical, magnetic, and optical properties. The film is formed speedily at atmospheric pressure, which is an advantage of this technique. This is also a low-cost technique. Williams et al. used this method to deposit films for large-scale applications, such as metal oxide-based gas sensors, optical gas sensors, and electrochemical gas sensors [85].

9.4.3 Screen printing

Screen printing is extensively used in industry for making metal sulfide semiconductor gas sensors. In the screen-printing method, ink is forwarded on the substrate, contain the material to be deposited. Most nanomaterial-based biosensors are manufactured using a screen-printing method. The screen-printing technique prints comparatively thick films, which may decrease the performance of biosensors [86,87].

9.4.4 Drop coating

Drop coating is a method in which a paste is formed of a target metal sulfide powder, and then paste is deposited on a substrate through controlled injection. The deposited layer is finally heated to remove the solvent and other contaminants. Combination of the paste and type of the dropping material can affect the film structure and sensor performance [88].

9.4.5 Spray pyrolysis

The spray pyrolysis technique consists of a heated chemical reaction between the target material and substrate. It involves spraying of a solution, generally aqueous, consisting of solvable salts of the given compound to be deposited on the substrate. The substrate provides thermal energy for thermal decay and, consequently, recombination of the desired materials. When the substrate temperature increases, a film is created that is used for the fabrication of the gas sensor [89,90].

9.5 Application in environmental science and technology

There are a number of environmental gases, such as CO, CO_2, NO, H_2S and NH_3, that have been detected by using nanomaterial-based sensors. In the next section, the operation of different gas sensors is discussed.

9.5.1 Carbon monoxide sensor

Carbon monoxide is a colorless, odorless, tasteless gas for humans and is one of the main causes of death in the United States and worldwide. When humans are exposed to CO gas, gaseous species replace oxygen in the red blood cells, which causes tissue damage and even death [91]. This gas is mostly produced by igniting gasoline, wood, chemical, and other related fuels. The concentration of CO is high in industrial zones and megacities with heavy traffic. Gas sensors are utilized in homes as monitoring systems to detect carbon monoxide gas [92,93]. The sensors can be divided into two main groups, the blob sensors and the electrical sensors. The blob sensors consist of a strip of metal oxide base salts that interact with the monoxide, which decreases the salt, making carbon dioxide (CO_2). The salt changes to a black color when it is decreased, and this color change is a warning for the observer. However,

the warning system needs the attention of the viewer to recognize the variation in concentration. The second type is electronic sensors consisting of two parts: a thermistor-based metal-oxide sensor that detects variation in heat as soon as carbon monoxide reaches the oxide base substrate, and an electrolytic sensor for detecting the variation in charge carriers while carbon monoxide reacts with the sensor electrode [12]. Carbon monoxide sensors possess multiple uses, not only for home care, but also in determining atmospheric concentrations and for monitoring in industrial plants. Pd-decorated ZnO nanowires have shown a promising response for the detection of CO gas, whereas the response of bare nanowires was very poor [94] (Fig. 9.5).

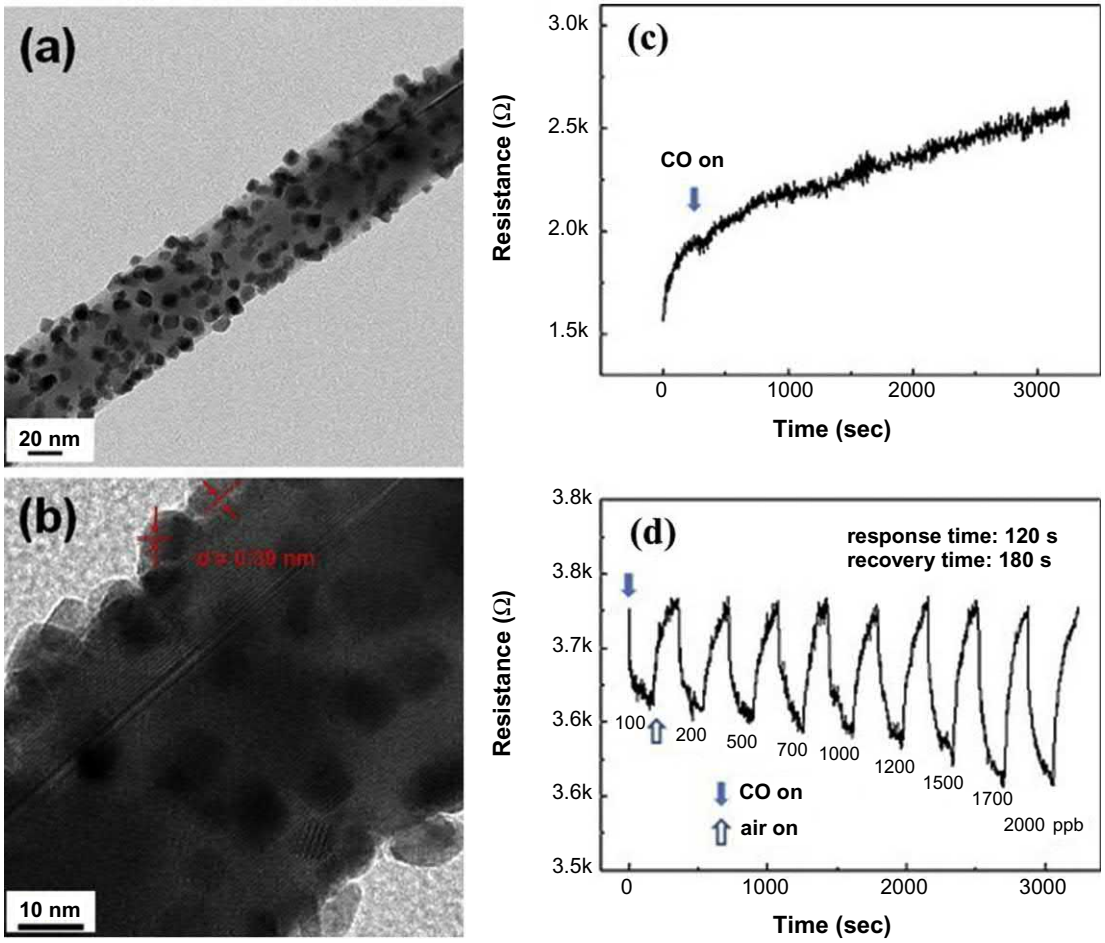

Fig. 9.5

(A and B) TEM images of Pd-decorated ZnO nanowires, (C) CO gas response of ZnO nanowires, (D) CO gas response of Pd functionalized ZnO nanowires. *Reprinted with permission from S.-W. Choi, S.S. Kim, Room temperature CO sensing of selectively grown networked ZnO nanowires by Pd nanodot functionalization, Sensors Actuators B Chem. 168 (2012) 8–13.*

9.5.2 Carbon dioxide sensor

Carbon dioxide (CO_2) is in the air, in concentrations of about 390 ppm. Carbon dioxide can be observed in many processes, such as carbonated drinks and atmospheric and photosynthesis processes. In the atmosphere, Co_2 is the major greenhouse gas that is increasing the climate temperature. Therefore, precise and effective sensors with correct temperature limits can be used to find the variation in gas concentration. Precise sensors can measure the production of CO_2 during combustion, hence giving a significant real-time report related to the quantity of carbon dioxide actually created by the activity of humans. Patel et al. [95] developed an indium tin oxide-based sensor that detected the presence of carbon dioxide. Some of the other metal oxide-based semiconductor materials were studied to find toxic gases, such as ITO, SnO_2 [96], $BaTiO_3$ [97] and TiO_2 but TiO_2 possess the extraordinary ability of sensing for CO_2 [98] (Fig. 9.6).

9.5.3 Nitrogen oxide sensor

NOx is a mixed group of gases with basic forms as nitric oxide, nitrogen dioxide, and nitrous oxide, etc. These gases are generally formed from the burning of fossil fuels inside ignition engines; the burning action helps to mix nitrogen and oxygen gas. Nitric oxide (NO) is a common constituent of photochemical smog, mixing hydrocarbons and oxygen that produce a dense cloud over industrial areas. Nitrogen dioxide (NO_2) is harmful if inhaled, but contrary to carbon monoxide (CO), this can easily be sensed by odor. The main hazards of nitrogen dioxide occur on the lungs. Animal lungs are also affected by the risk of NO_2 gas. The monitoring of NO_2 in the environment where it is a great hazard is necessary, so that effects on human health can be minimized [99]. Morito et al. [100] formed a thin film of WO_3 that has been found to respond correctly to NO and NO_2. This film was most sensitive in the detecting of NO at 473 K. For detection of NO_2 gas, the device provides good response at 573 K. Tamaki et al. [101] detected the effect of the nanoparticle size of WO_3 on the sensing properties of the sensor. In varying the shape of the nanoparticles, the response of the sensor also changed.

9.5.4 Ammonia sensor

Ammonia is an acidic and dangerous colorless gas with a typical pungent odor. International production of ammonia in 2008 was nearly 141 million tons, from just 2 million tons in 1945. About 84% of produced ammonia has been consumed in the fertilizer industry. Ammonia is both acidic and dangerous to humans, especially when its limit exceeds 25 ppm [102]. Wang et al. studied the response of WO_3 to the existence of NO and NH_3 [103]. A large number of materials were studied for the sensing of ammonia gas, such as ZnO [104], WO_3 [105], and TiO_2 [106]. Thin films-based sensors showed enhanced response for extremely small ammonia concentrations [107] (Fig. 9.7).

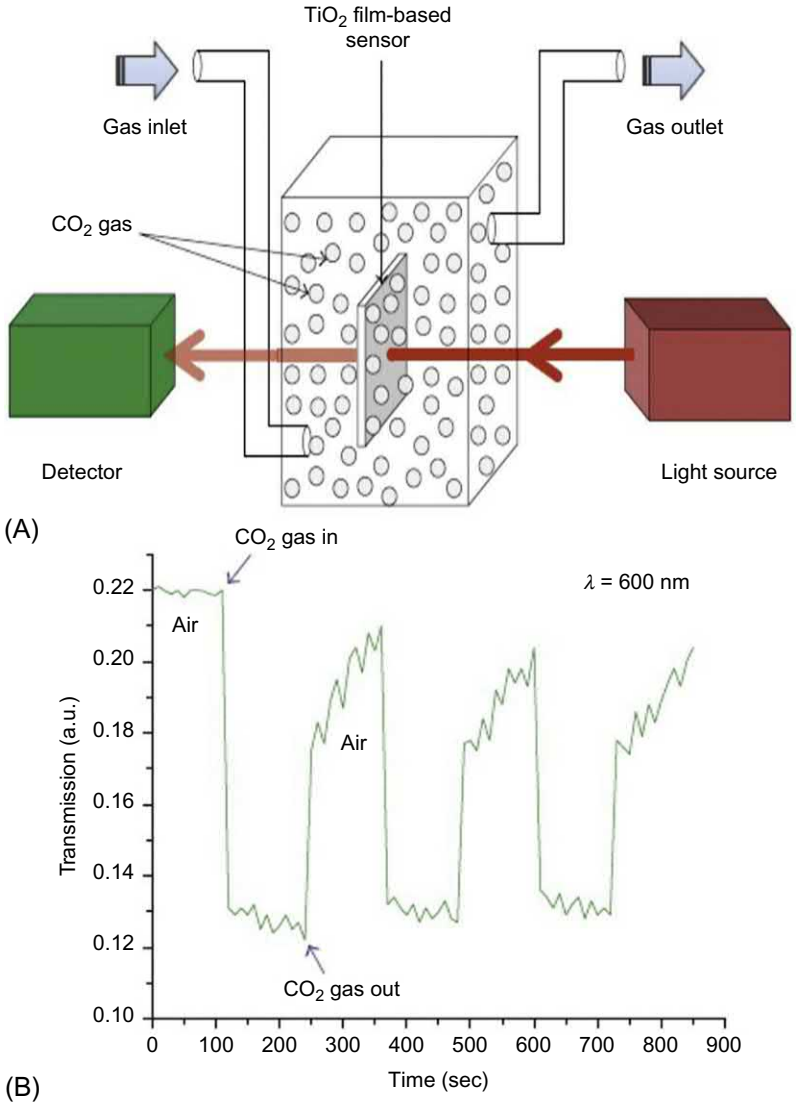

Fig. 9.6

(A) Schematic representation of CO_2 detection system. (B) CO gas response Au decorated TiO_2 thin films. *Reprinted from M.A. Raza, et al., Optical CO_2 gas sensing based on TiO2 thin films of diverse thickness decorated with silver nanoparticles, Adv. Mater. Sci. Eng. 2018 (2018) 12.*

9.5.5 Hydrogen sulfide sensor

Hydrogen sulfide is a naturally poisonous and toxic gas, due to its direct chemical reaction with blood's hemoglobin, which stops oxygen to basic organs and tissues. H_2S gas is mainly produced by the anaerobic breakdown of organic matter, also present in volcanos and natural gas. It has a typical rotten-egg smell that can be sensed at low concentrations. From a safety point of view, in situ sensing and monitoring of H_2S gas is necessary in coal

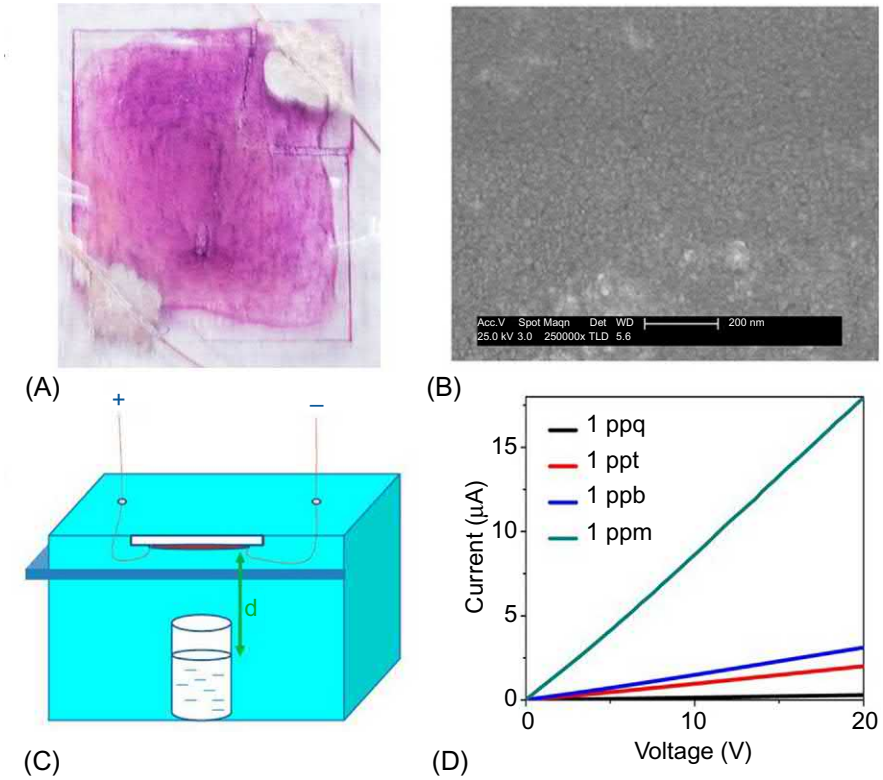

Fig. 9.7

Thin film-based sensor for ammonia vapors detection. (A and B) Digital and SEM image of the film, (C) Pictorial representation of gas testing cavity, (D) Current-voltage characteristics of polysaccharide-Au composite films for different ammonia concentrations. *Reprinted with permission from S. Pandey, K.K. Nanda, Au nanocomposite based chemiresistive ammonia sensor for health monitoring, ACS Sens. 1 (1) (2016) 55–62.*

manufacturing industries [108]. Several metal oxides were analyzed for H_2S sensing, among those, In_2O_3 whiskers formed by a carbothermal technique showed extraordinary performance for H_2S at room temperature [109]. WO_3 films produced using electrostatic spraying were also considered to be good H_2S sensors that react well at low concentrations [110]. The films also presented lower gas response to other gases referred for selective sensing of H_2S from a mixture of different gases. Hematite nanoparticle-based gas sensors have a detection limit of as low as 1 ppm of H_2S [111] (Fig. 9.8). The best H_2S response has been recently attained from a good SnO_2 thin film prepared with 16 nm silver nanoparticles at 200°C [112].

9.6 Conclusion and future perspectives

Detection of different gases released from industries and chemical processes is an important issue. Currently, nanomaterial-based gas sensors are a major area of research so that more economical, user-friendly, and efficient gas sensing systems can be developed. The gas sensing

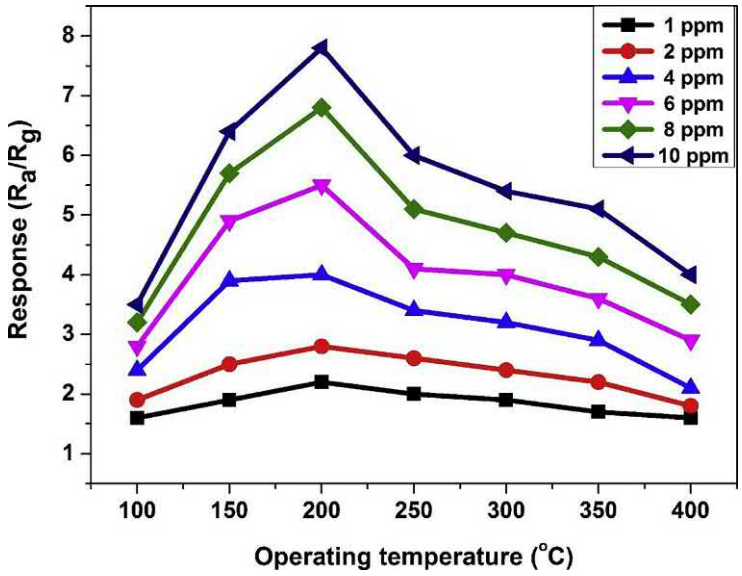

Fig. 9.8

Response of α-Fe_2O_3 nanoparticle-based sensor for different H_2S concentrations. *Reprinted with permission from Z. Li, et al., A fast response & recovery H2S gas sensor based on α-Fe2O3 nanoparticles with ppb level detection limit, J. Hazard. Mater. 300 (2015) 167–174.*

process involves surface reactions between gas species and a material surface, which activates changes in the properties of the materials. This indicates that small size and porous structures are efficient for gas detection. Additionally, the small size of nanomaterials can enhance sensitivity. This chapter provides insights in the different nanomaterials and their applications in detection of gaseous species. Metal sulfides, oxides, and noble metal properties have been discussed in detail. At high temperatures, grain size increases, which decreases surface area and catalytic response; therefore, a balance between grain size and stability is necessary. More stable materials with specific morphologies and porous surfaces can be more suitable as gas sensors.

References

[1] E. Comini, et al., Metal oxide nanoscience and nanotechnology for chemical sensors, Sensors Actuators B Chem. 179 (2013) 3–20.
[2] K. Kalantar-zadeh, B. Fry, Nanotechnology-Enabled Sensors, Springer Science & Business Media, 2007.
[3] S. Su, et al., Nanomaterials-based sensors for applications in environmental monitoring, J. Mater. Chem. 22 (35) (2012) 18101–18110.
[4] A. Chen, S. Chatterjee, Nanomaterials based electrochemical sensors for biomedical applications, Chem. Soc. Rev. 42 (12) (2013) 5425–5438.
[5] X. Du, Y. Du, S. George, CO gas sensing by ultrathin tin oxide films grown by atomic layer deposition using transmission FTIR spectroscopy, J. Phys. Chem. A 112 (39) (2008) 9211–9219.
[6] Y. Zhang, et al., New gold nanostructures for sensor applications: a review, Materials 7 (7) (2014) 5169–5201.

[7] Z. Li, et al., Advances in designs and mechanisms of semiconducting metal oxide nanostructures for high-precision gas sensors operated at room temperature, Mater. Horiz. 6 (3) (2019) 470–506.
[8] E. Comini, Metal oxide nanowire chemical sensors: innovation and quality of life, Mater. Today 19 (10) (2016) 559–567.
[9] N. Barsan, U. Weimar, Conduction model of metal oxide gas sensors, J. Electroceram. 7 (3) (2001) 143–167.
[10] I. Simon, et al., Micromachined metal oxide gas sensors: opportunities to improve sensor performance, Sensors Actuators B Chem. 73 (1) (2001) 1–26.
[11] C. Wang, et al., Metal oxide gas sensors: sensitivity and influencing factors, Sensors 10 (3) (2010) 2088–2106.
[12] G.F. Fine, et al., Metal oxide semi-conductor gas sensors in environmental monitoring, Sensors 10 (6) (2010) 5469–5502.
[13] A. Dey, Semiconductor metal oxide gas sensors: a review, Mater. Sci. Eng. B 229 (2018) 206–217.
[14] X. Gao, T. Zhang, An overview: facet-dependent metal oxide semiconductor gas sensors, Sensors Actuators B Chem. 277 (2018) 604–633.
[15] Z. Hua, et al., A theoretical investigation of the power-law response of metal oxide semiconductor gas sensors I: Schottky barrier control, Sensors Actuators B Chem. 255 (2018) 1911–1919.
[16] V.K. Tomer, et al., Noble metals–metal oxide mesoporous nanohybrids in humidity and gas sensing applications, in: Noble Metal-Metal Oxide Hybrid Nanoparticles, Elsevier, 2019, , pp. 283–302.
[17] J. Zhang, et al., Metal-oxide-semiconductor based gas sensors: screening, preparation, and integration, Phys. Chem. Chem. Phys. 19 (9) (2017) 6313–6329.
[18] P. Mehrotra, Biosensors and their applications–a review, J. Oral Biol. Craniofac. Res. 6 (2) (2016) 153–159.
[19] T. Pasinszki, et al., Carbon nanomaterial based biosensors for non-invasive detection of cancer and disease biomarkers for clinical diagnosis, Sensors 17 (8) (2017) 1919.
[20] A. Mokhtarzadeh, et al., Nanomaterial-based biosensors for detection of pathogenic virus, TrAC Trends Anal. Chem. 97 (2017) 445–457.
[21] Z. Wang, Z. Dai, Carbon nanomaterial-based electrochemical biosensors: an overview, Nanoscale 7 (15) (2015) 6420–6431.
[22] S. Kumar, et al., Graphene, carbon nanotubes, zinc oxide and gold as elite nanomaterials for fabrication of biosensors for healthcare, Biosens. Bioelectron. 70 (2015) 498–503.
[23] P. Ramnani, N.M. Saucedo, A. Mulchandani, Carbon nanomaterial-based electrochemical biosensors for label-free sensing of environmental pollutants, Chemosphere 143 (2016) 85–98.
[24] X. Kang, et al., Glucose oxidase–graphene–chitosan modified electrode for direct electrochemistry and glucose sensing, Biosens. Bioelectron. 25 (4) (2009) 901–905.
[25] C. Zhu, et al., Electrochemical sensors and biosensors based on nanomaterials and nanostructures, Anal. Chem. 87 (1) (2014) 230–249.
[26] X. Zhang, Q. Guo, D. Cui, Recent advances in nanotechnology applied to biosensors, Sensors 9 (2) (2009) 1033–1053.
[27] S. Zeng, et al., Nanomaterials enhanced surface plasmon resonance for biological and chemical sensing applications, Chem. Soc. Rev. 43 (10) (2014) 3426–3452.
[28] V. Biju, Chemical modifications and bioconjugate reactions of nanomaterials for sensing, imaging, drug delivery and therapy, Chem. Soc. Rev. 43 (3) (2014) 744–764.
[29] M.A. Carpenter, S. Mathur, A. Kolmakov, Metal Oxide Nanomaterials for Chemical Sensors, Springer Science & Business Media, 2012.
[30] J. Chen, J.X. Zhao, Upconversion nanomaterials: synthesis, mechanism, and applications in sensing, Sensors 12 (3) (2012) 2414–2435.
[31] F.-G. Banica, Chemical Sensors and Biosensors: Fundamentals and Applications, John Wiley & Sons, 2012.
[32] G. Neri, First fifty years of chemoresistive gas sensors, Chem. Aust. 3 (1) (2015) 1–20.
[33] R.R. Pradhananga, et al., Fabrication and applications of silver sulphide based ion sensors, in: Advanced Materials Research, Trans Tech Publ, 2010.
[34] S. Chaudhary, et al., Chemical sensing applications of ZnO nanomaterials, Materials 11 (2) (2018) 287.
[35] A. Waheed, M. Mansha, N. Ullah, Nanomaterials-based electrochemical detection of heavy metals in water: current status, challenges and future direction, TrAC Trends Anal. Chem. 105 (2018) 37–51.

[36] S.H. Jalalian, et al., Electrochemical and optical aptamer-based sensors for detection of tetracyclines, Trends Food Sci. Technol. 73 (2018) 45–57.
[37] T.A. Sheikh, et al., Sensitive 3-chlorophenol sensor development based on facile Er2O3/CuO nanomaterials for environmental safety, New J. Chem. 42 (5) (2018) 3936–3946.
[38] P. Samorì, F. Biscarini, Nanomaterials properties tuned by their environment: integrating supramolecular concepts into sensing devices, Chem. Soc. Rev. 47 (13) (2018) 4675–4676.
[39] A. Umar, et al., Enhanced photocatalytic degradation of harmful dye and phenyl hydrazine chemical sensing using ZnO nanourchins, Chem. Eng. J. 262 (2015) 588–596.
[40] S.I. Sadovnikov, Synthesis, properties and applications of semiconductor nanostructured zinc sulfide, Russ. Chem. Rev. 88 (6) (2019) 571.
[41] P. Hariharan, et al., A facile method for the synthesis fluorescent zinc chalcogenide (ZnO, ZnS and ZnSe) nanoparticles in PS and PMMA polymer matrix, J. Fluoresc. 26 (2) (2016) 703–707.
[42] S. Hussain, et al., Highly reactive 0D ZnS nanospheres and nanoparticles for formaldehyde gas-sensing properties, Sensors Actuators B Chem. 239 (2017) 1243–1250.
[43] L. Zhang, et al., Au nanoparticles decorated ZnS hollow spheres for highly improved gas sensor performances, Sensors Actuators B Chem. 245 (2017) 112–121.
[44] R. Mendil, Z.B. Ayadi, K. Djessas, Effect of solvent medium on the structural, morphological and optical properties of ZnS nanoparticles synthesized by solvothermal route, J. Alloys Compd. 678 (2016) 87–92.
[45] I. Parvaneh, S. Samira, N. Mohsen, Characterization of ZnS nanoparticles synthesized by co-precipitation method, Chinese Phys. B 24 (4) (2015), 046104 https://doi.org/10.1088/1674-1056/24/4/046104.
[46] X. Xu, et al., Controlled growth from ZnS nanoparticles to ZnS–CdS nanoparticle hybrids with enhanced photoactivity, Adv. Funct. Mater. 25 (3) (2015) 445–454.
[47] N. Vishwakarma, et al., Morphological and optical properties of pure and doped ZnS nanoparticles: a review, J. Nanosci. Nanoeng. Appl. 8 (1) (2018) 1–4.
[48] D. Bharti, A.V. Bharati, A.V. Wankhade, Synthesis, characterization and optical property investigation of CdS nanoparticles, Luminescence 33 (8) (2018) 1445–1449.
[49] R. Banerjee, R. Jayakrishnan, P. Ayyub, Effect of the size-induced structural transformation on the band gap in CdS nanoparticles, J. Phys. Condens. Matter 12 (50) (2000) 10647.
[50] J. Rockenberger, et al., EXAFS studies on the size dependence of structural and dynamic properties of CdS nanoparticles, J. Phys. Chem. B 101 (14) (1997) 2691–2701.
[51] H. Sekhar, D.N. Rao, Spectroscopic studies on Fe3+ doped CdS nanopowders prepared by simple coprecipitation method, J. Alloys Compd. 517 (2012) 103–110.
[52] P. Mandal, et al., Orange-red luminescence from Cu doped CdS nanophosphor prepared using mixed Langmuir–Blodgett multilayers, J. Chem. Phys. 128 (11) (2008) 114703.
[53] M. Kuzmanović, et al., Sodium-alginate biopolymer as a template for the synthesis of nontoxic red emitting Mn 2+−doped CdS nanoparticles, RSC Adv. 7 (84) (2017) 53422–53432.
[54] S. Muruganandam, G. Anbalagan, G. Murugadoss, Structural, electrochemical and magnetic properties of codoped (Cu, Mn) CdS nanoparticles with surfactant PVP, Optik 131 (2017) 826–837.
[55] K. Kaviyarasu, E. Manikandan, M. Maaza, Synthesis of CdS flower-like hierarchical microspheres as electrode material for electrochemical performance, J. Alloys Compd. 648 (2015) 559–563.
[56] M. Gao, et al., Synthesis of PbS nanoparticles in polymer matrices, J. Chem. Soc. Chem. Commun. 24 (1994) 2779–2780.
[57] A.A. Patel, et al., Synthesis, optical spectroscopy and ultrafast electron dynamics of PbS nanoparticles with different surface capping, J. Phys. Chem. B 104 (49) (2000) 11598–11605.
[58] D. Yu, et al., Synthesis of closed PbS nanowires with regular geometric morphologies, J. Mater. Chem. 12 (3) (2002) 403–405.
[59] S. Zhou, Y. Feng, L. Zhang, Sonochemical synthesis of large-scale single-crystal PbS nanorods, J. Mater. Res. 18 (5) (2003) 1188–1191.
[60] Y.-X. Pang, X. Bao, Aluminium oxide nanoparticles prepared by water-in-oil microemulsions, J. Mater. Chem. 12 (12) (2002) 3699–3704.
[61] A. Rai, et al., Understanding the mechanism of aluminium nanoparticle oxidation, Combust. Theory Model. 10 (5) (2006) 843–859.

[62] T. Seiyama, S. Kagawa, Study on a detector for gaseous components using semiconductive thin films, Anal. Chem. 38 (8) (1966) 1069–1073.
[63] T. Okabayashi, et al., High sensitive hydrocarbon gas sensor utilizing cataluminescence of γ-Al2O3 activated with Dy3+, Sensors Actuators B Chem. 64 (1–3) (2000) 54–58.
[64] W. Shi, et al., Hexagonal nanodisks of cadmium hydroxide and oxide with nanoporous structure, Cryst. Growth Des. 6 (4) (2006) 915–918.
[65] A. Heidari, C. Brown, Study of composition and morphology of cadmium oxide (CdO) nanoparticles for eliminating cancer cells, J. Nanomed. Res. 2 (5) (2015) 20.
[66] N.A. Shad, et al., Photocatalytic investigation of cadmium oxide nanosheets prepared by hydrothermal method, Arab. J. Sci. Eng. 44 (2019) 6669–6675.
[67] N. Dhineshbabu, et al., Study of structural and optical properties of cupric oxide nanoparticles, Appl. Nanosci. 6 (6) (2016) 933–939.
[68] D.I. Son, C.H. You, T.W. Kim, Structural, optical, and electronic properties of colloidal CuO nanoparticles formed by using a colloid-thermal synthesis process, Appl. Surf. Sci. 255 (21) (2009) 8794–8797.
[69] A. Kołodziejczak-Radzimska, T. Jesionowski, Zinc oxide—from synthesis to application: a review, Materials 7 (4) (2014) 2833–2881.
[70] S. Chah, M.R. Hammond, R.N. Zare, Gold nanoparticles as a colorimetric sensor for protein conformational changes, Chem. Biol. 12 (3) (2005) 323–328.
[71] I. Karaduman, et al., Room-temperature ammonia gas sensor based on reduced graphene oxide nanocomposites decorated by Ag, Au and Pt nanoparticles, J. Alloys Compd. 722 (2017) 569–578.
[72] H. Jiang, H. Ju, Electrochemiluminescence sensors for scavengers of hydroxyl radical based on its annihilation in CdSe quantum dots film/peroxide system, Anal. Chem. 79 (17) (2007) 6690–6696.
[73] M. Zubair, et al., Fabrication of CdSe/ZnS quantum dots thin film by electrohydrodynamics atomization technique for solution based flexible hybrid OLED application, Chem. Eng. J. 253 (2014) 325–331.
[74] I.L. Medintz, et al., Quantum dot bioconjugates for imaging, labelling and sensing, Nat. Mater. 4 (6) (2005) 435.
[75] N.S.A. Eom, et al., Room-temperature H2 gas sensing characterization of graphene-doped porous silicon via a facile solution dropping method, Sensors 17 (12) (2017) 2750.
[76] S.E. Lewis, et al., Sensitive, selective, and analytical improvements to a porous silicon gas sensor, Sensors Actuators B Chem. 110 (1) (2005) 54–65.
[77] L. Pancheri, et al., Very sensitive porous silicon NO2 sensor, Sensors Actuators B Chem. 89 (3) (2003) 237–239.
[78] D.M. Mattox, Handbook of Physical Vapor Deposition (PVD) Processing, William Andrew, 2010.
[79] Z.R. Dai, Z.W. Pan, Z.L. Wang, Novel nanostructures of functional oxides synthesized by thermal evaporation, Adv. Funct. Mater. 13 (1) (2003) 9–24.
[80] P.J. Kelly, R.D. Arnell, Magnetron sputtering: a review of recent developments and applications, Vacuum 56 (3) (2000) 159–172.
[81] D. Depla, S. Mahieu, Reactive Sputter Deposition, Vol. 109, Springer, 2008.
[82] S. Xu, et al., RF plasma sputtering deposition of hydroxyapatite bioceramics: synthesis, performance, and biocompatibility, Plasma Process. Polym. 2 (5) (2005) 373–390.
[83] K. Iwata, et al., Growth and electrical properties of ZnO thin films deposited by novel ion plating method, Thin Solid Films 445 (2) (2003) 274–277.
[84] E. Zhang, L. Xu, K. Yang, Formation by ion plating of Ti-coating on pure Mg for biomedical applications, Scr. Mater. 53 (5) (2005) 523–527.
[85] J.-H. Park, T. Sudarshan, Chemical Vapor Deposition, Vol. 2, ASM International, 2001.
[86] B. Ismail, M. Abaab, B. Rezig, Structural and electrical properties of ZnO films prepared by screen printing technique, Thin Solid Films 383 (1–2) (2001) 92–94.
[87] T. Ma, et al., Preparation and properties of nanostructured TiO2 electrode by a polymer organic-medium screen-printing technique, Electrochem. Commun. 5 (4) (2003) 369–372.
[88] R. Danzebrink, M.A. Aegerter, Deposition of micropatterned coating using an ink-jet technique, Thin Solid Films 351 (1–2) (1999) 115–118.
[89] P.S. Patil, Versatility of chemical spray pyrolysis technique, Mater. Chem. Phys. 59 (3) (1999) 185–198.

[90] D. Perednis, L.J. Gauckler, Thin film deposition using spray pyrolysis, J. Electroceram. 14 (2) (2005) 103–111.
[91] N.Y. Amponsah, et al., Greenhouse gas emissions from renewable energy sources: a review of lifecycle considerations, Renew. Sust. Energ. Rev. 39 (2014) 461–475.
[92] M. Hjiri, et al., Al-doped ZnO for highly sensitive CO gas sensors, Sensors Actuators B Chem. 196 (2014) 413–420.
[93] C. Li, et al., SnO2 highly sensitive CO gas sensor based on quasi-molecular-imprinting mechanism design, Sensors 15 (2) (2015) 3789–3800.
[94] S.-W. Choi, S.S. Kim, Room temperature CO sensing of selectively grown networked ZnO nanowires by Pd nanodot functionalization, Sensors Actuators B Chem. 168 (2012) 8–13.
[95] N. Patel, K. Makhija, C. Panchal, Fabrication of carbon dioxide gas sensor and its alarm system using indium tin oxide (ITO) thin films, Sensors Actuators B Chem. 21 (3) (1994) 193–197.
[96] Y. Xiong, et al., Effective CO_2 detection based on LaOCl-doped SnO_2 nanofibers: insight into the role of oxygen in carrier gas, Sensors Actuators B Chem. 241 (2017) 725–734.
[97] D.N. Suryawanshi, et al., Preparation, characterization and gas sensing performance of $BaTiO_3$ nanostructured thin films, in: AIP Conference Proceedings, AIP Publishing, 2018.
[98] M.A. Raza, et al., Optical CO_2 gas sensing based on TiO_2 thin films of diverse thickness decorated with silver nanoparticles, Adv. Mater. Sci. Eng. 2018 (2018) 12.
[99] S. Saad, et al., Classifying sources influencing indoor air quality (IAQ) using artificial neural network (ANN), Sensors 15 (5) (2015) 11665–11684.
[100] A. Morito, et al., Tungsten oxide-based semiconductor sensor highly sensitive to NO and NO_2, Chem. Lett. 20 (9) (1991) 1611–1614.
[101] J. Tamaki, et al., Grain-size effects in tungsten oxide-based sensor for nitrogen oxides, J. Electrochem. Soc. 141 (8) (1994) 2207–2210.
[102] B. Timmer, W. Olthuis, A. Van Den Berg, Ammonia sensors and their applications—a review, Sensors Actuators B Chem. 107 (2) (2005) 666–677.
[103] X. Wang, N. Miura, N. Yamazoe, Study of WO3-based sensing materials for NH_3 and NO detection, Sensors Actuators B Chem. 66 (1–3) (2000) 74–76.
[104] J.-M. Tulliani, et al., Room temperature ammonia sensors based on zinc oxide and functionalized graphite and multi-walled carbon nanotubes, Sensors Actuators B Chem. 152 (2) (2011) 144–154.
[105] E. Llobet, et al., Fabrication of highly selective tungsten oxide ammonia sensors, J. Electrochem. Soc. 147 (2) (2000) 776–779.
[106] B. Karunagaran, et al., TiO_2 thin film gas sensor for monitoring ammonia, Mater. Charact. 58 (8–9) (2007) 680–684.
[107] S. Pandey, K.K. Nanda, Au nanocomposite based chemiresistive ammonia sensor for health monitoring, ACS Sens. 1 (1) (2016) 55–62.
[108] W. Jaeschke, H. Claude, J. Herrmann, Sources and sinks of atmospheric H_2S, J. Geophys. Res. Oceans 85 (C10) (1980) 5639–5644.
[109] M. Kaur, et al., Room-temperature H_2S gas sensing at ppb level by single crystal In_2O_3 whiskers, Sensors Actuators B Chem. 133 (2) (2008) 456–461.
[110] C.M. Ghimbeu, et al., Electrosprayed metal oxide semiconductor films for sensitive and selective detection of hydrogen sulfide, Sensors 9 (11) (2009) 9122–9132.
[111] Z. Li, et al., A fast response & recovery H_2S gas sensor based on α-Fe_2O_3 nanoparticles with ppb level detection limit, J. Hazard. Mater. 300 (2015) 167–174.
[112] R. Niranjan, et al., High H2S-sensitive copper-doped tin oxide thin film, Mater. Chem. Phys. 80 (1) (2003) 250–256.

CHAPTER 10

Hybrid nanocomposites and their potential applications in the field of nanosensors/gas and biosensors

Periasamy Palanisamy[a], Murthy Chavali[b,c,d], Enamala Manoj Kumar[e], Krishna Chitanya Etika[f]

[a]*Department of Physics, Gnanamani College of Engineering, Namakkal, Tamil Nadu, India*
[b]*Shree Velagapudi Rama Krishna Memorial College (PG Studies), Affiliated to Acharya Nagarjuna University, Nagaram, Andhra Pradesh, India*
[c]*PG Department of Chemistry, Dharma Appa Rao College, Affiliated to Krishna University, Nuzvid, Andhra Pradesh, India*
[d]*NTRC, MCETRC, Tenali, Andhra Pradesh, India*
[e]*Bioserve Biotechnologies (India) Private Ltd., Hyderabad, Telangana, India*
[f]*Department of Chemical Engineering, Birla Institute of Technology and Science, Pilani, Rajasthan, India*

10.1 Introduction

Nanotechnology has been recognized as a key technology leading to innovations in almost all branches of science and technology research. Nanotechnology involves the structures of materials with sizes from 1 to 100 nm, and they describe the interdisciplinary and cross-sector research area with a clear and distinct definition [1]. The effects and phenomena of nanotechnology have been realized in biotechnology, electronics, optics, and new materials that are found only at nanoscale [2].

A formal definition for nanotechnology is not yet framed internationally, but the International Organization for Standardization (ISO) has led the way in this area. Their portrayal of basic principles and research approaches at nanoscale plays a vital role in this connection. Basically, the nanotechnological process is not a new one. Some ancient monuments have clearly revealed nano-effects realized without knowledge of the physicochemical principles behind them [3]. Examples are the red stain in church windows from finely distributed gold colloids and the toughening of Damascene steel sword blades using carbon nanotubes. Thus the spirit of nanotechnology involves the limited exploitation of nanosize structures and accepting of the principles involved at the molecular level.

Nanofabrication for Smart Nanosensor Applications. https://doi.org/10.1016/B978-0-12-820702-4.00011-8
© 2020 Elsevier Inc. All rights reserved.

"Nanotechnologies designate the formation, analysis and application of structures, molecular materials, inner interfaces and surfaces with at least one key measurement or with manufacturing tolerances (usually) below 100 nanometers" [4]. The significant aspects are the novel properties and functionalities at nanoscale of components that can be used for advancements in prevailing products or innovations leading to new products and their application options. Such novel special effects and potential applications are mostly based on the surface-to-volume ratio of atoms and on the quantum-mechanical behavior of the material elements [5]. Nanomaterials display drastically tailored properties pertaining to biological, chemical, and physical features.

The physical material properties of a solid, for instance hardness, electrical conductivity, fluorescence, and magnetism, change vitally in compliance with the arrangement of interconnecting atoms, ions, and molecules. The electrons in nanoscale materials can adopt only definite "quantized" energy states, contrary to macroscopic solids that are influenced by interacting atoms. Significantly, chemical properties of a nanomaterial strongly depend on its atomic arrangement and structure of the molecule [6]. Furthermore, the materials are broken into nanoscale substructures that exhibit effectively improved ratio of reactive surface atoms to interior particles, which also contributes to achieving a high level of chemical reactivity. For example, in a particle of 20 nm diameter, roughly only 10% of the atoms are on the surface of the particle, while in a 1 nm particle 99% of the atoms are on the surface. A comparison of the surface-to-volume ratio of bulk materials to nanomaterials is illustrated in Fig. 10.1.

Most of the atoms in the 1 nm particle are situated on the reactive surface area of the particle (blue) in comparison to the more inert center of the 20 nm particles (red). Fig. 10.1 shows a clear picture of the considerable variation of the ratio of surface atoms to the total number of inert atoms. Thus, nanomaterials have opened the door for "smart" material design, with the

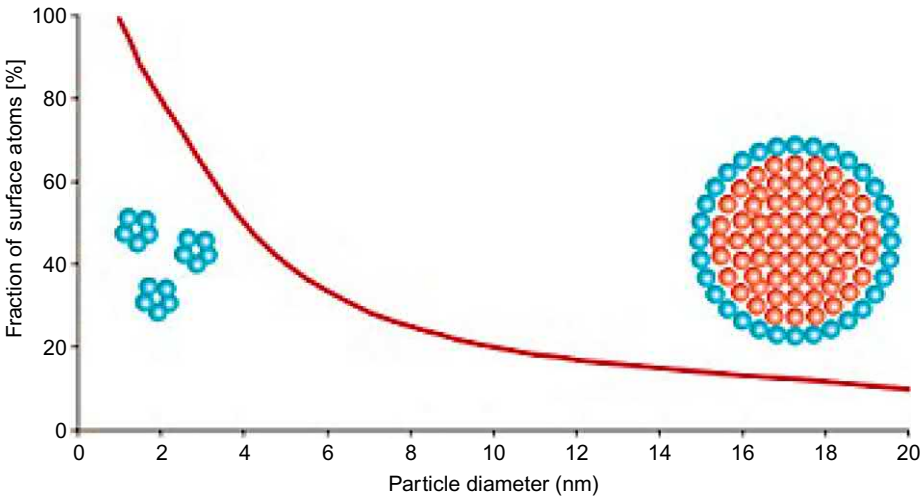

Fig. 10.1
Comparison of the surface-to-volume ratio of bulk materials to nanomaterials.

option of combining and adjusting the anticipated materials to meet particular technical applications.

10.2 Structures of nanomaterials

The reduction of the spatial dimensions of a material, or particle and/or quasiparticle confinement in a particular direction in the crystallographic structure, lead to revolutionized changes in various nanomaterial properties in that direction. Based on the reduction of confinement, nanostructures are classified as having zero-dimensional, one-dimensional, two-dimensional, and three-dimensional structure [7].

10.2.1 Zero-dimensional structure (0-D)

When the dimensions of a material are all confined and are also measured in the range of 1–100 nm, or nanoscale, it can be considered a zero-dimensional material. The nanoparticles are the most general illustration of zero-dimensional nanomaterials. The 0-D particles can be amorphous or crystalline, composed of single or multiple elements, be any shape or form, present individually or be built into a matrix, or be metallic, ceramic or polymeric; examples are colloidal particles, fullerenes, nanocapsules, nanoparticles, and nanograins.

10.2.2 One-dimensional structure (1-D)

When two dimensions of a material are confined for electron movement, then those materials can be considered as a one-dimensional material. The length of these materials is several micrometers, whereas the diameter is only a few nanometers. The 1-D material surface-to-volume ratio is higher than that of 2-D and 3-D materials, which is favorable for energy storage and other electronic applications. The 1-D nanomaterials can be amorphous or crystalline, chemically pure or impure, single-crystalline or polycrystalline, present as individual materials or be embedded in a matrix, and can be metallic, ceramic, or polymeric: examples are nanowires, nanotubes, and nanorods.

10.2.3 Two-dimensional structure (2-D)

In materials with two-dimensional structure, electrons are confined in one dimension and the remaining two dimensions are not narrowed to the nanoscale. The length of 2-D nanomaterials is large, several square micrometers, whereas its thickness remains in the nanoscale range, exhibiting plate-like shapes. The 2-D nanomaterials can be amorphous or crystalline, fabricated by various chemical compounds, be a single layer or multilayer structure, be deposited over a substrate, be incorporated in an adjoining matrix material, and can be metallic, ceramic, or polymeric: Examples are nanofilms, nanocoatings, and nanolayers.

10.2.4 Three-dimensional structure (3-D)

A material in which all three dimensions are not confined for electron transition is considered a 3-D nanomaterial, also known as a bulk material. Therefore, 3-D materials are characterized by possessing three arbitrary dimensions beyond 100 nm. The 3-D nanomaterials may include various structures such as bundles of nanowires, dispersions of nanoparticles, multi-nanolayers, and nanotubes. The 3-D nanomaterials can be amorphous or crystalline, constructed by different chemical compounds, and can be metallic, ceramic, or polymeric: examples are polycrystals, graphite, and mesoporous and microporous composite electrodes.

Examples of 0-D, 1-D, 2-D, and 3-D nanomaterials are shown in Fig. 10.2.

10.3 Preparation of hybridized nanocomposites

Materials researchers are engaged in development of new nanocomposites, novel materials that have excellent properties, additional functionality, and relatively low cost compared to already existing materials. Several synthesizing approaches have been proposed to meet the high-performance supercapacitance. Some of these approaches are listed and described briefly in the following paragraphs.

10.3.1 Solid-state synthesis

The most common method used to synthesize polycrystalline materials is the solid-state reaction method, particularly for a mixture of solid compounds [8, 9]. It has been observed that at normal temperature the solids do not react with other materials, so it is necessary to take them

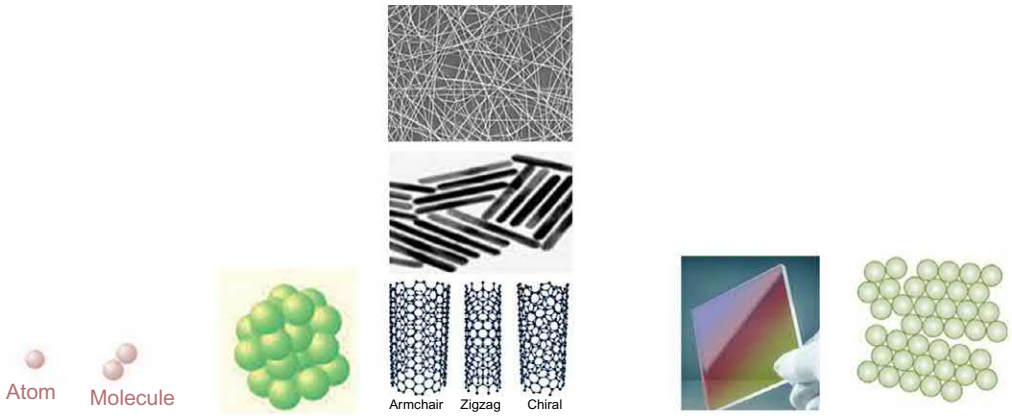

Fig. 10.2
Structures of 0-D, 1-D, 2-D, and 3-D nanomaterials.

to a higher temperature, such as 1000 °C to 1500°C, where the reaction can take place at the appropriate rate. This method offers the following advantages: simple process, controllable size, uniform particle size distribution, high yield and selectivity, and, mainly, less contamination. It can also decrease the agglomeration in the liquid phase and the number of particles originating from the process during an intermediate step at high temperature. The synthesizing (Fig. 10.3) procedure comprises four steps: diffusion, reaction, nucleation, and growth. The speed of the nucleus's growth should be dominated by the nucleation rate, which is beneficial to achieve the desired nanocrystallites.

10.3.2 Hydro-/solvothermal synthesis

Hydrothermal synthesis (Fig. 10.4) is usually carried out in an autoclave (pressurized vessel), particularly for reactions in solution [10]. The temperature in the autoclave can be raised beyond the boiling point of water whereas, in the solvothermal method, the nonaqueous solvent is used in the reaction medium. This method has been extensively used for synthesizing nanoparticles of various metal oxides by hydrothermal treatment of precipitates of respective precursor solutions [11, 12]. The hydrothermal synthesizing method can be used to change particle morphology and to control grain size, surface chemistry, and crystalline phase, by optimizing certain parameters such as the reaction temperature, pressure, solution composition, solvent, surfactant, and aging time [13]. Various types of autoclaves and their functions are

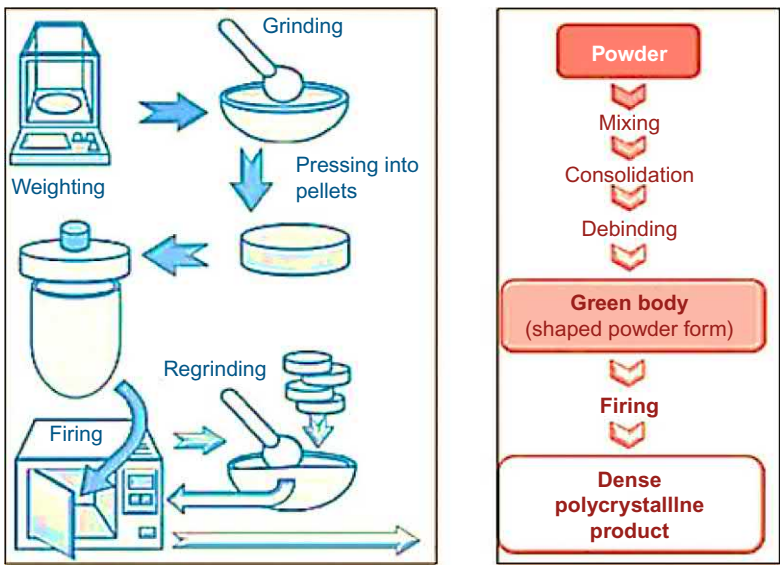

Fig. 10.3
Schematic representation of sold state synthesis. (A) Procedure and (B) flowchart.

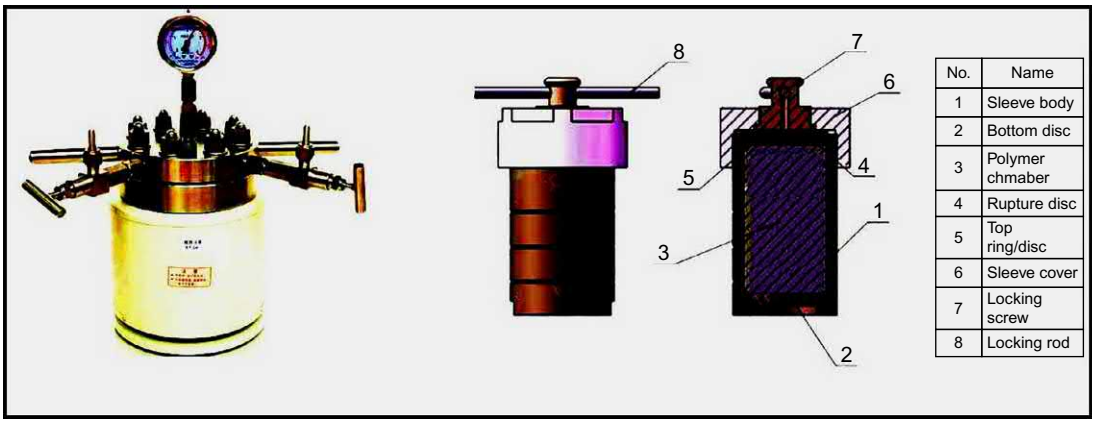

Fig. 10.4
Schematic representation of (A) commercially available autoclaves for hydrothermal synthesis, and (B) high-temperature autoclave.

intensely discussed by Hakuta et al. [14] and Rabenau [15]. The Teflon-lined autoclave is an ideal container to carry out the reaction under preferred conditions.

10.3.3 Sol-gel synthesis

The sol-gel method is a resourceful scheme for synthesizing different metal oxide nanostructures [16]. This synthesis method permits us to control the chemical properties, texture, and the structure and morphology of the material. Also, this method offers many advantages over other synthesizing approaches such as coprecipitation or impregnation, which allow us to add dopants. The foremost benefits of the method include purity of precursor, homogeneity, and mixing the compound on a molecular scale. The products of the sol-gel technique are highly unique, having high standards of structure and morphology, and peculiar physical and chemical properties of materials [17a, b]. The colloidal suspension/sol are derived by hydrolysis of precursor and aged for a few hours, depending on the desired morphology of the material. In this stage, the kind of solvent, the concentration of precursor solution, the amount of acid or base addition, and temperature directly affect the properties of materials (Fig. 10.5).

10.3.4 Chemical vapor deposition technique

In the semiconductor fabrication industry, this technique is commonly used to construct semiconducting thin films of high purity and superior performance. In this method, the desired substrate is exposed to the precursor solution and the thickness of the thin film also can be adjusted. The deposited thin film quality strongly depends on precursor concentration, reaction

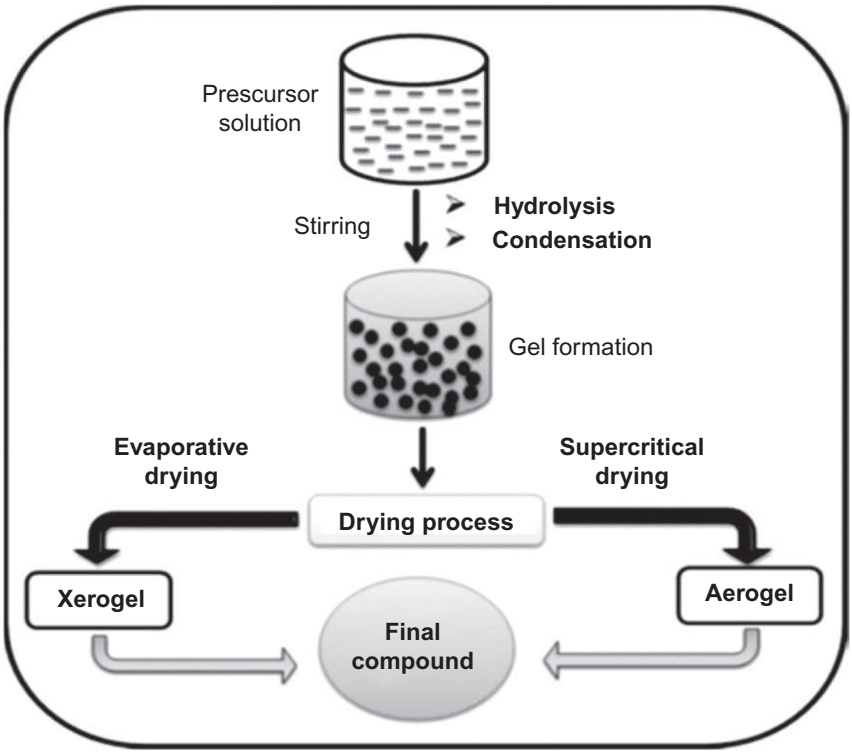

Fig. 10.5
Schematic representation of sol-gel synthesis.

rate, and temperature of the atmosphere [18]. This method offers many advantages, including high purity, uniform coating, and thickness-controlled thin film.

10.3.5 Microwave-assisted wet chemical method

The microwave-assisted wet chemical method is an effective method for nanostructure preparation. The method offers superior physicochemical properties, development of new phase material, and high reaction acceleration; thereby the yield product performance is improved. In addition, this method saves both energy and time, since less than an hour is needed to complete the reaction at low temperatures [19a]. This method exhibits higher heating rates, since the microwave can activate dipole rotation and ionic conduction. Therefore, the rapid heating in this method brings good results. To facilitate industrial applications, a clear distinction should be made between the microwave thermal effects (not excited by heat) from the microwave-induced thermal (temperature rise) effect.

Normally, nanocomposites for optoelectronics applications have been prepared by conventional methods. These methods entail complex procedures and can even require several

days to a week to complete the electrode preparation. It was observed through experimentation that the microwave-assisted method could minimize the nanostructure preparation time, to about 30 min, and long-time microwave irradiation could initiate new dimensional material structures. Hence, the implementation of a microwave-assisted method for electrode material synthesis has found support, not only for developing highly efficient and lower cost processing, but also to provide an opportunity to construct new types of nanomaterials that possibly could not be obtained from conventional heating methods.

Crystalline molecules have a channel of uniform micro −/mesoporous size, intraframework cages, high thermal stability, and tailor-made acidity or basicity. Due to these peculiar structures, nanomaterials have found varied applications, including as an energy storage device. The microwave-assisted (Fig. 10.6, [19b]) method has been employed to synthesize nanomaterials with low dimensions and high surface area structures. A glass reaction container offers the significant feature of uniform heating using microwave irradiation on a precursor solution, yielding additional homogeneous nucleation and smaller crystallization time when compared with conventional heating. In addition to this, microwave dielectric heating is perhaps a superior synthesizing approach, when taking into account its simple execution, energy efficiency, rapidity, and uniformity. Consequently, the microwave-assisted wet chemical technique is favorable for the realization of metal colloids. A few reports were found to be published on the effect of microwaves on particle size and particularly on the capacitance of nanoparticles.

10.4 Invasion of hybridized nanocomposite materials

The hybridized nanocomposite is simply defined as intimately mixed organic and inorganic components with metal oxides, or polymers and graphene materials. In order to make use of new and synergistic properties that are not possible in a single nanoparticle system,

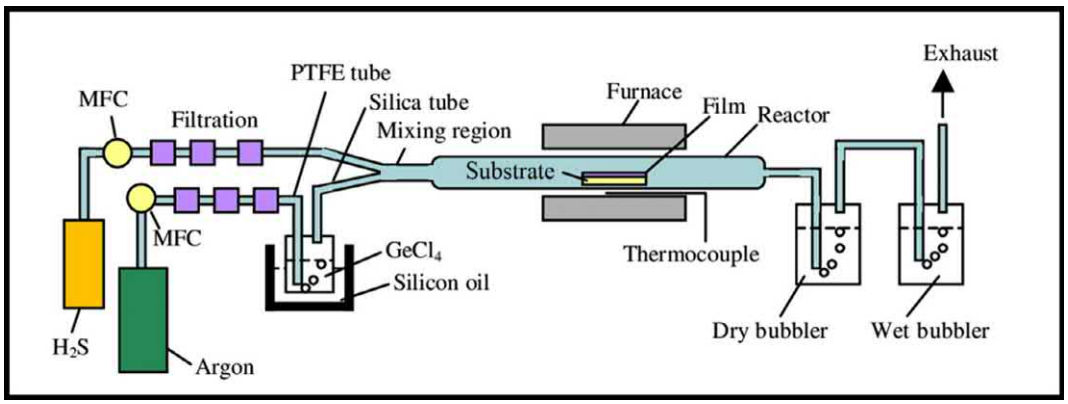

Fig. 10.6
Schematic diagram of the chemical vapor deposition apparatus.

hybridization is necessitated at present in all areas of materials research [20]. Typically, hybrids are a homogeneous system or heterogeneous system in which one component has the dimensions of a few angstroms to several nanometers. Certainly, the final material properties may depend on the chemical nature of the composition. Obviously, it is quite difficult to estimate the synergistic effect arising from the blend of different components. Hybrid nanocomposites are generally classified into many groups but are divided into two basic categories of weak chemical bonding and strong chemical bonding. The weak chemical bonding (ionic, hydrogen, and van der-Waals bonds) composites are composed of organic or inorganic materials mixed with an inorganic or organic matrix. The strong chemical bonding composites are combinations of diverse components which are associated at the molecular level [21].

The proposed mechanism for hybrid nanocomposites is as follows: the conduction band and valence band level of one compound in composite would be more negative than other corresponding bands such as the conduction band and valance band [22a], and the electron-hole pairs are produced upon increasing the applied current and concentration of the chemical compound ratio. These excited electrons in one component are confidently transferred from the conduction band of the other compound in the composite because of the potential difference; consecutively the recombination of the electron-hole pairs is promoted, and they perform as a catalyst for the reductive reaction (Fig. 10.7, [22b]). Instead, generated holes moving in the reverse direction from the valance band take part in an opposite manner and the electron-hole

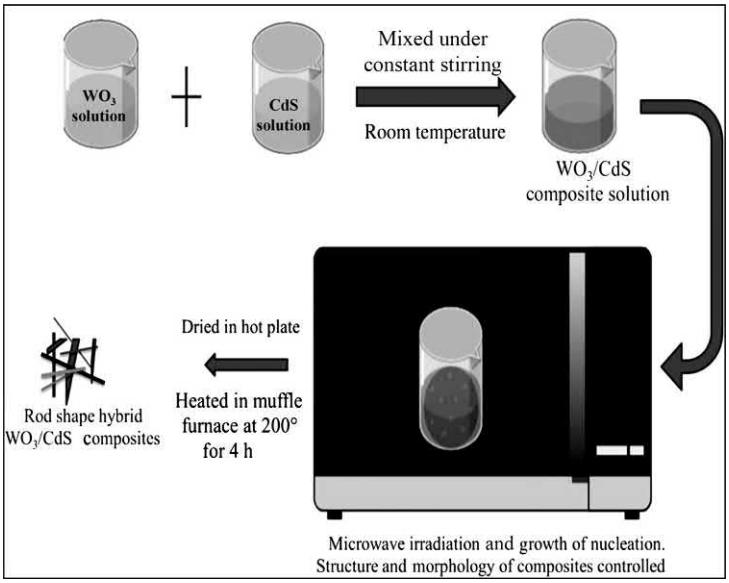
WO_3 solution
CdS solution
Mixed under constant stirring
Room temperature
WO_3/CdS composite solution
Microwave irradiation and growth of nucleation. Structure and morphology of composites controlled
Dried in hot plate
Heated in muffle furnace at 200° for 4 h
Rod shape hybrid WO_3/CdS composites

Fig. 10.7
Schematic diagram of the microwave-assisted method.

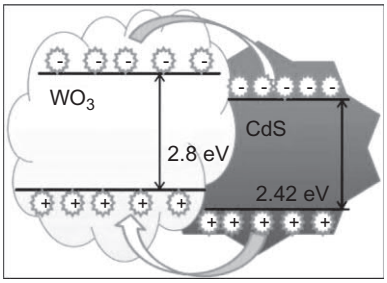

Fig. 10.8
Hybrid WO_3-CdS composite energy level diagram.

recombination possibility is reduced. The efficient charge transfer at the interface of the nanocomposite decreases the possibility of charge carrier recombination and results in the simplistic charge transport of electrons through the active material [23–25] (Fig. 10.8).

10.4.1 Classification of hybrid nanocomposites

A hybrid nanocomposite (NC) is a material fashioned by dispersing inorganic nanoparticles into a macroscopic organic matrix. Hybrid nanocomposites can be distributed into three classes: binary hybrid nanocomposites, ternary hybrid nanocomposites, and multiple hybrid nanocomposites (see Fig. 10.9). A binary hybrid nanocomposite comprises two components containing one nanomaterial; ternary is a composite of three components with one in the nanoscale; and a multiple hybrid comprises more than three components, with at least one of them in the nanoscale.

10.5 Role of the gas sensor in various fields

Recently, a report appeared on the mushrooming start-ups of new industries manufacturing a variety of products for machines, medicine, and combustible gases. Occasional incidents occurring worldwide, like asphyxiations, explosions, and loss of human life, have raised the

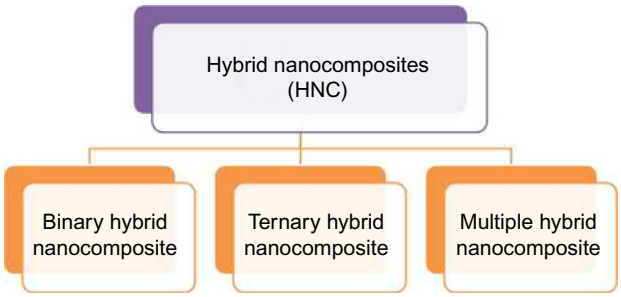

Fig. 10.9
Classification of hybrid nanocomposites.

alarm as to the significance of sensors in industries, and even in the home. The gas sensor is a necessity in helping to prevent such hazards. Gas sensors are used prominently in various fields such as petrochemical industries, scientific research organizations, paramedical industries, food processing, electronic device manufacturing industries, and manufacturing industries such as the motor, power generation, ship, and aircraft industries.

The primary gases released from automobiles are carbon monoxide and nitrogen oxides. Moreover, sulfur oxides released from coal-fired stations cause acid rain and environmental pollution. These factors should be monitored and controlled. Gas sensors in combustion industries provide better monitoring and control of CO, NOx, O_2, CO_2, HCs, and VOC gases and help us to determine the level of toxic gases and save energy. Apart from the manufacturing industries, gas sensors are widely and effectively utilized in food processing. A gas sensor, otherwise known as an e-nose, is used to analyze aromas of prepared and packed food items. The e-nose incorporates some major organizational components, such as artificial neural networks, reference-library databases, and software with digital pattern-recognition algorithms [26–28].

Further, the e-nose is used in analytical chemistry facilities, automobile manufacturing, cosmetics, packing, drugs, and the biomedical field for the advantage of quality control of raw and mass-produced products, and microbial pathogen detection. In addition, gas sensors are now gaining importance in agriculture for the detection of contaminants and pathogens in meat, milk, and milk-related food items; diagnosis of countless diseases in plants and animals; and determination of the quality of agricultural products [29]. Medicine and pharmaceutics are other significant fields in which gas sensors are now being employed. The significant application of gas sensors in medicine is the breath analyzer, in which patient feedback about current state and results of therapy provided can be obtained immediately [30, 31].

10.6 Requirements for a gas sensor

The most important function of any kind of gas sensor is to provide consistent real-time information regarding gas composition in the nearby surroundings. Hence, preferably, a device designed for gas sensing ought to function constantly and also reversibly, exclusive of not disturbing the analytes. Further, the ideal gas sensor should be available at an economical cost and be free of errors, functioning with flawless and instant selectivity with reference to a specific targeted gas in the immediate environs. The device is expected to generate a computable signal output for any optional gas concentration [32]. Fast response, relative temperature and humidity insensitivity, attainment of minimal measuring uncertainty, good resistance to contagion and toxicity, simple fabrication, and low noise are the required useful characteristics of the gas sensor. It is further expected that the ideal gas sensor would be

comfortable for practical usage, such as being portable and compact, not prone to explosions, having low energy consumption, and being suitable for hazardous and harsh locations [33].

As well, employees who are handling the sensor should need only minimal training to carry out the sensor's procedures and care. The gas sensor is supposed to supply repetitive measurements of analytes for a long time. Generally, it is expected that the ideal sensor should provide continuous reliable information without recalibration for at least 30 days. The lifetime of such an ideal gas sensor should be in the range of 2 years, and it should be low in cost and easy to replace. In an environmental monitoring sensor, control over any specified harmful gas is required. Hence, the long-time availability of control and suitability for varying environmental conditions like humidity and temperature, and specific requirements like different gas sensitivity and selectivity, may be imposed on the operation of the gas sensor [34].

10.7 Materials suitable for a gas sensor

Various materials have been extensively researched for the architecture of gas sensors, based on their physicochemical properties [35]. Prototypes of gas sensors based on covalent semiconductors, ionic salts, ionic membranes, semiconducting metal oxides (MOx), polymers, solid electrolytes, organic semiconductors, have been investigated [36–39]. Various materials have shown suitability for gas sensors in a successful manner. The optimization of the gas sensor is carried out by selecting the suitable sensing materials and modeling them into good gas sensing devices. Here, the term optimization has been used in the sense of good selectivity, sensitivity, and quick gas response time of sensors at the expected operating/ambient conditions. Though the requirements of gas sensors have become more multifaceted and specific, and perceptions on the nature of gas-sensing effects more essential, we must consider the following parameters to fully ddunderstand gas sensor implementation:

(a) Low cross-sensitivity
(b) Strong response to the target agent
(c) Low signal sensitivity to a change in air humidity
(d) Short time to operate
(e) Effective economical technology
(f) Broad measuring range
(g) High reproducibility

There has been an increasing demand for a gas sensor with the highest selectivity for the industry and in the home, for security purposes. Therefore, the prime importance is to be given the selection of the materials for gas sensor design (Tables 10.1 and 10.2).

Table 10.1: Comparative analysis of sensors intended for numerous applications of significance.

Analyte	Type of sensor	Reference
CH_4	Semiconductor oxides	[40]
CO	Semiconductor oxides	[41]
CO_2	Solid electrolyte, semiconductor oxides	[34]
Formaldehyde	Polymer and solid-state sensors	[42]
H_2	Semiconductor oxides	[41]
H_2S	Optical	[43]
NH_3	All types of sensors	[44]
NO	Solid electrolyte, semiconductor oxides	[45]
NO_2 (NO_x)	Solid electrolyte, semiconductor oxides	[34]
O_2 (HT)	Solid electrolyte	[46]
O_2 (RT)	Biosensor and electrochemical	[47]
O_3	Optical, electrochemical	[48]
SO_2	Solid electrolyte, semiconductor oxides	[49]
VOCs (hydrocarbons)	All types of sensors	[50]

Table 10.2: Typical materials used in gas sensor.

Material	Examples	Analyte
Cage compounds	Calixarenes, cyclodextrins, crown ethers, cyclophanes, zeolites, etc.	Gases, vapors
Carbon	Black carbon, carbon nanotubes, diamond, graphene, fullerenes	Gases, vapors
Ionic compounds	Ionic conductors [LaF_3, CaF_2, Na_2CO_3, AgCl, etc.]	Gases (CO_2, SO_2, CO), ions
Langmuir-Blodgett films	Phthalocyanines, polydiacetylenes	Gases (NO_2, NH_3, Cl_2), vapors
Metals	Ag Pt, Ni Pd, Au, Rh, Sb	Gases (H_2, O_2, etc.)
Metal oxides	Electronic conductors (SnO_2, TiO_2, In_2O_3, etc.); ionic conductors (ZrO_2, CeO_2, etc.); mixed conductors (Ga_2O_3, WO_3, $SrTiO_3$); metal oxides with metallic-type conductivity (RuO_2, Co_3O_4, PbO*x*, etc.)	Gases (CO, H_2, CH_4, NO_x, O_2, Cl_2, etc). vapor, alcohol; dissolved O_2, Cl_2 in solutions
Molecular crystals	Phthalocyanines [PbPc, $LuPc_2$, LiPc, FePc, etc.]	Gases, vapors
Membranes	Ion-exchange membranes; neutral-carrier membranes; charged carrier membrane	Cations, anions in solutions; gas filtration
Polymers, organic semi-conductors	Polyethers, polyurethanes, polythiophenes, polyolefins, polyphenyl acetylene, polysiloxanes, polypyrroles, etc.	Gases (CO, CO_2, CH_4, NO_x etc.), H_2O, chlorinated, hydrocarbons, etc.
Semi-conductors	Si, GaAs, InP, SiC, GaN, etc.	Gases (O_2, CO_2, H_2S, CH_4, NO_2, O_3, etc.)

10.8 Recent developments in hybrid nanocomposite-based gas sensors

Semiconducting metal oxides are being widely investigated for sensor applications due to their stability, high sensitivity towards target gas, quick response, and low cost. Several metal oxides have been identified as suitable materials for the detecting of combustible, oxidizing, and reducing gases. Although metal oxides have exhibited high sensitivity and chemical stability, two major drawbacks of metal oxides, high intrinsic resistance and low sensitivity at low temperature, highlight the need for alternatives. These drawbacks impede practical implementation, or we could even say they lead to unsafe conditions, due to a lacking in the detection of flammable H_2 gas.

The hybridization of composite materials would satisfy researchers' requirements by combining some extraordinary properties of metal oxides, carbon, and polymers and also some unique features from the hybridization. The as-prepared hybrid nanocomposites are not simply mixes of some individual components but rather are new entries of composite materials with novel properties. Several reports have been published stating improved chemical and gas-sensing properties of hybridized nanocomposites, with excellent recovery time, fast response, and enhanced sensitivity.

10.8.1 Ammonia gas sensor

Ammonia gas (NH_3) is a foremost hazardous gas due to its toxicity; it causes severe health problems to humans, including respiratory system irritation, damage to eyes, and skin problems. The main source of NH_3 gas is industry, mainly chemical manufacturing and refineries and agricultural production. Thus it is most important to detect any leakage or presence of NH_3 gas, in the view of a healthy environment and human safety. Several types of research have been conducted to sense the presence of ammonia in a specified place, such as a factory or even in homes [51–54]. Lin et al. [55] have prepared polyaniline (PANI) @ tungsten oxide (WO_3) nanocomposites by a facile in situ chemical oxidation polymerization method with diverse mole percentages of WO_3 (2%–50%). The gas-sensing performances of as-prepared composites have been demonstrated. The 10 mol% WO_3 loaded PANI showed a maximum response of more or less 20.1–100 ppm of NH_3 at RT, which was six times higher than the response of pure PANI. Further, as-synthesized composites have shown poor detection limits at 500 ppb to NH_3. In addition, PANI@WO_3 composites exhibited fast response and recovery rates around 13 and 49 s. Sakthivel et al. [56] used the surfactant-free hydrothermal method to synthesize a CuO and rGO-CuO nanocomposite for ammonia sensors. The pristine CuO and rGO-CuO composites were subjected to various parameters such as temperature, concentration, and time-dependent NH_3 sensing studies. The rGO-CuO nanocomposite showed increased gas-sensing performance of 13 ppm @RT, and this was 10 times greater than a pristine CuO nanostructure. The rGO-CuO nanocomposite was also taken to test the response of

methanol, ethanol, acetone, and ammonia gases, but it showed the highest response to NH_3 gas compared to the other gases, as shown in Fig. 10.10.

Satish et al. [57] reported a reduced graphene oxide (rGO)-$CuFe_2O_4$ nanocomposite using a one-step and combustion route. Its electrical properties and gas-sensing functions were investigated. The electrical properties of GO, rGO, and $CuFe_2O_4$ nanocomposites were analyzed and the GO had poorer conductivity than the remaining composites (see Fig. 10.11). The reduction of the O^- functional group increased the conductivity of rGO and the $CuFe_2O_4$

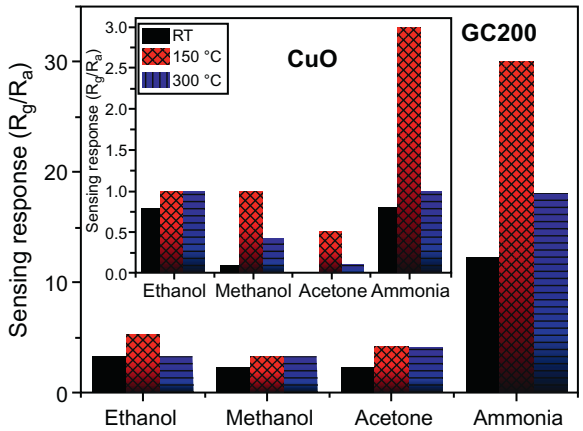

Fig. 10.10

Sensing response of GC200 device to 600 ppm of different gases (inset—sensing response of pristine CuO to different gases).

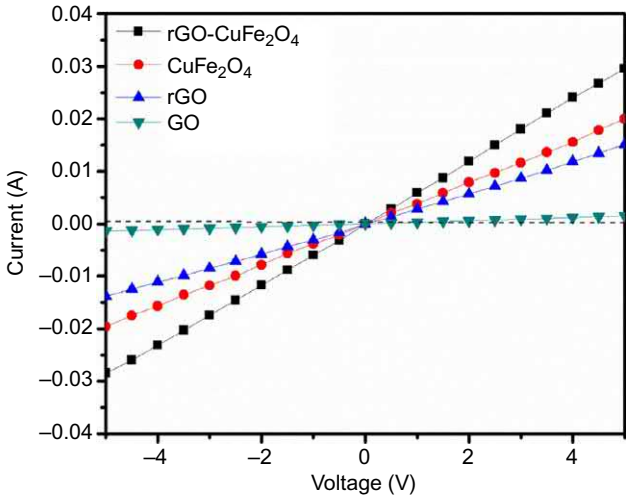

Fig. 10.11

I-V curves of GO, rGO, $CuFe_2O_4$, and rGO-$CuFe_2O_4$ composite-based sensor at RT.

composites demonstrated lower conductivity than rGO-$CuFe_2O_4$. The rGO-$CuFe_2O_4$ nanocomposite showed an NH_3 detection level of 5 ppm (low concentration) at room temperature. These enhanced gas-sensing properties were ascribed to the synergistic effect of the rGO and $CuFe_2O_4$ components.

Paul Le Maout et al. [58] designed a portable ammonia sensor to analyze breath. An increase in the amount of NH_3 gas in human breath indicates several diseases, mainly kidney failure, which is clinically silent and difficult to detect. For this study, they framed a portable system and 11 different polyaniline nanocomposites of a conductometric array sensor were used. This method allows determining the ammonia in human breath in a range of 500 ppb–2100 ppb. Titanium dioxide and CNT loaded polyaniline provided different sensitivities and response times. From the response curve, the maximum variation in resistance and derivative are extracted.

Poloju et al. [59] prepared ZnO (NPs), ZnO/CuO, and Al-ZnO/CuO nanocomposites by coprecipitation trailed by the sol-gel method for NH_3 gas sensing. The Al-ZnO/CuO composite showed an enhanced sensing response upon increasing the concentration of NH_3 gases and it was drastically increased over ZnO and CuO/ZnO nanocomposites. Further, the sensing response of an AlZnO/CuO composite estimated for 200 ppm of different VOC gases at room temperature was also examined, as shown in Fig. 10.12. An essential parameter of gas sensor is long-term stability, which determines the practical applications, and the Al-ZnO/CuO composite sensor test was conducted for 12 days under 500 ppm concentrated ammonia at RT. The response of the Al-ZnO/CuO composite towards NH_3 gas was nearly constant and indicated excellent stability of as-prepared nanocomposites.

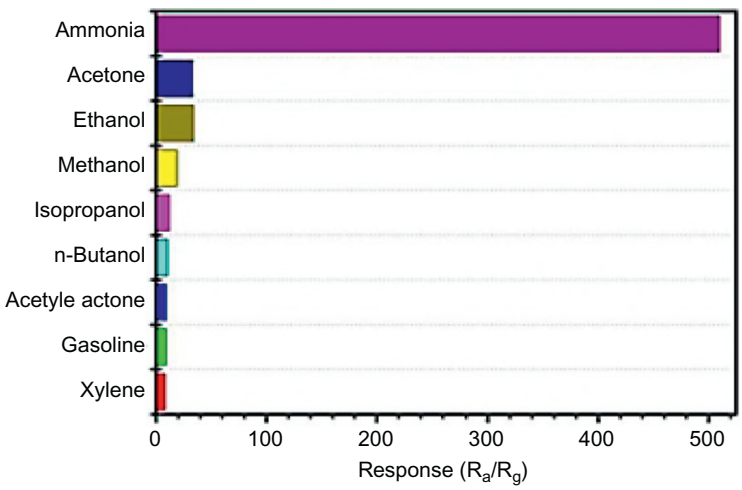

Fig. 10.12
The response of the Al-ZnO/CuO at a concentration of 200 ppm of different VOC gases.

Kulkarni et al. [60] reported that a flexible NH_3 gas sensor using a polyaniline and PANI-WO_3 hybrid nanocomposite was efficaciously prepared using the in-situ chemical oxidative polymerization process. The NH_3 gas analysis showed pure PANI having a moderate response, 53%, towards 100 ppm of NH_3 gas, and a poor response towards other gases, including NO_2, H_2S, CH_3OH, and C_2H_5OH vapors, was observed. Interestingly, the PANI-WO_3 flexible sensor showed higher selectivity concerning ammonia gas. Further, it was observed that 50 wt% WO_3 content showed excellent selectivity to ammonia gas and the PANI-WO3 hybrid sensor detected 1 ppm concentration of NH_3 with good stability and reproducibility.

Abdulla et al. [61] prepared a PANI/MWCNTs nanocomposite for trace level detection of NH_3 gas by in-situ chemical oxidative polymerization (iCOP). The I-V characterization of C-MWCNT and PANI/MWCNT showed ohmic behavior in the range of −1 to +1 V and evidenced that the charge carrier flows between sensing material to the gold electrode material. Gas analysis of a C-MWCNT and PANI/MWCNTs nanocomposite to ammonia at 2–10 ppm was conducted. The response time of the C-MWCNT sensor was estimated to be 965 s and for the PANI/MWCNT sensor was reduced to 6 s. A PANI-CeO_2 nanocomposite thin film [62] was prepared for a resistive-type flexible NH_3 sensor. CeO_2 nanoparticles have helped to modify the microstructures of PANI and enhanced its degree of protonation and oxidation. Ammonia gas-sensing performance was conducted at room temperature and sensing analysis showed that the PANI-CeO_2 film exhibited good response, good reproducibility, reduced recovery time, perfect response to concentration linearity, excellent selectivity, ultralow concentration detection (16 ppb), noteworthy long-term stability, and outstanding flexibility (Fig. 10.13).

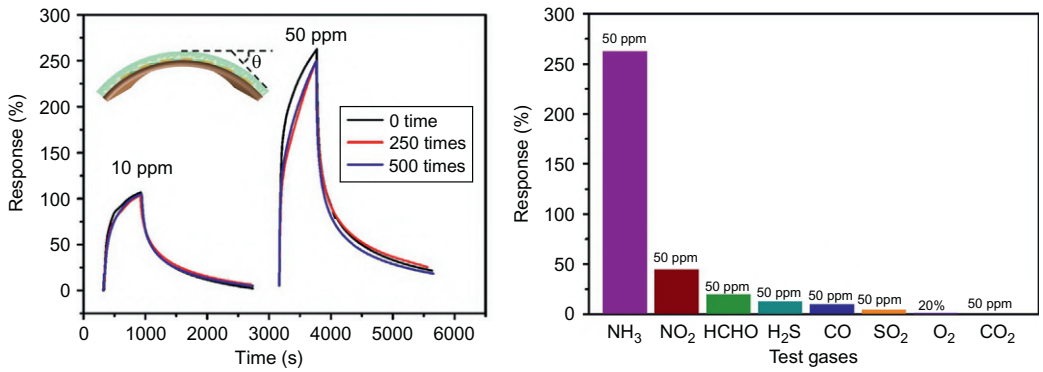

Fig. 10.13
The dynamic response-recovery curves of PANI-CeO_2 film sensor towards NH_3 and various gases at 10 and 50 ppm concentrations.

Andre et al. [63] reported the hybrid nanocomposite (NFI-rGO) combining In_2O_3 ceramic nanofibers (NFI) and reduced graphene oxide (rGO) prepared by the electrospinning (ES) technique was shadowed by calcination treatment. The gas-sensing performance was analyzed at room temperature for different gas ranges (1–60 ppm). The hybrid nanocomposite displayed higher electrical properties and selectivity than any other distinct material. The NFI-rGO showed the best performance, with a quicker response of 10 times, than NFI and rGO materials. This points out that NFI-rGO is more suitable for NH_3 sensing than pure NFI and rGO. This relates to the formation of the p-n heterojunction and synergistic effect amid NFI and rGO sheets.

Kulkarni et al. [64] lucratively synthesized PAni-WO_3 hybrid nanocomposites by the in-situ chemical oxidative polymerization process. The PAni matrix porosity was increased by loading the WO_3 nanoparticle, which supported the enhanced gas sensing properties. The as-prepared PAni-WO_3 hybrid nanocomposite was exposed to various oxidizing and reducing gases at the range of 5–100 ppm concentration. The PAni-WO_3 hybrid nanocomposites exhibited good stability, selectivity, sensitivity, and reproducibility when compared to pure PAni and WO_3. The 50% loaded WO_3 hybrid nanocomposite showed a maximum response of 158% for 100 ppm of NH_3 gas and was able to respond to the 5 ppm NH_3 gas with a rational response of 24%. The selectivity of PAni, WO_3, and PAni-WO_3 is shown in Fig. 10.14.

Huang et al. [65] invented a 3D framework of rGO by a combination of a 3D structural design and chemical functionalization techniques. At room temperature, the chemical modification was carried out in order to improve the selectivity and sensitivity of NH_3. The gas-sensing test was conducted for SiO_2-CRGO, SiO_2-TRGO, and bare CRGO for the various NH_3 gas concentrations in the range of 5 to 100 ppm. The CRGO sensor showed 0.5% of the response to 5 ppm of NH_3 gas and the SiO_2-TRGO composite showed 2.5% of the response. But, when NH_3 concentrations were increased to 100 ppm, the CRGO response was increased to 12.5%, and SiO_2-TRGO showed only 7.6%. The oligomer layers produced in the reducing process were deduced to be the important factor for improved performance of the doping/dedoping mechanism. Consequently, the selectivity of NH_3 was significantly improved.

10.9 Hybrid nanocomposites as biosensors

Biosensors with the benefits of sensitivity, robustness, swiftness, and suitability were established in various analyses. Modified nanomaterials were considered for the phenomenon of biosensing for their accuracy and ease of analysis. Nevertheless, the nanomaterials are typically functionalized or combined with other inorganic and organic functional materials/nanomaterials to form the nanocomposites for advanced practical applications. Hybrid nanocomposites that are superior to solitary nanomaterials have been used as superior modifications instead of nanomaterials for biosensors. This section explores the latest available current and selective hybrid nanocomposite-based biosensors.

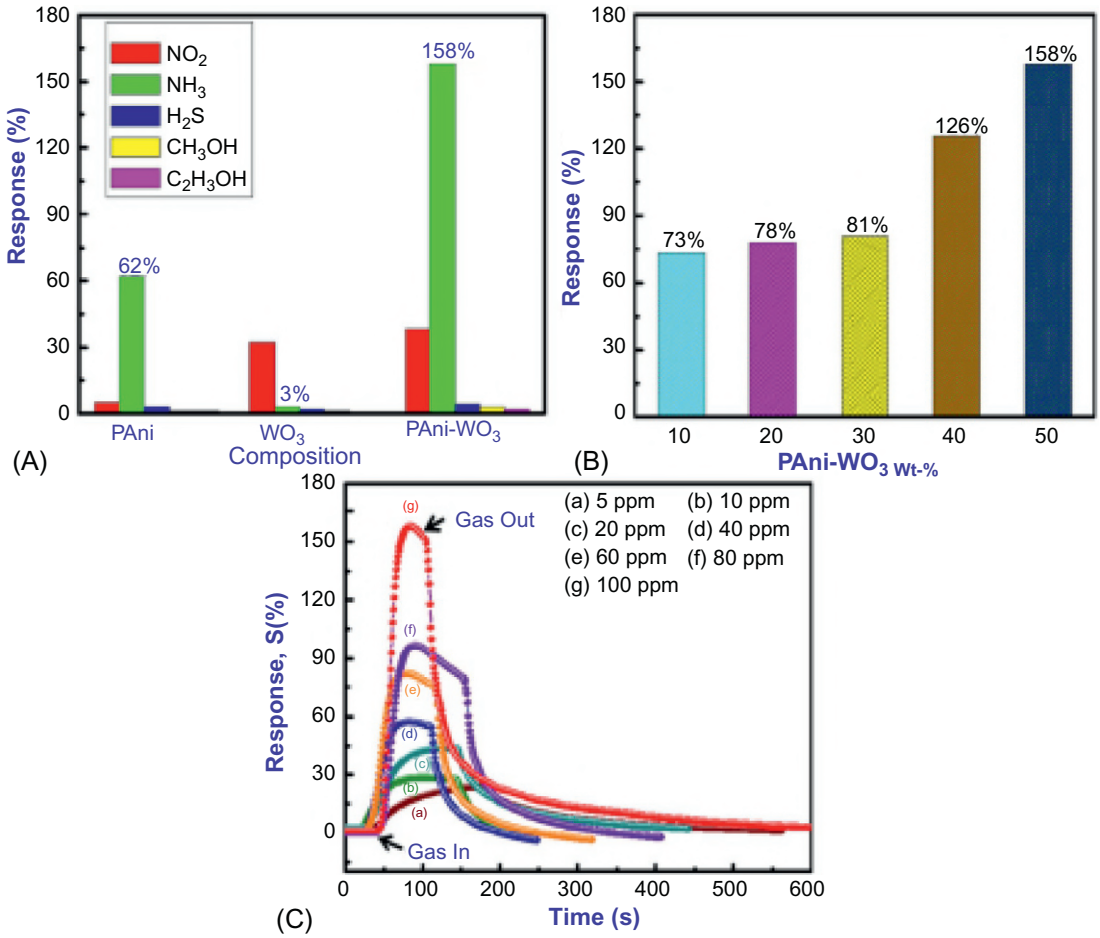

Fig. 10.14

(A) Selectivity of PAni, WO_3, and PAni-WO_3 (50%) for different test gases. (B) The response of PAni-WO_3 (10%–50%) hybrid NCs. (C) The response of PAni-WO_3 (50%) hybrid NCs to 5–100 ppm of NH_3 gas.

10.9.1 Electrochemical/glucose/graphene-based biosensors

Hybrid nanocomposites are widely used for biomedical applications developed using modified Au NP-graphene oxide sheet (AuNP-GO) nanocomposite, detecting two different interactions between proteins and hybrid nanocomposites. GO sheets have great bioaffinity, and they also enable the binding of biomolecules to carboxyl groups, which led to the development of precise sensing mechanisms. GO sheets, when decorated with AuNPs, bring together localized surface plasmon resonance (LSPR) in the resonance energy transfer of spectral changes. The results obtained by the modified AuNP-GO sheet in the detection of antiBSA (10 ng/mL of hCG nonspecific interfering protein) had dynamic responses ranging from 1.45 nM to 145 fM, and an LOD of 145 fM [66].

A hybrid nanocomposite consisting of Cu nanowires (Cu NWs) and graphene (GR)/CTS served as an outstanding catalyst for methyl parathion electrooxidation, prepared via a modest approach to achieve mixed Cu NWs/GNs-Chit hybrid nanocomposites. The combination then formed an assembly similar to an overhead network, providing an advantageous platform for the electrochemical methyl parathion detection. The electrochemical characterization of the Cu NWs/GNs-Chit modified electrode via specific adsorption was estimated using cyclic voltammetry (CV) and square wave voltammetry (SWV). The results highlight the applicability of CuNWs/GNs-Chit hybrid nanocomposites for fast, simple, sensitive, and selective analysis, opening a new avenue in monitoring offering precise detection of methyl parathion residues with good reproducibility and stability. The sensor shows specific and outstanding performance, with high sensitivity, high selectivity, and wide dynamic range in the quantification of methyl parathion [67].

Recently, the development of rare-earth metal nanocomposites has gained attention. Noble metals have been used in most graphene–metal nanocomposites for biosensing. Mediator-free enzymatic biosensors have a nanoceria–nano platinum–graphene hybrid nanocomposite as a base transducing layer. The hybrid nanocomposite exhibited improved detection of superoxide or hydrogen peroxide compared to other carbon-metal hybrid nanocomposites. Glucose biosensors demonstrated sensitivity (66.2 ± 2.6 μAm/M/cm^2), with 6.3 ± 3.4 s response time and 1.3 ± 0.6 μM as the limit of detection, which was analogous to other graphene-mediated electrodes from the latest literature. Strangely, an XOD biosensor with 1164 ± 332 μAm/M sensitivity, 5.0 ± 1.5 s response time, and 0.2 ± 0.1 μM as a limit of detection was higher than any stated biosensors using analogous metal-decorated carbon nanomaterials [68].

Chitin and chitosan are noticeably versatile and promising biomaterials as nanoparticles (NP) and nanocomposites (NC). These nanostructured composites are applied for the determination of biologically important analytes such as cholesterol; dopamine, glucose, urea and hydrogen peroxide are reported. Moreover, chitosan-based hybrid nanocomposite biosensors are swift, economical, highly durable, and offer precise measurements, providing exciting new opportunities for the growth of biosensor capabilities [69]. A high-performance multifunctional biosensor was prepared from Fe_3O_4 (magnetite) nanoparticle-modified chitosan/graphene nanocomposites. This biosensor exhibited good glucose detection with a low detection limit of 16 μM, a sensitivity of 5.658 mA/cm^2/M, and a linear detection as high as 26 mM glucose.

Creation of multifunctional MNP/CG nanocomposites offers extra advantages for applications in more clinical areas, such as in vivo biosensors and MRI agents [70]. Another study reports glucose oxidase (GO_x) immobilized cellulose–tin oxide (SnO_2) HNC as a glucose biosensor. The enzyme (GO_x) was immobilized into a cellulose–SnO_2 hybrid nanocomposite by the physical absorption method [71]. A simple electrochemical biosensor for 4-chlorophenol based on laccase immobilized on a hybrid nanocomposite (ZnO nanoparticles/chitosan) and combined in a carbon paste electrode was developed. Differential pulse voltammetry was used

for constructing a calibration curve for 4-chlorophenol and a linear response was obtained from 1 to 50 μM, with a lower detection limit of 0.75 μM. The attained biosensor showed extraordinary accuracy [72].

The huge surface area and decent electrical conductivity of graphene suggest that graphene is a prospective candidate as a sensor material. A bionanocomposite film sensor containing glucose oxidase/Pt/functional graphene sheets/chitosan (GOD/Pt/FGS/chitosan) for sensing glucose was established with good reproducibility, long-term stability, and nearly zero to insignificant interfering signals from ascorbic acid or uric acid, compared with the response to glucose. This novel complex hybrid nanocomposite glucose sensor provides new possibilities in clinical diagnosis and point-of-care uses [73].

Using a glucose oxidase (GOx) immobilized TiO_2-cellulose hybrid nanocomposite, a conductometric glucose biosensor was developed. A cellulose solution was prepared by dissolving cotton pulp with lithium chloride/*N*, *N*-dimethyl acetamide solvent. TiO_2 NPs blended with cellulose solution to produce a TiO_2-cellulose hybrid nanocomposite. TiO_2-cellulose hybrid material serves as a probable candidate for developing an inexpensive disposable glucose biosensor having a linear response in the range 1–10 mM and a correlation coefficient of 0.9993 [74].

10.9.2 Xanthine biosensors

Hybrid nanocomposite-containing multiwalled carbon nanotubes (MWCNTs), Pt nanoparticles (PtNPs), and gold nanoparticles (AuNPs) were used as a xanthene biosensor in synthetic serum samples; the biosensor was fabricated by dropping AuNP/PtNP/MWCNT onto a xanthine oxidase (XO) modified glassy carbon paste electrode (GCPE). The XO/AuNP/PtNP/MWCNT/GCPE biosensor showed linearity between 2.0 and 50 μM and 0.25 and 6.0 mM for xanthene [75].

A chitosan-polypyrrole-gold bionanocomposite for construction of a highly sensitive amperometric biosensor that has been developed for the determination of xanthine in fish and beef samples and chicken real-sample measurements. The biosensor exhibited a very good linear range of 1–200 μM, a low detection limit of 0.25 μM, an average response time of 8 s, and was not prone to significant interference from uric acid, ascorbic acid, glucose, and sodium benzoate [76]. NiONPs/GO with polyaniline had an active surface area of 0.378 cm^2 for glucose sensing [77a].

In the layout of the amperometric xanthine biosensor, chitosan/polypyrrole/gold nanoparticles synthesized by an in situ chemical synthesis method on a GCE surface was used to enhance electron transfer and to provide good enzyme affinity. A novel xanthine biosensor, based on a hybrid bionanocomposite platform, has been successfully designed in the evaluation of freshness of meat. The electrochemical biosensor exhibited a very good linear range of

1e200 mM, with a low detection limit of 0.25 mM and an average response time of 8 s, and was not prone to any noteworthy interference from uric acid [77b].

10.9.3 Cancer biosensor

Cancer markers (especially prostate-specific antigen, PSA) are specific molecules existing in blood or tissue, whose measurement or identification is considered very critical and efficient in cancer prediction, diagnosis, and monitoring. Reports have suggested three types of Gr-based composites were synthesized (from pure to hybrid) for the production of PSA biosensors. The self-assembled graphene biosensor established the finest detection limits and sensitivity, while the pure graphene with microfluidic induced graphene biosensor displayed better accuracy and stability [78].

10.9.4 Food biosensors

The quantitative determination of nitrite, aspartame, and vitamin B9 was carried out using ZnONPs/CNTs composites. ZnO nanoparticles with an average size of 100–200 nm form due to the hydrogen bonds between the carboxyl groups and oxygen of electrodeposited ZnO. [79] The surface of MWCNTs developed thousands of carboxyl terminals after acidification and was fully concealed by dispersible ZnO NPs.

Coapplicable nanocomposites (CANCs) were formed between graphene and metals/MOx. Nanometals such as Cu, Pt, Ni, Au, and their metal oxides were used for the cohesion with the graphene family to form CANCs. The charge transfer resistance [80] value was the lowest for CuNPs/NGr and with greatest electrochemical response intensity, showing that electron transfer was easier due to the presence of Cu NPs onto nitrogen-doped graphene towards glucose.

A cssDNA/GO/CS/GCE biosensor using differential pulse voltammetry (DPV) to distinguish complementary, 1-base mismatched DNA, 2-base mismatched DNA, and multibase mismatched DNA shown decent specificity and outstanding ability. This developed research strategy exposed that the GO/CS modified electrode holds an admirable performance in identifying *Escherichia coli* O157:H7 DNA [81].

10.10 Conclusions, outlook, and future scope

Materials science and engineering are playing a very important role in our day-to-day life, especially in the development of new materials. With nanotechnology infiltrating into the market for some niche applications, it may take another decade before it has a major impact on the market. There have been several exciting advancements in the field of materials science in the past quarter-century, with many researchers generating enthusiasm and excitement in

different materials research, especially hybrids, composites, and hybrid nanocomposites. Hybrid nanocomposite materials hold the potential to redefine the field of traditional composite materials, both in terms of performance and prospective applications. It is virtually certain that hybrid nanocomposites have a tremendous market potential, both as replacements for current composites and in the creation of new markets through their outstanding properties.

Hybrid nanocomposites find their place in different sectors of research and application, which is highly promising and are also drawing increasing investment from governments and businesses in many parts of the world. Nanocomposites are being increasingly developed for precise, steadfast, accurate chemical and biosensing, and also for the diagnosis of manifold infections and diseases in health care, promising new horizons for novel functions with a variety of applications in gas sensing and biosensing in clinical and nonclinical diagnostics. Hybrid nanocomposites show encouraging growth in technology and applications, while emerging as one of the priority materials, both as a material and as a composite. However, many challenges still remain to be addressed and resolved before realizing these nanocomposites' utilization to their fullest potential, regarding synthesis methods, costs, and applications.

Graphene-based hybrid nanocomposites have displayed many extraordinary properties, while graphene-based materials have a wide range of potential applications, such as a flexible transparent electrode, sensors, and electronic components. Due to the high diversity, properties, and advantages of graphene, a multitude of nanocomposite-based practical applications have been envisioned. Applications of graphene-based polymer nanocomposites are multidirectional, in almost all the fields. Moreover, the scale-up of fabricating graphene-based materials at reasonable cost is still extremely challenging. However, these multifunctional graphene composites at affordable cost will soon be seen in the global market. Essentially, the potential health risks of graphene-based hybrid nanocomposite materials need to be evaluated before large-scale utilization. Hybrid nanocomposites are among the top 10 breakthroughs in materials science; some of the trending areas of discovery, application, and commercial interest are:

- Research in materials science will continue, to identify the countless applications of hybrid nanocomposites.
- Present commercial applications of carbon nanotube-based composites in combination with other materials will likely play a central role in emerging nanoscience, engineering, and technology.
- Hybrid nanocomposites will be used in racecars and bikes, among other engineering applications.
- Academics often lead the way in this research, with breakthroughs.
- Allocation of government research funding for innovations will take place.
- Outside of governments, industries, and institutions of higher education, direct investment in materials science research could come from corporations.

The dominance of hybrid nanocomposites stems from easy admission of diverse materials as precursor materials, the cost, and its orientation flexibility (morphology). Hybrid nanocomposites' current potential applications are astounding and could revolutionize many products, markets, and fields, which could include waterproofing materials, energy storage, electronics, sensing, water purification, biomedical, medicine, air filters for purification, biofilters, potential material for applications in 3D printing, potential applications in optoelectronic and photovoltaic fields, and even computing to some extent. In this chapter, from the field of materials science, hybrid nanocomposites have been highlighted and reviewed for their applications and for the most promising developments, in an attempt to introduce all the latest and potential applications of hybrid nanocomposites as nanosensors, both for gases and bio-related molecules.

Conflicts of interest

The authors declare no conflicts of interest.

References

[1] E.L. Wolf, Nanophysics and Nanotechnology, Wiley-VCH, Weinheim, 2004.
[2] B. Bhushan (Ed.), Springer Handbook of Nanotechnology, Springer, 2017.
[3] D. Schaming, H. Remita, Nanotechnology: from the ancient time to nowadays, Found. Chem. 17 (3) (2015) 187–205.
[4] N. Malanowski, T. Heimer, W. Luther, M. Werner (Eds.), Growth Market Nanotechnology: An Analysis of Technology and Innovation, John Wiley & Sons, 2008.
[5] Y. Chen, Z. Fan, Z. Zhang, W. Niu, C. Li, N. Yang, B. Chen, H. Zhang, Two-dimensional metal nanomaterials: synthesis, properties, and applications, Chem. Rev. 118 (13) (2018) 6409–6455.
[6] K. Jagiello, B. Chomicz, A. Avramopoulos, A. Gajewicz, A. Mikolajczyk, P. Bonifassi, M. G. Papadopoulos, J. Leszczynski, T. Puzyn, Size-dependent electronic properties of nanomaterials: how this novel class of nanodescriptors supposed to be calculated? Struct. Chem. 28 (3) (2017) 635–643.
[7] L.E. Murr, L.E. Murr, Classifications and structures of nanomaterials, in: Handbook of Materials Structures, Properties, Processing and Performance, Springer, 2017, pp. 1–29.
[8] R. Zhang, J. Jia, J.L. Cao, Y. Wang, SnO_2/graphene nanoplatelet nanocomposites: solid-state method synthesis with high ethanol gas-sensing performance, Front. Chem. 6 (2018) 337.
[9] Y. Cao, D. Jia, J. Zhou, Y. Sun, Simple solid-state chemical synthesis of $ZnSnO_3$ nanocubes and their application as gas sensors, Eur. J. Inorg. Chem. 2009 (27) (2009) 4105–4109.
[10] Y. Tang, X. Wang, Q. Zhang, Y. Li, H. Wang, Solvothermal synthesis of $Co1-xNixFe_2O_4$ nanoparticles and its application in ammonia vapours detection, Prog. Nat. Sci. Mater. Int. 22 (1) (2012) 53–58.
[11] J.W. Gong, X.F. Wan, Hydrothermal synthesis of different nanostructure MoO3 sensing materials: application for transformer fault diagnosis, Mater. Technol. 30 (6) (2015) 332–337.
[12] W. Chen, H. Gan, W. Zhang, Z. Mao, Hydrothermal synthesis and hydrogen sensing properties of nanostructured SnO_2 with different morphologies, J. Nanomater. 2014 (2014) 7.
[13] A. Boudiba, C. Zhang, C. Bittencourt, P. Umek, M.G. Olivier, R. Snyders, M. Debliquy, Hydrothermal synthesis of two dimensional WO3 nanostructures for NO_2 detection in the ppb-level, Procedia Eng. 47 (2012) 228–231.
[14] H. Hayashi, Y. Hakuta, Hydrothermal synthesis of metal oxide nanoparticles in supercritical water, Materials 3 (7) (2010) 3794–3817.

[15] A. Rabenau, The role of hydrothermal synthesis in preparative chemistry, Angew. Chem. Int. Ed. Eng. 24 (12) (1985) 1026–1040.
[16] M. Fernandez-Garcia, A. Martinez-Arias, J.C. Hanson, J.A. Rodriguez, Nanostructured oxides in chemistry: characterization and properties, Chem. Rev. 104 (9) (2004) 4063–4104.
[17] (a)D. Susanti, A.G.P. Diputra, L. Tananta, H. Purwaningsih, G.E. Kusuma, C. Wang, S. Shih, Y. Huang, WO_3 nanomaterials synthesized via a sol-gel method and calcination for use as a CO gas sensor, Front. Chem. Sci. Eng. 8 (2) (2014) 179–187. (b)B.G. Rao, D. Mukherjee, B.M. Reddy, Novel approaches for the preparation of nanoparticles, in: D.F.A. Grumezescu (Ed.), Nanostructures for novel therapy, Synthesis, Characterization and Applications, first ed., Elsevier, hardcover, ISBN: 9780323461429, 2017, pp. 1–36.
[18] C.S. Kim, K. Okuyama, K. Nakaso, M. Shimada, Direct measurement of nucleation and growth modes in titania nanoparticles generation by a CVD method, J. Chem. Eng. Japan 37 (11) (2004) 1379–1389.
[19] (a)in: S. Horikoshi, N. Serpone (Eds.), Microwaves in Nanoparticle Synthesis: Fundamentals and Applications, John Wiley & Sons, 2013. (b)P. Periasamy, T. Krishnakumar, M. Sandhiya, M. Sathish, M. Chavali, P. F. Siril, V.P. Devarajan, Electrochemical investigation of hybridized WO_3–CdS semiconducting nanostructures prepared by microwave-assisted wet chemical route for supercapacitor application, J. Mater. Sci. Mater. Electron. 30 (10) (2019) 9231–9244.
[20] N. Aich, J. Plazas-Tuttle, J.R. Lead, N.B. Saleh, A critical review of nanohybrids: synthesis, applications, and environmental implications, Environ. Chem. 11 (6) (2014), https://doi.org/10.1071/EN14127.
[21] M.A. Aegerter, N. Leventis, M.M. Koebel, Advances in sol-gel derived materials and technologies, in: Aerogels Handbook, Springer, New York, NY, 2011.
[22] (a)M.A. Butler, D.S. Ginley, Prediction of flat band potentials at semiconductor-electrolyte interfaces from atomic electronegativities, J. Electrochem. Soc. 125 (2) (1978) 228–232. (b)P. Periasamy, T. Krishnakumar, M. Sandhiya, M. Sathish, M. Chavali, P.F. Siril, V.P. Devarajan, Electrochemical investigation of hybridized WO 3–CdS semiconducting nanostructures prepared by microwave-assisted wet chemical route for supercapacitor application, J. Mater. Sci. Mater. Electron. 30 (10) (2019) 9231–9244.
[23] H. Kim, Y. Tak, K. Senthil, J. Joo, S. Jeon, K. Yong, Novel heterostructure of CdS nanoparticle/WO_3 nanowhisker: synthesis and photocatalytic properties, J. Vac. Sci. Technol. B 27 (5) (2009) 2182–2186.
[24] S.J. Hong, S. Lee, J.S. Jang, J.S. Lee, Heterojunction $BiVO_4$/WO_3 electrodes for enhanced photoactivity of water oxidation, Energy Environ. Sci. 4 (5) (2011) 1781–1787.
[25] P. Prasannalakshmi, N. Shanmugam, A.S. Kumar, Electrochemistry of TiO_2/CdS composite electrodes for supercapacitor applications, J. Appl. Electrochem. 47 (8) (2017) 889–903.
[26] B.R. Kowalski, C.F. Bender, Pattern recognition. A powerful approach to interpreting chemical data, J. Am. Chem. Soc. 94 (16) (1972) 5632–5639.
[27] M.S. Freund, N.S. Lewis, A chemically diverse conducting polymer-based "electronic nose", Proc. Natl. Acad. Sci. U. S. A. 92 (7) (1995) 2652–2656.
[28] A. Wilson, M. Baietto, Applications and advances in electronic-nose technologies, Sensors 9 (7) (2009) 5099–5148.
[29] R.F. Taylor, Chemical and Biological Sensors: Markets and Commercialization, Institute of Physics, Philadelphia, PA, 1996, pp. 553–579.
[30] K.L. Moskalenko, A.I. Nadezhdinskii, I.A. Adamovskaya, Human breath trace gas content study by tunable diode laser spectroscopy technique, Infrared Phys. Technol. 37 (1) (1996) 181–192.
[31] S.A. Kharitonov, P.J. Barnes, Clinical aspects of exhaled nitric oxide, Eur. Respir. J. 16 (4) (2000) 781–792.
[32] C.K. Ho, M.T. Itamura, M. Kelley, R.C. Hughes, Review of chemical sensors for in-situ monitoring of volatile contaminants (Sandia report), (2001) 28.
[33] J. Chou, Hazardous Gas Monitors: A Practical Guide to Selection, Operation and Applications, McGraw-Hill Professional Publishing, 2000.
[34] N. Yamazoe, N. Miura, Environmental gas sensing, Sensors Actuators B Chem. 20 (2–3) (1994) 95–102.
[35] G. Korotcenkov, B.K. Cho, Porous semiconductors: advanced material for gas sensor applications, Crit. Rev. Solid State Mater. Sci. 35 (1) (2010) 1–37.

[36] W. Göpel, Ultimate limits in the miniaturization of chemical sensors, Sensors Actuators A Phys. 56 (1–2) (1996) 83–102.
[37] J.E. Haugen, K. Kvaal, Electronic nose and artificial neural network, Meat Sci. 49 (1998) S273–S286.
[38] B. Adhikari, S. Majumdar, Polymers in sensor applications, Prog. Polym. Sci. 29 (7) (2004) 699–766.
[39] G. Eranna, B.C. Joshi, D.P. Runthala, R.P. Gupta, Oxide materials for the development of integrated gas sensors—a comprehensive review, Crit. Rev. Solid State Mater. Sci. 29 (3–4) (2004) 111–188.
[40] S. Basu, P.K. Basu, Nanocrystalline metal oxides for methane sensors: role of noble metals, J. Sensors 2009 (2009).
[41] V. Aroutiounian, Metal oxide hydrogen, oxygen, and carbon monoxide sensors for hydrogen setups and cells, Int. J. Hydrog. Energy 32 (9) (2007) 1145–1158.
[42] J. Flueckiger, F. Ko, K. Cheung, Microfabricated formaldehyde gas sensors, Sensors 9 (11) (2009) 9196–9215.
[43] M.M. Choi, P. Hawkins, Development of an optical hydrogen sulphide sensor, Sensors Actuators B Chem. 90 (1–3) (2003) 211–215.
[44] S.G. Sazhin, E.I. Soborover, S.V. Tokarev, Sensor methods of ammonia inspection, Russ. J. Nondestruct. Test. 39 (10) (2003) 791–806.
[45] F. Menil, V. Coillard, C. Lucat, A critical review of nitrogen monoxide sensors for exhaust gases of lean-burn engines, Sensors Actuators B Chem. 67 (1–2) (2000) 1–23.
[46] W.C. Maskell, Inorganic solid-state chemically sensitive devices: electrochemical oxygen gas sensors, J. Phys. E 20 (10) (1987) 1156.
[47] A.M. Azevedo, D.M.F. Prazeres, J.M. Cabral, L.P. Fonseca, Ethanol biosensors based on alcohol oxidase, Biosens. Bioelectron. 21 (2) (2005) 235–247.
[48] D.D. Parrish, F.C. Fehsenfeld, Methods for gas-phase measurements of ozone, ozone precursors and aerosol precursors, Atmos. Environ. 34 (12–14) (2000) 1921–1957.
[49] N. Yamazoe, N. Miura, Prospect and problems of solid electrolyte-based oxygenic gas sensors, Solid State Ionics 86 (1996) 987–993.
[50] B. Pejcic, P. Eadington, A. Ross, Environmental monitoring of hydrocarbons: a chemical sensor perspective, Environ. Sci. Technol. 41 (18) (2007) 6333–6342.
[51] B. Timmer, W. Olthuis, A. Van Den Berg, Ammonia sensors and their applications—a review, Sensors Actuators B Chem. 107 (2) (2005) 666–677.
[52] A. Kaushik, R. Kumar, S.K. Arya, M. Nair, B.D. Malhotra, S. Bhansali, Organic-inorganic hybrid nanocomposite-based gas sensors for environmental monitoring, Chem. Rev. 115 (11) (2015) 4571–4606.
[53] C.M. Leung, C.L. Foo, Mass ammonia inhalational burns-experience in the management of 12 patients, Ann. Acad. Med. Singap. 21 (5) (1992) 624–629.
[54] N. Docquier, S. Candel, Combustion control and sensors: a review, Prog. Energy Combust. Sci. 28 (2) (2002) 107–150.
[55] S. Li, P. Lin, L. Zhao, C. Wang, D. Liu, F. Liu, P. Sun, X. Liang, F. Liu, X. Yan, Y. Gao, The room temperature gas sensor based on polyaniline@ flower-like WO3 nanocomposites and flexible PET substrate for NH_3 detection, Sensors Actuators B Chem. 259 (2018) 505–513.
[56] B. Sakthivel, G. Nammalvar, Selective ammonia sensor based on copper oxide/reduced graphene oxide nanocomposite, J. Alloys Compd. 788 (2019) 422–428.
[57] L.S.K. Achary, A. Kumar, B. Barik, P.S. Nayak, N. Tripathy, J.P. Kar, P. Dash, Reduced graphene oxide-$CuFe_2O_4$ nanocomposite: a highly sensitive room temperature NH_3 gas sensor, Sensors Actuators B Chem. 272 (2018) 100–109.
[58] P. Le Maout, J.
L. Wojkiewicz, N. Redon, C. Lahuec, F. Seguin, L. Dupont, S. Mikhaylov, Y. Noskov, N. Ogurtsov, A. Pud, Polyaniline nanocomposites based sensor array for breath ammonia analysis. Portable e-nose approach to the non-invasive diagnosis of chronic kidney disease, Sensors Actuators B Chem. 274 (2018) 616–626.
[59] M. Poloju, N. Jayababu, M.R. Reddy, Improved gas sensing performance of Al-doped ZnO/CuO nanocomposite based ammonia gas sensor, Mater. Sci. Eng. B 227 (2018) 61–67.

[60] S.B. Kulkarni, Y.H. Navale, S.T. Navale, F.J. Stadler, N.S. Ramgir, V.B. Patil, Hybrid polyaniline-WO3 flexible sensor: a room temperature competence towards NH_3 gas, Sensors Actuators B Chem. 288 (2019) 279–288.

[61] S. Abdulla, T.L. Mathew, B. Pullithadathil, Highly sensitive, room temperature gas sensor based on polyaniline-multi walled carbon nanotubes (PANI/MWCNTs) nanocomposite for trace-level ammonia detection, Sensors Actuators B Chem. 221 (2015) 1523–1534.

[62] C. Liu, H. Tai, P. Zhang, Z. Yuan, X. Du, G. Xie, Y. Jiang, A high-performance flexible gas sensor based on self-assembled PANI-CeO_2 nanocomposite thin film for trace-level NH_3 detection at room temperature, Sensors Actuators B Chem. 261 (2018) 587–597.

[63] R.S. Andre, L.A. Mercante, M.H. Facure, L.H. Mattoso, D.S. Correa, Enhanced and selective ammonia detection using In2O3/reduced graphene oxide hybrid nanofibers, Appl. Surf. Sci. 473 (2019) 133–140.

[64] S.B. Kulkarni, Y.H. Navale, S.T. Navale, N.S. Ramgir, A.K. Debnath, S.C. Gadkari, S.K. Gupta, D. K. Aswal, V.B. Patil, Enhanced ammonia sensing characteristics of tungsten oxide decorated polyaniline hybrid nanocomposites, Org. Electron. 45 (2017) 65–73.

[65] D. Huang, X. Li, S. Wang, G. He, W. Jiang, J. Hu, Y. Wang, N. Hu, Y. Zhang, Z. Yang, Three-dimensional chemically reduced graphene oxide templated by silica spheres for ammonia sensing, Sensors Actuators B Chem. 252 (2017) 956–964.

[66] N.-F. Chiu, C.-C. Chen, C.-D. Yang, Y.-S. Kao, W.-R. Wu, Enhanced plasmonic biosensors of hybrid gold nanoparticle-graphene oxide-based label-free immunoassay, Nanoscale Res. Lett. 13 (2018) 152, https://doi.org/10.1186/s11671-018-2565-7.

[67] M. Chen, C. Hou, D. Huo, H. Fa, M. Yang, A novel electrochemical biosensor based on graphene and Cu nanowires hybrid nanocomposites, in: The 229th Electrochemical Society Meeting, San Diego, CA, 2016. Abstracts, Article: MA2016-01 2230.

[68] P. Chaturvedi, D.C. Vanegas, M. Taguchi, S.L. Burrs, P. Sharma, E.S. McLamore, A nanoceria–platinum–graphene nanocomposite for electrochemical biosensing, Biosens. Bioelectron. 58 (2014) 179–185.

[69] E. Muthusankar, D. Ragupathy, Chitosan based nanocomposite biosensors: a recent review, Sens. Lett. 16 (2) (2018) 81–91, https://doi.org/10.1166/sl.2018.3925.

[70] W. Zhang, X. Li, R. Zou, H. Wu, H. Shi, S. Yu, Y. Liu, Multifunctional glucose biosensors from Fe_3O_4 nanoparticles modified chitosan/graphene nanocomposites, Nat. Sci. Rep. 5 (2015)11129, https://doi.org/10.1038/srep11129.

[71] S.K. Mahadeva, J. Kim, Conductometric glucose biosensor made with cellulose and tin oxide hybrid nanocomposite, Sensors Actuators B Chem. 157 (1) (2015) 177–182.

[72] R.K. Mendes, et al., Determination of chlorophenol in environmental samples using a voltammetric biosensor based on hybrid nanocomposite, J. Braz. Chem. Soc. 28 (7) (2017) 1212–1219, https://doi.org/10.21577/0103-5053.20160282.

[73] H. Wu, J. Wang, X. Kang, C. Wang, D. Wang, J. Liu, I.A. Aksay, Y. Lin, Glucose biosensor based on immobilization of glucose oxidase in platinum nanoparticles/graphene/chitosan nanocomposite film, Talanta 80 (1) (2009) 403–406, https://doi.org/10.1016/j.talanta.2009.06.054.

[74] M. Maniruzzaman, S.K. Mahadeva, A.H. Khondoker, J. Kim, Titanium dioxide-cellulose hybrid nanocomposite based conductometric glucose biosensor, in: SPIE Proceedings volume 8344, Nanosensors, Biosensors, and Info-Tech Sensors and Systems 2012, 2012. https://doi.org/10.1117/12.915759.

[75] S. Çevik, Xanthine biosensor based on XO/AuNP/PtNP/MWCNT hybrid nanocomposite modified GCPE, Biotechnol. Bioprocess Eng. 21 (2) (2016) 314–320, https://doi.org/10.1007/s12257-016-0014-y.

[76] M. Dervisevic, E. Dervisevic, E. Çevik, M. Şenel, Novel electrochemical xanthine biosensor based on chitosan–polypyrrole–gold nanoparticles hybrid bio-nano composite platform, J. Food Drug Anal. 25 (3) (2017) 510–519, https://doi.org/10.1016/j.jfda.2016.12.005.

[77] (a)X.M. Zhuang, C.Y. Tian, F. Luan, X.R. Wu, L.X. Chen, One-step electrochemical fabrication of a nickel oxide nanoparticle/polyaniline nanowire/graphene oxide hybrid on a glassy carbon electrode for use as a non-enzymatic glucose biosensor, RSC Adv. 6 (2016) 92541–92546. (b)M. Dervisevic, E. Dervisevic, E. Çevik, M. Şenel, Novel electrochemical xanthine biosensor based on chitosan-polypyrrole-gold nanoparticles

hybrid bio-nano composite platform, J. Food Drug Anal. 25 (3) (2017) 510–519, https://doi.org/10.1016/j.jfda.2016.12.005.

[78] B. Zhang, T. Cui, Cancer sensors based on graphene and graphene composites, in: 17th International Conference on Miniaturized Systems for Chemistry and Life Sciences, μTAS 2013 Conference, Oct. 2013 Freiburg, Germany, (MicroTAS 2013) (3 Vol's), ISBN: 9781632666246, 2013, pp. 203–206.

[79] F. Khaleghi, A.E. Irai, R. Sadeghi, V.K. Gupta, Y.P. Wen, A fast strategy for the determination of vitamin B9 in food and pharmaceutical samples using an ionic liquid-modified nanostructure voltammetric sensor, Sensors 16 (2016) 747–758.

[80] L. Shabnam, S.N. Faisal, A.K. Roy, E. Haque, A.I. Minett, V.G. Gomes, Doped graphene/Cu nanocomposite: a high sensitivity non-enzymatic glucose sensor for food, Food Chem. 221 (2017) 751–759.

[81] S. Xu, Y. Zhang, K. Dong, J. Wen, C. Zheng, S. Zhao, Electrochemical DNA biosensor based on graphene oxide-chitosan hybrid nanocomposites for detection of *Escherichia coli* O157:H7, Int. J. Electrochem. Sci. 12 (2017) 3443–3458, https://doi.org/10.20964/2017.04.16.

CHAPTER 11

Design and fabrication of CNT/graphene-based polymer nanocomposite applications in nanosensors

Irene S. Fahim[a], **Ahmed M. Hassanein**[b], **Lobna A. Said**[b], **Ahmed H. Madian**[b,c]

[a]*Industrial Engineering Department, Smart Engineering Systems Research Center (SESC), Nile University, Giza, Egypt*
[b]*Nanoelectronics Integrated Systems Center (NISC), Nile University, Giza, Egypt*
[c]*Radiation Engineering Department, NCRRT, Egyptian Atomic Energy Authority, Cairo, Egypt*

11.1 Introduction

Nanosensors are classified into mechanical and chemical types. Chemical nanosensors sense chemical materials by determining the electrical conductivity of the nanomaterial. Mechanical nanosensors also operate by spotting a modification in the electrical conductivity of a solid substance, but their detection mechanism is unique. Nanomaterials used as mechanical nanosensors modify their electrical conductivity when the material is used, producing a detectable response, which is measured using a capacitor. Both sensors have a varied range of applications, from monitoring gas concentrations to identifying faces; electrochemical sensors contain nanomaterials that have enhanced sensitivity to detect metals or pesticides in various samples. Nanosensors can also be used for light sensing by detecting UV radiation. Additionally, we can combine nanosensors with microelectromechanical systems (MEMS) for more effective chemical sensing applications [1].

This chapter focuses on a specific application of nanosensors, which is monitoring a number of gas emissions, of either harmful or useful gases. This application is exceedingly important for human safety, since individuals are exposed to hard-to-detect and dangerous gases such as carbon monoxide, the flammable gases formaldehyde, nitrogen oxides, and methane, and volatile organic compounds (VOCs). Gas sensors are critical in several applications, such as air quality monitoring, healthcare, food damage, and industrial safety. In order to make the gas sensors more efficient—in other words, be able to detect at low limits—nanotechnology is used. The nanomaterials used in the sensor being studied have a large surface-to-bulk ratio

Nanofabrication for Smart Nanosensor Applications. https://doi.org/10.1016/B978-0-12-820702-4.00012-X
© 2020 Elsevier Inc. All rights reserved.

compared to granular materials, thus allowing a sensor to be constructed with high surface energy and motion [2].

There are several ways to fabricate gas sensors. One of the fabrication techniques commonly used to produce many gas units in one batch is integrating a microheating platform with a nanopore array constructed within a silicon substrate. The dynamic region of gas sensing contains several layers: a supporting layer, microheater for thermal stability, an isolation layer, and interdigital electrodes [3]. Another method for fabricating gas sensors is mixing tin dioxide (SnO_2) powder with deionized water to produce a form of paste. This paste is coated on a ceramic pipe with a couple of platinum (Pt) wires wrapped on gold (Au) electrodes, followed by drying in the air. The electrodes are then connected on a base, and a Ni-Cr heating wire is merged into a ceramic tube. The gas sensors are kept at 300°C for 10 h to enhance their steadiness [4].

A new concept for identifying gas molecules was presented in [5]. The concept was based on detecting the gas rotational-vibrational modes after recording the infrared (IR) transmission spectra of the gas using graphene (G) plasmon. Graphene is considered a favorable nanofiller owing to its exceptional electrical and mechanical properties, due to its elevated surface area and its affinity to organic compounds [6]. Graphene exhibits physical and electrical changes when exposed to different gases; that is why it is applied in fabricating gas sensors [7]. In [8], two new gas-sensing materials were proposed. The materials were based on carbon nanosheets, graphene quantum dots, and nitrogen doped-carbon nanoparticles. That experiment included sensing methanol, ethanol, and propanol vapors. Improvements in using carbon nanotubes (CNTs) for gas sensors were presented in [9]. The improvement was attempted through designing a graphene-constructed surface plasmon separation waveguide. The results of that work improved detecting trace gases of NO2, CO or ammonia, and a mixture of numerous contaminated gases in a specific environment. Also, that proposed work was claimed to overcome the shortcomings of the trace gas sensors. The work in [10] was concerned with developing materials for gaseous ethanol sensors. The proposed material was chemically prepared graphene oxide sheets draped with tin dioxide nanoparticles (SnO2-GO 4:1, 8:1, and 16:1). The sample SnO2-GO 16:1 was the only compound that had a significant response to gaseous ethanol for 150o and ultraviolet light. Another study concerned with sensing toxic gases, specifically HF and H2S, using graphene was conducted in [11]. The sensor was based on the adsorption behavior of the gases, as mentioned earlier, on pristine and Ti-inserted twin graphene. The results of that work claimed increased adsorption of the Ti-inserted twin graphene as compared to the graphene. In [12], the performance of sensing CO_2 gas using graphene oxide (GO)- and vanadium dioxide (VO2)-based gas sensors was monitored. Also, that work presented a synthesis method to prepare GO and VO2 materials. An electrochemical nitrite sensor was presented in [13]. The sensor was based on carbon nanotubes and graphene oxide decorated with cobalt oxide. New improved material based on GO for gas sensors was presented in [14]. This new material was

claimed to have high-level sensitivity, rapid response and recovery, and high steadiness when used to detect volatile organics like acetone and ammonia. In [15], an alternating-current electroluminescent (AC-EL) based gas sensor was introduced. That sensor was fabricated using a graphene layer instead of the normal dielectric layer. Also, it was applied to detect carbon dioxide (CO_2) at 25°C. The mechanism of such sensors differs on the charge shift interaction between the graphene layer and CO_2, which causes a change in the graphene layer resistance. That sensor was claimed to achieve good sensitivity and measurement accuracy. Detection of hydrogen (H_2) under ultraviolet radiation and room temperature using gold-decorated nanocomposite sheets based on graphene/zinc oxides (rGO/ZnO) was investigated in [16]. The comparison between that work and the former (H_2) detection research in the literature highlighted the high response for that work. The sensing mechanism was based on releasing the trapped electrons to the sensor bulk after a chemical reaction between the hydrogen and the ionized oxygen under ultraviolet radiation; this, in turn, decreased the measured resistance of the sensor material. Considering sensors that are based on biomaterials, the authors in [17] used three-dimensional reduced graphene oxide (3D-rGO) to polymerize polypyrrole (PPy). The polymerization idea was inspired from olfactory cells of mice. That nanocomposite material was proved to have high sensitivity for sensing gases at room temperature. That material was used to detect NH3 at room temperature, and good reversibility, stability, and selectivity were claimed. The importance of detecting ethylene (C2H4) in agriculture inspired the work in [18] to synthesize material for better ethylene detection in low concentrations and under lower temperature. The proposed material was a composite of palladium (Pd) nanoparticles, (rGO) reduced graphene oxide, and porous α-Fe_2O_3. The material mentioned earlier was claimed to be a superior material for ethylene sensors compared to other sensors due to the excellent sensing performance, especially, the ability to sense low-concentration ethylene, which was of agricultural benefits. In [19], a composite material (a composite of double-layer Co3O4 and rGO) was presented as a gas-sensing material. The material was tested on triethylamine, and it was claimed to give better performance than the conventional Co3O4 sensor for the same operating temperature (200°C). The work in [20] proposed a way to compound metal-organic frameworks (MOFs) and graphene aerogels (GAs). The work stated that this material provided an electrochemical sensing policy for detecting the extremely toxic 2,2-methylenebis (4-chlorophenol). That sensor was stated to have high sensitivity towards dichlorophenol (Dcp), and it also was stated to be able to detect it in lake water. Some sensors were designed based on quantum capacitance, such as those in [7]. In [21], a reduced graphene oxide (rGO) film was made up as a bridge between interdigitated electrodes (IDEs) and polyethylene terephthalate (PET). The aim behind that fabricated material was for use in gas sensing. The sample gases used were isoprene, hydrothion, and odor emissions of different fruit maturity stages. The effect of graphene intensity and film thickness on chemiresistive polymer-based gas sensors was investigated in [22]. Table 11.1 summarizes the sample gases used in the literature survey based on previously mentioned detection mechanisms.

Table 11.1 List of the sample gases used in the gas sensors survey.

Reference	Sample gases used	Reference	Sample gases used
[5,7]	SO_2, NO_2, N_2O, and NO	[15]	CO_2
[8]	Ethanol, methanol, and propanol vapors	[16]	H_2
[9]	NO_2, CO, ammonia, and toxic gases	[17]	NH_3
[10]	Gaseous ethanol	[18]	Ethylene
[11]	Toxic gases specifically HF and H_2S	[19]	Triethylamine
[12]	CO_2	[20]	Dichlorophenol
[13]	Nitrite	[21]	Isoprene, hydrothion and odor emissions of fruits
[14]	volatile organics like acetone and ammonia	[22]	Methanol

In this chapter, the authors are suggesting a novel detecting layer of polymer nanocomposites in a gas sensor that depends on two detection mechanisms in which the proposed layer acts as a barrier for gas diffusion. The first detecting mechanism depends on the concentration gradient measurements for different gases. The concentration gradient is the movement of gas particles from high-density areas to lower-density ones. Having the proposed layer as a barrier, the rate at which the gas molecules move through the layer depends mainly on the gas molecule size. The second mechanism depends on measuring the electrical resistivity of the proposed layer. This mechanism is based on two facts: first, the graphene layer has improved the porous chitosan layer electrical conductivity; and second, the movements of free electrons depend mainly on the molecule type of the detected gas. The physical interface of the gas sensor might look like that in Fig. 11.1.

In this work, we used oxygen gas as a sample gas to illustrate our detection mechanism. The suggested polymer in this research is chitosan, and the nanofiller is graphene. Chitosan is a polymer formed by the deacetylation of chitin from shrimp shells. It is a linear polysaccharide;

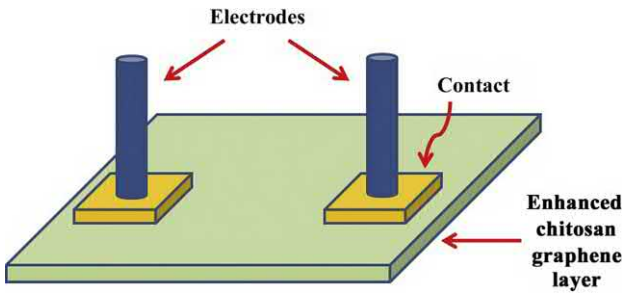

Fig. 11.1
Block diagram for the chitosan polymer nanocomposite graphene layer.

its mechanical strength differs with the degree of deacetylation [23]. The advantage of using chitosan lies in its nontoxicity, biodegradability, and capability of attachment with other functional groups. The mechanical strength and electrical conductivity of pure chitosan are enhanced by the addition of different concentrations of graphene. Additionally, the scattering of graphene into the chitosan polymer affects the rate of diffusion of gases. Consequently, the characterization techniques in this chapter include tensile strength, permeability, electrical conductivity, and finite elements testing. The results obtained from the characterization techniques provide a roadmap on how to use this nanopolymeric layer for gas detection. The proposed detection mechanisms could be mechanical or electrical. The mechanical technique depends on the concentration gradient of the detected gas flow through the holes of the chitosan layer. Considering a fixed number of holes and hole sizes, the concentration gradient would be different for each gas molecule, and it would be dependent on the gas molecule size, considering constant flow for all samples. This sensing mechanism would be suitable only for single-gas detection, as compound gases could be confused with a single gas of the same molecular size. On the other hand, an electrical test could be carried out to detect different gases. The mechanism depends on the interaction nature of the layer with gas molecules under some temperature and pressure conditions. As the graphene layer dramatically enhanced the conductivity of the porous chitosan, more electron flow could be induced on the interaction surface, which in turn makes the change in the layer resistivity detectable. The number of electrons and the layer resistivity depend on the nature of the interaction between the detected gas and the layer, which in turn depends on the gas molecule itself.

11.2 Materials and methods

11.2.1 Materials

11.2.1.1 Preparation of chitosan

The shrimp waste was purchased from a regional fish marketplace in Al-Obour City, Egypt. Shrimp shell waste was washed and dried at room temperature. Chitin was obtained from the shrimp waste by deproteinization and demineralization steps. The chitin formed was deacetylated using 50% NaOH to produce chitosan. All chemicals used were purchased from Sigma-Aldrich: acetic acid (CH3COOH), hydrochloric acid (HCl), and sodium hydroxide (NaOH). Graphene was purchased from Sky Spring Nanomaterials.

11.2.1.2 Addition of graphene nanofiller

The chitosan solution was mixed with graphene (G) at 0.1, 0.5, 1 wt% by wet mixing. Blending was carried out by continuous stirring for 1 h using a VWR Standard Analog Shaker to produce a transparent, consistent solution.

11.2.2 Thin film processing

The mixture was poured into a flat plate. The samples were dried at room temperature.

11.2.3 Characterization techniques

11.2.3.1 Scanning electron microscopy (SEM)

Nanocomposite membranes were examined using an FESEM: Leo Supra 55 (Zeiss Inc., Germany). The secondary electron (SE2) lens (6–8 KV) was utilized to avoid damage of the polymer.

11.2.3.2 Pore size characterization

The porosimeter was used for defining the average pore size of the chitosan and nanocomposite membranes. The pore size experiments were done by utilizing a porosimeter (Micrometrics ASAP 2020) [24]. The preparation of samples for the porosimeter was simple. The samples were sliced to the size of 1 mm and arranged in a glass tube. The technique uses condensed nitrogen gas in the pores and calculates the pore volume from the gas that turned into a liquid.

11.2.3.3 Gas permeability characterization

Gas permeability determination was completed using Type GDP-E (Brugger Feinmechanik GmbH) permeability testing apparatus. The membranes were analyzed to determine the permeability. Oxygen gas was used for permeability tests.

11.2.3.4 Mechanical properties characterization

Tests of tensile strength and percent elongation (ductility) of chitosan films were conducted using a universal testing machine (Instron, 100 KN, strain 1.8, strain rate of 10 mm/min). The samples were cut according to the ASTM Standard Method D 882-91 [25].

11.2.3.5 Resistance measurement

A high resistance meter (HP-4329A, Agilent, CA) with a two-point probe method was used to measure resistivity. The face of the specimen was prepared by brushing with distilled water according to ISO 3915:1981 [26]. The specimens were coated to guarantee good electrical contact. Resistance values were recorded after 60 s (time of electrification). The resistivity (R) was computed through the slope of $I-V$ curves, with Ohm's law; thus, electrical conductivity was measured. The test voltage is adjustable between 10 and 1000 V. The current must be within 50 fA and 20 μA and the thickness of the sample is 2 mm. The resistivity of the sample could be measured up to 1014 Ω cm.

11.2.4 Finite element analysis

The comprehension of gas mass transfer vehicle through films has turned out to be progressively significant in mechanical applications. Permeability is measured when particles move inside the polymer from the "outside" condition to the "inside" condition. The main thrust for mass transfer vehicle incorporates diffusivity and permeability. As per Fick's law, the dispersion motion corresponds to the concentration gradient. The estimation of diffusivity is extremely entangled, and finite element analysis (FEA) will be utilized to ascertain the dispersion [27]. Abaqus is a software application utilized for displaying and investigating mass concentration gradients. Permeability is characterized in Abaqus as an element of the void proportion and the pore size. The fundamental arrangement variable is the standardized fixation (C/S), S is dissolvability in the base material, and C is the mass concentration of the diffusing material [28].

11.2.5 Results and discussion

11.2.5.1 Pore size morphology of chitosan and graphene

The SEM image of chitosan is illustrated in Fig. 11.2A. A slightly porous network structure can be observed. The pore size of the chitosan membrane was calculated using ASAP 2020 software: the membranes had a pore size of 10 nm. The graphene, shown in Fig. 11.3, consists of carbon atoms, organized in a honeycomb crystal pattern. The flaky nanocluster size of the graphene has a substantial effect on the barrier and tensile properties of thin films. In particular, it decreases the pore sizes in chitosan membranes.

Upon adding the graphene nanofiller to chitosan, SEM images showed considerable variations in the pore size morphology of the membranes, as demonstrated in Fig. 11.4. The SEM image of chitosan membranes showed a pore size of 10 nm, and upon adding graphene nanofillers with

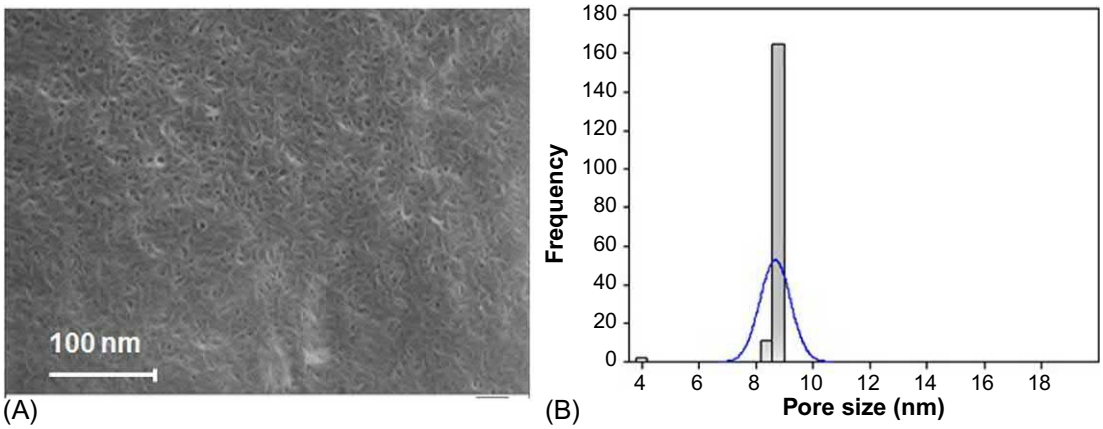

Fig. 11.2
(A) SEM images of chitosan membrane; (B) the pore size distribution.

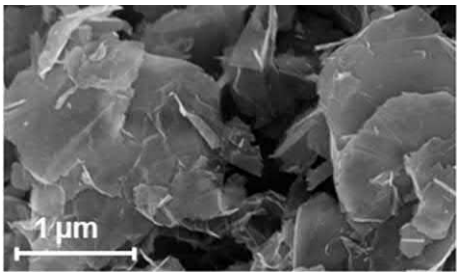

Fig. 11.3
SEM image of G nanofiller.

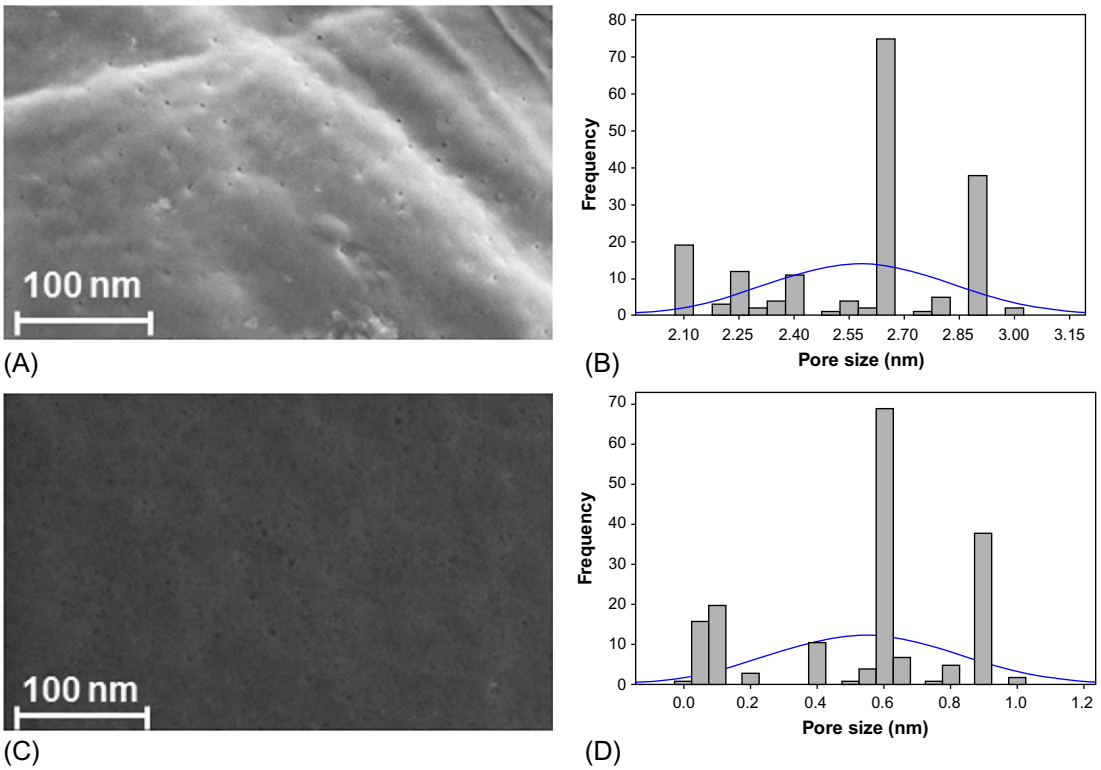

Fig. 11.4
SEM, the pore size distribution of (A and B) chitosan/0.1 wt% G, and (C and D) chitosan/1 wt% G.

0.1 and 1 wt%, the pore size reduced to 3 nm. However, by adding 1 wt% G, the pore size reached 0.6 nm. There was a reduction in the pore size by 70% at 0.1 wt% G and 90% at 1 wt% G. This was primarily owing to the hindrance effect of the G nanofiller morphology and size. The nanofiller percentage by weight performed a vital role in managing the membrane pores [29]. Fig. 11.5 shows the influence of G nanofiller on the chitosan pores that led to

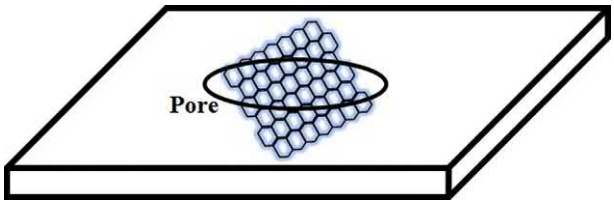

Fig. 11.5
Chitosan membranes and pore sizes upon addition of G nanofiller.

their buildup inside the pores of the membranes. The pores in the scheme in Fig. 11.5 were scaled according to the achieved pore sizes.

11.2.5.2 Gas permeability of chitosan membranes and their nanocomposites

It was detected from Fig. 11.6 that the oxygen transmission rate through the chitosan and nanocomposite membrane is a function of the nanofiller percentage. The oxygen transmission rate of chitosan membranes reached 70 cm^2/cm^2 d bar. For the G addition, a constant reduction in oxygen transmission occurred up to 1 wt% G, reaching 50 cm^2/cm^2 d bar. The adding of G nanofiller had an excellent impact on the oxygen transmission rate. The G nanofiller lessened the rate by 29%, since the spaces in the pores were blocked with the G nanofiller addition.

11.2.5.3 Tensile properties of chitosan membranes and their nanocomposites

Chitosan nanocomposite thin films with G nanofillers were synthesized and their mechanical properties were examined. The tensile behavior versus strain of chitosan was 24 MPa. After the G nanofiller addition, the tensile strength of chitosan with 0.1 wt% G was 30 MPa, highlighting an increase in the tensile strength. The strength was enlarged by adding 1 wt% of G till it reached 40 MPa, as illustrated in Fig. 11.7. Hence, the addition of G nanofiller (1 wt%) caused a 40% rise in tensile strength. It was stated by Chaharmahali et al. that G enhanced the mechanical properties of polymers up to 29%. This improvement was easily understandable,

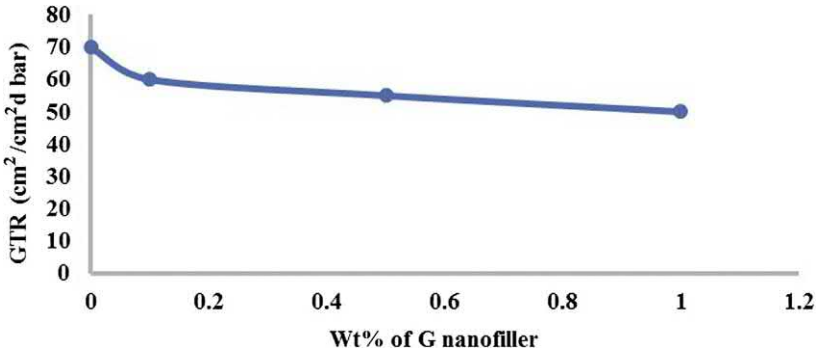

Fig. 11.6
Oxygen transmission rate for chitosan nanocomposite membranes.

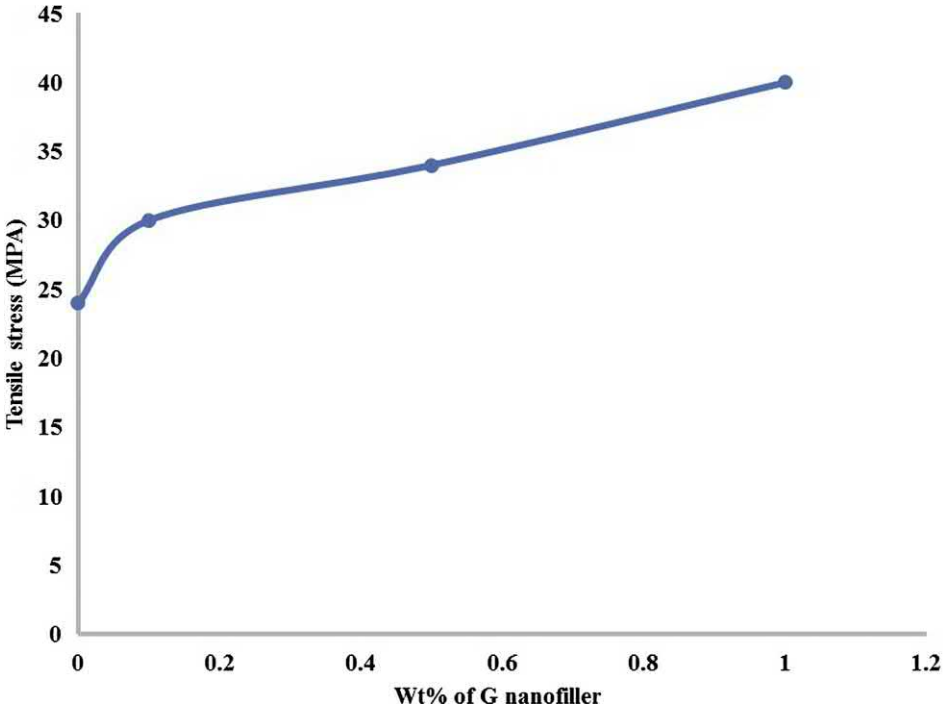

Fig. 11.7

Stress-strain curve for chitosan membranes as a function of increasing the percentage by weight of G nanofiller.

with the huge aspect ratio and elevated interfacial area of G nanoparticles with the chitosan [30].

The rise in tensile strength with the addition of different percentages by weight of G recommended that G nanofiller be spread into the chitosan during the solvent-mixing procedure, creating a carbon network in the chitosan structure. Furthermore, the dispersion of the hydrogen bonds in chitosan with the carbonyl functional group together with the G nanoparticles produced a detectable improvement in mechanical properties [31]. The decrease in the ductility of the composite with an increase in G nanofillers is owing to the deformation of the stiff interfacial interaction between G and chitosan. The stiffness of the connection between G and chitosan led to a low percentage of elongation [32].

11.2.5.4 The electrical conductivity of chitosan membranes and their nanocomposites

The electrical conductivity of the membranes was enhanced. It was observed that electrical resistivity values increased with G content, as demonstrated in Fig. 11.8. There is a noticeable increase with adding 0.5 wt% and 1 wt% G. Reviewing the electrical properties of chitosan and G nanofiller revealed substantial improvement in electrical conductivity, thus extending the

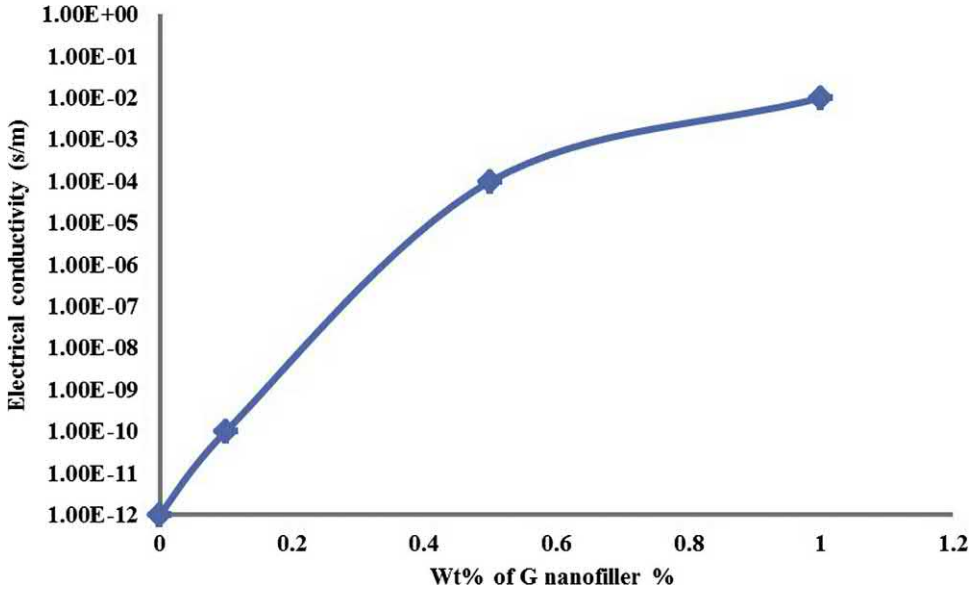

Fig. 11.8

Electrical conductivity for chitosan membranes as a function of adding percentage by weight of G nanofiller.

applications to nanosensors. The extremely dispersed G nanoparticles in the chitosan/G nanocomposite expressively enhanced the electronic conductivity and permitted the electrochemical activity of the polymer nanocomposite to be ultimately used. The G nanofiller acts as an electron transport pathway and allows fast charge transfer, compared to those reinforced with carbon nanotubes. Carbon nanotubes have an uneven arrangement, dropping the conductivity of the nanocomposite. The increase in G content allows the development of a conducting network with a bulky number of charge carriers moving through the entire network, achieving an active material utilization ratio [33]. Furthermore, the linear region of the electrical conductivity of the G nanofiller was found to be between 0 and 0.5 wt%. This region could be of interest in sensing applications, as it provides a tunable G-nanofiller conductivity in a linear manner with the graphene weight. This, in turn, gives more flexibility in sensing constraints and could cover different conductivity ranges: hence, more gases to sense.

11.2.5.5 Finite element analysis

Abaqus/Standard modeled the steady-state diffusion via the fabricated membranes. The software illustrated the change in concentration with regards to time. The basic contributions were solubility and diffusivity. Fick's equations permitted the nonuniform solubility. The fundamental response was normalized concentration ($Ø = c/s$), where c is the mass concentration of the diffusing particles and s is solubility [27]. The response was estimated at the specified nodes for chitosan membranes, as shown in Fig. 11.9.

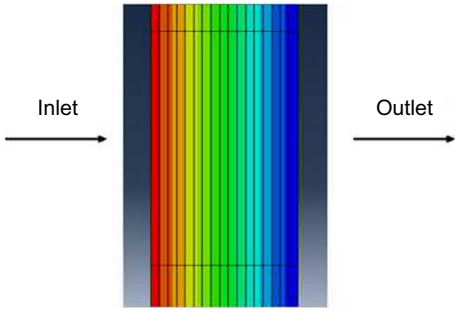

Fig. 11.9
Normalized concentration through the chitosan membrane thickness.

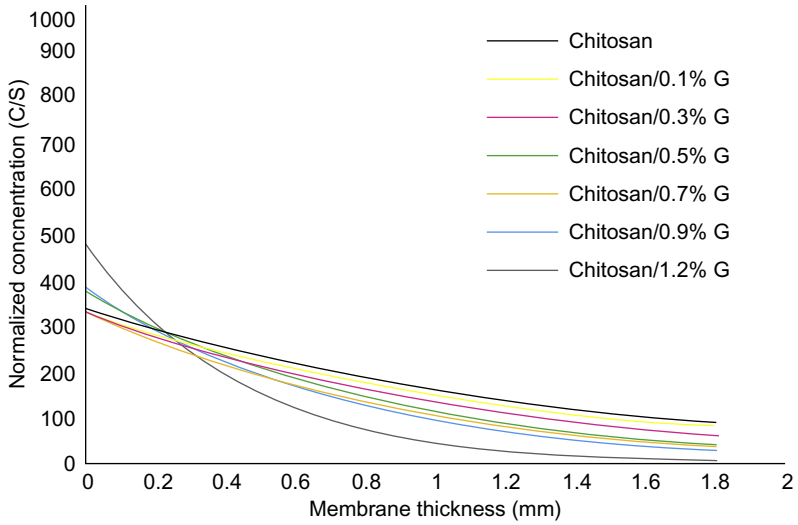

Fig. 11.10
Normalized mass concentration for chitosan and G nanofiller.

Fig. 11.10 highlights the deviation of normalized concentration of oxygen across the chitosan membrane thickness due to nanofiller concentration and the thickness of the membrane. There was a reduction in normalized mass concentration due to the addition of G nanofiller. The existence of nanofillers obstructed mass diffusion. The normalized concentration declined by adding 1 wt% G nanofiller from 500 to 100 c/s. This emphasized a minor diffusion rate through chitosan/G nanofiller membranes, which agreed with experimental results of gas diffusion measurement. Other gases would have different diffusion rates according to their particle size. In some other materials, like graphene nanoplatelets, the concentration directly affects the material sensing response, which is increased with increasing concentration [22].

11.2.5.6 Recommendation

Further tests are needed to measure the layer conductivity under certain conditions for different gas flows, to detect and sense the effect of the gas molecule interactions with the layer surface. In this way, a unique footprint for different gases could be deduced, and the gas sensor could be acquired.

References

[1] R. Bogue, Nanosensors: a review of recent research, Sens. Rev. 29 (4) (2009) 310–315.
[2] N.M. Julkapli, S. Bagheri, Nanosensor in gas monitoring: a review, Nanotechnol. Environ. Sci. (2018) 443–472.
[3] L. Xu, Z. Dai, G. Duan, L. Guo, Y. Wang, H. Zhou, et al., Micro/nano gas sensors: a new strategy towards in-situ wafer-level fabrication of high-performance gas sensing chips, Sci. Rep. 5 (2015) 10507.
[4] Anon, Electron. Suppl. Mater. CrystEngComm (2012).
[5] H. Hu, X. Yang, X. Guo, K. Khaliji, S.R. Biswas, F.J.G. de Abajo, et al., Gas identification with graphene plasmons, Nat. Commun. 10 (1) (2019) 1131.
[6] E.K. Wujcik, C.N. Monty, Nanotechnology for implantable sensors: carbon nanotubes and graphene in medicine, Wiley Interdiscip. Rev. Nanomed. Nanobiotechnol. 5 (3) (2013) 233–249.
[7] A.H. Pourasl, S.H.S. Ariffin, M.T. Ahmadi, N. Gharaei, R.A. Rashid, R. Ismail, Quantum capacitance model for graphene FET based gas sensor, IEEE Sens J. (2019).
[8] R. Parvizi, S. Azad, K. Dashtian, M. Ghaedi, H. Heidari, Natural source-based graphene as sensitising agents for air quality monitoring, Sci. Rep. 9 (1) (2019) 3798.
[9] J. Zhu, Z. Xu, D. Fu, D. Wei, et al., Sense trace gases based surface plasmon polarization waveguide of graphene, Measurement 144 (2019) 67–71.
[10] E. Pargoletti, A. Tricoli, V. Pifferi, S. Orsini, M. Longhi, V. Guglielmi, et al., An electrochemical outlook upon the gaseous ethanol sensing by graphene oxide-SnO2 hybrid materials, Appl. Surf. Sci. 483 (2019) 1081–1089.
[11] R. Majidi, A. Ramazani, Detection of HF and H2S with pristine and Ti-embedded twin graphene: a density functional theory study, J. Phys. Chem. Solids 132 (2019) 31–37.
[12] S.E. Zaki, M.A. Basyooni, M. Shaban, M. Rabia, Y.R. Eker, G.F. Attia, et al., Role of oxygen vacancies in vanadium oxide and oxygen functional groups in graphene oxide for room temperature CO_2 gas sensors, Sensors Actuators A Phys. 294 (2019) 17–24.
[13] Z. Zhao, J. Zhang, W. Wang, Y. Sun, P. Li, J. Hu, et al., Synthesis and electrochemical properties of Co3O4-rGO/CNTs composites towards highly sensitive nitrite detection, Appl. Surf. Sci. 485 (2019) 274–282.
[14] H. Song, S. Yan, Y. Yao, L. Xia, X. Jia, J. Xu, 3D $α$-Fe2O3 nanorods arrays@ graphene oxide nanosheets as sensing materials for improved gas sensitivity, Chem. Eng. J. (2019).
[15] Y. Seekaew, C. Wongchoosuk, A novel graphene-based electroluminescent gas sensor for carbon dioxide detection, Appl. Surf. Sci. 479 (2019) 525–531.
[16] Q.A. Drmosh, A.H. Hendi, M.K. Hossain, Z.H. Yamani, R.A. Moqbel, A. Hezam, et al., UV-activated gold decorated rGO/ZnO heterostructured nanocomposite sensor for efficient room temperature H_2 detection, Sensors Actuators B Chem. (2019).
[17] Y. Qin, B. Zhang, Z. Zhang, Combination of PPy with three-dimensional rGO to construct bioinspired nanocomposite for NH3-sensing enhancement, Org. Electron. 70 (2019) 240–245.
[18] B. Li, M. Li, F. Meng, J. Liu, Highly sensitive ethylene sensors using Pd nanoparticles and rGO modified flower-like hierarchical porous $α$-Fe_2O_3, Sensors Actuators B Chem. 290 (2019) 396–405.
[19] Z. Yuan, J. Zhao, F. Meng, W. Qin, Y. Chen, M. Yang, et al., Sandwich-like composites of double-layer Co3O4 and reduced graphene oxide and their sensing properties to volatile organic compounds, J. Alloys Compd. (2019).

[20] Y. Xie, X. Tu, X. Ma, M. Xiao, G. Liu, F. Qu, et al., In-situ synthesis of hierarchically porous polypyrrole@ZIF-8/graphene aerogels for enhanced electrochemical sensing of 2, 2-methylenebis (4-chlorophenol), Electrochim. Acta 311 (2019) 114–122.
[21] Q. Chen, D. Liu, L. Lin, J. Wu, Bridging interdigitated electrodes by electrochemical-assisted deposition of graphene oxide for constructing flexible gas sensor, Sensors Actuators B Chem. 286 (2019) 591–599.
[22] M.S. Wiederoder, M. Weiss, B. Yoon, R.C. Paffenroth, M.G. SK, J.R. Uzarski, Impact of graphene nanoplatelet concentration and film thickness on vapor detection for polymer based chemiresistive sensors, Curr. Appl. Phys. 19 (2019) 978–983.
[23] G. D'Angelo, A. Elhussieny, M. Faisal, I. Fahim, N. Everitt, Mechanical behavior optimization of chitosan extracted from shrimp shells as a sustainable material for shopping bags, J. Funct. Biomater. 9 (2) (2018) 37.
[24] ASAP2020-Physisorption Analyzer, [Internet]. Available from: https://www.micromeritics.com/Product-Showcase/ASAP-2020a.aspx, 2020.
[25] ASTM International, West Conshohocken P, ASTM D882-18, Standard Test Method for Tensile Properties of Thin Plastic Sheeting [Internet], Available from: www.astm.org.
[26] International Organization For Standardization, ISO 3915:1981 [Internet], Available from: https://www.iso.org/standard/9547.html, 2015.
[27] B. Duncan, J. Urquhart, S. Roberts, Review of Measurement and Modelling of Permeation and Diffusion in Polymers, National Physical Laboratory Middlesex, UK, 2005.
[28] M.H. Choi, K.U. Kwon, C.H. Park, S.W. Kim, S.H. Hahn, D.J. Seong, et al., Estimate of the thermal diffusivity of films with a sandwich structure by using pulsed transient analysis and AC calorimetry, J. Korean Phys. Soc. 34 (6) (1999) 514–518.
[29] R.K. Bharadwaj, Modeling the barrier properties of polymer-layered silicate nanocomposites, Macromolecules 34 (26) (2001) 9189–9192.
[30] M. Chaharmahali, Y. Hamzeh, G. Ebrahimi, A. Ashori, I. Ghasemi, Effects of nano-graphene on the physico-mechanical properties of bagasse/polypropylene composites, Polym. Bull. 71 (2) (2014) 337–349.
[31] S. Bhuvaneshwari, D. Sruthi, V. Sivasubramanian, K. Niranjana, J. Sugunabai, Development and characterization of chitosan films, Int. J. Eng. Res. Appl. 1 (2) (2011) 292–299.
[32] V. Siracusa, P. Rocculi, S. Romani, R.M. Dalla, Biodegradable polymers for food packaging: a review, Trends Food Sci. Technol. 19 (12) (2008) 634–643.
[33] C.-W. Nan, Y. Shen, J. Ma, Physical properties of composites near percolation, Annu. Rev. Mater. Res. 40 (2010) 131–151.

CHAPTER 12

Nanomaterials dispersed liquid crystalline self-assembly of hybrid matrix application towards thermal sensor

Asiya S.I.[a], **Kaushik Pal**[b,c], **Samo Kralj**[d], **Sabu Thomas**[e]

[a]*Bharath Institute of Higher Education and Research (BIHER), Bharath University, Chennai, Tamil Nadu, India*
[b]*International and Inter University Centre for Nanoscience and Nanotechnology (IIUCN), School of Energy Materials, Mahatma Gandhi University, Kottayam, Kerala, India*
[c]*Wuhan University, Wuchang District, Wuhan, Hubei Province, Republic of China*
[d]*Faculty of Natural Sciences and Mathematics, University of Maribor, Maribor, Slovenia*
[e]*International and Inter University Centre for Nanoscience and Nanotechnology (IIUCN), School of Chemical Sciences, Mahatma Gandhi University, Kottayam, Kerala, India*

12.1 Introduction

Nanotechnology is a branch of technology that deals with dimensions less than 100 nm, particularly the manipulation of matter on an atomic or molecular scale. This branch of technology has provided significant opportunities for the design and fabrication of novel materials at nanoscale. From home to industry, this small but mighty technology plays a vital role. According to Baletto and Ferrando [1], design of nanomaterials and tailoring of their properties are the main task in the development of nanotechnologies. There has been a tremendous growth in nanotechnology over the last few years, mainly due to the development of new techniques for the synthesis, designing, characterization, and manipulation of nanomaterials [1]. Research attention has been focused on nanomaterials, as it is possible to control a material's structure and properties on an atomic scale. For more than 25 years, carbon nanomaterials have gained much research interest due to the range of allotropes that can be derived from the three bonds (sp^2 hybridized bonds, sp^3 hybridized bonds, sp^2 and sp^3 hybridized bonds) that carbon can make [2]. Undoubtedly, these nanostructured materials have acquired a wealth of academic and industrial attention due to their size-dependent electronic, optical, magnetic, and chemical properties, which are in essence not the same as those of the bulk materials [3–10]. They have found extensive applications in all areas of science, including biotechnology, optics, medicine, and energy.

Nanofabrication for Smart Nanosensor Applications. https://doi.org/10.1016/B978-0-12-820702-4.00013-1
© 2020 Elsevier Inc. All rights reserved.

Researchers have observed some fascinating facts when these nanomaterials are embedded with LCs, leading to an abundance of interesting new and potential applications. Hybrid nanocomposite compounds produced by the addition of nanomaterials to liquid crystal have improved macroscopic properties. These composite materials exhibit high performance and are considered as a probable substitution for microcomposites and monolithitics, owing to their outstanding properties. The main objectives in developing a nanomaterial dispersed liquid crystal are to modify the physical or chemical properties of the liquid crystal, modify the properties of the nanomaterials by manipulating and ordering the nanomaterials into liquid crystal, and to take advantage of properties that are not available in either liquid crystals or the nanomaterials in their pure states [11–13]. A robust impact of nanomaterials on the liquid crystal properties, and vice-versa, is observed on the composite material due to long-range orientation and interactions in mesophases. In composites formed by doping different sorts of nanomaterials in LCs, the coupling of long-range ordering in liquid crystal and the exceptional properties of the nanomaterials can change or develop new physical properties in the liquid crystal nanocomposite [14].

Gerasin and his co-researchers proposed that a zero-dimensional (0D) nanocomposite encompass a filler of 1 nm in all three dimensions, in a one-dimensional (1D) nanocomposite two dimensions of the filler are 1 nm, and two-dimensional (2D) nanocomposites consist of layers of nanometer thickness [15]. The physical and chemical properties of the nanomaterial dopant and their interaction with liquid crystal play a vital role in determining the enhanced physical characteristics and novel functionalities of the nanocomposite obtained [16–21]. Researchers have identified that the mechanical, electrical, thermal, optical, electrochemical, and catalytic properties of the composite material are highly dependent on the type of the nanomaterial dopant, its size, and the method of preparation. The most commonly used nanomaterial dopants are carbon, ferroelectric, metal, and semiconductor nanomaterials. Nanocomposites find extensive applications in many fields due to their exceptional properties and are a good substitute for conventional composites. The high surface area-to-volume ratio of the dispersed nanomaterials and their extremely high aspect ratio find more potential applications for nanocomposites than for conventional composites.

This chapter deals with the recent development of the potential application of nanomaterial dispersed LC optical materials as thermal sensors. Liquid crystal and its features, classification, and properties are explained in the first section, followed by the characteristics of nanomaterials, and the interaction of nanomaterials with LC, mainly focusing on the functionalities of nanomaterial dispersed into LC. The next section emphasizes the application of LC nanocomposite, particularly its application as thermal sensors.

12.2 Overview of liquid crystals

Liquid crystals (LCs), often referred to as the fourth state of matter, are soft-materials that show both order and mobility on a molecular, supramolecular, and macroscopic levels. They are identified as a group of functional materials that find application in various fields,

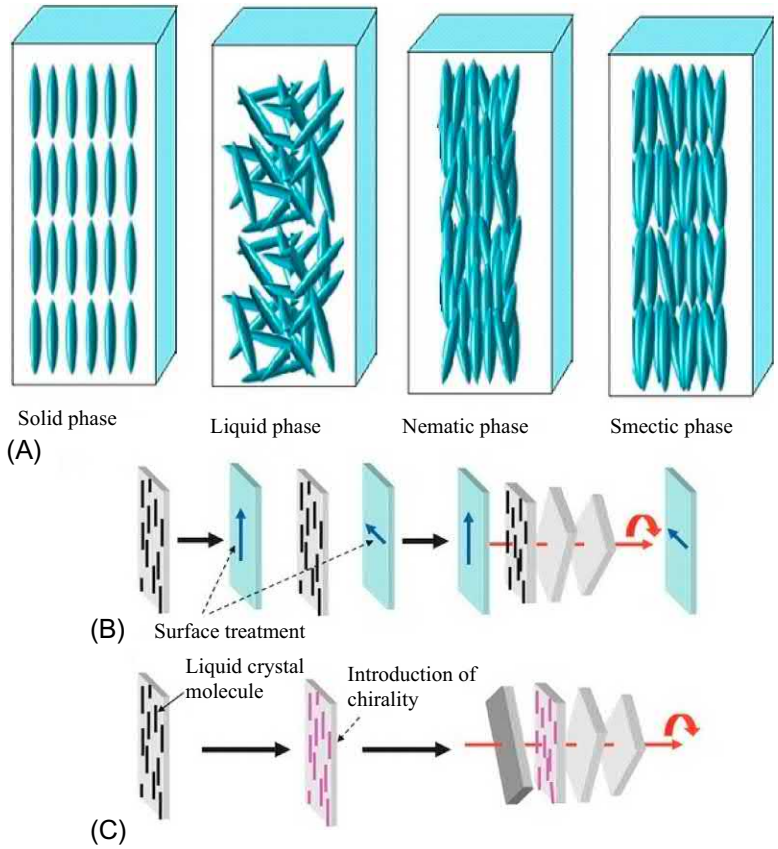

Fig. 12.1

(A) Different states of matter and ordering of molecules in those state, (B) surface treatment of two surfaces to form a helical structure, (C) spontaneous alignment of LC molecules by the introduction of chirality [22]. *Copyright @ Springer Japan, 2016.*

such as: information, health care, energy, and environment. Fig. 12.1A illustrates the different states of matter and the molecular arrangements in those states. Their capability to occur as a crystalline phase and an isotropic liquid phase leads to the existence of mesophases. The steady unit that is accountable for the establishment of the liquid crystalline phase is called a "mesogen." Being a thermodynamically stable state of matter, it is constituted of organic or inorganic mesogens or metallomesogens [23]. They can also be defined as anisotropic fluids that are thermodynamically positioned between the isotropic liquid and the crystalline phase, exhibiting the fluidity of liquids as well as the long-range lattice order of crystalline solids [24, 25]. Thus molecules with greater anisotropy are expected to produce a liquid crystal phase. Liquid crystals are built of rod- or disc-shaped anisotropic units that are oriented along an axis called the director "*n*" [26]. The director of liquid crystals, influenced by numerous external stimuli such as mechanical, magnetic, electrical, optical, and thermal, makes LCs attractive to both industry and academia

[27–31]. Recently, liquid crystals have been finding heightened interest for other applications, e.g. photonics, biosensor, slide projection system, light modulator, temperature sensor, and even LC laser [31–34].

Fig. 12.1B and C indicate the two different factors that determine the alignment styles. In Fig. 12.1B it is the surface treatment of the liquid crystal cell due to the surrounding environmental conditions that, determines the alignment, and in Fig. 12.1C the spontaneous alignment of liquid crystal cell is exhibited. In the surface treatment, the LC molecules are placed between two surfaces and the alignment direction is twisted 90° to form a helical structural arrangement. This is considered to be a frustrated structure, as the bulk molecules have a "desire" to align in parallel. This liquid crystal property is the underlying technology of flat panel display [22].

12.3 Taxonomy of liquid crystals

Liquid crystals fall into various categories depending upon certain factors, such as:

(i) Molar mass of the constituent molecules—a liquid crystal with low molar mass is known as monomeric and oligomeric, whereas LC with high molar mass is known as polymeric liquid crystal.
(ii) Depending on the formation of LC—Thermotropic LC is formed by varying the temperature, and lyotropic LC is formed by adding solvent.
(iii) According to the nature of the constituent molecules, LCs are classified as organic, inorganic, and organometallic.
(iv) Rod-like, disc-like, and bent core liquid crystals exist due to the geometric shape of the molecules.
(v) Based on the arrangement of the molecules in the liquid crystalline phase, LCs are classified as nematic, smectic, columnar, helical, B phases, etc.

Fig. 12.2A shows briefly the various classifications of liquid crystal.

According to Chandrasekhar et al. [36], mesophases can be formed by calamitic molecules as well as disc-like molecular shape compounds. It was discovered in 1996 that banana-shaped molecules, also known as "bent-shape molecules," exhibit a liquid crystal phase and provide access to mesophases with polar order and supramolecular chirality. However, thermotropic LCs and lyotropic LCs are the most commonly used LCs. An amphotropic liquid crystal phase contains both thermotropic and lyotropic liquid crystalline phases. Recent research in the field of liquid crystals has proposed a novel technique of switching the molecular orientation of nematic and chiral liquid crystal by radical polymers, as shown in Fig. 12.2B. A helical structured chiral nematic LC exhibits excellent optical properties that find application in optical fibers, displays, and lasers. Compared to the normal nematic phase,

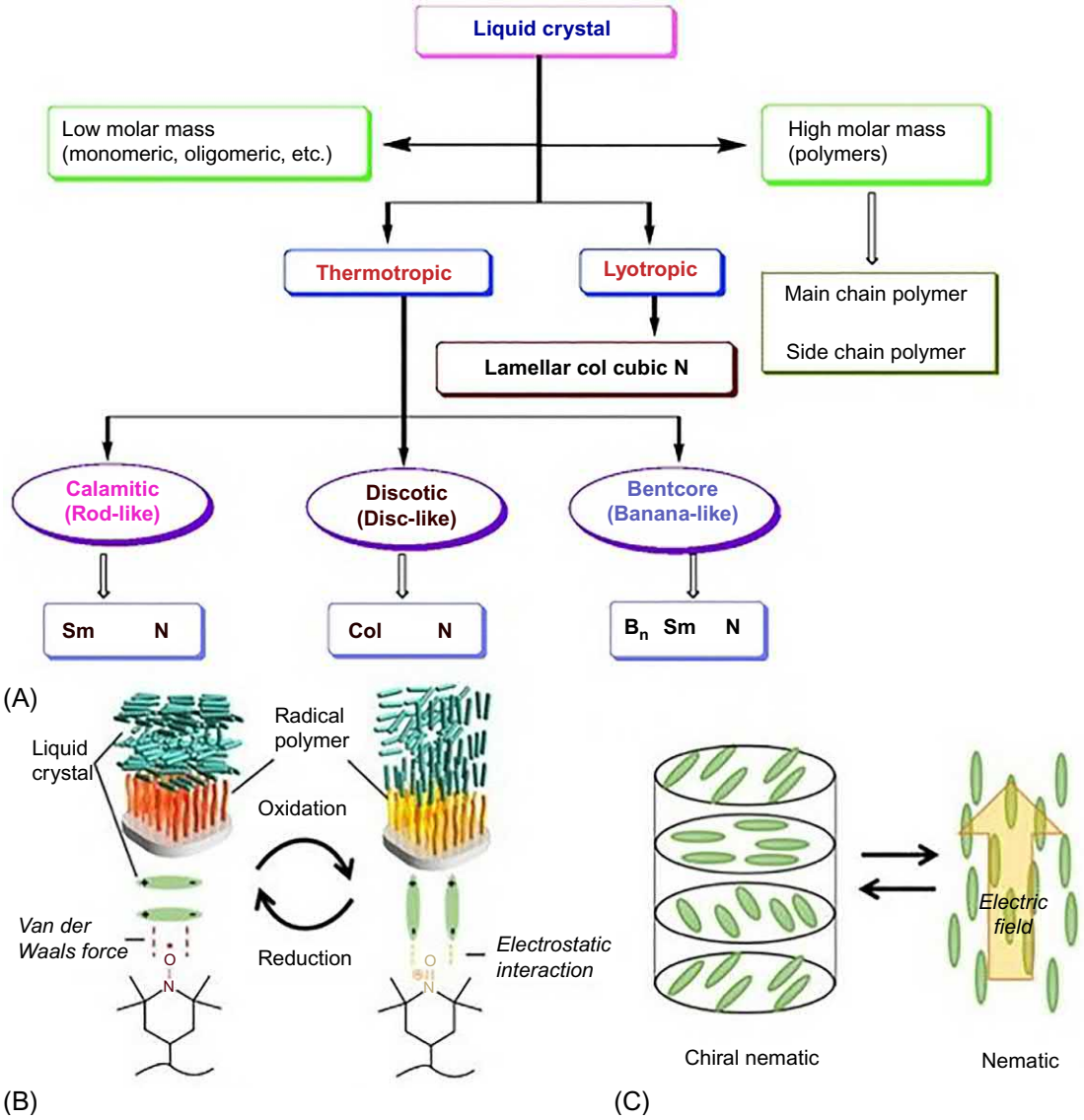

Fig. 12.2

(A) Classification of liquid crystal, (B) switching of chiral nematic LC by radical polymers and by (C) an external electric field [35]. *Copyright @ 2017, Polymer Journal.*

the control of molecular alignment is more challenging for the chiral nematic phase. The anisotropic electromagnetic properties of the LC molecules enable the switching of the orientation of the nematic phase by the external application of a magnetic or electric field. As shown in Fig. 12.2C, the applied electric field could easily break the helical structures of the chiral nematic phases [35].

12.3.1 Thermotropic liquid crystal

In thermotropic liquid crystals, temperature determines the order of the components. As illustrated in Fig. 12.3, thermotropic liquid crystal falls into further classification as calamitic for rod-like shape, discotic for disk-like shape, and bent-core for banana-like shape, based on the shape of their constituent molecule mesogens [38]. The calamitic is highly important for applications, due to its response to electrical and magnetic fields.

Fig. 12.3A shows the main-chain liquid crystal polymer (MC-LCP) and Fig. 12.3B shows side-chain liquid crystal polymers (SC-LPs). Here the mesogens are tightly bound to each other or with a flexible spacer, which is more often an alkyl chain by which the mesogens are linked to the polymer backbone. The mesogens are connected to the polymer backbone either by one side or laterally in SC-LCP, whereas in MC-LCP, the mesogens are connected to the flexible spacer by their ends or laterally. A few LC materials undergo changes in phase before reaching a real isotropic phase, depending on the structure and the chemical properties of the mesogens [37].

Fig. 12.4 illustrates the various phases of a calamatic LC obtained upon heating. With increase in temperature, a thermotropic LC passes through higher-ordered phases, the fluid smectic phases ('Sm C' and "Sm A"), which exhibit both positional and orientation order, and finally passes to the nematic phase (N), characterized by purely orientation order with molecules arranged in the direction along the director axis, into the isotropic phase. The symmetry, order, and chemical composition of the liquid crystal molecules are the various factors that determine the different liquid crystal phases. The type of smectic phase is determined by the direction of the director as compared to the normal layer. An orthogonal smectic phase (Sm A) appears when the director "*n*" is parallel to the smectic layer normal, and a smectic phase (Sm C) is observed if the director is tilted by an angle "θ."

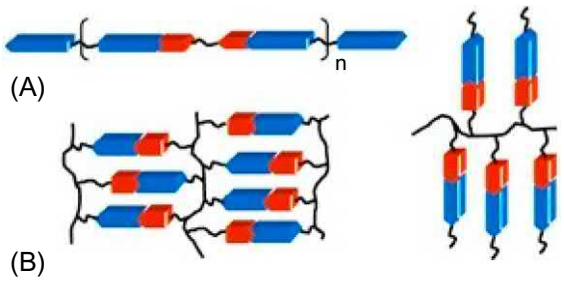

Fig. 12.3

Architecture of thermotropic liquid crystalline polymer [37]. Designing of hydrogen bonded liquid crystal assembly of polymer chain. (A) LC-state and (B) isotropic-state. *Copyright @ 2007, Springer.*

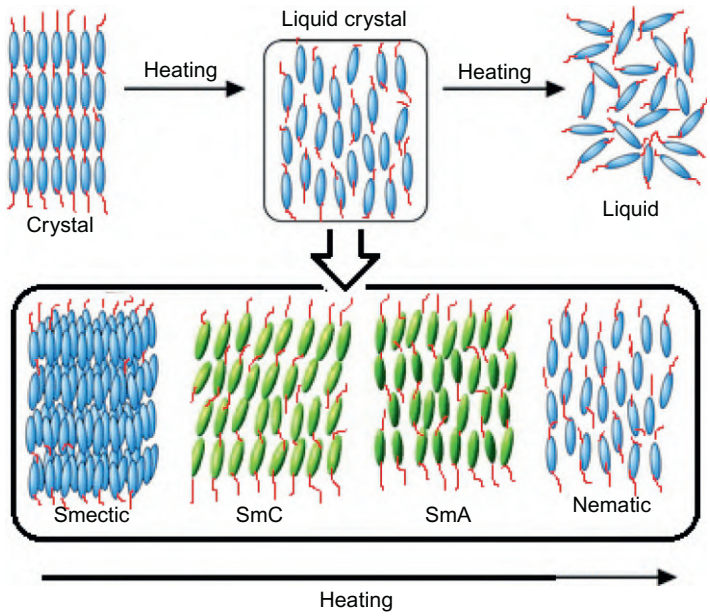

Fig. 12.4
Different thermotropic LC phases observed on heating from crystalline state.

12.3.2 Lyotropic liquid crystal

On the other hand, a lyotropic liquid crystal is formed when, under certain circumstances of pressure, temperature and concentration, an amphiphilic molecule is melted in an appropriate solvent medium. The "lyotropic" liquid crystal mixture is controlled by varying the concentration of the solvent. A thermotropic LC undergoes phase change with change in temperature, whereas lyotropic LC phase changes are dependent on temperature of the system and the concentration of the components. As indicated in Fig. 12.5, different lyotropic LC phases are formed by increasing the amphiphile concentration. The high amphiphile liquid crystal concentration separate hydrophobic and hydrophilic regions that lead to the molecular arrangements into spherical or rod-like micelles, then form a hexagonal phase. Sometimes the micelles combine together in a cubic arrangement, to form a phase known as the cubic "lyotropic" LC phase, and the increase in concentration leads to the formation of yet another phase, known as the "lamellar" phase [40]. The lyotropic LCs can be inorganic when they occur in colloidal size [41] and the solute component consists of anisotropic-shaped, much larger solid particles.

12.3.3 Functional properties and application of liquid crystal

Liquid crystal, a soft condensed-matter material, presents various anisotropic physical properties while retaining its capability to flow: for instance, magnetic susceptibility, electric conductivity, viscosity, elastic constant, and refractive index [42–46]. Researchers found

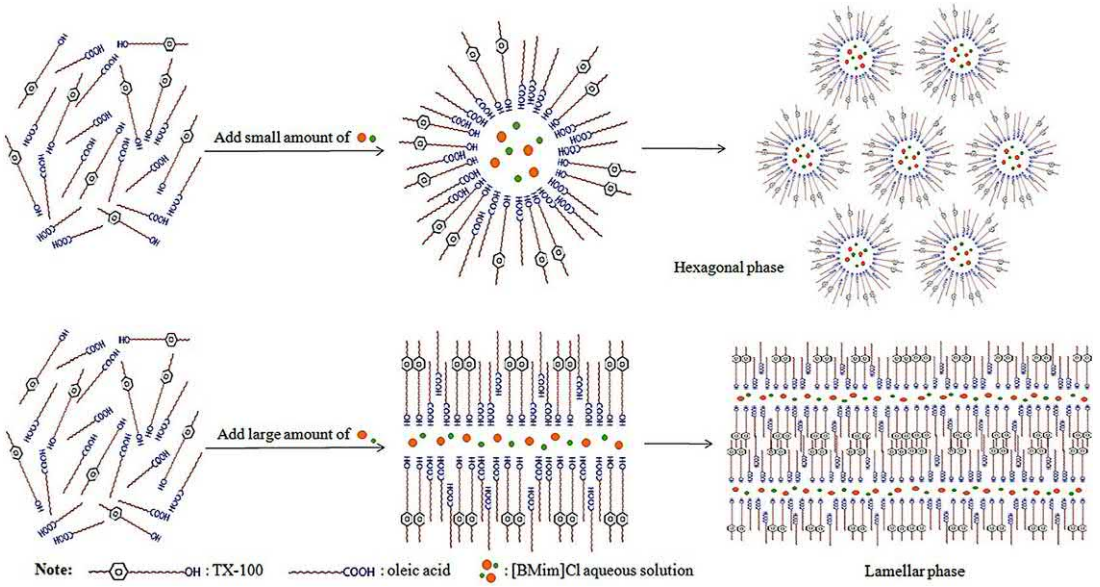

Fig. 12.5

Lyotropic LC phase diagram of amphiphilic molecules dissolved in a solvent [39]. *Copyright @ 2019, Elsevier, Journal of Molecular Liquids.*

extensive applications for liquid crystal, as the macroscopic properties of the crystal can be altered by external perturbations such as electric and magnetic fields. Anisotropic molecules of the liquid crystal react to external fields and interact with surfaces to manipulate their structure and properties [47]. The speed of the molecular alignment due to the influence of external field is an important property of the liquid crystal that is of high interest in industrial applications. Distinctive surface treatment or magnetic, electric, optic stimuli, and temperature can easily influence the orientation of the director of the liquid crystal. Recently, rod-like and disc-like mesogens have led to the development of nonconventional chemical structures for liquid crystals [25, 48]. The bent-core LC has emerged with a unique ferroelectric property and exhibits spontaneous polarization and polar switching in the liquid crystal phase [49].

A diversity of phase transition properties such as crystal– liquid crystal, liquid crystal-liquid crystal, and liquid crystal-isotropic transitions are observed in liquid crystal matrix. These order-order and order-disorder transitions are essential for the proper functioning of liquid crystals [25, 50, 51]. Researchers' attention has been strongly focused on numerous external stimuli: for instance, the photo, mechanical, or electric field that triggers the phase transition in thermotropic LC, in addition to thermal stimuli. The molecular order of the LC can be effectively manipulated with a photo-stimuli [52]. Mechanical stimuli induce a phase transition in liquid crystal and also help to acquire macroscopically oriented LC to form a columnar liquid crystal phase that enhances the transport properties of charge and ions and polarized

photoemission [53, 54]. Electric-field stimuli have been used as a significant force to align liquid crystal molecules. The columnar LC molecules can be easily oriented by the application of electric fields [55].

The discovery of liquid crystal as a display device in 1970, has led to it becoming the most popular display material around the world [56]. The molecular motion and orientation theories of liquid crystal have gained widespread attention in numerous fields, including bioscience and information technology, finding application in sensors, medicines, photonics, electrooptical devices, and many others [57]. Thermotropic liquid crystals find extensive application in electrooptic displays, temperature sensors, and selective reflective pigments. Lyotropic LCs, on the other hand, are widely used in the cleaning and cosmetic industries. They are also used in the preparation of mesoporous materials. Liquid crystals are exceptionally varied, as there are varieties of LCs found in DNA, synthetic polymers, and small organic molecules like alkyl and alkoxy cyanobiphenyls group exists into the host material.

Over the last decades, liquid crystal science has stimulated the area of Nanoscience and advanced technology, promising a new era of Materials Science. Recent developments in the field of Nanotechnology have mainly been focused on synthesis of nanomaterials using liquid crystals, the design and fabrication of liquid crystal nanomaterials, and alignment and self-assembly of nanomaterials using liquid crystal phases. Revolutionary developments in nanotechnology were evident with the birth of new devices and products obtained by appropriate control of the properties of the nanostructured materials. The main challenge faced by researchers in the field of nanotechnology is to realize new methodologies for assembling nanostructured building blocks into functional bulk materials. Hence, much current research is focused on designing nanomaterials that are capable of self-assembly into bulk structures. Liquid crystalline materials have proved to be a perfect solution for the production of nanostructured materials, and their self-assembly in the LC state combines order and mobility at the nanoscale level.

12.4 Important exploration of nanoscience and nanotechnology

The study of the manipulation of materials at the atomic, molecular, and macromolecular scales is referred to as nanoscience, whereas nanotechnology refers to constructing and engineering functional systems at a very micro level, or even at a molecular level. The fast-growing fields of Nanoscience and Nanotechnology have demanded that researchers explore the primary chemical and physical properties of nanomaterials by manipulating their shape and size, leading to the birth of a series of novel nanomaterials whose size is in the range from 1 to 100 nm [58]. Hence, nanotechnology is opening up many innovations in materials that are lighter, stronger, and more flexible, with high sensitivity, multifunctionality, and intelligence. Currently, the principal objective of nanotechnology is to manipulate the molecular structure and explore the characteristics to develop novel devices.

12.5 Drawbacks of nanomaterials

Nanomaterials are particles that exhibit extremely small dimensions that benefit their unique physical and chemical properties at the nanoscale. Nanomaterials are referred to as materials with dimensions on the order of a few nanometers. The physical and chemical properties of these nanostructured materials are entirely different from the bulk particles due to their unique size, and they behave in a way that is not seen in their bulk materials. More precisely, materials less than 100 nm in at least one dimension are referred to as nanomaterials. The definition of nanomaterial accepted by the European Commission on October 18, 2011 is "a natural, incidental or manufactured material containing particles, in an unbound state or as an aggregate or as an agglomerate and for 50% or more of the particles in the number size distribution, one or more external dimensions is in the size range 1 nm – 100 nm. In specific cases and where warranted by concerns for the environment, health, safety or competitiveness the number size distribution threshold of 50% may be replaced by a threshold between 1% and 50%." Fig. 12.6 illustrates, a comparison of macroscale and microscale particles with

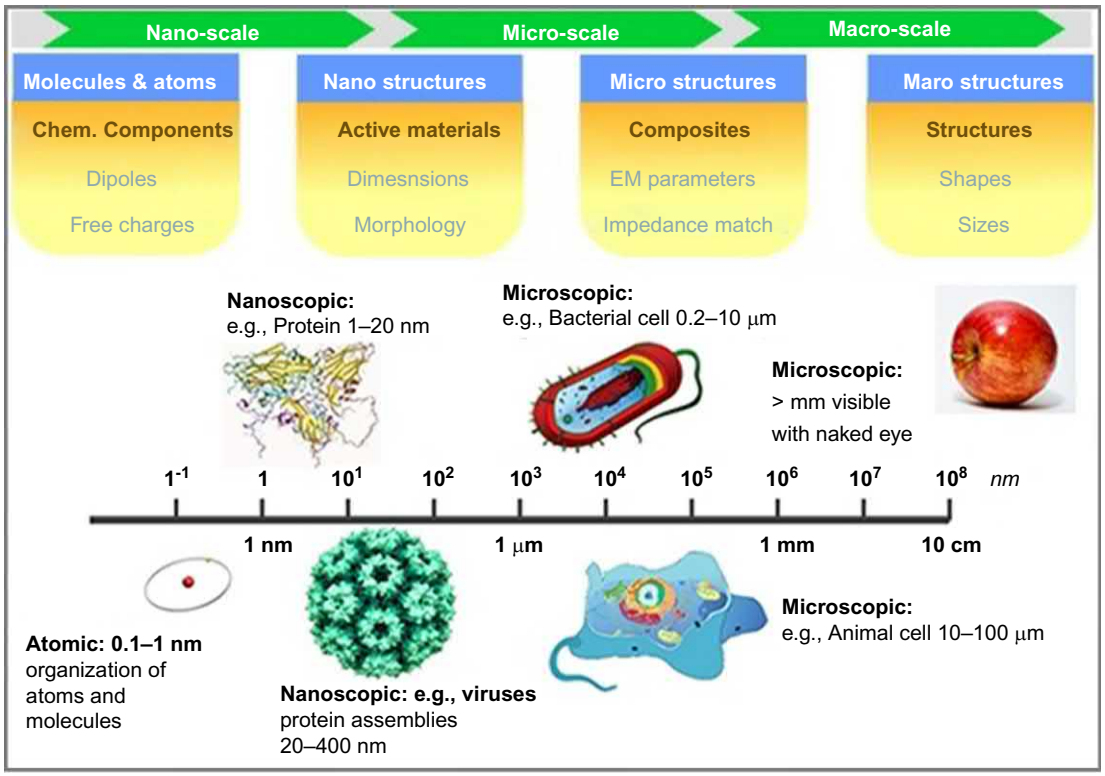

Fig. 12.6

Illustrates the macroscale to microscale and nanoscale comparison [59]. *Copyright @ 2012, Elsevier.*

particles of nanoscale. The diameter of human hair is 15×10^4 nm, indicating that nanomaterials are too small to be seen with the human eye [59].

Many properties of a material turn into highly noticeable phenomena as the material size diminishes. Some commonly observed properties of nanomaterials are: conductivity of metal nanoparticles decreases as the size of the material is reduced significantly; an antibacterial property has been seen in silver nanomaterials; gold nanoparticles reveal catalytic properties; nanostructured metal enhances optical absorption and florescence properties, as compared to their bulk materials [3, 60, 61]. The latest developments in technology such as the scanning tunneling microscope (STM), atomic force microscopy (AFM), high-resolution transmission electron microscope (HR-TEM), and field emission scanning electron microscope (FE-SEM) enable researchers to observe the size and shape of nanomaterial with high accuracy. Recent years have witnessed tremendous growth in nanomaterials and many novel nanomaterials, such as: graphene, metallic nanomaterials, fullerene, semiconductor quantum dots, nanorods, and carbon nanotubes, have been developed.

12.5.1 Evaluation of nanomaterials from bulk materials

Elevated surface area and quantum effects that can alter or improve the properties of nanomaterials, such as their strength, reactivity, and electrical properties, are the two main features that distinguish nanomaterials from their bulk material. Extensive research on nanomaterials led to the discovery that, with reduced particle size, more atoms accumulate on the surface than in the inner part. It has been observed that 5% of atoms are found on the surface of a particle with dimension 30 nm, while 20% of atoms accumulate on the surface when the particle size diminishes to 20 nm, and 50% are on the surface for a particle size of 3 nm. This proves that nanoparticles possess much higher surface area per unit mass than their bulk materials, and for a given mass they are more reactive than the same mass of bulk material, as most of the chemical reaction takes place at the surface. The high surface area effect of nanomaterials can improve the optical, electrical, and magnetic properties of the material.

12.5.2 Varieties of nanomaterials and their applications

Nanomaterials are generally classified based on the mode of fabrication, into natural and artificially fabricated nanomaterials. Materials that incorporate a biological system within them come under the category of natural nanomaterials, whereas nanomaterials developed by performing various laboratory-based experiments are known as artificial nanomaterials. They fall under four subdivisions:

(i) **Carbon based:** These nanomaterials are composed mostly of carbon, most commonly taking the form of hollow spheres, ellipsoids, or tubes. Spherical and ellipsoidal carbon

nanomaterials are referred to as fullerenes, while cylindrical ones are called nanotubes, or carbon nanotubes (CNTs).

(ii) **Metal based:** These nanomaterials include quantum dots, nano-gold, nano-silver, and metal oxides, such as titanium dioxide.

(iii) **Dendrimers:** These nanomaterials are nanosized polymers built from branched units. The surface of a dendrimer has numerous chain ends, which can be tailored to perform specific chemical functions. This property can also be useful for catalysis. Also, because three-dimensional dendrimers contain interior cavities into which other molecules can be placed, they may be useful for drug delivery.

(iv) **Composites:** They are obtained by combining nanoparticles with other nanoparticles or with larger, bulk-type materials. The composites may be any combination of metal-based, carbon-based, or polymer-based nanomaterials with any form of metal, ceramic, or polymer bulk materials.

Some of the common applications of nanomaterials are illustrated in Fig. 12.7.

12.5.3 Dimensions of nanomaterials

This classification is based on the number of dimensions of a material outside the nanoscale (<100 nm) range. Accordingly, in zero-dimensional (0-D) nanomaterials, all the dimensions are measured within the nanoscale (no dimensions are larger than 100 nm). Most commonly, 0-D nanomaterials are nanoparticles. In one-dimensional nanomaterials (1-D), one dimension is outside the nanoscale. This class includes nanotubes, nanorods, and nanowires. In two-dimensional nanomaterials (2-D), two dimensions are outside the nanoscale. This class exhibits plate-like shapes and includes graphene, nanofilms, nanolayers, and nanocoatings.

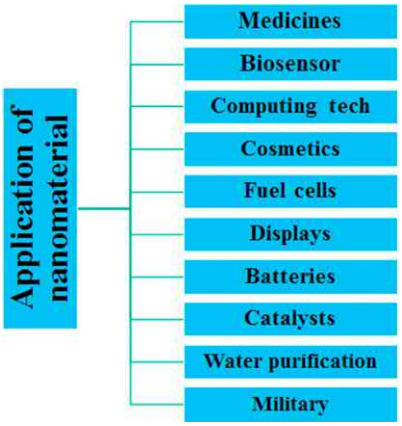

Fig. 12.7
Applications of nanomaterials in various aspect.

Three-dimensional nanomaterials (3-D) are materials that are not confined to the nanoscale in any dimension. This class can contain bulk powders, dispersions of nanoparticles, bundles of nanowires, and nanotubes as well as multi-nanolayers [62].

Fig. 12.8 illustrates the various epitaxial hybrid nanostructures with differing architectures. The core shell nanostructure as shown in Fig. 12.8A is made by growing a shell or a multilayer of shell on a seed nanocrystal. Examples include quantum rods, nanorods, nanowires, etc. The nanoparticle-based hybrid nanostructures in Fig. 12.8B are made by the epitaxial deposition of spherical nanoparticles on the surface of other types of nanostructures, such as nanocubes, nanorods, nanowires, etc. Well-defined heterostructures are constructed by epitaxially aligning two nanocrystals in an ordered manner; see Fig. 12.8C. Hierarchical heterostructures as shown in Fig. 12.8D are usually produced by the epitaxial growth of 1-D nanorods on the surfaces of nanoparticles, nanowires, or nanoplates, or by the epitaxial growth of 2-D nanoplates or nanosheets on the surface of 1-D nanostructures. The 2D-2D heterostructures shown in Fig. 12.8E have been extensively explored in recent years in the fields of electronics and optoelectronics, as they can be considered as atomically thin 2-D p-n junctions. These 2D-2D heterostructures can be further classified into 2-D lateral heterostructures and 2-D vertical heterostructures.

12.6 Nanomaterial dispersed liquid crystal

With the rapid growth and remarkable advantages of nanomaterials, many technologists have focused their attention on developing a diversity of hybrid nanocomposites by dispersing nanomaterials on liquid crystal to enhance their functionality other than the display property [64]. The uniform scattering of nanomaterials on liquid crystal improves the optical and electronic properties, thereby promising a wide range of uses in various applications. It was observed that in composite liquid crystalline materials, long-range orientation and interactions in the mesophase could develop a strong impact on the properties of liquid crystals or on the properties of nanomaterials. These hybrid nanocomposites exhibit novel functions and physical characteristics, depending on the features of the dopants and the interaction between the liquid crystal and nanomaterials [16–18]. Accordingly, four groups of nanomaterials that are used as dopant in liquid crystals are (i) metal nanoparticles, (ii) ferroelectric nanoparticles, (iii) semiconductor nanoparticles, and (iv) carbon nanoparticles. The nanocomposite material properties depend on certain features of the dopants, such as size, type of material, time taken, and preparation conditions.

To stabilize the mesophase, researchers disperse metal and semiconducting nanoparticles to the LC. It has been noticed that silica, ferroelectric, and metal nanoparticles create a strong impact on the electrooptical response of the nematic liquid crystal and produce a memory effect without applying any external electric field [65–67]. Also, the dispersion of metal nanoparticles on nematic LCs induces a frequency-dependent electrooptical response, owing to the

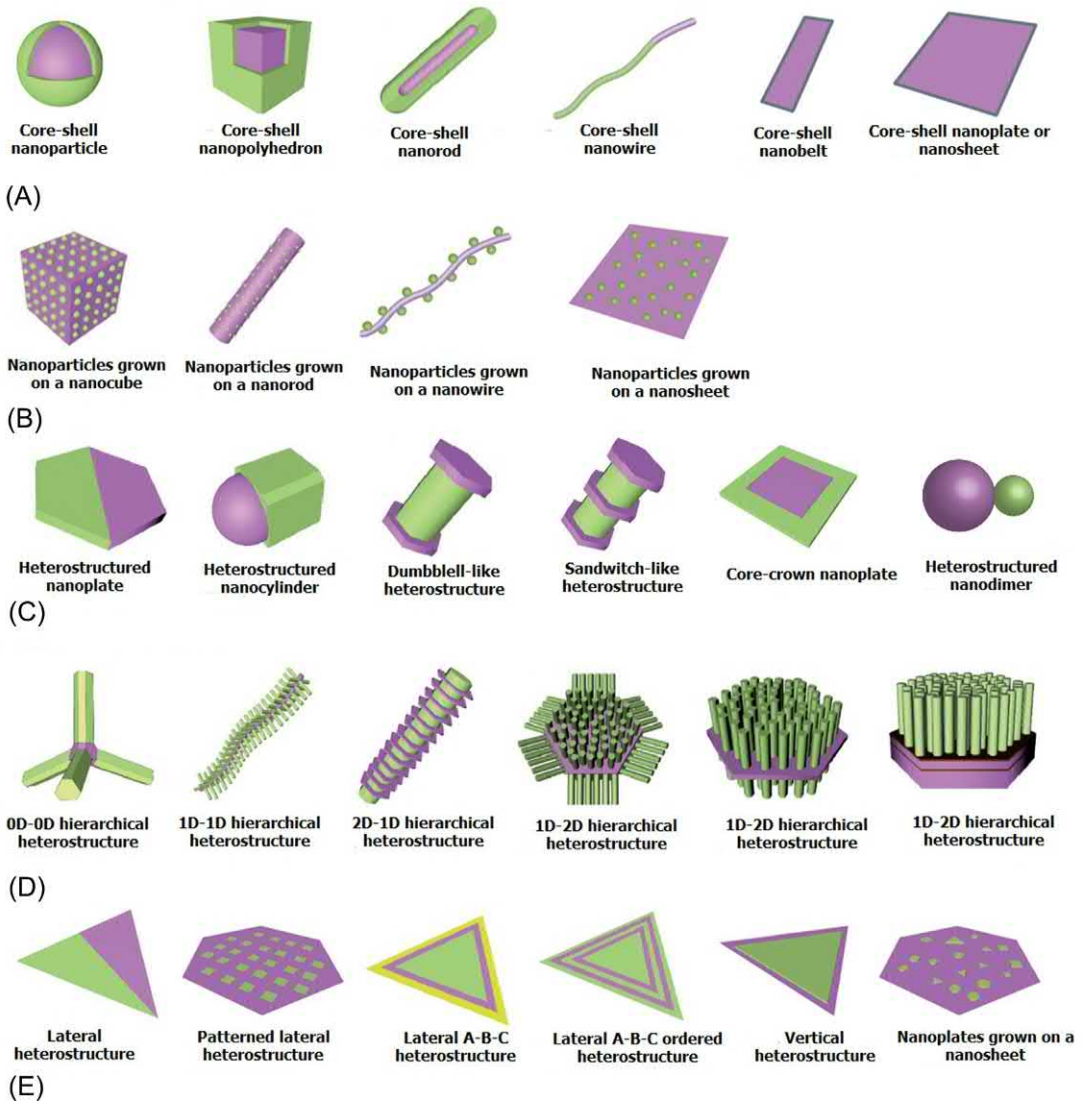

Fig. 12.8

Architectures of epitaxial hybrid nanostructures [63]. (A) Core-shell nanostructures, (B) nanoparticle-based hybrid nanostructures, (C) well-defined heterostructures, (D) hierarchical heterostructures, (E) 2D-2D heterostructures. *Copyright @ 2018, Nature Reviews Material.*

combination of the dielectric properties of the nanoparticles and the liquid crystals [68, 69]. Extensive research in the area of Nanotechnology has led to some interesting observations: the addition of carbon nanotubes to nematic liquid crystal enhances the electrical conductivity based on the orientation of the tubes along the direction of the director of liquid crystal [70];

dispersion of fullerenes improves the switching speed of liquid crystal and adding graphene to liquid crystals boosts the electrooptic switching characteristics [71]. The thriving development in the field of Nanotechnology has led to different categories of novel nanomaterials whose size, shape anisotropy, surface structure, etc. can be well controlled and this has caused a dramatic improvement in the usage of nanocomposite LCs, which are complemented by some rather amazing physical properties. The attention of this chapter is thus mainly concentrated on the functionalities of nanomaterial-dispersed LCs and principally their use as a thermal sensor.

12.7 Liquid crystal-based temperature sensor

Temperature changes are inevitable in various biological processes, industries, control systems, automobiles, energy, food, and a wide variety of other applications, which ensures the importance of temperature sensors to enable operations in diversified temperature conditions. Among the available temperature sensors that work on different theoretical concepts, the most popular are thermocouples, resistor temperature detectors, optical-fiber temperature sensors, thermistors, and integrated circuit temperature sensors. Recent research has discovered that an extremely capable temperature sensor can be designed and fabricated by using liquid crystals. Such LC thermal sensors require a nematic phase of the LC and contain a high thermooptic coefficient and elongated organic molecules of nanometric scale that produce an orientational order. The liquid crystal material and its characteristic parameters such as cell thickness and alignment play vital roles in influencing the sensitivity of the sensor. LC temperature sensors offer a wide temperature range, from 35°C to more than 170°C, depending on the choice of the LC material [72].

12.7.1 Scope of sensor

The anisotropic properties of liquid crystal that can be controlled electrically have led to the development of innovative devices for extensive and varied fields of applications. Moreover, the temperature dependence of nematic liquid crystal parameters has revolutionized the design of nematic liquid crystal devices into the development of temperature sensors. Most of these sensors make use of the optical properties of the nematic liquid crystal device. A chiral nematic liquid crystal temperature sensor measures the temperature change by monitoring the color change. The major disadvantage of this system is its low sensitivities and range of temperature. Marcos et al. [73] described a frequency temperature LC transducer that depends on the change in permittivity with temperature. A wide range of temperature and high sensitivity has been reported for this particular sensor.

12.7.2 Design and fabrication of nanomaterial dispersed liquid crystal (NLC) temperature sensor

This novel sensor consists of a micrometer-sized indium tin oxide (ITO) comb electrode structure and a thin-film in which the temperature change is presented as a hyperbolic cosine function that leads to high sensitivity. The high efficiency of the sensor is owed to the dispersion of metal nanomaterial (nickel) on the surface of the indium tin oxide comb electrode. The high voltage output depends on the structure and dimensions of the liquid crystal device [74]. The confined geometry of photo-refractive ITO coated LC cell decoration as displayed in Fig. 12.9A shows the cross-sectional view of the sensor, and Fig. 12.9B illustrates two electrodes (comb 1 and 2) connected at the conducting junction.

Among the two electrodes, the voltage source is the electrode Comb 1 and Comb 2 is responsible for determining the voltage drop at the midpoint of two teeth of Comb 1. Comb electrodes are made up of a chrome mask that has soda lime glass and synthetic quartz as the base material. They are designed for use in high-resolution lithography. The glass substrate is coated with indium tin oxide and has electrodes with a width of 20 μm. There are approximately 51 electrodes in each comb. Deposition of nickel nanoparticles onto the silicon dioxide (SiO_2) layer by the process of evaporation increases the conductivity of the device. A spacer of 40 μm is incorporated to provide a separation between the glass substrates. Nematic liquid crystal (MDA-98-1602) fills in the resultant cavity [74]. The equivalent electric circuit of the sensor set-up is as shown in Fig. 12.10.

The voltage between the electrodes is given by the equation:

$$\frac{\partial V^2(x)}{\partial x^2} = \frac{\frac{1}{R_{LC2}} + j\omega C_{LC2}}{\frac{1}{R_{SqNi}} + j\omega C_{LC1}} . V(x) \tag{12.1}$$

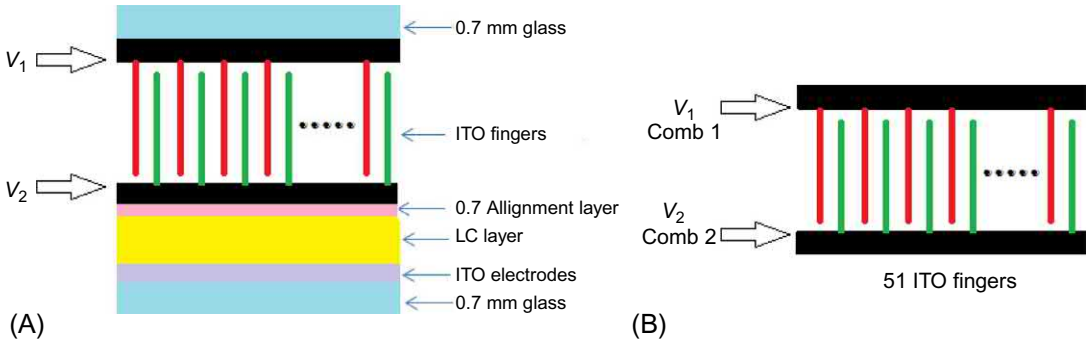

Fig. 12.9

Liquid crystal temperature sensor. (A) A cross-sectional view of the sensor showing the electrodes and glass base coated with indium tin oxide; (B) combination of two electrodes system.

where R_{sqNi} is the resistance of the nickel layer, R_{LC} is the resistance of the liquid crystal, C_{LC} is the capacitance of the liquid crystal, and V_1 and V_2 are the voltages measured at the electrodes as a function of $V(x)$.

The parallel R_{LC1} and C_{LC1} of the circuit are neglected, as they are much higher than the resistor R_{SqNi} and this increases the sensitivity of the circuit. In the frequency range of 100 Hz to 10 kHz, the resistance R_{LC2} is higher than the impedance of C_{LC2} and it can be neglected. The C_{LC2} is related to the structure of the sensor by the equation:

$$C_{LC2} = \varepsilon_0 . \frac{\varepsilon'_{LC2}}{t_{LC}},$$

where ε_0 is the permittivity of the vacuum, t_{LC} is the thickness of the liquid crystal, and $\varepsilon'_{LC2}$is the average real permittivity. Substituting $V(x = -r) = V(x = r) = V_1$, and $V(x = 0) = V_2$, where r is the distance between electrodes, then the following equation is obtained:

$$V_2 = \frac{V_1}{\cosh\left(\sqrt{\frac{R_{sqNi}\varepsilon_0\varepsilon' t_{LC2}\omega}{2t_{LC}}}.r\right)} \tag{12.2}$$

The sensitivity of the sensor is determined by the parameter ε'_{LC2}. As the applied voltage rises, the real permittivity also increases its value to an extraordinary permittivity ε'_e from its ordinary permittivity ε'_o and vice versa. The parameter ε'_e varies highly with change in temperature and the sensitivity increases with increase in the input voltage. Sensitivity can be determined using the relation $S = \Delta V_2/\Delta T$ (mV/°C). Thus it can be concluded that the sensitivity of the sensor is directly proportional to the applied voltage. Experiments also reveal that the minimum operating temperature possible for this nematic liquid crystal temperature sensor is −20°C.

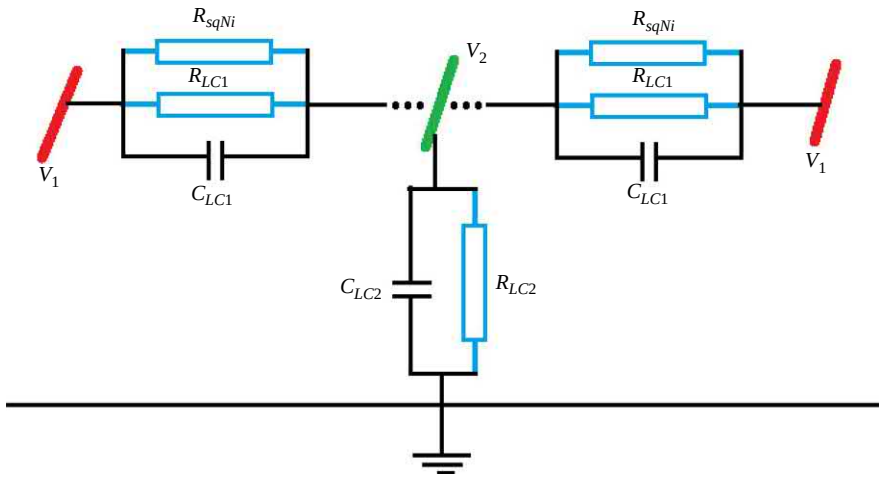

Fig. 12.10
Equivalent electric circuit.

12.7.3 Experimental set-up, observation, and results

The experimental set-up is devised by a heating and freezing stage LT350, inside of which the sensor is placed, operated by a system controller TP94. Two additional silicon temperature sensors, LM35, are employed on both sides of the substrate to obtain better control of temperature by avoiding the losses in calibration of the system controller, TP94, considering the possible change in temperature due to uneven thickness of the liquid crystal sensor. An automated MATLAB program was developed to control the set-up, evaluate the measured data, and provide graphical representation of temperature and voltage dependence.

As shown in Fig. 12.11, the input AC voltage is controlled by a waveform generator along with a high voltage broadband amplifier. An AC square signal of variable frequency and amplitude is generated by the waveform generator. An increase in temperature at a rate of 1°C is produced by the heating stage. The output of the silicon sensors is directed to the two analog inputs of the ATMEGA 2560 microcontroller. The data output obtained through the USB port is processed at the rate of 3 samples per minute by the MATLAB program. It is observed that the permittivity changes according to the change in temperature and subsequently changes the output voltage V_2. The output voltage, which is approximately 10 times the input voltage, is then coupled to a buffer amplifier (TL081) employing an operational amplifier. The AC output of the buffer is converted to DC by using an AC-to-DC converter (AD536). This DC output is then directed to the analog input of the microcontroller and is processed by MATLAB.

Eq. (12.2) indicates that the output voltage is directly related to the distance between the electrode (r) and the thickness of the sample (t_{LC}). It was observed that $V_2 = 0.1\ V_1$ at a temperature of 25°C and when the relation between two electrodes the permittivity becomes 0.4.
The experiments confirmed that the liquid crystal has a high permittivity anisotropy that is dependent on the voltage.

In the next trial, input voltage with varying frequency and constant amplitude was applied to the system and measurements were taken by increasing and decreasing the temperature; no hysteresis was observed, which implies that there is no difference on the offset error.

Among the output voltages measured for three different frequencies at 1, 10, and 100 kHz, it was noticed that highest sensitivity was obtained at 1 kHz input voltage. The real permittivity ε'_{LC2} predominates at this frequency because of its greater temperature dependence. Among the responses obtained for three different frequencies (100 Hz, 1 kHz, and 10 kHz), the best linearity was indicated by the responses at 1 and 10 kHz. It was also observed that the voltage's sensitivity to temperature was predominant at higher voltages.

To understand the significance of the nanomaterial effect on the temperature sensor, a similar device without the Ni layer was fabricated and tested for high input voltage. The highest

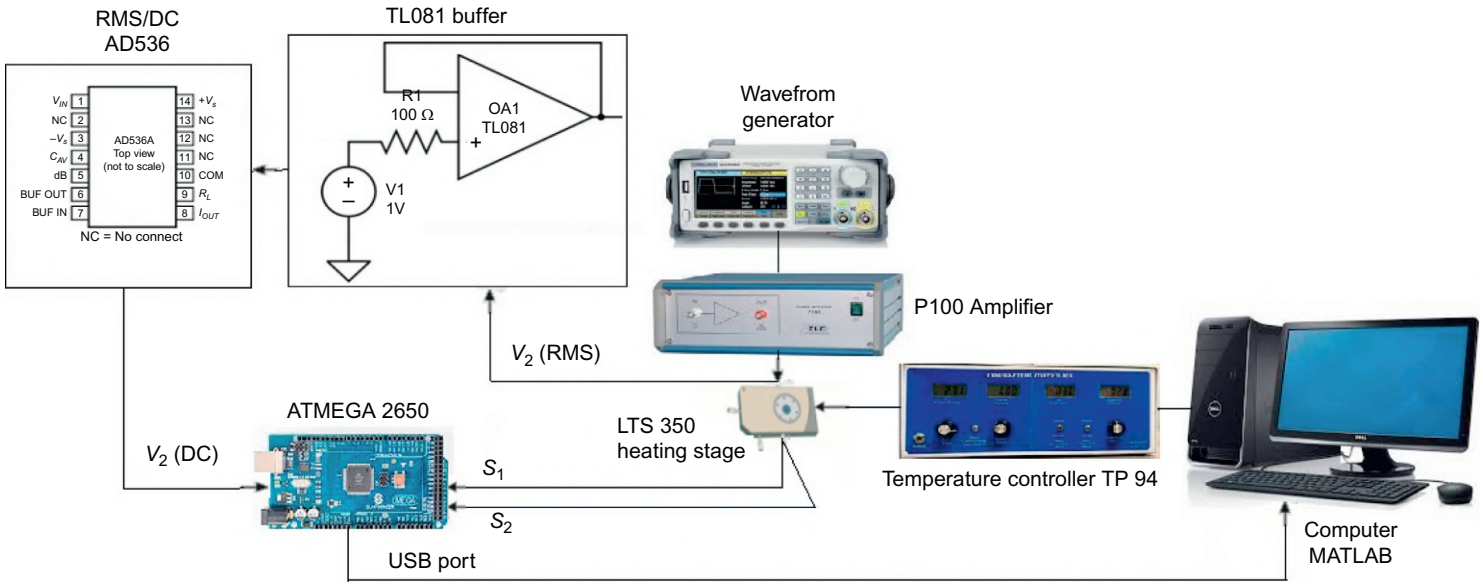

Fig. 12.11
Liquid crystal temperature sensor experimental set-up.

sensitivity obtained for the temperature between 60°C and 95°C was 33 mV/°C. For the temperature sensor with the Ni layer, higher sensitivity is expected than for a sensor without a Ni layer. This layer allows maximum current, which in turn allows more input voltage to be applied. The sensitivity is affected by the applied voltage, as the extraordinary permittivity is highly dependent on the temperature. This proves that homogeneous alignment of molecules is the principal factor in determining higher sensitivity at low voltages. Results obtained by the application of 2 and 4 V to the sensor circuit with and without the Ni layer in the temperature range of 20–100°C confirm that the use of the Ni layer increases the sensitivity and also sensitivity is directly related to increase in temperature.

The temperature sensitivity of the device with the "Ni" layer is approximately six times greater than in the sensor without the "Ni" layer. The introduction of RsqNi increases the sensitivity. The sensor could follow the temperature with high sensitivities in this specific range. Considering the high sensitivity obtained, the LC temperature sensor has numerous benefits over the other available sensors. Yet another noticeable feature of the LC temperature sensor is the reduced power consumption, which depends on the impedance of the LC cell at the particular voltage applied as input. Impedance of the liquid crystal temperature sensor was measured for various frequencies between 100 Hz and 1 kHz for the input voltage of 2 and 30 V_{rms}. It is evident from the graph that high impedance is observed for low applied input voltage (2 V_{rms}). Power consumed calculated by the formula, $P = \frac{V^2}{Z}$ indicates that the power consumption is low for high impedance. This relation concludes that for low applied input voltages, the power consumed by the liquid crystal temperature sensor is very low and this property is highly applicable for portable devices. Low power consumption of the sensor also prevents the device from overheating during its operation.

This particular sensor can be easily integrated in LC displays due to the simplicity and similarity of these two technologies. This technology helps to fabricate miniaturized, reproducible, and low-cost devices by introducing very small-dimension coplanar electrodes. It is also evident that the magnitude or the frequency of the applied input voltage can be used to control the sensitivity of output voltage. Low power consumption and high temperature sensitivity enable this sensor to be used in a wide variety of applications, such as LCDs, LCD projectors, LCDs used in extreme environmental conditions, portable devices, and so forth. It is also concluded that the addition of a layer of nanomaterial Ni improves the sensitivity of the sensor by six times.

12.8 Wireless liquid crystal temperature sensor

Today, the sensor industry is vibrant and demands more flexible features that are not possible with a wired approach. The novel discovery of wireless sensors represents a long-awaited invention foreseen by e-medicine [75] and the Internet of Things (IoT). Wireless technology allows the sensor to operate in challenging environmental conditions with less power

consumption. In this section of the chapter, a wireless temperature sensor that exploits the capacitance of the liquid crystal cell as a sensing element is discussed. An inductive capacitive resonant circuit including this sensor promises the wireless connection.

12.8.1 Design of sensor

The main part of the sensor is the resonant circuit that contains the capacitive element coupled to the inductor. As shown in Fig. 12.12, this circuit is excited by the oscillating magnetic field sent out by the remote antenna. The variation of the capacitance caused by the change in temperature sets up a resonant frequency shift, which in turn causes changes in the impedance and is detected by the reader [76].

A nematic liquid crystal cell having a positive dielectric anisotropy ($\Delta\varepsilon$)10 at low frequencies and a clearing point of 104°C is inserted between indium tin oxide film-coated glass plates with an area of 1 cm^2. This set-up acts as a flat parallel plate capacitor, where the nematic liquid crystal is a dielectric and capacitance is given by the equation, $C = \frac{\varepsilon_0 \varepsilon' A}{d}$, where ε_0 is the dielectric permittivity of the vacuum, ε' is the relative permittivity of the dielectric. A is the area of the electrodes, and d is the distance between the cells. This expression shows that the gap between the parallel plates is a major factor in determining the capacitance. Hence for the experimental set-up the cell gap is fixed to 1.5 μm using a spacer, as illustrated in Fig. 12.13, to gain high temperature sensitivity [77].

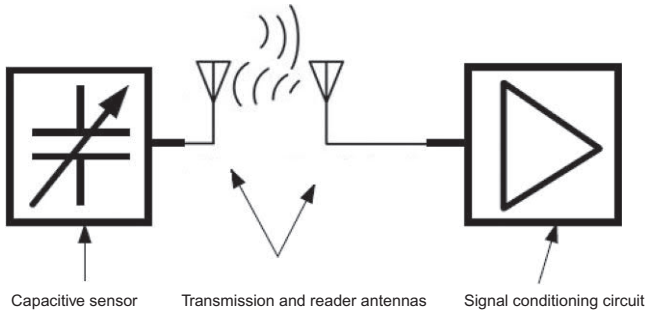

Fig. 12.12
Layout of the wireless temperature sensor circuit.

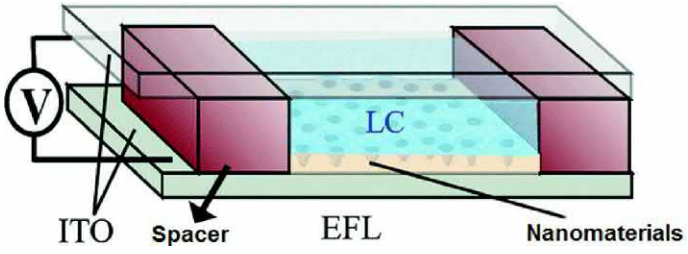

Fig. 12.13
Capacitive arrangement of nematic LC cell with spacer to fix the cell gap.

The homeotropic alignment of the LC cell is due to its larger sensitivity to change in temperature [78]. The capacitance of this liquid crystal arrangement varies as the dielectric permittivity changes with temperature and the dielectric permittivity is highly dependent on the molecular orientation of the liquid crystal material. Let the dielectric permittivity be ε when the electric field applied to the liquid crystal cell is zero and the molecular orientation is parallel to the substrate. Due to the application of a high electric field the molecular orientation now changes to be perpendicular to the substrate, with permittivity of ε'. A dielectric permittivity between ε and ε' is obtained by the application of an electric field.

12.8.2 Results and discussions

The frequency response obtained was nonlinear with sensitivity around 24.8 Hz/°C with a nonlinearity of 18.35%. To obtain the experimental results, both the antennas were fabricated with an inductance of 55.888 mH. Hence the values of both k and n are approximately 1. The capacitances at different temperatures are obtained by characterization of the NLC. The simulated resonant frequency response shows a close agreement between the experimental and theoretical results. These experiments conclude that the resonant frequency varies, as the capacitance of the liquid crystal cell changes, as a function of temperature.

The liquid crystal doped with dye is of huge interest, as it has a wide variety of applications. Doping with a florescent dye enhances various important parameters of the nematic liquid crystal, such as the changes in the molecular dynamics, which have a direct influence on the performance of the practical device. The temperature dependence of birefringence for pure nematic liquid crystal and dye-doped NLC is shown in Fig. 12.14A. An increase in temperature increases the output intensity for pure NLC and dye composite NLC, due to change in their molecular orientation, as indicated in Fig. 12.14B. Fig. 12.14C illustrates that dispersion of disc-shaped dye into a nematic liquid crystal structure enhances the molecular orientation. Experimental results also confirm that the relative permittivity increases with the doping of dye into NLC [79].

Easy availability and reduced cost of the liquid crystal cell, the accurate operation of the wireless connectivity, and high sensitivity make this wireless liquid crystal temperature sensor suitable for potential use in a wide variety of applications.

12.9 Conclusions and outlook

The temperature dependence of nematic liquid crystal parameters has revolutionized the design of nematic liquid crystal devices for the development of temperature sensors. The high efficiency of the sensor is owed to the dispersion of metal nanomaterial into the crystal structure. The high voltage output depends on the structure and dimensions of the liquid crystal device. A homeotropic alignment would make better use of the temperature permittivity

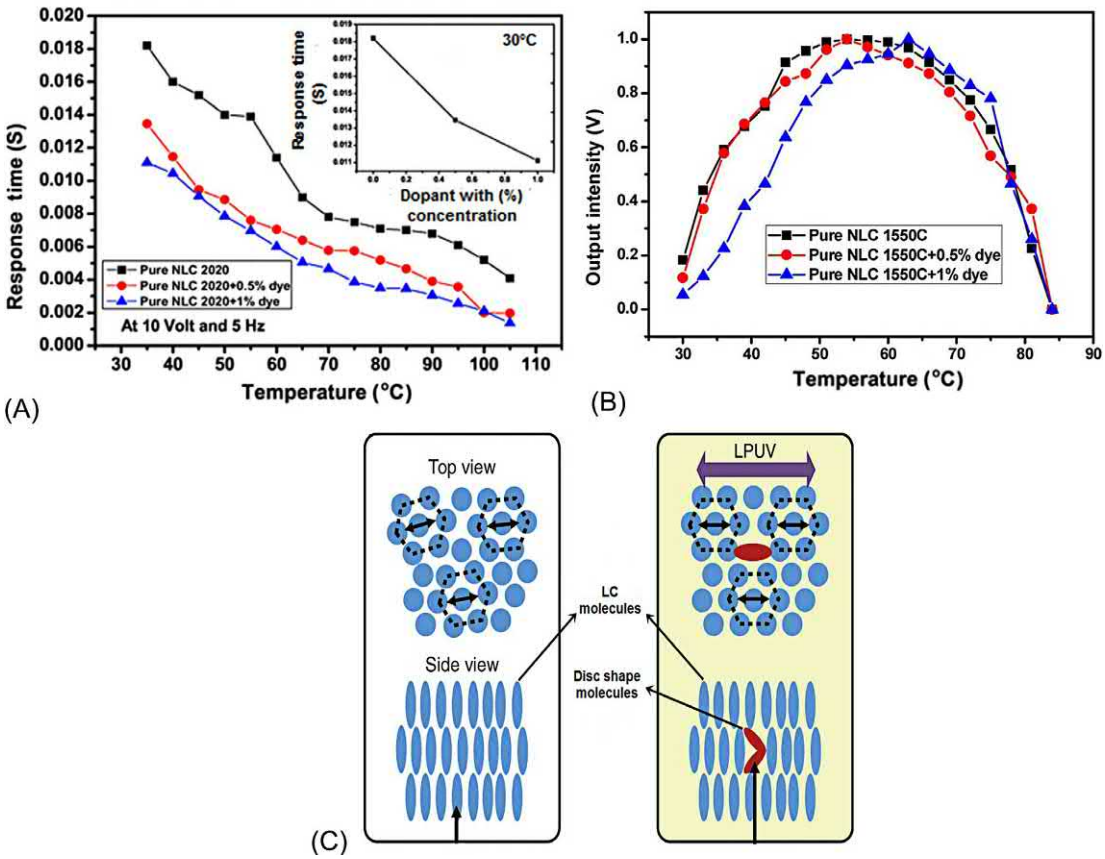

Fig. 12.14

(A) Variation in birefringence for pure and dye composite nanolaterials dispersed liquid crystal (NLC); (B) output intensity variation with respect to temperature; (C) change in molecular orientation with the addition of dye [79]. *Copyright @ 2018,Opto-Electronics Review.*

dependence of the LC cell. The high impedance input reduces the power dissipation and makes it a suitable device for a wide variety of novel applications. Reduced cost and high sensitivity promise acceptance of the LC temperature sensor in the field of Nanotechnology.

12.10 Benefits and future aspects

Nanotechnology is playing a vital role in many areas, with the invention of novel devices. The liquid crystal temperature sensor explored in this chapter is one such unique and novel piece of technology that utilizes the liquid crystal permittivity, which depends on temperature, to sense the variations in temperature. Among the other numerous benefits, high sensitivity and linearity improve the characteristics of LC temperature sensors, exceeding the capabilities of commercial sensors now available in the market. The unique feature of this novel device is

the possible integration of this LC temperature sensor in other switchable devices. The wireless LC temperature sensor improves flexibility, simplifies production, and is offered for many applications that were impossible with a wired approach. The wireless connectivity of this particular sensor reveals potential applications in biomedical, portable devices, devices operating in diverse environments and operational conditions, as well as many other areas.

References

[1] F. Baletto, R. Ferrando, Structural properties of nanoclusters: energetic, thermodynamic, and kinetic effects, Rev. Mod. Phys. 77 (1) (2005) 371.

[2] S. Nasir, et al., Carbon-based nanomaterials/allotropes: a glimpse of their synthesis, properties and some applications, Materials 11 (2) (2018) 295.

[3] C. Burda, et al., Chemistry and properties of nanocrystals of different shapes, Chem. Rev. 105 (4) (2005) 1025–1102.

[4] J. Liu, et al., Recent advances of plasmonic nanoparticles and their applications, Materials 11 (10) (2018) 1833.

[5] S. Zhang, et al., Directed assembly of hybrid nanomaterials and nanocomposites, Adv. Mater. 30 (18) (2018) 1705794.

[6] Q.-B. Meng, et al., Assembly of highly ordered three-dimensional porous structure with nanocrystalline TiO_2 semiconductors, Chem. Mater. 14 (1) (2002) 83–88.

[7] A. Furube, et al., Ultrafast plasmon-induced electron transfer from gold nanodots into TiO_2 nanoparticles, J. Am. Chem. Soc. 129 (48) (2007) 14852–14853.

[8] I. Robel, M. Kuno, P.V. Kamat, Size-dependent electron injection from excited CdSe quantum dots into TiO_2 nanoparticles, J. Am. Chem. Soc. 129 (14) (2007) 4136–4137.

[9] B.-R. Hyun, et al., Electron injection from colloidal PbS quantum dots into titanium dioxide nanoparticles, ACS Nano 2 (11) (2008) 2206–2212.

[10] A.K. Tripathi, et al., Study of structural transformation in TiO_2 nanoparticles and its optical properties, J. Alloys Compd. 549 (2013) 114–120.

[11] X. Li, et al., Enhanced birefringence for metallic nanoparticle doped liquid crystals, Opt. Commun. 286 (2013) 224–227.

[12] S.Y. Park, D. Stroud, Surface-enhanced plasmon splitting in a liquid-crystal-coated gold nanoparticle, Phys. Rev. Lett. 94 (21) (2005) 217401.

[13] P.A. Kossyrev, et al., Electric field tuning of plasmonic response of nanodot array in liquid crystal matrix, Nano Lett. 5 (10) (2005) 1978–1981.

[14] I. Dierking, Nanomaterials in Liquid Crystals, Multidisciplinary Digital Publishing Institute, 2018.

[15] V. Gerasin, et al., New approaches to the development of hybrid nanocomposites: from structural materials to high-tech applications, Russ. Chem. Rev. 82 (4) (2013) 303.

[16] A. Lapanik, et al., Electrooptical and dielectric properties of alkylthiol-capped gold nanoparticle–ferroelectric liquid crystal nanocomposites: influence of chain length and tethered liquid crystal functional groups, Soft Matter 8 (33) (2012) 8722–8728.

[17] R. Shukla, et al., Influence of different amount of functionalized bulky gold nanorods dopant on the electrooptical, dielectric and optical properties of the FLC host, Chem. Phys. Lett. 599 (2014) 80–85.

[18] T. Joshi, et al., Low power operation of ferroelectric liquid crystal system dispersed with zinc oxide nanoparticles, Appl. Phys. Lett. 96 (25) (2010) 253109.

[19] N. Lebovka, et al., Phase transitions in smectogenic liquid crystal 4-butoxybenzylidene-4′-butylaniline (BBBA) doped by multiwalled carbon nanotubes, Phase Transit. 86 (5) (2013) 463–476.

[20] U. Singh, et al., Enhanced electro-optical properties of a nematic liquid crystals in presence of $BaTiO_3$ nanoparticles, Liq. Cryst. 41 (7) (2014) 953–959.

[21] S. Bronnikov, et al., Dielectric study of side-chain liquid crystalline polyazomethine/fullerene C 60 nanocomposite, J. Polym. Res. 23 (3) (2016) 54.

[22] N. Koide, Liquid Crystal Display Story, Springer, 2016.

[23] T. Kato, et al., Molecular self-assembly of liquid crystalline side-chain polymers through intermolecular hydrogen bonding. Polymeric complexes built from a polyacrylate and stilbazoles, Macromolecules 25 (25) (1992) 6836–6841.
[24] H.K. Bisoyi, S. Kumar, Liquid-crystal nanoscience: an emerging avenue of soft self-assembly, Chem. Soc. Rev. 40 (1) (2011) 306–319.
[25] T. Kato, N. Mizoshita, K. Kishimoto, Functional liquid-crystalline assemblies: self-organized soft materials, Angew. Chem. Int. Ed. 45 (1) (2006) 38–68.
[26] T. Ohzono, J.-i. Fukuda, Zigzag line defects and manipulation of colloids in a nematic liquid crystal in microwrinkle grooves, Nat. Commun. 3 (2012) 701.
[27] Z.-G. Zheng, et al., Three-dimensional control of the helical axis of a chiral nematic liquid crystal by light, Nature 531 (7594) (2016) 352.
[28] Y. Shen, et al., Photoalignment of dye-doped cholesteric liquid crystals for electrically tunable patterns with fingerprint textures, Opt. Express 26 (2) (2018) 1422–1432.
[29] H.K. Bisoyi, A.M. Urbas, Q. Li, Soft materials driven by photothermal effect and their applications, Adv. Opt. Mater. 6 (15) (2018) 1800458.
[30] Y. Lin, et al., Magnetic nanoparticle-assisted tunable optical patterns from spherical cholesteric liquid crystal Bragg reflectors, Nanomaterials 7 (11) (2017) 376.
[31] M. O'Neill, S.M. Kelly, Ordered materials for organic electronics and photonics, Adv. Mater. 23 (5) (2011) 566–584.
[32] B. Dan, et al., Liquid crystals of aqueous, giant graphene oxide flakes, Soft Matter 7 (23) (2011) 11154–11159.
[33] J.E. Kim, et al., Graphene oxide liquid crystals, Angew. Chem. Int. Ed. 50 (13) (2011) 3043–3047.
[34] Z. Xu, C. Gao, Aqueous liquid crystals of graphene oxide, ACS Nano 5 (4) (2011) 2908–2915.
[35] K. Sato, et al., Grafted radical polymer brush for surface-driven switching of chiral nematic liquid crystals, Polym. J. 49 (10) (2017) 691.
[36] S. Chandrasekhar, B. Sadashiva, K. Suresh, Liquid crystals of disc-like molecules, Pramana 9 (5) (1977) 471–480.
[37] S.J. Rowan, P.T. Mather, Supramolecular interactions in the formation of thermotropic liquid crystalline polymers, in: Liquid Crystalline Functional Assemblies and Their Supramolecular Structures, Springer, 2007, pp. 119–149.
[38] I. Dierking, Textures of Liquid Crystals, John Wiley & Sons, 2003.
[39] Y. Fang, et al., Effect of 1-butyl-3-methylimidazolium chloride on the lyotropic liquid crystal structure and properties of TX-100/oleic acid/water system, J. Mol. Liq. (2019) 111637.
[40] D. Lombardo, et al., Amphiphiles self-assembly: basic concepts and future perspectives of supramolecular approaches, Adv. Condens. Matter Phys. 2015 (2015).
[41] I. Dierking, S. Al-Zangana, Lyotropic liquid crystal phases from anisotropic nanomaterials, Nanomaterials 7 (10) (2017) 305.
[42] R.A. Jones, Soft Condensed Matter, vol. 6, Oxford University Press, 2002.
[43] K. Salikhov, M. Kleman, O.D. Lavrentovich, Soft matter physics. An introduction, Appl. Magn. Reson. 27 (3) (2004) 563–564.
[44] L.S. Hirst, Fundamentals of Soft Matter Science, CRC Press, 2012.
[45] E.M. Terentjev, D.A. Weitz, The Oxford Handbook of Soft Condensed Matter, Oxford University Press, USA, 2015.
[46] P. De Gennes, J. Prost, The Physics of Liquid Crystals, second ed., Clarendon, Oxford, 1993.
[47] J. Banerjee, D. Bose, S.K.H. Rahaman, R.D.B. Walsh, M.J. Zaworotko, B.K. Ghosh, Indian J. Chem. 43 (2004) 1119–1122.
[48] M. Prehm, et al., New liquid crystalline phases with layerlike organization, J. Am. Chem. Soc. 124 (41) (2002) 12072–12073.
[49] T. Niori, et al., Distinct ferroelectric smectic liquid crystals consisting of banana shaped achiral molecules, J. Mater. Chem. 6 (7) (1996) 1231–1233.
[50] Y. Sagara, T. Kato, Mechanically induced luminescence changes in molecular assemblies, Nat. Chem. 1 (8) (2009) 605.

[51] O. Ikkala, G. ten Brinke, Functional materials based on self-assembly of polymeric supramolecules, Science 295 (5564) (2002) 2407–2409.
[52] D.H. Wang, et al., Photomechanical response of glassy azobenzene polyimide networks, Macromolecules 44 (10) (2011) 3840–3846.
[53] M. Yoshio, et al., One-dimensional ion transport in self-organized columnar ionic liquids, J. Am. Chem. Soc. 126 (4) (2004) 994–995.
[54] M.L. Bushey, T.-Q. Nguyen, C. Nuckolls, Synthesis, self-assembly, and switching of one-dimensional nanostructures from new crowded aromatics, J. Am. Chem. Soc. 125 (27) (2003) 8264–8269.
[55] N. Hu, et al., An electric-field-responsive discotic liquid-crystalline hexa-peri-hexabenzocoronene/oligothiophene hybrid, Adv. Mater. 26 (13) (2014) 2066–2071.
[56] S. Sano, et al., Enhancement of the characteristics of LCDs by doping nanoparticles: reduction of the operating voltage, viscosity, and response times, in: Liquid Crystal Materials, Devices, and Applications XI, International Society for Optics and Photonics, 2006.
[57] T. Hegmann, H. Qi, V.M. Marx, Nanoparticles in liquid crystals: synthesis, self-assembly, defect formation and potential applications, J. Inorg. Organomet. Polym. Mater. 17 (3) (2007) 483–508.
[58] M.A. Elkodous, et al., Therapeutic and diagnostic potential of nanomaterials for enhanced biomedical applications. Colloids Surf. B: Biointerfaces 180 (2019) 411–428, https://doi.org/10.1016/j.colsurfb.2019.05.008.
[59] A.Z. Wilczewska, et al., Nanoparticles as drug delivery systems, Pharmacol. Rep. 64 (5) (2012) 1020–1037.
[60] M.-C. Daniel, D. Astruc, Gold nanoparticles: assembly, supramolecular chemistry, quantum-size-related properties, and applications toward biology, catalysis, and nanotechnology, Chem. Rev. 104 (1) (2004) 293–346.
[61] C. Rao, A. Müller, A.K. Cheetham, Moving nanoparticles around: phase–transfer processes in nanomaterials synthesis, in: The Chemistry of Nanomaterials: Synthesis, Properties and Applications in 2 volumes, Wiley-VCH, Weinheim, 2004.
[62] Y.A. Garbovskiy, A.V. Glushchenko, Liquid crystalline colloids of nanoparticles: preparation, properties, and applications, in: Solid State Physics, Elsevier, 2010, pp. 1–74.
[63] C. Tan, et al., Epitaxial growth of hybrid nanostructures, Nat. Rev. Mater. 3 (2) (2018) 17089.
[64] P. Poulin, et al., Novel colloidal interactions in anisotropic fluids, Science 275 (5307) (1997) 1770–1773.
[65] J. Prakash, et al., Nonvolatile memory effect based on gold nanoparticles doped ferroelectric liquid crystal, Appl. Phys. Lett. 93 (11) (2008) 112904.
[66] R. Basu, Soft memory in a ferroelectric nanoparticle-doped liquid crystal, Phys. Rev. E 89 (2) (2014) 022508.
[67] R. Kempaiah, et al., Giant soft-memory in liquid crystal nanocomposites, Appl. Phys. Lett. 108 (8) (2016) 083105.
[68] T. Miyama, et al., Fast switching of frequency modulation twisted nematic liquid crystal display fabricated by doping nanoparticles and its mechanism, Jpn. J. Appl. Phys. 43 (5R) (2004) 2580.
[69] Y. Shiraishi, et al., Frequency modulation response of a liquid-crystal electro-optic device doped with nanoparticles, Appl. Phys. Lett. 81 (15) (2002) 2845–2847.
[70] I. Dierking, et al., Aligning and reorienting carbon nanotubes with nematic liquid crystals, Adv. Mater. 16 (11) (2004) 865–869.
[71] Ş. Özgan, H. Eskalen, Y. Tapkıranlı, Thermal and electro-optic properties of graphene oxide-doped hexylcyanobiphenyl liquid crystal, J. Theor. Appl. Phys. 12 (3) (2018) 169–176.
[72] H.S. Nalwa, Handbook of Advanced Electronic and Photonic Materials and Devices, Ten-Volume Set, vol. 1, Academic Press, 2000.
[73] C. Marcos, et al., Temperature-frequency converter using a liquid crystal cell as a sensing element, Sensors 12 (3) (2012) 3204–3214.
[74] J.F. Algorri, et al., Liquid crystal temperature sensor based on a micrometric structure and a metallic nanometric layer, IEEE Electron Device Lett. 35 (6) (2014) 666–668.
[75] S. Nakata, et al., Wearable, flexible, and multifunctional healthcare device with an ISFET chemical sensor for simultaneous sweat pH and skin temperature monitoring, ACS Sens. 2 (3) (2017) 443–448.
[76] S. Woodard, et al., LC measurement acquisition method for aerospace systems, in: AIAA's 3rd Annual Aviation Technology, Integration, and Operations (ATIO) Forum, 2003.

[77] J. Torres, et al., Wireless temperature sensor based on a nematic liquid crystal cell as variable capacitance, Sensors 18 (10) (2018) 3436.
[78] Z. Zhang, Z. You, D. Chu, Fundamentals of phase-only liquid crystal on silicon (LCOS) devices, Light Sci. Appl. 3 (10) (2014) e213.
[79] G. Pathak, et al., Dispersion of fluorescent dye in the nematic liquid crystal: enhanced photoluminescence and high birefringence, Opto-Electron. Rev. 26 (4) (2018) 317–324.

CHAPTER 13

Carbon-based nanomaterials as novel nanosensors

Shreya Sharma[a], Shashank Shekhar[a], Sanjeev Gautam[a], Bhasha Sharma[a], Amit Kumar[b], Purnima Jain[a]

[a]*Netaji Subhas University of Technology, Delhi, India*
[b]*Dyal Singh College, University of Delhi, Delhi, India*

13.1 Introduction

Nanotechnology is an emerging field that focuses on creation, manipulation, exploitation, and engineering of atoms, molecules, and supramolecular structures, i.e., matter and particle structures on the nanometer scale. These nanomaterials range from 1 to 100 nm in size and are known for remarkably changing their characteristics in the nanorange with outstanding properties, thus offering the possibility of implementation in newer domains with improved performance.

A sensor is a device that measures and detects changes in a somatic stimulus that translate into a human-readable display at the sensor location or an evaluable signal that can be recorded for further processing (e.g., electrical, optical, or mechanical). High sensitivity and authenticity, quicker recovery, faster response, reduced size, minimal cost, simple operations, and in-situ analysis are the major attractions of sensor systems. However, most current sensors come with pretreatment needs, difficult operation, slow response, and no ideal limits of detection, sensitivity to sensory stimuli, and/or selectivity, all of which demands an alternative approach. Nanosensors are nanosized sensing tools. Their expanding role in physical and chemical sensing is wide-ranging, including biochemical diagnosis in tissues and quantification of nanoscale particles and surroundings, and has led scientists to perform more incremental research in this sector. An overview of a variety of sensors in use is displayed in Fig. 13.1.

Carbon-based materials are among the most researched and currently used materials in the nanotechnology field, because of their impressive characteristics. Carbon materials present innumerable benefits over other conventionally used materials. Their inherent electrical characteristics, sensitive to alterations in the chemical surroundings, single them out as the most

Nanofabrication for Smart Nanosensor Applications. https://doi.org/10.1016/B978-0-12-820702-4.00014-3
© 2020 Elsevier Inc. All rights reserved.

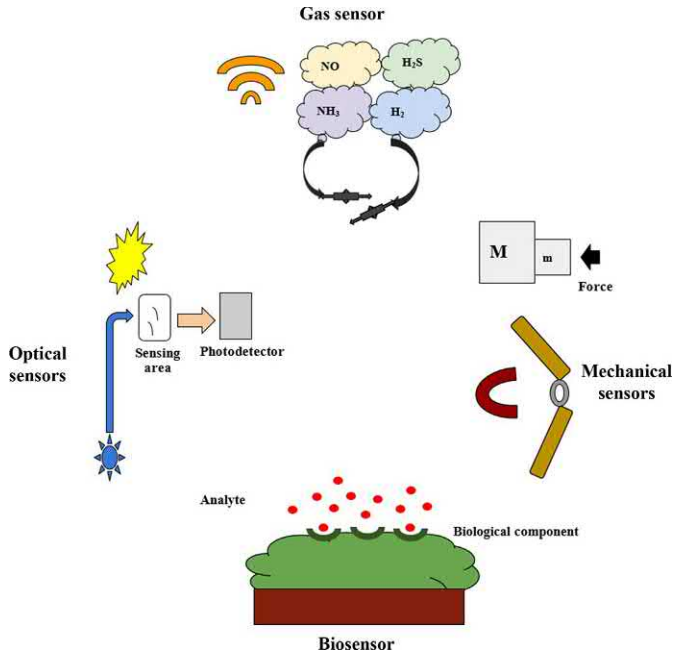

Fig. 13.1
Some sensor devices in use.

significant and hopeful option for sensor production. Moreover, properties such as poor water solubility and low fluorescence, acceptable thermal and chemical consistency, and functionalization make them appropriate for high-efficiency chemical sensing. Their hybridization property, allowing formation of many different chains with different lengths and electronic configurations, makes it possible to form more than a hundred million compounds with different properties.

13.1.1 Carbon-based nanomaterials

13.1.1.1 Carbon nanotube

The carbon nanotube (CNT) is a type of 1D tubular hollow cylindrical nanomaterial made from graphite sheets. It exhibits excellent chemical, thermal, electrical, and mechanical properties. It represents a progressively essential group of nanosubstances that has received impressive consideration since its first isolation in 1991. A tabulated form of characteristics of nanofillers used in sensors is shown in Table 13.1.

CNTs are obtained from fullerenes and therefore are also referred to as buckytubes [2]. When compared to fullerenes, curvature is absent in the axial direction of nanotubes, where fullerenes are positively curved molecules in all three directions in space. CNTs are composed of sp^2 hybridized carbon atoms; the nanotubes exhibit extraordinarily unique strength. The 2D sheets

Table 13.1: Overview of carbon-based nanofillers used in sensor applications [1].

Characteristics	Carbon nanotube	Graphene	Graphene oxide	Reduced graphene oxide
Synthesis	Chemical vapor deposition	Chemical vapor deposition Graphite exfoliation	Oxidation of graphite followed by exfoliation	Thermal or chemical reduction of graphene oxide
C:O ratio	No oxygen	No oxygen	2–3	8–246
Young's Modulus (TPa)	1–1.5	1–2	2–4	2–4
Electron Mobility ($cm^2v^{-1}\ s^{-1}$)	10,000	10,000–50,000	Insulator	0.05–200
Thermal Conductivity (W/mK)	3500	$4.84–5.30 \times 10^{-3}$	1500–5800	0.1–2
Electrical Conductivity (S/m)	3000–4000	7200	$1–5 \times 10^{-5}$	$2–7 \times 10^{-3}$
Production cost	High	High	Low	Low

built from sp^2 hybridized carbon can roll like paper and form tubular structures; π-π interaction, which is another basic essential feature of graphite, can be seen in multiwalled nanotubes (MWNTs) attached to the neighboring sheets. These amazing structures exhibit superconductive properties; prodigious strength (at least 100 times stronger than steel); and are efficient conductors of heat, which makes them potentially applicable for implementation in optics, electrochemistry, electronics, nanotechnology, and other fields.

Based on the number of walls, CNTs can be classified into single-walled CNTs (SWCNTs), which is a hollow cylinder of a graphite sheet, and multiwalled CNTs (MWCNTs), which consist of a number of coaxial SWCNTs [2, 3]. Single-walled nanotubes are made from solitary graphene sheets, which are composed of a hexagonal type benzene ring of carbon atoms curled up to form a cylinder that encompasses the longitudinal hub of the tube (diameter varies between 1 and 2 nm). MWCNTs comprise cylinders with interlayer spacing of graphite (diameter varies between 2 and 100 nm). The chirality and diameter affect the tubes in such a way that the SWCNTs exhibit metallic or semiconducting electronic properties, whereas MWCNTs have metallic electronic properties [4]. CNTs are synthesized using three major methods: laser ablation, arc discharge, and catalyst-assisted chemical vapor deposition (CVD).

13.1.1.2 Graphene

A planar, layered structure of hexagonal rings of sp^2 hybridized carbon atoms, graphene (GPN) is deemed a supermaterial, as it is the basic structural element for carbon structures of different functionalities. From wrapping up into 0D fullerenes to rolling up into 1D carbon nanotubes or vertically stacked 3D graphites [5], carbon materials contain graphene as the primary building

block of their structure. The ambipolar characteristic that demonstrates graphene to be electrically sensitive to both electron-withdrawing and electron-releasing species comes from the fact that the charge carriers in graphene are continuously tunable between holes and electrons in concentrations ranging up to 1013 cm^{-2} with mobilities above 15,000 cm^2v^{-1} s^{-1} in ambient conditions [4]. Each carbon atom forms a covalent bond with the three neighboring carbon atoms, which further take part in generation of chemical bonds. In addition, the free moving fourth electron renders graphene conductive. Graphene and its derivatives can be found in single, double, or multilayered forms like graphene oxide or reduced graphene oxide, etc. The layers of graphene and its derivatives have Van der Waal forces of interactions, having 3.35 Å interlayer spacing [6]. Synthesis of graphene takes place using two approaches: top-down and bottom-up techniques. The top-down technique involves electrochemical methods as well as a chemical and physical exfoliation process. In addition, the bottom-up technique involves chemical vapor deposition (CVD) which has very low yield. Graphene, a wonder material, has excellent elasticity, high strength, and outstanding thermal conductivity, followed by incomparable mechanical characteristics that have prompted its propelled implementation in medicine, electronics, optics, and thermal therapy [5]. In contrary to CNTs, graphene exhibits abundant functional moieties, easy dispersion, high specific surface area, and abundant surface functional groups, all of which are beneficial for use in a variety of sensor arrays.

Graphene oxide (GO) is synthesized by oxidation of exfoliated graphite using vigorous oxidizing agents for, e.g., phosphoric acid, sulfuric acid, and nitric acid (Hummer's method). The higher hydrophobic behavior and interlayer distance exhibited by GO is attributed to higher oxygen content. Also, the presence of various functional moieties like epoxide groups, hydroxyl groups, carboxylic groups, and phenols provides pathways for aptamers/DNA, proteins, and antibodies, with biosensor implications [6].

GO is reduced to reduced graphene oxide (rGO) using chemical agents like hydrazine, electrochemically by directly applying a reduction potential, or thermally at elevated temperature. Reduction helps in the removal of chemical and structural defects in GO and thus helps in restoring the semiconductor properties for applications in electronics, especially for field-effect transistor (FET)-based biosensing.

13.1.1.3 Diamond

Diamond, a solid form of the element carbon, is the hardest material in the world. It is characterized by its low current, high electrical stability, and excellent biocompatibility. Diamond is the best-known electrochemical transducer. Large overpotentials for oxygen and hydrogen evolution are related to the wide working window of diamond. A typical window of 3.25 V or greater is normal for high-quality films. The surfaces of diamond nanostructures play an important role in determining the utility and biocompatibility of these nanostructures in biological and medical applications, such as targeted drug delivery, selective biosensing, and effective therapy. The electronic properties of the solid/electrolyte surface can be optimized due to the surface termination with hydrogen, oxygen, and the OH group. The surface of

diamond is hydrophobic for hydrogen termination and hydrophilic for oxygen termination [7]. Noticeably, diamond exhibits the strongest bonding stability to deoxyribonucleic acid (DNA). Diamond can be prepared by a high-pressure, high-temperature method (HPHT) and a low-pressure CVD technique.

A vacancy defect in the lattice can be produced by irradiation of elevated energy particles such as neutrons, electrons, protons, neutrons, gamma particles, and ions. At 800 °C, some strain is produced in the diamond lattice, attributed to the existence of nitrogen atoms and coupled with vacancies (a migration and capture mechanism), which forms a nitrogen-vacancy (NV) color center. However, in the CVD technique diamond films thrive in the existence of a gas mixture having 0.7% CH_4,0–0.1% N, and 99.2% H_2, which leads to the formation of NV centers [8].

Nanodiamonds are small-sized diamonds with the same superlative properties. Nanodiamonds have emerged as cogent nanomaterials owing to their low and stable background current, high mechanical and thermal properties, wide working potential window, and excellent corrosion resistance. Each particle of nanodiamond has sp^3 bonded carbon atoms covered by sp^2. They are very tiny particles, with an average diameter of 4–6 nm and a specific surface area of 300 m^2/g. Nanodiamonds have high biocompatibility in comparison to other carbon-based materials, for example carbon black, SWNTs, and MWNTs, with no cytotoxicity to different cell lines.

Diamond nanowires (DNWs) have a cross-sectional area of 4.58 nm^2 at room temperature ($300K$) with Young's modulus, yield strength, and fracture strength as high as 688, 63, and 91 GPa, respectively. When compared to bulk diamond, they can be used as a single photon source with greater flux and less power. DNWs have motivated considerable interest in the applications of microelectromechanical systems (MEMS), quantum information processing applications, electrochemical gene sensing platforms, and others.

In the subsequent sections, recent progress in the utilization of two types of diamond nanostructures, namely diamond nanoparticles and vertically aligned 1D diamond nanostructures, is discussed.

13.2 Sensing properties

A sensor is a device that perceives change in a physical or chemical stimulus, generating a signal that can be measured or recorded, i.e., that can be electronically analyzed. A sensor consists of two fundamental components: a receptor that interacts with a specific analyte and a transducer that transmites the identification that happens between receptor and analyte into an accessible detection signal. The selection of an appropriate sensor is based on the possibility of quick response to external stimulus, the ability to detect an analyte in proportions as low as possible, the ability to provide the result with high accuracy and precision, and minimal recuperation time. Furthermore, eco-friendly and cheap devices are a current focus. Therefore,

research is accelerating in the field to improve existing systems and find promising alternatives that allow for changing technologies.

Specifically, nanomaterials based on carbon are the most widely exploited, reported, and studied nanomaterials [9] due to their impressive characteristics. The typical characteristics of each carbonaceous nanostructure enable it to be utilized in a particular sensor model. For instance, an appealing defect of diamond is its carbon vacancy adjacent to a nitrogen atom, called an NV center. These NV centers have applications in quantum sensing and quantum technology, having optically active properties. They can be used to monitor electrical or magnetic fields and external perturbations, which has implications in the biological environment [10].

The quasi-one-dimensional shape of a CNT along with its very large surface area in comparison to the volume and the hollow framework make it ideal for producing nanomaterials useful for a range of sensor applications. CNTs are considered good candidates for the production of chemical and biological sensors, because of their property of absorbing a high number of molecules onto their surface through interactions between molecular electronic states. Their advantageous ability to transfer ballistic electrical charge, quantum conduction, and the ultrathin body allow applications at a sub-8 nm scale, which is a limit for development of semiconductors. Also, CNTs can withstand high current densities up to 1010 A/cm^2, which is three to four orders of magnitude higher than most metals. These unique properties have led to their use in actuators, field-effect transistors, and energy and gas storage. Table 13.2 exhibits the nature, applications, and characteristics of some sensor devices used and reported earlier.

Graphene and its derivatives have become the most used raw materials for sensors in different applications, due to their peculiar characteristics, like outstanding mechanical flexibility, high thermal conductivity, fast electron transfer, optical transparency, good mechanical strength, and enhanced biocompatibility [6]. However, controlling the number of layers of graphene, profitable synthesis, and manipulation of its intrinsic chemical responses are still challenges to be met.

Fullerenes (FLNs), a category of allotrope of 60 carbon atoms arranged in a structure like a soccer ball, have been extensively studied for producing sensors to analyze a variety of molecules such as glucose, fluoride ion, hydrogen peroxide, licit and illicit drugs, DNA, adenosine triphosphate (ATP), and various organic vapors. The C-60 molecule has high symmetry, which is a very important characteristic. Fullerene contains fused rings and conjugated double bonds that lead to remarkable electronic properties and strong reduction-activation activity. FLNs exhibit optical and photoelectrical properties, which have additionally been investigated for innovations in color-sensing materials. Chemical functionalization increases the ability to dissolve in various solvents and helps in combinations of the characteristics with those of other compounds, thus expanding their probable applications.

Table 13.2: Some sensor devices and their characteristics.

Carbon-based sensor components	Target analyte	Application and its area of implementation	Sensitivity/limit of detection	Ref
CNT as field emission cathode	Temperature from 20°C to 110°C	Gas identification and temperature measurement	Sensitivity $= 4.74\ \mu A°C^{-1}$ (air) and $22.72\ \mu A°C^{-1}$ (N2)	[11]
Graphene oxide nanosheets	Hg2+	Heavy metal detection for biological and environmental analysis	LOD = 25 pM	[12]
Glassy carbon electrode modified with nitrogen-doped carbon nanotube	Theophylline (THEO) and caffeine (CAF)	Electrochemical sensor for healthcare	Linear dynamic range from 0.10 to 70.0 μM and 0.40–140.0 μM Low detection limit (S/N = 3) of 0.033 μM and 0.20 μM respectively	[13]
SWCNT and graphene	Prostate specific antigen complexed with α1-antichymotrypsin (PSA-ACT)	FET biosensor for cancer diagnosis	LOD = 1.0 ng/mL	[4]
NV center of nanodiamond Cu1 − xNix magnet nanoparticle on a diamond nanopillar	Magnetic phase transition of a single magnetic nanoparticle	Hybrid nanothermometer for in situ and real-time observation of nonuniform heat dissipation of microelectronic or nanoelectronic devices, nanoplasmonics, subcellular thermal processes, and chemical reaction at nanoscale	Sensitivity $=11\ mK/\sqrt{Hz}$	[14]
Boron-doped diamond nanoforest electrodes	Glucose	Electrochemical sensing for diabetes monitoring	Sensitivity $= 8.1\ \mu A\ mM^{-1}\ cm^{-2}$ LOD = 0.2 ± 0.01 μM	[15]
Carbon dots as fluorophore	Vitamin B12	Inner field effect-based sensing for pharmaceutical analysis	LOD = 0.1 μM	[16]
MWCNT arrays	Micropressure from touch	Tactile sensor for applications in robotics, prosthesis, and a variety of human-machine interface implementations	Sensitivity $=9.95\ kPa^{-1}$ (ultrahigh)	[10]
Graphene nanostructure	*E. coli* O157:H7	Electrochemical biosensor for pathogen detection	Sensitivity = 10–100 cells/mL	[17]
Fullerene/graphene oxide nanocomposites	Humidity	For food production storage, laboratorial and industrial processes, textiles	Sensitivity = 31 Hz/% RH	[18]

Carbon dots and carbon nanohorns have also become prominent as sensor materials. Carbon nanohorns, an attractive alternative to CNT-based structures, have a spherical shape that benefits different electronic properties. They lack intrinsic fluorescence, but the existence of reactive sp^3 hybridized carbon edge sites permits labeling of various moieties. Also, their metal free property helps in avoiding residual metal impurity interference. Hence, these structures are proving to have a remarkable dominance over CNTs in fabrication of electrochemical sensors [9].

Carbon nanomaterials have potential for routine sensing, as they can be integrated into various sensing devices that can exploit their high surface area and increased conductivity. Several examples of carbon-based nanosensor devices that are well-studied and researched and in practical use are presented in the following sections.

13.3 Nanosensors

13.3.1 Optical nanosensors

Optical sensors are powerful tools equipped for providing information on an analyte remotely [19]. They are composed of signal transducers and molecular recognition elements. The nanomaterial-based optical sensors show specific and selective response to the target molecule. The detectable changes are transduced in quantified optical signals, useful for the multimodal and remote detection preferred for biological and biological applications. The most popular optical sensing techniques include fluorescence, Raman scattering, and surface plasmon resonance (SPR).

SWCNTs are sensitive to changes in the surface chemistry and 800–1600 nm wavelength range in near-infrared (NIR) emissions. The near-infrared window in biological tissue called the "biological window" lies in the range of 700–1300 nm, in which scattering, absorption, and autofluorescence by water, blood, and tissues are minimal [19]. Also, they do not blink or bleach for a long period of time, thus making SWCNTs applicable for use in biological environments. For a given intensity, the signals produced from sensors can be determined by the fluorescence quantum yield of SWCNTs and therefore it is a crucial factor in materials science and sensor-based applications. Graphene possesses a number of optoelectronic properties, and graphene derivatives are known to interact with virtually the whole spectrum, i.e., from UV rays to terahertz radiation. In QDs, Förster resonance energy transfer (FRET) donors, GO is almost a robust material, which opens the way to its application in novel lab-on-chip (LOC) platforms and QD FRET-based microarrays, as compared with carbon nanotubes and graphite carbon nanofibers (CNFs) [20]. This proves useful for GO quantification during its use as DNA labels, or protein/cell sensing. The ability to decrease the intensity of fluorescence of a sample inspired scientists to use it practically in the detection of DNA (5 nM) with a detection limit of 2 nM. Also, development of a GO-based colorimetric technique for detecting

damaged DNA was also reported [20]. As an efficient fluorescence quencher, GO or graphene has been broadly utilized for successive detection of metal ions (heavy metal ions such as Ag^{+}, $Hg^{2+,}$ Pb^{2+}, Cd^{2+}, Ni^{2+}). Most GO-based biosensing devices exploit photoluminescence, excited via UV light (around 365 nm).

In graphene-based nanomaterials, the optical method has been developed as a promising technique. The technique based on superresolution often suffers from a restricted photostability of fluorophores [21]. For example, NV centers, near-infrared emitters providing a broad emission peak with a maximum at ~700 nm, provide exceptionally stable fluorescence and do not photobleach or blink even after extreme continuous excitation. The photostability of color centers also offers new possibilities for advances in FRET sensing [21], another very powerful approach for sensing at nanoscale. Fluorescent nanodiamonds are among the few types of nanosensors synthesized that enable direct optical reading of noncovalent binding events based on modulation of fluorescence.

13.3.2 Electromagnetic nanosensors

Two types of nanosensors are described in order to categorize them based on their physical mechanics: detection via electricity measurement or via magnetism measurement [10]. The sensitivity of electron density of states to external influences (chemical, mechanical, magnetic, etc.) proffered the analysis of elementary electromagnetic characteristics of CNTs and graphene nanoribbons for nanosensor applications. Recent research states that the electronic densities of graphene and CNTs have sensitivity to conductivity. The sensitivity implies that graphene and CNT-derived nanodevices can conceivably be utilized as nanosensor frameworks, in which electronic density is influenced by external factors. The creation of nanodevices that store and transfer information using the spin and charge of electrons, e.g., nanomemory devices, was made possible with nanocarbon magnetic metal interfaces [22].

13.3.3 Gas nanosensors

Owing to their reduced dimensionality and high surface-to-volume ratio, carbon nanostructures are considered exemplary for gas detection and quantification. Gas selectivity further increases due to the good possibility of functionalization provided by the sensors. Carbonaceous nanomaterials offer higher sensitivity, selectivity, reliability, fast response, and stability and therefore are employed in a range of sensor models (capacitance, ionization, sorption, or resonance frequency shift). The encounter with a gas molecule causes a change in potential difference, which is further converted into an electrical signal. Carbonaceous nanoparticles can detect different kinds of gases, especially hydrogen sulfide, carbon monoxide, carbon dioxide, nitrogen oxide, ammonia, and methane.

GPN, GO, CNTs, and FLN help in production of sensors to monitor environmental pollutants that are a threat to both the environment and human health. NO_2 is a nasty-smelling gas responsible for acid rain and respiratory problems in humans and leading to reduced immunity in lung infections. A gas sensor whose output readily changes with a corresponding change in input at room temperature depositing a GPN bilayer onto Ni electrodes was developed with a sensibility range of 1409 ppm^{-1} towards NO_2 over a concentration range of 1–25 ppm. In another work, rGO with high sensitivity (25.5 ppm) and a remarkably low LOD (9.1 ppb) was used for NO_2 detection [10]. The rGO proved to be advantageous over GO, as the functional groups such as carboxylic, epoxide, and hydroxyl responsible for decreasing the conductance of graphene and making it vulnerable towards humidity were now absent. Gas absorption is also promoted due to the presence of a large number of defects over an increased surface area.

Exposure to H_2S can lead to immediate loss of consciousness, coma, and respiratory paralysis. Concentrations above the 100-ppm level can induce an immediate collapse with loss of breathing and eventually lead to death. A graphene-based nanosensor doped with Ag nanoparticles displayed a fast response ($\sim$1 s) and short recuperation time ($\sim$20 s), allowing real-time H_2S monitoring [10]. A nanohybrid tin oxide quantum dots-C60 FLN was synthesized using a hydrothermal method to be used as a gas sensor.

Li^+ doped CNTs were used for methane (CH_4) detection. A component of natural gas, CH_4 has high global warming potential (21 times that of CO_2) and can cause asphyxiation and eruptions when existing in significant amounts in nonventilated areas. Under CH_4 exposure, the conductivity of this sensor changed through an electrochemical reaction. A change in hybridization state from sp^2 to sp^3 was produced with the binding of CH_4 to π bonds of CNT, which intervened with the resistance offered by the system. A 14.5% sensitivity response to 500 ppm of CH_4 indicated the suitability of this nanomaterial to be more exploited and applied.

Accurate detection and monitoring of hydrogen is an important issue. Hydrogen is a colorless and odorless gas highly flammable in nature. CNT- and GPN-based sensors decorated with platinum were produced. A resistance change of the film on switching the gas environment from air to H_2 in the cycling regime was used for gas sensing. Multiwalled CNTs with a mixture of graphite and ferrocene exhibited high sensitivity (maximum sensitivity of 239%) susceptible to a 20–1000 ppm mixture of H_2-N_2 [10] and under a voltage of 0.05 V.

The effect of absorption of various hazardous molecules, including sarin, a nerve agent gas used in chemical welfare whose exposure can lead to death in a minute, and dimethyl methyl phosphonate, a simulant of sarin generally used as flame retardant, were also studied. Carbonaceous nanoparticles have also been designed for the detection of ethanol, oxygen, and rare gases.

Besides the identification and quantification of gas, carbon-based materials are also used to determine the temperature of ionized gas. Sensors able to discern temperatures from 20°C to

110°C with a sensitivity of 4.74 μA°C^{-1} (air) and 22.72 μA°C^{-1} (N_2), both at 110°C, have been reported [10]. The system doesn't involve absorption and desorption of gas molecules but instead features an electrical breakdown in which CNTs play an essential role. The degree of ionization and the emission current are affected by the temperature of the gas. Other research on NO produced under the same guidelines exhibited the highest sensitivity of 5.5 nAppm^{-1} at 330 ppm of NO, with fast response and short recovery time [11].

13.4 CNT-based nanosensors

As described earlier, carbon nanotubes present a seamless structure and are built from sp^2 hybridized carbon units. CNTS are known to exhibit moderate chemical stability combined with unique electronic and mechanical properties. An electron band, formed from the free-moving π-electrons present above and below the hexagonal layer, delivers the semimetal electrical properties of graphite. CNTs are small in size with high sensitivity, fast response, and larger surface area, which gives them an advantage over other bulky materials to be used as a gas sensor. CNTs decorated with metal Ti and Cu were studied to detect oxygen. Vertically aligned carbon nanotube (VACNT) based NH_3 sensors and formaldehyde sensors using VACNTs modified by amino groups have been developed. MWCNT synthesized on an oxidized silicon substrate used to detect ethanol gas, Au-nanoparticle functionalized MWCNT used to detect NO_2, NH_3, and H_2S, and SWCNT-based NO_2 sensors are among the research papers published lately [23]. CNT-based nanosensors are widely used in chemical sensors, field emission particles, hydrogen energy storage, catalyst support, and electronic devices.

The ultralow variation in sensitivity (less than 6%), comparable with metal oxide sensors or polymer microfilms, presents a series of advantages for chemical sensing. Gases and organic vapors in the same sampling environment can be detected. The ability of CNTs in sensing both forms is specifically attributed to the electron-hopping between the tubular structures, which otherwise does not occur in polymer microfilms or in monolayer metal oxides. However, they are progressively productive when chirally uniform, which is related to their uniform bandgaps that otherwise vary with small changes in the nanotube diameter [24].

When used as an electrode, CNTs have the ability to mediate electron transfer reactions with electroactive species in solution, making them appropriate for combinations of electrochemical and electronic biosensors. The high surface area provides enough accessible dynamic destinations for analyte detection, and thus improves the detection sensitivity, which lessens the point of confinement of discovery. Numerous CNT-based sensors for determination of glucose based on the conjugation of glucose oxidase have been designed. Electrochemical biosensors based on CNTs have been designed for the detection of nitric oxide and epinephrine sensing. A dramatic increase in the sensitivity of detection of DNA with CNT electrodes has also been reported. The label-free detection of individual protein efflux from *Escherichia coli* (bacteria) and Pichia pastoris (yeast) in real time was made possible

by using SWCNT [2]. Due to the similarity of carbon and nitrogen atomic in valence electron layer structure and size, nitrogen-doped carbon nanotubes combined with polymer were used in the electrochemical detection of caffeine and theophylline with a low detection limit (S/N = 3) of 0.033 μM and 0.20 μM, and a wide linear dynamic range from 0.10 to 70.0 μM and 0.40 to 140.0 μM, respectively [13]. PANI composites (produced by polymerization of aniline, mostly in acid solution) and MWCNT powder underwent electrochemical polymerization to produce a pH sensor for marine water. Surface functionalization not only tunes the sensing properties but aims at the modification of surface chemistry to enhance the interactions of CNTs with polymers in the realization of functional nanocomposites [25].

CNTs show the highest elastic modulus and tensile strength ever recorded, but their properties are emphatically subject to the structure. Excellent photostability and photophysical properties such as fluorescence emission in the NIR region make the SWCNT an effectual optical probe in biomedicine (single-stranded DNA functionalized SWCNTs were designed to measure the lipid content in the endosomal lumen of live cells [26]; and a label-free multiplexed microarray platform using fluorescent single-walled carbon nanotubes was constructed for quantitative detection of antibody molecules, including human IgD, mouse IgM, and rat IgG) [27]. Their strong NIR light absorption capability makes CNTs efficient photothermal agents with applications in anticancer drugs, genes, and protein for chemotherapy [28].

One of the principal advantages of CNTs are their ability to assemble into free-standing films, sponges, and arrays with high mechanical strength and impressive electrical conductivity, thus opening doors for opportunities in decentralized assay and microscale analysis.

CNT-based field-effect transistors utilize a single carbon nanotube or an array of carbon nanotubes in the traditional MOSFET structure. Their natural ultrathin body, efficient electron and hole transport properties, and reasonable energy gap offer superior solutions when compared to other semiconductors scaled to the sub-10 nm regime. An SWCNT-based bio-FET was demonstrated for sensing nucleic acid-based analytes and proteins. Applications include: ultrasensitive detection of a broad range of ctDNA in human blood; KRAS G12DM as low as 0.3 fM with a detection of 5.0 μL of sample volume could be sensed through the T-rich deoxyribonucleic acid (DNA)-mediated surface enhanced Raman scattering (SERS) of SWNTs; diagnosis of prostate cancer by detection of prostate specific antigen/α1-antichymotrypsin (PSA-ACT) complex; a label-free protein biosensor for IgE and IgG detection; electronic detection of biotin-streptavidin and pig serum albumin; a carbon nanotube transistor array to detect DNA hybridization.

Large stiffness-to-mass ratio and slight structural damping are two exceptional features found in nanotubes; these features have accelerated research and become the focus for many design engineers for use in precise mass sensors. Some researchers have reported the behavior of a carbon nanotube-based mass nanosensor based on a nonlocal elastic foundation investigated through an efficient finite element model, including the integral form of nonlocal elasticity

[29]. In another study, the application of heterojunction CNTs (composed of two CNTs with different chirality) as a mass sensor using nonlocal gradient theory is discussed. The results reported in the paper introduce HJCNTs as new mass sensors that can operate more efficiently than CNTs [30].

13.5 Graphene-based nanosensors

As defined earlier, graphene is an auxiliary and essential kind of carbonaceous substance usually made by mechanical exfoliation of graphite. It can be produced using methods such as shear exfoliation using surfactants, reduction of carbon dioxide, laser scribing, and unzipping nanotubes; however, the most common approach is the use of chemical vapor deposition (CVD) or through production of GO (graphene oxide), which includes carboxylic, phenol, hydroxyl, and epoxide groups usually produced by Hummer's method. Graphene has a sheet-like structure that makes it appropriate for sensing mechanisms that rely on semiconductive films or conductive interfaces, which either transfer an electrical impulse via two adjoining electrodes or take place in an electrochemical reaction with a binding molecule via the contribution of π-electrons in the highest occupied molecular orbital (HOMO) [24]. This property has been researched intensively for a broad range of applications in the field of electrochemical sensors. Graphene-based electrochemical sensors are used in immunosensors for early detection of diseases [17].

The absorptive properties of graphene make it superior for sensing functions related to planar molecules, such as polycyclic molecules and molecular species with few rings, such as benzene or naphthalene, which are often found in pollutants from exhaust emissions and fuel combustion processes. The tremendous surface area of graphene augments the surface loading of desired organic or biomolecules (such as hydrogen peroxide, urea, uric acid, glucose, dopamine, glutamate, ascorbic acid, xylene, benzene, protein biomarkers, hemoglobin, immunoglobulin G and E, cholesterol, nicotinamide, saccharides, and amino acid) [31] through either chemical or physical adsorption. The high detection sensitivity, reaching concentrations as low as 32 nmol/L of the target molecule with a reproducibility of 5.2%, makes it suitable for environmental samples (in pH sensors, detection of environmental contaminants such as hydrazine, hydroquinone, paraoxon, catechol, and nitromethane) [31]. Also, graphene-based sensors provide quick recovery after usage (with over 96% recuperation).

The forms of graphene used in sensors play a crucial role as well. For example, functionalized graphene is a form of graphene with a particularly high electrochemical response towards electron transfer reactions, which makes it ideal for detecting bound molecules under the effect of electric current. In a recent paper that reports the detection of HIV, CVD, and RA biomarkers using amine-functionalized graphene conjugated with specific antibodies, graphene-based field-effect transistors were used, which exhibited a clear advantage over conventional techniques with a high POCT potential for the on-site detection of HIV, CVD, and RA

biomarkers in real samples, because of its quick response time and increased selectivity and sensitivity [32]. Graphene's ultrathin characteristics respond to effects from the surroundings, which makes it ideal as a conductive component in field-effect transistors. Graphene field-effect transistors act as highly sensitive electrical sensors for detecting biomolecule concentration. Electric detection of protein absorption, with effective separation of the current signals of the four bases guanine (G), adenine (A), thymine (T), and cytosine (C), was studied based on the properties of GFTs. A novel FET nanobiosensor based on a chemical vapor deposition (CVD)-grown monolayer of graphene was also reported; the sensor turned out ultrasensitive, label-free, and highly specific for detection of DNA.

It was also reported that functionalized graphene possesses innumerable advantages for sensor-based applications due to the presence of a large number of prominent structural defects, as physical defects led to higher binding potential than ultrauniform graphene material. An increase in the occurrence of hinges and clefts caused by the natural conformation flexibility of graphene contributed to binding more molecules of the target molecule, as the surface morphology adapts to molecule-to-molecule interactions more easily.

Graphene and its derivatives are also considered a promising tool in gas sensing for detection of carbon monoxide, oxygen, ethanol, chlorine, hydrogen, water vapor, iodine, methane, nitrogen oxide, cyanide, etc. [20]. It can be used as an ideal platform for transporting other components for a particular role. The high conductivity and ballistic nature of charge transport ensure that graphene manifests very small interferences as a chemical sensor and does not require an auxiliary heating device because of its excellent chemical stability at ambient temperature [33]. The hexagonal moieties of carbon are stabilized by one another in the cyclic π electron configuration, making it suitable for sensing corrosive and reactive gases without being damaged. Fluorographene is considered to be an effective electronic sensor for the detection of toxic gaseous molecules such as NH_3, CH_3NH_2, $(CH_3)_2NH$, and $(CH_3)_3N$ [34].

Graphene has outstanding optoelectronic properties. Noticeably, reduction of GO results in production of an optically transparent and electrically conductive nanomaterial. GO is fluorescent among a wide range of wavelengths and can quench molecules that are fluorescent, such as quantum dots and dyes. The high quenching efficiency of GO may open the way to novel QD FRET-based microarrays and lab-on-chip (LOC) platforms, by employing GO as a platform for transducing, which has proved to be a vital element for GO quantification in DNA labels, cell sensing, or protein [20].

The ability of graphene and its derivatives to act as an efficient fluorescence quencher has been utilized for construction of sensing platforms for metal ion detection. Heavy metal ions of, e.g., Ag^+, Hg^{2+}, Pb^{2+}, Cd^{2+}, Ni^{2+} in food resources and water are attributed to increased industrial effluents as well as the wastewater release of metal ions. Because of their high degree of toxicity, they are a threat to both human health and the environment [35].

13.6 Diamond-based nanosensors

Diamond, a metastable state of carbon with exceptionally high bulk modulus and hardness, is the hardest material available. It consists of a 3D cubic lattice with a 3.57 Å lattice constant along a C—C bond length of 1.54 Å [36], and it is characterized by its hardness, inertness, biocompatibility, high thermal conductivity, and optical transparency. The sp^3 carbon units can be synthesized by using a low-pressure CVD technique or a high-pressure high-temperature technique. [2].

Nanodiamonds (NDs) are nanoparticles of diamond with a size below 1 μm, investigated for their applications in nanostructures and nanodevices because of their outstanding corrosion resistance, microstructural stability at extreme anodic and cathodic potentials, wide working potential window, high mechanical and thermal properties, low and stable background current, fluorescent capability, noncytotoxicity, and biocompatibility.

A diamond crystal that is transparent to visible light (optical bandgap of E = 5.48 eV, which corresponds to a 1226 nm wavelength) is known to display vivid colors on rare occasions. However, elements like boron, nickel, silicon, and nitrogen give rise to impurity defects in the lattice structure, capable of emitting and absorbing light in the visible spectrum. The most commonly found nitrogen vacancy center is a point defect that exists in the diamond lattice formed by replacement of nitrogen atoms directly alongside the lattice vacancy, which is oriented along [111] direction in crystal. The NV center can exist as a neutral charge state NV0, positive charge state NV+, and a negatively charged state NV−.

The nanosensing applications of the NV center include locating single elementary charges, performing thermometry within living cells, and realizing nanoscale MRI in ambient conditions. The low sensitivity of MRI is due to low temperature and low polarization of nuclear spins, which can be further improved using (DNP) dynamic nuclear spin polarization of nanodiamonds. The presence of NV defects permit the utilization of similar NV centers to polarize multiple nuclear spins over short timescales in a low field at ambient temperature without performance loss. NV centers are considered as point dipoles in which the energy can be reconstructed in the existence of external spins. The aforementioned changes in energy can be accessed via optically perceived magnetic resonance of NV center spins [21]. The detection of external electron spins by using a diamond magnetometer was made possible. Detection of proteins attached to paramagnetic ions and magnetic proteins such as ferritin by using magnetic noise has also been reported. Diamond nanospin mechanical sensors capable of both nanomechanical sensing and quantum nanosensing of electric fields, magnetic fields, and temperature, were recognized. The sensors had high potential for force microscopy and mass spectroscopy capable of providing unprecedented AC force images of cellular biomechanics and of the inertial imaging of distribution of mass in single molecules [37]. A recently published paper described a hybrid nanothermometer composed of NV centers and

a magnetic nanoparticle (MNP). With its superb sensitivity and designable working temperature range, the hybrid nanothermometer enabled in situ and real-time observation of nonuniform heat dissipation of microelectronic or nanoelectronic devices, nanoplasmonics, subcellular thermal processes, and chemical reactions at nanoscale [14].

Cathodoluminescence (CL), a powerful technique to analyze materials with nanometric resolution, could help in achieving molecular localization with drug delivery implications, and it also reveals structural details within organisms or live cells. Fluorescent nanodiamonds have been demonstrated for CL imaging which, unlike fluorescence, imparts much better spatial resolution, i.e., $\sim$5 nm, and is not restricted by diffraction of light.

Boron added to diamond (boron-doped diamond, or BDD), due to its extraordinary chemical resistance has continued to find numerous, wide-ranging applications in the electrochemical field in recent years. Its properties, such as high chemical and physical stability, background currents, and wide potential window, provide selectivity for detection of heavy metal ions such as Al, In, Pb, Fe, brass, Hg^{2+}, Cu^{2+}, and Ag^{+}. BDD modifications with redox-active compounds including gold, bismuth, antimony, and iridium for the detection of As^{3+} and As^{2+}, Se^{4+} and Se^{6+}, Cd^{2+} and Pb^{2+} have also been reported.

The electron transfer between the substrate electrode and analytes is facilitated by redox active sites with a considerable reduction in overpotential activation [38]. Recent papers have also discussed the application of nanocrystalline BDD and diamond-like carbon for the detection of trace metals. BDD is used in neurotransmitter sensing (dopamine detection by BDD arrays; detection of 5-HT, a signaling molecule in the CNS as well as the gastrointestinal tract known to regulate mood and sleep, by BDD microelectrodes; combined detection of KCl-stimulated secretion and corresponding intracellular Ca^{2+} transients in chromaffin cells on BDD nanocrystalline arrays were all reported) [39].

DNWs, the diamond analog of CNTs, represent phenomena for selectrochemical sensing applications (including nonenzymatic detection of glucose; and an electrical immunosensor that detects the binding of IgG by electrochemical impedance spectroscopy measurements, for immobilization of peptides) [15]. Due to their high surface area, DNWs are anticipated to exhibit much higher selectivity and sensitivity than planar BDD electrodes.

13.7 Biosensors

As a part of global efforts towards the improvement of healthcare along with adequate progress in pharmaceutics, illness treatment, and prevention, portable diagnostic devices are being developed to provide fast and reliable detection of biomarkers. Bionanosensors are considered as an alternative to conventional methods of clinical analysis utilizing immunochemical approaches. They are engineered for the detection of infectious mediums and bioagents, signal detection in bionanosystems for pesticide and pollutant detection, sampling of chemical

compounds, detection of DNA in samples, as well as sensing of biomaterials based on chemiluminescence and fluorescence. The present-day advances suggest the use of quantum dots, graphene, carbon nanotubes (CNTs), fullerenes, nanohorns, and conductive polymers for use in therapeutic applications, environmental analyses, and other applications in sensing [24].

A range of drugs, including antineoplastic drugs such as flutamide and chlorambucil, tuberculosis drugs such as pyrazinamide (PZA), tranquilizers such as diazepam, phenylpropanolamine, illicit drugs, and amphetamines can be detected using nanostructures based on carbon nanotubes, nanodiamonds, FLNs, and GPNs. The anticancer drug chlorambucil (CHB) was detected using electroactive C60 monoadduct-micellar molecularly imprinted polymer grafted on an ionic liquid-based carbon ceramic electrode (ILCCE). An overdose of flutamide, another anticancer drug, causes hepatitis, and MWCNT-based sensors were used to monitor this drug. MWCNT exhibited a potent ability to catalyze the oxidation or reduction of the methodically examined drug. Human serum and biological urine samples were studied for PZA determination using an ND-GCE electrochemical sensor.

FLN is reported as a promising substance to be utilized in electroactive sensors, due to its strong interaction with drugs, including methyldopa, metoprolol, enalapril, tolazoline, tyramine, and dextroamphetamine. FLN is also used as a sensor for the detection of illicit drugs that need significant attention. The detection of amphetamine and phenylpropanolamine using pristine C60 FLN and C60 reinforced with Al, Si, Ga, Ge, and Be was studied by various researchers. A sensor modified electrode with CNTs, 1-butyl-3-methylimidazolium tetrafluoroborate ionic liquid (IL) and C60 was used to detect diazepam in samples, which included urine, tablets, and serum. The carbon nanotubes improved the dispersion of C60 and helped in retaining the mechanical, electrical, and thermal properties of ILs.

In order to retard the rate of development of antibacterial resistance, accurate and rapid diagnosis of pathogenic bacteria is crucial in medical diagnostics. Due to low sensitivity and delays in detection results with classical approaches, nanoparticles and ceramic nanospheres were investigated. The use of nanowire field effect transistors helped in real-time electrical diagnosis of viruses [40]; the influenza A virus was detected using CNT field-effect transistors (CNTFETs).

The nonenzymatic examination of glucose for diabetes screening and diagnosis was performed by GPN-, FLN-, and CNT/GPN-based hybrid sensors. A glucose biosensor developed using 3-amino-capto-1,2,4-triazole functionalized C-60-based gold nanocomposite presented good selectivity and stability; remarkable electrocatalytic activity was revealed by cyclic voltammetry and amperometric techniques, and the high surface area of the composite favored the electrochemical oxidation of glucose. A GPN/Au enhanced plastic-clad silica fiber-optic surface plasmon resonance (SPR) sensor, developed by Wei et al., was used to evaluate a solution of standard glucose, presenting the scope of usage for other biomolecules. The large

surface area of GPN resulted in outstanding reusability (3.5% of fluctuation) of the sensor and twice the sensibility of a conventional Au film SPR fiber optic sensor.

A fluorescent carbon dots nanosensor based on the inner filter effect (IFE) was constructed for effective determination of vitamin B12. All the other methods attempted for the determination of vitamin B12, including microbiological analysis, atomic absorption spectroscopy (AAS), high performance liquid chromatography (HPLC), enzyme-linked immunosorbent assay, chemiluminescence, coupled plasma mass spectrometry (ICP-MS), surface-enhanced Raman spectroscopy (SERS), electrochemical analysis, and capillary electrophoresis, had poorer performance than the new nanosensor. Also, IFE-based sensors do not initiate any covalent linking between the quencher and fluorophore. Therefore, this technique has been widely used for optical sensing [16].

13.7.1 Graphene-based electrochemical biosensors

Electrochemical nanosensors detect a signal at the interface of electrode and solution (dynamic/static). The interaction involves a reduction-oxidation reaction process followed by the transfer of electrons in a voltammetric nanosensor (dynamic method). A potentiometric nanosensor (static method) monitors the charged species concentration as a function of the electrochemical potential. The static method is applicable to species carrying charge (electrons and ions), whereas in the case of organic pharmaceutical species, voltammetric sensors must be subjected to a redox reaction via an electroactive center at working potential [2].

A biosensor using electrochemical transduction comprises a biorecognition element embedded in the electrochemical signal transducer (e.g., FET or electrode). The recognition of the analyte by the biorecognition molecules produces a change in current or voltage, which forms the basic principle of operation of electrochemical biosensors. As indicated by the electrochemical biosensors, signal transport behavior can be categorized into voltammetric/amperometric, impedimetric, potentiometric, FET biosensor, and conductometric.

Its remarkably large values of electron mobility (at RTP), with experimental values in excess of 15,000 cm^2V^{-1} s^{-1}, minimal Johnson noise, large surface area of 2620 m^2/g, and low resistivity (10–6 Ω-cm) combine to make graphene suitable for use in next-generation electronic devices [31]. Different biofunctionalization patterns arise through physical entrapment, cross-linking, or adsorption of biological interfaces onto the so-modified electrode surface due to the presence of functional groups (e.g., OH, COOH, OCH_3, and NH_2), due to which GLNs and graphene play a crucial role in biosensor construction.

Graphene-based materials have proved to be an excellent substrate for enzymatic immobilization and activity as well as thermal stability, along with exhibiting high rectangular distribution of electrochemical active sites, as compared with different carbonaceous structures

including graphite, fullerenes, or CNTs. Graphene-based materials are used as effective transducers, as they allow direct electron transfer between enzymes and electrodes.

Enzymatic biosensors work via two-step mechanisms:

(i) Based on the catalytic ability of an enzyme towards analyte from its undetectable form to a detectable form.
(ii) Based on inhibition/moderation of the enzyme activity.

Model enzymes are utilized for the development of these sensors, which are used for the detection of a large number of different compounds. Catechols and phenols are determined using laccase, known to catalyze the four electron reduction of oxygen to water; 17 β-estradiol was detected using a laccase-based electrochemical biosensor. Hydrogen peroxide concentrations can be determined using HRP immobilized on porous calcium carbonate microspheres encapsulated with graphene capsules, even under complex test conditions. Glucose oxidase is used to develop biosensors to monitor glucose levels, proving highly efficient for diabetic patients.

In the electrochemical detection of DNA hybridization, there are two main types of sensors: electrochemical sensors, which depend on estimations of the adjustment in current, voltage, or impedance caused due to variation in electrochemical variables, including DNA hybridization causing conductivity or capacitance changes, electron loss, or oxidation of adenine (A), guanine (G), cytosine (C), and thymine (T) of DNA; and fluorescent sensors, which are based on the principle of hybridization of two single-stranded DNA in which ssDNA is labeled with a fluorescent dye and the second one is the complementary DNA corresponding to the target DNA. In the electrochemical approach, the π-π surface interactions of graphene-based nanomaterials are utilized for the immobilization of DNA. EDC/NHS is the most usual chemistry utilized for immobilization of DNA on graphene-based nanomaterials. G edges and GO or rGO with their functional groups (carboxylic, hydroxyl, and epoxide groups) can likewise be used to covalently interact with the DNA.

Graphene nanowalls (realize quantities as small as 0.1 fM) are the best material identified for detection of dsDNA, whereas rGO sensors modified with labeled single-stranded DNA and gold nanoparticles (ssDNA–AuNPs–ERGO) are considered best for detection of ssDNA. A GO-based fluorescence biosensor with sequence-specific DNA detection using multicolor DNA probes displays an excellent emission signal and low background fluorescence from specific targets when the hybridization occurs. The fluorescence resonance energy transfer (FRET or Förster) is another approach to the fluorescence sensing method. This detection method incorporates the quenching of the fluorescent labeled DNA probe to the surface of graphene-based nanomaterial through FRET, which turns the fluorescent signal off, upon which hybridization releases the fluorescent molecule along with the dsDNA. The fluorescent signal is then turned on for optical detection. The FRET strategy was used to build a biosensor

for detection of HIV-1; GO and a nanocomposite of gold nanoparticles (AuNPs) was fabricated and used as a quencher (nanoquencher) with the use of a DNA probe and fluorescent carbon dots (CDs) [17].

Graphene-based immunosensors have been developed for various kinds of pathogens, such as bacteria and virus detection (antibody nanosensors with G to detect the Zika virus and *E. coli*; GO for detection of DENV, rotavirus, and heart- and blood-related diseases [17]; influenza virus H7 detection and diagnosis/prognosis; detection of celiac disease, HIV, and cholera toxin through dendrimer modified G), and cancer therapy (curcumin-loaded graphene quantum dots for synergistic chemotherapy, GQD capped magnetic mesoporous silica nanoparticles for chemo-photothermal therapy and magnetic hyperthermia, because of the ability to produce heat under alternating magnetic field (AMF) and/or under NIR irradiation). Graphene and GO offer the lowest detection limit (10 times less) for detection of bacterial pathogens in comparison to rGO. For viruses, graphene modified with particles of Au and Ag in the nanorange by covalent attachment of an antibody, which allows the detection of concentrations as low as picograms per milliliter (pg/mL) of virus. In the case of investigation of tumor cells, graphene oxide modified by functionalization with magnetic Fe_3O_4 particles allows detection limits in femtograms (fg) [17].

13.8 Potential applications of carbon-based nanosensors

13.8.1 Pharmaceutical analysis

Carbon-based nanomaterials have been extensively investigated in biomedical applications with potential use in pharmaceutical analysis. In addition, for some applications like tablets, drugs, human serum, etc., Fatehy M. Abdel-Haleem et al. in their work constructed a potentiometric sensor for the determination of salicylate anion in pharmaceutical formulations. The rGO in the electrode caused better performance of the sensor, with a detection limit of 1×10^{-5} mol L^{-1} in the concentration range of 10^{-1}–10^{-5} mol L^{-1} in a very short response time of 6 s [41]. An electroanalytical resolution of anxiolytic buspirone hydrochloride using MWCNTs with lengths of 0.1–10 μm on a glassy carbon electrode was accomplished. In another study, bromhexine was detected using MWCNTs functionalized with nickel nanoparticles in the range of 5.0×10^{-6} to 2.3×10^{-4} M with an LOD value of 3.0×10^{-6} M. Zhai et al. developed an electrochemical nanosensor using sulfonated graphene sheets/oxygen-functionalized MWCNTs for the determination of β2-adrenergic agonists, clenbuterol [2]. A differential pulse voltammetric method was used to detect clenbuterol with an LOD of 0.0046 μM in the range of 0.01–5.0 μM. For the determination of thioridazine, nanodiamond decorated with Ag particles in the nanorange was used for the construction of the nanosensor. Thioridazine was determined between 0.08 and 100 mM with an LOD of 0.01 mM and was applied in pharmaceutical and clinical samples.

13.8.2 Bioimaging and biosensing applications

Carbon nanoparticles are engineered for their application in imaging and biosensing for diagnostic purposes. CNTs exhibit astonishing electrochemical properties, making them a popular form of biosensor. With the ability to undergo fast electron transfer, they are able to refute most of the drawbacks put forward by other carbon or metal electrodes in amperometric or voltammetric analyte detection. As optical biosensors, they are used to design new infrared fluorescence and Raman scattering in sensors [5]. When we talk about graphene, two types of frameworks are utilized for biosensing: the first uses a probe molecule to communicate with the analyte, while the second measures the change in the electrical properties and how it interacts with the analyte [5]. CNT and graphene selectively accumulate in tumors through enhanced permeability and retention effect as well as demonstrate extremely high levels of intrinsic absorbance in the biological transparency window located near the NIR region [42–44].

Nanodiamonds are studied for their potential as high-quality bioimaging agents. They are used as fluorescent probes for in vivo studies because of low toxicity. A published work discusses the entry of nanodiamonds into the cell, mainly via endocytosis and by using a clathrin-mediated pathway, during which larger nanodiamonds localize in vesicles while small nanodiamonds appear to be in the cytoplasm.

13.9 Limitations and drawbacks of carbon-based nanosensors

General drawbacks are discussed in the following paragraphs.

13.9.1 Sample preparation

Surfactants play a major role in the preparation of nanoparticles. The high surface-active nanomaterials increase sensitivity towards species present in a test solution/media. Henceforth, the false-positive signals and the cross-interference should be reduced.

For instance, the prerequisite for the detection and analysis of complex analytes, including food toxins, microorganisms, pathogens, and others, is the isolation and purification of the suitable analyte [45, 46]. Preliminary sample preparation and preconcentration steps would not only make the system inconvenient for use but would also increase the cost of the whole process.

Currently, incorporation of the microfluidic channels to purify and obtain the preconcentration of the samples is a general practice. Robust packaging is still required in such cases.

13.9.2 Lack of self-validation and standardization with real-life samples

The validity of nanosensors with real samples under real conditions has become a significant aspect that has gone astray with their advancements in research and applied science. With a major emphasis on disposability, the interassay precision of sensor chips/electrodes/test kits are usually ignored in their implementation in routine analysis. In addition to their functioning under laboratory conditions in synthetic solution/media, complex examinations in conditions like river and municipal supply (for heavy metal sensing, pesticides, and pathogen detection for bacteria), the outside environment (for gas sensing), and food (for heavy metals, pathogens, and toxin detection) should also be reported, as this would raise the reliability of the final evaluated outcomes [16, 46, 47].

Also, standardization would lead to a straightforward transition from testing grounds to the marketplace.

13.9.3 Nanotoxicity

Nanomaterials should be characterized accurately for comprehensive knowledge about their toxicity prior to their implementation in biological matrices or any in vitro applications, including ascertainment of the acceptable concentration amounts in environmental nanotoxicology, which involves the interactions of nanomaterials with the environment and environmentally relevant species [48].

13.9.4 The risk assessment of exposures

Detailed studies on transformation, transport, fate in the environment, and uptake on cellular membranes and cell walls should be researched, discussed, and made available to the concerned industries as well as to the public. The dumping of sensors along with municipal waste should be avoided, and properly accepted and diagnosed protocols should be implemented for their safe use and disposal [24].

13.9.5 Product cost

The techniques used in synthesis and the characterization of nanomaterial-based sensors are relatively costly. Despite the outstanding performance of carbon-based nanosensors, they show some limitations in their outcomes [49]. The implementation of FLN-based sensor systems presents some limitations associated with the fabrication process (different stable C60, C70, C20 and other impurities in manufacturing result) and the gas sensing models (various types of gases sometimes absorb each other, producing lack of selectivity, and exposure to air for a long time can result in instability of the sensor.) The structural properties of CNTs limit their usage. The metallic properties exhibited by CNTs limit their direct implementation in biomedical

applications. CNT-BioFETs exhibit outstanding performance in determination of biomolecules, but the background noise produced turns out to be a limitation, as it can phase out reliable data being recorded and measured. The presence of defects in the structure can affect the Young's modulus and yield several problems. The graphene-based nanosensors are reactive towards the oxidative environment, which affects their performance. The surface chemistry of nanodiamonds must be taken care of, particularly the specific functionalization, as it affects the luminescence and the quantum sensing directly. The interaction between the surface chemistry of nanodiamonds and bulk nanodiamonds requires better performance.

13.10 Conclusion

Carbon nanomaterials are growing as promising materials, due to their inherent mechanical, optical, electrochemical, and electrical properties. The recent increase in the number of articles and publications in this field is due to the existence of both the inorganic semiconducting property and organic π-π stacking character. Different carbon allotropic forms discussed in this chapter have the potential for routine sensing as can be seen through their widespread integration into sensing devices. As outlined in the chapter, carbon nanostructures have a high degree of selectivity, particularly when functionalized. Advances in the carbon-based model to ease out contaminants as well as to improve the surface modification and characterization process will assist in enhancing the sensor's selectivity. The chapter has introduced several applications of carbon-based nanomaterials. With the popularity of CBNs as highly versatile and useful nanomaterials, we expect to see continued use of CBNs in many facets of biomedical engineering, with great promise in applying their biocompatible and multifunctional nature to the areas that interconnect mechatronics and biology, such as microelectromechanical systems for biological sensors and actuators. Efforts are required in the areas of size selective synthesis, purification, and separation.

Acknowledgment

The authors would like to thank Netaji Subhas University of Technology for providing facilities and financial support.

References

[1] B. Sharma, P. Malik, P. Jain, Biopolymer reinforced nanocomposites: a comprehensive review, Mater. Today Commun. 16 (2018) 353–363.
[2] S. Kurbanoglu, S.A. Ozkan, Electrochemical carbon based nanosensors: a promising tool in pharmaceutical and biomedical analysis, J. Pharm. Biomed. Anal. 147 (2018) 439–457.
[3] Y. Yang, X. Yang, Y. Yang, Q. Yuan, Aptamer-functionalized carbon nanomaterials electrochemical sensors for detecting cancer relevant biomolecules, Carbon 129 (2018) 380–395.
[4] T.-T. Tran, A. Mulchandani, Carbon nanotubes and graphene nano field-effect transistor-based biosensors, TrAC Trends Anal. Chem. 79 (2016) 222–232.

[5] A. Rifai, E. Pirogova, K. Fox, Diamond, carbon nanotubes and graphene for biomedical applications, in: Encyclopedia of Biomedical Engineering, Elsevier, 2019, pp. 97–107.
[6] S. Shekhar, A. Sarkar, B. Sharma, P. Jain, Electrochemical evaluation of functionalized graphene oxide filled PVA-chitosan biohybrid for supercapacitor applications, J. Appl. Polym. Sci. (2019) 48610.
[7] A. Qureshi, W.P. Kang, J.L. Davidson, Y. Gurbuz, Review on carbon-derived, solid-state, micro and nano sensors for electrochemical sensing applications, Diam. Relat. Mater. 18 (12) (2009) 1401–1420.
[8] X. Chen, W. Zhang, Diamond nanostructures for drug delivery, bioimaging, and biosensing, Chem. Soc. Rev. 46 (3) (2016) 734–760.
[9] F.R. Baptista, S.A. Belhout, S. Giordanib, S.J. Quinn, Recent developments in carbon nanomaterial sensors, Chem. Soc. Rev. 44 (2015) 4433–4453.
[10] V.D.N. Bezzon, T.L.A. Montanheiro, B.R.C. de Menezes, R.G. Ribas, V.A.N. Righetti, K.F. Rodrigues, G.P. Thim, Carbon nanostructure-based sensors: a brief review on recent advances, Adv. Mater. Sci. Eng. 2019 (2019) 4293073 21 pages.
[11] H. Song, Y. Zhang, J. Cao, Sensing mechanism of an ionization gas temperature sensor based on a carbon nanotube film, RSC Adv. 7 (84) (2017) 53265–53269.
[12] W. Yuna, W. Xiong, H. Wua, M. Fua, Y. Huang, X. Liu, L. Yang, Graphene oxide-based fluorescent "turn-on" strategy for Hg2+ detection by using catalytic hairpin assembly for amplification, Sensors Actuators B Chem. 249 (2017) 493–498.
[13] Y. Wang, Y. Ding, L. Li, P. Hu, Nitrogen-doped carbon nanotubes decorated poly (L-cysteine) as a novel, ultrasensitive electrochemical sensor for simultaneous determination of theophylline and caffeine, Talanta 178 (2018) 449–457.
[14] N. Wang, G.-Q. Liu, W.-H. Leong, H. Zeng, X. Feng, S.-H. Li, F. Dolde, H. Fedder, J. Wrachtrup, X.-D. Cui, S. Yang, Q. Li, R.-B. Liu, Magnetic criticality enhanced hybrid nanodiamond thermometer under ambient conditions, Phys. Rev. X 8 (1) (2018) 011042.
[15] S. Szunerits, Y. Coffinier, R. Boukherroub, Diamond nanowires: a recent success story for biosensing, in: Carbon-Based Nanosensor Technology, Springer, Cham, 2018, pp. 1–18.
[16] L. Ding, H. Yang, S. Ge, J. Yu, Fluorescent carbon dots nanosensor for label-free determination of vitamin B12 based on inner filter effect, Spectrochim. Acta A Mol. Biomol. Spectrosc. 193 (2018) 305–309.
[17] J. Peña-Bahamonde, H.N. Nguyen, S.K. Fanourakis, D.F. Rodrigues, Recent advances in graphene-based biosensor technology with applications in life sciences, J. Nanobiotechnol. 16 (1) (2018) 75.
[18] X. Ding, X.D. Chen, X. Chen, X. Zhao, N. Li, A QCM humidity sensor based on fullerene/graphene oxide nanocomposites with high quality factor, Sensors Actuators B Chem. 266 (2018) 534–542.
[19] J. Pan, T.-G. Cha, H. Chen, J.H. Choi, Carbon nanotube-based optical platforms for biomolecular detection, in: Carbon Nanotubes and Graphene for Photonic Applications, Elsevier, 2013, pp. 270–297.
[20] A.K. Sundramoorthy, T.H. Vignesh Kumar, S. Gunasekaran, Graphene-based nanosensors and smart food packaging systems for food safety and quality monitoring, in: Graphene Bioelectronics Advanced Nanomaterials, Elsevier, 2018, pp. 267–306 (Chapter 12).
[21] Y. Wu, F. Jelezko, M.B. Plenio, T. Weil, Diamond quantum devices in biology, Angew. Chem. Int. Ed. 55 (23) (2016) 6586–6598.
[22] Y. Shunin, S. Bellucci, Y. Zhukovskii, V. Gopeyenko, N. Burlutskaya, T. Lobanova-Shunina, Nanocarbon electromagnetics in CNT-, GNR- and aerogel-based nanodevices: models and simulations, Comput. Model. New Technol. 19 (1A) (2015) 35–42.
[23] M.M. Rana, D.S. Ibrahim, M.R.M. Asyraf, S. Jarin, A. Tomal, A review on recent advances of CNTs as gas sensors, Sens. Rev. 37 (2) (2017) 127–136.
[24] S. Manzetti, D. Vasilache, E. Francesco, Emerging carbon-based nanosensor devices: structures, functions and applications, Adv. Manuf. 3 (1) (2015) 63–72.
[25] A. Grozdanov, A. Petrovski, P. Paunovik, A.T. Dimitrov, M. Avella, MWCNT/polyaniline nanocomposites used for ph nanosensors of marine waters, in: Proceedings of the International Conference on Microplastic Pollution in the Mediterranean Sea, 2017.
[26] P.V. Jena, D. Roxbury, T.V. Galassi, L. Akkari, C.P. Horoszko, D.B. Iaea, J. Budhathoki-Uprety, N. Pipalia, A.S. Haka, J.D. Harvey, J. Mittal, F.R. Maxfield, J.A. Joyce, D.A. Heller, A carbon nanotube optical reporter maps endolysosomal lipid flux, ACS Nano 11 (11) (2017) 10689–10703.

[27] J. Dong, D.P. Salem, J.H. Sun, M.S. Strano, Analysis of multiplexed nanosensor arrays based on near-infrared fluorescent single-walled carbon nanotubes, ACS Nano 12 (4) (2018) 3769–3779.
[28] K. Yang, D. Maiti, X. Tong, X.Z. Mou, Carbon based nanomaterials for biomedical applications: a recent study, Front. Pharmacol. 9 (2019) 1401.
[29] M. Fakher, S. Rahmanian, S. Hosseini-Hashemi, On the carbon nanotube mass nanosensor by integral form of nonlocal elasticity, Int. J. Mech. Sci. 150 (2019) 445–457.
[30] M. Mohammadian, M.H. Abolbashari, S.M. Hosseini, Application of hetero junction CNTs as mass nanosensor using nonlocal strain gradient theory: an analytical solution, Appl. Math. Model. 76 (2019) 26–49.
[31] S.J. Rodríguez, L. Makinistian, E.A. Albanesi, Graphene for amino acid biosensing: theoretical study of the electronic transport, Appl. Surf. Sci. 419 (2017) 540–545.
[32] S. Islam, S. Shukla, V.K. Bajpai, Y.-K. Han, Y.S. Huh, A. Kumar, A. Ghosh, S. Gandhi, A smart nanosensor for the detection of human immunodeficiency virus and associated cardiovascular and arthritis diseases using functionalized graphene-based transistors, Biosens. Bioelectron. 126 (2019) 792–799.
[33] K. Xu, C. Fu, Z. Gao, F. Wei, Y. Ying, C. Xu, G. Fu, Nanomaterial-based gas sensors: a review, Instrum. Sci. Technol. (2017) 115–145.
[34] M. Rouhani, Fluoro-functionalized graphene as a promising nanosensor in detection of fish spoilage: a theoretical study, Chem. Phys. Lett. 719 (2019) 91–102.
[35] L. Zhang, D. Peng, R.-P. Liang, J.-D. Qiu, Graphene-based optical nanosensors for detection of heavy metal ions, TrAC Trends Anal. Chem. 102 (2018) 280–289.
[36] R. Mishra, J. Militky, Carbon based nanomaterials, in: Nanotechnology in Textiles: Theory and Application, Elsevier, 2019.
[37] M.S.J. Barson, P. Peddibhotla, P. Ovartchaiyapong, K. Ganesan, R.L. Taylor, M. Gebert, Z. Mielens, B. Koslowski, D.A. Simpson, L.P. McGuinness, J. McCallum, S. Prawer, S. Onoda, T. Ohshima, A.C. Bleszynski Jayich, F. Jelezko, N.B. Manson, M.W. Doherty, Nanomechanical sensing using spins in diamond, Nano Lett. 17 (3) (2017) 1496–1503.
[38] T.A. Ivandini, Y. Einaga, Heavy metal sensing based on diamond electrodes, in: Carbon-Based Nanosensor Technology, Springer, Cham, 2018, pp. 67–82.
[39] A. Pasquarelli, F. Picollo, V. Carabelli, Boron-doped diamond and graphitic multiarrays for neurotransmitter sensing, in: Carbon-Based Nanosensor Technology, Springer, Cham, 2018, pp. 19–65.
[40] S. Mojtaba Mousavi, S. Alireza Hashemi, M. Zarei, A.M. Amani, A. Babapoor, Nanosensors for chemical and biological and medical applications. Med. Chem. 8 (8) (2018). https://doi.org/10.4172/2161-0444.1000515.
[41] F.M. Abdel-Haleem, A. Salah, M.S. Rizk, H. Moustafa, M. Bechelany, A. Barhoum, Carbon-based nanosensors for salicylate determination in pharmaceutical preparations, Electroanalysis (2019).
[42] B. Sharma, S. Shekhar, P. Malik, P. Jain, Study of mechanism involved in synthesis of graphene oxide and reduced graphene oxide from graphene nanoplatelets, Mater. Res. Express 5 (6) (2018) 065012.
[43] B. Sharma, S. Shekhar, S. Gautam, A. Sarkar, P. Jain, Nanomechanical analysis of chemically reduced graphene oxide reinforced poly (vinyl alcohol) nanocomposite thin films, Polym. Test. 70 (2018) 458–466.
[44] B. Sharma, S. Shekhar, S. Gautam, P. Jain, Dynamic shear rheology behavior and long term stability kinetics of reduced graphene oxide filled poly (vinyl alcohol) biofilm, Polym. Test. 69 (2018) 583–592.
[45] S. Lu, D. Wu, G. Li, Z. Lv, Z. Chen, L. Chen, G. Chen, L. Xia, J. You, Y. Wu, Carbon dots-based ratiometric nanosensor for highly sensitive and selective detection of mercury (II) ions and glutathione, RSC Adv. 6 (105) (2016) 103169–103177.
[46] Q. Li, Q. Huang, J.-J. Zhu, W.-G. Ji, Q.-X. Tong, Carbon dots–quinoline derivative nanocomposite: facile synthesis and application as a "turn-off" fluorescent chemosensor for detection of Cu 2+ ions in tap water, RSC Adv. 6 (90) (2016) 87230–87236.
[47] F. Yan, Z. Bai, F. Liu, F. Zu, R. Zhang, J. Xu, L. Chen, Ratiometric fluorescence probes based on carbon dots, Curr. Org. Chem. 22 (1) (2018) 57–66.
[48] A.-E. Al Moustafa, E. Mfoumou, D.E. Roman, V. Nerguizian, A. Alazzam, I. Stiharu, A. Yasmeen, Impact of single-walled carbon nanotubes on the embryo: a brief review, Int. J. Nanomedicine 11 (2016) 349.
[49] R. Kaur, S.K. Sharma, S.K. Tripathy, Advantages and limitations of environmental nanosensors, in: Advances in Nanosensors for Biological and Environmental Analysis, Elsevier, 2019, pp. 119–132.

CHAPTER 14

Polymerized hybrid nanocomposite implementations of energy conversion cells device

Nidhi Asthana[a], **Kaushik Pal**[b,c]

[a]*National Centre of Experimental Mineralogy and Petrology, University of Allahabad, Allahabad, India*
[b]*International and Inter University Centre for Nanoscience and Nanotechnology (IIUCN), School of Energy Materials, Mahatma Gandhi University, Kottayam, Kerala, India*
[c]*Wuhan University, Wuchang District, Wuhan, Hubei Province, Republic of China*

14.1 An overview of environmental science innovations

The term environment is derived from the French word *environner*, which means to encircle or surround. All the biological and nonbiological things surrounding an organism are thus included in the environment. Therefore, the environment can be considered as the sum of water, air, and land, and the interrelationships among them, humans, and other living organisms. Thus in order to study the environment, one needs knowledge input from various disciplines of science, including botany, zoology, microbiology, genetics, biochemistry, and biotechnology, which help in understanding the biotic components and their interaction. The physical and chemical structure of the abiotic components, energy transfer, and its flow are understood with the help of basic concepts of physics, chemistry, geology, atmospheric science, oceanography, and geography. Mathematics, statistics, and computer science serve as effective tools in environmental modeling and management. Subjects like education, economics, sociology, and mass communication provide the inputs for dealing with the socioeconomic aspects associated with various developmental activities [1–4]. Synthesis with environmental engineering, civil engineering, hydraulics, and chemical engineering form the basis for various technologies dealing with the control of environmental pollution, waste treatment, and development of cleaner technologies, which are important for protection of the environment. Environmental laws provide the tools for effective management and protection of the environment. Environmental studies, therefore, are a multidisciplinary subject in which different aspects are dealt with in a holistic approach.

Nanofabrication for Smart Nanosensor Applications. https://doi.org/10.1016/B978-0-12-820702-4.00015-5
© 2020 Elsevier Inc. All rights reserved.

The scope of environmental studies is broad-based and it encompasses a large number of areas and aspects, as listed here:

- Natural resources
- Ecology and biodiversity
- Environmental pollution and control
- Social issues in relation to development and environment
- Human population and environment.

The environment belongs to all and is therefore important to all. Thus the environment is a subject that is actually global in nature. For example, the atmosphere has no boundaries and the pollutants produced at one place can be dispersed and transported to another place. The environment is a closely and intricately woven network of components and functions. There are some environmental issues that may be of localized importance, but there are also major issues like global warming, depletion of ozone layer, dwindling forest and energy resources, loss of global biodiversity, etc. that affect mankind as a whole and for that we have to think globally.

Environmental studies are very important, since they deal with the most fundamental issues like safe and clean drinking water, hygienic living conditions, and clean and fresh air. There is need for trained manpower at every level to deal with environmental issues. Hazardous chemical abundance and diversity are major environmental challenges of today. Pollution is the issue of "dirtying" the environment in several ways, such as illegally disposing of waste or the excessive cutting of trees [5]. There are many forms of pollution, namely noise pollution, water pollution, air pollution, light pollution, visual pollution, thermal pollution, soil contamination, radioactive contamination, and so forth. These pollutions usually create negative effects on human health and environment.

- *Noise pollution*: This kind of pollution is an excessive amount of noise produced by something or someone. This usually affects or harms our hearing.
- *Air pollution*: This is caused by entities that release harmful gases and other emissions such as carbon monoxide and CFC into the air, which can harm humans and the earth.
- *Water pollution*: This is the contamination of water bodies by toxic/oil spills, littering, or other harmful activities. It not only affects us, but it also affects marine life, endangering their habitat.
- *Land pollution*: This occurs when harmful substances such as acid rain and pesticides seep into the soil and contaminate it. This can affect plant growth rate and the soil's fertility negatively.
- *Thermal pollution*: This involves the temperature variation of air and water bodies caused by human activities, e.g., water as a coolant in a power plant.

Air pollution and global warming are two of the major threats to human and animal health. To check air pollution and to reduce the current emission of greenhouse gases, factories and power plants need to be equipped in such a way as to meet the current air emission standards stated in

the Environmental Pollution Control Regulation 2000 [6]. Major pollutants of the air are carbon monoxide (CO), carbon dioxide (CO_2), chlorofluorocarbons (CFCs), lead, ozone, and nitrogen oxide (NOx).

Energy and environmental pollution are the two most challenging issues faced by our society. With the production of oil predicted to decline and the number of vehicles and their pollution impact to increase globally, safe, low-cost, highly efficient, and environmentally friendly alternative power sources have become a most urgent need of today. Solar energy, H_2 energy, fuel cells, and batteries are attracting considerable interest as alternative power sources, to reduce dangerous anthropogenic emissions that interfere with the climate system. Energy insecurity and rising prices of conventional energy sources are also major threats to our economic and political stability.

Many alternatives to conventional energy sources have been proposed, but analyses of such options have been limited in breadth and depth. At the heart of modern society lies an economy driven by energy use. Unfortunately, the same energy that brings us comfort, convenience, and prosperity also brings us pollution, impoverishment, and global warming. Our challenges are to maximize the benefits gained from energy consumption while minimizing the cost incurred. The primary global warming pollutants are, in order, carbon dioxide gas, fossil-fuel plus biofuel soot particles, methane gas, [7, 8] halocarbons, troposphere ozone, and nitrous oxide gas. This alone indicates that addressing global warming quickly is critical, because air pollution and global warming problems are caused primarily by exhaust from solid, liquid, and gas combustion during energy production and use. Therefore, such problems can be addressed only with large-scale changes to the energy sector. The work carried out in this chapter was motivated by the need to assist the ever-changing and ever-improving nanotechnologies related to miniaturization of electronic devices, which are environmentally friendly. Here, environmentally friendly means such a device that does not harm the surroundings, i.e., atmosphere, nature (land, water, air, and plants), animals, etc. The environment provides resources that support life on the earth and that also help in the growth of a relationship of interchange between living organisms and the environment in which we live. There are actually two types of environment. One is the natural environment of the air, water, solid wastes, noise, radiation, soil, timber, wildlife, and living space. The second one is the manmade environment that deals with work environment, housing, technology, aesthetics, transportation, utilities, settlement, urbanization, and so on. The natural environmental components are considered as the resources and are mostly exploited and utilized by humans to fulfil our daily basic physical needs. However, natural resources are finite, which means that if we use them continuously, we will eventually exhaust them. Moreover, the environmental pollution due to manmade technologies is the main cause of degradation of our natural resources. In order to preserve our natural resources, humans require alternatives to natural resources, which includes technologies for generation of energy by means of solar, hydrogen, batteries, hydrocarbons, wind, etc. However, at present, most of the technologies used for the betterment of our lives have been based on inorganic metallic semiconductors, which does not protect our

surroundings from pollution caused by carbon dioxide emissions and the lack of biocompatibility of materials. Therefore, research is growing in areas related to environmentally friendly materials due to concerns with increasing carbon emissions and the limited sources of petroleum and natural gas resources.

These environmentally friendly materials contain polymers and possibly fillers that are either biodegradable or from renewable resources. The life cycle of renewable polymeric materials is a carbon-neutral process, and their use in environmentally friendly devices in nanotechnology may reduce carbon dioxide accumulation in the atmosphere. Nanotechnology has now been recognized as one of the most promising technologies of the 21st century and new materials (organic, inorganic, semiconductor, polymer, nanocomposite, graphene, etc.) have been used for many device applications [9]. Among the various materials research, polymers [10] have emerged as a new attractive material, with multidisciplinary research activity focused on them. Results obtained through the research on polymer nanocomposites discussed in this chapter will broaden the applications of polymers. In addition, we have also improved the ionic/transport properties of polymer electrolytes with the use of different filler groups, plasticizers, salts, etc., useful for device fabrication [11]. The details of polymers, polymer nanocomposites, their properties and applications are described in the next section.

14.2 Polymers

Polymers are substances whose molecules have high molar masses and that are composed of a large number of repeating units. There are both naturally occurring and synthetic polymers. Among naturally occurring polymers are proteins, starches, cellulose, and latex. Polymers are generally classified as [12]:

(1) Natural polymers: The polymers that occur in nature, also known as biopolymers, e.g., starch, rubber, etc.
(2) Half synthetic polymers: The chemically modified natural polymers, such as hydrogenated polymers, e.g., cellulosic, methyl cellulose, etc.
(3) Synthetic polymers: The polymers that have been synthesized in the laboratory, e.g., polyvinyl alcohol, polyethylene, etc.

14.2.1 Structure of polymers

Polymeric macromolecules can be linear or branched and may be cross-linked. Three types of macromolecules are shown in Fig. 14.1 [13]:

(a) Linear polymers: if the monomer units are joined in a linear fashion, the polymer is said to be a linear polymer.
(b) Branched polymers: when the monomer units are joined in a branched manner, it is called a branched polymer.

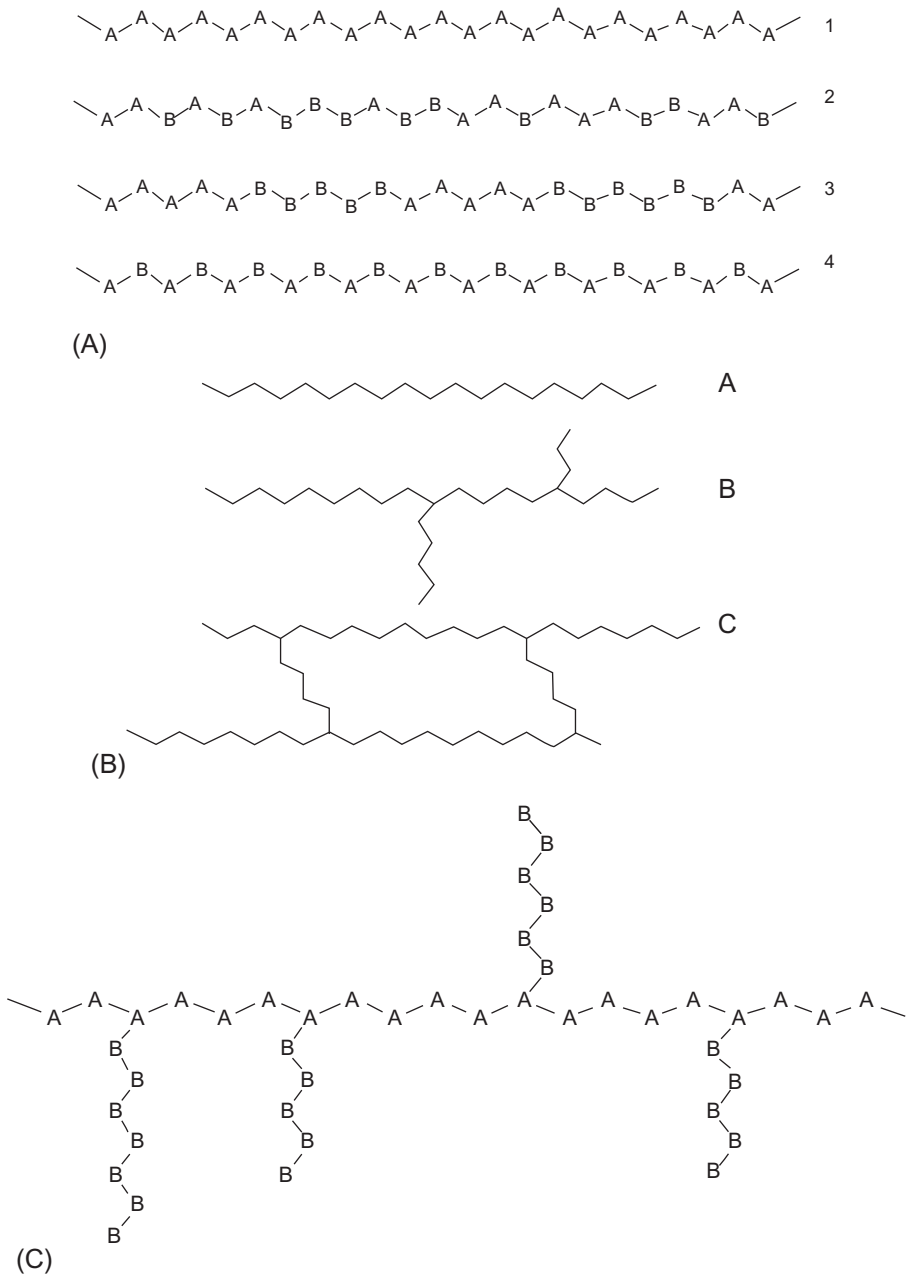

Fig. 14.1
Structure of different polymers: (A) linear polymer; (B) branched polymer; (C) cross-linked polymer.

(c) Cross-linked polymers: a polymer is said to be a cross-linked polymer if the monomer units are joined together in a cross-linked chain fashion.

Polymers can be composed of just one type of monomer (homopolymer) or of different types (copolymer).

The different monomer units in copolymers can basically be arranged in three different ways:

- *Random copolymer*: There is no regularity in the arrangement of the two different monomers in the polymer.
- *Block copolymer*: Blocks of pure oligomer alternate with blocks of another pure oligomer.
- *Alternating copolymer*: The monomers alternate within the composition of the polymer.

14.2.2 Properties of the polymer

The building principle of a polymer is extreme flexibility, so that polymers with an extensive range of properties and combinations can be produced. Polymers in the shape of objects, fibers, or films may be rigid or flexible; transparent, translucent or opaque; hard or soft; weather resistant or degradable; or resistant to either high or low temperature. In addition, they may be compounded with fillers and blended with other products, forming so-called composites. A certain polymer is usually applicable in more than one field of application. Polymers can be used in a number of applications.

14.2.3 Thermal properties of polymers

Substances can exist in three possible physical states: solid, liquid, and gas. In polymeric materials, most polymers decompose before they boil and cross-linked polymers decompose before they melt. According to their basic thermal properties, four different types of polymers are distinguished:

Thermoplastics: These polymeric materials are more or less rigid at room temperature and can be melted by heat.
Thermosets: These materials are also rigid at room temperature, but due to the cross-links in their molecular structure, they cannot be melted.
Rubbers or elastomers: Rubbers are flexible at room temperature; most of them are amorphous materials and do not show a melting point. They have a glass transition point instead, which is well below room temperature. Below this glass transition temperature, they are rigid.
Thermoplastic elastomers: Thermoplastic elastomers are block copolymers or polymer blends that are flexible and have properties similar to vulcanized rubbers at room

temperature, but which can be softened or melted by heat. This process is reversible, so the products can be reprocessed and remolded.

14.3 Composites

Over the past few decades, composite materials, plastics, and ceramics have been dominant emerging materials undergoing research. The volume and number of applications of composite materials have grown steadily, penetrating and conquering new markets relentlessly. Modern composite materials constitute a significant proportion of the engineered materials on the market, ranging from everyday products to sophisticated niche applications. As composites have already proven their worth as weight-saving materials, the current challenge is to make them more ecofriendly and cost effective. The efforts to produce economically attractive composite components have resulted in several innovative manufacturing techniques currently being used in the composites industry. It is obvious, especially for composites, that the improvements in manufacturing technology alone are not enough to overcome the cost hurdle. It is essential that there be an integrated effort in design, material, process, tooling, quality assurance, manufacturing, and even program management for composites to become competitive with metals. The composites industry has begun to recognize that the commercial applications of composites could offer much larger business opportunities than the aerospace sector, due to the sheer size of the transportation industry. Thus the shift of composite applications from aircraft to other commercial uses has become prominent in recent years. Increasingly enabled by the introduction of newer polymer resin matrix materials and high-performance reinforcement fibers of glass, carbon, and aramid, the penetration of these advanced materials has witnessed a steady expansion in uses and volume. This increased volume has resulted in the expected reduction in costs. In certain applications, the use of composites rather than metals has in fact resulted in savings of both cost and weight. Further, the need for composites to be used as lighter construction materials and in more seismic-resistant structures has placed strong emphasis on the potential of new and advanced materials that not only decrease dead weight but also absorb shock and vibration through tailored microstructures. Composites are now extensively being used for rehabilitation/strengthening of preexisting structures that have to be retrofitted to make them seismic resistant, or to repair damage caused by seismic activity.

Unlike conventional materials (e.g., steel), the properties of composite materials can be designed considering the structural aspects. The design of a structural component using composites involves both material and structural design. Composite properties (e.g., stiffness, thermal expansion, etc.) can be varied continuously over a broad range of values under the control of the designer. Careful selection of reinforcement type enables the finished product characteristics to be tailored to almost any specific engineering requirement.

14.4 Types of composite materials

14.4.1 Fiber-reinforced composites

Reinforced composites are popular for use in many industrial applications, because of their inherent high specific strength and stiffness. Due to their excellent structural performance, the composites are gaining ground also in biological applications. In this type of composite the second phase is in the form of fibers dispersed in the matrix, which could be either plastic or metal. The volume fraction (Vf) varies from a few percent to as high as 70%. Usually the purpose of the fiber reinforcement is to obtain high strength and high modulus.

14.4.2 Particulate composite

In this type of composite, 1 μm to 200 μm size particles are dispersed in the matrix and the volume fraction (Vf) is generally between 0.01 Vf to 0.85 Vf. This is classified as: (a) random fiber (short fiber) reinforced; (b) particles as the reinforcement composites (particulate composites); (c) continuous fiber (long fiber) reinforced; (d) flat flakes as the reinforcement composites (flake composites); (e) fillers as the reinforcement (filler composites).

14.5 Electrolytes

An electrolyte is a substance that ionizes when dissolved in suitable solvents. In other words, electrolytes are substances that conduct electricity as a result of dissociation of salt into its constituents. The solution of an electrolyte is ionic in nature [14].

Electrolytes can be divided into five major categories, depending upon the physical nature of the electrolyte used in the devices.

(i) Liquid electrolyte
(ii) Solid electrolyte
(iii) Gel electrolyte
(iv) Polymer electrolyte
(v) Polymer gel electrolyte.

14.5.1 Liquid electrolyte

A liquid electrolyte is formed when a salt dissolves in a solvent (which can be water or a polar solvent), e.g., NaCl dissolved in H_2O to form a liquid electrolyte. The most appreciable property of a liquid electrolyte is its high ionic conductivity, on the order of 10^{-2} Scm^{-1} [15]. Most primary and secondary lithium ion batteries are basically designed using liquid electrolytes, containing a lithium salt, such as $LiPF_6$, $LiBF_6$, $LiClO_4$, $LiBC_4O_8$, or Li

$[PF_3(C_2CF_5)_3]$, dissolved in organic alkyl carbonate solvent. However, high sensitivity to moisture and high oxidation of anions have caused some safety issues in such batteries.

14.5.2 Solid electrolyte

The solid nature of an electrolyte that shows high ionic conductivity (10^{-6} Scm^{-1}) is known as a solid electrolyte or a super-ion conductor [16]. The advantage of a solid electrolyte over a liquid electrolyte is:

(i) High ionic conductivity (10^{-1} to 10^{-4} Scm^{-1}),
(ii) Low electronic conductivity ($<10^{-6}$ Scm^{-1}),
(iii) Low activation energy (Ea < 0.3 eV) and ionic charge carriers which are principal charge carrier (i.e. ionic transport number ($t_{ion} \approx 1$)) are the essential features of an ideal solid electrolyte.

Gel electrolytes are synthesized by incorporating liquid electrolyte into polymer base membranes by soaking the membranes in lithium-based organic electrolytes. Although solid electrolytes are used in various fields, they also possess some drawbacks.

14.5.2.1 Classification of solid electrolytes

On the basis of microstructure and physical properties; solid electrolytes are divided into the following categories:

(i) Framework crystalline materials,
(ii) Amorphous-glassy electrolytes,
(iii) Composite electrolytes,
(iv) Polymer electrolytes.

Amorphous glassy and polymer electrolytes are microscopically disordered, whereas composite electrolytes are macroscopically disordered, but the framework crystalline materials are ordered in structure [17].

14.5.3 Polymer electrolyte

Polymer electrolytes are usually formed by complexing polar polymers like PEO, PVdF, PPO, and PEG with ionic salts of monovalent alkali metal or divalent transition metal ammonium salts. Polymer electrolytes are mostly prepared by the solution cast method or the electrodeposition method. Polymer electrolytes have several advantages over liquid electrolytes, such as freedom from leakage, good processibility, design flexibility, space casing, light weight, and the possibility of high energy and power density [18].

For the purpose of application in solid electrochemical devices, a polymer electrolyte should possess the following properties [19, 20]:

(i) high ionic conductivity and high transference number;
(ii) high chemical and thermal stabilities;
(iii) good compatibility with the electrode.

Classification of polymer electrolytes

On the basis of the synthesis technique of electrolytes, polymer electrolytes can be classified into the following categories:

Conventional polymer salt complex or solid polymer electrolyte (SPE) SPEs are prepared by dissolving ionic salts into polar polymer hosts, namely polyethylene oxide (PEO), polypropylene oxide (PPO), and polyvinylidene fluoride (PVdF). The film synthesis is carried out either by the solution cast method, electrodeposition method, or sol gel method.

Plasticized polymer salt complex The plasticized polymer salt complex is prepared by adding plasticizers into SPEs. The plasticized polymer salt complex possesses both liquid- and solid-like behavior. By this process, the ambient conductivity is substantially enhanced.

Composite polymer electrolyte (CPE) CPEs are basically analogs to phase composite solid electrolyte systems. They are also prepared simply by dispersing a small fraction of micro/nanosize inorganic or organic filler particles into the conventional SPE host. As a result, the ionic conductivity, the mechanical stability, and the interfacial activity are usually enhanced substantially.

14.5.4 Gel and polymer gel electrolyte

Gels are the three-dimensional network structures of polymers and their swollen mattes. They possess both the cohesive properties of solids and the diffusive transport properties of liquids. Their properties vary from viscous liquid to hard solid, according to chemical composition [21]. The properties of polymer gel electrolytes have been found to depend upon the structure of the polymer network that makes up the gel, as well as on the interaction of the network and the solvent. As the polymer networks are solvated by a large amount of the trapped solvent, so the gels generally possess high mobility. The polymer gel electrolyte is usually formed by adding the polymer into a solvent-salt solution. Compared to solid electrolytes and liquid electrolytes, gel electrolytes have several advantages, including no shape restrictions, faster charging/discharging, and higher power density. The best way to achieve high conductivity in gel-based electrolytes is to use polymer host materials. The term polymer gel electrolyte includes three terms: polymer, gel, and electrolyte. Polymers are substances of high molecular weight formed by the union of small molecular substances known as monomers held together by covalent bonds. Gels are substances with jellylike structures. In the steady state a gel does not flow. Gels are liquid, but due to the presence of a 3D cross-link network, they behave as a solid. They can be formed by mixing organic liquid solvent

with a salt and then polymer is added to give mechanical stability, which results in the formation of a gel. The solvent used here is called a liquid plasticizer, the salt used is usually an alkali metal salt, and the polymer used can be PEO, PVC, PMMA, PVdF, and so forth. Propylene carbonate (PC), ethylene carbonate (EC), dimethyl formamide (DMF), diethyl carbonate (DEC), and dimethyl carbonate (DMC) are usually used as plasticizers. The salt can be an alkali metal salt having low lattice energy and bulky anions. Polymers like polyacrylonitrile (PAN), poly(methyl methacrylate) (PMMA), polyvinylidene fluoride (PVdF), and others are used as a polymer host. They act as a gelling agent in the preparation of polymer gel electrolytes. Polymer gel electrolytes usually possess high electrical conductivity as compared to solid polymer electrolytes. In this chapter, nanocomposite polymer electrolytes are discussed.

14.5.5 Polymer nanocomposite and their classifications

However, first of all it is essential to understand the terms polymer, composite, nanocomposite, and the properties that make them superior to other materials. The polymers are compounds containing a large number of structural units joined by the same type of linkage, which often form into a chain-like structure. Polymers already have a wide range of applications that far exceed those of any other class of material available to man, such as adhesives, coatings, foams, and packaging materials, to textile and industrial fibers, electronic devices, biomedical devices, optical devices, and their precursors.

Thus the composite materials combine two or more different materials that are mixed in an effort to get the best properties out of all. However, a nanocomposite is a composite material in which one of the components has at least one dimension that is nanoscopic (10^{-9} m) in size. It is well established that by reducing the physical dimensions of the compound down to the nanometer length scale, unusual and often enhanced properties can be realized, because many chemical and physical interactions are governed by the surface properties and nanoparticles have large surface-to-volume ratio.

There are generally three main structures (conventional, intercalated, and exfoliated) of polymer nanocomposites that can be synthesized, as shown in Fig. 14.2.

Thus a nanocomposite material consists of an assemblage of two materials of different natures, completing and allowing us to obtain a material for which the set of characteristic properties is greater than that of the components taken separately. In general, such a material consists of one or more discontinuous phases, distributed in one continuous phase. The discontinuous phase is usually harder and with superior mechanical properties than the continuous phase, and it is usually called reinforcement, or reinforcing material, whereas the continuous phase is called a matrix. Both reinforcement and matrix materials in the composite materials have different roles and sets of properties, making them superior over

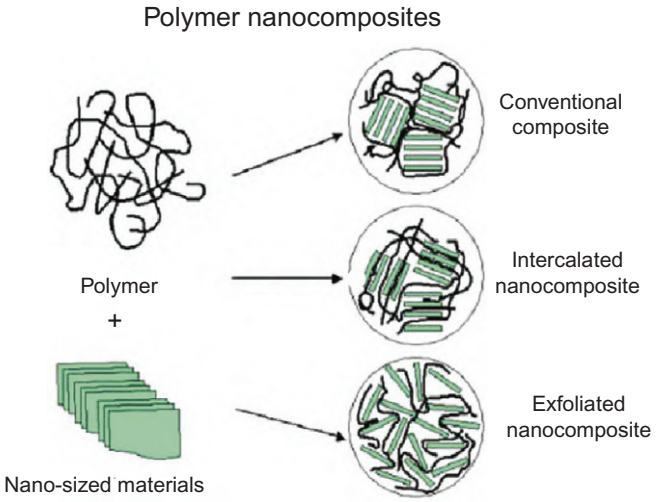

Fig. 14.2
Schematic diagram of the formation of polymer nanocomposite compound and their structures.

other polymer compounds. The reinforcement brings to the composite material its greater mechanical performance, whereas the role of the matrix is to transmit to the fiber the external mechanical load and protect the fibers against external attack. The type of reinforcement-matrix association depends upon the type of application for which the nanocomposite material has been designed. On the bases of their specific applications and properties, nanocomposites can be classified as in the schematic diagram shown in Fig. 14.3. Therefore, these materials offer improvements over conventional composites in

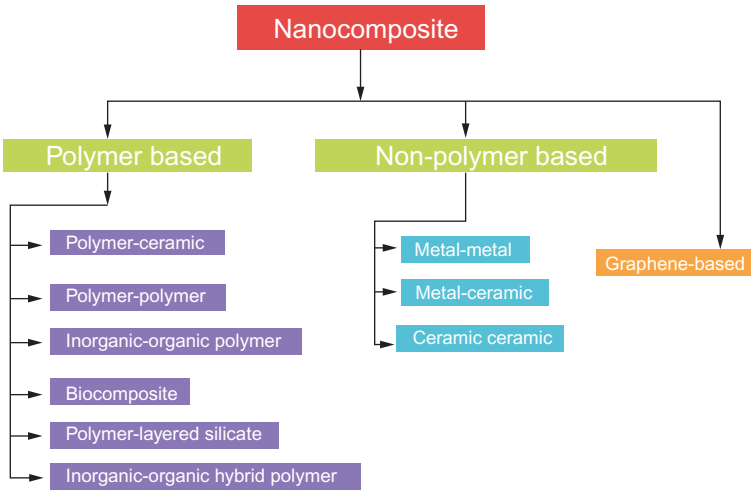

Fig. 14.3
Nanocomposite compounds and their classifications.

mechanical, thermal, electrical, and barrier properties. Furthermore, they can reduce flammability significantly and maintain the transparency of the polymer matrix.

Polymer nanocomposites have become ubiquitous in modern life because they are lightweight, durable, flexible, and simple to process. Moreover, their wide range of thermomechanical properties, low-cost feedstock, and chemical resistance make these materials useful for many applications, including solar cells, rechargeable battery materials, actuators and capacitors, sporting goods, aerospace components, and automobiles. However, synthesis of nanocomposite polymers with the desired properties for a specific application requires a lot of research to tune their physical properties for a specific application. This chapter discusses the synthesis, characterization, and improved physical properties of polymer nanocomposite-based devices, particularly those using polyvinylidene fluoride (PVdF) and polyethylene oxide (PEO) materials.

14.5.6 Investigation of polymer nanocomposites

The study of PEO-based polymer electrolytes was initiated by Fenton and his coworker [22]. However, PEOs became technologically important due to their ionic conductive properties after 1978 [23]. The chemical structure of PEO is depicted in Fig. 14.4. The polymer chain has two terminal groups, –H and –OH, with n representing the polymerization degree, which is the number of repeating units.

The repeating unit contains a hydrophobic ethylene unit and hydrophilic oxygen, which is also a hydrogen bond site. PEO is prepared by polymerization of ethylene oxide (EO) using a suitable catalyst. Low molecular weight PEOs (MW $<$ 20,000) are colorless liquids or waxy solids depending on their molecular weights. High molecular weight PEOs (MW $>$ 20,000) are highly crystalline thermoplastic solids. They have a high solvating power along with high chemical and thermal stability. Due to the flexibility of PEO from the lack of double bonds, it is possible to coordinate with a number of different metal ions at the electron lone pair of the ether oxygen. It has been found that PEO can form coordinates with alkali metal ions and attain conductivities in the region of 1×10^{-8} S/cm. PEOs are commercially available in a very wide range of molecular weights from 200 to 7106 g/mol. Often narrow polydispersity products are available. PEOs have good mechanical properties, even though they have a low glass transition temperature, $T_g = -52°C$.

They are completely soluble in cold and warm water. The pH of PEO solutions is in the range from 6.5–7.5 [24]. PEO complexed with alkali metal salts showed high ionic conductivity at ambient and elevated temperatures. Although PEO can solvate many types of salts, it crystallizes with age. Various other polymers like polyacrylonitrile (PAN), polyvinylidene fluoride (PVdF), polyvinyl chloride (PVC), and poly(methyl methacrylate) (PMMA) have been studied. Compared to solid electrolytes and liquid electrolytes, gel polymer electrolytes (GPEs)

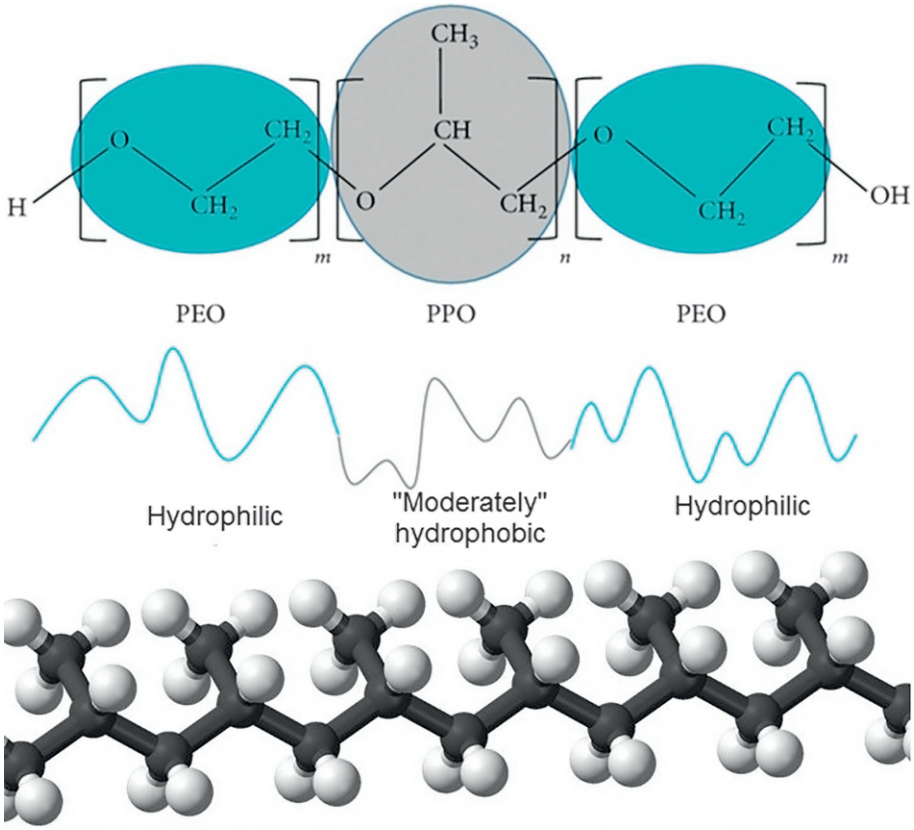

Fig. 14.4
Structural formula and atomic arrangement in PEO compound.

have several advantages, including no shape restrictions, faster charging/discharging, and higher power density.

Periasamy et al. [25] reported that in lithium metal batteries using PVdF-based electrolytes a passivation layer is formed between the lithium anode and the electrolyte. The resistance of this film continuously increases with increasing concentration of salt and polymer. This leads to a decrease in the capacity-rate behavior of the battery. It indicates that the concentration of PVdF should be low, which could result in mechanical instability of the electrolyte. Ramesh et al. showed that PVC copolymerized with PMMA could increase the conductivity of GPEs. The porous PDMS-CNT nanocomposites with PMMA could improve the flexibility and successfully control the degree of phase separation between PDMS and PMMA [26, 27]. The chemical structure of PVdF is shown in Fig. 14.5. PVdF is a semicrystalline thermoelastic polymer with abundance of its polymeric form. It has a chemical composition of $(\text{-}CH_2\text{-}CF_2)_n$ and is more formally known as 1, 1-difluoroethylene [28].

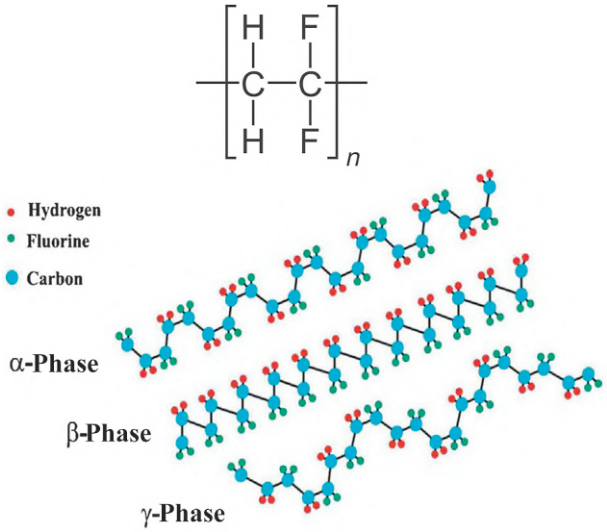

Fig. 14.5
Chemical structural formula and atomic representation of α,β,γ-phase deviation of PVdF compound.

14.6 Transport mechanism in nanocomposite polymer electrolyte

Defects play an essential role for ionic conduction in polymer electrolytes or gel polymer electrolytes. Variation of ionic conduction with temperature can be explained by two mechanisms, using either the Vogel-Tammann-Fulcher (VTF) equation or the Arrhenius equation [29].

14.6.1 VTF equation

One group of polymer electrolytes obeys a VTF-type relation, expressed by the following equation:

$$\sigma = \sigma_0 T^{-1/2} \exp\left[-E_a/(T - T_0)\right] \tag{14.1}$$

where E_a is the preexponential factor and T_0 the equilibrium glass transition temperature. In the VTF relation (shown in Fig. 14.6), conductivity against reciprocal of temperature plot is typically nonlinear in sense, indicating conducting mechanism that involving in a hopping motion coupled with relaxation/breathing or segmental motion.

14.6.2 Arrhenius equation

On the other hand, some polymer electrolytes obey the Arrhenius equation for the ion conduction mechanism, which is given by

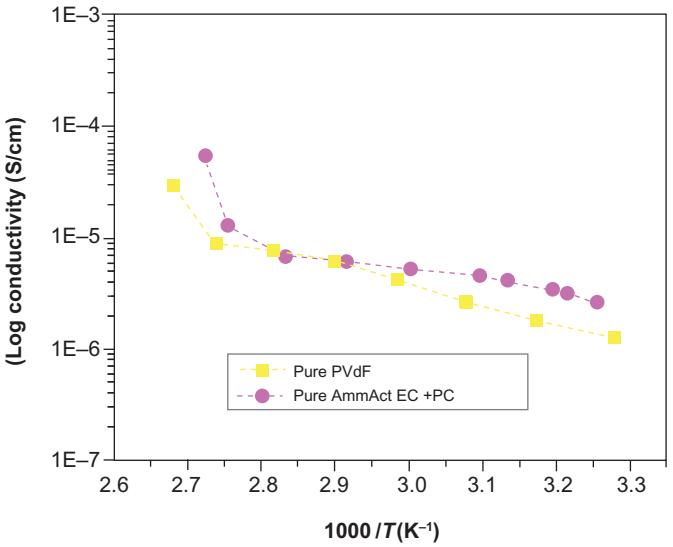

Fig. 14.6
Graphical representation of VTF equation.

$$\sigma = \sigma_0 \exp\left(-E_a/KT\right) \tag{14.2}$$

where E_a is the activation energy, which can be calculated from the linear least-square fit of the data from logσ versus the 1000/T curve. The material exhibiting a linear Arrhenius equation (shown in Fig. 14.7) indicates ion transport via a simple hopping mechanism decoupled from the polymer chain breathing.

14.7 Applications of nanocomposite polymer-gel electrolytes in environmentally friendly devices

Due to the unique properties of polymer electrolytes such as good process ability, flexibility, light weight, moldability, and transparency, polymer electrolytes have attained an important position in the development of ionic devices, a feature not exhibited by any other class of superionic solids. Superionic solids have immense potential applicability in developing solid-state electrochemical devices, such as solid-state batteries, sensors, fuel cells, memory devices, supercapacitors, electrochemical display devices (ECDs), smart windows, solar cells, and others [30].

14.7.1 Hydrogen–oxygen fuel cell

A fuel cell is an electrochemical device that converts electrical energy into chemical energy (as shown in Fig. 14.8). A hydrogen fuel cell uses hydrogen as its fuel and oxygen as its oxidant. Hydrogen and oxygen combine to produce electricity with water and heat as its

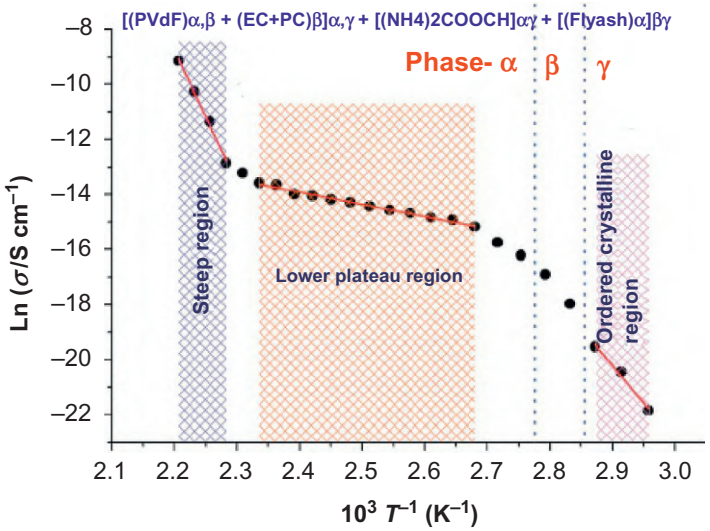

Fig. 14.7
Graphical representation of Arrhenius equation exhibited phase—α,β,γ.

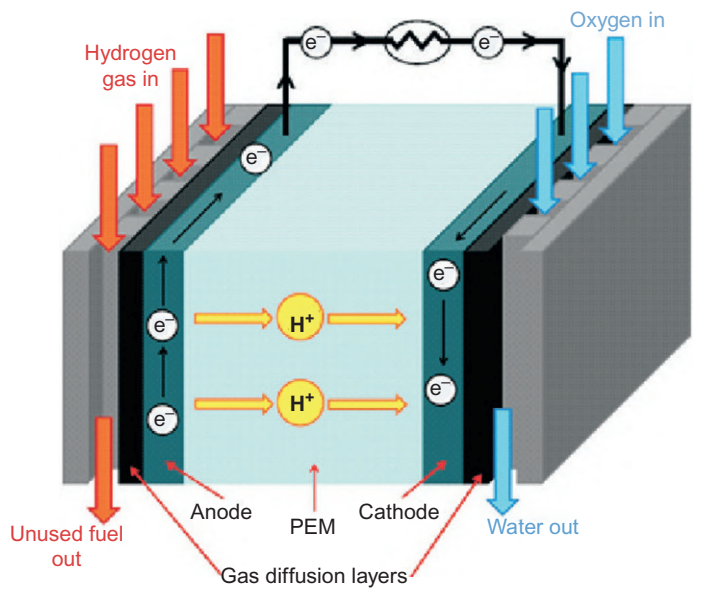

Fig. 14.8
Schematic diagram of typical polymer nanocomposite-based fuel cell.

byproduct. The hydrogen ions move through the electrolyte membrane to the cathode electrode, where they combine with oxygen and the electrons to produce water [31].

In addition to low or zero emission, the benefits include high efficiency and reliability, multifuel capability, sitting flexibility, durability, scalability, and ease of maintenance.

14.7.2 Solid-state rechargeable battery

Batteries, continuous sources of power and integral components of electronic circuitry as well as a wide variety of digital/analog appliances, basically work on the principle of chemical to electrical energy conversion. The battery industry is presently the only industry producing products with exceptionally wide energy range, i.e., 0.1 W to 100 MW [32].

Polymer electrolyte batteries offer improved performance by having higher average output voltage and lighter weights, thus a higher energy density and longer cycling life. They can be recharged for various cycles.

14.7.3 Sensors

Many modern equipment plant processes use a wide variety of sensors. The sensor device essentially measures the level of a chemical or physical quantity for efficient control of the process and environmental monitoring. These sensors are attractive because chemical quantities are directly transduced into electrical signals. Some important solid polymer electrolyte and gel electrolyte based sensors are hydrogen sensors, humidity sensors, carbon monoxide sensors, and biosensors [33].

14.7.4 Supercapacitors

Supercapacitors have drawn the attention of scientists and technologists in recent years with the developments made in the field of ion/electron conducting polymers [34]. They provide higher power density in comparison to batteries, on the one hand, and higher energy densities than found in the case of conventional dielectric capacitors, on account of higher capacitances (see Fig. 14.9).

14.7.5 Photoelectrochemical cells

Photoelectrochemical cells are solar cells that generate electrical energy from light, including visual light. Some photoelectrochemical cells simply produce electrical energy, while others produce hydrogen in a process similar to the electrolysis of water. Polymer electrolytes have been successful in eliminating the usual problem of photocorrosion and side reactions in photoelectrochemical cells and hence replace the conventional liquid electrolytes used in this device [36].

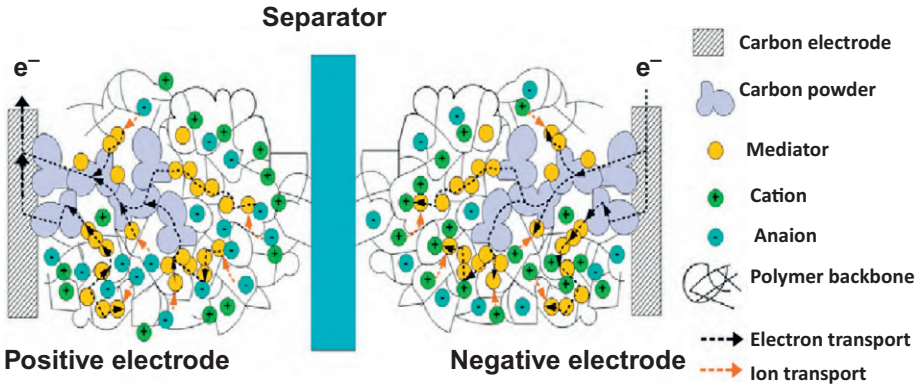

Fig. 14.9
Illustration of formation of nanocomposite-based molecular capacitor and charging process in proposed supercapacitors [35].

14.7.6 Solar cells

Polymer nanocomposites also have applications in the field of organic solar cells. Single-layer organic photovoltaic cells are the simplest of the various forms of organic photovoltaic cells. These cells are made by sandwiching a layer of organic electronic materials between two metallic conductors, typically a layer of indium tin oxide (ITO) with its high work function and a layer of a low work function metal, such as Al, Mg or Ca [37]. Another type of inorganic material and polymer-based solar cell known as hybrid-polymer based solar cells, which use a combination of a conjugated organic polymer and an inorganic semiconductor, are potentially interesting alternatives to silicon-based devices. Fig. 14.10 depicts an example of a simple polymer and hybrid polymer nanocomposite-based solar cell.

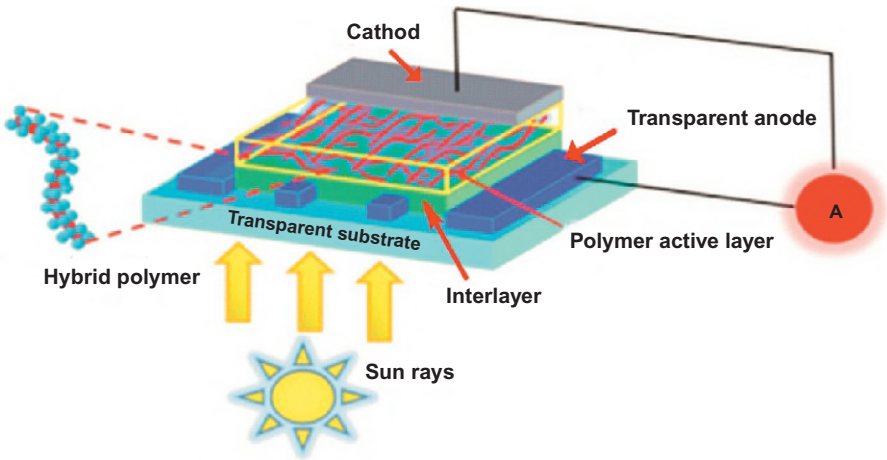

Fig. 14.10
Simple device structure of an inorganic hybrid polymer solar cell.

14.7.6.1 Objectives

Keeping all these observation and facts in mind, an experimental investigation was carried out with the following objectives:

To develop free-standing films of proton-conducting mechanically stable nanocomposite polymer electrolyte (NCPE) employing a polyvinylidene difluoride (PVdF) host matrix.

(a) Host polymer is soaked in liquid electrolyte of proton/NH_4^+ conducting salt to form proton-conducting pristine electrolytes.
(b) Addition of filler particle of nanometric dimensions to synthesize the second phase.
(c) Through solution cast technique, the NCPEs are synthesized.

To characterize the nanocomposite polymer electrolytes structurally, electrochemically, and electrically to understand the structure, morphology, and nature of ion behavior of these materials.

14.8 Structural and ion transport studies in (100-x) PVdF + xNH_4SCN gel electrolyte

Gel polymer electrolytes have high technical interest for fabrication of electrochemical devices. These materials have properties of both solids and liquids, and they have been introduced as a novel electrolyte material in the field of electrochemical device applications [20, 38]. In GPEs, the polymer matrix is swelled in solvents containing ions and so can be thought of as a nonaqueous liquid electrolyte immobilized by a polymer matrix. The solvent helps in the dissolution of salt and provides the medium for ion conduction. In recent years, polymers such as polyvinyl alcohol (PVA), poly(vinylidene fluoride) (PVdF), polyethylene glycol (PEG), poly(vinyl chloride) (PVC), poly(acrylonitrile) (PAN), poly(vinyl pyrrolidone) (PVP), and poly(vinyl sulfone) (PVS) have been prominently used in the development of GPEs [39–42]. These electrolytes have been found to possess ionic conductivity, electrochemical stability, and transport properties similar to their liquid counterparts, along with better dynamical properties suitable for electrochemical applications. Among the listed polymeric hosts, poly(vinylidene fluoride) has been intensely investigated because of its interesting ferroelectric properties and technological applications. PVdF is a commercially available fluoropolymer with low surface energy and good physical, chemical, and mechanical properties. Therefore, it is reasonable to expect that the PVdF membrane with a porous surface structure should have enhanced hydrophobicity. It can exist in at least five different crystalline phases, known as Form I (β) Form II (α), Form III (γ) polar II (α_p) and polar form III (γ_p) [43–45]. Form I (β) is distinguished from the others by very important properties for application: piezoelectricity and pyroelectricity. These are closely related to ferroelectricity. PVdF can exist in several crystal modifications. Crystallization of PVdF from the melt at conventional cooling rate leads to the formation of three crystal modifications, either non-polar α or polar β and γ forms, depending

on the temperature. At crystallization temperatures below 425 K, only α crystals are formed, while at higher temperature a mixture of β and γ phases are detected. The γ crystal converted into the α form when the crystallization temperature was higher than 435 K [46]. The crystalline α,β,γ, α_p, and γ_p phases of PVdF carry a permanent polarization, which is beneficial for a number of technical applications. The permanent polarization changes after mechanical distortions like tension, compression, or action of hydrostatic pressure, and their strengths are roughly proportional to the permanent polarization. Further, PVdF is a semicrystalline polymer and the electrolytes based on PVdF are expected to have high anodic stabilities due to strong electron withdrawing functional groups. The PVdF-based gel electrolytes, with high permittivity and relatively low dissipation factor, assist with the higher ionization of salts, providing higher concentration of charge carriers [47] and thus rendering high electrical conductivity. PVdF is also a very attractive polymer for its piezoelectric and pyroelectric characteristics, which have been exploited in the development of electrochemical devices [48–51]. In view of the preceding discussion, a detailed experimental study (structural, thermal, and electrical) on poly(vinylidene fluoride) (PVdF) based gel polymer electrolytes with ammonium thiocyanate salt has been carried out in this investigation.

14.8.1 Membrane fabrication

Poly(vinylidene fluoride) (PVdF; Aldrich sigma) with an average molecular weight of ($\sim 5.34 \times 10^5$) and ammonium thiocyanate (NH_4SCN; Ranken India) were used for the preparation of the polymer electrolyte. NH_4SCN salt was used after drying at 70°C under vacuum for 24 h and PVdF without any further purification. Distilled tetrahydrofuran (THF) and dimethyl sulfoxide (DMSO) in a suitable ratio were used as solvent. The dissolved polymer and salt solutions were mixed and the resulting solution was stirred continuously to obtain a homogeneous mixture. The polymer solution was allowed to evaporate at 35°C until the achievement of a gel state. Extraordinary thin-film of solvent free layers thus obtained when poured the desired polymeric solution into accessioned cleaned glass Petri dish.

14.8.2 Results and discussions

14.8.2.1 Structural characterization

X-ray diffraction (XRD)

The X-ray diffraction patterns of the pure PVdF and composite gel electrolyte system, namely [90PVdF + 10NH_4SCN], are shown in Fig. 14.11.

In pure PVdF, three intense characteristic peaks located at 19.6° (110), 23.5° (200) and 26.6° (021) along with one small peak at 18° are observed. All the three major peaks correspond to the orthorhombic α-phase of PVdF. A few dull reflections appearing near these intense peaks show the possibility of formation of γ crystals in PVdF simultaneously. The formation of

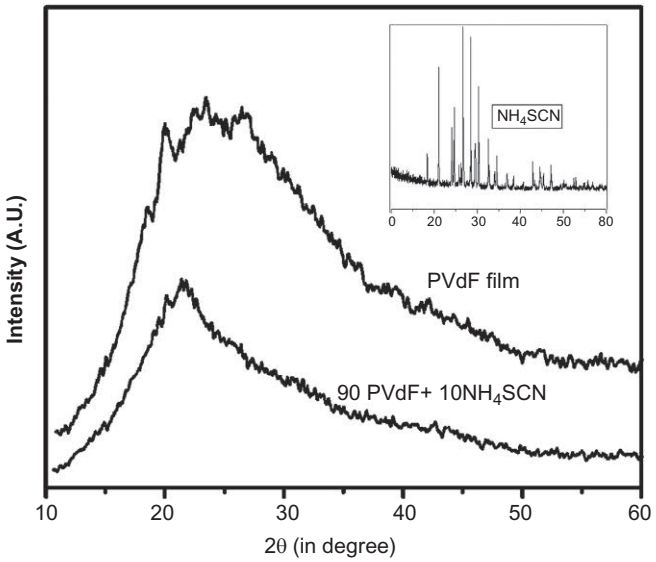

Fig. 14.11
X-ray diffraction patterns of different polymer electrolytes (inset: small-angle XRD reveals high crystalline smooth peaks distribution of NH_4SCN).

different phases in PVdF (α, β, and γ, etc.) mostly depends upon the film formation condition and synthesis techniques. The PVdF film prepared by the solution cast technique at room temperature in THF and DMSO show prominence of α and β crystallinity [51]. In the 90PVdF + 10NH_4SCN polymer electrolyte film, a diffraction peak at $2\theta = 18°$ and 19.6° in pure polymer merged in a single peak with downsizing of intensities, along with its shifting towards high 2θ values (20.1°). The peak area enhanced in the complexes system with respect to the pure PVdF. This change in XRD peaks shows a possible interaction of polymer with the doped salt NH_4SCN. Similarly, the characteristic peaks of pure PVdF (i.e., 23.5° and 26.6°) completely vanish after the complexation of NH_4SCN with the polymer matrix; a similar result has been reported by Park et al. [52] for a PVdF-based system. The XRD pattern of the electrolyte did not reveal any new peak corresponding to the NH_4SCN salt (the XRD pattern of NH_4SCN is shown in the inset of Fig. 3.1) [52a], thereby indicating an absence of uncomplexed salt in the composite polymer electrolyte film. Comparative studies of the XRD pattern of the pure PVdF and composite electrolyte show a decrease in the intensity of the main peak. This reduction and enhancement in peak area reveal the increase in amorphousness and thus are expected to cause a higher conducting region. These observations apparently suggest that the polymer undergoes significant structural reorganization upon the addition of salt. The sample with higher weight content of NH_4SCN gives a completely amorphous film. XRD studies give evidence regarding the change in crystallinity after the complexation of salt. The average crystallite size in the composite polymer electrolyte was calculated using the Scherrer equation, which can be written as:

$$\tau = \frac{K\lambda}{\beta Cos\theta}$$

where τ is the mean size of the ordered (crystalline) domains, which may be smaller or equal to the grain size. K is a dimensionless shape factor, with a value close to unity. The shape factor has a typical value of 0.94 (the value of the shape factor varies with the actual shape of the crystallite). λ is the X-ray wavelength (in this case λ is 1.542 Å for Cu K_α); β is the line broadening at half the maximum intensity (FWHM) in radians; and θ is the Bragg angle.

The average calculated crystallite size in the 90PVdF + 10NH_4SCN composite polymer electrolyte is 35–40 nm.

Scanning electron microscopy (SEM)

The SEM image of pure PVdF and different PVdF + NH_4SCN based gel electrolyte systems were recorded and are shown in Fig. 14.12 to assess the morphology.

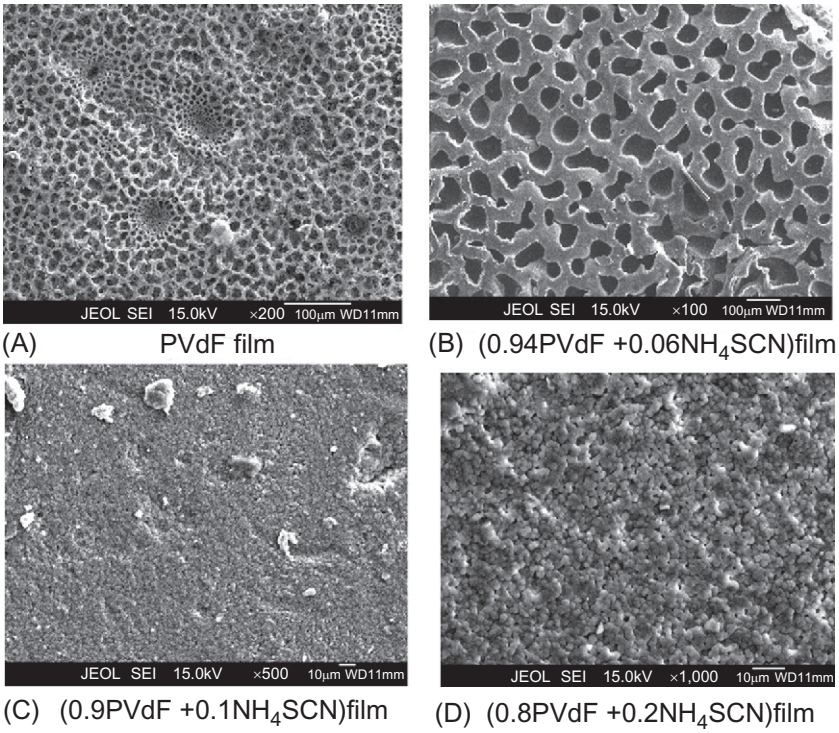
JEOL SEI 15.0kV ×200 100μm WD11mm
(A) PVdF film
JEOL SEI 15.0kV ×100 100μm WD11mm
(B) (0.94PVdF +0.06NH4SCN)film
JEOL SEI 15.0kV ×500 10μm WD11mm
(C) (0.9PVdF +0.1NH4SCN)film
JEOL SEI 15.0kV ×1,000 10μm WD11mm
(D) (0.8PVdF +0.2NH4SCN)film

Fig. 14.12
Typical SEM micrographs of (A) pure PVdF film, at specific concentration of composite electrolyte films architectural execution at (B) (0.94 PVdF + 0.06 NH_4SCN), (C) (0.9 PVdF + 0.1 NH_4SCN) film, and (D) (0.8 PVdF + 0.2 NH_4SCN) film.

In pure PVdF film [Fig. 14.12A], several pores with a lamellar distribution of polycrystalline domain and traces of two polymorphic phases (α and β) are observed [53]. The crystalline structure formed due to longer evaporation time. Furthermore, the original structural entity lose this character due to addition of salt adapt in host solution, and it also drastically changes the PVdF microstructure [Fig. 14.12B]. It clearly shows bimodal morphology with the modified crystalline domain. The addition of salt (NH_4SCN) connects these pores to each other due to induced delay in phase relation or lower surface energy. In the polymer composite film [Fig. 14.12C] containing 10% of the salt, gives a slightly smooth and better structure with some aggregation. At very high salt content, the pores disappear giving rise to the smooth morphology of films. The disappearance of porosity and enhancement of grains are advantageous for interfacial contact between the polymer and salt. This connectivity of the pores is favorable for the protons transport and thus enhancement of ionic conductivity [54]. [Fig. 14.12D] presents the film containing higher NH_4SCN ratio (i.e., 20 wt%) in PVdF, becoming homogeneous followed by cluster formation, which produces a hindrance for the ionic movement. The same ratio films also show the sticky behavior. Scanning electron images show that the addition of salt disturbs the crystalline nature of the pure matrix.

14.8.2.2 Infrared spectroscopy (IR) characterization

The IR spectra of pristine PVdF and (90PVdF + 10NH_4SCN) electrolyte films are shown in Fig. 14.13. Pertinent peaks were analyzed and have been summarized in Table 15.1.

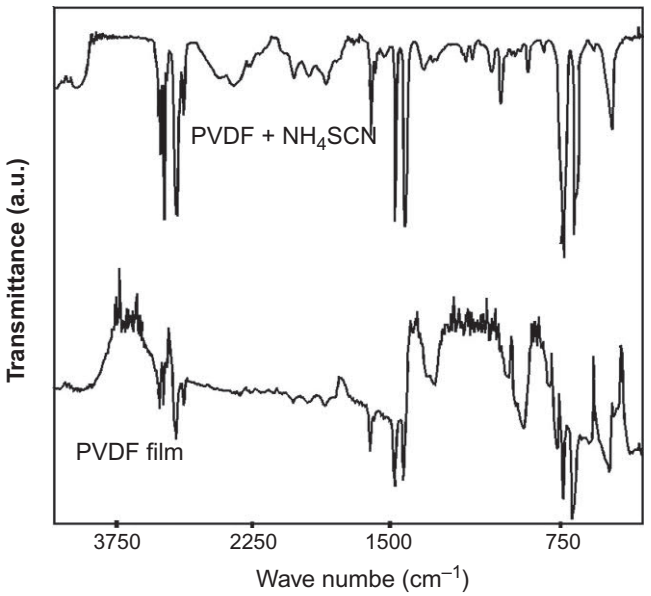

Fig. 14.13
FTIR spectra of PVdF and composite electrolyte films.

Table 15.1. Peak positions and their assignment for PVdF and 90PVdF + 10NH_4 SCN electrolytes.

Peak positions (cm^{-1})		
Pure PVDF	**Pure PVdF + NH_4SCN**	**Assignments**
510	–	β-phase of PVdF
532	532	α-phase
612	–	α-phase of PVdF (mixed mode of CF_2)
706	706	ν_{as} (S = O) of DMSO
763	764	α-phase (rocking vibration)
860	848	β-phase (out of phase combination)
	988	α-phase
1024	1024	ν_{as} (C = S) of DMSO
1210	–	α-phase of PVdF
1234	–	α-phase of PVdF
1286	1268	β-phase
1310	1310	DMSO in liquid state
1383	1336	α-phase
1431	1428	β-phase, in plane bending or scissoring
1839	–	Pure PVDF
2000–2200	2000–2200 (intense and sharp)	Characteristic peaks of NH_4SCN
2910	2910	CH_2 Asymmetric stretching
3020	3020	CH_2 Symmetric stretching
3250	3280	N–H stretching
3600	3600	–OH bending

Pristine PVdF is characterized by the presence of vibrational bands at 612 and 763 cm^{-1} that are related to CF_2 with skeleton bending, respectively. The presence of peaks at 532, 1210, 1383, 1432 cm^{-1} shows dominance of the crystalline α phase in PVdF film. This spectrum also exhibits a moderately intense band at 840 and 510 cm^{-1}, indicating the existence of the β form of polymer film [55]. Similarly, the presence of the γ phase (in trace) is indicated by the appearance of the 1234 cm^{-1} absorption peak. In PVdF film, a peak at 840 cm^{-1} is always visible and its intensity is not much affected by the sample preparation condition, and thus it can be used as an internal reference for evaluation of the fraction of α and β phase in the film. Another important feature in PVdF film is the presence of a CH_2 group 3020 cm^{-1} (υ_a CH_2) and symmetric vibration at 2970 cm^{-1} (υ_s CH_2). Symmetric vibrations are weaker than asymmetric vibrations, since the former lead to less change in dipole moment. In the 90PVdF + 10NH_4SCN gel electrolyte system, a few peaks related to α and β phases are slightly shifted to the lower wave number side along with a change in intensity. The intense and broad absorption peak related to the –CH_2 rocking vibration at 874 cm^{-1} in pure PVdF weakens significantly after complexation with NH_4SCN, possibly due to replacement of fluorine atoms with SCN^-. A few peaks (706, 1024 and 1310 cm^{-1}) related to DMSO are also visible in the pure as well as gel

polymer film. But the intensity in complexed film decreases with respect to the pure and the peak area broadens. All three peaks of DMSO are present in both systems, but the intensity of peaks becomes prominent and at 1310 cm^{-1} the peak area also increases and new peaks are formed. The absorption peak at 677 cm^{-1} shows the presence of head to head and tail to tail configurations, but the intensity of this peak enhances after the addition of salt, indicating a strong salt-polymer interaction. The addition of NH_4SCN gives a few new peaks at 2000–2200 cm^{-1}, which indicates formation of a PVdF-NH_4SCN crystalline complex [56, 57]. The new peaks formed in the range of 2000 cm^{-1} to 2200 $cm^{-1}$are 2100 cm^{-1}, 2150 cm^{-1} and 2200 cm^{-1}; after complexation these peaks are very strong and broad due to symmetric SCN stretching vibration. These peaks are mostly weak doublets, and indication of polymer salt interaction. The new peaks at 2100 cm^{-1} are ascribable to the contact ion pair and solvent separated dimer. The characteristic peaks of NH_4SCN (i.e., 2050 cm^{-1}, 1406 cm^{-1}, and 780 cm^{-1}) have been visualized in spectra of the composite electrolyte. The intensity of these characteristic peaks with respect to the pure NH_4SCN reduced after the interaction of PVdF polymer. In the higher wave number, the intensities of peaks 2910 cm^{-1}, 3020 cm^{-1} and 3250 cm^{-1} become more prominent in the composite electrolyte.

14.8.2.3 Electrochemical characterization

Cyclic voltammetric study

The cyclic voltammetric curves for different ratios of polymer composite electrolyte systems, i.e., (100 − x) PVdF + xNH_4SCN, are shown in Fig. 14.14.

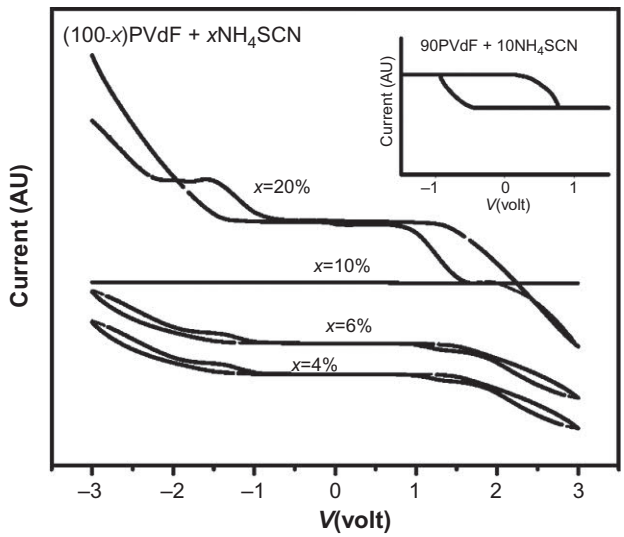

Fig. 14.14
Variation of current with voltage of PVdF and composite electrolyte films.

Cyclic voltammetry (CV) is arguably the most widely used technique for the characterization of redox systems. It can provide qualitative information about the number of oxidation states and their stability, as well as the rate of heterogeneous electron transfer reactions. It can also be used in studies to calculate rates of homogeneous and heterogeneous reactions. Such studies typically involve varying the scan rate [58] as well as other conditions and examining low characteristic features such as the peak current and peak potential. To study the chemical stability, we have used the following cell configuration:

$$\text{Pt//CPE//Pt}$$

where Pt is the standard platinum electrode. In cyclic voltammetric measurements, we use the sweep voltammetric technique in the potential range ± 3 V on the different synthesized electrolytes. The current vs. voltage measurements of $[(100 - x)\ \text{PVdF} + x\text{NH}_4\text{SCN}]$/Pt (where $x = 4, 6, 10, 20$) cell at a scan rate of 0.1 mV/s were identified. Among these, the entire system of the gel polymer electrolyte containing 10 wt% NH_4SCN shows highly stable behavior. To ascertain this fact, the plot was expanded (inset of Fig. 14.14). In this curve a loop is visible, which is related to the oxidation reduction process of the electrolyte. The onset current in the anodic high voltage range is assumed to result from a decomposition process associated with the electrode as upper limit of the electrolyte stability range. This voltage is generally located as the point of interaction of the extrapolated linear current in the high-voltage region with the voltage axis. For the electrolyte system, the current response is better at ±1.5 V. This implies that there is no decomposition of any components in this potential region.

14.8.2.4 Electrical characterization

Ionic conducting studies

The changes in bulk electrical conductivity of the pristine polymer electrolyte film as a function of variation of salt (NH_4SCN) in the $[(100 - x)\ \text{PVdF} + x\text{NH}_4\text{SCN}]$ system are given in Fig. 14.14 (with respect to frequency and composition) and Fig. 14.15 (variation of bulk electrical conductivity evaluated by Cole–Cole plot).

The addition of NH_4SCN increases the conductivity of the PVdF film by more than two orders of magnitude, attains a maximum, and then starts decreasing. The increase in conductivity can be attributed to the increase in numbers of transporting ions or ion–ion interactions and some amount of liquid trapped within the polymer matrix. Initially, as the salt concentrations increase, there is an increase in free ions, due to which the electrical conductivity increases. Another possible reason for the increase in conductivity is the presence of trapped liquid within the pores of the polymer matrix. In Fig. 14.14 the conductivity initially increases with the rapid increment of salt concentration, as well as frequency. In Fig. 14.15 the increase in the electrical conductivity reaches a maximum value (10 wt% of salt) and thereafter it starts to decrease. Beyond a limit (12 wt% salt concentration) the film becomes fully sticky and is extremely difficult to handle for further measurements. The increase in bulk electrical conductivity of

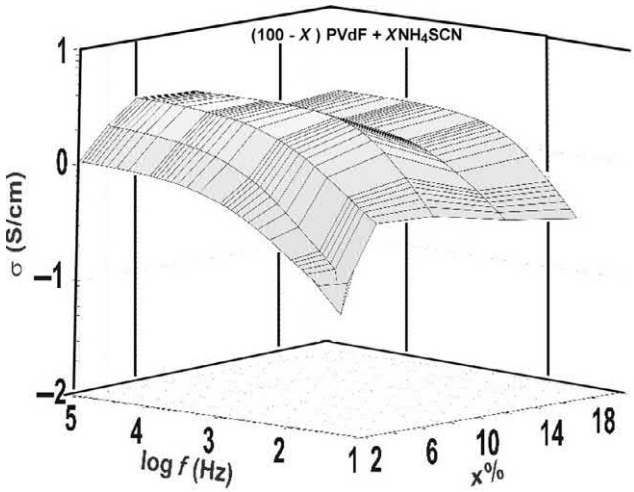

Fig. 14.15
Variation of conductivity with respect to frequency and composition.

pristine electrolyte with salt concentration can be attributed to the increase in the number of charge carriers and enhancement in the amorphous behavior of the system. The decrease in conductivity at higher salt concentrations can be explained with the help of the ion association effect in the PVdF chain [59]. As evidenced in XRD and IR studies, the interaction between salt with fluorine group in the PVdF matrix is likely to enhance the conductivity of the gel electrolyte. In addition, the mechanical stability of the composite materials has also been found to improve with increasing concentration (10 wt%) of salt. Because the morphology of the film is directly linked to mobility of charge carriers to migrate upon the application of an electric field, ionic conductivity of the polymer electrolyte is bound to be influenced by the morphology of the system. As the concentration of salt increases significantly, the mutual distance between ions decreases until ion–ion interaction becomes significant. Therefore, the higher the concentration, the stronger is the ion–ion interaction which results in the change of free ions to ion pairs or the formation of higher aggregates. Consequently, the ionic conductivity decreases as a result of the decrease of mobility or/as well as the number of charge carriers.

The changes in electrical conductivity with temperature of pristine polymer electrolyte film as a function of variation of salt (NH_4SCN) in the [$(100 - x)$ PVdF + $x NH_4SCN$] system are given in Fig. 14.16 (change in conductivity with respect to frequency and temperature) and Fig. 14.17 (variation of electrical conductivity evaluated by Cole–Cole plot) (Fig. 14.18). After the addition of salt (NH_4SCN) Fig. 14.15 represents the variation in temperature-dependent conductivity with frequency, which shows that as the frequency increases the conductivity also increases along with temperature. Fig. 14.17 also shows the nonlinear increase in conductivity with temperature up to 340 K. Above 340 K, the gel electrolyte shows a sudden change of slope in conductivity response. This increase has been explained on the basis of a semicrystalline to amorphous phase transition. The almost linear variation in conductivity

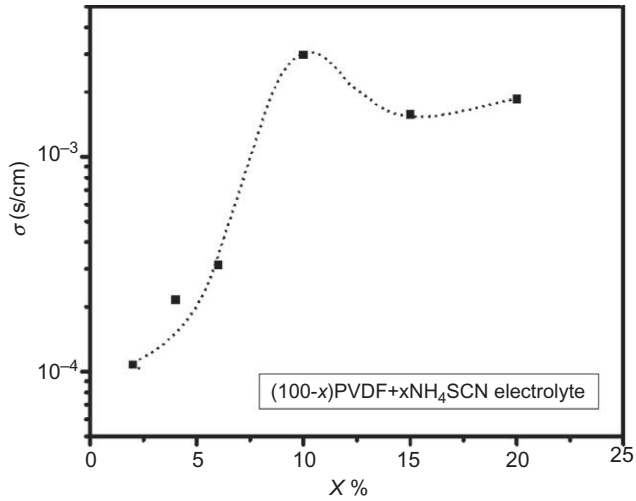

Fig. 14.16
Variation of bulk electrical conductivity evaluated through Cole-Cole.

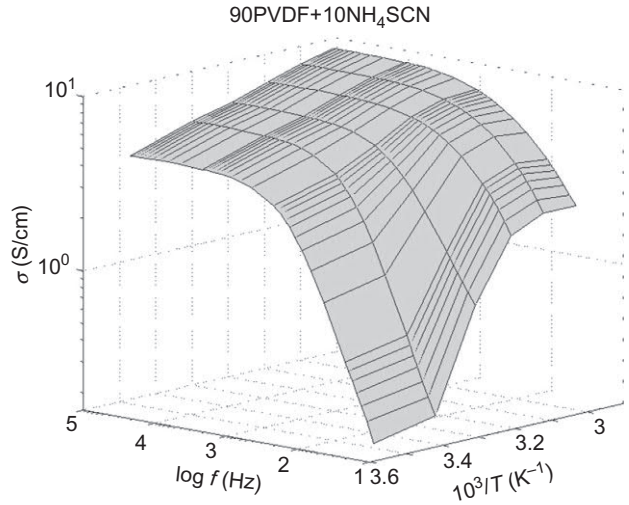

Fig. 14.17
Variation of electrical conductivity with respect to frequency and temperature.

and positive curvature in the curve indicates that ionic conduction obeys the Vogel–Tammann–Fulcher (VTF) relationship, which describes the transport properties in viscous matrix and is mathematically represented as:

$$\sigma = \sigma_0 T^{-1/2} \exp\left[-E_a/(T - T_0)\right] \tag{14.3}$$

where E_a is a constant related to activation energy and T_0 is reference temperature associated with ideal T_g. The motion is strongly decoupled from the segmental motion of

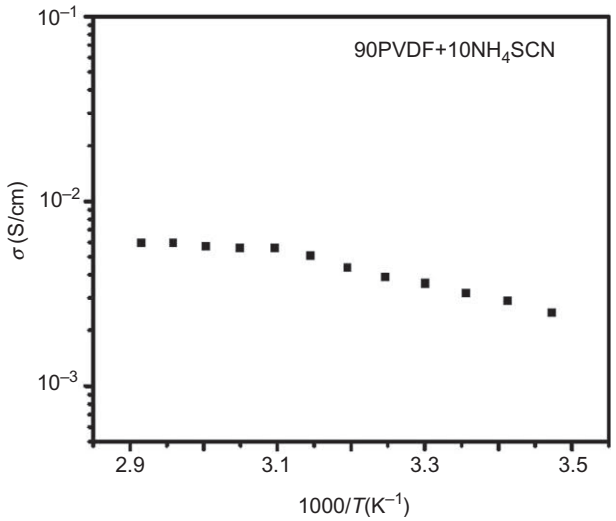

Fig. 14.18
Variation of electrical conductivity evaluated by Cole–Cole plot.

the polymer backbone, thus finally demonstrating that the ionic transport in the gel membranes occurs mainly within the liquid solvent. The curvature at 70°C is possibly due to transition of polymorphic phase ($-\alpha_c$ phase) in poly(vinylidene fluoride). Such features are generally observed in a highly amorphous polymeric system. The α_c relaxation may have an important implication in determining the viscoelastic properties of polymeric systems. The conductivity behavior below 70°C may be due to the beginning of a crystallization process occurring due to orientation-induced stretching in the electrolyte film [60]. The increase in conductivity with temperature is interpreted as a hopping mechanism between coordinated sites, local structural relaxation, and segmental motion of the polymer. As the amorphous region progressively increases, however, the polymer chain acquires faster internal motion and bond rotations (segmental motions). This in turn favors the hopping of interchain and intrachain movement and the ionic conductivity of the polymer electrolyte becomes high.

It is very beneficial to note that an AC conductivity measurement is important to characterize the nature of the conduction process. Frequency-dependent conductivity of $(100 - x)$ (PVdF+ xNH_4 SCN) is shown in Fig. 14.19. The AC conductivity has been calculated from the dielectric constant and tan δ. The AC conductivity of the gel electrolyte has been evaluated using the relation

$$\sigma_{ac=} \varepsilon' \varepsilon_o \omega \tan\delta \tag{14.4}$$

where ε_o is the vacuum permittivity and ω is the angular frequency.

It can be assumed that the AC conductivity (σ_{ac}) of the samples depends on the frequency (ω) according to the well-known universal power law, [61]

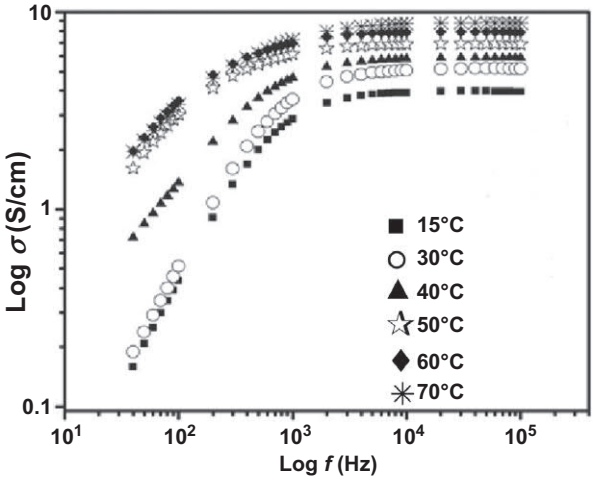

Fig. 14.19
Variation of frequency-dependent conductivity.

$$\sigma_{ac} = \sigma_o A\,\omega^n \tag{14.5}$$

where σ_{ac} is the DC conductivity (the extrapolation of the plateau region to zero frequency gives the value of DC ionic conductivity), A is the preexponential factor and n is a fractional exponent lying between 0 and 1.

The ω^n power law is very frequently observed in a wide range of materials, among which are polymers. The conductivity of the NCPE film increases slowly with increasing frequency at different temperatures. This suggests temperature-independent relaxation dynamics of the system, and thus it can be assumed that the AC conductivity (σ_{ac}) of the samples depends on the frequency. The frequency-dependent conductivity at various temperatures has a resemblance to the typical nature of conductivity in the polymer electrolyte. In all, the temperature conductivity follows the universal power law. Conductivity initially increases with frequency up to 1 kHz and thereafter tends to attain a plateau in all compositions. The initial increase in conductivity with frequency is due to the relaxation effect of the polymer. The frequency-independent behavior of conductivity in the high-frequency region has been reported in other polymeric electrolytes and has been well explained by Ramesh and Arof [62]. It has been observed that the maximum value of conductivity is 1×10^{-2} S/cm for samples synthesized with 10 wt% NH_4SCN concentration.

Dielectric studies

Thin polymers are known to be a mixture of amorphous and crystalline regions. The amorphous regions are the areas in which chains are irregular and entangled, whereas in crystalline regions the chains are regularly folded or orderly arranged. In the crystalline areas, because of the presence of

hindering structural units (due to greater density of the region), the polymeric chains move with much greater difficulty than in the amorphous region. The hindrance can be assumed to possess a certain potential energy. When the polymer is heated, the movement of the main chain sets in and maximizes at T_g, with losses corresponding to α-relaxation. This relaxation, corresponding to T_g, may also be understood by the free volume theory, according to which the molecular mobility depends mainly on free volume. The dielectric dispersion appearing at higher temperature is generally connected to the ordinary motion of the molecules from one quasi-stable position to another around the skeletal bond, involving large-scale conformational rearrangement of the main chain, and is known as the primary dispersion region or the α-relaxation. The low-temperature dielectric dispersion is attributed to the dielectric response of the side group, which is considered to be more mobile, or the small displacement of the dipoles near the frozen-in position, known as the secondary dispersion region. In the case of polar polymers, the dielectric constant begins to drop at a certain frequency. This decrease with frequency is attributed to electrical relaxation or inability of the dipole to rotate rapidly to follow the applied field. In the low-frequency region, ion aggregation at the interface leads to a net polarization, which allows formation of a space charge region at the electrode-electrolyte interface.

Variation of dielectric constant (ε') of the (90PVdF + 10NH_4SCN) electrolyte system as a function of frequency for different temperatures is shown in Fig. 14.20. Strong frequency dispersion in dielectric constant and dielectric loss was recorded in the lower-frequency region followed by frequency-independent behavior at higher frequencies (above 10 kHz) in the case of the polymer electrolyte as well. The dielectric constant and loss value initially increase with temperature up to 70°C and then start decreasing. The decrease in dielectric constant beyond 70°C could be due to onset of some crystallization processes, as observed by Gregorio and Cestari [63]. The change in the

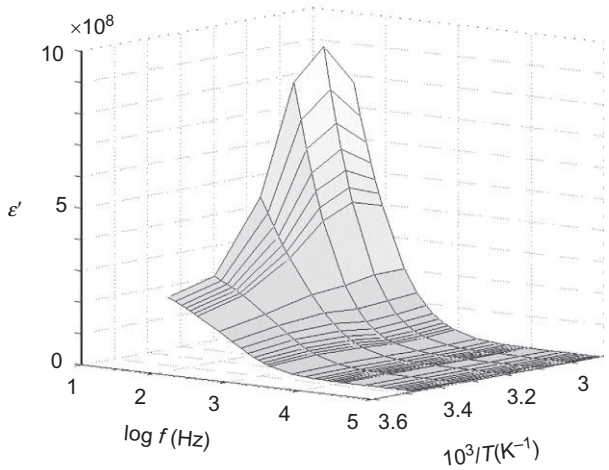

Fig. 14.20
Variation of dielectric constant with frequency at various temperatures.

imaginary part of dielectric permittivity (ε'') (or dielectric loss) with frequency at different temperature of (90PVdF + 10NH_4SCN) is shown in Fig. 14.21. The dielectric study gives a single maximum for dielectric loss. The entire response reflects a non-Debye relaxation in the nanocomposite polymer electrolyte. The variation of tangent loss (tanδ) with frequency at different temperatures of (90PVdF + 10NH_4SCN) is shown in Fig. 14.22. The higher value of tangent loss can be attributed to segmental diffusion motion in the amorphous region. At 70°C a relaxation

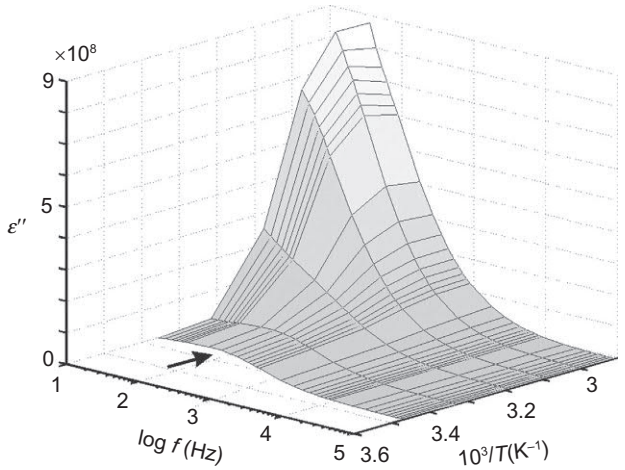

Fig. 14.21
Variation of dielectric loss with frequency at various temperatures.

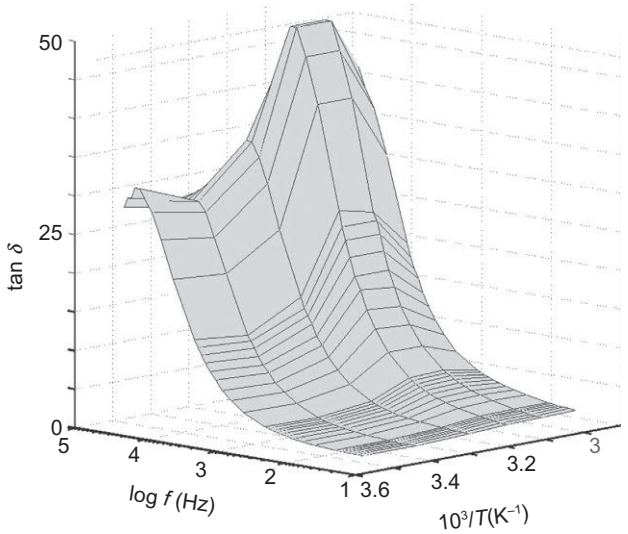

Fig. 14.22
Variation of tan δ with frequency at various temperatures.

process is observed in the temperature-dependent tan δ curve. This is similar to dielectric loss and labeled as α or α_c and can be associated with motion within the crystalline region [64]. It should be noticed that this relaxation is not clearly observed as a peak in the figure.

14.8.3 Application of polymer nanocomposites in environmentally friendly devices

In modern society, humankind is critically dependent on energy and requires environmentally sustainable methods for the conservation, storage, conversion, and production of energy. New conversion technologies and new sources are a continuous quest for many researchers. The Earth holds all forms of energy rather ecological conditions always precepts the lives. While, it will claim 90 billion of oil and 7 billion ton of coal due to the provision of exceeding energies. The developing world consumes more energy, so 50% of the energy will be required in the developing world [65]. The consumption of energy is coupled with GDP growth requirements. The energy shortage expansion will be 7%–8% and peak load shortage shall be 13%, these additional energy requirement will be reasonable occurrence. There are two key problems with continued use of fossil fuels, which meet about 80% of the world energy demand today. The first problem is that they are limited in amount and sooner or later will be depleted. The second problem is that fossil fuels are causing serious environmental problems, such as global warming, climate changes, melting of ice caps, rising sea levels, acid rain, pollution, ozone layer depletion, oil spills, forest and agricultural land damage caused by surface mining of coal, and so on. Early in the 1970s, a hydrogen energy system was proposed as a solution for these two interconnected global problems [66]. Hydrogen is an excellent energy carrier with many unique properties. It is the lightest, most efficient, and cleanest fuel. One of its unique properties is that, through electrochemical processes, it can be converted to electricity in a fuel cell with higher efficiencies than conversion of fossil fuels to mechanical energy in internal combustion engines or to electrical energies in thermal power plants [67]. The hydrogen fuel cells utilized for automotive power plant project due to unique properties of hydrogen has been made. The reason for the higher efficiency of hydrogen fuel cells is that they are electrochemical engines, not heat engines, and as such they are not subject to Carnot cycle limitations [68].

14.8.4 Basics of fuel cells

A device that converts chemical energy into electrical energy using a chemical reaction is known as a fuel cell. [69] (Fig. 14.23).

In the chemical reactions of a fuel cell, positively charged hydrogen ions interact with oxygen or an oxidizing agent. However, fuel cells require a continuous source of fuel and oxygen to maintain the chemical reaction, unlike a battery, where chemicals present in the battery react with each other to generate electricity. In the simplest way, a fuel cell is an electrochemical device that directly converts chemical energy into electrical energy by utilizing various fuels, such as hydrogen, methanol, ethanol, methylene blue, glucose, natural gas, etc.,

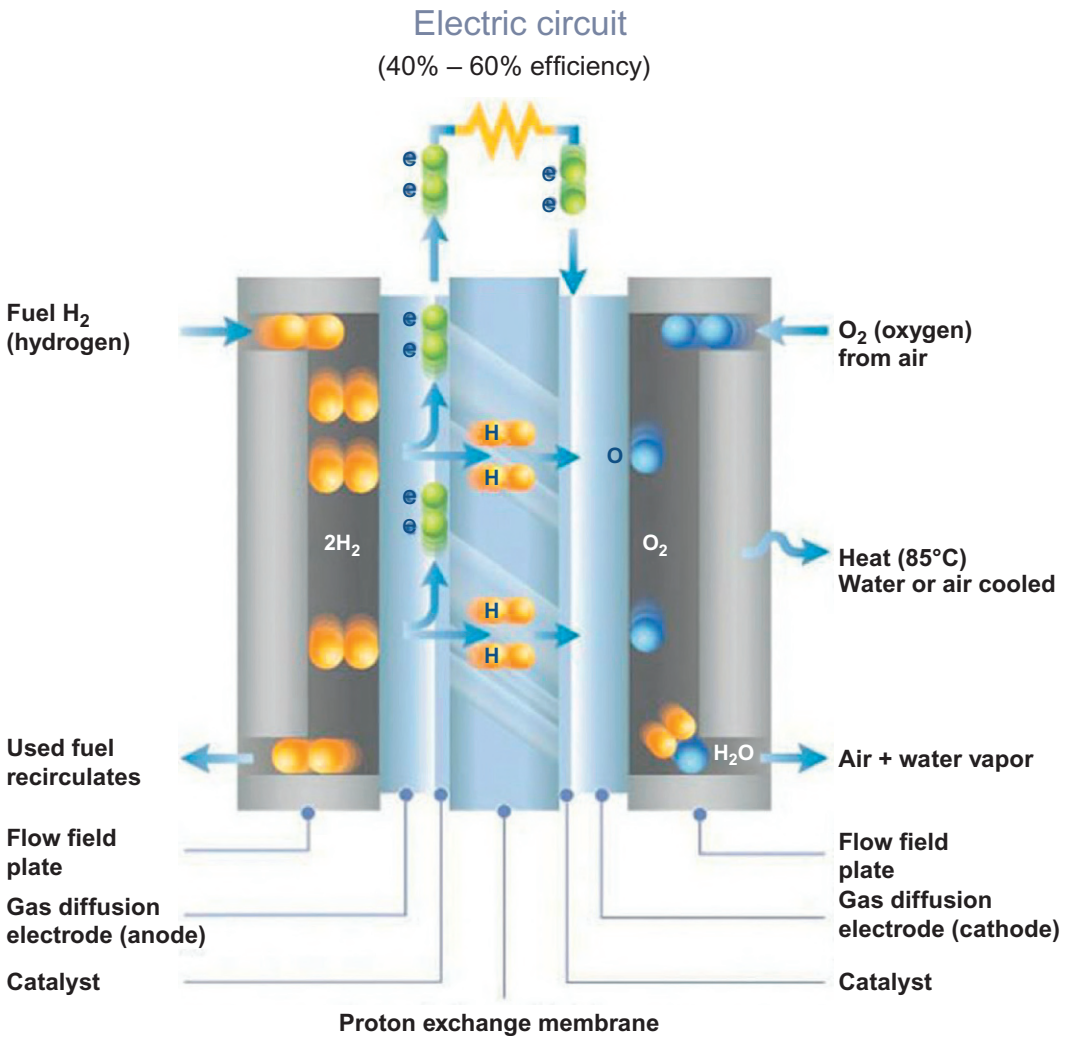

Fig. 14.23
Schematic diagram of basic fuel cell.

in a reaction with an oxidant (oxygen) Research on fuel cells has been carried out for many decades, with the first fuel cell invented in 1838, and they are still a topic of current scientific interest [70, 71]. The fuel cell has many technological applications, such as power generation for industries, vehicle propulsion, generating water and heat, etc. A fuel cell consists of an anode, a cathode, and an electrolyte that allows positively charged hydrogen ions (or protons) to move between the two sides of the fuel cell. The anode and cathode contain a catalyst that is responsible for the fuel undergoing an oxidation reaction, i.e., generation of hydrogen ions and electrons. The hydrogen ions are collected through the electrolyte, while the electrons are drawn from the anode to the cathode through an external circuit, producing electricity. At the cathode, hydrogen ions, electrons, and oxygen react to form water (shown in Fig. 14.24).

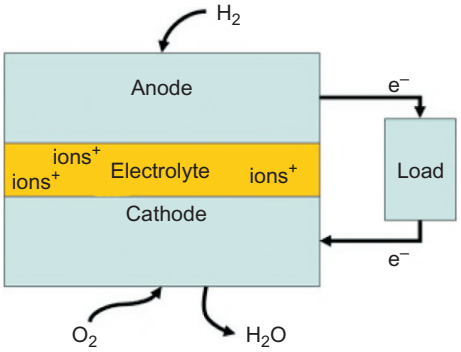

Fig. 14.24
Block diagram of fuel cell.

Depending upon the types of electrolytes used in fuel cells, they are classified into different categories. On the basis of temperature of operation, fuel cells can be broadly divided into three categories:

(1) Low temperature fuel cell (RT-100 °C)
(2) Intermediate temperature fuel cell (100–400°C)
(3) High temperature fuel cell (400–1500°C).

Various types of fuel cells are available currently, depending upon the types of electrolyte used for fabrication [72]. Several types of fuel cells are listed here.

- *Proton exchange membrane fuel cell*
  In this type of fuel cell, a proton-conducting polymer membrane (typically Nafion) contains the electrolyte solution that separates the anode and cathode sides.
- *Phosphoric acid fuel cell (PAFC)*
  In these cells, phosphoric acid is used as a nonconductive electrolyte to pass positive hydrogen ions from the anode to the cathode.
- *Solid oxide fuel cells (SOFCs)*
  Solid oxide fuel cells (SOFCs) use a solid material, most commonly a ceramic material called yttria-stabilized zirconia (YSZ), as the electrolyte. Because SOFCs are made entirely of solid materials, they are not limited to the flat plane configuration of other types of fuel cells and are often designed as rolled tubes. They require high operating temperatures (800–1000°C) and run on a variety of fuels, including natural gas.
- *Hydrogen-oxygen fuel cell*
  This type of fuel cell consists of two porous carbon electrodes impregnated with a suitable catalyst such as Pt, Pd, etc. The space between the two electrodes is filled with a concentrated solution of KOH or NaOH, which serves as an electrolyte.

- *Molten carbonate fuel cells (MCFCs)*
  Molten carbonate fuel cells (MCFCs) require a high operating temperature, 650°C (1200 °F), similar to SOFCs. MCFCs use lithium potassium carbonate salt as an electrolyte, and this salt liquefies at high temperatures, allowing for the movement of charge within the cell – in this case, negative carbonate ions.
- *Polymer nanocomposite-based fuel cell*
  In this class of fuel cells, a polymer nanocomposite membrane is used for the electrolyte. The electrolyte membranes act as a separator between the electrodes and determine the overall performance of fuel cells. Such fuel cell includes polymer electrolyte membrane (PEMFC) and directs methanol fuel cells (DMFC) such as gas diffusion layer (GDL), membrane electrode assembly (MEA), bipolar plates, stack, catalysts, and electrolyte membranes.

14.8.5 Working principle of fuel cells

The main components of any fuel cell are the anode, the electrolyte, and the cathode. There are two chemical reactions that occur at the interfaces between these electrodes.

At the anode the hydrogen is oxidized:

$$H_2\,(g) \rightarrow 2H^+ + 2e^-$$

The electrons pass through the load to provide the desired current and end up at the cathode, where the matching reduction reaction occurs:

$$2e^- + \tfrac{1}{2}O_2\,(g) \rightarrow {O_2}^-$$

Electrostatic balance is reached as the hydrogen ion diffuses through the electrolyte to get to the cathode:

$$2H^+ + {O_2}^- \rightarrow H_2O\,(l)$$

The thermal energy release of the overall reaction is determined by the enthalpy change.

These reactions in which a fuel is consumed and water or carbon dioxide is created result in generation of electric current, which can be used to power electrical devices, normally referred to as the load. A catalyst oxidizes the fuel (usually hydrogen) at the anode, resulting in a positively charged ion and a negatively charged electron. Then, an electrolyte between the cathode and anode passes the ions only through it to the cathode. Here, the ions and electrons react with a third chemical, usually oxygen, to create water or carbon dioxide. The electrons that cannot pass through the electrolyte travel through a wire, creating the electric current.

An electrolyte physically separates the two reactants and also prevents electronic conduction, while allowing ions to pass through; the electrons travel through an external loop to supply the load (shown in Fig. 14.25). Electrodes are attached to either side of the electrolyte.

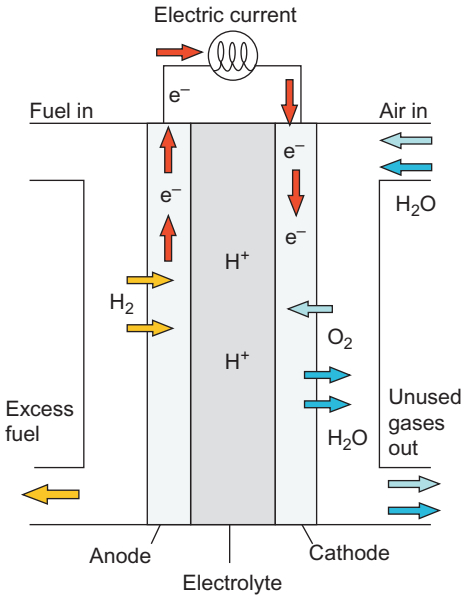

Fig. 14.25
Mechanism of fuel cell.

14.8.6 Polymer electrolyte membrane fuel cell (PEMFC)

A polymer electrolyte fuel cell has the ability to operate at a low temperature range (RT–80°C). This is the main attraction of a PEM fuel cell; since they have the ability to deliver such high power densities at this temperature, they can be made smaller, which reduces the overall weight, the cost to produce, and specific volume. It reduces corrosion and provides a longer stack life [73]. The PEM, like all fuel cells, consists of three basic parts: the anode, the cathode, and the membrane (shown in Fig. 14.26).

PEMs are being actively pursued for use in automobiles, buses, and portable applications. Today industry has great hope for the PEM, with some even predicting that it exceeds all other electrical energy generating technologies in the breadth of scope and possible applications [74]. The PEM is named for the solid-state exchange membrane that separates its electrodes. The membrane allows for the transfer of protons and thus permits the general fuel cell process. Hydrogen at the anode separates the electron and proton, freeing them to travel throughout the fuel cell. The electron and proton then meet at the cathode, where water is formed, in the presence of oxygen. Since high temperatures are not necessary to hydrate the membrane, the PEM can be run at very low temperature, typically at 80°C or lower.

The main concern to be considered in the polymer electrolyte membrane is the management of water. This is an issue because liquid is produced as a final product, as opposed to steam; since this water product is formed, it is important not to flood the electrolytes. Flooding of the

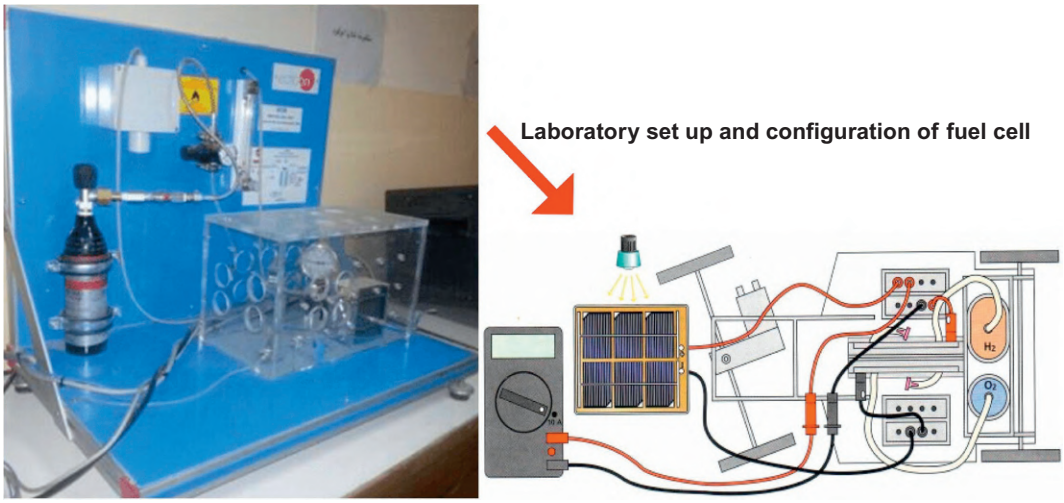

Fig. 14.26
Laboratory-based experimental set up of fuel cell and schematics of its operational configuration.

electrodes causes a decrease in surface area in which the separation of hydrogen or the formation of water takes place. The water cannot be simply removed, since the membrane needs to be hydrated; thus a balance must be regulated by a removal or retention technique. Since the electrode is very thin (50 μm) it is possible for the water to leak back to the anode, which would be the ideal situation if the exact amount were to migrate. This is ideal since the electrode needs to remain hydrated to promote the high levels of proton transfer; the water transfers the protons through the membrane. Several complications arise in this process. The first is that the water naturally moves towards the cathode, about 1 to 2.5 molecules per proton. This "electro-osmotic drag" is problematic at high current densities because all the water can be removed from the anode, thus causing an abrupt loss in fuel pressure, since no water will be present to transfer new protons (this is a form of a mass transportation loss). A further problem in water management is the susceptibility of the air drying the water out at high temperatures. Studies have shown that at temperatures over 60°C the air dries out the cathode. To solve this problem, it is necessary to add water to the system to keep everything hydrated; the trick is not to overhydrate the cell.

14.8.6.1 Applications of polymer nanocomposites in fuel cells

In this chapter, we have worked on various types of polymer nanocomposites, examining their physical and chemical investigations and their applications in environmental devices. The polymer nanocomposites are polymer matrices reinforced with nanometric inorganic fillers that possess remarkable optical, electrical, thermal, magnetic, physical, chemical, and conductive properties. Because of these extraordinary properties, polymer nanocomposite membranes are fascinating to the fuel cell field. However, the prerequisite requirements for

using suitable polymer electrolyte membranes are to find the best combination of both organic and inorganic nanomaterials. The prepared composite material, therefore, has enhanced properties compared with the single organic or inorganic material. The main idea of using nanocomposite membranes in fuel cells is to combine the best properties of individual components. Moreover, the advantages of having nanocomposites can be listed as follows [75, 76]:

(i) Using organic and inorganic components influences the electrochemical stability.
(ii) The hygroscopic characteristics of nanocomposites adsorb water molecules to a greater extent, being thus responsible for the lower humidity operation.
(iii) They help to improve the surface chemistry, as a high surface area of fillers increases the surface area of the membrane.
(iv) Ceramic properties of the nanofillers influence higher temperature applications.
(v) Polymer nanocomposite material influences high temperature and lower humidity operation of fuel cells with extended durability.

14.8.6.2 EMF measurement of fuel cell testing

This is one of the standard procedures for identifying the mobile species [77]. The electrolyte acts as a separating membrane between the anode/cathode compartment having different electrochemical activity. The electrochemical EMF so generated is measured and interpreted thermodynamically (shown in Fig. 14.27).

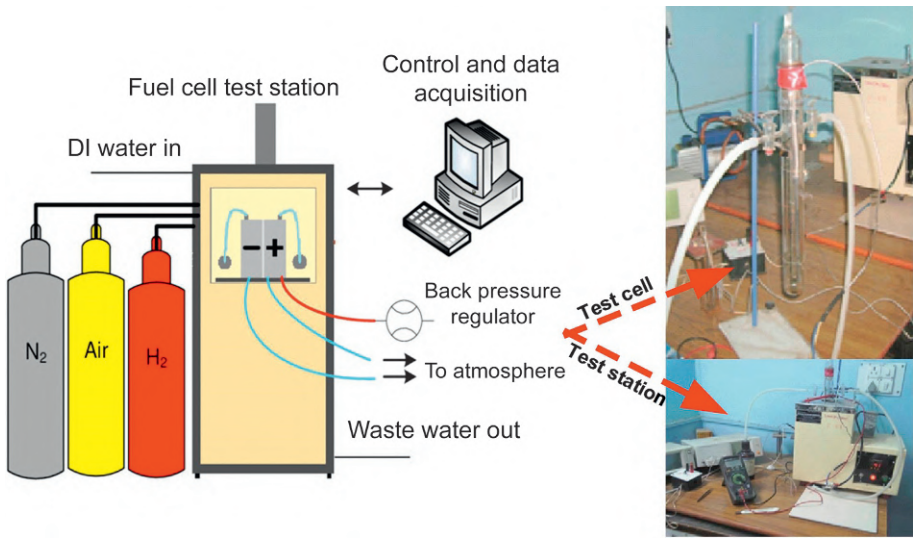

Fig. 14.27
Laboratory-based fuel cell testing platform.

The electrochemical EMF measurement across the concentration cell is a good method, particularly at higher temperature.

Suppose the concentration cell has the configuration:

$$Pt = PH_2(P') \,||\, \text{proton conductor} \,||\, PH_2(P'')$$

The potential difference developed across it is given by the Nernst equation:

$$E = t\frac{RT}{2F} \ln\left[\frac{p'}{p''}\right]$$

where t is the transference number, p' and p'' are the partial pressure of gases. By this method, the presence of protonic conduction can be demonstrated. [78] The actual experimental arrangement used in the present investigation is shown in Fig. 14.28.

Two types of concentration cells were used for the present study:

Electrolyte used:

Polymer nanocomposite electrolyte

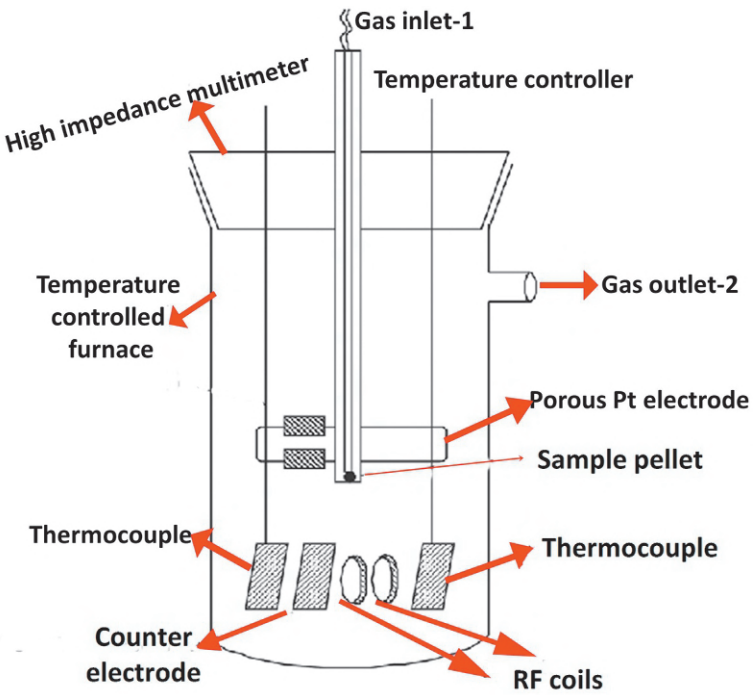

Fig. 14.28
Schematic representation of the EMF measurement cell.

Electrode used:

$$\text{Pd.Paste (Alfa Asar)}$$

Cell configuration:

$$P_{H2}(P') \text{ Pd.I}^{st} \text{ ambient}//\text{NCPE}//\text{II}^{nd} \text{ ambient Pd.}P_{H2}(P'')$$

Concentration Cell

$$\text{Wet air, Pd/Polymer film (PVdF : Amm Act : Fillar)/Pd, dry air}$$

$$\text{EMF Obtained} = 34 - 120\,\text{mV}\ (0.8\,\text{cm}^2 \text{ area up to } 80°\text{C})$$

Concentration Cell

$$H_2 \text{ Pd.Polymer Film (PVdF : Amm Act : filler)/Pd, dry air}$$

$$\text{EMF Obtained} = 100 - 300\,\text{mV}\ (\text{on } 0.8\,\text{cm}^2 \text{ area up to } 80°\text{C})$$

14.8.7 Application of fuel cell

As we have discussed, due to the size flexibility of fuel cells, the technology may be used in various applications in power needs. Fuel cells are applicable in mobile or stationary applications (shown in Fig. 14.29).

Some automobile manufacturers (Toyota, Ford) have chosen to feed their fuel cells with methanol, while others have preferred to use pure hydrogen (Opel has used liquid hydrogen, General Motors has stored hydrogen in hydride form). Ballard Power Systems in Canada uses fuel cells for cars, buses, and trucks. Toyota introduced its new Mirai, which means "future." The vehicle can travel 300 miles on a single hydrogen tank.

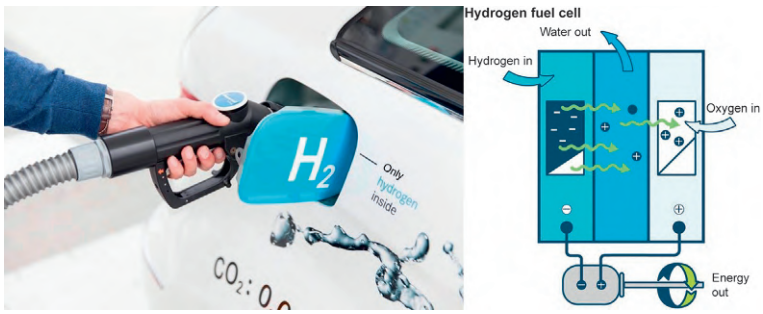

Fig. 14.29
Application of fuel cell in hydrogen fueling station.

The primary stationary application of fuel cell technology is for the combined generation of electricity and heat for building industrial facilities or standby generators; because the efficiency of fuel cell power systems is nearly unaffected by size, the initial stationary plant development has focused on smaller, several hundred kilowatt to low megawatt capacity plants. The plants are fueled primarily with natural gas, and operation of complete, self-contained, stationary plants has been demonstrated using PEMFC, AFC, PAFC, MCFC, and SOFC technology [79].

14.9 Conclusions and outlook

Nanocomposite polymer electrolyte (NCPE) materials have received recent prominence in recent times, particularly in the field of the environment, owing to their potential applications in advanced ionic devices such as high-performance batteries, fuel cells, supercapacitors, sensors, smart windows, and drug targeting. Essentially, NCPEs are a class of materials in which nanosized particles are molecularly dispersed within a polymer matrix. Commercial interest in these NCPEs arises from the fact that they exhibit distinct advantages over liquid electrolytes, such as good mechanical property, easy moldability, light weight, and better thermal stability, among others. Within the framework of nanocomposite polymer electrolytes, poly(vinylidene fluoride) [PVdF] based polymeric nanocomposite electrolytes are the most extensively investigated systems, as PVdF is a semicrystalline polymer at room temperature. Further, it has a low glass transition temperature and melting point. It has an exceptional property to dissolve high concentrations of a wide variety of dopants. Moreover, it possesses a single helical structure, which supports fast ion transport. Prompted by these considerations, attempts have been made as described in this chapter to develop a proton/ammonium ion conducting nanocomposite electrolyte based on the polymer PVdF. Within the gambit of different proton-conducting polymer electrolytes, NH_4SCN and ammonium acetate salt have been considered as a favorable solute owing to the small cationic/larger anionic size, which allows greater mobility in transporting ions.

As mentioned earlier, a variety of inorganic/organic filler particles have been used to develop composite systems. Among them, SiO_2 has been popularly used as a third component, owing to ease of SiO_2 synthesis and its availability in abundance. In addition, ferrite and ferroelectric nanoparticles, which possess unique magnetic properties and are usually characterized by a high dielectric constant and relative high permeability below Curie temperature, have lately been suggested as potent active fillers in the development of NCPEs. It is pertinent to note that nanoparticles differ from their bulk counterparts in the sense that they contain single domain in contrast to multidomain structure of bulk magnetic materials. Such nanoparticle-based systems exhibit superparamagnetic behavior and coactivity while keeping a very high saturation magnetization. Such systems have potential application in biomedicine, magnetic drug delivery, and magnetic refrigeration technology. Synthesis and structural characterization of [90PVdF:

$10NH_4SCN$], and ([PVdF $_{0.3}$+ (EC + PC) $_{0.7}]_{0.9}$ + $[(NH_4)_2COOCH_2]_{0.1}$) + filler based nanocomposite polymer electrolytes have been carried out under the following conditions.

a. Varying salt (NH_4SCN) concentration in a PVdF +NH_4SCN composite system.
b. Varying concentration of nanosized oxides/ferrite powder as filler in polymer matrix, keeping the stoichiometry of the pristine electrolyte fixed.

The salient features recorded during structural characterization of the as-synthesized nanocomposite polymer electrolytes are as follows:

I. The X-diffraction pattern of a pure PVdF and composite gel electrolyte system, i.e., [90PVdF +$10NH_4SCN$]. In pure PVdF, three intense characteristic peaks located at 19.6° (110), 23.5° (200), and 26.6° (021) along with one small peak at 18° are observed. The existence of broad peaks, in addition to a few sharp reflections, affirmed its partial crystalline and partial amorphous nature. In 90PVdF + $10NH_4SCN$ polymer electrolyte film, diffraction peaks at $2\theta = 18°$ and 19.6° in pure polymer merged in a single peak with downsizing of intensities, along with its shifting towards high 2θ values (20.1°). The addition of ceramic fillers (SiO_2, Al_2O_3, fly ash, and Li-ferrite) in a polymer host reduced the intensity of the main peak followed by broadening of the peak area, which is an indication of reduction in degree of crystallinity. A comparison shows that the broadness of the 20° peak (i.e., the main peak of PVdF) with the different filler groups increases 2%–5% with respect to the original size.
II. The optical micrograph of the ([PVdF $_{0.3}$+ (EC + PC) $_{0.7}]_{0.9}$ + $[(NH_4)_2COOCH_2]_{0.1}$) gel electrolyte system was recorded to assess the morphology of the gel electrolyte. In polymeric material, two mechanisms of phase separation are known: nucleation and growth, and spinodal decomposition. The first process starts with formation of nuclei of new components, whereas in spinodal decomposition the system behaves differently. The spinodal decomposition structure is a stable structure at room temperature.
III. The SEM image of pure PVdF and different PVdF + NH_4SCN based gel electrolyte systems clearly shows bimodal morphology with a modified crystalline domain. The addition of salt (NH_4SCN) connects the pores to each other, due to induced delay in phase relation or lower surface energy. The addition of filler and salt drastically changes the microstructure of the pristine electrolyte. The comparative look of SEM images of different filler system provides more smoothness with more grains.
IV. The IR spectrum of pristine PVdF and (90PVdF + $10NH_4SCN$) electrolyte films. PVdF electrolyte is characterized by the presence of vibrational bands at 612 and 763 cm^{-1} that are related to CF_2 with skeleton bending, respectively. The peaks at 532, 1210, 1383, 1432 cm^{-1} show dominance of the crystalline α phase in PVdF film. The addition of NH_4SCN gives a few new peaks in the region 2000–2200 cm^{-1}, which indicates formation of a PVdF-NH_4SCN crystalline complex. The IR spectra of ($[PVdF_{0.3}$ + (EC + PC)$_{0.7}]_{0.9}$+

$[(NH_4)_2COOCH_2]_{0.1}$) with different filler. In the SiO_2 system the prominent peak presents at 807 cm^{-1}, due to existing silica peak compared which shows the effect of filler, and the original peaks are reducing and chain flexibility is increasing.

V. Cyclic voltammetry (CV) of the Pt/NCPEs/Pt cell at room temperature was performed to assess the electrochemical stability of nanocomposite polymer electrolytes. It can be seen that electrovoltammograms of better ion-conducting films exhibit very good reversibility. The current voltage measurements on Pt/(100 − x) PVdF + xNH_4SCN/Pt (where x = 4, 6, 10, 20) cell at a scan rate of 0.1 mV/s were taken. Among these gel polymer electrolyte systems, the electrolyte containing 10 wt% NH_4SCN shows highly stable behavior. In the ($[PVdF_{0.3}$ + (EC + PC) $_{0.7}]_{0.9}$ + $[(NH_4)_2COOCH_2]_{0.1}$) electrolyte, after the introduction of fillers the electrochemical window enhanced drastically and reached ±8 V. This means that the effect of different groups of filler is clearly visible on the pristine electrolyte.

VI. Wagner's polarization methods have been used to assess the nature of ion transport and evaluate total ionic transference number. Experimental results show that PVdF with ammonium thiocyanate (NH_4SCN) has a completely ionic nature. But after the addition of filler SiO_2, ferrite, Al_2O_3 and fly ash, the composite electrolyte shows the ionic behavior. These result coupled with IR investigation indicate proton as the likely specie which is mobile in these electrolytes.

VII. Electrical characterization of ionic materials is an important factor to establish utility in electrochemical devices. Keeping this in mind electrical characterization on developed NCPEs was pursued and the results have been presented in the following paragraphs.

Composition dependence of the conductivity of pristine electrolyte shows that bulk electrical conductivity increases with increasing concentration of salt up to 10 wt% and thereafter it decreases. Above 10 wt%, the films become sticky in nature, reflecting the upper limit of salt absorption in a polymer host, as far as formation of free-standing films is concerned. The optimum conductivity of pristine electrolyte (1.5×10^{-4} S/cm) was obtained for the 90PVdF + $10NH_4SCN$ system. Similarly, the optimum conductivity of [($[PVdF_{0.3}$ + (EC + PC) $_{0.7}]_{0.9}$ + $[(NH_4)_2COOCH_2]_{0.1}$)] is 1.3×10^{-4} S/m. The addition of fillers in pristine electrolyte (($[PVdF_{0.3}$ + (EC + PC) $_{0.7}]_{0.9}$ + $[(NH_4)_2COOCH_2]_{0.1}$)) provides the better thermal, mechanical, and electrical behavior. The electrolyte with Al_2O_3 shows the highest conductivity in the group of oxide fillers. The higher conductivity in {($[PVdF_{0.3}$ + (EC + PC) $_{0.7}]_{0.9}$ + $[(NH_4)_2COOCH_2]_{0.1}$)}$_{0.99}$:{Al_2O_3}$_{0\cdot01}$ electrolyte is probably due to the small ionic size of the Al^{+++} ion among the other two, i.e., SiO_2 and fly ash.

In another group, the Li-ferrite filler-based electrolyte possesses the higher conductivity among the different systems; the Li-ferrite-based NCPE exhibits the highest AC conductivity values, possibly due to the creation of extra hopping sites assisting ion hop. This is possibly due to greater interaction among components in the presence of reactive Li ions.

During dielectric spectroscopic investigations on all the NCPEs, a strong frequency dispersion in relative permittivity (ε') was recorded in the low-frequency region followed by a nearly frequency-independent nature at higher frequencies. The low-frequency dispersion has been linked to the electrode polarization effect in the polymer electrolyte. Low-temperature dispersion in ε' has once again been correlated to electrode polarization effects, while high-temperature behavior has been attributed to thermally activated polarization behavior. After doping of SiO_2/ferrites in the pristine electrolyte system, the dielectric parameter (ε') increases with increasing filler content.

The imaginary part of dielectric permittivity (ε'') recorded a high value in the low-frequency region followed by a nearly frequency-independent nature in the high-frequency regime in all the nanocomposite polymer electrolytes. A higher value of dielectric loss (ε'') at low frequency is essentially due to the electrode-electrolyte interfacial polarization. All the curves display the so-called β-relaxation peak in polyethylene oxide. The β-relaxation is usually detected in the range 250–300 K and is associated with local motion of chain segments or side group (short-range bond rotation in polymer chain).

The variation of dielectric loss (ε'') at different temperatures is seen to increase with increasing temperature. The observed behavior has been explained by considering the system to be formed of molecular dipoles, which remain frozen when the temperature is low. As the temperature increases, the dipoles become thermally more activated, having more rotational freedom, which leads to the observed increase in the dielectric parameter.

Tangent loss results show that enhancement of oxide/ferrite content tends to lose the segmental packing in the chain, thereby increasing the free volume for dipolar relaxation. This shows that the peak in the tanδ curve can be attributed to segmental diffusion motion in the amorphous region and is assignable to the β (beta) relaxation process. To prove the worth of investigated electrolytes in electrochemical devices, PEM fuel cells were fabricated for optimally conducting electrolyte systems.

14.10 Remarks and future prospects

It is concluded from the present work that ferrites are one of the better options for synthesis of nanocomposite polymer electrolytes, due to their unique properties such as high dielectric constant, superparamagnetic behavior, and possibility of intercalation. These so-called magneto ionic polymer electrolytes (*smart material*) with higher ionic conductivity, better morphology, and thermal, mechanical and electrochemical stability are likely to generate new application areas of electrochemical devices. Present experimental investigations show that the developed nanocomposite polymer electrolyte (NCPE) containing Li-ferrite is a better conducting system among the investigated fillers, having better morphology, and thermal, mechanical and electrochemical stability. The interaction of a polymer (PVdF) with salt

(NH_4SCN) and fillers (ferrites) suggests the role of nanoferrites as that of an *active filler*, whereas silica performed the role of an *inert filler* in the electrolyte system, as evidenced through XRD studies. The optical micrography studies highlight the change in system morphology for all the composite electrolyte systems in a favorable manner. IR studies indicate interaction of polymer with salt and filler particles in NCPEs. The greater interaction among constituents in the Li-ferrite-based system reaffirms the active role of Li-ferrite filler particles in control of electrical properties. Wagner's polarization study for all NCPEs shows that "ferrite fillers affect ionic transference number" and thus control the ion conduction property of composite electrolytes. The bulk electrical conductivity response of NCPE shows that both salt and fillers (silica/ferrites) are able to increase the ionic conductivity of the electrolyte system.

Finally, the applicability of these nanocomposite polymer electrolytes has been tested in a PEM fuel cell.

References

[1] K. Andy, J.C. Cleveland, Environmental Information Coalition, National Council for Science and the Environment, 2007.
[2] L. Bian, Annuals of the Association of American Geographers, 97 (2007), p. 267.
[3] A. Brimicombe, GIS, Environmental Modelling and Engineering, second ed., Taylor and Francis Group, 2009.
[4] I. Ferencika, T. Niemia, A. Jolmaa, On site environmental modeling and monitoring: the Nordic Scenario in Hydrosys Project, in: D.A. Swayne, W. Yang, A. Voinov, A. Rizzoli, T. Filatova (Eds.), International Congress on Environmental Modelling and Software, International Environmental Modelling and Software Society (iEMSs), 2010.
[5] Pollution-Definition from the Merriam-Webster Online Dictionary, Merriam-webster.com. 13 August 2010. Retrieved 26 August 2010.
[6] M. Brauer, G. Hoek, H.A. Smith, J.C. de Jongste, J. Gerritsen, D.S. Postma, European Society for Clinical Respiratory Physiology, 29 (2007), p. 879.
[7] J. Colls, Air Pollution, Spon Press, New York, 2002.
[8] J. Serra, Alternative Fuel Resource Development, Clean and Green Fuels Fund, 2006.
[9] S. Bilgen, K. Kaygusuz, Energy Sources 26 (p) (2004) 1119.
[10] J. De Barteleven, Eastern Europe's Environmental Crisis, Johns Hopkins Press, 1992.
[11] E.K. Drexler, Engines of Creation: The Coming Era of Nanotechnology, Doubleday Publisher, 1986.
[12] H.K. Joseph, H. Mcgraw, Nanoscience and Technology Series, (2006).
[13] F.W. Bill Meyer Jr., Textbook of Polymer Science, John Wiley and Sons, 1984, p. 578.
[14] S. Glasstone, An Introduction to Electrochemistry, Litton Educational Publisher, 1974, p. 11.
[15] M.A. Taige, D. Hilbert, T.J.S. Schubert, Phys. Chem. 226 (p) (2011) 129.
[16] N. Shukla, A.K. Thakur, A. Shukla, D.T. Marx, Int. J. Electrochem. Sci. 9 (p) (2014) 7644.
[17] R.C. Agrawal, R.K. Gupta, J. Mater. Sci. 34 (p) (1999) 1131.
[18] P.G. Bruce, C.A. Vincent, J. Chem. Soc. Faraday Trans. 89 (1993) 3187.
[19] F.M. Gray, Materials monographs, in: Polymer Electrolytes, The Royal Society of Chemistry, 1997.
[20] J.Y. Song, Y.Y. Wang, J. Power Sources 77 (p) (1999) 183.
[21] S.S. Sekhon, Bull. Mater. Sci. 26 (p) (2003) 331.
[22] D.E. Fenton, J.M. Parker, P.V. Wright, Polymer 14 (1973) 589.
[23] M.B. Armand, J.M. Chabagno, M.J. Duclot, 2nd International Meeting on Solid Electrolytes, St. Andrews, Scotland, (1978).
[24] S. Dhawan, M. Varma, V.R. Sinha, Pharm. Technol. 5 (2005) 72.

[25] P. Periasamy, K. Tatsumi, M. Shikano, T. Fujieda, T. Sakai, Y. Saito, M. Mizuhata, A. Kajinami, S. Deki, Solid State Ionics 126 (1999) 285.
[26] S. Ramesh, K.H. Leen, K. Kumutha, A. Arof, Spectrochim. Acta A Mol. Biomol. Spectrosc. 66 (2007) 1237.
[27] H. Lee, J.K. Yoo, J.H. Park, J.H. Kim, K. Kang, Y.S. Jung, Adv. Energy Mater. 2 (2012) 976.
[28] D.M. Esterly, Manufacturing of Poly (Vinylidene Fluoride) and Evaluation of Its Mechanical Properties, Virginia Tech, 2002.
[29] S. Panero, B. Sacrosati, J. Power Sources 90 (p) (2000) 13.
[30] B. Sacrosati, Application of Electroactive Polymers, Chapman and Hall, London, 1993.
[31] D.J. Jones, J. Roziere, J. Fuel Cells 215 (p) (2008) 219.
[32] A. Volta, Philos. Trans. R. Soc. Lond. 90 (1800) 403.
[33] J. Wood, Mater. Today 10 (p) (2005) 219.
[34] B.B. Owens, G.R. Argue, Science 157 (1967) 308.
[35] Y. Yijing, Open access dissertations, University of Miami paper 440, (2010).
[36] J.S. Wagner, C. Wagner, J. Chem. Phys. 26 (p) (1957) 1597.
[37] C.W. Tang, Appl. Phys. Lett. 48 (p) (1986) 183.
[38] S.S. Sekhon, Bull. Mater. Sci. 26 (p) (2003) 321.
[39] P. Ueberschlag, Sens. Rev. 21 (p) (2001) 118.
[40] M. Gilbert, Polym. Rev. 34 (1994) 77.
[41] A.A. Awadhi, S.K. Patel, S.L. Agrawal, Prog. Cryst. Growth Charact. Mater. 52 (2006) 61.
[42] S.K. Patel, A. Awadhia, S.L. Agrawal, Phase Transit. 82 (2009) 421.
[43] V. Neburchilov, J. Martin, H. Wang, J. Zhang, J. Power Sources 169 (2007) 221.
[44] H. Zhang, J. Wang, Spectrochim. Acta A Mol. Biomol. Spectrosc. 71 (2009) 1927.
[45] D.R. Dillon, K.K. Tenneti, C.Y. Li, F.K. Ko, I. Sics, B.S. Hsiao, Polymer 47 (p) (2006) 1678.
[46] J.B. Lando, H.G. Olf, A. Petrlin, Polym. Chem. 4 (1966) 941.
[47] S.S. Sekhon, H.P. Singh, Solid State Ionics 169 (2002) 152.
[48] B.K. Cho, P.C. Canfield, D.C. Johnston, Phys. Rev. B 52 (1995) 3844.
[49] J.G. Bergman, J.H. Mc Fee, G.R. Crane, Appl. Phys. Lett. 18 (1971) 203.
[50] J.H. Mc Fee, J.G. Bergman, G.R. Cron, Ferroelectrics 3 (1972) 305.
[51] R.G. Kepler, R.A. Anderson, J. Appl. Phys. 49 (1978) 1232.
[52] B.A. Newman, C.H. Yoon, K.D. Pae, J. Appl. Phys. 50 (1979) 6095.
[52a] S.L. Agrawal, M. Singh, M. Tripathi, et al., Dielectric relaxation studies on [PEO–SiO_2]:NH_4SCN nanocomposite polymer electrolyte films, J. Mater. Sci. 44 (2009) 6060–6068.
[53] J.P. Youn, S.K. Yong, P. Cheolmin, Eur. Polym. J. 41 (2005) 1002.
[54] K. Kimmerle, H. Strathmann, Desalination 79 (1990) 283.
[55] L. Jian, X. Jingu, S. Quing, J. Xiaozhen, Chin. Sci. Bull. 50 (2005) 368.
[56] M.M. Dwivdi, N. Asthana, S.K. Chaturvedi, K. Pandey, J. Nanosci. Nanoeng. 1 (2015) 265.
[57] S.L. Agrawal, A. Awadhia, Bull. Mater. Sci. 27 (2004) 523.
[58] K. Pandey, M.M. Dwivedi, M. Singh, S.L. Agrawal, J. Polym. Res. 17 (2010) 127.
[59] G. Mago, M.K. Dilhan, T.F. Frank, J. Nanomater. 2008 (2008) 8.
[60] M.K. Song, Y.T. Kim, B.W. Cho, B.N. Popov, H.W. Rhee, J. Electrochem. Soc. 150 (2003) 439.
[61] K. Pandey, M.M. Dwivedi, I.M.L. Das, M. Singh, S.L. Agrawal, J. Electroceram. 25 (2009) 99.
[62] A.K. Jonscher, Nature 267 (1977) 673.
[63] S. Ramesh, A.K. Arof, Mater. Sci. Eng. B 85 (2001) 11.
[64] R. Gregoria Jr., M. Cestari, J. Polym. Sci. 32 (1994) 859.
[65] T.G. Fox, P.J. Flory, Am. Chem. Soc. 70 (1950) 12384.
[66] Energy and Environment: Mission Statement, Multi-Science Publishing, 2012 Retrieved.
[67] D.L. Johnson, S.H. Ambrose, T.J. Bassett, M.L. Bowen, D.E. Crummey, J.S. Isaacson, D. N. Johnson, P. Lamb, M. Saul, A.E. Winter-Nelson, J. Environ. Qual. 26 (1997) 581.
[68] N. Rajab, N. Saad, S. Prakash, Int. J. Electr. Electron. Telecommun. Eng. 44 (2013) 625.
[69] N. Giordano, College Physics: Reasoning and Relationships, Cengage Learning, 2009, p. 510.

[70] R.S. Khurmi, Material Science, S. Chand and Co., 1987.
[71] A.J. Appleby, F.R. Foulkes, N.V. Reinhold, Fuel Cell Handbook, S. Chand Publishing, 1993.
[72] J.M.J. Blomen, M.N. Mugerwa, Fuel Cell Systems, Plenum Press, 1993.
[73] S.G. Kordesch, Fuel Cells and Their Applications, VCH, 1996.
[74] EGandG Services Parsons, Inc., Science Applications International Corporation, Fuel Cell Handbook, fifth ed., National Energy Technology Laboratory, 2000.
[75] J. Larminie, A. Dicks, Fuel Cell Systems Explained, John Wiley and Sons, Ltd, Chichester, England, 2000.
[76] Z.M. Huang, Y.Z. Zhang, M. Kotaki, S. Ramakrishna, Compos. Sci. Technol. 63 (2003) 2223.
[77] R. Bogue, Assem. Autom. 31 (2011) 106.
[78] S. Chandra, Super Ionic Solids—Principle and Application, North-Holland, Amsterdam, 1981.
[79] T. Takahashi, O. Yamamoto, F. Matsuyama, Y. Noda, J. Solid State Chem. 16 (1976) 35.

CHAPTER 15

Smart polymer systems as concrete self-healing agents

Vítor Corrêa da Costa[a], Mostafa G. Aboelkheir[a], Kaushik Pal[b,c], Romildo Dias Toledo Filho[d], Fernando Gomes[a,d]

[a]*Macromolecule Institute Professor Eloisa Mano, Technology Center - University City, Federal University of Rio de Janeiro, Rio de Janeiro, Brazil*
[b]*International and Inter University Centre for Nanoscience and Nanotechnology (IIUCN), School of Energy Materials, Mahatma Gandhi University, Kottayam, Kerala, India*
[c]*Wuhan University, Wuchang District, Wuhan, Hubei Province, Republic of China*
[d]*Civil Engineering Program, COPPE, Technology Center - University City, Federal University of Rio de Janeiro, Rio de Janeiro, Brazil*

15.1 Introduction

Concrete is a resistant and relatively cheap material, and it is one of the most used construction materials of all time [1]. Concrete presents good compression strength but lacks good tensile strength. This last property can be compensated for by the incorporation of steel fibers in the final product, producing reinforced concretes [2]. Concrete properties can vary considerably [3], with prior adjustments being needed to produce the right composition for specific applications. In that way, concrete can be used in a variety of structural applications [4].

Cracks in concrete materials are recurring problems, which are not necessarily considered prejudicial if they retain a certain thickness [5]. However, they can allow penetration of water and other deteriorating materials, destroying the structure. Consequently, oxidative expansion of steel used in reinforced concretes might occur, making the crack thickness control a crucial problem [6].

Costs relative to concrete repair can be enormous, on the order of trillions of dollars [7]. Besides high costs, concrete repair causes many environmental problems, as it is one of the leading causes of CO_2 emissions worldwide [8] and the source of the generation of tons of waste.

To face those economic and environmental problems, new technologies allowing the production of more durable concrete are needed. One of those technologies is self-healing

Nanofabrication for Smart Nanosensor Applications. https://doi.org/10.1016/B978-0-12-820702-4.00016-7
© 2020 Elsevier Inc. All rights reserved.

concrete, in which the material can restore its mechanical properties after a crack appears, acting as a smart polymer system [9].

The self-healing process has been increasingly studied in the last few decades. Scientific papers related to "concrete self-healing" keywords from 1999 to 2019 in the Google Academic database have grown exponentially ($r^2 = 0.97$), showing the importance of this mechanism in current research. An exponential fitting relating the article number increase over the years is shown in Fig. 15.1.

After comparing the number of scientific papers containing the keywords "concrete self-healing" and "concrete self-healing polymer" on Google Academic, one can conclude that around 40% of 33,400 articles are related to polymer-based self-healing systems, highlighting the importance of polymeric materials in this process.

Thus polymers are strongly associated with the concrete self-healing process, indicating the significance of this chapter, which elaborates the main mechanisms related to the process, the main polymers used in each mechanism, and the most current trends in the field.

15.2 Self-healing property

Self-healing is a process in which a material regenerates itself, without the addition of any external agent after the defect, restoring its properties entirely or partially, and increasing its lifespan [10]. This process may occur due to intrinsic properties of the material [11] or due to previously added components [12].

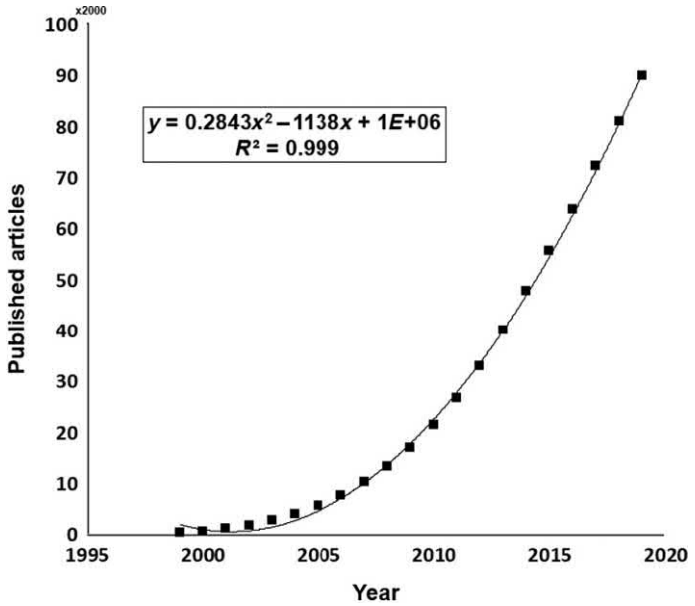

Fig. 15.1
Integrated growth of studies related to the keywords "concrete self-healing." *Google Academic, 06/08/19.*

Most of the materials with a self-regenerating capacity are polymers, such as hydrogels [13], polyurethanes [14], and epoxy resins [15]. Some of these materials may form hybrid complexes [16] or nanocomposites [17]. Asphaltenes also have this capacity, although its mechanism is not apparent yet [18].

Notably, the self-healing of concrete is becoming a sustainable possibility to be employed, restoring cracks from 50 μm [19] to 450 μm [20], depending on the agents used in the process. Concrete properties can be almost completely restored, with its regeneration occurring more than one time [21].

Comparing the search for the keywords "self-healing" and "concrete self-healing" in Google Academic, one can observe that the self-healing mechanism applied to concrete materials represents about 10% of 385,000 total reported research studies.

The numbers of lab-based research studies investigating concrete self-healing were reported [22]; however, research investigations based on larger scales are being developed, indicating promising results [23]. Concrete with regeneration properties promotes a considerable increase in the material's lifetime [24]. However, it is necessary to evaluate the cost/benefit at amplified scale, to optimize the systems and make the regeneration process more efficient without an excessive increase in costs.

Fig. 15.2 compares the life of an ordinary material and a self-healing one. It is depicted that the self-healing material, while having a higher initial cost in relation to the regular material, maintains the material performance, being cost-effective in the long term.

15.3 Concrete self-healing mechanisms

As with other materials, the self-healing property in concrete can be caused by an intrinsic capacity of the material or by the addition of another component into the system. The intrinsic mechanism is defined as "autogenous self-healing" (*autós* + *génos*, "generated by itself", from

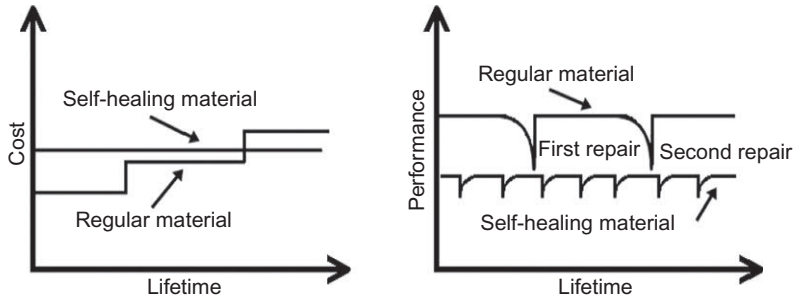

Fig. 15.2
Lifetime comparison between a conventional material and a self-healing material, relating it to cost (left) and performance (right).

Greek). The cases in which the addition of another material is necessary can be divided into three categories: mineral admixture systems, bacterial systems, and adhesive materials systems [25–27]. The primary mechanisms are shown in Fig. 15.3.

15.3.1 Autogenous

Although it was already known, the autogenous mechanism was explained in detail by Edvardsen [28], who discovered the calcite ($CaCO_3$) formation in the healed part of concrete. Portlandite [$Ca(OH)_2$] recrystallization found in the cement and the hydration of unhydrated cement particles are also considered related mechanisms to this technique. Cement hydration tends to happen instantaneously with water penetration into the crack, while the portlandite and calcite mechanisms proceed in slower steps [29]. Calcite tends to be formed next to the crack, since CO_3^{2-} anions come from the environment, while portlandite is formed inside the crack [30].

15.3.2 Mineral admixtures

Mineral admixtures can be divided into expansive and crystalline additives. The first consists of the production of expansible material, while the second consists of the formation of crystalline products, which crystallize along the cracks [31]. Some downsides with this kind of mechanism include: minerals can react as soon as the hydration happens, even before the application; expansion can happen inside the material, causing damage; and there is a constant need for water. So, encapsulation methodologies using polymeric materials are combined with this technique [32].

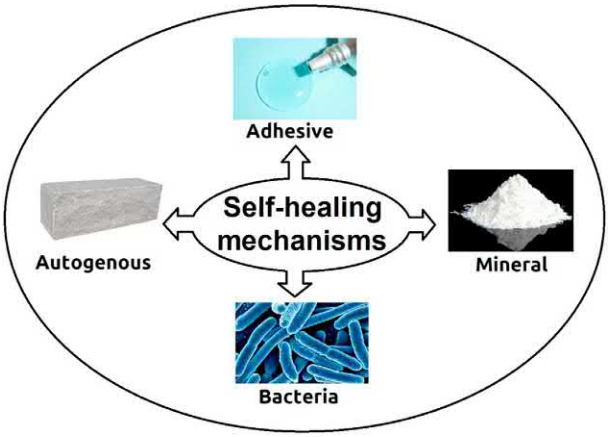

Fig. 15.3
Self-healing mechanisms.

15.3.3 Bacteria

Bacteria can be used to precipitate $CaCO_3$ through their metabolism and can be added into concrete to increase the self-healing capacity [33]. Urea hydrolysis is the most rigorous pathway due to its capability of producing high quantities of calcite quickly [34]. Some aspects of this mechanism have to be considered. The first one is to protect the species from the highly alkaline environment inside the concrete [35] and the reduction of the available space inside the concrete when it starts to hydrate [20]. In most cases, encapsulation via polymeric materials is applied [36].

15.3.4 Adhesive materials

Adhesive agents can seal cracks, connecting two crack surfaces. These materials can have one, two, or multiple agents in their composition. Their properties vary greatly with the different materials used [37]. Due to their adherent properties, polymers, such as epoxy [38], polyacrylates [39], silicon [40], and others, are utilized for this application. These materials can also be encapsulated as prepolymers, and, once they are liberated, they start to polymerize, leading to gluing of cracks [41].

According to Huang [42], the four different mechanisms present different conditions to be utilized in the best possible way. These conditions are as follows: (i) water presence, (ii) CO_3^{2-} presence, (iii) crack thickness, and (iv) agent availability (that is, the need to use another agent to make the regenerative additive available). In addition, water is desirable in the first three mechanisms, since it facilitates the obtaining of CO_3^{2-}, while it can disturb the adhesive mechanism. In turn, the CO_3^{2-} presence is desirable in bacteria and autogenous mechanisms, since it tends to accelerate them, if they are based on calcite production. Regarding crack size, autogenous systems can only heal up to 50 μm, while other mechanisms can heal much thicker cracks. Also, as stated before, minerals, bacteria, and adhesive-based systems need encapsulation methods. On the other hand, the absence of water makes the adhesive treatment better suited for internal elements or open sky structures, while the other three mechanisms are applicable to submerged and subsoil structures, since they need a water supply [42].

There is no need for polymeric encapsulations in autogenous systems, since this mechanism is inherent in concrete [28], while in both mineral [43] and bacteria-based mechanisms [44] polymers can be used as encapsulation agents. As for adhesive material mechanisms, as stated before, they are polymers themselves with adhesive properties [45]. The relationship between the different mechanisms of concrete self-healing and the different polymers in use during this process are summarized in Table 15.1.

Table 15.1: Polymer use in different self-healing systems.

Mechanisms	Polymer use	References
Autogenous	Not necessary	[30, 46, 47]
Minerals	Encapsulation agent	[31, 48, 49]
Bacteria	Encapsulation agent	[36, 50, 51]
Adhesive	Polymers with adhesive properties	[38, 40, 52]

15.4 Polymers in concrete self-healing

In this section, the main polymers used in the self-healing mechanism of concrete are described, together with recent studies on their applications.

Fig. 15.4 shows the percentages of the total number of articles related to the subject for each of the main polymers used in this application, according to Google Academic. The keywords used as the 100% criteria were "concrete self-healing" (total of 33,600 articles), and, to specify the percentage of the studies related to each polymer, their names were added as a keyword. Considering that many studies work with more than one polymeric system, the studies may be repeated.

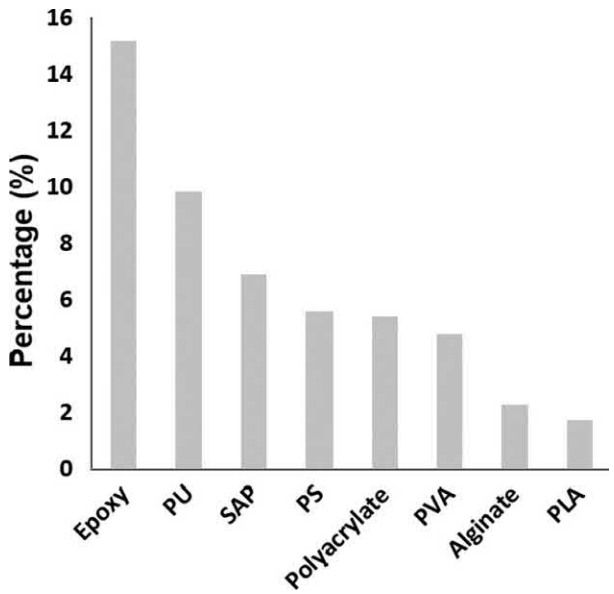

Fig. 15.4
Comparison of "concrete self-healing" and "concrete self-healing + *polymer name*" keywords. *Google Academic, 06/08/2019.*

It is necessary to keep in mind that the polymers cited in Fig. 15.4 are not all the unique materials used in the preparation of self-healing systems. Some other polymers are used, such as urea-formaldehyde resin [53], gelatin [54], and silicon [55]. The graphical abstract shows the formulae of the primary polymer used in this novel application. Fig. 15.5 presents the chemical structure of the polymers mentioned in the current review.

15.4.1 Poly (vinyl alcohol) (PVA)

PVA is known by its solubility in water and is commonly used in papermaking, coating, and textile applications [56]. Algharmi *et al*. [43] used this polymer to coat mineral aggregates, so they could resist the concrete moisture and cure, avoiding interaction with the concrete before crack formation. Snoeck et al. added PVA fibers to increase cement tenacity and control its crack thickness, meaning that this polymer can be utilized to help in test procedures [57].

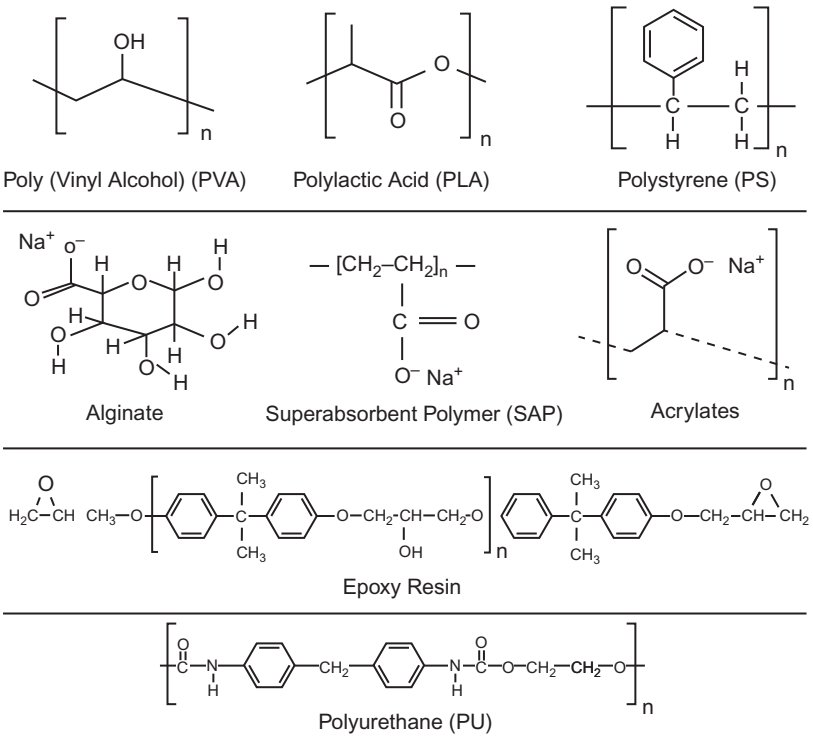

Fig. 15.5
The chemical structures of polymers applied in concrete self-healing systems.

15.4.2 Poly (lactic acid) (PLA)

PLA exhibits a biodegradability property [58]. It is commonly used in 3D printers [59]. Hilloulin and collaborator used this polymer to coat healing agents to substitute for glass capsules, which did not last within the concrete mixture. The material had a better malleability and stayed intact, while the concrete maintained its mechanical properties [60]. Savija et al. [61] have shown that PLA has good interaction with adhesive agents.

15.4.3 Polystyrene (PS)

One of the most useful polymers in the world, PS is used as a sheet/molded, as foams, or as expanded material [62]. Illouling et al. used PS to encapsulate self-healing agents, which resisted the mixture procedure and retained the concrete mechanical properties [60]. Dong *et al*. [63] encapsulated concrete self-healing agents with PS to protect the concrete from corrosion. Results varied, depending on the material thickness.

15.4.4 Polyurethanes (PUs)

PUs are polymers composed of carbamate units, which are used as foams, adhesives, and others [64]. Feiteira et al. [37] compared two PUs, one flexible and one rigid, to regenerate concrete, claiming that the application of the flexible one was preferable due to a better interface property. Van Tittelboom et al. [65] carried out a large-scale test to analyze a PU capsule, which they claimed to be applicable in dry environments.

15.4.5 Epoxy resin

Polymers that contain the epoxy group are applied as coatings, adhesives, and in electronic applications [66]. Guadagno et al. [38] used epoxy resins to act as self-healing agents, which presented in the form of nanotubes, showing good mechanical and thermal properties. Doug et al. [53] used epoxy to promote cross-linking in an encapsulation agent, which successfully protected the healing agents.

15.4.6 Polyacrylates

Polyacrylates are a group of polymers that contain the acrylate group and are employed as a substitute for glass and as an adhesive [67]. Araújo et al. [68] used acrylate prepolymers as adhesive materials to promote self-healing by polymerizing when their capsules broke. The best outcomes came from an epoxy resin/dimethylsiloxane system. Perez et al. [69] developed a

system containing acrylates and silica and claimed that the material had a good interaction with cement and satisfactory morphology and particle size.

15.4.7 Alginates

Alginates are polysaccharides with varying properties produced by algae, used in healthcare and food applications [70]. Palin et al. [47] developed a self-healing system encapsulated by alginate. The material swelled by 300% and had a high yield. The authors claimed that it can be used in low-temperature submersed materials. Mignon et al. [71] produced alginate to use in concrete self-healing capsules. It swelled 600%, and the mechanical properties remained the same, presenting good properties and low cost.

15.4.8 Superabsorbent polymers (SAPs)

SAPs are a class of materials characterized by the capacity to swell hundreds of times their weight, acting as adhesive agents that attach themselves along the crack [57]. Mignon et al. [45] developed an SAP sensitive to pH. This material was very swellable in alkaline pH, being compatible with the alkaline environment in concrete. Snoeck et al. [57] compared two SAPs to evaluate their self-healing properties. Both succeeded in regenerating submersed and outdoor structures by absorbing air humidity.

15.5 Trends in concrete self-healing

This section presents an evaluation of the main recent articles produced about the subject, in order to see future trends in the field.

Kua et al. [72] used a self-healing system composed of superabsorbent polymers, $CaCO_3$, and precipitating bacteria to increase the lifespan of a PVA-fiber reinforced concrete. We think this is a brilliant example of the technique of combination to further improve self-healing capacities, thus improving the material lifetime.

Mullem et al. [73] studied the effects of crack width variation and geometry in self-healing concrete materials. We believe that understanding physical mechanisms in self-healing concrete is a recent trend that can enrich our comprehension of it.

Mauludin et al. [74] studied PMMA capsules containing self-healing agents using algorithms in a computational model. Mauludin's work shows the increasing relevance of computer models to simulate concrete self-healing systems. This might help future researchers to avoid time-consuming adjustments and waste of material.

Van den Heede et al. [22] carried out a large-scale test to evaluate the efficiency of different prepolymer systems in tests similar to real-life applications. This study shows concrete healing

systems being tested at larger scales, which constitutes excellent progress, since many research studies on the use of polymers in concrete are still on a laboratory scale.

Van den Heede et al. [75] tested encapsulated polymers to inhibit carbonation-induced corrosion in steel-reinforced concrete. A PU precursor was used, and the results showed that the concrete could remain repair-free for at least 100 years. The system produced shows the potential applications at a large scale.

Dong et al. [72] compared two kinds of chemically triggered self-healing systems using X-ray microcomputed tomography (XCT) and environmental scanning electron microscopy (ESEM) equipped with texture element analysis microscopy (TEAM). Dong's work proved that researchers must study microchanges that happen in self-healing systems.

Teall et al. [76] studied the use of shape memory polymers (SMPs) activated by electricity as self-healing agents in concrete by autogenous boosting. Teall's study allows us to believe that electricity-activated polymers have many promising applications in concrete healing. However, one could question whether it is worth it to use this advanced technology instead of using cheaper and simpler technologies.

Nguyen et al. [77] performed a detailed study of the atomic phenomena related to the self-healing mechanism in concrete-polymer composites. Those studies are essential in order to potentialize the mechanisms related to concrete self-healing and avoid mechanisms that are detrimental to it. We believe those studies will be even more critical in the future to produce more efficient systems.

New studies also indicate that self-healing concrete technology is proving itself suitable for large-scale applications, once problems regarding the upscale are dealt with.

Promising technologies would allow cost reduction of the materials, besides improving the efficacy of these systems. The knowledge of physical and atomic mechanisms seems to be a key factor.

We strongly recommend that the main focus in the field should be the production of environmentally friendly and cheaper materials, which could present an excellent cost-benefit relationship. Materials such as polar and biodegradable natural polymers could be the future of this kind of application.

15.6 Final considerations

As proved in the text, the exponential increase in the number of research articles published dealing with self-healing demonstrates the massive interest in this subject. The mechanisms of self-healing can be improved with the use of polymers. Among them, hydrophilic polymers, such as PVA, PLA, SAPs, polyurethanes, and polyacrylates, are relevant materials for this

novel application. Two groups can be highlighted: the first group (PVA, PLA, SAPs) presents a good interaction with the concrete matrix, while the second one (polyurethanes and polyacrylates) contains materials that are more durable. We also believe that the development of materials that are sustainable and cost-effective, and that exhibit suitable properties, is the key to the success of self-healing systems over the next few years.

References

[1] V. Afroughsabet, G. Geng, A. Lin, L. Biolzi, C.P. Ostertag, P.J.M. Monteiro, The influence of expansive cement on the mechanical, physical, and microstructural properties of hybrid-fiber-reinforced concrete, Cem. Concr. Compos. 96 (2019) 21–32, https://doi.org/10.1016/j.cemconcomp.2018.11.012.

[2] J.C. McCormac, R.H. Brown, Design of Reinforced Concrete, John Wiley & Sons, 2015.

[3] P.K. Mehta, P.J. Monteiro, Concrete Microstructure, Properties and Materials, 2017.

[4] Q. Fu, D. Niu, D. Li, Y. Wang, J. Zhang, D. Huang, Impact characterization and modelling of basalt–polypropylene fibre-reinforced concrete containing mineral admixtures, Cem. Concr. Compos. 93 (2018) 246–259, https://doi.org/10.1016/j.cemconcomp.2018.07.019.

[5] G. Rastiello, S. Dal Pont, J.-L. Tailhan, P. Rossi, On the threshold crack opening effect on the intrinsic permeability of localized macro-cracks in concrete samples under Brazilian test conditions, Mech. Res. Commun. 90 (2018) 52–58, https://doi.org/10.1016/j.mechrescom.2018.04.008.

[6] W. Nguyen, J.F. Duncan, G. Jen, C.P. Ostertag, Influence of matrix cracking and hybrid fiber reinforcement on the corrosion initiation and propagation behaviors of reinforced concrete, Corros. Sci. (2018), https://doi.org/10.1016/j.corsci.2018.06.004.

[7] B. Kiani, R.Y. Liang, J. Gross, Material selection for repair of structural concrete using VIKOR method, Case Stud. Constr. Mater. 8 (2018) 489–497, https://doi.org/10.1016/j.cscm.2018.03.008.

[8] A. Souto-Martinez, J.H. Arehart, W.V. Srubar, Cradle-to-gate CO2e emissions vs. in situ CO2 sequestration of structural concrete elements, Energy Build. 167 (2018) 301–311, https://doi.org/10.1016/j.enbuild.2018.02.042.

[9] L. Ferrara, V. Krelani, F. Moretti, M. Roig Flores, P. Serna Ros, Effects of autogenous healing on the recovery of mechanical performance of high performance fibre reinforced cementitious composites (HPFRCCs): part 1, Cem, Concr. Compos. 83 (2017) 76–100, https://doi.org/10.1016/j.cemconcomp.2017.07.010.

[10] H. Siad, M. Lachemi, M. Sahmaran, H.A. Mesbah, K.A. Hossain, Advanced engineered cementitious composites with combined self-sensing and self-healing functionalities, Constr. Build. Mater. 176 (2018) 313–322, https://doi.org/10.1016/j.conbuildmat.2018.05.026.

[11] S.A. Ponnusami, J. Krishnasamy, S. Turteltaub, S. van der Zwaag, A cohesive-zone crack healing model for self-healing materials, Int. J. Solids Struct. 134 (2018) 249–263, https://doi.org/10.1016/j.ijsolstr.2017.11.004.

[12] L. Zhang, Q. Liu, S. Wu, Y. Rao, Y. Sun, J. Xie, P. Pan, Investigation of the flow and self-healing properties of UV aged asphalt binders, Constr. Build. Mater. 174 (2018) 401–409, https://doi.org/10.1016/j.conbuildmat.2018.04.109.

[13] M. Kang, S. Liu, O. Oderinde, F. Yao, G. Fu, Z. Zhang, Template method for dual network self-healing hydrogel with conductive property, Mater. Des. 148 (2018) 96–103, https://doi.org/10.1016/j.matdes.2018.03.047.

[14] T. Wan, D. Chen, Mechanical enhancement of self-healing waterborne polyurethane by graphene oxide, Prog. Org. Coat. 121 (2018) 73–79, https://doi.org/10.1016/j.porgcoat.2018.04.016.

[15] Z. Ding, L. Yuan, Q. Guan, A. Gu, G. Liang, A reconfiguring and self-healing thermoset epoxy/chain-extended bismaleimide resin system with thermally dynamic covalent bonds, Polymer 147 (2018) 170–182, https://doi.org/10.1016/j.polymer.2018.06.008.

[16] G. Yıldırım, A.H. Khiavi, S. Yeşilmen, M. Şahmaran, Self-healing performance of aged cementitious composites, Cem. Concr. Compos. 87 (2018) 172–186, https://doi.org/10.1016/j.cemconcomp.2018.01.004.

[17] R. Bayan, N. Karak, Bio-derived aliphatic hyperbranched polyurethane nanocomposites with inherent self healing tendency and surface hydrophobicity: towards creating high performance smart

materials, Compos. A: Appl. Sci. Manuf. 110 (2018) 142–153, https://doi.org/10.1016/j.compositesa.2018.04.024.
[18] T. Al-Mansoori, J. Norambuena-Contreras, R. Micaelo, A. Garcia, Self-healing of asphalt mastic by the action of polymeric capsules containing rejuvenators, Constr. Build. Mater. 161 (2018) 330–339, https://doi.org/10.1016/j.conbuildmat.2017.11.125.
[19] S. van der Zwaag, Self Healing Materials-An Alternative Approach to 20, Sybrand van der Zwaag, Springer, 2007. www.springer.com/la/book/9781402062490. (Accessed 19 October 2017).
[20] H.M. Jonkers, A. Thijssen, G. Muyzer, O. Copuroglu, E. Schlangen, Application of bacteria as self-healing agent for the development of sustainable concrete, Ecol. Eng. 36 (2010) 230–235, https://doi.org/10.1016/j.ecoleng.2008.12.036.
[21] F.A. Gilabert, K. Van Tittelboom, E. Tsangouri, D. Van Hemelrijck, N. De Belie, W. Van Paepegem, Determination of strength and debonding energy of a glass-concrete interface for encapsulation-based self-healing concrete, Cem. Concr. Compos. 79 (2017) 76–93, https://doi.org/10.1016/j.cemconcomp.2017.01.011.
[22] P. Van den Heede, B. Van Belleghem, M.A. Araújo, J. Feiteira, N. De Belie, Screening of different encapsulated polymer-based healing agents for chloride exposed self-healing concrete using chloride migration tests, in: Key Eng. Mater., Trans Tech Publ, 2018, pp. 152–158.
[23] E. Gruyaert, B. Debbaut, M. Kaasgaard, H. Erndahl Sorensen, J. Pelto, V. Branco, F. Malm, C. Grosse, E. Price, M. Krüger, Evaluation of the performance of self-healing concrete at small and large scale under laboratory conditions, in: 14th Int. Conf. Durab. Build. Mater. Compon. XIV DBMC, RILEM Publications, 2017, pp. 1–12.
[24] M. Al-Ansari, A.G. Abu-Taqa, M.M. Hassan, A. Senouci, J. Milla, Performance of modified self-healing concrete with calcium nitrate microencapsulation, Constr. Build. Mater. 149 (2017) 525–534, https://doi.org/10.1016/j.conbuildmat.2017.05.152.
[25] L. Ferrara, T. Van Mullem, M.C. Alonso, P. Antonaci, R.P. Borg, E. Cuenca, A. Jefferson, P.-L. Ng, A. Peled, M. Roig-Flores, M. Sanchez, C. Schroefl, P. Serna, D. Snoeck, J.M. Tulliani, N. De Belie, Experimental characterization of the self-healing capacity of cement based materials and its effects on the material performance: a state of the art report by COST action SARCOS WG2, Constr. Build. Mater. 167 (2018) 115–142, https://doi.org/10.1016/j.conbuildmat.2018.01.143.
[26] W. Tang, O. Kardani, H. Cui, Robust evaluation of self-healing efficiency in cementitious materials—a review, Constr. Build. Mater. 81 (2015) 233–247, https://doi.org/10.1016/j.conbuildmat.2015.02.054.
[27] S. Gupta, H.W. Kua, S.D. Pang, Healing cement mortar by immobilization of bacteria in biochar: an integrated approach of self-healing and carbon sequestration, Cem. Concr. Compos. 86 (2018) 238–254, https://doi.org/10.1016/j.cemconcomp.2017.11.015.
[28] C. Edvardsen, Water permeability and autogenous healing of cracks in concrete, Mater. J. 96 (1999) 448–454, https://doi.org/10.14359/645.
[29] B. Hilloulin, F. Grondin, M. Matallah, A. Loukili, Modelling of autogenous healing in ultra high performance concrete, Cem. Concr. Res. 61 (2014) 64–70.
[30] H. Huang, G. Ye, L. Pel, New insights into autogenous self-healing in cement paste based on nuclear magnetic resonance (NMR) tests, Mater. Struct. 49 (2016) 2509–2524.
[31] P. Escoffres, C. Desmettre, J.-P. Charron, Effect of a crystalline admixture on the self-healing capability of high-performance fiber reinforced concretes in service conditions, Constr. Build. Mater. 173 (2018) 763–774, https://doi.org/10.1016/j.conbuildmat.2018.04.003.
[32] A. Kanellopoulos, T.S. Qureshi, A. Al-Tabbaa, Glass encapsulated minerals for self-healing in cement based composites, Constr. Build. Mater. 98 (2015) 780–791.
[33] K. Vijay, M. Murmu, S.V. Deo, Bacteria based self healing concrete—a review, Constr. Build. Mater. 152 (2017) 1008–1014, https://doi.org/10.1016/j.conbuildmat.2017.07.040.
[34] M. Luo, C. Qian, R. Li, Factors affecting crack repairing capacity of bacteria-based self-healing concrete, Constr. Build. Mater. 87 (2015) 1–7, https://doi.org/10.1016/j.conbuildmat.2015.03.117.
[35] E. Tziviloglou, K. Van Tittelboom, D. Palin, J. Wang, M.G. Sierra-Beltrán, Y.Ç. Erşan, R. Mors, V. Wiktor, H. M. Jonkers, E. Schlangen, Bio-based self-healing concrete: from research to field application, in: Self-Healing Materials, Springer, 2016, pp. 345–385.

[36] D. Palin, V. Wiktor, H.M. Jonkers, A bacteria-based bead for possible self-healing marine concrete applications, Smart Mater. Struct. 25 (2016) 084008.
[37] J. Feiteira, E. Tsangouri, E. Gruyaert, C. Lors, G. Louis, N. De Belie, Monitoring crack movement in polymer-based self-healing concrete through digital image correlation, acoustic emission analysis and SEM in-situ loading, Mater. Des. 115 (2017) 238–246, https://doi.org/10.1016/j.matdes.2016.11.050.
[38] L. Guadagno, M. Raimondo, C. Naddeo, P. Longo, A. Mariconda, W.H. Binder, Healing efficiency and dynamic mechanical properties of self-healing epoxy systems, Smart Mater. Struct. 23 (2014) 045001.
[39] A.B.W. Brochu, Self-Healing Poly (Methyl Methacrylate) Bone Cement Utilizing Embedded Microencapsulated 2-Octyl Cyanoacrylate Tissue Adhesive, Duke University, 2013.http://search.proquest.com/openview/24d71bdfe0b851d6561da9392bca32a1/1?pq-origsite=gscholar&cbl=18750&diss=y. (Accessed 11 October 2017).
[40] A. Behnood, K. Van Tittelboom, S. Chatrabhuti, J.-M. Raquez, P. Dubois, N. De Belie, Comparative study on different polymer tubes as carriers of healing agent for self-healing concrete, in: 5th Int. Conf. Self-Heal. Mater. ICSHM 2015, Duke University, 2015.
[41] T.-C. Tseng, F.-Y. Hsieh, P. Theato, Y. Wei, S. Hsu, Glucose-sensitive self-healing hydrogel as sacrificial materials to fabricate vascularized constructs, Biomaterials 133 (2017) 20–28, https://doi.org/10.1016/j.biomaterials.2017.04.008.
[42] H. Huang, G. Ye, C. Qian, E. Schlangen, Self-healing in cementitious materials: materials, methods and service conditions, Mater. Des. 92 (2016) 499–511, https://doi.org/10.1016/j.matdes.2015.12.091.
[43] R. Alghamri, A. Kanellopoulos, A. Al-Tabbaa, Impregnation and encapsulation of lightweight aggregates for self-healing concrete, Constr. Build. Mater. 124 (2016) 910–921, https://doi.org/10.1016/j.conbuildmat.2016.07.143.
[44] J.Y. Wang, H. Soens, W. Verstraete, N. De Belie, Self-healing concrete by use of microencapsulated bacterial spores, Cem. Concr. Res. 56 (2014) 139–152, https://doi.org/10.1016/j.cemconres.2013.11.009.
[45] A. Mignon, G.-J. Graulus, D. Snoeck, J. Martins, N.D. Belie, P. Dubruel, S.V. Vlierberghe, pH-sensitive superabsorbent polymers: a potential candidate material for self-healing concrete, J. Mater. Sci. 50 (2015) 970–979, https://doi.org/10.1007/s10853-014-8657-6.
[46] A.R. Suleiman, M.L. Nehdi, Effect of environmental exposure on autogenous self-healing of cracked cement-based materials, Cem. Concr. Res. (2018) https://doi.org/10.1016/j.cemconres.2018.05.009.
[47] D. Palin, V. Wiktor, H.M. Jonkers, Autogenous healing of marine exposed concrete: characterization and quantification through visual crack closure, Cem. Concr. Res. 73 (2015) 17–24.
[48] X.F. Wang, C. Fang, D.W. Li, N.X. Han, F. Xing, A self-healing cementitious composite with mineral admixtures and built-in carbonate, Cem. Concr. Compos. (2018), https://doi.org/10.1016/j.cemconcomp.2018.05.013.
[49] T.S. Qureshi, A. Kanellopoulos, A. Al-Tabbaa, Encapsulation of expansive powder minerals within a concentric glass capsule system for self-healing concrete, Constr. Build. Mater. 121 (2016) 629–643, https://doi.org/10.1016/j.conbuildmat.2016.06.030.
[50] H. Kalhori, R. Bagherpour, Application of carbonate precipitating bacteria for improving properties and repairing cracks of shotcrete, Constr. Build. Mater. 148 (2017) 249–260, https://doi.org/10.1016/j.conbuildmat.2017.05.074.
[51] U.U. Jadhav, M. Lahoti, Z. Chen, J. Qiu, B. Cao, E.-H. Yang, Viability of bacterial spores and crack healing in bacteria-containing geopolymer, Constr. Build. Mater. 169 (2018) 716–723, https://doi.org/10.1016/j.conbuildmat.2018.03.039.
[52] Y. Xu, D. Chen, A novel self-healing polyurethane based on disulfide bonds, Macromol. Chem. Phys. 217 (2016) 1191–1196, https://doi.org/10.1002/macp.201600011.
[53] B. Dong, G. Fang, Y. Wang, Y. Liu, S. Hong, J. Zhang, S. Lin, F. Xing, Performance recovery concerning the permeability of concrete by means of a microcapsule based self-healing system, Cem. Concr. Compos. 78 (2017) 84–96, https://doi.org/10.1016/j.cemconcomp.2016.12.005.
[54] J. Song, X. Cui, G. Jin, Z. Cai, E. Liu, X. Li, Y. Chen, B. Lu, Self-healing conversion coating with gelatin–chitosan microcapsules containing inhibitor on AZ91D alloy, Surf. Eng. 34 (2018) 79–84.
[55] H. Mihashi, T. Nishiwaki, Development of engineered self-healing and self-repairing concrete-state-of-the-art report, J. Adv. Concr. Technol. 10 (2012) 170–184.

[56] T. Gao, Z. Yang, C. Chen, Y. Li, K. Fu, J. Dai, E.M. Hitz, H. Xie, B. Liu, J. Song, Three-dimensional printed thermal regulation textiles, ACS Nano 11 (2017) 11513–11520.
[57] D. Snoeck, K. Van Tittelboom, S. Steuperaert, P. Dubruel, N. De Belie, Self-healing cementitious materials by the combination of microfibres and superabsorbent polymers, J. Intell. Mater. Syst. Struct. 25 (2014) 13–24, https://doi.org/10.1177/1045389X12438623.
[58] J. Gu, P. Xiao, P. Chen, L. Zhang, H. Wang, L. Dai, L. Song, Y. Huang, J. Zhang, T. Chen, Functionalization of biodegradable PLA nonwoven fabric as superoleophilic and superhydrophobic material for efficient oil absorption and oil/water separation, ACS Appl. Mater. Interfaces 9 (2017) 5968–5973.
[59] J.P. Bustillo, R. Tumlos, R.Z. Remoto, Intensity modulated radiotherapy (IMRT) phantom fabrication using fused deposition modeling (FDM) 3D printing technique, in: World Congr. Med. Phys. Biomed. Eng. 2018, Springer, 2019, pp. 509–515.
[60] B. Hilloulin, K. Van Tittelboom, E. Gruyaert, N. De Belie, A. Loukili, Design of polymeric capsules for self-healing concrete, Cem. Concr. Compos. 55 (2015) 298–307, https://doi.org/10.1016/j.cemconcomp.2014.09.022.
[61] B. Šavija, J. Feiteira, M. Araújo, S. Chatrabhuti, J.-M. Raquez, K. Van Tittelboom, E. Gruyaert, N. De Belie, E. Schlangen, Simulation-aided design of tubular polymeric capsules for self-healing concrete, Materials 10 (2016) 10.
[62] A. Pczieczek, A. Schackow, C. Effting, I.R. Gomes, T.F. Dias, Properties of mortars containing tire rubber waste and expanded polystyrene (eps), J. Urban Environ. Eng. 11 (2018) 224–230.
[63] B. Dong, Y. Wang, W. Ding, S. Li, N. Han, F. Xing, Y. Lu, Electrochemical impedance study on steel corrosion in the simulated concrete system with a novel self-healing microcapsule, Constr. Build. Mater. 56 (2014) 1–6, https://doi.org/10.1016/j.conbuildmat.2014.01.070.
[64] V. Guilamo-Ramos, M. Reading, A.S. Bowman, D.C. Perlman, S. Barrett, Multipurpose prevention technologies: a global sexual and reproductive health priority, J. Assoc. Nurses AIDS Care 29 (2018) 6–9.
[65] K. Van Tittelboom, J. Wang, M. Araújo, D. Snoeck, E. Gruyaert, B. Debbaut, H. Derluyn, V. Cnudde, E. Tsangouri, D. Van Hemelrijck, N. De Belie, Comparison of different approaches for self-healing concrete in a large-scale lab test, Constr. Build. Mater. 107 (2016) 125–137, https://doi.org/10.1016/j.conbuildmat.2015.12.186.
[66] B. Xiong, W. Zhong, Q. Zhu, K. Liu, M. Li, G. Sun, D. Wang, Highly transparent and rollable PVA-co-PE nanofibers synergistically reinforced with epoxy film for flexible electronic devices, Nanoscale 9 (2017) 19216–19226.
[67] C. Li, H. Xiao, X. Wang, T. Zhao, Development of green waterborne UV-curable vegetable oil-based urethane acrylate pigment prints adhesive: preparation and application, J. Clean. Prod. 180 (2018) 272–279, https://doi.org/10.1016/j.jclepro.2018.01.193.
[68] M. Araújo, K.V. Tittelboom, P. Dubruel, S.V. Vlierberghe, N.D. Belie, Acrylate-endcapped polymer precursors: effect of chemical composition on the healing efficiency of active concrete cracks, Smart Mater. Struct. 26 (2017) 055031. https://doi.org/10.1088/1361-665X/aa64cb.
[69] G. Perez, E. Erkizia, J.J. Gaitero, I. Kaltzakorta, I. Jiménez, A. Guerrero, Synthesis and characterization of epoxy encapsulating silica microcapsules and amine functionalized silica nanoparticles for development of an innovative self-healing concrete, Mater. Chem. Phys. 165 (2015) 39–48, https://doi.org/10.1016/j.matchemphys.2015.08.047.
[70] J. Yao, Y. Zhou, X. Chen, F. Ma, P. Li, C. Chen, Effect of sodium alginate with three molecular weight forms on the water holding capacity of chicken breast myosin gel, Food Chem. 239 (2018) 1134–1142.
[71] A. Mignon, J. Vermeulen, D. Snoeck, P. Dubruel, S. Van Vlierberghe, N. De Belie, Use of methacrylated alginate for self-healing concrete, in: Heal.-Conf.-Self-Heal. Concr. Prolong. Lifetime, 2016, pp. 1–5.
[72] B. Dong, W. Ding, S. Qin, N. Han, G. Fang, Y. Liu, F. Xing, S. Hong, Chemical self-healing system with novel microcapsules for corrosion inhibition of rebar in concrete, Cem. Concr. Compos. 85 (2018) 83–91.
[73] T. Van Mullem, E. Gruyaert, B. Debbaut, R. Caspeele, N. De Belie, Novel active crack width control technique to reduce the variation on water permeability results for self-healing concrete, Constr. Build. Mater. 203 (2019) 541–551, https://doi.org/10.1016/j.conbuildmat.2019.01.105.
[74] L.M. Mauludin, X. Zhuang, T. Rabczuk, Computational modeling of fracture in encapsulation-based self-healing concrete using cohesive elements, Compos. Struct. 196 (2018) 63–75.

[75] P. Van den Heede, B. Van Belleghem, M.A. Araújo, J. Feiteira, N. De Belie, Screening encapsulated polymeric healing agents for carbonation-exposed self-healing concrete, service life extension, and environmental benefit, in: Int. Congr. Polym. Concr., Springer, 2018, pp. 83–89.
[76] O.R. Teall, M. Pilegis, R. Davies, J. Sweeney, A. Jefferson, R. Lark, D. Gardner, A shape memory polymer concrete crack closure system activated by electrical current, Smart Mater. Struct. 27 (7) (2018) 1361–1373.
[77] M.-T. Nguyen, Z. Wang, K.A. Rod, M.I. Childers, C. Fernandez, P.K. Koech, W.D. Bennett, R. Rousseau, V.-A. Glezakou, Atomic origins of the self-healing function in cement–polymer composites, ACS Appl. Mater. Interfaces (2018). https://doi.org/10.1021/acsami.7b13309.

Further reading

H.A. Abdel-Gawwad, E. Heikal, H. El-Didamony, F.S. Hashim, A.H. Mohammed, Recycling of concrete waste to produce ready-mix alkali activated cement, Ceram. Int. 44 (2018) 7300–7304, https://doi.org/10.1016/j.ceramint.2018.01.042.
H.W. Kua, S. Gupta, A.N. Aday, W.V. Srubar, Biochar-immobilized bacteria and superabsorbent polymers enable self-healing of fiber-reinforced concrete after multiple damage cycles, Cem. Concr. Compos. 100 (2019) 35–52, https://doi.org/10.1016/j.cemconcomp.2019.03.017.
D. Gardner, R. Lark, T. Jefferson, R. Davies, A survey on problems encountered in current concrete construction and the potential benefits of self-healing cementitious materials, Case Stud. Constr. Mater. 8 (2018) 238–247.
D.W. Fowler, Concrete-polymer materials: how far have we come, and where do we need to go? in: Int Congr. Polym. Concr. ICPIC, 2018 Springer, Cham, 2018, pp. 3–13. https://doi.org/10.1007/978-3-319-78175-4_1.

CHAPTER 16

Chemical engineering of protein cages and nanoparticles for pharmaceutical applications

Alaa A.A. Aljabali[a], Mazhar S. Al Zoubi[b], Lorca Alzoubi[a,e], Khalid M. Al-Batanyeh[c], Mohammad A. Obeid[a], Murtaza M. Tambwala[d]

[a]*Department of Pharmaceutics and Pharmaceutical Technology, Faculty of Pharmacy, Yarmouk University, Irbid, Jordan*
[b]*Department of Basic Medical Studies, Yarmouk University, Irbid, Jordan*
[c]*Department of Biological Sciences, Yarmouk University, Irbid, Jordan*
[d]*SAAD Centre for Pharmacy and Diabetes, School of Pharmacy and Pharmaceutical Science Ulster University, Coleraine, United Kingdom*
[e]*Medicinal Chemistry and Pharmacognosy Department, Faculty of Pharmacy, Yarmouk University, Irbid, Jordan*

16.1 Introduction to chemical modification of proteins

The term *protein cage* designates a proteinaceous structure that self-assembles into a hollow structure. Protein cages are often classified as virus-like particles (VLPs) and nonviral cages, and are regarded primarily as well-defined hollow spherical capsule-like 3D structures with unmatched monodispersity within the artificial nanoparticle (NP) formation. They are assembled from repetitive units, known as asymmetric units, that come together (self-assemble) within the host cell to form the whole virion structure. The static pores of well-defined size and polarity that are located between the asymmetric units allow accessibility to the interior of the protein cages [1]. These pores range from 0.4 nm for ferritin [2, 3] to approximately 3 nm for heat-shock proteins [4], and the P22 capsid is 10 nm [5]. These pores act as channels connecting the inside cavity with the exterior encompassing surroundings. Small therapeutic molecules smaller than the pore size can diffuse through them and can be entrapped within the capsid cavity [6–8]. In some viruses, the pores are lined with hydrophobic amino acid side chains, which act as gating mechanisms discriminating between molecules based on their charge and polarity [9]. However, one of the primary and attractive properties for some of the macromolecule cages (such as cowpea chlorotic mottle virus, CCMV) is their intrinsic dynamic

Nanofabrication for Smart Nanosensor Applications. https://doi.org/10.1016/B978-0-12-820702-4.00017-9
© 2020 Elsevier Inc. All rights reserved.

structure that can be assembled and disassembled in vitro in response to external stimuli, mainly pH [10]. Other protein cages undergo conformational changes that allow the closed pores to open in response to chelating agents [1]. The process was used to encapsulate molecules or NPs within the CCMV capsid that are larger, to fit through the swelling process of the CCMV capsid. On the other hand, over the past decades, these asymmetric units have been subjected to both chemical and genetic modification to introduce new functionalities. The wealth of information generated from understanding the pathogenicity of viruses as a pathogenic agent has led to the generation of a massive amount of information on the structure and the assemblies of such NPs [11].

In general, protein cages are considered to be robust, naturally occurring NPs. Viruses undergo structural changes as part of their life cycle from assembly to disassembly, to release their nucleic acid within the host cells. Therefore, they evolve to survive in a harsh environment during this cycle. They are capable of withstanding temperatures of up to 85°C [12]. In addition, as they move between different cellular environments, they also evolve to survive in a pH range of 2–10 and 6 M guanidine at pH 7.0 [13]. Moreover, protein cages preserve their structural integrity in the organic solvents DMSO and DMF for levels up to 50% *v*/v [14, 15].

The chemical engineering of proteins and protein cages is one of the most critical tools for introducing novel therapeutic conjugates in a predetermined position. The exterior and interior of asymmetric units, as well as between them, have been explored for chemical and genetic engineering of the viral capsids. Investigations have been made of the chemical selectivity of amino acid side chains under ambient and neutral pH while preserving the 3D architecture of the protein. Such hollow, naturally occurring NPs play a pivotal role in the bionanomedicine area of research, as templates for the synthesis of mineralization and metallization coatings [6, 14–19], reaction vesicles, and controlled drug release NPs [7, 8].

Protein cages that are extensively investigated in pharmaceutical and medical nanotechnology include ferritins [20], vaults [21], chaperones [22, 23], heat-shock proteins [24–26], encapsulins [27, 28], and bacterial microcompartments [29, 30]. Most of those macromolecule protein cages are spherical in their structural arrangement, with a size varying between 9 nm to 80–150 nm for the bacterial microcompartments, whereas viruses exist in various morphologies. For example, TMV [31] and the M13 bacteriophage are rod-shaped viruses, while cowpea chlorotic mottle virus (CCMV) [32, 33], cowpea mosaic virus (CPMV) [11, 14, 15], MS2 bacteriophage [34], and adenovirus [35] are sphere-shaped viruses. Rod-shaped viruses do not have a large internal cavity for the packaging of materials of interest. However, their external area has been developed as a template for inorganic material coatings through the metallization process or coating with polymeric-based materials [36–38]. Viral protein cages have a broad range of internal cavities; for example, bacteriophage ΦX174 has an inner diameter of 26 nm [39]. This expands in the Mimivirus and Megavirus chilensis to more than 500 nm [40, 41]. Spherical viruses assemble from a minimum of 60 asymmetric units that

arrange into 12 pentamers, whereas larger viruses assemble from a more significant asymmetric unit, which might reach 180 units or even more. These asymmetric units assemble around the nucleic acid in specific points of interaction between the protein capsids and the nucleic acid. However, as the VLPs have the same structure as the native viruses but lack the genetic materials, their formation is somehow different, depending on the expression system used for that purpose.

Various amino acid side chains on the outside or inside of the macromolecule cages are used as anchoring points to impart new functionalities. The side chains of lysine, cysteine, tyrosine, and histidine have been utilized for various applications. The many applications of chemically engineered proteins include in vivo and in vitro tracking of fluorophore-labeled proteins [42], polyethylene glycol (PEG)ylation of therapeutics to reduce immunogenicity [43], and cell-targeting molecules or drug molecules [7]. Surface alteration of the protein cage allows for the precise location of molecules of concern on all atoms, and for every amino acid side chain, specific chemicals can also be used. Herein is a detailed description of certain macromolecule cages together with polymers or therapeutic molecules.

16.2 Uncommon viral protein cages

Viral cages are one of the essential natural nanotemplates that have been developed over the past decades. There are three available routes for their engineering: their exterior, interior, and interspaces. Viral protein cages can be generated from plant or animal viruses, enveloped or nonenveloped, infectious or noninfectious, encapsidated nucleic acid, or virus-like particles (VLPs). Virus-based nanomaterials have attractive properties; they are exceptionally robust, with the ability to tolerate different environments during their life cycle. Viruses as natural nanomaterials are biodegradable and biocompatible, making them ideal as nanomedicine tools and for pharmaceutical applications. A large number of virus-based nanomaterials are available for a broad range of applications. However, as our space is limited here, we will attempt to highlight some of the least common viral-based systems, as presented in Fig. 16.1.

16.2.1 Adenovirus

Human adenovirus (Adv) is a double-stranded DNA (dsDNA) and is nonenveloped, with approximately 95 nm diameter from vertex (protein fiber) to vertex, with the spherical capsid measuring 70–75 nm in diameter. The Adv capsid consists of 252 capsomers (240 called hexons and 12 called pentons), arranged in an icosahedron with geometries of pseudo-$T = 3$ symmetry with 20 triangular facets and 12 vertices. The Adv capsid has 20 facets, and each facet has a surface pore (channel) of 5 nm that allows the attachment of the fiber shaft on the capsid. These fibers are essential in the viral-host cell interaction.

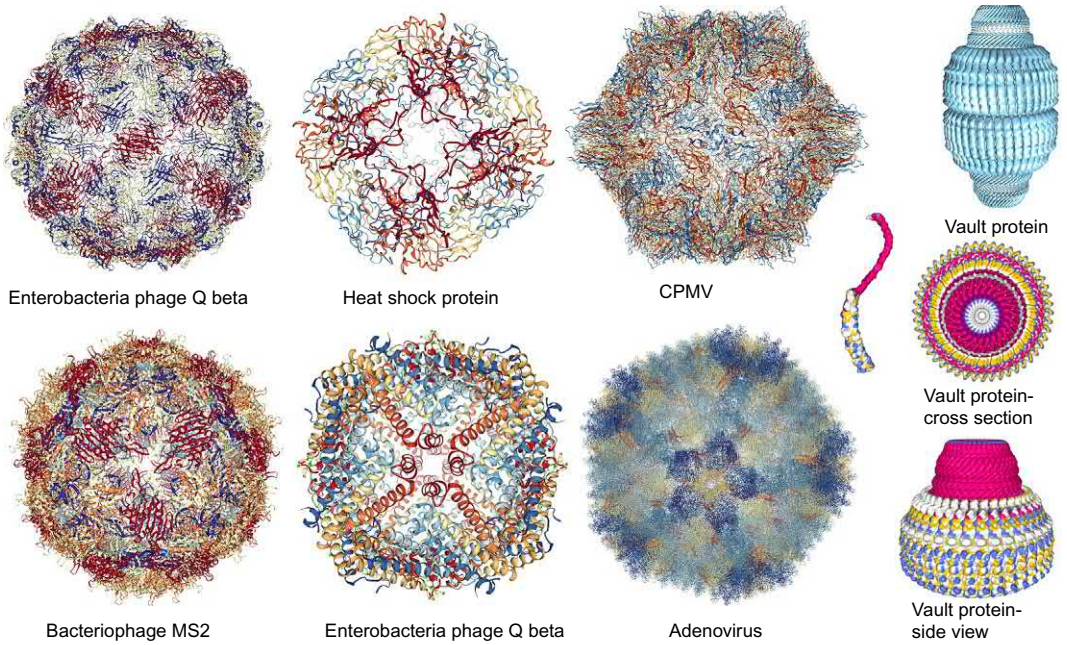

Fig. 16.1

An array of protein cages generated from the protein data bank with the accession numbers as follows: adenovirus (6CGV); ferritin (2FHA); CPMV (1NYY); vault protein (6BP7); heat-shock protein (3VQK); MS2 bacteriophage (2B2C); and Q-Beta bacteriophage (1QBE). Images were generated with PyMol software for protein rendering.

16.2.2 Viruses as protein cages

In the last 60 years, since the first published report described cowpea mosaic virus (CPMV), the virus has evolved to become one of the foremost intensely studied plant viruses [44]. Initially, the CPMV capsid was utilized to present peptides on its surface, and this has evolved to using the protein cage as a template for a broad range of applications, from metallization, mineralization, enzyme surface decoration, and therapeutics carrier, to clinical imaging tools [6, 7, 14–19]. CPMV belongs to the order *Picornavirales* and is a member of the Comoviridae family, a nonenveloped capsid with a positive-sense single-stranded RNA genome. The RNA is encapsidated separately (bipartite). The capsid is assembled in $T = 3$ symmetry from 60 copies of the asymmetric subunits to form a spherical structure of 30 nm. The encapsidation pattern gives rise to two slightly different densities upon the separation of the particles on cesium chloride or sucrose gradients.

Plant and animal viruses have been significantly reviewed, both through chemical and genetic manipulations. Therefore, due to limited chapter space, we have only highlighted some of the relevant and uncommon protein cages.

16.2.3 Qβ bacteriophage

Qβ-phage is one of the RNA phages that infect *Escherichia coli,* and it belongs to the *Leviviridae* family with an icosahedral capsid with $T = 3$ quasisymmetry. Qβ self-assembles from 180 coat protein subunits. In pentamers and hexamers, the Qß subunits are combined in an extraordinarily stoichiometric 12:20 ratio that differs from icosahedral symmetry, to form the full virion [45, 46].

16.3 Nonviral protein cages

16.3.1 Heat-shock proteins (Hsps)

Cells tend to produce more Hsps when they are under stress conditions, for example, cell exposure to high temperatures (168–169). For cells, Hsps are classified as chaperones that partially replenish cellular proteins and thus prevent physiological and environmental stresses from cellular bioavailability. One of the earliest examples used as a protein cage was the small heat-shock protein (sHsp) that was isolated from *Methanococcus jannaishii*. The sHsp protein is composed of 24 hollow devices of approximately 6.5 nm in diameter and an external 12 nm in diameter [47]. The assembled sHsp has eight pores, each of 3 nm in diameter, at the threefold symmetry axis, with an additional six pores (1.7 nm) with a diameter along the fourfold symmetry axis [48, 49].

16.3.2 Ferritin

Ferritins are abundant in animals, bacteria, and plants. The biomineralization $Fe_2{}^{+}$ to Fe_2O_3. H_2O involves the use of ferritins to store iron bioavailable in the cell. Ferritins play a pivotal role in regulation of the iron levels. Ferritin from mammalian origin consists of 24 protein subunits that assemble to form a spherical cage with an 8 nm internal cavity and 12 nm external dimensions. There are eight hydrophilic channels of 0.4 nm and 1.5 nm on the 3-fold symmetry axes connecting the inner and outer parts of the protein. Such channels are essential in the free movement of Fe^{2+} ions between the inside and the outside of the protein cage. Furthermore, ferritin possesses six hydrophobic channels that exist around the 4-fold symmetry axes.

16.3.3 Vault proteins (VPs)

VPs are known to exist only in higher eucaryotes as ribonucleoproteins [50]. The name is indicative of the particles' 3D barrel-like structure, which resembles a vaulted design. VPs have a size of 41×73 nm and an overall molecular mass of about 1.3×10^7 g mol^{-1} (vault poly(ADP ribose) polymerase and, therefore, the telomerase-associated protein 1 with the

RNA) [51]. VPs can self-assemble from 96 copies of a single protein (major protein with approximately 100 kDa) with a large hollow interior large enough to accommodate whole enzymes and abundant proteins. In mammalian cells, there are 10^4–10^6 VPs per cell.

Their precise function within the cell is not clear. However, some research shows that they may be playing a role in cellular shielding from toxins [50]. In addition, VPs have been utilized as a nanotemplate for drug delivery, in which VPs were used with the cell-penetrating peptide, TAT, to show an elevation in the binding and the uptake in an in vitro study [52]. C-termini of both the VPs have been altered with cell surface receptors to direct the cellular adhesion of the modified VPs to a HeLa cell surface receptor in vitro [53]. Furthermore, another research study utilized the chemical modification of surface-exposed amino acids (3354 lysine and 1092 cystines) dual surface modification for penetration and uptake studies [51].

16.3.3.1 Background and rationale

Protein cages are still seen as optimal building blocks in bionanotechnology as a consequence of their very well-defined geometries (monodispersed in both structure and composition), and their safety and nontoxicity, biodegradability, and metastability (chemical integrity in the cell, under laboratory conditions, or in different environments) [54–56].

16.3.3.2 Significance and selectivity

A significant challenge in the area of bioconjugation is that, in the presence of thousands competing for amino acid side chains of exposed proteins or macromolecules, the chemical reaction used must selectively alter the residual amino acids of significance. The selected reaction conditions must not affect the protein and must prevent the denaturation of or structural changes to the protein from causing function loss. Furthermore, the reaction condition must occur at near-neutral pH and at ambient temperature to eliminate protein degradation [57]. In addition, proteins are typically extracted in low quantities, and therefore the reaction must proceed very quickly to generate the desired product. The points mentioned here represent considerable challenges in protein modifications.

16.3.3.3 Chemical modification

Protein cages and their architectures have several copies of functional groups, which are mostly spatially dispersed across the structure. The required molecules of value may be paired with protein cages inside and outside. Some of the reported literature discusses the conjugation of a high number of contrast agents, drug molecules, and enzymes [7, 11, 58].

16.4 Residue-specific amino acid modification strategies

16.4.1 Lysine

Lysine is a crucial amino acid that carries protonated amine in a physiological pH and retains its reactivity. One of the simplest and easiest methods for amine functionalization is the use of N-hydroxysuccimide (NHS) esters. In such a reaction, NHS esters form an amide bond irreversibly in the presence of primary amine-containing molecules, which is shown in Fig. 16.2. The reagent isothiocyanates interact with the primary amines in the macromolecule/protein to determine the number of the primary amine in a given molecule by releasing thiourea quantitatively. However, the isothiocyanate reaction requires a pH range between 9 and 9.5,

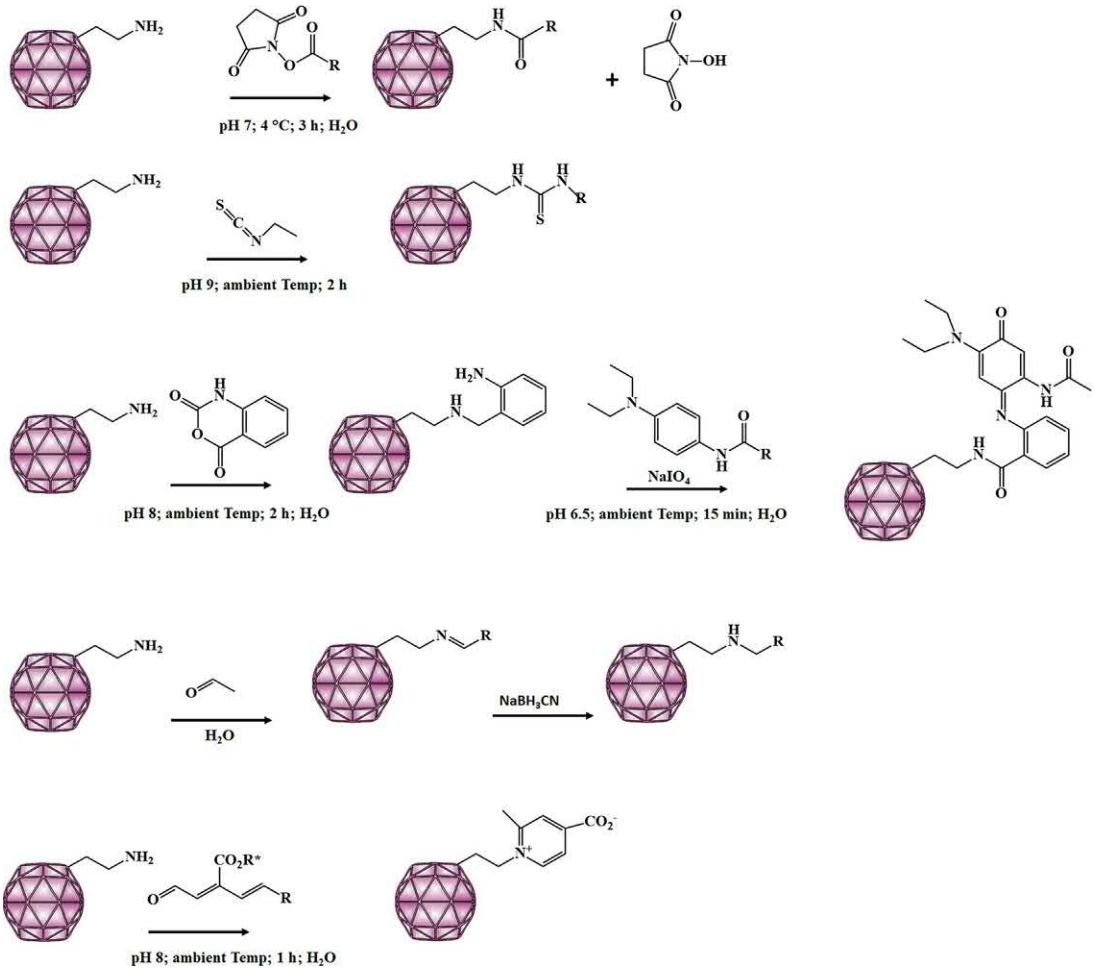
pH 7; 4 °C; 3 h; H2O
pH 9; ambient Temp; 2 h
pH 8; ambient Temp; 2 h; H2O
NaIO4
pH 6.5; ambient Temp; 15 min; H2O
H2O
NaBH3CN
pH 8; ambient Temp; 1 h; H2O

Fig. 16.2
Chemical conjugation of surface-exposed lysines.

which is a lot higher than the NHS ester at 8–9. The primary concern in such strategies is whether the elevated pH level affects protein structure and folding. Additionally, NHS-esters and isothiocyanate reactions are challenging to achieve in living cells, as the reaction of such chemicals to the first lysine may irreversibly release 1H-benzo[d][1,3]oxazine-2,4-dione, contributing to ortho-aminobenzamide formation [59]. Hooker and colleagues identified a different strategy to change lysine protein primarily with sodium periodate salt ($NaIO_4$) [60]. Furthermore, an imine or Schiff base was utilized for the labeling of the protein N-terminus and the surface-exposed lysines [61].

The early reports of lysine manipulation are the mixture from the PEG chain with the surface of μ bacteriophages to attack transmitting receptors, often overexpressed in various lines of human cancer [62–64].

16.4.2 Carboxyl

The existence of glutamate, aspartate, C-terminus of proteins is one of the main strategies in protein bioconjugation [65]. This technique is fundamental but relies upon stimulating the groups of carboxylates on the protein surface of an ester that is conjugated to molecules that produce amide by forming a bond. The process profits from the use of water-soluble reagents, including N-ethyl-3-*N*-dimethyl aminopropyl carbodiimide (EDC), as shown in Fig. 16.3. The EDC reagent is not stable, regardless of the reaction pH [66]. To stabilize this reaction, an NHS reagent is used to form a stable ester, which will rapidly react with amine-containing moieties.

16.4.3 Cystine

Cystine is considered one of the most convenient targets for protein modification. The sulfhydryl side chain of cysteine is considered an active nucleophilic moiety. Generally speaking, cystines are some of the lowest abundant surface-exposed amino acids [67]. Cysteine is a more nucleophilic moiety in comparison to the primary amines, and this allows selective modifications of cystines over lysines [59]. However, surface-exposed cysteines are rarely present on the exterior of the proteins, as they embed their side chain within the hydrophobic region of the protein. For example, once cysteines are on the surface of exposed proteins, this contributes to the forming of disulfide associations and ultimately to protein aggregation (agglomeration). This scheme is vital for protein stabilization. Maleimide chemistries are some of the most common approaches to labeling the side chain of cysteine, as they selectively react with the thiol group. The maleimide reaction is stable under physiological conditions, while lysines fail to react and the same reaction conditions. Thiols are recognized in oxidative terms to create disulfide ties. This oxidative reaction is involved in the cystine-cystine equilibrium, which is pivotal in the configuration of the 3D structure of the proteins, as the reaction conditions are very mild and do not affect the structural stability. The reaction is reversible and can be achieved through the addition of mercaptoethanol or dithiothreitol to decouple the disulfide bond, as shown in Fig. 16.4 [68].

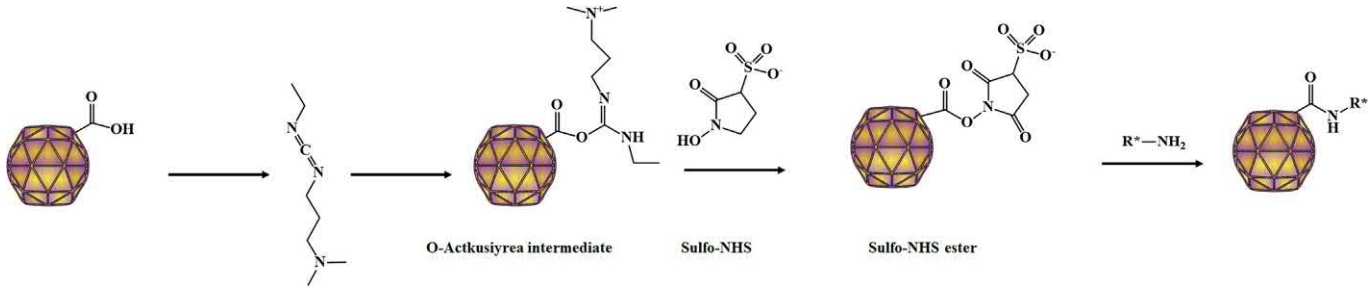

Fig. 16.3
Chemical conjugation of carboxy-terminated amino acids.

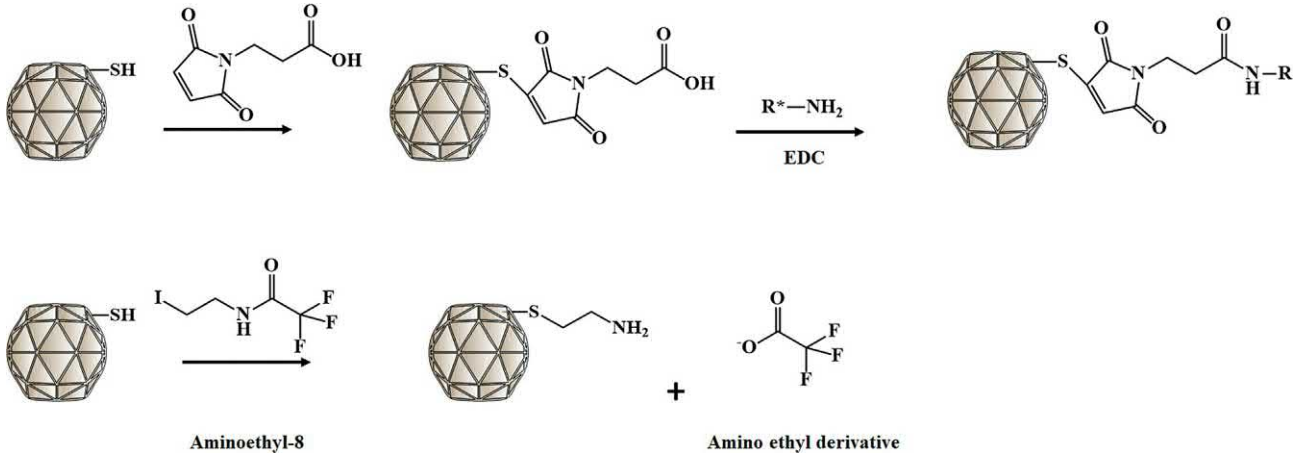

Fig. 16.4
Chemical modification of surface/internal modification of cystines.

In 1935, keratin was one of the earliest proteins to be modified; the surface-exposed cysteine was modified with iodoacetamide as reaction reagent [69].

Furthermore, terminal cysteines of papain, a proteolytic enzyme, were modified by Clark and Lowe using an α-bromoacetophenone reagent to alkylate cystines, which in turn were reduced to glycine and serine [70]. The same approach of α-bromoacetophenone was used for the conjugation of flavin to the accessible cystine of papain [70–72]. Several colorimetric procedures have been reported in the literature for estimating the number of thiol groups in any protein. This is due to the ease of oxidation of the sulfhydryl side chain using, for example, 5,5′-dithiobis(2-nitrobenzoic acid) (DTNB), commonly referred to as Ellman's reagent [73]. The colored thionitrobenzoate anion was released as each thiol group reacted with DTNB and was measured spectrophotometrically at λ_{412} nm with $\varepsilon = 1.36 \times 10^4\ M^{-1}\ cm^{-1}$ at pH 8 [74].

The ability to conjugate molecules of interest to the native cysteine through the formation of sulfur-sulfur bonds can be exploited to engineer new functionalities. Some of the significant chemistries that have been reported in the literature are the use of an aminomethylation reaction [75–77], iodoacetamide [78], and maleimides [79, 80].

16.4.4 Tyrosines

The phenol group of the nitrogen-containing tyrosine's was modified using diazonium salts. Even though the reaction was established for the synthesis of azo compounds in the pigment industries. The conversion of the azo bond into aniline occurred via the reduction cycle and the intermediates were converted into stable benzocaine with just a substituted acrylamide. This reaction was utilized to modify 180 tyrosine residues from the interior capsid of the bacteriophage MS2 [81].

Alternatively, ketone-derived aryl diazonium salts were used to generate stable oxime ethers, as shown in Fig. 16.5. This approach was used to modify surface-exposed tobacco mosaic virus [82]. A Mannich three-component approach was also utilized for tyrosine side chain modification with high selectivity of tyrosines. The reaction conditions were mild with low concentrations of the reagents and the reaction was carried out at a pH between 5.5 and 6.5. The surfaces of tyrosines, lysozymes, and chymotrypsinogen A were adjusted successfully. The same strategy struggled to change the tyrosine levels in horse myoglobin, as it was embedded widely in the protein [83]. Also, tyrosines were used to examine protein-protein interactions in which the phenol group was oxidized to produce a reactive tyrosyl radical. This radical was subsequently reacted with nucleophile present on the second protein within the spatial vicinity of amino acids, such as cysteine or a tyrosine [84].

16.4.5 Arginine

Arginine modification is based on the reaction of two of guanine's three nitrogens into the ring so that the reaction reagents can thoroughly make pyrimidine [84a]. Although a reaction with the arginine side chain is possible, the reaction time is lengthy, and the reactions require

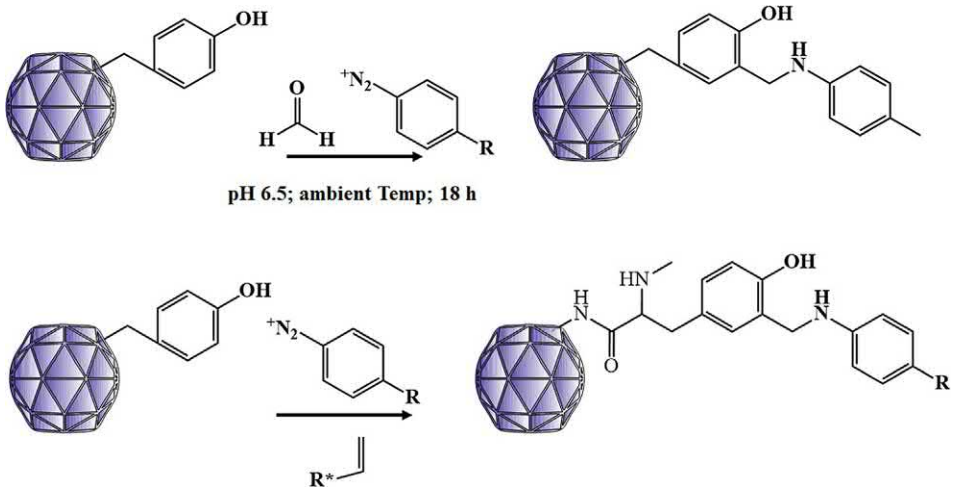

Fig. 16.5
Chemical conjugation of surface-exposed tyrosines.

100 mM concentrations at 37°C in phosphate buffer pH 7.4. Surface-exposed arginines of the bovine serum albumin proved that this reaction can be used selectively to modify surface-exposed arginine. However, the reaction took 14 days for completion, which makes it challenging to apply the approach to live cells.

16.4.6 Tryptophan

Some of the most common approaches adopted for tryptophan modification are through photooxidation, iodination, ozonization or the use of N-bromosuccinimide chemistries. One of the best-known reactions of tryptophan in proteins is with 2-hydroxynitrobenzyl bromide (HNBB) to generate colored products. The HNBB reaction is reported to be limited to tryptophan and cysteine residues [85, 86]. Furthermore, it has been reported that tryptophan residues can be converted to a l-formyl derivative in anhydrous formic acid that is saturated with gaseous HCl, with no effect or destruction of the native protein form [87]. Tryptophan oxidation was thoroughly reviewed in the literature, examining various reaction conditions, and the biological consequences were elaborated [88, 89].

16.4.7 Methionine

The alkylation of proteins with α-halocids or methyl iodide has developed three significant chemicals to modify methionine; (a) low-temperature photo-sensitized acetic acid photo-photooxidation (b) mild oxidation [90, 91]. Furthermore, a relatively new approach has been

reported to target methionine selectively using redox-based methods, known as ReACT, for the chemoselectivity of the reaction, which has been utilized to label in vivo antibodies precisely [92].

16.5 Nanoparticles targeted for drug delivery

Free and unencapsulated chemical therapeutics have low pharmacokinetic profiles and a nonspecific distribution in the human body, often leading to systemic toxic and adverse consequences [93]. Consequently, a substantial focus is now being placed on the practical and realistic implementation of these chemotherapeutic agents, utilizing drug delivery mechanisms to improve the concentration of the active drug in its targeted tumor site.

The success of any nanoparticle delivery system will depend on its ability to be accumulated into the targeted diseased tissues and avoid unwanted distribution into the healthy tissues. This is of great importance when dealing with toxic therapeutic agents, such as chemotherapeutic agents [94, 95]. The ability to direct a specific drug into its target using a nanocarrier will not only reduce the drug's side effects but also will ensure that the drug is available at the target site for the required duration and at the required concentration to ensure the best therapeutic outcomes. Therefore, the use of nanomaterials will improve the pharmacokinetics and pharmacodynamics characteristics of the encapsulated drug. This will enable the formulation of a controlled release profile, improving the specificity of the encapsulated drug toward the cancer cells and enhancing the cellular uptake of the drug into the intracellular matrices [96, 97].

In the scope of the drug target, dual types of drug targeting could be achieved using nanocarriers: active and passive targeting. Both active and passive drug targeting nanoparticle delivery systems to cancer tissues may help to improve drug accumulation at the target location, improve therapeutic efficacy, improve the delivery of poorly water-soluble drugs, and reduce drug accumulation at the target site.

16.5.1 Passive targeting

Diseased tissues, such as a tumor or inflamed tissues, usually have specific changes in their pathophysiology resulting in the formation of leaky blood vessels and widening of the tight endothelial junctions [98]. This enhances the penetration of larger molecules in a variety of sizes between 100 and 200 nm to the diseased tissues, which at the same time cannot penetrate the healthy tissues with the normal tight junctions that have limited permeability to molecules within this size range [99]. Moreover, tumor tissues also have a limited lymphatic drainage system, which reduces the alimentation rate of any molecule in these tissues [98]. Such pathophysiologic improvements allow the passive aggregation and persistence of nanoparticles inside the tumor or diseased tissues and prevent tissue protection when using a nanoparticle that is 100–200 nm for the distribution of therapeutic agents. This forms the concept of the enhanced

permeability and retention (EPR) phenomena on which the passive targeting of nanoparticle delivery systems is based [100, 101]. Several researchers have developed drug delivery models based on passive targeting. In a work by Obeid et al., niosome nanoparticles were created for the delivery of short interfering RNA (siRNA) to a cancer cell melanoma model. In this work, the average particle size was around 60 nm and the formulation was able to successfully deliver the loaded siRNA in vivo in mouse models [102].

16.5.2 Active targeting

The design of nanoparticles based on passive targeting ensures the accumulation of these carriers of the loaded drug in the diseased tissues, without any specificity of binding to a specific target or receptor. However, these nanocarriers have an exciting feature that allows their outer surfaces to be modified or decorated with certain ligands, which can distinguish and bind to specific overexpressed markers on the surface of the diseased cells. This approach is referred to as active targeting of the nanocarriers. Active targeting enhances the selectivity of the nanoparticles with the loaded drug for specific cells or tissues. Tumor cells have certain receptors that are overexpressed on their surfaces to meet their needs for a high rate of multiplication and growth. Designing an NP-based formulation with active targeting starts by studying the target tissue and detaining the type of overexpressed receptors on the surface of the target cells. Then the ligand that will be explicitly bound to these receptors is determined and attached to the surface of the nanoparticles that are loaded with the drug to be delivered. Different types of ligands can be used in the active targeting approach, such as monoclonal antibodies, small molecules such as folic acid and peptides, and proteins such as transferrin (TF) and aptamers [99]. Some of the most widely studied surface receptors for successful transmission of nanomaterials to cancer cells are TF receptors, folate receptors, epidermal factor development receptors, and cell surface glycoproteins [93, 102, 103]. Karim et al. has developed a multilamellar vesicle for the delivery of tocotrienol using transferrin as an active targeting moiety, and they were able to achieve significant tumor suppression without visible toxicity in mouse models with B16-F10 tumor [104].

16.5.3 Advantages and disadvantages

One of the significant challenges in protein alteration is that hundreds to thousands of amino acid side chains of the protein cage or macromolecules during reaction can selectively manage the reactions. Such selectivity may occur under mild conditions, to preserve the 3D protein architect at low levels of reagents and near physiological pH [46, 71].

16.5.4 Applications

Protein modification and engineering have led the development of some of the applications that are listed in this section, although these are only a few examples. Protein microarrays are driven by the ability to immobilize a protein on a reliable support (mica, gold, or commercial chips). Protein microarrays are essential in drug development and pharmaceutical applications, in which they select the molecules from a library and find out which molecules bind selectively with the protein of interest. The majority of enzyme inhibitors are discovered through this method. Some of the protein arrays developed in this area measure the levels of protein expression in a given cell or tissue; a cellular lysate is added to the protein array for subsequent detection of fluorescently labeled antibodies.

Protein surface modifications have allowed the study of some of the complex processes of posttranslational modifications (PTM). To this end, oligosaccharides or oligonucleotides were chemically incorporated into proteins. For example, bovine hemoglobin glycosylation (Hb) took place through lactose derivative conjugation into cystine 93 Hb [105]. Another active research region for protein alteration through the application of carbohydrates on protein surfaces is cancer vaccines through reductive amination. The Mannich reaction was utilized for the conjugation of peptides to the N-termini using the tyrosine amino acid. This approach enhanced protection against cellular enzymatic hydrolysis [106].

References

[1] K. Renggli, P. Baumann, K. Langowska, O. Onaca, N. Bruns, W. Meier, Selective and responsive nanoreactors, Adv. Funct. Mater. 21 (7) (2011) 1241–1259.
[2] R. Indra, T. Cerna, Z. Heger, J. Hrabeta, M. Wilhelm, S. Dostalova, A. Lengalova, M. Martinkova, V. Adam, T. Eckschlager, H.H. Schmeiser, V.M. Arlt, M. Stiborova, Ellipticine-loaded apoferritin nanocarrier retains DNA adduct-based cytochrome P450-facilitated toxicity in neuroblastoma cells, Toxicology 419 (2019) 40–54.
[3] A.I. Kuruppu, L. Zhang, H. Collins, L. Turyanska, N.R. Thomas, T.D. Bradshaw, An Apoferritin-based drug delivery system for the tyrosine kinase inhibitor Gefitinib, Adv. Healthc. Mater. 4 (18) (2015) 2816–2821.
[4] E.M. Fonseca, V. Scorsato, M.L. Dos Santos, A.T. Junior, S.F. Tada, C.A. Dos Santos, M.A. de Toledo, A. P. de Souza, I. Polikarpov, R. Aparicio, Crystal structure of a small heat-shock protein from Xylella fastidiosa reveals a distinct high-order structure, Acta Crystallogr. F Struct. Biol. Commun. 73 (Pt 4) (2017) 222–227.
[5] C.M. Teschke, A. McGough, P.A. Thuman-Commike, Penton release from P22 heat-expanded capsids suggests importance of stabilizing penton-hexon interactions during capsid maturation, Biophys. J. 84 (4) (2003) 2585–2592.
[6] A.A. Aljabali, F. Sainsbury, G.P. Lomonossoff, D.J. Evans, Cowpea mosaic virus unmodified empty virus like particles loaded with metal and metal oxide, Small 6 (7) (2010) 818–821.
[7] A.A. Aljabali, S. Shukla, G.P. Lomonossoff, N.F. Steinmetz, D.J. Evans, CPMV-DOX delivers, Mol. Pharm. 10 (1) (2013) 3–10.
[8] A.A.A. Aljabali, D.J. Evans, Internal deposition of cobalt metal and iron oxide within CPMV eVLPs, Methods Mol. Biol. 1776 (2018) 189–201.

[9] S. Abe, J. Niemeyer, M. Abe, Y. Takezawa, T. Ueno, T. Hikage, G. Erker, Y. Watanabe, Control of the coordination structure of organometallic palladium complexes in an apo-ferritin cage, J. Am. Chem. Soc. 130 (32) (2008) 10512–10514.
[10] R.M. Putri, J.J. Cornelissen, M.S. Koay, Self-assembled cage-like protein structures, ChemPhysChem 16 (5) (2015) 911–918.
[11] A.A. Aljabali, J.E. Barclay, N.F. Steinmetz, G.P. Lomonossoff, D.J. Evans, Controlled immobilisation of active enzymes on the cowpea mosaic virus capsid, Nanoscale 4 (18) (2012) 5640–5645.
[12] S. Stefanini, S. Cavallo, C.Q. Wang, P. Tataseo, P. Vecchini, A. Giartosio, E. Chiancone, Thermal stability of horse spleen apoferritin and human recombinant H apoferritin, Arch. Biochem. Biophys. 325 (1) (1996) 58–64.
[13] I. Listowsky, G. Blauer, S. Enlard, J.J. Betheil, Denaturation of horse spleen ferritin in aqueous guanidinium chloride solutions, Biochemistry 11 (11) (1972) 2176–2182.
[14] A.A. Aljabali, J.E. Barclay, J.N. Butt, G.P. Lomonossoff, D.J. Evans, Redox-active ferrocene-modified cowpea mosaic virus nanoparticles, Dalton Trans. 39 (32) (2010) 7569–7574.
[15] A.A. Aljabali, J.E. Barclay, G.P. Lomonossoff, D.J. Evans, Virus templated metallic nanoparticles, Nanoscale 2 (12) (2010) 2596–2600.
[16] A.A. Aljabali, D.J. Evans, Polyelectrolyte-modified cowpea mosaic virus for the synthesis of gold nanoparticles, Methods Mol. Biol. 1108 (2014) 97–103.
[17] A.A. Aljabali, D.J. Evans, Templated mineralization by charge-modified cowpea mosaic virus, Methods Mol. Biol. 1108 (2014) 89–95.
[18] A.A. Aljabali, G.P. Lomonossoff, D.J. Evans, CPMV-polyelectrolyte-templated gold nanoparticles, Biomacromolecules 12 (7) (2011) 2723–2728.
[19] A.A. Aljabali, S.N. Shah, R. Evans-Gowing, G.P. Lomonossoff, D.J. Evans, Chemically-coupled-peptide-promoted virus nanoparticle templated mineralization, Integr. Biol. 3 (2) (2011) 119–125.
[20] E.C. Theil, Ferritin: the protein nanocage and iron biomineral in health and in disease, Inorg. Chem. 52 (21) (2013) 12223–12233.
[21] L.H. Rome, V.A. Kickhoefer, Development of the vault particle as a platform technology, ACS Nano 7 (2) (2013) 889–902.
[22] C. Dekker, K.R. Willison, W.R. Taylor, On the evolutionary origin of the chaperonins, Proteins 79 (4) (2011) 1172–1192.
[23] A.L. Horwich, W.A. Fenton, E. Chapman, G.W. Farr, Two families of chaperonin: physiology and mechanism, Annu. Rev. Cell Dev. Biol. 23 (2007) 115–145.
[24] H. Bausinger, D. Lipsker, D. Hanau, Heat-shock proteins as activators of the innate immune system, Trends Immunol. 23 (7) (2002) 342–343.
[25] H. Singh-Jasuja, N. Hilf, D. Arnold-Schild, H. Schild, The role of heat shock proteins and their receptors in the activation of the immune system, Biol. Chem. 382 (4) (2001) 629–636.
[26] M.F. Tsan, B. Gao, Heat shock proteins and immune system, J. Leukoc. Biol. 85 (6) (2009) 905–910.
[27] H. Moon, J. Lee, J. Min, S. Kang, Developing genetically engineered encapsulin protein cage nanoparticles as a targeted delivery nanoplatform, Biomacromolecules 15 (10) (2014) 3794–3801.
[28] R. Rahmanpour, T.D. Bugg, Assembly in vitro of Rhodococcus jostii RHA1 encapsulin and peroxidase DypB to form a nanocompartment, FEBS J. 280 (9) (2013) 2097–2104.
[29] J.L. Corchero, J. Cedano, Self-assembling, protein-based intracellular bacterial organelles: emerging vehicles for encapsulating, targeting and delivering therapeutical cargoes, Microb. Cell Factories 10 (2011) 92.
[30] M.C. Thompson, C.S. Crowley, J. Kopstein, T.A. Bobik, T.O. Yeates, Structure of a bacterial microcompartment shell protein bound to a cobalamin cofactor, Acta Crystallogr. F Struct. Biol. Commun. 70 (Pt 12) (2014) 1584–1590.
[31] K. Namba, G. Stubbs, Structure of tobacco mosaic virus at 3.6 A resolution: implications for assembly, Science 231 (4744) (1986) 1401–1406.
[32] C.G. Sonwane, Q. Li, Guest-host encapsulation of microporous zeolites in ordered mesoporous materials by molecular simulations, Phys. Chem. Chem. Phys. 7 (19) (2005) 3501–3506.

[33] S. Tomaselli, U. Giovanella, K. Pagano, G. Leone, S. Zanzoni, M. Assfalg, F. Meinardi, H. Molinari, C. Botta, L. Ragona, Encapsulation of a rhodamine dye within a bile acid binding protein: toward water processable functional bio host-guest materials, Biomacromolecules 14 (10) (2013) 3549–3556.
[34] K. Valegard, L. Liljas, K. Fridborg, T. Unge, The three-dimensional structure of the bacterial virus MS2, Nature 345 (6270) (1990) 36–41.
[35] H. Liu, L. Jin, S.B. Koh, I. Atanasov, S. Schein, L. Wu, Z.H. Zhou, Atomic structure of human adenovirus by cryo-EM reveals interactions among protein networks, Science 329 (5995) (2010) 1038–1043.
[36] E.N. Banadda, I.Y. Smets, R. Jenne, J.F. Van Impe, Predicting the onset of filamentous bulking in biological wastewater treatment systems by exploiting image analysis information, Bioprocess Biosyst. Eng. 27 (5) (2005) 339–348.
[37] J.N. Culver, A.D. Brown, F. Zang, M. Gnerlich, K. Gerasopoulos, R. Ghodssi, Plant virus directed fabrication of nanoscale materials and devices, Virology 479-480 (2015) 200–212.
[38] G. Stephanopoulos, H. Alper, J. Moxley, Exploiting biological complexity for strain improvement through systems biology, Nat. Biotechnol. 22 (10) (2004) 1261–1267.
[39] R. McKenna, D. Xia, P. Willingmann, L.L. Ilag, S. Krishnaswamy, M.G. Rossmann, N.H. Olson, T. S. Baker, N.L. Incardona, Atomic structure of single-stranded DNA bacteriophage phi X174 and its functional implications, Nature 355 (6356) (1992) 137–143.
[40] D. Arslan, M. Legendre, V. Seltzer, C. Abergel, J.M. Claverie, Distant Mimivirus relative with a larger genome highlights the fundamental features of Megaviridae, Proc. Natl. Acad. Sci. U. S. A. 108 (42) (2011) 17486–17491.
[41] C. Xiao, M.G. Rossmann, Structures of giant icosahedral eukaryotic dsDNA viruses, Curr. Opin. Virol. 1 (2) (2011) 101–109.
[42] J.A. Prescher, D.H. Dube, C.R. Bertozzi, Chemical remodelling of cell surfaces in living animals, Nature 430 (7002) (2004) 873–877.
[43] H. Cho, T. Daniel, Y.J. Buechler, D.C. Litzinger, Z. Maio, A.M. Putnam, V.S. Kraynov, B. C. Sim, S. Bussell, T. Javahishvili, S. Kaphle, G. Viramontes, M. Ong, S. Chu, G. C. Becky, R. Lieu, N. Knudsen, P. Castiglioni, T.C. Norman, D.W. Axelrod, A.R. Hoffman, P.G. Schultz, R. D. DiMarchi, B.E. Kimmel, Optimized clinical performance of growth hormone with an expanded genetic code, Proc. Natl. Acad. Sci. U. S. A. 108 (22) (2011) 9060–9065.
[44] A.A.A. Aljabali, A. Berardi, D.J. Evans, Nature's nanoparticles: using viruses as nanomedicines and for bioimaging, in: A. Barhoum, A.S.H. Makhlouf (Eds.), Fundamentals of Nanoparticles, Elsevier, 2018, pp. 29–50 (Chapter 2).
[45] R. Golmohammadi, K. Fridborg, M. Bundule, K. Valegard, L. Liljas, The crystal structure of bacteriophage Q beta at 3.5 A resolution, Structure 4 (5) (1996) 543–554.
[46] R.L.C. Leung, M.D.M. Robinson, A.A. A. Ajabali, G. Karunanithy, B. Lyons, R. Raj, S. Raoufmoghaddam, S. Mohammed, T.D.W. Claridge, A. J. Baldwin, B.G. Davis, Monitoring the disassembly of virus-like particles by (19)F-NMR, J. Am. Chem. Soc. 139 (15) (2017) 5277–5280.
[47] K.K. Kim, H. Yokota, S. Santoso, D. Lerner, R. Kim, S.H. Kim, Purification, crystallization, and preliminary X-ray crystallographic data analysis of small heat shock protein homolog from Methanococcus jannaschii, a hyperthermophile, J. Struct. Biol. 121 (1) (1998) 76–80.
[48] M.L. Flenniken, L.O. Liepold, B.E. Crowley, D.A. Willits, M.J. Young, T. Douglas, Selective attachment and release of a chemotherapeutic agent from the interior of a protein cage architecture, Chem. Commun. (Camb.) (4) (2005) 447–449.
[49] K.R. Krishnapriya, M. Kandaswamy, Synthesis and characterization of a crosslinked chitosan derivative with a complexing agent and its adsorption studies toward metal(II) ions, Carbohydr. Res. 344 (13) (2009) 1632–1638.
[50] M. Rother, M.G. Nussbaumer, K. Renggli, N. Bruns, Protein cages and synthetic polymers: a fruitful symbiosis for drug delivery applications, bionanotechnology and materials science, Chem. Soc. Rev. 45 (22) (2016) 6213–6249.

[51] N.L. Benner, X. Zang, D.C. Buehler, V.A. Kickhoefer, M.E. Rome, L.H. Rome, P.A. Wender, Vault nanoparticles: chemical modifications for imaging and enhanced delivery, ACS Nano 11 (1) (2017) 872–881.
[52] J. Yang, A. Srinivasan, Y. Sun, J. Mrazek, Z. Shu, V.A. Kickhoefer, L.H. Rome, Vault nanoparticles engineered with the protein transduction domain, TAT48, enhances cellular uptake, Integr. Biol. (Camb.) 5 (1) (2013) 151–158.
[53] V.A. Kickhoefer, M. Han, S. Raval-Fernandes, M.J. Poderycki, R.J. Moniz, D. Vaccari, M. Silvestry, P. L. Stewart, K.A. Kelly, L.H. Rome, Targeting vault nanoparticles to specific cell surface receptors, ACS Nano 3 (1) (2009) 27–36.
[54] J.G. Heddle, Protein cages, rings and tubes: useful components of future nanodevices? Nanotechnol. Sci. Appl. 1 (2008) 67–78.
[55] C.R. Kaiser, M.L. Flenniken, E. Gillitzer, A.L. Harmsen, A.G. Harmsen, M.A. Jutila, T. Douglas, M. J. Young, Biodistribution studies of protein cage nanoparticles demonstrate broad tissue distribution and rapid clearance in vivo, Int. J. Nanomedicine 2 (4) (2007) 715–733.
[56] N.M. Molino, S.W. Wang, Caged protein nanoparticles for drug delivery, Curr. Opin. Biotechnol. 28 (2014) 75–82.
[57] F. Perez-Balderas, S.I. van Kasteren, A.A. Aljabali, K. Wals, S. Serres, A. Jefferson, M. Sarmiento Soto, A. A. Khrapitchev, J.R. Larkin, C. Bristow, S.S. Lee, G. Bort, F. De Simone, S.J. Campbell, R.P. Choudhury, D. C. Anthony, N.R. Sibson, B.G. Davis, Covalent assembly of nanoparticles as a peptidase-degradable platform for molecular MRI, Nat. Commun. 8 (2017) 14254.
[58] A.A.A. Aljabali, E. Hussein, O. Aljumaili, M.A. Zoubi, B. Altrad, K. Albatayneh, M.A. Abd Al-razaq, Rapid magnetic Nanobiosensor for the detection of Serratia marcescen, IOP Conf. Ser. Mater. Sci. Eng. 305 (2018) 012005.
[59] E. Basle, N. Joubert, M. Pucheault, Protein chemical modification on endogenous amino acids, Chem. Biol. 17 (3) (2010) 213–227.
[60] J.M. Hooker, A.P. Esser-Kahn, M.B. Francis, Modification of aniline containing proteins using an oxidative coupling strategy, J. Am. Chem. Soc. 128 (49) (2006) 15558–15559.
[61] Y. Tanaka, J.J. Kohler, Photoactivatable crosslinking sugars for capturing glycoprotein interactions, J. Am. Chem. Soc. 130 (11) (2008) 3278–3279.
[62] T.R. Daniels, E. Bernabeu, J.A. Rodriguez, S. Patel, M. Kozman, D.A. Chiappetta, E. Holler, J. Y. Ljubimova, G. Helguera, M.L. Penichet, The transferrin receptor and the targeted delivery of therapeutic agents against cancer, Biochim. Biophys. Acta 1820 (3) (2012) 291–317.
[63] C. Dufes, M. Al Robaian, S. Somani, Transferrin and the transferrin receptor for the targeted delivery of therapeutic agents to the brain and cancer cells, Ther. Deliv. 4 (5) (2013) 629–640.
[64] K.J. Koudelka, S. Ippoliti, E. Medina, L.P. Shriver, S.A. Trauger, C.E. Catalano, M. Manchester, Lysine addressability and mammalian cell interactions of bacteriophage lambda procapsids, Biomacromolecules 14 (12) (2013) 4169–4176.
[65] A.A.A. Aljabali, M.S.A. Zoubi, K.M. Al-Batanyeh, A. Al-Radaideh, M.A. Obeid, A. Al Sharabi, W. Alshaer, B. Abu Fares, T. Al-Zanati, M.M. Tambuwala, N. Akbar, D.J. Evans, Gold-coated plant virus as computed tomography imaging contrast agent, Beilstein J. Nanotechnol. 10 (2019) 1983–1993.
[66] M.A. Gilles, A.Q. Hudson, C.L. Borders Jr., Stability of water-soluble carbodiimides in aqueous solution, Anal. Biochem. 184 (2) (1990) 244–248.
[67] M.N. Fodje, S. Al-Karadaghi, Occurrence, conformational features and amino acid propensities for the pi-helix, Protein Eng. 15 (5) (2002) 353–358.
[68] J.M. Chalker, Y.A. Lin, O. Boutureira, B.G. Davis, Enabling olefin metathesis on proteins: chemical methods for installation of S-allyl cysteine, Chem. Commun. (Camb.) (25) (2009) 3714–3716.
[69] D.R. Goddard, L. Michaelis, Derivatives of keratin, J. Biol. Chem. 112 (1) (1935) 361–371.
[70] P.I. Clark, G. Lowe, Chemical mutations of papain. The preparation of ser 25- and gly 25-papain, J. Chem. Soc. Chem. Commun. (24) (1977) 923–924.
[71] J.M. Chalker, G.J. Bernardes, Y.A. Lin, B.G. Davis, Chemical modification of proteins at cysteine: opportunities in chemistry and biology, Chem. Asian J. 4 (5) (2009) 630–640.

[72] E.T. Kaiser, D.S. Lawrence, Chemical mutation of enzyme active sites, Science 226 (4674) (1984) 505–511.
[73] G.L. Ellman, Tissue sulfhydryl groups, Arch. Biochem. Biophys. 82 (1) (1959) 70–77.
[74] A.S. Nashef, D.T. Osuga, R.E. Feeney, Determination of hydrogen sulfide with 5,5′-dithiobis-(2-nitrobenzoic acid), N-ethylmaleimide, and parachloromercuribenzoate, Anal. Biochem. 79 (1–2) (1977) 394–405.
[75] C. Chatterjee, T.W. Muir, Chemical approaches for studying histone modifications, J. Biol. Chem. 285 (15) (2010) 11045–11050.
[76] M.D. Simon, F. Chu, L.R. Racki, C.C. de la Cruz, A.L. Burlingame, B. Panning, G.J. Narlikar, K. M. Shokat, The site-specific installation of methyl-lysine analogs into recombinant histones, Cell 128 (5) (2007) 1003–1012.
[77] M.D. Simon, Installation of site-specific methylation into histones using methyl lysine analogs, Curr. Protoc. Mol. Biol. (2010) Chapter 21: Unit 21 18 21-10.
[78] N. Lundell, T. Schreitmuller, Sample preparation for peptide mapping—a pharmaceutical quality-control perspective, Anal. Biochem. 266 (1) (1999) 31–47.
[79] J.E. Moore, W.H. Ward, Cross-linking of bovine plasma albumin and wool keratin, J. Am. Chem. Soc. 78 (11) (1956) 2414–2418.
[80] M.E. Smith, F.F. Schumacher, C.P. Ryan, L.M. Tedaldi, D. Papaioannou, G. Waksman, S. Caddick, J. R. Baker, Protein modification, bioconjugation, and disulfide bridging using bromomaleimides, J. Am. Chem. Soc. 132 (6) (2010) 1960–1965.
[81] J.M. Hooker, E.W. Kovacs, M.B. Francis, Interior surface modification of bacteriophage MS2, J. Am. Chem. Soc. 126 (12) (2004) 3718–3719.
[82] T.L. Schlick, Z. Ding, E.W. Kovacs, M.B. Francis, Dual-surface modification of the tobacco mosaic virus, J. Am. Chem. Soc. 127 (11) (2005) 3718–3723.
[83] N. Jentoft, D.G. Dearborn, Protein labeling by reductive alkylation, Methods Enzymol. 91 (1983) 570–579.
[84] S. Adhikari, Y. Xia, S.A. McLuckey, Top-down analysis of disulfide-linked proteins using photoinduced radical reactions and ET-DDC, Int. J. Mass Spectrom. 444 (2019) 116173–116180.
[84a] T. Oya, N. Hattori, Y. Mizuno, S. Miyata, S. Maeda, T. Osawa, K. Uchida, Methylglyoxal modification of protein chemical and immunochemical characterization of methylglyoxal-arginine adducts, J. Biol. Chem. 274 (26) (1999) 18492–18502.
[85] H.R. Horton, W.P. Tucker, Dimethyl(2-hydroxy-5-nitrobenzyl)sulfonium salts. Water-soluble environmentally sensitive protein reagents, J. Biol. Chem. 245 (13) (1970) 3397–3401.
[86] A.K. Nagaich, K. Misra, Highly efficient synthesis of oligodeoxyribonucleotides using alpha-phenyl cinnamoyl group for selective amino protection, Nucleic Acids Res. 17 (13) (1989) 5125–5134.
[87] A. Previero, M.A. Coletti-Previero, J.C. Cavadore, A reversible chemical modification of the tryptophan residue, Biochim. Biophys. Acta 147 (3) (1967) 453–461.
[88] M.J. Davies, R.J. Truscott, Photo-oxidation of proteins and its role in cataractogenesis, J. Photochem. Photobiol. B 63 (1–3) (2001) 114–125.
[89] M. Ehrenshaft, L.J. Deterding, R.P. Mason, Tripping up Trp: modification of protein tryptophan residues by reactive oxygen species, modes of detection, and biological consequences, Free Radic. Biol. Med. 89 (2015) 220–228.
[90] G. Jori, G. Galiazzo, A. Marzotto, E. Scoffone, Dye-sensitized selective photooxidation of methionine, Biochim. Biophys. Acta 154 (1) (1968) 1–9.
[91] C. Lockhart, A.K. Smith, D.K. Klimov, Methionine oxidation changes the mechanism of Abeta peptide binding to the DMPC bilayer, Sci. Rep. 9 (1) (2019) 5947.
[92] S. Lin, X. Yang, S. Jia, A.M. Weeks, M. Hornsby, P.S. Lee, R.V. Nichiporuk, A.T. Iavarone, J.A. Wells, F. D. Toste, C.J. Chang, Redox-based reagents for chemoselective methionine bioconjugation, Science 355 (6325) (2017) 597–602.
[93] M.A. Obeid, I. Khadra, A. Albaloushi, M. Mullin, H. Alyamani, V.A. Ferro, Microfluidic manufacturing of different niosomes nanoparticles for curcumin encapsulation: physical characteristics, encapsulation efficacy, and drug release, Beilstein J. Nanotechnol. 10 (1) (2019) 1826–1832.

[94] A.A.A. Aljabali, Y. Akkam, M.S. Al Zoubi, K.M. Al-Batayneh, B. Al-Trad, O. Abo Alrob, A. M. Alkilany, M. Benamara, D.J. Evans, Synthesis of gold nanoparticles using leaf extract of Ziziphus zizyphus and their antimicrobial activity, Nanomaterials (Basel) 8 (3) (2018) 174–190.
[95] M.A. Obeid, A.M. Gebril, R.J. Tate, A.B. Mullen, V.A. Ferro, Comparison of the physical characteristics of monodisperse non-ionic surfactant vesicles (NISV) prepared using different manufacturing methods, Int. J. Pharm. 521 (1–2) (2017) 54–60.
[96] H. Alyamani, M.A. Obeid, R.J. Tate, V.A. Ferro, Exosomes: fighting cancer with cancer, Ther. Deliv. 10 (1) (2019) 37–61.
[97] M.A. Obeid, I. Khadra, A.B. Mullen, R.J. Tate, V.A. Ferro, The effects of hydration media on the characteristics of non-ionic surfactant vesicles (NISV) prepared by microfluidics, Int. J. Pharm. 516 (1–2) (2017) 52–60.
[98] A.G. Kohli, P.H. Kierstead, V.J. Venditto, C.L. Walsh, F.C. Szoka, Designer lipids for drug delivery: from heads to tails, J. Control. Release 190 (2014) 274–287.
[99] M.A. Obeid, R.J. Tate, A.B. Mullen, V.A. Ferro, Lipid-based nanoparticles for cancer treatment, in: Lipid Nanocarriers for Drug Targeting, Elsevier, 2018, pp. 313–359.
[100] B. Al-Trad, A. Aljabali, M. Al Zoubi, M. Shehab, S. Omari, Effect of gold nanoparticles treatment on the testosterone-induced benign prostatic hyperplasia in rats, Int. J. Nanomedicine 14 (2019) 3145–3154.
[101] M.A. Obeid, A. Elburi, L.C. Young, A.B. Mullen, R.J. Tate, V.A. Ferro, Formulation of nonionic surfactant vesicles (NISV) prepared by microfluidics for therapeutic delivery of siRNA into Cancer cells, Mol. Pharm. 14 (7) (2017) 2450–2458.
[102] M.A. Obeid, C. Dufès, S. Somani, A.B. Mullen, R.J. Tate, V.A. Ferro, Proof of concept studies for siRNA delivery by nonionic surfactant vesicles: in vitro and in vivo evaluation of protein knockdown, J. Liposome Res. (2018) 1–10.
[103] P. Yingchoncharoen, D.S. Kalinowski, D.R. Richardson, Lipid-based drug delivery systems in cancer therapy: what is available and what is yet to come, Pharmacol. Rev. 68 (3) (2016) 701–787.
[104] R. Karim, S. Somani, M. Al Robaian, M. Mullin, R. Amor, G. McConnell, C. Dufès, Tumor regression after intravenous administration of targeted vesicles entrapping the vitamin E α-tocotrienol, J. Control. Release 246 (2017) 79–87.
[105] Y. Zhang, V.S. Bhatt, G. Sun, P.G. Wang, A.F. Palmer, Site-selective glycosylation of hemoglobin on Cys β93, Bioconjug. Chem. 19 (11) (2008) 2221–2230.
[106] R. Tugyi, G. Mezo, S. Gitta, E. Fellinger, D. Andreu, F. Hudecz, Effect of conjugation with polypeptide carrier on the enzymatic degradation of herpes simplex virus glycoprotein D derived epitope peptide, Bioconjug. Chem. 19 (8) (2008) 1652–1659.

Index

Note: Page numbers followed by *f* indicate figures and *t* indicate tables.

A

Abaqus, 287, 291
Acetamiprid, 21, 72–73
Acetylcholinesterase (AChE) biosensor, 74, 193–194, 196–197
Acoustic detection biosensors, 166–167
Acoustic wave nanobiosensor, 170
Activated gold, 2–3
Active targeting, nanoparticle delivery systems, 426–427
Adenosine triphosphate (ATP), 180, 328
Adenovirus (Adv), 416–417, 418*f*
Adhesive materials, 403, 406–407
A-fetoprotein (AFP), 103–104
Affibody-based biosensors, 54–57
Affinity sensor, 72, 166
AGE. *See* Alternating group explicit (AGE)
AgNPs. *See* Silver nanoparticles (AgNPs)
Agriculture
  development, 151
  nanobiosensors in, 140–141, 152*t*
  wireless nanosensors, 22
Agrofood sector, nanosensors in, 147–153
Agro-Micron, 155–156
Air pollution, 350–352
Alcohol
  adsorption of, 131–132
  alcoholic compounds, 125–126
  oxidation of, 130–131
Alginates, 407
α-Fe_2O_3 nanoparticle-based sensor, 246–247, 248*f*
Alternating group explicit (AGE), 27–30, 31*f*
Aluminum nanolayer, food packaging, 153
Aluminum oxide (Al_2O_3), 205, 236
Alzheimer's disease, 206, 211
Al-ZnO/CuO nanocomposites, 268, 268*f*
3-Aminopropyltriethoxysilane (APTES), 73–74
Ammonia gas (NH_3) sensor
  Al-ZnO/CuO nanocomposites, 268, 268*f*
  C-MWCNT and PANI/MWCNTs nanocomposite, 269
  environmental science and technology, application in, 245, 247*f*
  GO, rGO, and $CuFe_2O_4$ nanocomposites, 267–268, 267*f*
  NFI-rGO materials, 270
  PANI-CeO_2 film sensor, 269, 269*f*
  PAni, WO_3, and PAni-WO_3 hybrid nanocomposites, 270, 271*f*
  PANI@WO_3 composites, 266–267
  PANI-WO_3 hybrid nanocomposite, 269
  portable ammonia sensor, 268
  pristine CuO and rGO-CuO nanocomposite, 266–267, 267*f*
  rGO-$CuFe_2O_4$ composite-based sensor, 267–268, 267*f*
  SiO2-TRGO composite, 270
  source of, 266–267
  ZnO and CuO/ZnO nanocomposites, 268
Ammonium pyrrolidine dithiocarbamate (APDC), 68–71
Amorphous-glassy electrolytes, 357
Amperometric xanthine biosensor, 273–274
Antibody-antigen interaction, 232
Aptameric biosensor, 197
Aptamer modified carbon nanotubes, 204
Aptamer modified graphene, for immunoglobulin E protein detection, 204
Aptamers
  definition, 149–151
  DNA aptamers, 58–61, 68
  thiolated aptamers, 76
Aptasensors, 54–57, 149–151
Arc vapor deposition method, 242
Arginine, 424–425
Arrhenius equation, 363–364, 365*f*
Artificial nanomaterials, 305–306
Aspergillus, 146
Asphaltenes, 401
Atomic force microscopy (AFM), 97, 305

Atrazine, 72
nanoencapsulated atrazine, 198–199
nanopesticides, 148, 154*f*
AuNPS. *See* Gold nanoparticles (AuNPS)
Au@Pt nanoparticles (Au@PtNPs), 71
Autoclaves, hydrothermal synthesis, 257–258, 258*f*
Autogenous self-healing, 401–402
Azo-bis-isobutyronitrile (AIBN), 93–96, 98–99

B

Batch-binding method, 98–99
β-cyclodextrin-graphene modified glassy carbon electrode (β-CD-rGO/GCE), 72–73, 73*f*
Beta-cyfluthrin (BC), 108–110
Binary hybrid nanocomposites, 262, 262*f*
Bioimaging, 343
Biomedical applications, nanobiosensors, 168–169
BioMEMs-MIP sensors, 115–116
Biomolecular detection, nanomaterial-based biosensors
carbon-based nanomaterials, 189–192*t*, 194–196
Convolvulus pluricaulis leaf extracts and polyphenol oxidase from *Manilkara zapota* synthesized silver nanoparticles, 189–192*t*, 199
DNA-modified three-dimensional reduced graphene oxide-chitosan nanocomposites, 189–192*t*, 199
double stranded DNA-poly (L-cysteine)-iron oxide nanoparticles-graphene oxide, 189–192*t*, 199
electrochemical biosensors, 200–202*t*, 202–204
field effect transistor biosensors, 200–202*t*, 204–205
gold nanoparticles-DNA supersandwiches, 189–192*t*, 199
graphene oxide-gold nanoparticles, 207
graphene oxide nanohybrid, 207
indium nitride plasmonic nanoparticles, 207
metal and metal oxide nanomaterials, 188, 189–192*t*, 192–194
microneedle-based biosensors, 207
nanocomposites, 189–192*t*, 196–199
polymeric nanoparticles, 207
polystyrene embedded carbon nanoparticles, 207
Saccharomyces cerevisiae extract synthesized gold nanoparticles, 189–192*t*, 199
spectroscopic biosensors, 200–202*t*, 205–207
terahertz metamaterials, 207
Bionanocomposites, 144–145, 149*f*
Bioreceptor, 151*f*, 163–165, 188, 231
Biosensors, 128–129, 164, 338–342. *See also* Nanobiosensors
applications, 231
biomolecular detection (*see* Biomolecular detection, nanomaterial-based biosensors)
carbon-based nanosensors, 343
components, 188, 231
definition, 89
diagnostic applications (*see* Diagnosis, biosensors)
enzyme sensors, 231
fundamental blocks of, 164–165, 165*f*
graphene-based electrochemical biosensors, 340–342
hybrid nanocomposites
cancer biosensor, 274
electrochemical/glucose/graphene-based biosensors, 271–273
food biosensors, 274
xanthine biosensors, 273–274
types, 165–167
acoustic detection biosensors, 167
affinity sensor, 166
catalytic sensor, 166
electrochemical detection biosensors, 166
metabolism sensor, 166
optical detection biosensors, 167
working process of, 164, 165*f*
Biotinylated quantum dots-manganese dioxide nanosheet composites, 198
Black phosphorus nanosheets, 205
Block copolymer, 354
Blood glucose detection, nanobiosensors in, 178
Boronate-affinity sandwich assay (BASA), 103–104, 103*f*
Boron-doped diamond (BDD), 338
Boron nitride quantum dots, 211
Bottom-up approach, 13, 14*f*
Branched polymers, 352, 353*f*
Breath analyzer, 263
Brunauer, Emmett and Teller (BET) analysis, 97
Bulk acoustic wave (BAW) transducers, 167

C

Cadmium (Cd), 68–71, 236
Cadmium oxide (CdO), 236
Cadmium selenide (CdSe), 237–239, 239*f*
Cadmium selenide quantum dots-chitosan nanocomposite, 198
Cadmium sulfide (CdS), 234–235
Calcite ($CaCO_3$), 402
Cancer
biosensor, 274
detection, nanobiosensors in, 179
diagnosis

MIPs, optical-based nanosensors, 100–105
nanomaterial-based biosensors, 208–209*t*, 209–210
Cantilever-based sensors, 173–174
Carbon-based nanocomposites, 197
Carbon-based nanomaterials, 7, 7*f*, 13, 210–211, 295, 305, 323–324
biomolecular detection, 189–192*t*, 194–196
carbon nanotube (CNT) (*see* Carbon nanotubes (CNTs))
diamond, 326–327
graphene, 325–326
sensing properties, 327–330
Carbon-based nanosensors
limitations and drawbacks
exposures, risk assessment of, 344
nanotoxicity, 344
product cost, 344–345
sample preparation, 343
self-validation, lack of, 344
standardization, 344
potential applications
bioimaging and biosensing, 343
pharmaceutical analysis, 342
Carbon dioxide (CO_2) sensor, 245, 246*f*
Carbon monoxide (CO), 243–244, 263
air pollution, 350–351
sensor, 243–244
Carbon nanotube-field-effect transistor (CNT-FETs), 8*f*, 328, 339
Carbon nanotube-nickel nanocomposites, 197–198
Carbon nanotubes (CNTs), 4–5, 8, 13, 146, 155, 168, 171–172, 195, 197–198, 282–283, 305, 324–325, 328, 331, 343
advantages of, 334
nanosensors, 333–335
sensors, 171–172
Carbon-neutral process, 352
Carbon paste electrode (CPE), 11
Carbothermal technique, 246–247
Carboxy-terminated amino acids, 422, 423*f*
Carcinoembryonic antigen (CEA), 71
Cardiovascular diseases, 211
Catalysis based enzymatic biosensors, 54–57
Catalytic sensor, 166
Cathodoluminescence (CL), 338
CCMV. *See* Cowpea chlorotic mottle virus (CCMV)
Characterization techniques
gas permeability characterization, 286
mechanical properties characterization, 286
pore size characterization, 286
resistance measurement, 286
scanning electron microscopy (SEM), 286
Chemical modification, protein. *See* Protein cages
Chemical sensor, 127
affinity interaction, 232
definition, 231–232
functions, 231–232
ion sensor, 232
transducer and sensing element, 231–232
ZnO-based chemical sensors, 232, 233*f*
Chemical vapor deposition (CVD) technique, 325–327, 335, 337
gas sensors, 242
hybrid nanocomposites, preparation of, 258–259, 260*f*
Chemiresistors, 52–53
Chitin, 272, 284–285
Chitosan
advantages, 284–285
graphene nanofiller, addition of, 285
nanocomposites
electrical conductivity and, 290–291
gas permeability and, 289, 289*f*
graphene layer, 284–285, 284*f*
hybrid nanocomposite biosensors, 272
tensile properties and, 289–290
pore size morphology of, 287–289
preparation, 285
scanning electron microscopy images of, 287–289, 287*f*
Chitosan-polypyrrole-gold bionanocomposite, 273
Chitosan-titanium dioxide-graphene nanoparticles, 197
Chlorambucil (CHB), 339
Cholera, 64–66
Cholera toxin (CT), 64–66
Chromatographic method, 98–99
Chromium (Cr), 67–68
Clothlanidin, 72–73
CNTs. *See* Carbon nanotubes (CNTs)
Coapplicable nanocomposites (CANCs), 274
Cocaine, 106–107
Codeine, 106–107
Cole–Cole plot, 376–378, 377–378*f*
Colorimetric biosensor, 209–210
Colorimetric (absorption) sensing, 53
Complementary metal oxide semiconductor (CMOS) approach, 173
Composite electrolytes, 357
Composite materials
commercial applications of, 355
fiber-reinforced composites, 356
particulate composite, 356
preexisting structures, rehabilitation/strengthening of, 355
properties of, 355
Composite polymer electrolyte (CPE), 358
Comsol Multiphysics, 27
Concrete self-healing
chemical structure of, 405, 405*f*
cracks in, 399
mechanisms, 401–403, 402*f*
adhesive materials, 403

Concrete self-healing *(Continued)*
autogenous, 402
bacteria, 403
mineral admixtures, 402
polymers in, 404–407, 404*t*
alginates, 407
epoxy resin, 406
poly (lactic acid) (PLA), 406
poly (vinyl alcohol) (PVA), 405
polyacrylates, 406–407
polystyrene (PS), 406
polyurethanes (PUs), 406
superabsorbent polymers (SAPs), 407
property, 400–401, 401*f*
trends in, 407–408
Conjugated polyelectrolytes (CPs), 63, 64*f*
Conventional fertilizer applications, 135, 136*t*, 149, 150*t*
Convolvulus pluricaulis leaf extracts and polyphenol oxidase from *Manilkara zapota* synthesized silver nanoparticles, 189–192*t*, 199
Copper-hemin-metal organic framework-chitosan reduced graphene oxide nanocomposite, 196–197
Copper nanofibers, 194
Copper nanoparticles, 142, 169–170, 192–193
Copper nanorods, 194
Copper nanowires, 194
Copper oxide, 236–237
nanoparticles, 193–194
Copper oxide nanowire-single walled carbon nanotubes, 197–198
Covalent molecular imprinting method, 91–94, 93*f*
Cowpea chlorotic mottle virus (CCMV), 415–417
Cowpea mosaic virus (CPMV), 416–418, 418*f*
CPE. *See* Composite polymer electrolyte (CPE)
Crank-Nicolson schemes, 26, 46–47, 47*f*
Cross-linked polymers, 353*f*, 354
cssDNA/GO/CS/GCE biosensor, 274
Cupric oxide (CuO), 236–237
CVD. *See* Chemical vapor deposition (CVD) technique
Cyanazine, 72
Cyclic voltammetry (CV), 374–375, 374*f*, 393
Cystines, 422–424, 423*f*

D

Dendrimers, 306
Dextrin-capped gold nanoparticles (d-AuNPs), 61–63
Diabetes diagnosis, nanomaterial-based biosensors, 208–209*t*, 210–211
Diagnosis, biosensors
conventional biosensors, limitations of, 187–188
nanobiosensors, 178
blood glucose detection, 178
cancer detection, 179
drug discovery, 180
HIV detection, 179
immunoassays, 179
nanostructured sensing electrodes, 180
pathogenic bacteria, detection of, 180
nanomaterial-based biosensors
Alzheimer's disease, 211
cancer, 208–209*t*, 209–210
cardiovascular diseases, 211
challenges, 211–213
diabetes, 208–209*t*, 210–211
futuristic biosensor design, 212–213, 213*f*
microbial infection, 208–209*t*, 210
neurodegenerative diseases, 211
Parkinson's disease, 211
typhoid, 211
research, 188
Diamond, 326–327
nanoparticles, 195–196
nanosensors, 337–338
Diamond nanowires (DNWs), 327, 338
Diclofenac, 107–108, 107*f*
Differential pulse voltammetry (DPV), 274
Dimethylformamide (DMF), 93–94
Dimethyl sulfoxide (DMSO), 369–371, 373–374
Dimetridazole (DMZ), 106–107
Directs methanol fuel cells (DMFC), 385
5,5′-Dithiobis(2-nitrobenzoic acid) (DTNB), 424
DNA biochips, 156
DNA hybridization, electrochemical detection of, 341
DNA-modified three-dimensional reduced graphene oxide-chitosan nanocomposites, 189–192*t*, 199
Dose-response curve, 177
Double stranded DNA-poly (L-cysteine)-iron oxide nanoparticles-graphene oxide, 189–192*t*, 199
Douglas-Rachford (DR) variant, 30
Drop coating, 243
Drug delivery, nanoparticles for, 426
active targeting, 426–427
advantages and disadvantages, 427
applications, 428
passive targeting, 426–427
Drug discovery, nanobiosensors, 180
Durethan, 155

E

EBL. *See* Electron beam lithography (EBL)
Elastomers, 354
Electrical-based nanobiosensors, 142
Electrical signal transduction, 52–53

Electrochemical biosensors, 166, 211–212, 333–334
biomolecular detection, 197–198, 200–202*t*, 202–204
cancer, 209–210
graphene-based, 340–342
microbial infection, detection of, 210
microRNA detection, 192–193
Electrochemical impedance spectroscopy (EIS), 100–101
Electrochemical nanobiosensor, 142, 170–171
Electrochemical nanosensors, 2, 77, 340, 342
Electrochemical nitrite sensor, 282–283
Electrochemical reduced graphene oxide-gold nanoparticles-beta-cyclodextrin-Prussian blue-chitosan nanocomposites, 197
Electrochemical sensors, 52–53, 74, 124, 129–132, 211–212, 341
Electrochemical transducer, 124, 326–327
Electrolytes
definition, 356
gel and polymer gel electrolyte (*see* Gel polymer electrolytes (GPEs))
liquid electrolyte, 356–357
polymer electrolytes (*see* Polymer electrolytes)
solid electrolyte, 356–357
Electromagnetic nanosensors, 331
Electron beam lithography (EBL), 12, 16
Electronic tongue, 115–116
Electrospinning (ES) technique, 270
Electrospun manganese (III) oxide nanofiber, 61–63
Electrostatic spraying, 246–247
Energy and environmental pollution, 351–352
Enhanced permeability and retention (EPR), 426–427
E-nose. *See* Gas sensors
Environmental applications, nanosensors
challenges and future direction, 76–77
heavy metal detection
cadmium (Cd), 68–71
chromium (Cr), 67–68
lead, 68, 69–70*f*
mercury, 71
high sensitivity, 57–58, 59*t*
nanomaterials, 54–57, 55–56*t*
pathogen detections, 61–63
Escherichia coli, 63, 64*f*
Legionella pneumophila, 66–67
Pseudomonas aeruginosa, 67
Salmonella typhi, 63–64
signal transduction modes, 61, 62*f*
Vibrio cholerae, 64–66, 65*f*
pesticide detection
neonicotinoids, 72–73, 73*f*
organochlorines, 74–76
organophosphates (OPs), 74
pyrethroids, 73–74, 75–76*f*
triazines, 72
portability, 58–61
recognition elements, 54–57
response time, 57–58
selectivity, 58–61
sensitivity/resolution, 58–61
signal transduction mechanism
electrical signal transduction, 52–53
magnetic signal transduction, 53–54
optical signal transduction, 53
Environmental pollutants
highly sensitive nanosensors, 57–58, 59*t*
SERS-based sensing of, 53
Environmental pollution, 350–352
Environmental Pollution Control Regulation 2000, 350–351
Environmental scanning electron microscopy (ESEM), 408
Environmental science and technology, gas sensors application in
ammonia sensor, 245, 247*f*
carbon dioxide (CO_2) sensor, 245, 246*f*
carbon monoxide sensor, 243–244
hydrogen sulfide (H_2S) sensor, 246–247, 248*f*
nitrogen oxide (NOx) sensor, 245
Environmental studies, 349–350
Enzymatic biosensors, 54–57, 341
Enzyme glucose oxidase (GOX), 231
Enzyme sensors, 231
Epoxy resin, 406
Escherichia coli, 63, 64*f*, 155
Ethanol, 125–126, 195
4-Ethylaniline (EA), 95–96
Ethylene detection, 282–283
Ethylene glycol dimethacrylate (EGDMA), 93–94, 98–99

F

Ferritins, 415–416, 418*f*, 419
Ferromagnetic nanoparticles, 169–170
Field-effect transistor (FET), 52–53
biosensors, 200–202*t*, 204–205
CNT-FETs, 8, 334
Finite difference method (FDM), 26
Finite element analysis, 287, 291–292
FLNs. *See* Fullerenes (FLNs)
Fluorescein isothiocyanate (FITC), 68–71
Fluorescence-based optical sensors, 237–239
Fluorescence nanosensor, 101–103
Fluorescence resonance energy transfer (FRET), 68, 341–342
Fluorescence switch sensing mechanism, 108–110
Fluorescent MIP (FMIPs), 108–110
Fluorescent sensors, 341
Fluorographene, 336
Focused ion beam lithography, 16–17, 17*f*
Food and environmental sensing, MIPs, 108–111, 113*t*
Food biosensors, 274
Food packaging, nanosensors in, 153–156
life cycle of, 153–154, 154*f*
nanobiosensors in, 151, 152*t*

Food processing, nanobiosensors, 151, 152*t*
Food sectors, nanobiosensors in, 144–147
Fossil fuels, 382
Fourier transform infrared (FTIR) spectroscopy, 229–230
FRET. *See* Fluorescence resonance energy transfer (FRET)
Fuel cell
  application of, 390–391, 390*f*
  chemical reactions, 382–383
  components of, 382–383, 384*f*, 385
  definition, 382
  directs methanol fuel cells (DMFC), 385
  high temperature fuel cell, 384
  hydrogen-oxygen fuel cell, 384
  intermediate temperature fuel cell, 384
  low temperature fuel cell, 384
  molten carbonate fuel cells (MCFCs), 385
  phosphoric acid fuel cell (PAFC), 384
  polymer electrolyte membrane (*see* Polymer electrolyte membrane fuel cell (PEMFC))
  proton exchange membrane fuel cell, 384
  schematic diagram of, 383*f*
  solid oxide fuel cells (SOFCs), 384
  working principle of, 385, 386*f*
Fullerenes (FLNs), 195–196, 328, 339

G

Gas chromatography, 229–230
Gas sensors, 128, 281–282
  applications of, 262–263
  bulk and surface characteristics, 230
  carbon nanotubes (CNTs) for, 282–283
  environmental pollution monitoring, 230–231
environmental science and technology, application in
  ammonia sensor, 245, 247*f*
  carbon dioxide (CO_2) sensor, 245, 246*f*
  carbon monoxide sensor, 243–244
  hydrogen sulfide (H_2S) sensor, 246–247, 248*f*
  nitrogen oxide (NOx) sensor, 245
fabrication techniques, 282
  chemical vapor deposition (CVD) technique, 242
  drop coating, 243
  physical vapor deposition (PVD) (*see* Physical vapor deposition (PVD) technique)
  screen printing, 243
  spray pyrolysis, 243
features, 229–230
function of, 263–264
hybrid nanocomposites, ammonia gas sensor (*see* Ammonia gas (NH_3) sensor)
low-dimensional nanoparticles, 229
materials, selection of, 264–265, 265*t*
metal oxide nanomaterials, 230
  aluminum oxide (Al_2O_3), 236
  cadmium oxide (CdO), 236
  copper oxide, 236–237
  zinc oxide (ZnO), 237
metal sulfide semiconductors
  cadmium sulfide (CdS), 234–235
  lead sulfide (PbS), 235
  zinc sulfide (ZnS), 232–234
nanosensors, 331–333
noble metal nanoparticles, 237, 238*f*
optimization of, 264
porous silicon (PSi), 239, 240*f*
quantitate techniques, 229–230
quantum dots (QDs), 237–239, 239*f*
requirements for, 263–264
response time, 230–231
  selectivity, 230–231
  semiconducting metal oxides, 266
  sensitivity, 230–231
  survey, 282–283, 284*t*
  thin gas sensors, 230
Gel polymer electrolytes (GPEs), 356–359, 361–362
  advantages, 361–362
  environmentally friendly devices, applications in, 391
    hydrogen–oxygen fuel cell, 364–366, 365*f*
    photoelectrochemical cells, 366
    sensors, 366
    solar cells, 367–368, 367*f*
    solid-state rechargeable battery, 366
    supercapacitors, 366, 367*f*
  (100-*x*) PVdF+ $x$$NH_4SCN$ gel electrolyte systems, 368–369, 391–392
    cyclic voltammetry (CV), 374–375, 374*f*, 393
    dielectric studies, 379–382, 380–381*f*, 394
    infrared spectroscopy (IR) characterization, 372–374, 372*f*, 373*t*, 392
    ionic conducting studies, 375–379, 376–379*f*, 393
    membrane fabrication, 369
    scanning electron microscopy (SEM), 371–372, 371*f*, 392
    Wagner's polarization methods, 393
    X-ray diffraction (XRD), 369–371, 370*f*, 392
Gene therapy, 181–182
Genosensors, 54–57
Global warming, 350–352
Glove biosensor (GB), 74
Glucose biosensors, 193–195, 197, 272–273
Glucose monitoring tattoos, 212–213
Glucose oxidase, 172, 195, 197–198, 341

Glucose oxidase (GOx)
immobilized TiO_2-cellulose hybrid nanocomposite, 273
Glycoproteins, 101–104, 103*f*, 232
Gold nanofilms, 194
Gold nanoparticle-aptamer, 205–206
Gold nanoparticle-carbon nanosphere, 203–204
Gold nanoparticle-doped beta-cyclodextrin-lead metal-organic framework, 210–211
Gold nanoparticle-molybdenum sulfide nanosheet, 203–204
Gold nanoparticle-polyaniline-titanium dioxide nanotube, 206
Gold nanoparticles (AuNPS), 52–53, 142, 144–146, 149, 195, 211, 237
antigen-antibody detection, 207
biochemical detection, 192–193
cancer biomarkers, detection of, 209–210
catechol detection in water samples, 192–193
choline detection, 192–193
chronic lymphocytic leukemia, sequence specific DNA detection of, 205–206
for *Clostridium difficile* toxin detection, 205–206
complementary oligonucleotide sequence detection, 205–206
C-reactive protein detection, 206
dehydrogenase enzyme detection, 202–203
DNA detection, 203–204
DNA supersandwiches, 189–192*t*, 199
enzyme conjugated, 170–171
genomic DNA of *Brucella* species, 192–193
glucose detection, 192–193
hydrogen peroxide detection, 207
impedance and capacitance biosensors, 205–206
lactate detection, 207
mathematical model (*see* Mathematical model, of gold nanoparticle fabrication)
methyl parathion detection, 192–193
microbial infection, detection of, 210
microRNA detection, 192–193
oral malignant epithelial HOC 313 clone 8 and HSC 3 cell line detection, 206
polynucleotide kinase detection, 203–204
prostate specific antigen detection, 192–193
protein detection, 207
two-dimensional molybdenum disulfide nanosheets, 203–204
Gold nanoparticles-three-dimensional zinc oxide nanostructures, 210–211
Gold nanorods, 194
Gold nanosheets, 194
Gold nanowires, 52–53
Gold-platinum metal organic framework nanocomposites, 196–197
GPEs. *See* Gel polymer electrolytes (GPEs)
GQDs. *See* Graphene quantum dots (GQDs)
Grafting approach, 174
Graphene, 4–5, 282–283, 325–326, 328
electrochemical biosensors, 340–342
hybrid nanocomposites, 275–276
immunosensors, 342
nanofiller
chitosan, addition to, 285, 289*f*
scanning electron microscopy images of, 287, 288*f*
nanosensors, 335–336
nanowalls, 341–342
pore size morphology of, 287–289
protein, 205
sensors, 175–176
Graphene-carbon nanotubes, 195
Graphene-copper nanoparticle, 206–207
Graphene oxide (GO), 71, 326, 330–331, 336
Graphene oxide-gold nanoparticles, 204, 206–207
Graphene oxide-gold nanowires, 211
Graphene oxide-magnetic nanoparticles, 197
Graphene oxide-single stranded DNA-poly L-lactide nanoparticles, 203–204
Graphene oxide supported carbon quantum dots (GO/C-dots), 108–110
Graphene quantum dots (GQDs), 106–107, 195–196
Graphene quantum dots-embedded silica molecular imprinted polymer (GQDs-SMIP) nanosensor, 106–107, 109*t*
Graphyne nanosheets, 194–195
Green fluorescent protein (GFP) reporter sequence, 181–182

H

Half synthetic polymers, 352
Heat-shock proteins (Hsps), 415–416, 418*f*, 419
Heavy metals
cadmium (Cd), 68–71
chromium (Cr), 67–68
lead, 68, 69–70*f*
mercury, 71
Hematite nanoparticle-based gas sensors, 246–247
Hemoglobin glycosylation (Hb), 428
Highly sensitive nanosensors, 57–58, 59*t*
High-performance liquid chromatography, 115–116
HIV detection, nanobiosensors in, 179
HNC. *See* Hybrid nanocomposites (HNC)
Horseradish peroxidase (HRP), 101–104

Hsps. *See* Heat-shock proteins (Hsps)
Human papilloma virus detection, 194
Hybrid molybdenum sulfide nanoparticle-graphene oxide, 203–204
Hybrid nanocomposites (HNC)
  ammonia gas sensor (*see* Ammonia gas (NH_3) sensor)
  biosensors
    cancer biosensor, 274
    electrochemical/glucose/graphene-based biosensors, 271–273
    food biosensors, 274
    xanthine biosensors, 273–274
  classification of, 262, 262*f*
  definition, 260–261
  graphene-based hybrid nanocomposites, 275–276
  preparation of
    chemical vapor deposition technique, 258–259, 260*f*
    hydro-/solvothermal synthesis, 257–258, 258*f*
    microwave-assisted wet chemical method, 259–260, 261*f*
    sol-gel synthesis, 258, 259*f*
    solid-state synthesis, 256–257, 257*f*
  research, applications, and commercial interest, areas of, 275–276
  strong chemical bonding, 260–261
  weak chemical bonding, 260–261
  WO_3-CdS composite energy level, 261–262, 262*f*
Hybrid-polymer based solar cells, 367, 367*f*
Hydrazine, 125–126
Hydrogen, 229–230, 332
  energy system, 382
  fueling station, fuel cell application in, 390, 390*f*
Hydrogen–oxygen fuel cell, 364–366, 365*f*, 384
Hydrogen sulfide (H_2S) sensor, 246–247, 248*f*
Hydrothermal synthesizing method, 257–258, 258*f*
Hydroxyl fullerenes-titanium dioxide nanoparticles, 197–198
6-Hydroxynicotinic acid (6-HNA), 110–111
2-Hydroxynitrobenzyl bromide (HNBB), 425

I

Imidacloprid, 72–73
Immunoassays, nanobiosensors in, 179
Immunochemical biosensors, 211–212
Immunosensors, 54–57
Impedance biosensors, 205–206, 211–212
Impedance spectroscopy, 205–206
Indium nitride plasmonic nanoparticles, 207
Indium tin oxide (ITO), 108–110
  comb electrodes, 310, 310*f*
  sensor, 245
Infrared spectroscopy (IR) characterization, 372–374, 372*f*, 373*t*, 392
Inhibition based enzymatic biosensors, 54–57
Inner filter effect (IFE), 340
In situ biochips, 212–213
In-situ chemical oxidative polymerization (iCOP), 269
Interlamellar polymerization technique, 154
Internet of Things (IoT)-enabled water sensing, 77, 78*f*
Inverse mini-emulsion polymerization method, 107–108
Ion imprinting, 91–93
Ion plating, 242
Ion sensor, 232
Iron oxide-based magnetic nanoparticles, 205–206
Iron oxide-chitosan-graphene nanocomposites, 197
Iron oxide nanoparticle-polyvinyl alcohol composite, 203–204
Isopropyl alcohol (IPA), 125–126
ITO. *See* Indium tin oxide (ITO)

J

Jacobi method (JB), 27–30, 32–33, 37*t*
Janus nanoparticles, 157

L

Lab-on-a-chip portable nanosensor, 58–61, 60*f*
Land pollution, 350
Lanthanum hydroxide nanostructure, 192–193
Lateral flow immunochromatographic assay (LFIA), 146, 150*f*
LCs. *See* Liquid crystals (LCs)
Lead, 68, 69–70*f*
Lead sulfide (PbS)
  colloidal nanoparticle of, 169–170, 169*f*
  as gas sensors, 235
Legionella pneumophila, 66–67
LFIA. *See* Lateral flow immunochromatographic assay (LFIA)
Li^+ doped CNTs, 332
Limit of detection/determination (LOD), 177
Linear polymers, 352, 353*f*
Linear system equations (LSEs), 22, 27
Linux Fedora 21 operating system, 34
Liquid chromatography (LC), 107–108
Liquid crystals (LCs)
  applications, 296–298, 303
  categories, factors, 298
  classifications of, 298, 299*f*
    lyotropic liquid crystal, 298–299, 301, 302*f*
    thermotropic liquid crystals, 298–300, 300–301*f*

external electric field, 298–299, 299*f*
functional properties, 301–303
mesogen, 296–298
nanomaterial dispersed liquid crystal (NLC), 296, 307–309
spontaneous alignment of, 297*f*, 298
states of matter and molecular arrangements, 296–298, 297*f*
surface treatment, 297*f*, 298
thermal sensor (*see* Temperature sensor, liquid crystals)
Liquid electrolyte, 356–357
Liquid plasticizer, 358–359
Lithography, 16
Localized surface plasmon (LSP), 4
Localized surface plasmon resonance (LSPR), 53, 67, 179
Low-dimensional nanoparticles, 229
LSEs. *See* Linear system equations (LSEs)
Lyotropic liquid crystal, 298–299, 299*f*, 301, 302*f*, 303
Lysine, 421–422, 421*f*

M

Magnetic iron oxide nanoparticles, 193–194, 210
Magnetic nanobiosensor, 170
Magnetic nanoparticles (MNPs), 53–54, 55–56*t*, 211, 337–338
CD81 surface marker, annexin V and cholera toxin B detection, 205–206
Listeria monocytogenes detection, 205–206
urease nanosensors, 61–63
Magnetic nanosensors, 5–7
Magnetic nickel ferrite nanoparticles, 204
Magnetic polymeric nanoparticles (MPNPs), 64–66, 65*f*
Magnetic resonance imaging (MRI), 5–7
Magnetic signal transduction, 53–54
Magnetic silica beads/graphene quantum dots/molecularly imprinted polypyrrole (mSGP) sensor, 110–111, 112*f*
Magneto-PCR-colorimetry technique, 64–66, 65*f*
Main-chain liquid crystal polymer (MC-LCP), 300, 300*f*
Manganese dioxide nanoparticles, 204
Mannich three-component approach, 424
Mass spectroscopy (MS), 107–108, 229–230
Mathematical model, of gold nanoparticle fabrication, 24
applications, 23
discretization using finite difference method for, 26
governing equation, 24–25
growth of, 23–24
linear system equation formulation, 27
nondimensionalized parameters, 25–26
numerical implementation, 28–47
alternating group explicit (AGE), 30, 31*f*
Jacobi method (JB), 32–33
Red-Black Gauss-Seidel method (RBGS), 30–32, 32–33*f*
parallelization, 28–47
of iterative methods, 33–40
1D parallel alternating group explicit method (1D PAGE), 37–38
1D parallel Jacobi method (1D PJB), 39–40
1D parallel Red-Black Gauss-Seidel method (1D PRBGS), 38–39
performance evaluation, 40–47
partial differential equations (PDEs), 22
photochemical synthesis of, 28
as substrates, 22
visualization, 27–28, 28–29*f*
Matlab R2013b, 27
MC-LCP. *See* Main-chain liquid crystal polymer (MC-LCP)
Mechanical nanosensors, 281
Medicine, gas sensors in, 263
Melt processing, 154
4-Mercaptophenyl-boronic acid (MPBA), 103–104
Mercury intrusion porosimetry, 97
Mercury ion detection, 197
Metabolism sensor, 166
Metal nanoparticles, 9–10, 144, 307–309
Metal organic framework-carbon nanocomposites, 197
Metal oxide nanomaterials
in biosensor fabrication, 188, 189–192*t*, 192–194
for gas sensors, 266
aluminum oxide (Al_2O_3), 236
cadmium oxide (CdO), 236
copper oxide, 236–237
zinc oxide (ZnO), 237
Metal-oxide nanostructures, 130
Metal oxide semiconductors, 124–125
Metal sulfides
cadmium sulfide (CdS), 234–235
lead sulfide (PbS), 235
zinc sulfide (ZnS), 232–234
Methacrylic acid (MAA), 93–94
Methane, 229–230
Methanol, 125–126
Methionine, 425–426
Methyl parathion detection, 192–193
Metronidazole (MNZ), 106–107
Microbial infection, 208–209*t*, 210
Microcontact imprinting, 101, 102*f*
Microelectromechanical systems (MEMS), 281
Microneedle-based biosensors, 207
Microwave-assisted wet chemical method, 259–260, 261*f*
Mineral admixtures, 402
MNPs. *See* Magnetic nanoparticles (MNPs)

Molecularly imprinted polymers (MIPs), 54–57, 206–207
characterization of, 97–99
definition, 89–90
optical-based nanosensors, applications in
cancer diagnosis, 100–105
challenges, 111–115
developments, 115–117
food and environmental sensing, 108–111, 113*t*
optical sensors, 99–100, 100*f*
pharmaceuticals and drugs, detection of, 106–108, 109*t*
production methods, 90–91, 90*f*
non-free radical techniques, 91–93
phase inversion precipitation polymerization, 91–96, 95*f*
soft lithography/surface stamping, 91–93, 96–97, 96*f*
template-monomer method, 91–94, 92*f*
properties, 89–90
qualities, 89–90
three-dimensional bioMEMs-based MIP sensor, 115–116
Molecular self-assembly, 13–14
Molten carbonate fuel cells (MCFCs), 385
Molybdenum disulfide-gold nanoparticle, 205
Molybdenum sulfide nanosheets, 211
Morphine, 106–107
Multiple hybrid nanocomposites, 262, 262*f*
Multiplex detection, 177–178
Multiwalled carbon nanotube (MWCNTs), 8, 11, 146–147, 171–172, 171*f*, 195, 198–199, 269, 325, 333, 339, 342
Mycobacterium avium spp. paratuberculosis (MAP), 180
Mycotoxin, 146

N

Nanobiosensors, 54, 55–56*t*, 138–139, 178, 231
advantages, 140
in agriculture, 140–142, 143*t*
agrofood sector, development in, 147–153
Au nanoparticles in, 144–145
in biomedical applications, 168–169
cantilever-based sensors, 173–174
characteristics of, 139–140
components, 140
detection by, 142–144
diagnostic purpose, 178
blood glucose detection, 178
cancer detection, 179
drug discovery, 180
HIV detection, 179
immunoassays, 179
nanostructured sensing electrodes, 180
pathogenic bacteria, detection of, 180
in different food sectors, 144–147
environmental monitoring, 181
inorganics detection, 181
toxicants detection, 181
in food packaging, 153–156
gene therapy, 181–182
graphene-based sensors, 175–176
history of, 137
nanomedicine, 181
nanoparticle-based sensors, 169–171
acoustic wave nanobiosensor, 170
electrochemical nanobiosensor, 170–171
magnetic nanobiosensor, 170
nanotube-based sensors, 171–172
nanowire-based sensors, 172–173
performance parameters, 176–178
dose-response curve, 177
dynamic range, 177
multiplex detection, 177–178
selectivity, 176
sensitivity, 176–177
small objects *vs.* microorganisms, 137*f*
types, 140
Nanocomposite polymer electrolyte (NCPE)
Arrhenius equation, 363–364, 365*f*
Li-ferrite filler-based electrolyte, 393–395
nanocomposite polymer gel electrolytes, applications in, 391
hydrogen–oxygen fuel cell, 364–366, 365*f*
photoelectrochemical cells, 366
sensors, 366
solar cells, 367–368, 367*f*
solid-state rechargeable battery, 366
supercapacitors, 366, 367*f*
objectives, 368
polymer electrolyte fuel cell (*see* Polymer electrolyte membrane fuel cell (PEMFC))
(100-*x*) PVdF+ $x$$NH_4SCN$ gel electrolyte systems, 368–369, 391–392
cyclic voltammetry (CV), 374–375, 374*f*, 393
dielectric studies, 379–382, 380–381*f*, 394
infrared spectroscopy (IR) characterization, 372–374, 372*f*, 373*t*, 392
ionic conducting studies, 375–379, 376–379*f*, 393
membrane fabrication, 369
scanning electron microscopy (SEM), 371–372, 371*f*, 392
Wagner's polarization methods, 393
X-ray diffraction (XRD), 369–371, 370*f*, 392
Vogel-Tammann-Fulcher (VTF) equation, 363, 364*f*

Nanocomposites, 153–154
applications, 296
biomolecular detection, 189–192*t*, 196–199
chitosan
electrical conductivity, 290–291
gas permeability and, 289, 289*f*
graphene layer, 284–285, 284*f*
hybrid nanocomposite biosensors, 272
tensile properties, 289–290
hybrid nanocomposites (*see* Hybrid nanocomposites (HNC))
one-dimensional (1D) nanocomposite, 296
polymer nanocomposites, 359
applications, 361
classifications, 359–361, 360*f*
environmentally friendly devices, applications in, 382
nanocomposite polymer electrolyte (NCPE) (*see* Nanocomposite polymer electrolyte (NCPE))
polyethylene oxide (PEO), 361–362, 362*f*
polyvinylidene fluoride (PVdF), 362, 363*f*
reinforcement and matrix materials, 359–361
structures, 359, 360*f*
two-dimensional (2D) nanocomposites, 296
zero-dimensional (0D) nanocomposite, 296
Nanodiamonds (NDs), 327, 337, 343
Nanofertilizers, 135, 136*t*, 149, 150*t*
Nanofillers, carbon-based, 324, 325*t*
Nanolithography, 12
Nanomanufacturing, 11–14
bottom-up approach, 13
molecular self-assembly, 13–14
for nanosensors, 15–17
electron beam lithography (EBL), 16
focused ion beam lithography, 16–17
X-ray lithography (XRL), 17
top-down approach, 12–13
Nanomaterial-coated fabrics, 212–213
Nanomaterial dispersed liquid crystal (NLC), 296
carbon nanoparticles, 307–309
ferroelectric nanoparticles, 307–309
metal nanoparticles, 307–309
semiconductor nanoparticles, 307–309
temperature sensor, 310–311, 316, 317*f*
Nanomaterials, 2–3, 254
applications, 295, 306*f*
biomolecular detection, biosensors for (*see* Biomolecular detection, nanomaterial-based biosensors)
bulk materials
evaluation, 305
surface-to-volume ratio of, 254–255, 254*f*
carbon nanomaterials (*see* Carbon-based nanomaterials)
composites, 306
definition of, 304–305
dendrimers, 306
diagnostic applications, biosensors for (*see* Diagnosis, biosensors)
electrochemical sensors, 129–130
epitaxial hybrid nanostructures, 307, 308*f*
in food sector, 144*t*
liquid crystals, 303
macroscale, microscale and nanoscale comparison, 304–305, 304*f*
metal based, 306
nanobiosensors, 54–57, 55–56*t*
nanosensors, 2–11, 281
one-dimensional (1-D) nanomaterials, 255, 256*f*, 306–307
properties of, 135–137, 305
research, 295
three-dimensional (3-D) nanomaterials, 256, 256*f*, 306–307
two-dimensional (2-D) nanomaterials, 255, 256*f*, 306–307
virus-based nanomaterials, 417
zero-dimensional (0-D) nanomaterials, 255, 256*f*, 306–307
Nanoparticles, 9–10, 168–169, 182
aptasensors, 149–151
crop plants, effect in, 149–151
drug delivery system, 426
active targeting, 426–427
advantages and disadvantages, 427
applications, 428
passive targeting, 426–427
in food sector, 144*t*
gold nanoparticles (AuNPS) (*see* Gold nanoparticles (AuNPS))
hybrid nanostructures, 307, 308*f*
magnetic nanoparticles (MNPs) (*see* Magnetic nanoparticles (MNPs))
properties of, 135–137
sensors, 169–171
silver nanoparticles (AgNPs) (*see* Silver nanoparticles (AgNPs))
Nanoporous alumina membrane-magnetic nanoparticles, 205–206
Nanorobots, 212–213
Nanorods, 168–169
Nanoscale field effect transistor biosensors, 204
Nanoscale semiconductor crystals, 171
Nanoscience, 303
Nanosensors, 1–2, 167–168, 323. *See also* Nanobiosensors
applications, 2
carbon-based nanosensors (*see* Carbon-based nanosensors)

Nanosensors *(Continued)*
electrochemical, 2
electromagnetic, 331
environmental perspective (*see* Environmental applications, nanosensors)
gas sensors (*see* Gas sensors)
history of, 3
nanomaterials, 2–11
carbon nanotube, 8
electronic properties, 4–5
fullerenes, 11
magnetic properties, 5–7
nanoparticles, 9–10
nanowires, 8–9
optical properties, 4
properties of, 3–7
optical (*see* Optical nanosensors)
Nanostructured sensing electrodes, 180
Nanotechnology, 253–254, 295, 303, 352
applications of, 141, 141*f*, 153*f*
benefits, in food industry, 150*f*, 151
exploration of, 303
in food science and technology, 136*f*, 136*t*, 139*t*
impact of, 142–144, 145*f*
objective of, 303
research publications on, 142–144, 147*f*
Nanotoxicity, 344
Nanowalls, graphene, 341–342
Nano-wheels, 155
Nanowire-based sensors, 172–173
Nanowires, 8–9, 168–169
Natural polymers, 352
Natural receptors, 89
NCPE. *See* Nanocomposite polymer electrolyte (NCPE)
Neel relaxation, 5–7
Neonicotinoids, 72–73, 73*f*
Neurodegenerative diseases, 211
NH_3 gas sensor. *See* Ammonia gas (NH_3) sensor
N-hydroxysuccimide (NHS) esters, 421–422
Nickel-iron-mesoporous carbon nanocomposites, 197
Nicotinamide adenine dinucleotide (NADH) based biosensors, 195
Niosome nanoparticles, 426–427
N-isopropylacrylamide (NIPAAm), 101–103
Nitenpyram, 72–73
Nithiazine, 72–73
Nitrile, 146
Nitrogen dioxide (NO_2), 245
Nitrogen-doped graphene-gold nanoparticles, 203–204
Nitrogen oxide (NOx) sensor, 245
Nitrogen sorption porosimetry, 97
Nitrogen-vacancy (NV) centers, 327–328, 331, 337–338
NLC. *See* Nanomaterial dispersed liquid crystal (NLC)
Noble metal nanoparticles, 4, 53, 237, 238*f*
Noise pollution, 350
Noncovalent molecular imprinting method, 91–94, 93*f*
Nondimensionalized parameter, 25–26
Non-free radical polymerization methods, 91–93
Nonimprinted polymers (NIPs), 106–107
Nonviral protein cages, 418*f*
ferritins, 415–416, 419
heat-shock proteins (Hsps), 415–416, 419
vault proteins (VPs), 419–420
Numerical implementation, for gold nanoparticle fabrication, 28–47

O

Ochratoxin-A, 146
Ocimum tenuiflorum leaf extract synthesized zinc oxide nanoparticles, 193–194
Octadecyl-p-vinylbenzyldimethy lammonium chloride (OVDAC), 101–103
One-dimensional (1D) nanocomposite, 296
One-dimensional (1-D) nanomaterials, 255, 256*f*, 306–307
One-dimensional parabolic PDEs, 22, 24, 27
One-dimensional parallel alternating group explicit method (1D PAGE), 36*t*, 37–38, 38*f*, 43–47
One-dimensional parallel Jacobi method (1D PJB), 37*t*, 39–40, 44
One-dimensional parallel Red-Black Gauss-Seidel method (1D PRBGS), 36*t*, 38–39, 39*f*
Optical detection biosensors, 167
Optical nanosensors, 2
carbon nanomaterials, 330–331
MIPs applications
cancer diagnosis, 100–105
challenges, 111–115
developments, 115–117
food and environmental sensing, 108–111, 113*t*
optical sensors, 99–100, 100*f*
pharmaceuticals and drugs, detection of, 106–108, 109*t*
Optical signal transduction, 53
Optical spectroscopy sensing system, 99–100, 100*f*
Organochlorines, 74–76
Organophosphate (OP) pesticides, 52–53, 74, 197
Ornidazole (ONZ), 106–107
Oxygen (O_2), 71, 130–131
gas, 284–286
sensors, 230–231

P

Palladium nanoparticles, 9–10, 192–193
Papain, 424
Paper-based optical biosensor-green algae *Chlamydomonas reinhardtii*, 198–199
Parallelization, for gold nanoparticle fabrication, 28–47

Parallel Virtual Machine (PVM), 23, 28–30, 34, 35*f*, 40–41, 47
Parkinson's disease, 211
Partial differential equations (PDEs), 22, 24
Particulate composite, 356
Passive targeting, nanoparticle delivery systems, 426–427
Pathogen detection, nanosensors for, 61–63
  Escherichia coli, 63, 64*f*
  Legionella pneumophila, 66–67
  nanobiosensors, 180
  Pseudomonas aeruginosa, 67
  Salmonella typhi, 63–64
  signal transduction modes, 61, 62*f*
  Vibrio cholerae, 64–66, 65*f*
Patulin (PAT), 110–111, 111*f*
PbS. *See* Lead sulfide (PbS)
Pd-decorated ZnO nanowires, 243–244, 244*f*
PDEs. *See* Partial differential equations (PDEs)
Peclet number, 26
PEMFC. *See* Polymer electrolyte membrane fuel cell (PEMFC)
Penicillin G (PenG), 107–108
Penicillium, 146
PEO. *See* Polyethylene oxide (PEO)
Pesticide detection, nanosensors for, 142
  neonicotinoids, 72–73, 73*f*
  organochlorines, 74–76
  organophosphates (OPs), 74
  pyrethroids, 73–74, 75–76*f*
  triazines, 72
Phage biosensors, 54–57
Pharmaceutical analysis, 342
Pharmaceutical nanotechnology, 416–417
Pharmaceuticals and drug detection, MIPs, 106–108, 109*t*
Phase inversion method, 91–96, 95*f*
3-Phenoxybenzaldehyde (3-PBD), 73–74
Phenyltrimethoxysilane (PTES), 73–74
Phosphoric acid fuel cell (PAFC), 384
Photoelectrochemical cells, 366
Photo-induced electron transfer mechanism, 110–111
Photoluminescence (PL), 68–71
Photonic crystals, 156, 167, 193–194
Photopolymerization method, 107–108
Physical vapor deposition (PVD) technique, 241
  arc vapor deposition method, 242
  ion plating, 242
  sputtering, 241–242
  thermal evaporation, 241
Physicochemical transducer, 127, 231
PLA. *See* Poly (lactic acid) (PLA)
Plastic bottle beer packaging, 155
Plasticized polymer salt complex, 358
Platinum-conducting polymer hybrid nanoparticles, 205
Platinum nanoparticles, 192–193, 197, 205
Platinum nanowires, 194
Poly (lactic acid) (PLA), 406
Poly(methyl methacrylate) (PMMA), 358–359, 361–362, 407
Poly (vinyl alcohol) (PVA), 405
Polyacrylamide nanoparticle, 4
Polyacrylates, 406–407
Polyaniline (PANI) @ tungsten oxide (WO_3) nanocomposites, 266–267
Polybrominated diphenyl ethers (PBDEs), 58–61
Polycrystalline materials, 256–257
Polydimethylsiloxane (PDMS) microfluidic chip, 58–61
Polyethylene glycol (PEG) modified Mn-doped ZnS quantum dots, 106–107
Polyethylene oxide (PEO), 361–362, 362*f*
Polymer electrolyte membrane fuel cell (PEMFC), 385
  applications, 386–388
  EMF measurement of, 388–390, 388–389*f*
  experimental arrangement of, 386, 387*f*
  water management, problem in, 386–387
Polymer electrolytes, 356
  advantages, 357
  composite polymer electrolyte (CPE), 358
  nanocomposite polymer electrolyte (NCPE) (*see* Nanocomposite polymer electrolyte (NCPE))
  PEO-based polymer electrolytes, 361–362, 362*f*
  plasticized polymer salt complex, 358
  properties, 357–358
  PVdF-based electrolytes (*see* Polyvinylidene fluoride (PVdF))
  solid polymer electrolyte (SPE), 358
Polymer gel electrolyte. *See* Gel polymer electrolytes (GPEs)
Polymeric liquid crystal, 298
Polymers
  alternating copolymer, 354
  applications, 359
  block copolymer, 354
  branched polymers, structure of, 352, 353*f*
  in concrete self-healing, 404–407, 404*t*
    alginates, 407
    epoxy resin, 406
    poly (lactic acid) (PLA), 406
    poly (vinyl alcohol) (PVA), 405
    polyacrylates, 406–407
    polystyrene (PS), 406
    polyurethanes (PUs), 406
    superabsorbent polymers (SAPs), 407
  cross-linked polymers, structure of, 353*f*, 354
  definition, 352
  half synthetic polymers, 352

Polymers *(Continued)*
linear polymer, structure of, 352, 353*f*
nanocomposites, 198–199, 352, 359
applications, 361
classifications, 359–361, 360*f*
environmentally friendly devices, applications in, 382
nanocomposite polymer electrolyte (NCPE) (*see* Nanocomposite polymer electrolyte (NCPE))
polyethylene oxide (PEO), 361–362, 362*f*
polyvinylidene fluoride (PVdF), 362, 363*f*
reinforcement and matrix materials, 359–361
structures, 359, 360*f*
nanowires, 52–53
natural polymers, 352
properties of, 354
random copolymer, 354
synthetic polymers, 352
thermal properties of, 354–355
thermotropic liquid crystals, 300, 300*f*
Poly (glycidyl methacrylate-co-vinylferrocene)-multiwalled carbon nanotubes, 198–199
Polystyrene (PS), 406
Polystyrene embedded carbon nanoparticles, 207
Polyurethanes (PUs), 406, 408
Polyvinylidene fluoride (PVdF)
chemical structure and atomic representation of, 362, 363*f*
(100-*x*) PVdF+ $x$$NH_4SCN$ gel electrolyte systems, 368–369, 391–392
cyclic voltammetry (CV), 374–375, 374*f*, 393
dielectric studies, 379–382, 380–381*f*, 394
infrared spectroscopy (IR) characterization, 372–374, 372*f*, 373*t*, 392
ionic conducting studies, 375–379, 376–379*f*, 393
membrane fabrication, 369
scanning electron microscopy (SEM), 371–372, 371*f*, 392
Wagner's polarization methods, 393
X-ray diffraction (XRD), 369–371, 370*f*, 392
solid polymer electrolyte (SPE), 358
Porous silicon (PSi), 239, 240*f*
Porous silver nanofilms, 194
Portable nanosensors, 58–61, 60*f*
Posttranslational modifications (PTM), 428
Prostate-specific antigen (PSA), 101, 102*f*, 274
Protein cages, 416
asymmetric units, 415–416
definition, 415–416
nanoparticles, for drug delivery, 426
active targeting, 426–427
advantages and disadvantages, 427
applications, 428
passive targeting, 426–427
nonviral cages, 418*f*
ferritins, 415–416, 419
heat-shock proteins (Hsps), 415–416, 419
vault proteins (VPs), 419–420
residue-specific amino acid modification strategies, 417
arginine, 424–425
carboxyl, 422, 423*f*
cystines, 422–424, 423*f*
lysine, 421–422, 421*f*
methionine, 425–426
tryptophan, 425
tyrosines, 424, 425*f*
static pores, 415–416
viral protein cages, 416, 418*f*
adenovirus (Adv), 416–417
cowpea chlorotic mottle virus (CCMV), 415–417
cowpea mosaic virus (CPMV), 416–418
internal cavities, 416–417
*Q*β bacteriophage, 419
Proton exchange membrane fuel cell, 384
PS. *See* Polystyrene (PS)
Pseudomonas aeruginosa, 67
P-type semiconductors, 131, 234–235
PUs. *See* Polyurethanes (PUs)
PVA. *See* Poly (vinyl alcohol) (PVA)
PVD. *See* Physical vapor deposition (PVD) technique
PVdF. *See* Polyvinylidene fluoride (PVdF)
PVM. *See* Parallel Virtual Machine (PVM)
Pyrethroids, 73–74, 75–76*f*

Q

*Q*β bacteriophage, 418*f*, 419
Quantum dots (QDs), 106–107, 168, 198
CdSe/ZnS quantum dots, 237–239, 239*f*
definition, 237–239
Quartz crystal microbalance (QCM), 100–101
Quinoxaline-2-carboxylic acid, 146

R

Random copolymer, 354
Ratiometric colorimetric sensor, 71
Ratiometric sensor (RMS), 68–71
RBGS. *See* Red-Black Gauss-Seidel method (RBGS)
ReACT, 425–426
Reactive deposition, 241
Reactive ion plating, 242
Reactive sputter deposition, 242
Recognition elements, 54–57
Red-Black Gauss-Seidel method (RBGS), 27–32, 32–33*f*, 36*t*
Reduced graphene oxide (rGO), 326, 332
ammonia gas (NH_3) sensor
GO, rGO, and $CuFe_2O_4$ nanocomposites, 267–268, 267*f*

NFI-rGO materials, 270
pristine CuO and rGO-CuO nanocomposite, 266–267, 267*f*
rGO-$CuFe_2O_4$ composite-based sensor, 267–268, 267*f*
nanoparticles, 204
Reduced graphene sheets-gold nanoparticles, 205
Reflectometric interference spectroscopy (RIfS), 107–108
Reinforced composites, 356
Rolling circle amplification (RCA), 68
Rubbers, 354

S

Saccharomyces cerevisiae extract synthesized gold nanoparticles, 189–192*t*, 199
Salmonella typhi, 63–64
SAPs. *See* Superabsorbent polymers (SAPs)
SAXS. *See* Small angle X-ray scattering (SAXS)
Scanning electron microscopy (SEM), 97, 286, 371–372, 371*f*, 392
Scatchard analysis, 98–99, 98*f*
SC-LPs. *See* Side-chain liquid crystal polymers (SC-LPs)
Screen printing, 243
Selective detection, 58–61
SELEX, 149–151
SEM. *See* Scanning electron microscopy (SEM)
Semiconducting metal oxides
gas sensors, 266
nanostructures, 131–132, 230
Semiconductor-based nanowires, 172–173
Semicovalent imprinting, 91–93
Semorex, 115–116
Sensors, 3, 127, 163–164, 323
biosensors (*see* Biosensors)
chemical sensors, 127
affinity interaction, 232
definition, 231–232
functions, 231–232
ion sensor, 232
transducer and sensing element, 231–232
ZnO-based chemical sensors, 232, 233*f*
electrochemical (*see* Electrochemical sensors)
fabrication techniques
chemical vapor deposition (CVD) technique, 242
drop coating, 243
physical vapor deposition (PVD) (*see* Physical vapor deposition (PVD) technique)
screen printing, 243
spray pyrolysis, 243
gas (*see* Gas sensors)
LC thermal sensors (*see* Temperature sensor, liquid crystals)
nanobiosensors (*see* Nanobiosensors)
nanocomposite polymer gel electrolytes, 366
nanosensors (*see* Nanosensors)
SERS. *See* Surface-enhanced Raman spectroscopy (SERS)
Shape memory polymers (SMPs), 408
Short interfering RNA (siRNA), 426–427
Sialic acid (SA), 104–105
Side-chain liquid crystal polymers (SC-LPs), 300, 300*f*
Silicon dioxide nanoparticles, 193–194, 204
Silicon nanodots (Si NDs), 71
Silicon nanowire-gold nanoparticles, 205
Silicon nanowires (SiNWs)
biosensors, 172–173
for cellular recordingcellular recording, 204
field effect transistor-based miniature devices, 180
flu diagnosis, 52–53
gold nanoparticle electrodes, 211
sensor, 8–9, 9*f*
Silver-copper oxide-reduced graphene oxide nanocomposite, 206–207
Silver-multiwalled carbon nanotubes-iron oxide magnetic multilayered nanocomposites, 197
Silver nanofilms, 194
Silver nanoflower-reduced graphene oxide composite, 210–211
Silver nanoparticle-aptamer, 203–204
Silver nanoparticles (AgNPs), 103–105, 142, 237
acetylcholinesterase detection, 192–193
antibiotics detection, in milk, 192–193
beta-amyloid oligomer detection, 192–193
catechol detection, in green tea samples, 192–193
guanine and adenine detection, 192–193
human chorionic gonadotropin in human serum/urine samples, detection of, 192–193
human IgG detection, 192–193
poly-L-lysine and 11-mercaptoundecanoic acid detection, 206
Silver nanosheets, 194
Silver nanowires, 194
Simazine, 72
SIMD, 33, 34*f*
Single-walled carbon nanotubes (SWCNTs), 8, 57–61, 77, 146–147, 171–172, 171*f*, 197–198, 325, 330–331, 334
Small angle X-ray scattering (SAXS), 23–24
Small heat-shock protein (sHsp), 419
Soft lithography, 91–93, 96–97, 96*f*
Solar cells, 367–368, 367*f*
Sol-gel method, 91–93, 258, 259*f*, 268
Solid electrolyte, 356–357

Solid oxide fuel cells (SOFCs), 384
Solid polymer electrolyte (SPE), 358
Solid-state reaction method, 256–257, 257*f*
Solid-state rechargeable battery, 366
Solution method, 154
Solvothermal method, 257–258, 258*f*
SPE. *See* Solid polymer electrolyte (SPE)
Spectral absorption, 28, 28*f*
Spectroscopic biosensors, 200–202*t*, 205–207, 210
Spinodal decomposition, 392
SPR. *See* Surface plasmon resonance (SPR)
Spray pyrolysis, 229–230, 243
Sputtering deposition method, 241–242
Stainless steel-gold-palladium nanoparticles, 203–204
Streptavidin-coated gold nanoparticles, 206
Sulfonamides identification, 146, 150*f*
Sulfur oxides, 263
Superabsorbent polymers (SAPs), 407
Supercapacitors, 366, 367*f*
Superconducting quantum interference devices (SQUIDs), 5–7, 6*f*, 170
Surface acoustic wave (SAW) transducers, 167
Surface-enhanced Raman spectroscopy (SERS), 53, 67–68, 103–105, 105*f*, 142, 206–207
Surface plasmon resonance (SPR), 179, 206
  biosensor, 193–194
  sensor chip, 101, 102*f*
Surface stamping method, 91–93, 96–97, 96*f*
Surface-to-volume ratio, 254–255, 254*f*
Surface treatment, liquid crystals, 297*f*, 298
Surfactants, 343
Synthetic polymers, 352

T

Tattoos, 212–213
Teflon-lined autoclave, 257–258
Temperature sensor, liquid crystals
  benefits, 317–318
  chiral nematic liquid crystal temperature sensor, 309
  experimental set-up, observation, and results, 312–314, 313*f*
  nanomaterial dispersed liquid crystal (NLC), 310–311
  temperature range, 309
  wireless temperature sensor (*see* Wireless liquid crystal temperature sensor)
Template-monomer method, 91–94, 92*f*
Terahertz plasmonic metamaterials, 207
Ternary hybrid nanocomposites, 262, 262*f*
Tetraethoxysilane (TEOS), 110–111
Tetrahydrocannabinol (THC), 106–107
Tetrahydrofuran (THF), 95–96, 369–371
Texture element analysis microscopy (TEAM), 408
Thermal evaporation, 241
Thermal pollution, 350
Thermoplastic elastomers, 354
Thermoplastics, 354
Thermosets, 354
Thermotropic liquid crystals, 298–300, 300–301*f*, 303
Thiacloprid, 72–73
Thiamethoxam, 72–73
Thin films-based sensors, 245, 247*f*
Thioaniline, 145–146
Thionine-graphene nanocomposite, 202–203
Three-dimensional bioMEMs-based MIP sensor, 115–116
Three-dimensional graphene foam-silver nanoparticle, 206–207
Three-dimensional (3-D) nanomaterials, 256, 256*f*, 306–307
Thrombin binding aptamer (TBA), 68
Tin oxide-polyaniline-three-dimensional reduced graphene oxide, 198–199
Tissue engineering, bottom-up approach, 13, 14*f*
Titanium dioxide nanoparticles, 209–210
Titanium dioxide-silver nanoparticles, 206–207
Toluene, 229–230
Top-down approach, 12–13
Toxicants detection, 181
Transferrin (TF), 193–194, 427
Transition metal nanosheets, 189–192*t*, 194
Triangular silver nanoparticles, 206
Triazines, 72
Tributyltin pesticide (TBT), 110–111
Triethoxy orthosilicate (TEOS), 95–96
Trimethylolpropane trimethacrylate (TRIM), 108–110
Trinitrotoluene (TNT), 57–58
Tri-*O*-acetyladenosine (TOAA), 98–99, 98*f*
Tri-sodium citrate, 28
Tryptophan, 425
Two-dimensional metal nanostructures, 194
Two-dimensional (2D) nanocomposites, 296
Two-dimensional (2-D) nanomaterials, 255, 256*f*, 306–307
Typhoid, 211
Tyrosines, 424, 425*f*

U

Ultrasonic assisted nanomanufacturing process, 11, 12*f*
Up-conversion nanoparticles (UCNPs), 53, 55–56*t*

Urea hydrolysis, 403
Urease nanosensors, 61–63

V

Vault proteins (VPs), 418*f*, 419–420
Vertically aligned carbon nanotube (VACNT), 333
Vibrio cholerae, 64–66, 65*f*
4-Vinylphenylboronic acid (VPBA), 101–103
Viral protein cages, 416, 418*f*
  adenovirus (Adv), 416–417
  cowpea chlorotic mottle virus (CCMV), 415–417
  cowpea mosaic virus (CPMV), 416–418
  internal cavities, 416–417
  *Q*β bacteriophage, 419
Virginiamycin, 108–110, 110*f*
Virus-like particles (VLPs), 415–417
Vogel-Tammann-Fulcher (VTF) equation, 363, 364*f*
Volatile organic compounds (VOCs), 52–53, 268, 268*f*, 281–282

W

Wagner's polarization methods, 393–395
Water pollution, 350
Whole cell biosensors, 54–57
Wireless liquid crystal temperature sensor, 314–315
  applications, 317–318
  benefits, 317–318
  design of, 315–316, 315*f*
  pure and dye composite NLC, 316, 317*f*
  resonant frequency response, 316
Wireless nanosensors, 22, 142

X

Xanthine biosensors, 273–274
XO/AuNP/PtNP/MWCNT/GCPE biosensor, 273
XOD biosensor, 272
X-ray absorption near-edge structure (XANES), 23–24
X-ray diffraction (XRD), 369–371, 370*f*, 392
X-ray lithography (XRL), 12, 13*f*, 17
X-ray microcomputed tomography (XCT), 408

Z

Zero-dimensional (0D) nanocomposite, 296
Zero-dimensional (0-D) nanomaterials, 255, 256*f*, 306–307
Zero-dimensional nanostructures, 194–196
Zinc oxide (ZnO)
  chemical sensors, 232, 233*f*
  gas sensors, 237
  nanofilms, 194
  nanoparticles, 193–194
  nanorod arrays, 205
Zinc oxide nanorod modified nickel oxide quantum dots, 205
Zinc oxide-porous carbon nanocomposites, 197
Zinc selenium oxide perovskite nanomaterial, 211
Zinc sulfide (ZnS), 232–234
Zirconia (ZrO_2) nanoparticles, 74
ZnONPs/CNTs composites, 274

NANOFABRICATION FOR SMART NANOSENSOR APPLICATIONS

Edited by Kaushik Pal and Fernando Gomes

Nanofabrication for Smart Nanosensor Applications addresses the design, manufacture, and potentials of a variety of nanomaterial classics for sensing applications. In particular, the book explores simple and cost-effective nanofabrication techniques that are being used to create highly efficient nanosensors and examines their major applications in biomedicine and environmental science.

The book discusses the fundamentals of nanosensor performance, before going on to explain how novel architectures of sensors can be investigated, using a variety of different nanomaterial types. It then moves on to discuss different nanofabrication mechanisms, exploring the conditions under which different techniques should be applied and also outlining toxicity and safety issues related to the creation of nanosensors using certain branches of nanomaterials. A summary is also provided of the major challenges in employing various nanofabrication approaches to these nanomaterials for sensing applications.

This work provides an important resource for nanotechnologists, materials scientists, and engineers making material selection decisions for the new generation of nanosensor devices.

Key Features

- Summarizes current research and applications related to a variety of nanofabrication techniques for the creation of efficient sensing devices.
- Provides readers with an understanding of surfaces and interfaces, a key challenge for those working on hybrid nanomaterials, carbon nanotubes, graphene, polymers, and liquid crystal electrooptical imaging, where the analysis of spectroscopy and electron microscopy responses are vital.
- Discusses the variability and sight recognition of biopolymers, such as DNA molecules, which offer a wide range of opportunities for the self-organization of nanostructures into much more complex patterns.

About the Editors

Kaushik Pal served as Visiting Professor in the School of Energy Materials, International and Inter University Centre for Nanoscience and Nanotechnology (IIUCN), Mahatma Gandhi University, Kottayam, Kerala (India). His research focuses on nanofabrication, functional materials, carbon nanotubes, and nanosized sensing technology.

Fernando Gomes is Associate Professor in the Laboratory of Biopolymers and Sensors/*LaBioS Centro de Tecnologia* at the Federal University of Rio de Janeiro, Brazil. His research focuses on areas regarding the use of renewable resources and nanocomposites in sensors, drug delivery, and environmental recovery.

ELSEVIER elsevier.com/books-and-journals

Material Science

ISBN 978-0-12-820702-4